LEABHARLANN CHOLÁISTE NA TRÍONÓIDE, BAILE ÁTHA CLIATH | TRINITY COLLEGE LIBRARY DUBLIN
Ollscoil Átha Cliath | The University of Dublin

Terms and Conditions of Use of Digitised Theses from Trinity College Library Dublin

Copyright statement

All material supplied by Trinity College Library is protected by copyright (under the Copyright and Related Rights Act, 2000 as amended) and other relevant Intellectual Property Rights. By accessing and using a Digitised Thesis from Trinity College Library you acknowledge that all Intellectual Property Rights in any Works supplied are the sole and exclusive property of the copyright and/or other IPR holder. Specific copyright holders may not be explicitly identified. Use of materials from other sources within a thesis should not be construed as a claim over them.

A non-exclusive, non-transferable licence is hereby granted to those using or reproducing, in whole or in part, the material for valid purposes, providing the copyright owners are acknowledged using the normal conventions. Where specific permission to use material is required, this is identified and such permission must be sought from the copyright holder or agency cited.

Liability statement

By using a Digitised Thesis, I accept that Trinity College Dublin bears no legal responsibility for the accuracy, legality or comprehensiveness of materials contained within the thesis, and that Trinity College Dublin accepts no liability for indirect, consequential, or incidental, damages or losses arising from use of the thesis for whatever reason. Information located in a thesis may be subject to specific use constraints, details of which may not be explicitly described. It is the responsibility of potential and actual users to be aware of such constraints and to abide by them. By making use of material from a digitised thesis, you accept these copyright and disclaimer provisions. Where it is brought to the attention of Trinity College Library that there may be a breach of copyright or other restraint, it is the policy to withdraw or take down access to a thesis while the issue is being resolved.

Access Agreement

By using a Digitised Thesis from Trinity College Library you are bound by the following Terms & Conditions. Please read them carefully.

I have read and I understand the following statement: All material supplied via a Digitised Thesis from Trinity College Library is protected by copyright and other intellectual property rights, and duplication or sale of all or part of any of a thesis is not permitted, except that material may be duplicated by you for your research use or for educational purposes in electronic or print form providing the copyright owners are acknowledged using the normal conventions. You must obtain permission for any other use. Electronic or print copies may not be offered, whether for sale or otherwise to anyone. This copy has been supplied on the understanding that it is copyright material and that no quotation from the thesis may be published without proper acknowledgement.

INVESTIGATIONS OF PHYSICOCHEMICAL PROPERTIES OF SPRAY DRIED DRUG-EXCIPIENT COMPOSITES DIRECTED TO INHALABLE PRODUCTS

by

Lidia Tajber, M.Sc. (Pharm.), Dip. Stat. Q.I.

being a thesis submitted for the degree of
Doctor of Philosophy in Pharmaceutics

at
University of Dublin
Trinity College

under the supervision and direction of
Anne Marie Healy, B. Sc. (Pharm.), Ph.D., M.P.S.I.
and
Professor Owen I. Corrigan,
B.Sc. (Pharm.) (N.U.I.), M.A., Ph.D. (N.U.I.), F.T.C.D., F.P.S.I.

March 2005

TRINITY COLLEGE
0 5 AUG 2008
LIBRARY DUBLIN
A68 15
8528

DECLARATION

This thesis is submitted by the undersigned to the University of Dublin, Trinity College, for examination for the degree of Doctor of Philosophy. It has not been submitted for a degree at any other university. I myself carried out all the practical work except where duly acknowledged. This manuscript was written by me with the help of editorial advice from Dr. A. M. Healy and Prof. O.I. Corrigan.

Lidia Tajber

Lidia Tajber

TABLE OF CONTENTS

Acknowledgements i

Presentations and Publications associated with this thesis ii

Abbreviations and Symbols iii

Summary vii

INTRODUCTION

Origin and scope of the thesis 1

Chapter 1 Introduction 2

1.1 Spray drying 2

1.2 Pulmonary delivery 5

1.2.1 Delivery devices 6

1.2.1.1 Dry powder inhalers (DPIs) 6

1.2.1.2 Metered dose inhalers (MDIs) 7

1.2.1.3 Other devices (nebulisers) 8

1.3 Solid state properties of pharmaceutical materials 9

1.3.1 Polymorphism and pseudopolymorphism 9

1.3.2 Amorphous state 10

1.3.3 Solid dispersions 11

1.4 Characterisation of pharmaceutical powders 13

1.4.1 X-ray diffraction analysis (XRD) 13

1.4.2 Thermal analysis 14

1.4.3 Infrared spectroscopy 15

1.4.4 Particle size and size distribution 16

1.4.5 Particle shape 18

1.5 Characterisation of aerodynamic properties of medicinal aerosols 19

1.5.1 Twin stage impinger 19

1.5.2 Other in vitro devices 20

1.6 Background to drugs used in the current work 21

1.6.1 Budesonide 21

1.6.2 Salbutamol base 22

1.6.3 Formoterol 23

1.6.4 Bendroflumethiazide 23

1.6.5 Hydroflumethiazide 24

1.6.6 Hydrochlorothiazide 24

DECLARATION

This thesis has not been submitted as an exercise for a degree at any other university. Except where stated, the work described therein was carried out by me alone.

I give permission for the Library to lend or copy this thesis upon request.

Signed: Lidia Teyber

EXPERIMENTAL

Chapter 2 Materials and methods 25
2.1 Materials 25
2.2 Methods 28
2.2.1 Spray drying 28
2.2.2 Preparation of solid dispersions 28
2.2.2.1 Spray drying 28
2.2.2.2 Differential scanning calorimetry (DSC) 28
2.2.2.3 Melt method 28
2.2.3 Preparation of physical mixtures 28
2.2.4 Thermal methods 29
2.2.4.1 Differential scanning calorimetry (DSC) 29
2.2.4.2 Thermogravimetric analysis (TGA) 29
2.2.5 Density measurement 29
2.2.5.1 Helium pycnometry 29
2.2.5.2 Bulk (aerated) and tap densities 29
2.2.6 X-ray methods 29
2.2.6.1 Powder X-Ray diffraction (XRD) 29
2.2.6.2 Energy Dispersive X-Ray Analysis (EDXA) 30
2.2.7 Microscopy 30
2.2.7.1 Scanning Electron Microscopy (SEM) 30
2.2.7.2 Transmission Electron Microscopy (TEM) 30
2.2.8 Fourier transform infra-red spectroscopy (FTIR) 30
2.2.8.1 FTIR peaks deconvolution 30
2.2.9 High pressure liquid chromatography (HPLC) 30
2.2.9.1 Analysis of budesonide as well as budesonide and formoterol fumarate in samples containing a mixture of the two drugs 31
2.2.9.2 Analysis of formoterol fumarate 31
2.2.9.3 Stability indicating assay for formoterol fumarate dihydrate 31
2.2.10 Particle size characterisation 31
2.2.10.1 Malvern Mastersizer 2000 31
2.2.10.2 Sympatec 32
2.2.10.3 SEM 32
2.2.11 In vitro aerosol characterisation 32
2.2.12 pH measurement 33
2.2.13 Determination of water content in HFA 134a propellant 33
2.2.14 Preparation of MDI systems 33
2.2.15 Dispersibility study of MDIs 33

2.2.16 Chemical stability study of formoterol fumarate 34
2.2.16.1 Aqueous solution kinetic studies 34
2.2.16.2 Preparation of buffer solutions 34
2.2.16.2.1 Britton-Robinson buffer 34
2.2.16.2.2 Phosphate buffers 34
2.2.16.2.2 Citrate buffers 35
2.2.16.3 Solid state stability study 35
2.2.16.4 Stability of formoterol fumarate MDI formulations 36
2.2.17 Solubility study of surfactants in HFA-134a3 36
2.2.18 Statistical analysis and data fitting 36

RESULTS AND DISCUSSION

Chapter 3 Spray drying of salbutamol base and its excipient containing composites 37
3.1 Introduction 37
3.2 Spray dried salbutamol base 37
3.2.1 Physicochemical characteristics 39
3.2.2 Influence of the spray drying conditions on crystallinity of salbutamol base 43
3.3 Salbutamol base co-spray dried composites 44
3.3.1 Introduction 44
3.3.2 Co-spray dried salbutamol base and lactose monohydrate 45
3.3.3 Co-spray dried salbutamol base and trehalose dihydrate 48
3.3.4 Co-spray dried salbutamol base and maltodextrin 51
3.3.5 Co-spray dried salbutamol base and PVP 53
3.4 Conclusions 56

Chapter 4 Factorial design study of co-spray dried budesonide-formoterol fumarate dihydrate 100:6 58
4.1 Introduction 58
4.2 Design study – structure 59
4.3 The statistical analysis of the 25-1 factorial design 61
4.3.1 Experimental design: response "percentage yield" 61
4.3.2 Experimental design: response "median particle size" 65
4.3.3 Experimental design: response: "Carr's compressibility index" 68
4.3.4 Experimental design: response "in vitro respirable fraction" 72
4.3.5 Statistical analysis of the true density values 76
4.4 Physicochemical characterisation 77
4.4.1 Formoterol fumarate 77

4.4.2 Budesonide 81
4.4.3 Budesonide/formoterol fumarate dihydrate 100:6 83
4.5 Conclusions 86

Chapter 5 Co-spray dried formoterol fumarate dihydrate/excipient composites for use in DPIs 89
5.1 Introduction 89
5.2 Formoterol fumarate dihydrate and PEG 20000 systems 90
5.2.1 Spray dried PEG 20000 90
5.2.2 Co-spray dried formoterol fumarate/PEG 20000 94
5.3 Co-spray dried formoterol fumarate dihydrate and PVP 10000 systems 98
5.4 Co-spray dried formoterol fumarate dihydrate and trehalose dihydrate systems 102
5.5 Co-spray dried formoterol fumarate dihydrate and raffinose pentahydrate systems 105
5.6 Co-spray dried formoterol fumarate dihydrate and hydroxypropyl-β-cyclodextrin systems 109
5.7 Co-spray dried formoterol fumarate dihydrate and Brij 58 systems 114
5.8 Co-spray dried formoterol fumarate dihydrate and Myrj 59 systems 117
5.9 In vitro respirable fractions assessment by twin stage impinger 119
5.10 Conclusions 123

Chapter 6 Co-spray dried budesonide/excipient(s) systems for use in DPIs 125
6.1 Introduction 125
6.2 Co-spray dried budesonide and raffinose pentahydrate 30% system 126
6.3 Co-spray dried budesonide/hydroxypropyl-β-cyclodextrin 30% 128
6.4 Budesonide/stearic acid systems 129
6.4.1 Budesonide co-spray dried with PVP 10000 and stearic acid 132
6.5 Budesonide/ascorbyl palmitate systems 135
6.6 Budesonide/Aerosil 200 Pharma systems 137
6.7 Budesonide/microcrystalline cellulose systems 139
6.8 Evaluation of in vitro respirable fractions of the co-spray dried budesonide systems by twin stage impinger 142
6.9 Budesonide/magnesium stearate systems 144
6.9.1 Introduction 144
6.9.2 Physicochemical characterisation of the "as received" and spray dried magnesium stearate samples 145
6.9.3 Budesonide/magnesium stearate Élan systems 150
6.9.3.1 Co-spray dried budesonide/magnesium stearate Élan 150

6.9.3.2 Co-spray dried budesonide, PVP 10000 and magnesium stearate Élan 153
6.9.4 Co-spray dried budesonide/magnesium stearate Aldrich systems 154
6.9.4.1 Co-spray dried budesonide/magnesium stearate Aldrich 154
6.9.4.2 Co-spray dried budesonide, PVP 10000 and magnesium stearate Aldrich 157
6.9.5 Co-spray dried budesonide/magnesium stearate Riedel de Haën systems 157
6.9.5.1 Co-spray dried budesonide/magnesium stearate Riedel de Haën 157
6.9.5.2 Co-spray dried budesonide, PVP 10000 and magnesium stearate Riedel de Haën 158
6.10 Evaluation of in vitro respirable fractions of the co-spray dried budesonide/magnesium stearate systems by twin stage impinger 159
6.11 Production and characterisation of budesonide porous particles 161
6.11.1 Twin stage impinger studies 165
6.12 Crystallinity of co-spray dried budesonide systems by FTIR and XRD 168
6.13 Conclusions 171

Chapter 7 Stability of formoterol fumarate in MDI formulations 173
7.1 Introduction 173
7.2 Chemical stability of formoterol fumarate in solutions 174
7.2.1 Order of reaction 174
7.2.2 HPLC assay and degradation products of formoterol 175
7.2.3 pH-rate degradation profile 176
7.2.3.1 Britton-Robinson buffer at 40˚C 176
7.2.3.2 Britton-Robinson buffer at 25˚C 181
7.2.3.3 0.1 M solution of HCl at 25°C 182
7.2.3.4 Phosphate buffer at 25 °C 183
7.2.3.5 Citrate buffer at 25 °C 184
7.2.4 Buffer catalysis 185
7.2.4.1 Phosphate buffer 185
7.2.4.2 Citrate buffer 186
7.2.5 Stability study in ethanol-water mixtures 188
7.2.6 The effect of drug concentration 190
7.3 Spray drying of excipients and formoterol fumarate-excipient(s) systems 191
7.3.1 Introduction 191
7.3.2 Mannitol 192
7.3.3 Xylitol 198
7.3.4 Hydroxypropylmethylcellulose grade (HPMC) E5 199
7.3.5 PVP 202

7.3.6 Dispersibility study of the spray dried excipients in HFA-134a 205
7.3.7 Co-spray dried mannitol/HPMC 211
7.3.8 Co-spray dried mannitol/PVP 213
7.3.9 Co-spray dried mannitol/formoterol fumarate dihydrate 216
7.3.10 Solid state pH modification of formoterol fumarate 219
7.3.11 Introductory experiments-pH of concentrated and diluted buffer solutions 219
7.3.12 Co-spray drying of mannitol/formoterol fumarate dihydrate/ buffer salts composites 222
7.3.12.1 Mannitol/formoterol fumarate dihydrate 10%/citrate buffer (citric acid:tri-sodium citrate 1.5:8.5) 1% (w/w) 222
7.3.12.2 Mannitol/formoterol fumarate dihydrate 10%/phosphate buffer (sodium dihydrogen phosphate:di-sodium hydrogen phosphate 7:3) 1% (w/w) 224
7.3.13 Co-spray drying of mannitol/formoterol fumarate dihydrate/calcium chloride dihydrate composites 225
7.3.13.1 Mannitol/formoterol fumarate dihydrate 10%/calcium chloride dihydrate 5% (w/w) 225
7.3.13.2 Mannitol/formoterol fumarate dihydrate 10%/calcium chloride dihydrate 5% (w/w)/citrate buffer (citric acid:tri-sodium citrate 1.5:8.5) 1% (w/w) 225
7.3.14 Dispersibility study of formoterol fumarate dihydrate and co-spray dried systems in HFA134a 226
7.3.14.1 Binary co-spray dried mannitol/excipient mixtures 226
7.3.14.2 Formoterol fumarate dihydrate starting material and its co-spray dried systems 226
7.3.14.3 Conclusions from the dispersibility studies of formoterol fumarate dihydrate and co-spray dried composites 228
7.4 Solid state stability study of formoterol fumarate dihydrate and its co-spray dried composites 228
7.4.1 Stability study of formoterol fumarate composites at 25°C and 60% relative humidity 228
7.4.2 Stability study of formoterol fumarate composites at 40°C and 75% relative humidity 229
7.5 Chemical stability of formoterol fumarate in pMDI formulations 231
7.6 Conclusions 232

Chapter 8 Glass transition composition relationships of amorphous drug/PVP composites 234
8.1 Introduction 234
8.2 Theoretical background 235

8.3 Salbutamol base/PVP composites 239
8.3.1 Thermal analysis 239
8.3.2 FTIR analysis 241
8.4 Thiazide diuretics/PVP composites 243
8.4.1 Thermal analysis 244
8.4.2 FTIR analysis 249
8.4.2.1 Crystalline compounds 249
8.4.2.2 Amorphous compounds 251
8.4.2.3 Co-spray dried composites 251
8.5 Conclusions 254

Chapter 9 General discussion 255
9.1 Introduction 255
9.2 Morphology and aerolisation properties of systems for inhalation purposes 255
9.2.1 Dry powder inhalers 255
9.2.2 Metered dose inhalers 261
9.3 Crystallinity of spray dried systems 263
9.3.1 Systems spray dried alone 263
9.3.1.1 Drugs spray dried alone 263
9.3.1.2 Polymers spray dried alone 264
9.3.1.3 Excipients spray dried alone 265
9.3.2 Systems spray dried as mixtures 266
9.3.2.1 Formoterol fumarate systems 267
9.3.2.2 Budesonide systems 269
9.3.2.3 Mannitol systems 270
9.4 Interactions in co-spray dried polyvinylpyrrolidone (PVP) systems 270
9.5 Main findings 275
9.6 Future work 276

References 277

Appendices

Appendix I 301
Appendix II 309
Appendix III 310
Appendix IV 311
Appendix V 312
Appendix VI 313

ACKNOWLEDGEMENTS

I would like to thank my supervisors, Prof. Owen Corrigan and Dr. Anne Marie Healy for giving me this opportunity for doing a Ph.D. degree in the Trinity College. I am very grateful for your guidance and support during the course of my research and especially in the preparation of this thesis.

I am grateful to the academic, secretarial and technical staff of the School of Pharmacy, in particular Liesa, Derek Cos, Brian, Pat and Derek Bell. I would like to thank to Neal and Colin of the CMA for all their help with microscopy.

I wish to thank the Trinity Trust for the postgraduate award and for travel grants which allowed me to attend an international conference in Nuremberg.

My thanks also goes to my lab mate Deirdre D. for all the "serious" conversations and proof read of some of the chapters. Thanks to my fellow postgrads: Helena, Anne, Anthony, Mark, Fiona B., Karl, Len, Emma, Rob, Fiona N. Alamaith, Jenny, and the others for all the coffee breaks (too few!) and chatting in the hallway. I am very grateful for Katie, Alecia and Lorraine for correcting the language lapses in this thesis. Thanks to the Pharm Chem and Pharmacognosy people for the parties. Thanks to Carsten for sharing that lovely German music.

Special thanks for Deirdre Corrigan for being very, very helpful in year one and introducing me to the world of spray drying.

For my crowd back in Poland - Wielkie dzięki za wszystko!

My very special thanks to Sergey (Misiu Malinkowy) for his support.

Thanks to my parents and my sister Joanna for all their encouragement, love and support.

PRESENTATIONS AND PUBLICATIONS ASSOCIATED WITH THIS THESIS

Oral Presentation

"The use of statistical factorial design in the production of a spray dried powder" at the 2nd Advanced School for Pharmacutical Technology "Innovative therapeutics: from molecules to drugs", Italy, June, 2002. [Lidia Tajber, Anne Marie Healy, Owen I. Corrigan]

Poster Presentations

"Calculating the glass transition temperature of mixtures - a comparison of different approaches", at the Annual Postgraduate research Seminar, Trinity College Dublin, March 2003. [Lidia Tajber, Deirdre O. Corrigan, Sophia Berrada Souni, Owen I. Corrigan and Anne Marie Healy]

"The effect of polyvinylpyrrolidone content on the glass transition temperature of thiazide diuretics", at the International Meeting on Pharmaceutics, Biopharmaceutics and Pharmaceutical Technology, Nuremberg, Germany, March 2004. [Lidia Tajber, Anne Marie Healy and Owen I. Corrigan]

Publication

"Physicochemical evaluation of PVP–thiazide diuretic interactions in co-spray-dried composites—analysis of glass transition composition relationships", Eur. J. Pharm. Sci., 24 (2005) 553-563. [Lidia Tajber, Owen I. Corrigan and Anne Marie Healy]

ABBREVIATIONS AND SYMBOLS

-	to
%	percent
°	degree
°C	degree Celsius
~	approximately
$\Delta\alpha$	expansion coefficient
®	registered trademark
μm	micrometer
A	surface area
ACI	andersen cascade impactor
ANOVA	analysis of variance
B.P.	British Pharmacopoeia
BFMT	bendroflumethiazide
CFC	chlorofluorocarbon
cm	centimetre
cm^{-1}	frequency
COPD	chronic obstructive pulmonary disease
CPS	counts per second
CR	crystallisation
CYC	hydroxyproply-β-cyclodextrin
d	density
D	diffusion coefficient
D_{ae}	aerodynamic diameter
DE	desolvation
D_e	equivalent volume spherical diameter
dM/dt	rate of dissolution
DPI	dry powder inhaler
–dR/dt	rate of retreat of the droplet surface

DSC	differential scanning calorimetry
E.P.	European Pharmacopoeia
EDXA	energy dispersive X-ray analysis
ESV	exposure to solvent vapour
EtOH	ethanol
exo	exothermic direction
FD	freeze drying
FF	formoterol fumarate
FTIR	Fourier transform infrared spectroscopy
g	gram
g	gravitational acceleration constant
h	diffusion layer thickness
H	enthalpy
h	hour
H	hydrogen
H_20	water
HCl	hydrochloric acid
HE	heating
HFA-134a	hydrofluorocarbon propellant HFA-134a
HFA-277	hydrofluorocarbon propellant HFA-277
HFMT	hydroflumethiazide
HLB	hydrophilic lipophilic balance
HPLC	high performance liquid chromatography
IR	infrared
J.P.	Japanese Pharmacopoeia
J/g	joules per gram
K	degrees Kelvin
KBr	potassium bromide
k_{obs}	rate constant of the first-order reaction
M	mega
M	moles per litre
MDI	metered dose inhaler
ME	melting

mg	milligram
MI	milling
min	minute
ml	millilitre
MLI	multistage liquid impinger
mM	millimolar
mW	milliwatt
Nl/h	litres/hour
nm	nanometre
Pa	Pascal
PEG	polyethylene glycol
pH	minus log of hydrogen ion concentration
Ph.Eur	European Pharmacopoeia
PR	precipitation
PVP	polyvinylpyrrolidone
QC	quench cooling
R	ideal gas constant (8.314J/K/mol)
R^2	correlation coefficient
RAF	raffinose
RAW	unprocessed
RH	relative humidity
S.D.	standard deviation
SC	slurry conversion
SD	spray dried
SDSP	solid dispersion
SEM	scanning electron microscopy
t	time
$t_{1/2}$	half-life
t_{10}	shelf-life
TEM	transmission electron microscopy
T_g	glass transition temperature
TG	thermogravimetric analysis
TGA	thermogravimetric analysis

T_K	Kauzmann temperature
T_m	melting point
™	trademark
TRE	trehalose
USP	United States Pharmacopoeia
V	specific volume
v/v	volume in volume
w	weight fraction
w/v	weight in volume
w/w	weight in weight
WG	wet granulation
XRD	X-ray diffraction (powder)
α_s	polarizability
Δc_p	change in the heat capacities at the T_g
η	refractive index
κ	dynamic shape factor
λ	wavelength
μ	viscosity
ρ	density
σ	surface tension
φ	volume fraction
ΔH	change in enthalpy
θ	angle of incidence

SUMMARY

The studies in this thesis explored the solid state and inhalation properties of various systems produced by the spray drying technique. The work focused on the feasibility analysis of spray drying as a means of producing materials for pulmonary delivery. The chemical and physical stability of different processed systems have also been addressed. The drugs investigated were salbutamol base, formoterol fumarate dihydrate, budesonide, bendroflumethiazide, hydroflumethiazide and hydrochlorothiazide. In all cases the physicochemical characteristics were studied by differential scanning calorimetry (DSC), thermogravimetric analysis (TGA), infrared (IR) spectroscopy, powder X-ray diffraction (XRD) and scanning electron microscopy (SEM). The inhalation properties were investigated using the twin stage impinger. Different aspects of chemical and physical stability studies were examined.

Spray drying of salbutamol base alone resulted in predominantly amorphous powdered products and the degree of amorphicity depended on the spray drying conditions. Difficulties in processing were observed with the drug exhibiting stickiness due to its low glass transition temperature. Co-spray drying of salbutamol base with sugars and PVP resulted in composite particles that demonstrated a lesser degree of particle fusion.

Budesonide and formoterol fumarate dihydrate when spray dried alone were obtained in amorphous phases. The effect of five variables (air inlet temperature, airflow, pump feed rate, aspirator capacity and feed concentration) on the flowability and physicochemical properties of co-spray dried budesonide-formoterol fumarate dihydrate (100:6) systems were evaluated by a 2^{5-1} factorial experimental design. Amorphous particulate powders were formed in each process and the particles were in the inhalable range. Four responses were evaluated: yield, median particle size, Carr's index and *in vitro* respirable fraction. The sample processed from 1% (w/v) solution at the inlet temperature of 84°C, airflow 400 Nl/h, pump 10%, aspirator 70% gave a 2.6-fold increase in the respirable fraction when compared with the equivalent physical mixture.

Co-spray drying of formoterol fumarate dihydrate with excipients resulted in XRD amorphous systems, except for the drug/PEG 20000 30% sample which had weak peaks of the crystalline polymer. PEG 20000 when processed alone gave material with a reduced degree of crystallinity. The best emitted dose was discerned for spray dried formoterol fumarate/PVP 10000 10%, whereas the best respirable fraction was obtained with co-spray dried formoterol fumarate/hydroxypropyl- β-cyclodextrin 30%.

The particles of the budesonide co-spray dried systems were in the inhalable range. The budesonide/stearic acid and budesonide/magnesium stearate systems were crystalline. The best respirable fraction was achieved with the co-spray dried budesonide/hydroxypropyl-β-cyclodextrin 30% and budesonide/magnesium stearate/PVP 10000 samples. A novel method of preparation of porous particles made solely of budesonide, by spray drying from a solution containing an active and dissolved blowing agent, was presented with one of the porous systems giving an over 6-fold increase in the fine particle fraction compared to that of the budesonide starting powder.

Chemical stability studies of formoterol fumarate in buffered solutions revealed that the pH at which the drug was the most stable was 5.00-5.20, depending on the temperature and buffer used. The stability studies in the dry state showed that mannitol stabilised the drug at low relative humidity and temperature but when dispersed in the propellant (HFA-134a) the unprocessed drug had the best chemical stability. The optimum medium for physical stability in terms of suspension settling rates of the suspension inhaler formulations investigated was a mixture of HFA-134a/ethanol/PVP 40000.

Glass transition composition behaviour for amorphous drug/PVP composites investigated deviated from the predictions of the Gordon-Taylor equation. For the salbutamol base/PVP systems negative deviations were observed, while large positive deviations for the thiazide diuretics/PVP composites were attributed to interactions between the constituents. In the latter case the Schneider equation was used to provide the best fir to the glass transition temperature/composition profiles.

ORIGIN AND SCOPE

Spray drying has been established as a method of production of particles suitable for inhalation purposes (Vidgren *et al.,* 1987; Chawla *et al.* 1994). Co-spray drying may have the advantage that an intimate mixture of two or more compounds can be produced ensuring uniformity of the dose released from the inhaler (Corrigan, 2002). However, despite the usefulness of this technique, spray drying often results in the production of amorphous materials (Corrigan *et al.*, 1984) that may be physically unstable (Gibbs and DiMarzio, 1958). An appropriately selected excipient may be spray dried with the drug, thereby stabilising and improving the shelf-life of the active (Corrigan and Holohan, 1984). The highly disordered substances produced on spray drying tend to be also hygroscopic and difficult to disperse in air. The former problem may be overcome by co-spray drying with hydrophobic excipients, which may prevent moisture sorption, and poor flow predispositions may be improved by a change in the morphology of particles (Dellamary *et al.*, 2000). Other difficulties encountered in the production of medicinal inhalers may arise from reduced chemical stability of a drug, especially when formulated in metered dose inhalers (MDIs). In recent years, due to the elimination of Freon (CFC) gases, commonly used as propellants in MDI formulations, alternative compounds (HFA-134a and HFA-227) have emerged on the market. However, as the new propellants have different physicochemical properties (Zeng *et al.,* 2001), reformulation of the Freon-based MDIs is needed. No commercial formoterol fumarate dihydrate metered dose inhaler based on any of the new propellants has been released to date and moreover, this substance is known to possess low chemical stability (Lewis *et al.,* 2001) when formulated in MDIs. Physicochemical properties of spray dried active substances, excipients and their co-spray dried mixtures were also of interest.

The scope of this thesis was:

- to implement the co-spray drying technique to reduce stickiness and improve respirable fractions of various drugs from dry powder inhalers (DPIs);
- to investigate and characterise the influence of various spray dryer settings on the resulting product in terms of achieving the optimum product to be formulated in inhalers;
- to explore excipients that upon co-spray drying with drugs are potentially able to maximise the respirable fractions achieved when the powder is delivered from a DPI
- to investigate the feasibility and influence of co-spray drying with excipients on a model drug – formoterol fumarate dihydrate as a drug reported to possess poor chemical stability in new generation propellant MDIs and
- to examine the effect of polymers on the physical stability of two component co-spray dried composites.

INTRODUCTION

1.1 Spray drying

Spray drying is a technique whereby particles are produced by atomisation of a solution or slurry and evaporation the solvent from the resulting droplets by suspending them in a hot gas. It is a one step process and easy to control, which makes spray drying a unique and important unit operation. Figure 1.1 presents a schematic of a Büchi B-191 Mini Spray Dryer. The general procedure of spray drying as follows. The liquid feed is pumped to an atomiser, which breaks down the feed into a fine spray, which then enters into the drying chamber. In this chamber the spray is mixed with hot drying gas. The solvent vapour is removed from the spray and the droplets are transformed into dry particles. The separation of the particles from the drying gas takes place in the cyclone the subsequent collection of the product takes place in the collecting vessel.

The spray drying process consists of four steps (Masters, 1985):

- atomisation of the feed into a spray
- spray-air contact
- drying of the spray
- separation of the dried material from the drying gas

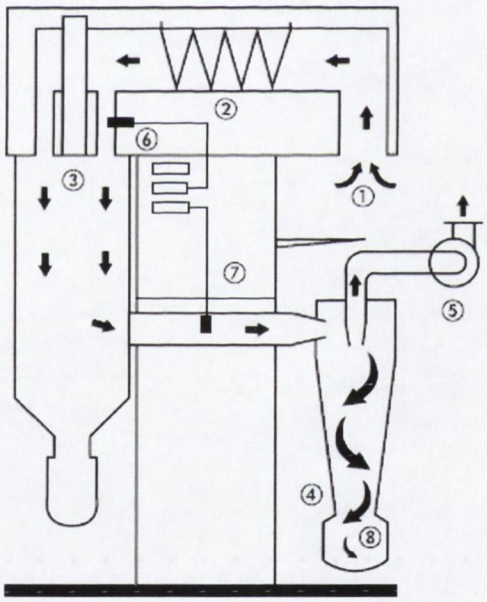

Figure 1.1 Diagram of the spray dryer and the drying medium flow pattern (indicated by arrows). Key : 1 – air intake, 2 – heater, 3 – drying chamber, 4 – cyclone (separation of the product from the drying medium), 5 – aspirator, 6 – temperature sensor for the inlet, 7 – temperature sensor for the outlet, 8 – collecting vessel. Taken from the technical specification on Büchi B-191 Mini Spray Dryer (Switzerland) with modification.

The atomiser is a key component of the spray drying process and its characteristics determine the properties of the dried particles and the design of the rest of the process (Oakley, 1997). Additionally, the droplet size, velocity and spray angle dictate the drying chamber size and shape needed to contain the spray and give the droplets sufficient drying time. Spray dryer atomisers must

deal with viscous solutions and slurries that may contain suspended particles. There is a variety of atomisation systems available, classified according to the nozzle design: rotary, pressure and two-fluid (pneumatic) atomisers (Broadhead *et al.*, 1992). In rotary atomisation the liquid to be atomised is fed onto a rapidly rotating wheel or disc. The liquid is accelerated outward by centrifugal forces and ejects as a thin sheet of liquid that is subsequently broken down into droplets (Oakley, 1997). A pressure nozzle atomiser is a much smaller device than the rotary atomiser and liquid introduced into the nozzle is swirled by a tangential inlet or slotted inserts. The spin has sufficient force to atomise the fluid leaving the nozzle. In two-fluid nozzles the feed and atomising medium are introduced separately to the nozzle, where they mix and the gas stream breaks down the liquid into small droplets (Broadhead *et al.*, 1992). Two-fluid nozzles are frequently used on small-scale production work such as with the Büchi B-191 spray dryer.

The main function of the drying (spray) chamber is to confine the spray and ensure that droplets are dried while still airborne (Oakley, 1997). It is crucial that the drying particles do not strike the walls of the chamber as this will results in deposits and complications in production. The construction of the drying chamber depends on whether a spray dryer operates in a co-current mode, counter-current mode or intermediate between co- and counter-current. With co-current chambers the spray and hot drying gas are both introduced at the top of the chamber and pass in the same direction through the chamber. This method is especially suitable for drying of heat-sensitive materials as they will be protected from the high inlet gas temperature by evaporative cooling (Oakley, 1997). The counter-current method of operation is the reverse arrangements, whereby spray and air enter at the opposite ends of the dryer.

The temperatures and drying conditions to which the drying droplets are subjected have an important effect on the final powder properties. Figure 1.2 shows a typical particle formation mechanism from a droplet containing dissolved solid.

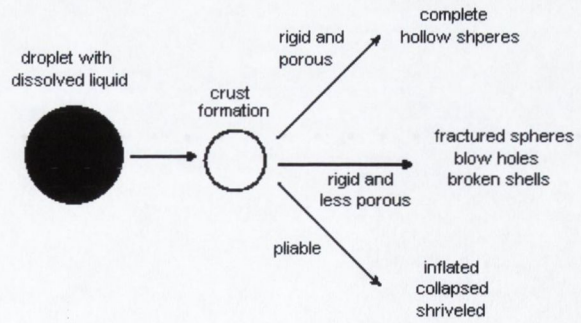

Figure 1.2 Particle formation from a drying droplet. Taken from Oakley (1997).

In the early stages of drying, the temperature on the surface of droplets is equal to that of the saturated solution, hence solvent evaporation is rapid. The depletion of liquid causes the solute to be more concentrated at the surface and this will depend on the speed of evaporation and the rate at which the liquid can be replenished from the interior of the droplet (Oakley, 1997). In spray drying

operations, where the gas temperature is above the boiling point of the droplet solution, vapour may be formed inside the droplets and when the solid phase has formed a crust around each droplet, pressure can be created inside the particle (Masters, 1985). When the forming crust is porous, hollow particles may be obtained (Figure 1.2). If the droplet temperature does not reach the boiling point, moisture movement within the droplet is by diffusional and capillary mechanisms (Masters, 1985). The thickness of the crust depends on the heating rate and high drying rates lead to larger particles with thin shells and low density (Oakley, 1997). Hollow particles may also be formed if a portion of the drying gas is confined within the droplets.

Morphological changes of particles composed of materials that are amorphous after spray drying can be dependent on the physicochemical properties of these substances. Alexander and King (1985) defined a dimensionless parameter θ that compares the relative rates of particle fold (defined as wrinkles on the surface) formation and fold smoothing (Equation 1.1):

$$\theta = \frac{(-dR/dt)\cdot\mu}{\sigma} \qquad \text{(Equation 1.1)}$$

where –dR/dt is the rate of retreat of the droplet surface due to the solvent loss, μ and σ are the viscosity and surface tension, respectively, of the material in the surface layer of the droplet. A folding criterion may be expressed as $\theta >> 1$ – large tendency toward folding and $\theta << 1$ – little or no tendency toward folding.

By modifying the spray drying process it is possible to alter and control physicochemical properties of the powder such as particle size and distribution, bulk density, porosity and flowability (Masters, 1985). For instance, the particle size is usually increased as the feed concentration or viscosity increases (Broadhead *et al.*, 1992). A decrease in the particle size will be achieved if the atomisation energy input is increased.

Spray drying has a wide range of applications in pharmaceutical processing (Broadhead *et al.*, 1992). During the process a polymorphic change often occurs that may lead to the production of amorphous substances (Corrigan *et al.*, 1984). Co-spray drying a drug with excipient(s) may result in the formation of solid dispersions and therefore an enhancement of the dissolution rate of the drug. Corrigan and Holohan (1984) spray dried hydroflumethiazide with 20% (w/w) PVP which allowed the drug apparent solubility to be increased by 4-5-fold compared to that of the corresponding physical mixture. Spray drying has extensively been used as a potential alternative to milling for the production of fine particles suitable for inhalation, but no commercial product containing spray dried particles of a drug has been reported to date. This technique has been used to produce carrier particles for DPIs such as spray dried lactose (Harjunen *et al.*, 2002a). Spray dried particles are often more spherical in shape than micronised powder particles and therefore are attractive for inhalation purposes e.g. disodium cromoglycate (Vidgren *et al.*, 1987) and salbutamol sulphate (Chawla *et al.*, 1994). Spray drying from non-aqueous liquids has been used to prepare porous particles suitable for aerosol delivery (Dellamary *et al.*, 2000). This manufacturing method

can also be employed to prepare protein powders for inhalation (Bot *et al.*, 2000; Ståhl *et al.*, 2002).

1.2 Pulmonary delivery

Inhaled medications have been available for many years for the treatment of lung diseases and are widely accepted as first-line therapy for asthma and chronic obstructive pulmonary disease (COPD) (Labiris and Dolovich, 2003a). The lung has also been considered as a possible route of administration for the treatment of systemic diseases. They are two primary modes of pulmonary administration: nasal and oral inhalation (Groneberg *et al.*, 2003).

Before the inhaled drug can be absorbed into the blood stream it has several barriers to overcome: lung surfactant, surface lining fluid, epithelium, interstitium and basement membrane and the endothelium (Labiris and Dolovich, 2003a). Drug absorption is regulated by a thin alveolar-vascular permeable barrier, but as the number of alveoli ranges from 200 to 600 million, the resulting epithelial surface area is enormous and consists only of a single cellular layer (Labiris and Dolovich, 2003a). Therefore, a rapid onset of the drug action can be achieved with this route of delivery. The high bioavailability of macromolecules deposited in lungs (10-200 times greater than gastrointestinal route) may be due to the vast surface area, very thin diffusion layer, low surface clearance and antiprotease defence system (Patton, 1996).

Aerosol particle size is one of the most important variables in determining the dose deposited and distributed in different parts of the lung. Particles may be deposited by inertial impaction, gravitational sedimentation and diffusion (Zeng *et al.*, 2001). Inertial impaction occurs during the passage through the oropharynx and large conducting airways if the particles have aerodynamic diameters above 3 μm (Groneberg *et al.*, 2003). The aerodynamic diameter is the diameter of a sphere with unit density that has aerodynamic behaviour identical to that of the particle in question. Larger particles are usually swallowed and their contribution to the therapeutic response is minimal. Gravitational sedimentation prevails in smaller bronchi and bronchioles, and the particles deposited in these regions normally have aerodynamic diameters of between 1 and 3 μm. Smaller particles are deposited in the alveolar region by both sedimentation and diffusion. Morphological, particle size and geometry aspects of inhaled particles together with ventilatory parameters have a crucial influence on the site, extent and efficacy of deposition in the lung (Groneberg *et al.*, 2003). Also, deposition is influenced by the particle source which can be a solution, powder or suspension (Martonen and Katz, 1993). A summary of factors affecting the pulmonary delivery of drugs is presented schematically in Figure 1.3.

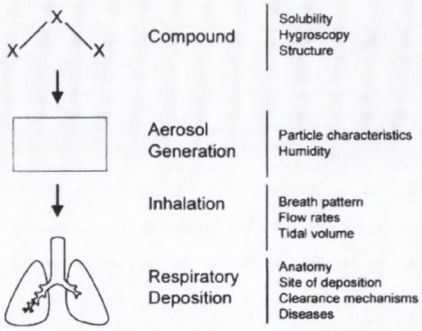

Figure 1.3 Factors affecting the pulmonary delivery of drugs (taken from Groneberg *et al.* (2003)).

1.2.1 Delivery devices

1.2.1.1 Dry powder inhalers (DPIs)

The first successful dry powder inhaler, the Spinhaler®, was introduced in the 1960s and was designed for the delivery of disodium cromoglycate (Bell *et al.*, 1971). Over recent years, dry powder inhalers (DPIs) have become more attractive and they have many advantages over MDIs and nebulisers. They contain no volatile propellants and dispersion of drug particles is caused by the inhalation efforts of the patient alone (Zeng *et al.,* 2001). Furthermore, DPIs are environmentally friendly, easy to use and handle and there is no issue of synchronisation of actuation and inhalation as is required to operate MDIs properly. The active is in the form of a micronised dry powder. Typically the particle size of the drug ranges between 1 μm and 5 μm in diameter. As drugs are kept in the solid state, it is expected that DPI formulations would exhibit a high physicochemical stability (Zeng *et al.,* 2001). An ideal DPI should be simple to use, compact, inexpensive, produce high aerolisation efficiency with low inspiratory effort, produce reproducible emitted and fine particle doses, preferably be a multidose device and maintain physicochemical stability of the powder formulations (Timsina *et al.*, 1994). Many types of DPI devices have been commercially available but none of them meets all the requirements of the ideal device. The most popular of them include: Spinhaler®, Rotahaler® and Turbohaler®. The Spinhaler® employs a gelatin capsule to contain the dose of the micronised drug particles mixed with lactose carrier particles. The capsule is placed in a rotor and before inhalation the drug particles are released from the capsule by actuating the device which pierces the capsule with metal needles (Zeng *et al.,* 2001). The Rotahaler® also uses gelatine capsules, but in this device the capsule is broken before inhalation by twisting the segments of the device. The first multidose device was Turbohaler® introduced by Astra Pharmaceuticals. In this device, a disposable reservoir is employed to meter the dose of the drug on priming the inhaler (Zeng *et al.,* 2001). They are also other devices on the market: Ultrahaler® (Fisons), Diskus® (GlaxoWellcome), Easyhaler® (Orion) and Clickhaler® (ML Laboratories).

Micronised powders used in DPI formulations are not easy to handle. A typical dose of the active may be only 100 micrograms, therefore the common approach is to mix the micronised drug with a bulking agent such as lactose. The bulking agent aids the delivery of the correct dose and the lactose/drug mixture has better flow properties than the pure micronised active. The lactose carrier has particles in the range 50 μm to 100 μm in diameter (Houzego, 2002). The formulations of the drug and excipient used in a DPI have a major impact on the performance of the inhaler. The excipient must be safe for inhalation and lactose monohydrate is used as the standard. Typically the formulations used in DPIs contain between 0.5% and 5% of the drug blended with lactose (Houzego, 2002). During inhalation it is necessary to separate the particles of the drug adhered to the carrier particles. This process is termed deagreggation. They are at least four different adhesion forces: surface tension if water is present between the particles, electrostatic if the particles have opposite charges, van der Waals at the contact point and chemical bonding (Hickey *et al.*, 1994). For the deagreggation process to occur, a means must be provided to detach the drug particles from the lactose. Two approaches are employed in DPIs and rely solely on the energy available in the airstream: aerodynamic – removal of the particles of the active using the turbulent air flowing over the lactose particles and inertial – removal of the drug particles by impact of the lactose particles onto a surface.

1.2.1.2 Metered dose inhalers (MDIs)

Metered dose inhalers (MDIs) were introduced in the 1950s (Zeng *et al.*, 2001). They were developed as locally administered aerosol delivery devices for the treatment of asthma and were the first and simplest examples of targeted drug delivery (Stefely, 2002). The therapeutic dose delivered by means of MDI can be substantially lower than that achieved by oral therapy. The negative side effects of drugs can also be minimised. Nowadays, inhalation delivery has expanded to treat not only pulmonary diseases, but also diseases requiring systemic delivery. These include systemic therapies requiring fast onset of action of the drug (e.g. pain management) and avoidance first-pass metabolism (e.g. delivery of protein and peptides). The first MDIs consisted of a pressurised container containing the drug dissolved or dispersed in a suitable liquid freon propellant. MDIs may also contain auxiliary materials such as solvents, solubilising agents, suspending agents and a lubricant to prevent blocking of the valve (Zeng *et al.*, 2001).

MDIs are small, portable and quick to use. Generally, every MDI is composed of four major elements. The vial and metered dose valve comprise the container closure systems. The actuator's purpose is to control the discharge of the device. The spray released from the MDI every time it is actuated consists of a metered volume of propellant containing a predetermined dose of the drug (Zeng *et al.*, 2001). The formulation is composed of the drug and the propellant, which plays a vital role in the performance of MDI. The propellant provides the energy needed to aerosolise the formulation (Stefeley, 2002).

They are two major drawbacks associated with the use of MDIs. First is poor coordination between actuation and inhalation. This problem is of most concern in clinical application, since many patients cannot operate the device properly even after extensive training (Zeng *et al.,* 2001). The second disadvantage is associated with the freon (CFC-chlorofluorocarbon) propellants employed in MDIs. These compounds are gradually decomposed in the upper atmosphere by solar ultraviolet radiation, the chlorine radicals are released and result in catalytic conversion of ozone to molecular oxygen and this leads to the depletion of the ozone layer (Vaswani and Creticos, 1998). The non-chlorine compounds that can be used as propellants in MDI formulations include hydrofluorocarbons: HFA-134a and HFA-227. However, they have very different physicochemical properties than the CFC propellants. Particularly, the polarity, vapour pressure and density are considerably different and the MDIs have to be reformulated (Zeng *et al.,* 2001). There have been numerous approaches taken to overcome the problems of drug particle stability in the HFA propellants and these include (Smith, 2002): increasing the solvency of the HFA propellant through the addition of a cosolvent, developing new surface active agents specifically for use with HFA propellants, modifying the particle surface properties of the drug to reduce the interfacial tension between the particle surface and HFA and particle engineering to produce more HFA propellant compatible materials.

The first CFC-free MDI products released to the UK market were salbutamol inhalers: Airomir™ (3M Healthcare, UK) and Ventolin Evohaler™ (Allen and Hanburys, UK). Also beclomethasone dipropionate was launched in 1998 as Qvar® (3M Healthcare, UK) (McDonald and Martin, 2000). Recent developments have been aimed at the production of drug particles with a microporous structure (Dellamary *et al.*, 2000) that allow the HFA propellant to diffuse into the particle surface to produce a 'homodispersion' (Smith, 2002). Such porous structures also have low densities and therefore the suspensions obtained may be more stable.

1.2.1.3 Other devices (nebulisers)

A nebuliser is a device that turns an aqueous solution of drug into a mist of droplets which are subsequently inhaled. They are two basic types of nebulisers: air-jet and ultrasonic nebuliser. The first class of devices utilises a compressed gas (air or oxygen) that passes through a narrow orifice creating an area of low pressure at the outlet of the adjacent liquid feed tube (Labiris and Dolovich, 2003b). The negative pressure draws up the liquid into the capillary and breaks down the solution into small droplets. The ultrasonic nebulisers do not require the use of a compressed gas and the solution is atomised by vibrations generated by a piezoelectric crystal (Zeng *et al.,* 2001). Nebulisers are not efficient devices as around 50% of the drug is wasted and only 10% of the total dose reaches the lungs. Main advantages of nebulisers are their simplicity of use, ease of generation of small droplets and the fact that doses as high as 1 g can be delivered (Zeng *et al.,* 2001).

1.3 Solid state properties of pharmaceutical materials

1.3.1 Polymorphism and pseudopolymorphism

Polymorphism is the ability of any element or compound to crystallise as more than one distinct crystalline type (Haleblian and McCrone, 1969). Different polymorphs of a given compound are as different in structure and properties as the crystals of two different compounds. As a result of this, polymorphs can have very different melting temperatures, densities, solubilities, dissolution rates and bioavailability as well as physical and chemical stabilities etc. (Ford, 1989). Polymorphs have different crystalline structures but are identical in the liquid and vapour states. Hydrates, solvates, desolvates and amorphous compounds are often referred to as pseudopolymorphs.

An extended definition of polymorphism includes true polymorphs (solvent-free crystals with different molecular packing), isomorphic desolvates (obtained by desolvation of a solvate and retaining the initial solvate crystal symmetry), liquid crystals, amorphous materials and mixtures thereof (Yu *et al.*, 1998b). The extended definition indicates a practical need to characterise all solid forms of a drug substance that can be produced by pharmaceutical processes such as crystallisation, milling, spray drying etc. (Figure 1.4).

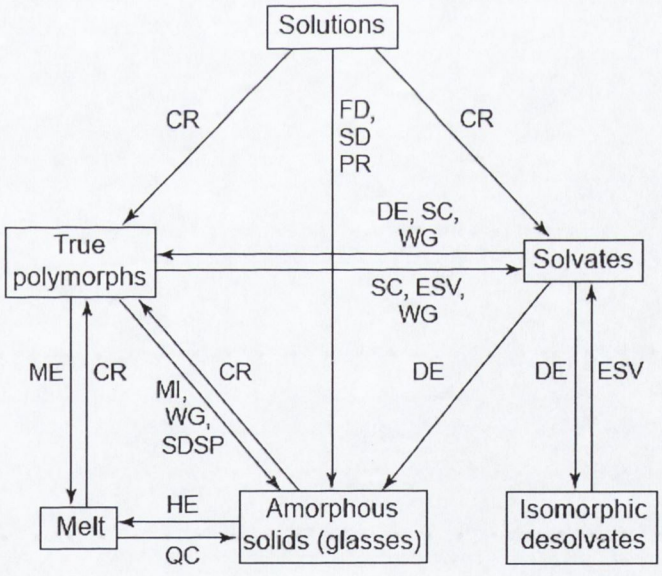

Figure 1.4 Types of polymorphs that can be produced by various pharmaceutical processes. Key : CR – crystallisation, DE – desolvation, ESV – exposure to solvent vapour, FD – freeze drying, HE – heating, ME – melting, MI – milling, PR – precipitation, QC – quench cooling, SC – slurry conversion, SD – spray drying, SDSP – solid dispersion and WG – wet granulation. Taken from Yu *et al.* (1998b).

Generally, polymorphs are divided into two groups: enantiotropic and monotropic (Ford, 1989; Byrn *et al.*, 1995). Monotropic polymorphs have only one stable crystal form and this form has a higher melting point and enthalpy of fusion than the less stable crystal form. When the higher melting form has a lower enthalpy of fusion, then the polymorphs are called enantiotropic.

The unforeseen appearance of a polymorphic form can lead to serious pharmaceutical consequences, which may result in setbacks in product development and disruption of commercial production. For instance, a thermodynamically more stable form of ritonavir, which has different dissolution and absorption characteristics, was discovered after the product (Norvir) was launched, causing production to stop completely (Bauer *et al.*, 2001).

There are specific guidelines on the control of physicochemical properties of polymorphs, presented and discussed in the form of decision trees, flow charts and algorithms (Byrn *et al.*, 1995; ICH, 1997).

1.3.2 Amorphous state

An amorphous solid (glass) has no long-range order of molecular packing and the position of molecules relative to one another is more random as in the liquid state. Therefore the molecules in the glassy state are conformationally flexible and have physical properties different from those of their corresponding crystalline states. Figure 1.5 presents a schematic diagram of the enthalpy (H) or specific volume (V) of a solid substance as a function of its temperature.

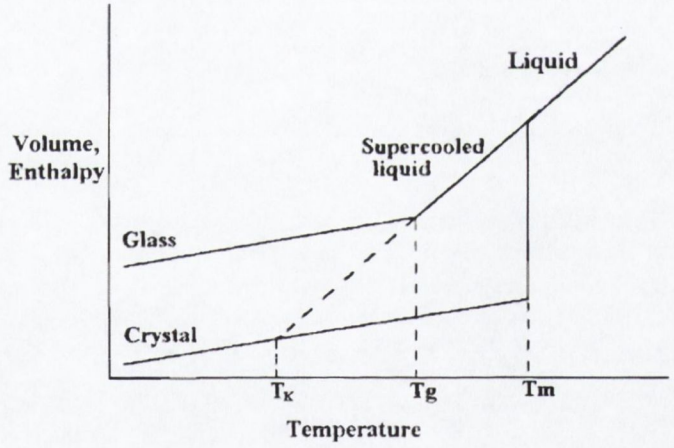

Figure 1.5 Schematic diagram of the variation of enthalpy (or volume) with temperature. Taken from Hancock and Zografi (1997).

For a crystalline material at very low temperatures there is a small increase in enthalpy and volume with respect to temperature. There is a discontinuity in both H and V at the melting temperature (T_m) representing the first-order phase transition to the liquid state (Hancock and Zografi, 1997). Upon rapid cooling of the melt H and V may follow the equilibrium line for the liquid beyond the melting temperature into the supercooled region. On further cooling a change in slope is seen at a characteristic temperature known as the glass transition temperature (T_g) (Hancock and Zografi, 1997). T_K is the critical temperature known as the Kauzmann temperature and is thought to indicate the point at which the configurational entropy of the system reaches zero.

The means by which amorphous character may be generated are summarised in Table 1.1.

Table 1.1 methods of producing amorphous pharmaceutical materials (adapted from Hancock and Zografi (1997); Hancock (2002)).

Form	Method	Process
Crystal	Disruption/energy input	Grinding/milling Compression Reaction Dehydration
Solution	Solvent removal	Freeze drying Spray drying Precipitation Reaction
Liquid	Cooling/energy removal	Rapid cooling Nucleation suppression Polymerisation
Vapour	Cooling/energy removal	Sublimation

In the case of pharmaceutical materials, the importance of amorphous solids originates from:

- higher apparent solubility and dissolution rates than their crystalline equivalents
- instability, as glassy solids are generally less stable than corresponding crystals
- common occurrence, as they can be produced by standard pharmaceutical processes and are the common form of certain materials (Yu, 2001).

Pharmaceutical materials may exist intrinsically in the amorphous state, for instance PVP, or they may be rendered amorphous deliberately and in the later case they have to be physically stabilised to prevent the reconvertion to the equivalent crystals. Many reviews have been devoted to the characterisation of pharmaceutical amorphous solids, including works of Saleki-Gerhardt and co-workers (1994), Hancock and Zografi (1997), Yu (2001) and Hancock (2002).

1.3.3 Solid dispersions

The term "solid dispersion" refers to the dispersion of one or more active ingredients in an inert carrier or matrix at solid state prepared by the melting, solvent or melting-solvent method (Chiou and Riegelman, 1971). Complexes, formed *in situ* by any of these processes may also be classified as solid dispersions but simple physical blends are not (Ford, 1986). Solid dispersions are prepared to overcome the limitations associated with the bioavailability of poorly water soluble drugs. The Nernst-Brunner equation (Equation 1.2, Nernst and Brunner, (1904)) describes how different factors influence the dissolution rate of a compound:

$$\frac{dM}{dt} = \frac{A \cdot D(C_S - C)}{h} \qquad \text{(Equation 1.2)}$$

where dM/dt is the rate of dissolution, A is the surface of the compound being dissolved, D is the diffusion coefficient, C_S is the solubility in the dissolution medium, C is the concentration of the drug in the medium at time t and h is the thickness of the diffusion boundary layer adjacent to the surface of the dissolving compound.

An improvement of the dissolution rate of a substance can be accomplished by decreasing the particle size of the compound, thereby increasing the surface area of the drug, optimising the wetting characteristics of the surface of the compound, decreasing the boundary layer thickness or by improving the apparent solubility of the drug. An increase in the surface area available for dissolution can be accomplished by commonly used methods such as grinding, but there is a practical limit to the degree of micronisation that can be achieved. Such fine powders may be problematic in handling and have poor wettability due to the aggregation tendency. Salt formation is one of the ways of improving solubility of a compound but it is not always feasible. Even when a salt is prepared, due to the reconversion into the original compound an increased dissolution rate in the gastrointestinal tract may not be achieved (Serajuddin, 1999). Improvement of the solubility through various formulation approaches seems to be the most attractive option. Formulating the compound as a molecular dispersion combines the benefits of a local increase in the solubility and maximising the surface area of the active that is created as the carrier dissolves by contact with the dissolution medium (Leuner and Dressman, 2000). Furthermore, an improvement in the wettability of the active can occur (Yamamura and Rogers, 1996). A further way in which the carrier may affect the dissolution of a drug is by a direct cosolubilisation or cosolvation effect (Leuner and Dressman, 2000). As the drug may not possess the crystal structure in the solid dispersion, no energy is needed to break down the crystalline lattice enhancing the dissolution rate. Following the dissolution process, the drug is present as a supersaturated solution and in some cases the carrier may act as a precipitation inhibitor (Usui *et al.*, 1997).

Solid dispersions may be produced using the following techniques:

- melting (fusion process), whereby the components are melted and rapidly solidify
- solvent method, whereby solid dispersions are prepared firstly by dissolving a physical mixture in a common solvent and then evaporation of the solvent
- melting-solvent method which is based on incorporation of a solution of the drug dissolved in a suitable liquid solvent into the melt of the carrier.

Solid dispersions can be divided into groups, based on the interactions between the carrier and drug (Chiou and Riegelman, 1971):

- simple eutectic mixtures – the components mix in the liquid state but show negligible solid-solid solubility
- solid solutions – only one phase is present – a solid solute dissolved in a solid solvent
- glass solutions – the solute and solvent molecules are dispersed molecularly, but irregularly and both do not possess a crystalline lattice
- glass suspensions – the drug and carrier do not show interactions and are immiscible in the liquid state
- amorphous precipitations of a drug in a crystalline carrier
- compound or complex formations
- combinations of the above.

1.4 Characterisation of pharmaceutical powders

1.4.1 X-ray diffraction analysis (XRD)

X-ray diffraction is a non-destructive analytical technique for the identification and quantitative determination of various crystalline compounds. Every nonamorphous material possesses a crystal lattice, which is a regular three-dimensional distribution of atoms in space. These are organised in a series of parallel planes separated from one another by a specific distance. This gap varies according to the nature of the material. When a focused X-ray beam interacts with these planes, a part of the beam is diffracted and the rest of the beam can be absorbed, refracted and scattered. The diffraction of X-rays by a crystal is described by Bragg's law (Equation 1.3):

$$n\lambda = 2d\sin\theta \qquad \text{(Equation 1.3)}$$

When a monochromatic X-ray beam with a wavelength λ is projected onto a crystalline material at an angle θ, diffraction occurs only when the distance travelled by the rays reflected from successive planes differs by a complete number, n, of wavelengths (Cullity, 1978). In this technique, the wavelength of the electromagnetical radiation is around 1 Å. XRD analysis can be carried out on a single crystal or a powder sample consisting of much small, randomly oriented crystallities. Preparation of single crystals of organic compounds is often problematic, which has made powder diffraction the most used technique for pharmaceutical applications (Klug and Alexander, 1974). For a powder XRD analysis a randomly orientated sample is prepared and therefore all the crystalline planes of the sample are exposed to the collimated X-rays. The scattering angle θ is determined by slowly rotating the sample and using a scintillation counter to measure the angle of the diffracted rays with respect to the angle of the incident beam. Alternatively, the sample is stationary in the horizontal position and the X-ray tube and detector moves simultaneously over the angular angle θ. By plotting the angular positions and intensities of the resultant diffracted peaks a pattern, which is characteristic of the sample, can be obtained. Knowing the wavelength of the beam, calculation of the d-spacing (spacing between the planes) of the material is possible. The characteristic set of d-spacings provides a unique fingerprint of the specimen and by comparison with a standard reference pattern the identification of the material is feasible. The technique is particularly suited to the quantitative identification of different polymorphic forms and the solvated and anhydrous forms of a compound (Black and Lovering, 1977). It has been used widely to measure the degree of crystallinity (Klug and Alexander, 1974; Black and Lovering, 1977), where the peaks heights or the integrated intensities of the peaks are compared and used as a measure of the crystallinity. Often, an internal standard such as lithium fluoride is included in the samples to correct for the absorption coefficient. XRD technique was successfully used by Phadnis *et al.* (1997) to unambiguously identify the active ingredient in a variety of pharmaceutical formulations such as tablets, capsules, suppositories and ointments. Two major drawbacks of this method were ascertained. The primary requirement was that the active compound investigated had to be

crystalline and it should have constituted at least 5% (w/w) of the formulation. Phadnis and Suryanarayanan (1997) developed a simple XRD method for the simultaneous quantification of an enantiomer and the racemic compound of ibuprofen, showing that this technique can potentially be utilised for other enantiomeric compounds. Chen *et al.* (2001) introduced a new X-ray method for the quantitation of the residual amount of an amorphous content in a pharmaceutical solid. Lactose monohydrate was a model system and the approach of whole pattern fitting was employed. The limit of detection was calculated to be 0.37% of the amorphous lactose content. The XRD method can be used to determine the different types of solid dispersion systems and a detailed description of this approach can be found in the work of (Chiou and Riegelman, 1971).

1.4.2 Thermal analysis

Thermal analysis includes a group of methods by which the physical and chemical properties of a substance or a mixture of substances are determined as a function of temperature or time, while the sample is subjected to a controlled temperature program. The program may involve heating or cooling (dynamic), or holding the temperature constant (isothermal), or any combination of these (Ford, 1989).

Differential scanning calorimetry (DSC) allows quantitative measurements of enthalpy changes to be made. The heat flow into and out of a sample and reference in a controlled atmosphere (air, nitrogen, helium) over a wide temperature is measured. Two types of instrumentation are available for obtaining DSC data: power compensated DSC and heat-flux DSC. Power compensated calorimeters possess two individual furnaces. By varying the heat required to keep both pans at the same temperature, the temperature differences between the sample and reference are compensated for. The energy difference is plotted as a function of sample temperature. Heat flux instruments utilise a single furnace and heat flows into both the sample and reference via electrically heated constantan thermoelectric disc and is proportional to the difference in output of the two thermocouple junctions (Ford, 1989). This technique is widely used for the characterisation of substances because almost every phase transition, chemical reaction, absorption or mixing is accompanied by an exchange of heat (Giron, 1998). The transitions detected by DSC can be endothermic (melting, vaporisation, sublimation, desorption, desolvation, decomposition, degradation, glass transition-as baseline shift, relaxation of glasses) and exothermic (crystallisation, condensation, solidification, adsorption, salvation, decomposition). Differential scanning calorimetry can be used to assess the degree of disorder in crystalline solids (Saleki-Gerhardt *et al.*, 1994) and to compare the solid state disorder of materials (Grant and York, 1986) among many other applications.

In modulated temperature DSC (MTDSC) the linear heating ramp is overlaid with a sinusoidal function defined by a frequency and amplitude to produce a sinus wave-shaped temperature versus time function (Giron, 1998). Using Fourier mathematics, the DSC signal is then split into two components: one reflecting nonreversible events and the other reversible processes. This technique allows for distinguishing overlapped thermal events and it has increasingly been used in the determination of the glass transition temperatures of compounds (Craig *et al.*, 2000). The MTDSC method has been demonstrated as successful in the quantitation of the amorphous content in samples of a micronised drug substance (Guinot and Leveiller, 1999).
High speed or high performance DSC (Hyper-DSC) operates at extremely high scanning rates (100-500°C/min range as opposed to typically 10°C/min in the conventional instruments). Recently, Saunders *et al.* (2004) have shown that Hyper-DSC can successfully be used to detect and quantify low levels of amorphous content in samples that are mostly crystalline. This method has also been presented as a useful tool to detect polymorphic impurities (McGregor *et al.*, 2004).

Isothermal microcalorimetry relies upon maintaining a constant temperature. The technique involves monitoring the heat conduction into and out of a measuring cell from or to the heat sink. The heat signal is recorded as the heat flow and is proportional to the reaction in the sample vessel. Isothermal microcalorimetry has been found to be applicable in the pharmaceutical field. Studies have been made on the stability and compatibility of compounds in the solid state drug development (Phipps and Mackin, 2000), changes in crystallinity of excipients (Briggner *et al.*, 1994) and actives (Buckton *et al.*, 1995). It has also been used in investigations on surfactant aggregation and surfactant-drug interactions in aerosol systems (Blackett and Buckton, 1995).

Thermogravimetry (TG or TGA) is based on the change of a sample mass as a function of temperature. Most instruments record the percentage of mass change. Balance sensitivity is usually around one microgram, with a total capacity of a few hundred milligrams. The thermal processes in which weight is gained are adsorption or absorption, whereas in desolvation, desorption, sublimation, vaporisation and decomposition weight is lost. TG has been applied extensively to studying hydrates (Henwood *et al.*, 2001) or solvates (Caira *et al.*, 1995).

1.4.3 Infrared spectroscopy

Infrared (IR) spectroscopy is a fundamental technique that can be used in the identification of functional chemical groups of a molecule. The vibrational modes of a molecule are used to deduce its structure. Infrared spectroscopy can be divided into three areas based on spectral region: the far-IR (100-400 cm^{-1}), mid-IR (400-4000 cm^{-1}) and near-IR (NIR) (4000-14000 cm^{-1}) (Socrates, 2001). Far-IR is used primarily for detection of very strong bonds such as metal-ligand interactions (Drożdżewski and Kordon, 2000) and has also been employed in hydrogen bonding investigations

of amorphous and crystalline sugars (Walther *et al.*, 2003). Mid-IR is the most commonly used form of infrared spectroscopy and has been used for the identification of organic compounds, as most of them can be identified by their very complex spectra taken as fingerprints. The main disadvantage of mid-IR is that samples must be prepared by mixing with an alkali halide compound (usually potassium bromide – KBr) and pressing the mixture into a pellet or by diluting the grounded sample with mineral oil to form a mull. Mid-IR samples have to be preferably free of moisture because water gives obstructive background and strong peaks (Socrates, 2001). A near-IR spectrum contains mainly overtones of C-H, N-H, and O-H vibrations. It is a rapid, non-invasive technique which requires minimal sample preparation. It has been proved successful in studies of polymorphism (Brittain, 1999) and water content of sugars (Kamat *et al.*, 1989). Near infrared spectroscopy has been used to detect changes between the crystalline and amorphous forms of pharmaceutical materials such as lactose (Buckton *et al.*, 1998) and raffinose (Hogan and Buckton, 2001b).

Infrared spectroscopy can be used in qualitative differentiations of various polymorphic forms of a substance (Chao and Vail, 1987), investigations of specific interactions between the molecules manifesting in shifts in the band positions (Anguiano-Igea *et al.*, 1995; Nair *et al.*, 2001) and studies on hydrogen bonding in pharmaceutical actives (Tang *et al.*, 2002a; Tang *et al.*, 2002b) and sugars (Wolkers *et al.*, 1998; Wolkers *et al.*, 2004). In addition to the qualitative infrared analysis, which is the most often performed, quantitative measurements utilising infrared spectroscopy are also possible. It has been used for quantitative analysis of mixtures of polymorphs (Hartauer *et al.*, 1992) and the determination of crystallinity of lactose monohydrate (Gombás *et al.*, 2003).

1.4.4 Particle size and size distribution

Changes in particle size are generally believed to also change the functional behaviour of most particle processes. The determination and control of particle size is a fundamental requirement in the formulation of pharmaceuticals. This is particularly important in the formulation of dry powder inhalers since the particle size of both carrier and drug particles determines powder performance affecting the flowability, fluidisation, separation and deposition of powders. The importance of particle size in the development of solid pharmaceutical dosage forms has long been appreciated and techniques for its measurement are well established (Zeng *et al.*, 2001). However, the particle size obtained is dependent on the principle of measurement (Allen, 1997).

A variety of methods have been employed to determine particle size and these include optical microscopy, laser light scattering, electrical sensing zone technique, sieve analysis and time of flight techniques. Each method is most appropriately used according to the intended application and each method may yield a different particle size. A good comparison of these techniques in relation to the primary particle size analysis for dry powder inhalation was presented by Bosquillon *et al.* (2001a). Both electrical sensing zone and laser diffraction analyses resulted in a good

assessment of the particle size of free-flowing and moderately aggregated dry powders. In the case of very cohesive powders, only laser diffraction was capable of producing reliable measurements when the sample was suspended in a liquid and ultrasonicated prior to the analysis. Microscopy allowed individual particles to be distinguished but it was extremely time consuming and the particle counts were small, reducing accuracy. Automated light microscopy was more rapid than electron microscopy, however particles < 1μm could not be detected resulting in an overestimation of the particle size. The mass median particle diameter measured by laser diffraction following dispersion with compressed air at a pressure of 3 bar gave a correct estimation of the particle size of the powders investigated. This pressure presented a good compromise between the separation of the agglomerates and breaking of the particles.

The particles of a powder are rarely uniform in size, hence it is useful to define an average particle size, which is then used to compare samples. In describing a representative diameter of particles of the sample, three parameters can be used: the mean, median and the mode. Furthermore, the distribution of sizes about the average is required. A number of mathematical functions have been proposed to represent the particle size distribution, among which the Gaussian (normal distribution) is the most commonly used (Allen, 1997). However, unless the range of particle sizes is extremely narrow, most powder samples cannot be described adequately by the normal distribution function. The size distribution of the majority of real powder samples (e.g. produced by milling or grinding) usually is skewed. Such powders are better described by the log-normal distribution type. When the particle distribution is plotted by means of the logarithm of the particle size, the skewed curve is transformed into one closely resembling a normal distribution. The distribution in a log-normal representation can be fully specified by two parameters: the geometric median particle size (d_g) and the standard deviation in the geometric mean (σ_g) (Brittain, 2001).

Laser diffraction represents a well-established method for determining particle size (Haynes *et al.*, 2004). Many theories have been generated to study light-scattering properties of particles, among which are the classical Mie theory and its simplification – Fraunhofer theory (Allen, 1997). According to Mie theory, the scattering of light by particles approaching the wavelength of incident radiation is a function of the angles of scattering, the wavelength of the incident light, differences in refractive indices and the diameter of the sphere. When particles are four or five times greater than the wavelength of the laser light, the Mie theory can be reduced to the Fraunhofer theory, also referred to as static light scattering (Zeng *et al.*, 2001). Light scattering is an absolute method, does not require calibration and is rapid to perform. Moreover, data obtained from this method also provide information on size polydispersity. The Malvern Mastersizer 2000 (Malvern Instruments, Malvern, UK) apply Mie scattering to derive the particle size distribution, whereas HELOS laser diffraction particle sizer (Sympatec GmbH, Germany) utilises the simplified Fraunhofer theory as the default evaluation method with the Mie calculations as an option.

The particles released from DPIs and sizes of droplets constituting the plumes discharged from MDIs and other medicinal aerosols containing liquids can also be measured by means of the laser diffraction technique. Using a Malvern 2600c laser diffractometer, Smyth and Hickey (2003) showed that the particles emitted from HFA-134a solution MDIs had apparent multimodal particle size distributions. Two dominant particle size modes were seen: the mode of the fine particles, which was independent of the measurement parameters and the mode of droplets exhibiting insufficient evaporation of the propellant. The Malvern Spraytec® with its inhalation cell, represents the newest diffraction-based device introduced by Malvern Instruments, which has been specifically modified for measuring the particle size distribution generated from medicinal aerosols, including MDIs, dry powder inhalers, and nebulisers (Haynes *et al.*, 2004).

1.4.5 Particle shape

It is not possible to reasonably discuss the size of a particle or any distribution associated with the sizes of a group of particles without first considering the three-dimensional characteristics of the particle itself. This is because the size of a particle is expressed either in terms of linear dimension characteristics derived from its shape or in terms of its projected surface or volume (Brittain, 2001). Static shape factors can be derived from direct imaging of particles. Initially shape factors were developed to demonstrate deviation from an ideal geometry, the sphere (Hickey and Concessio, 1997). One of the simplest shape expressions was developed by Heywood. This approach uses the ratio of particle length (L) measured along the longest axis and the breadth (width) (B) perpendicular to the length as an elongation ratio (Allen, 1997).

In recent years a number of mathematical approaches have been developed to define meaningful shape factors to describe particles. Among the most significant of these are Fourier (Beddow *et al.*, 1977) and fractal analyses (Kindratenko *et al.*, 1994).

Dynamic shape factors can be derived from comparison of various equivalent spherical diameters (Hickey and Concessio, 1997). They are number of dynamic shape factors and one of them - (κ) is that obtained from the expression for the terminal settling velocity of a particle (Hinds, 1999) (Equation 1.4):

$$V_t = \frac{g \cdot d \cdot C_e \cdot D_e^{\,2}}{18\eta \cdot \kappa} = \frac{g \cdot d_0 \cdot C_{ae} \cdot D_{ae}^{\,2}}{18\eta} \qquad \text{(Equation 1.4)}$$

where g is the acceleration due to gravity, η is the viscosity of air, D_e and D_{ae} are equivalent volume spherical diameter and aerodynamic diameter, respectively, C_e and C_{ae} are the Cunningham slip correction factors (account for molecular slip that occurs when the size of the particle is of the same magnitude as the distance between gas molecules) for each of the above diameters, d and d_0 are the true particle and unit (1 g/cm^3) densities, respectively and κ is the dynamic shape factor. The later can be defined by rearranging Equation 1.4 into Equation 1.5:

$$\kappa = \frac{d \cdot C_e \cdot D_e^{\,2}}{d_0 \cdot C_{ae} \cdot D_{ae}^{\,2}} \qquad \text{(Equation 1.5)}$$

Shape of particles is also a factor in the phenomenon of mechanical interlocking of particles and can cause significant cohesion in a powder bed or adhesion to surfaces (Hickey and Concessio, 1997). Flat and elongated crystals are less easily dispersed than spherical particles because of the greater area of contact between particles, which contributes to strong interparticulate forces (Hickey *et al.*, 1994).

1.5 Characterisation of aerodynamic properties of medicinal aerosols

The principle of formulation a drug as an inhaler is to deliver the active solely to the site of action to maximise the therapeutic effect and minimise the side-effects. The amount or percentage of the drug reaching the targets is one of the major factors to be considered in the design of a formulation for inhalation (Zeng *et al.*, 2001). Drug particles for inhalation must be in a size range suitable for the delivering to the lungs. It is generally assumed that particles <10 μm in aerodynamic diameter are suitable for lung deposition (Hickey and Concessio, 1997). Dry powder aerosols are unique in comparison with other forms of pharmaceutical aerosols. MDIs and nebulisers output particle/droplet size are predominantly <10 μm, but DPIs frequently contain an excipient, preferably lactose, acting as a carrier in a large, nonrespirable size range of 30-60 μm.
It has to be emphasized that the aerodynamic diameter rather than the geometric diameter is used to characterise the size of particles for inhalation.

1.5.1 Twin stage impinger

The two stage liquid impinger (twin impinger, glass impinger) was developed by Hallworth and Westmoreland (1987) for evaluation of pulmonary delivery of drugs from MDIs. This device was adopted by British Pharmacopoeia (apparatus A, Appendix XII F, 2004) and European Pharmacopoeia (apparatus A, Section 2.9.18, 5th Edition, 2004) which provide the exact specifications of each component of the impinger. The twin stage impinger operates on the inertial impaction principle. It consists of two impaction stages: the upper impinger (the round bottomed flask) that functions at low velocity and traps the large particles whilst the lower stage (the conical flask) operates at a much higher velocity (Zeng *et al.*, 2001). The schematic diagram of the twin impinger apparatus is presented in Figure 1.6.

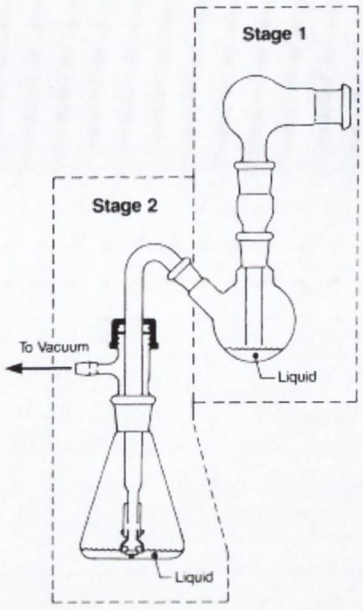

Figure 1.6 Schematic diagram of twin impinger (adopted from Miller *et al.* (1992) with modification).

During operation, air is drawn though the instrument at a flow rate 60 l/min by a means of a vacuum pump attached to the outlet of the lower impinger. The inhaler is discharged and the particle cloud is introduced at the inlet, then it passes though a glass throat simulating the oropharynx and travels into the upper impinger stage, which contains 7 ml of a suitable liquid able to dissolve the drug. The cut-off point of this stage is 6.4 μm (Hallworth and Westmoreland, 1987), therefore particles larger than this size should be collected in the liquid of the upper impinger. Smaller particles (<6.4 μm) proceed to the lower stage where they are trapped by 30 ml of the same liquid. The particles that reach the lower stage are defined as "respirable fraction" and are likely to penetrate into the deep lung (Zeng *et al.*, 2001). The main disadvantage of the twin stage impinger is that it cannot reveal the particle distribution of the inhaler cloud and it is not able to discriminate among distributions with specific combinations of varying aerodynamic size and spread of the particles (Miller *et al.*, 1992). The second disadvantage is that environmental conditions such humidity and temperature can affect the measurements. This was shown by Jashnani *et al.* (1995) who demonstrated that elevated relative humidity and temperature of the atmosphere significantly decreased both the emitted and fine particle doses of salbutamol base and sulphate. Despite these drawbacks, twin impinger analysis is a very quick analytical *in vitro* method of assessing the fine particle dose of inhalers.

1.5.2 Other *in vitro* devices

Another pharmacopoeial (B.P., E.P., 2004) device for aerodynamic assessment of distribution of particles and fine particle dose of inhalers is the multistage liquid impinger (MLI). The apparatus consist of a glass inlet throat, four impaction stages and an integral filter stage. To operate this

device, a suitable filter is placed in the filter stage and 20 ml of a suitable liquid is introduced to each impaction stage. Powder deposition is measured at 60 l/min but the impinger can operate at other flow rates, as it has been calibrated to measure the particle size at flow rates ranging from 30 to 100 l/min (B.P., 2004). The respirable dose is the total mass of the drug collected in the stages 3 to 5 (cut-off of the stage 3 is 3.1 μm).

Andersen cascade impactor (ACI) has also been characterised by both British and European Pharmacopoeias (apparatus D, 2004). It was designed to cover the particle size range from 0.1 μm to 10 μm. The instrument consists of a stack of plates, similar to a stack of sieves (Zeng *et al.*, 2001). There are eight aluminium stages together with a final filter. The stages are clamped together. A suitable mouthpiece adapter should be used to provide an airtight seal between the inhaler and the induction port (B.P., 2004). For measurements of DPIs, a pre-separator is placed above the top stage to collect large masses of non-respirable powder and this part is connected to the induction port. The impactor should be used at a low rate of 28.3 l/min for MDIs, whereas the flow rate used for DPIs depends on the inhalation device employed. This impactor is superior to both the twin impinger and multistage liquid impinger due to the fact that ACI can produce more detailed information about the particle size distribution (Zeng *et al.*, 2001). The problems associated with the use of this apparatus include particles bouncing against the impactor walls. This can be overcome by coating the impaction plates with a material (grease, oil) that ensures stickiness of the particles to the surfaces.

Other *in vitro* devices include the single stage metal impinger (Apparatus B of British and European Pharmacopoeias, 2004), Marple Miller cascade impactor (Apparatus 2 of United States Pharmacopoeia, 2004) and next generation pharmaceutical impactor (Apparatus 5 of United States Pharmacopoeia, 2004).

1.6 Background to drugs used in the current work

1.6.1 Budesonide

CAS number 51333-22-3, chemical formula $C_{25}H_{34}O_6$, chemical name *5-hydroxy-6b-hydroxyacetyl-4a,6a-dimethyl-8-propyl-4a,4b,5,6,6a,6b,9a,10,10a,10b,11,12-dodecahydro-7,9-dioxa-pentaleno[2,1-α]phenanthren-2-one,* molecular weight 430.54

Budesonide is a synthetic corticosteroid with mainly glucocorticoid activity. It acts by its broad anti-inflammatory efficacy, mediated in part by inhibition of production of inflammatory cytokines. Chronic use of corticosteroids effectively reduces symptoms and improves pulmonary function in patients with mild asthma (Katzung, 2001). Budesonide is a white or almost white crystalline

powder, practically insoluble in water, freely soluble in methylene chloride and sparingly soluble in alcohol (B.P., 2004). The structure of budesonide is shown in Figure 1.7.

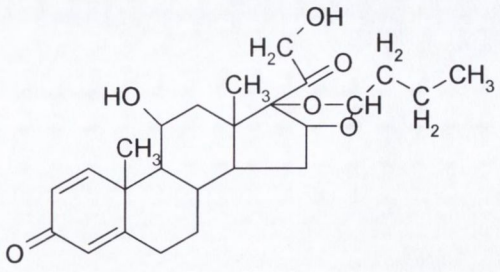

Figure 1.7 Chemical structure of budesonide.

1.6.2 Salbutamol base

CAS number 18559-94-9, chemical formula $C_{13}H_{21}NO_3$, chemical name *1-(3-hydroxymethyl-4-hydroxyphenyl)-2-tert-butylamino-ethanol*, molecular weight 239.31

Salbutamol is a one of the β_2-selective adrenoreceptor agonist drugs, which are the most widely used class for the treatment of asthma at the present time. Given by inhalation, salbutamol causes bronchodilation equivalent to that produced by isoproterenol. Bronchodilation is maximal by 30 min and persists for 3-4 hours (Katzung, 2001). Salbutamol is a white to off-white crystalline solid. It is soluble in ethanol, sparingly soluble in water, and very soluble in chloroform (B.P., 2004). Salbutamol has two isomers: R- and S-. R-salbutamol acts on β_2 adrenergic receptors and S-salbutamol is now thought to be the main cause of bronchial hyper responsiveness in the treatment of asthma with salbutamol. S-salbutamol acts on muscarinic receptor receptors.

Salbutamol is used mainly as a sulphate salt, however the synthesis of the novel salbutamol derivatives, adipate and stearate, has been reported in the literature (Jashnani *et al.*, 1993). It was shown that the stearate salt possesses a very slow dissolution rate compared to that of the free base and the sulphate salt which may suggest the utility of salbutamol stearate as an agent capable of producing sustained bronchodilation (Jashnani *et al.*, 1993). The structure of salbutamol base is shown in Figure 1.8.

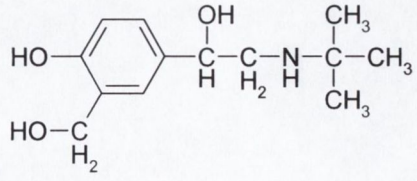

Figure 1.8 Chemical structure of salbutamol base.

1.6.3 Formoterol

CAS number 73573-87-2 (fumarate salt 43229-80-7), chemical formula $C_{19}H_{24}N_2O_4$, chemical name *N- (2- hydroxy-5-{1-hydroxy -2- [2- (4-methoxy-phenyl)-1 -methyl -ethylamino] -ethyl} -phenyl)- formamide*, molecular weight 344.41

Formoterol belongs to a new generation of long-acting β_2-selective agonists. It appears to achieve long duration of action (~12 hours) due to high lipid solubility, which permits formoterol to dissolve in the smooth muscle membrane in high concentration. Formoterol interacts with inhaled corticosteroids to improve asthma control. It is not recommended as the sole therapy for asthma (Katzung, 2001). The commercial form of formoterol is its fumarate salt. The structure of formoterol is shown in Figure 1.9.

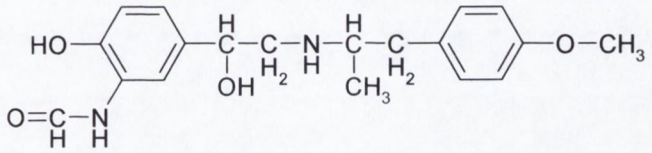

Figure 1.9 Chemical structure of formoterol.

1.6.4 Bendroflumethiazide

CAS number 73-48-3, chemical formula $C_{15}H_{14}F_3N_3O_4S_2$, chemical name *3-benzyl- 1,1-dioxo-6-trifluoromethyl-1,2,3,4-tetrahydro -1λ^6-benzo[1,2,4] thiadiazine-7-sulfonic acid amide,* molecular weight 421.41

Bendroflumethiazide belongs to the thiazide diuretics acting by inhibiting NaCl transport in the distal convoluted tubule. The daily oral dose is 2.5-10 mg. BFMT is a white or almost white crystalline powder, practically insoluble in water, freely soluble in acetone, soluble in alcohol (B.P., 2004). The formation of an amorphous phase of BFMT was reported by Corrigan *et al.* (1984) and the physicochemical properties of co-spray dried bendroflumethiazide with PEG 4000 were investigated by Corrigan and co-workers (2003). The co-spray dried composites produced from all BFMT/polymer solutions were amorphous. All BFMT/PEG systems showed initial increased release of BFMT compared to that of micronised BFMT alone, with the spray dried BFMT/PEG 4000 10% system showing initial rates two to three times that of BFMT alone. The structure of bendroflumethiazide is shown in Figure 1.10.

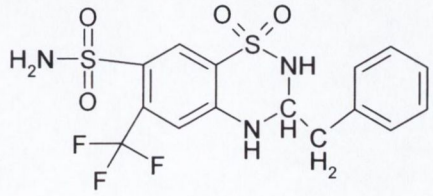

Figure 1.10 Chemical structure of bendroflumethiazide.

1.6.5 Hydroflumethiazide

CAS number 135-09-1, chemical formula $C_8H_8F_3N_3O_4S_2$, chemical name *1,1-dioxo-6-trifluoromethyl-1,2,3,4-tetrahydro-1λ^6-benzo[1,2,4]thiadiazine-7-sulfonic acid amide*, molecular weight 331.28

The mechanism of action results in an interference with the renal tubular mechanism of electrolyte reabsorption. Hydroflumethiazide is an odourless white to cream-colored, finely divided, crystalline powder. It has a melting point between 270°C and 275°C. Hydroflumethiazide is practically insoluble in water, soluble in ethanol 96%, practically insoluble in chloroform and in ether (B.P., 2004). Hydroflumethiazide was reported by Corrigan and Holohan (1984) to produce amorphous composites with PVP when spray dried. Furthermore, the apparent solubility of HFMT in spray dried systems increased with increasing PVP content (0-30%). The structure of hydroflumethiazide is shown in Figure 1.11.

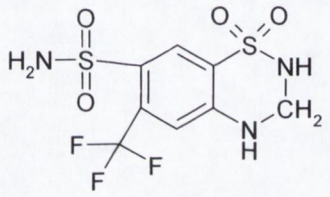

Figure 1.11 Chemical structure of hydroflumethiazide.

1.6.6 Hydrochlorothiazide

CAS number 58-93-5, chemical formula $C_7H_8ClN_3O_4S_2$, chemical name *1,1-dioxo-6-chloro-1,2,3,4-tetrahydro-1λ^6-benzo[1,2,4]thiadiazine-7-sulfonic acid amide*, molecular weight 297.73

Hydrochlorothiazide belongs to the same class of thiazide diuretics as bendroflumethiazide and hydroflumethiazide. The daily oral dose is 25-100 mg, given as a single dose (Katzung, 2001). It is a white or almost white, crystalline powder, very slightly soluble in water, soluble in acetone and sparingly soluble in alcohol. It dissolves in dilute solutions of alkali hydroxides (B.P., 2004). HCT on spray drying produced an unstable amorphous phase as shown by Corrigan *et al.* (1984). The structure of hydrochlorothiazide is shown in Figure 1.12.

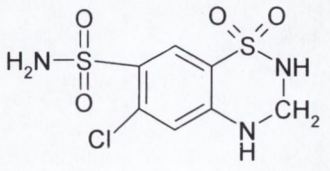

Figure 1.12 Chemical structure of hydrochlorothiazide.

EXPERIMENTAL

2 Materials and methods

2.1 Materials

Material (abbreviation or chemical formula)	Supplier/manufacturer
Acetic acid glacial (CH_3COOH)	BDH
Acetonitrile, HPLC grade	Lab-Scan
Aerosil 200 Pharma	Degussa, Germany
Ammonium carbonate (NH_4CO_3)	Sigma
Ascorbic acid 6-palmitate	Sigma
Bendroflumethiazide (BFMT)	Leo-Pharma, Ireland
Boric acid (H_3BO_3)	Merck
Budesonide	IVAX, Waterford, Ireland
Calcium chloride dihydrate ($CaCl_2 \cdot 2H_2O$)	BDH
Caprylocaproyl polyethylene-8 glycerides (Labrasol)	Gattefossé, France
Cellulose, microcrystalline, colloidal	Aldrich
Citric acid monohydrate ($C_6H_8O_7 \cdot H_2O$)	Sigma
Dichloromethane (CCl_2H_2)	Lab-Scan
Dioctyl sodium sulphosuccinate (Aerosol OT)	BDH
Ethanol	Cooley Distillery
Ethanol 99.9%, GC grade	Merck
Ethylenediaminetetraacetic acid (EDTA)	Aldrich
Formoterol fumarate dihydrate	IVAX, Waterford, Ireland
Glyceryl palmitostearate (Precirol ATO 5)	Gattefossé, France
HFA 134a (1,1,1,2-tertafluoroethane, MDIs propellant)	INEOS Fluor, UK
Hydranal (Karl-Fisher titration reagent)	Riedel de Haën
Hydrochloric acid 37% (HCl)	BDH
Hydrochlorothiazide (HCT)	Sigma
Hydroflumethiazide (HFMT)	Sigma
Hydroxypropyl-β-cyclodextrin	Aldrich
Hydroxypropylmethylcellulose E5 grade	ELAN, Athlone, Ireland
Lactose monohydrate	BDH
Magnesium chloride hexahydrate ($MgCl_2 \cdot 6H_2O$)	Merck

Material (abbreviation or chemical formula)	Supplier/manufacturer
Magnesium stearate	Aldrich
Magnesium stearate	Élan, Athlone, Ireland
Magnesium stearate	Riedel de Haën
Maltodextrin, dextrose equivalent 4.0-7.07	Aldrich
Mannitol	Sigma
Methanol, HPLC grade	Lab-Scan
Methanol anhydrous (Karl-Fisher titration reagent)	Merck
Phosphoric acid (H_3PO_4), 85%	BDH, Riedel de Haën
Polyethylene glycol 300 (PEG 300)	Riedel de Haën
Polyethylene glycol 1000 (PEG 1000)	Riedel de Haën
Polyethylene glycol 4000 (PEG 4000)	Riedel de Haën
Polyethylene glycol 6000 (PEG 6000)	Riedel de Haën
Polyethylene glycol 20,000 (PEG 20,000)	Fluka
Polyoxyethylene 10 oleyl ether (Brij 97)	Sigma
Polyoxyethylene 20 cetyl ether (Brij 58)	Aldrich
Polyoxyethylene 35 lauryl ether (Brij 35)	Aldrich
Polyoxyethylene 100 stearate (Myrj 59)	Sigma
Polyoxyethylene 50 stearate (Myrj 53)	Uniqema, Belgium
Polyoxyethylene 20 sorbitan monolaureate (Tween 20)	Sigma
Polyoxyethylene 20 sorbitan monooleate (Tween 80)	Croda chemicals, UK
Polyvinylpyrrolidone, Av. Mol. Wt. 10,000	Aldrich
Polyvinylpyrrolidone, Av. Mol. Wt. 40,000	Sigma
Potassium dihydrogen phosphate (KH_2PO_4)	Fluka
Potassium bromide (KBr), for IR spectroscopy	Spectrosol
Potassium chloride (KCl)	Merck
Propylene glycol monolaurate (Capmul PG-12)	Abitec Corp., USA
Raffinose pentahydrate	Aldrich
Salbutamol base	IVAX, Waterford, Ireland
Silica gel	Avonchem
Sodium acetate trihydrate ($NaC_2H_3O_2 \cdot 3H_2O$)	BDH
Sodium bromide ($NaBr$)	Aldrich
Sodium chloride ($NaCl$)	Merck
tri-Sodium citrate dihydrate ($Na_3C_6H_5O_7 \cdot 2H_2O$)	Sigma-Aldrich

Material (abbreviation or chemical formula)	Supplier/manufacturer
Sodium dihydrogen phosphate dihydrate ($NaH_2PO_4 \cdot 2H_2O$)	Merck
di-Sodium hydrogen phosphate dodecahydrate ($Na_2HPO_4 \cdot 12H_2O$)	Merck
Sodium hydrogen carbonate ($NaHCO_3$)	BDH
Sodium hydroxide ($NaOH$)	Riedel de Haën
Sodium hydroxide HPLC grade ($NaOH$)	Aldrich
Sodium sulphate anhydrous (Na_2SO_4)	Riedel-de Haën
Stearic acid	Merck
Stearoyl polyethylene-32 glycerides (Gelucire 50/13)	Gattefossé, France
Sulphadimidine	Schering Plough
Trehalose dihydrate	Aldrich
Water, deionised	Purite Prestige Analyst HP water purification system
Water, HPLC grade	Purite Prestige Analyst HP water purification system
Xylitol	Sigma

2.2 Methods

2.2.1 Spray drying

All systems were spray dried as solutions or suspensions using a Büchi 191 Mini Spray Dryer (Büchi Laboratoriums-Technik AG, Flawil, Swizerland). When an ethanol/water mixture was used as the solvent for the process, only the concentration of ethanol is given in the text e.g. 95% (v/v) ethanol indicates that the solution was made of 95% (v/v) ethanol and 5% (v/v) deionised water. The conditions used for spray drying various systems are presented in Appendix I.

2.2.2 Preparation of solid dispersions

2.2.2.1 Spray drying

The systems were spray dried as solutions using a Büchi 191 Mini Spray Dryer (Büchi Laboratoriums-Technik AG, Flawil, Swizerland). The conditions used for spray drying various systems are presented in Appendix I.

2.2.2.2 Differential scanning calorimetry (DSC)

The systems were prepared by loading portions of a physical mixture into aluminium DSC crucibles and subjecting them to a controlled heating programme in the DSC furnace (Mettler Toledo DSC 821^e, described in Section 2.2.4.1). The samples were melted just above the drug melting point or the T_g in the case of PVP, and immediately cooled down on a metal plate at 0°C. All solid dispersions prepared using this method are referred to as *in-situ* prepared melts.

2.2.2.3 Melt method

A portion of a physical mixture was melted in an evaporating dish over a hotplate while stirring. When a clear melt had formed the mixture was immersed in liquid nitrogen and the solid residue was milled with a mortar and pestle.

2.2.3 Preparation of physical mixtures

For comparison purposes, equivalent physical mixtures of co-spray dried composites were prepared. The substances prior to mixing were sieved and only the fractions of particles having the size sub 75 μm were used. Stoppered vials (10 ml), containing accurately weighted quantities of substances were placed in a Turbula mixer (Glen Greston Ltd., Middx, UK) and mixing was carried out for 15 min at 42 revolutions per min. Approximately 100 mg of each blend was prepared.

2.2.4 Thermal methods

2.2.4.1 Differential scanning calorimetry (DSC)

DSC experiments were conducted using a Mettler Toledo DSC 821^e with a refrigerated cooling system (LabPlant RP-100). Nitrogen was used as the purge gas. Hermetically sealed aluminium pans with three vent holes were used throughout the study and sample weights varied between 4 and 10 mg. DSC measurements were carried out at a heating/cooling rate of 10°C/min. The DSC system was controlled by Mettler Toledo STAR^e software (version 6.10) working on a Windows NT operating system.

2.2.4.2 Thermogravimetric analysis (TGA)

TGA was performed using a Mettler TG 50 module linked to a Mettler MT5 balance. Sample weights between 5 and 12 mg were used and placed into open aluminium pans. A heating rate of 10°C/min was implemented in all measurements. Analysis was carried out in the furnace under nitrogen purge and monitored by Mettler Toledo STAR^e software (version 6.10) with a Windows NT operating system.

2.2.5 Density measurement

2.2.5.1 Helium pycnometry

The true density was measured by an AccuPyc 1330 Pycnometer (Micromeritics®) using helium (99.995% purity) to determine the volume of the sample. The samples were dried for at least 24 hours prior to analysis using a vacuum oven (Gallencamp) operated at 50°C and -600mbar pressure. Either a 1 cm^3 or 0.1 cm^3 sample cup was used depending on the sample size available. The instrument was calibrated immediately before performing the analysis.

2.2.5.2 Bulk (aerated) and tap densities

A 5 cm^3 graduated cylinder was used in the bulk density determination of samples. The container was filled with accurately weighed sample and the top was levelled. The density was calculated as the ratio of the mass to the volume of the sample and called aerated density. The tap density was determined similarly to the aerated density, but the volume taken for calculations was that after 500 strokes. The work on bulk and tap densities carried out in our Pharmaceutics Laboratory by Bernard McDonald showed no significant differences in the density values obtained when different volumes graduated cylinders were used.

2.2.6 X-ray methods

2.2.6.1 Powder X-Ray diffraction (XRD)

Powder XRD analysis was conducted using nickel filtered CuKα (λ=1.54056) monochromatic radiation on a Siemens D500 Diffractometer with a DACO MP wide-range goniometer. The anode X-ray tube was operated at 40kV and 30mA. Measurements were taken from 5 to 40 on the 2 theta

scale at a step size of 0.05° per second. Low background silicon mounts (Bruker AXS) were used to support the sample during measurements.

2.2.6.2 Energy Dispersive X-Ray Analysis (EDXA)

EDXA was carried out using the Hitachi S-3500N variable pressure scanning electron microscope with the PGT Imix-PTS EDX analysis system with 10 mm^2 UTW detector. Point analysis was used for qualitative assessment of the elements present.

2.2.7 Microscopy

2.2.7.1 Scanning Electron Microscopy (SEM)

SEM analysis was performed using a Hitachi S-3500N variable pressure scanning electron microscope. Samples were glued onto aluminium stubs and sputter-coated with gold prior to analysis.

2.2.7.2 Transmission Electron Microscopy (TEM)

TEM analysis was carried out using a Hitachi H-7000 Scanning Transmission Electron Microscope. The accelerating voltage applied was 100 kV.

2.2.8 Fourier transform infra-red spectroscopy (FTIR)

Infrared spectra were recorded on a Nicolet Magna IR 560 E.S.P. spectrophotometer equipped with MCT/A detector, working under Omnic software version 4.1. A spectral range of 650-4000 cm^{-1}, resolution 2 cm^{-1} and accumulation of 64 scans were used in order to obtain good quality spectra. A KBr disk method was used with 0.5-1 % sample loading.

2.2.8.1 FTIR peaks deconvolution

FTIR spectra of spray dried thiazide diuretic-PVP samples were subjected to a peak deconvolution procedure, as the bands overlapped one another. A multiple-Gaussian function was used with five peaks allowing for an accurate separation of the bands. This was accomplished using Origin Software (Version 7.5, Aston Scientific Ltd.).

2.2.9 High pressure liquid chromatography (HPLC)

The HPLC system used was a Waters™ HPLC, which consists of a Waters™ 600E pump, Waters™ 717 Autosampler and a Waters™ 2487 Dual λ Absorbance Detector. Data collection and integration were accomplished using Waters™ 746 Data Module. The mobile phase was filtered before use and degassed under reduced pressure during the run using a Phenomenex Degasser, model DG-4000. The calibration curves are shown in Appendix II.

2.2.9.1 Analysis of budesonide as well as budesonide and formoterol fumarate in samples containing a mixture of the two drugs

The analytical column used was a Waters™ Spherisorb Cartridge (150mm length, diameter 4.6 mm, ODS1, particle size 5μm). The mobile phase consisted of methanol, acetonitrile and water (35:30:35 v/v). Separation was carried out isocratically at ambient temperature (about 22°C) and a flow rate of 0.5 ml/min, with UV detection at 230 nm (AUFS 0.5).

2.2.9.2 Analysis of formoterol fumarate

The analytical column used was a Jones Chromatography Genesis column (150mm length, diameter 4.6 mm, C18, particle size 4μm S/N 7091102). The mobile phase consisted of acetonitrile and 0.01M solution of HCl (25:75 v/v). Separation was carried out isocratically at ambient temperature (about 22°C) and a flow rate of 0.5 ml/min, with UV detection at 220 nm (AUFS 1.0).

2.2.9.3 Stability indicating assay for formoterol fumarate dihydrate

This separation technique is a modification of the stability indicating HPLC method supplied by IVAX Pharmaceuticals UK. The analytical column used was a Supelcosil LC-ABZ column (250mm length, diameter 4.6 mm, silica-based, particle size 5μm S/N 56642-02 and 61188-01). The mobile phase consisted of acetonitrile and phosphate buffer mixed in the ratio 17:83 v/v. The buffer was prepared by dissolving 3.35g of potassium dihydrogen phosphate and 0.1g EDTA in 1 litre of HPLC grade water. The pH of that prepared solution was adjusted to 5.60±0.10 with 0.2M solution of NaOH. Separation was carried out isocratically at 30°C and a flow rate of 1.5 ml/min, with UV detection at 242 nm or 280 nm (for some of the formoterol fumarate samples dissolved in citrate buffers).

2.2.10 Particle size characterisation

2.2.10.1 Mastersizer 2000

Measurements of particle size distributions were obtained using a laser diffraction particle sizer Mastersizer 2000 (Malvern Instruments, UK). Particles were dispersed using a Scirocco dry feeder instrument with 3 bar pressure unless stated otherwise. An obscuration rate of 0.5-6% was obtained under a vibration rate of 50-70%. The data were processed according to Mie theory, using a refractive index value appropriate for the material measured. The list of the refractive indices used is shown in Table 2.1. The values were taken either from the instruction manual of the Mastersizer 2000 or the Beilstein chemical database.

Table 2.1 Optical properties of substances.

Name	Refractivity index	Absorption index
Bendroflumethiazide	1.550	0.10
Budesonide	1.530	0.10
Cellulose	1.540	0.01
Formoterol fumarate dihydrate	1.520	0.10
HPMC	1.350	0.01
Lactose	1.347	0.10
Magnesium stearate	1.450	0.10
Mannitol	1.333	0.10
PEG	1.460	0.01
PVP	1.530	0.10
Sugars	1.510	0.01
Sulphadimidine	1.570	0.01

2.2.10.2 Sympatec

Particle size analysis was carried out using a Sympatec HELOS laser diffraction particle size analyser connected to a RODOS dry dispensing unit. The pressure applied to achieve a proper dispersion of particles was 3 bar and injector depression was 128 mbar. The feed rate used was 18%. Measurement was done using a lens with focal length equal to 100mm and 51ms measurement intervals. The particle size distribution was deconvoluted using Fraunhofer theory.

2.2.10.3 SEM

The mean particle diameter (Feret's diameter) of some of the spray dried systems was calculated using SEM photographs (Lee *et al.*, 1996). Graphical software, Adobe Photoshop version 6.0, and its measuring tool were used to measure the diameter of 200 particles. The mean particle diameter was taken as the average of 200 measurements.

2.2.11 In vitro aerosol characterisation

The apparatus used was a twin stage impinger conforming to the specification in the British Pharmacopoeia (2004) and European Pharmacopoeia (2004).

The powders were aerosolized using a dry powder inhalation device (Rotahaler®, Allen & Hanburys, U.K.). The aerodynamic particle deposition was investigated using the twin impinger (Model TI-2, Copley) containing 7 and 30 ml of appropriate collecting solvent (see below) for stage 1 and 2, respectively. A total of 50±1 mg of powder (35±2 mg for the porous budesonide systems) was loaded into a No.3 hard gelatin capsule. After the Rotahaler® was connected to the mouthpiece of the twin impinger, a capsule was placed in the holder of the device. An air stream of 60 l/min was produced throughout the system by attaching the outlet of the twin impinger to a vacuum pump for 3 s. The drug in stages 1 and 2, mouthpiece and device was collected by rinsing with fresh solvent. The rinsed solutions were diluted to appropriate volumes, filtered through 0.45 μm PVDF filters (Millipore) and the drug contents were determined by an appropriate HPLC method (see High Pressure Liquid Chromatography Section 2.2.10).

Collecting solvents:

- Budesonide, budesonide/excipient and budesonide/formoterol fumarate dihydrate samples - 80% (v/v) ethanol
- Formoterol fumarate and formoterol fumarate/excipient systems - 80% (v/v) methanol
- Co-spray dried salbutamol base/excipient – 0.02 M phosphate buffer, pH=3.00

2.2.12 pH measurement

An Orion pH meter (model 520A) equipped with an Orion Ross™ 8103SC glass body pH semi-micro electrode was used for pH measurements. The pH meter was calibrated using standard buffer solutions (Orion) of pH 4.00, 7.00 and 10.00 (±0.01).

2.2.13 Determination of water content in HFA 134a propellant

A Karl Fischer apparatus 701 KF Titrino (Metrohm) was used for this study. Each portion of propellant was introduced to the titration chamber by means of a long syringe needle inserted through the septum plug of the apparatus. The other end of the needle was inserted into the metering valve stem. The water content in the propellant was determined in triplicate and 40 discharges of propellant from the aerosol vial were used for each analysis.

2.2.14 Preparation of MDI systems

In order to prepare metered dose inhalers, 20 mg of powder was weighed into glass vials, obtained from IVAX Pharmaceuticals (UK). Afterwards a 25 μm metering valve (Bespak, UK) was crimped onto the glass vial and the liquid propellant HFA-134a was added through the nozzle. The final weight of each MDI (without the container and metering valve) was 10g. The last two steps were performed using a Pamasol P 2016 aerosol filling station (Pamasol Willi Mader AG, Pfäffikon, Switzerland). Prepared MDIs were homogenised in a Bransonic 220 ultrasonic bath (UK) for 1 min.

2.2.15 Dispersibility study of MDIs

The quality of MDIs formulations was assessed visually by means of time-lapse photography using a digital camera FinePix 410 (Fuji).

2.2.16 Chemical stability study of formoterol fumarate

2.2.16.1 Aqueous solution kinetic studies

Accurately weighed samples of formoterol fumarate dihydrate were transferred into glass volumetric flasks and diluted to volume with buffer solutions as described below in Section 2.2.16.2. The concentration of the drug was either 0.02% or 0.1% (w/v). Degradation was carried out in thermostatically controlled incubators (Gallenkamp, UK), protected from light at two temperatures: 25°C and 40°C. Controls were employed using distilled water instead of a buffer solution. Every pH point was duplicated. At appropriate time intervals two aliquots were withdrawn from each of the flasks and assayed according to Section 2.2.9.3.

2.2.16.2 Preparation of buffer solutions

Different buffered media were prepared and the effects of pH, concentration and temperature on the degradation of formoterol fumarate dihydrate were investigated.

2.2.16.2.1 Britton-Robinson buffer

This is a wide range buffered medium and consists of 0.04 M solutions of phosphate, boric and acetic acids mixed together in equal volumes and adjusted to the appropriate pH (between 2-10) with 0.2 M sodium hydroxide (NaOH) solution. The ionic strength of the buffer solution was kept constant at 0.1 M and was adjusted using sodium chloride (NaCl). Table 2.2 presents compositions of the Britton-Robinson buffer at different pH values.

Table 2.2 Composition of Britton-Robinson buffers.

pH at 25°C	pH at 40°C	ml of acids mixture	ml of 0.2M NaOH	g of NaCl
-	2.05	100.0	1.5	0.3404
-	3.00	100.0	6.0	0.3156
4.00	3.90	100.0	8.0	0.3039
5.20	5.00	100.0	12.0	0.2790
6.20	6.10	100.0	15.0	0.2637
6.95	6.70	100.0	17.5	0.2484
-	8.20	100.0	21.0	0.2279
-	8.70	100.0	23.5	0.2133
-	9.60	100.0	27.0	0.1929

2.2.16.2.2 Phosphate buffers

Sodium phosphate buffer solutions were prepared and Table 2.3 presents their compositions for different ionic strengths.

Table 2.3 Composition of phosphate buffers.

pH at 25°C	$NaH_2PO_4*2H_2O$ g per 500 ml	$Na_2HPO_4*12H_2O$ g per 500 ml
	ionic strength 0.1M	
4.75	7.7666	0.0823
4.90	7.7332	0.1632
5.10	7.6682	0.3236
5.40	7.5416	0.6357
5.65	7.3009	1.2277
5.95	6.8634	2.3037
6.25	6.1309	4.1056
	ionic strength 0.2M	
5.10	14.5831	0.7753
5.70	12.2092	2.5850
	ionic strength 0.5M	
5.10	34.2468	3.6331
5.70	26.5396	9.5441
	ionic strength 1 M	
5.10	64.2466	10.8048
5.70	46.0462	24.4924

2.2.16.2.3 Citrate buffers

Citrate buffer solutions were prepared using tri-sodium citrate dihydrate and citric acid monohydrate. Table 2.4 shows their compositions.

Table 2.4 Composition of citrate buffers.

pH at 25°C	$Na_3C_6H_5O_7*2H_2O$ g per 500 ml	$C_6H_8O_7*2H_2O$ g per 500 ml
	ionic strength 0.1M	
5.00	1.8265	0.7962
5.20	1.8415	0.6803
5.50	1.8640	0.5069
5.80	1.9310	0.3538
6.10	2.0700	0.2543
	ionic strength 0.2M	
5.20	3.9245	1.2933
5.80	4.1320	0.6196
	ionic strength 0.5M	
5.20	10.7975	2.7911
5.80	12.8485	1.3250
	ionic strength 1 M	
5.20	20.4230	4.9485
5.80	21.6945	2.0436

2.2.16.3 Solid state stability study

Solid state stability studies were conducted at two different conditions of temperature and humidity according to the ICH protocol (ICH, 2003). Solid samples were placed in weighing boats in glass chambers containing saturated solutions of:

- ❖ NaBr to maintain a constant relative humidity of 60% for long-term testing
- ❖ NaCl to maintain a constant relative humidity of 75% for accelerated testing (Nyqvist, 1983).

The glass chamber containing the NaBr solution was stored at 25°C and the glass chamber containing the NaCl solution was stored at 40°C in incubators (Gallenkamp, UK). At appropriate time intervals, duplicate samples of each solid formulation were removed from the ovens for analysis. All samples were reconstituted using distilled water. The samples were then analysed using the formoterol fumarate stability indicating HPLC method, as described in Section 2.2.9.3.

2.2.16.4 Stability of formoterol fumarate MDI formulations

The aerosol vials were prepared as described in Section 2.2.14 "Preparation of MDI systems" with the only difference being that 15 mg of a powdered system was taken. They were stored in a glass chamber at 40°C/75% RH. The storage environment was prepared as described in Section 2.2.16.3 "Solid state stability study". At the time of assaying, the MDI vial was removed from the chamber and cooled to room temperature. The suspension was quantitatively discharged to a glass beaker using an actuator. Then empty vial was cooled to 4°C in a cold room and the valve was separated using a cutting tool. The contents of the beaker and rinsings from the valve and the inside of the vial were made up to the required volume with deionised water in a volumetric flask. Analysis was performed using the HPLC method described in Section 2.2.9.3.

2.2.17 Solubility study of surfactants in HFA-134a

Accurately weighed aliquots of each surfactant were placed in a glass aerosol vial. Metering valves were crimped onto each aerosol vial and an appropriate amount of HFA-134a was filled through the valve using a small scale pressure filling machine (Pamasol Model P2016, Pamasol Willi Mader AG, Pfäffikon, Switzerland) such that the total weight of the content was 10g. Each assembled aerosol canister was sonicated for 5 min at room temperature. Solubility was determined visually. The observation of phase separation or cloudiness indicated that the surfactant was not completely dissolved in HFA-134a, and a clear solution indicated that the surfactant was dissolved in HFA-134a. The solubility of some of the surfactants investigated was determined with and without ethanol. Ethanol was added to the surfactant prior to the introduction of the HFA-134a.

2.2.18 Statistical analysis and data fitting

Statistical analysis was carried out using the following software:

- Minitab™ statistical software release 13.32, Minitab Inc.
- Origin® Software, version 7.5, Aston Scientific Ltd.
- Microsoft® Excel, Office package, version 2002, SP3

Data fitting to different models described in Chapter 8 was accomplished using Origin Software (Version 7.5, Aston Scientific Ltd.).

RESULTS AND DISCUSSION

SPRAY DRYING OF SALBUTAMOL BASE AND ITS EXCIPIENT CONTAINING COMPOSITES

3.1 Introduction

Previous attempts at spray drying of salbutamol base in order to achieve its amorphous counterpart did not succeed (Corrigan, 2002). The process resulted in a crystalline product with only some degree of amorphicity. The apparatus used was a Büchi B-190 Mini Spray Dryer and the solvent used was 95% (v/v) ethanol. The inlet temperature employed in that process varied between 78 and 79°C and, together with the pump rate of 6 (~700 ml/h) and airflow throughput of 500Nl/h, resulted in the outlet temperature of 48-50°C. The aspirator rate could not be modified and it was noticed that the aspiration output in the Büchi B-190 was lower than that in the newer model B-191 and furthermore, the construction of the latter allows regulation of the speed of the aspirator. As the amount of energy delivered needed for atomisation the feed depends on this parameter (Büchi B-191 technical specification) it was thought that using the Büchi B-191 or different operational conditions would help to produce an amorphous system of salbutamol base. Therefore, in the new trials a new Büchi device model B-191 was utilised and a range of different processing conditions was intended to apply. This decision was made on the basis of previous works of Dillen *et al.* (2004) and Billon *et al.* (2000) indicating that processing conditions can greatly influence the physicochemical properties of the output materials.

The second reason why salbutamol base was chosen was that no information about spray drying of this substance has been reported in the literature to date. The sulphate salt is the most commonly used in commercial formulations and it is the one that has been best characterised (Podczeck, 1998; Corrigan *et al.*, 2004). Processing of salbutamol sulphate by a spray drying technique has previously been described by (Chawla *et al.*, 1994). The free base salbutamol is less hygroscopic than the sulphate salt (Jashnani and Byron, 1996) and this feature may be advantageous on storage.

3.2 Spray dried salbutamol base

A range of conditions were used in order to study the feasibility of obtaining an amorphous form of salbutamol base. A statistical factorial study was undertaken. This allows the effects of more than one factor possibly influencing a response to be investigated simultaneously in all their possible combinations. The advantage of factorial designs over one-factor-at-a-time experiments is that they are more efficient and they allow interactions to be detected (Erden and Celebi, 1996). Furthermore, the conclusions hold for a wider range of conditions. In multi-factor experiments one can use fractional factorial designs, which involve only a fraction of full sets of runs.

The choice of experimental design depends on the objectives of the experiment and the number of factors to be investigated. If we wanted to investigate all the aspects having any impact on the spray drying process including: airflow, aspirator and feed rates, inlet temperature, diameter of the spraying nozzle as well as concentration of the feed, a full 2^6 factorial study would be necessary. With at least duplicate runs, we would have 128 runs, which is not feasible in a short period of time

and may be impractical due to financial limitations. A fractional factorial design would have been more appropriate, but for the reasons given below, a shorter version of a full factorial experiment was prepared and investigated.

Since, as the Büchi B-191 spray dryer is basically equipped with a 0.7 mm nozzle, the use of a nozzle with a different orifice diameter was abandoned. Ethanol 95% (v/v) instead of water was used as the solvent because of the low aqueous solubility of salbutamol base. The concentration of 1% (w/v) was used, which is quite a low feed concentration since concentrations of 20-50% are usually used (Chidavaenzi *et al.*, 1997). Therefore it was decided to keep the concentration constant at 1% (w/v) because lower solution concentrations would not significantly affect the product. Using ethanol as a solvent could increase the probability of an explosion during processing. Due to the lower boiling point of ethanol compared to water, the inlet temperature was set to 78°C.

Taking into consideration the above, the three remaining factors to be investigated were airflow, pump performance and aspirator speed. The appropriate ranges for the processing variables at which the spray drier was chosen to operate were selected on the basis of the technical specification of the Büchi B-191 Mini Spray Dryer (Büchi B-191 technical specification). The variable and constant parameters of the spray drier were as shown in Table 3.1.

Table 3.1 Processing parameters of salbutamol base.

		Parameter	Low level	Upper level
Variable	**A**	Airflow (Nl/h)	400	600
	B	Pump rate (%)	10	30
	C	Aspirator (%)	70	100
Constant	Inlet temperature (°C)		78	
	Feed concentration (%)		2.5	

The combination of manufacturing variables resulted in 8 runs which were not duplicated. Table 3.2 presents sample abbreviations and processing conditions at which these specimens were spray dried.

Table 3.2 Spray drying conditions for salbutamol base and the resulting outlet temperatures of the processes.

Sample abbreviation	**Parameter**			**Outlet temperature (°C)**
	A Airflow	**B Pump**	**C Aspirator**	
SB1	600	10	100	52
SB2	400	10	100	62
SB3	600	10	70	55-56
SB4	400	30	70	48-49
SB5	600	30	100	53-54
SB6	400	10	70	56-58
SB7	400	30	100	54-55
SB8	600	30	70	47-48

3.2.1 Physicochemical characteristics

Figure 3.1 compares the DSC thermograms of all spray dried samples of salbutamol base with that of the starting material. The latter appears to be crystalline, as only one endothermic event at ~158°C with the onset at ~156°C was recorded. It was ascribed to the melting process and confirmed by the literature value of 155°C for salbutamol base (B. P., 2004).

All processed samples exhibited two thermal events, namely an exotherm (peaking between 80°C-100°C) attributed to the recrystallisation of the amorphous material followed by an endotherm peaking at ~160°C, thus recognised as melting. Some of the spray dried specimens showed a weak baseline deflection at ~45°C, which can be classified as the glass transition of the drug (Figure 3.1).

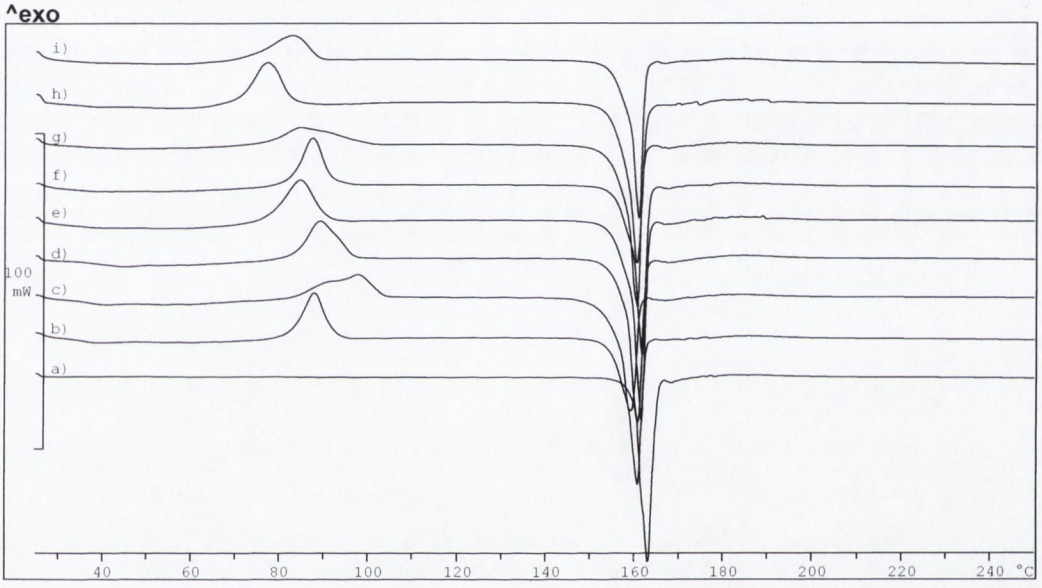

Figure 3.1 DSC scans of the (a) crystalline salbutamol base and its spray dried samples: (b) SB1, (c) SB2, (d) SB3, (e) SB4, (f) SB5, (g) SB6, (h) SB7 and (i) SB8.

It can be seen from Figure 3.1 that the recrystallisation peak had a different onset temperature and shape for different samples, indicating that the spray drying conditions had an influence on at least the thermal properties of the resulting materials. It is also confirmed by slight changes in the onset of melting of these samples from ~159°C for the crystalline salbutamol to ~155-158°C for the processed powders. The normalised heats of fusion were also reduced for the processed samples and were 175-198 J/g as opposed to 204 J/g for the crystalline counterpart. Yamaguchi *et al.* (1992) observed changes in the heat and temperature of the recrystallisation process of spray dried 4''-O-(4-methoxyphenyl)acetyltylosin (MAT) when various inlet temperatures of the process were used. It was concluded that the samples spray dried at the inlet temperature which was between the glass transition and recrystallisation temperatures of MAT had the greatest stability on storage. Here, the inlet temperature used was 78°C in all cases and it was between the glass transition and recrystallisation peak temperatures of salbutamol base, therefore it may be assumed that other

parameters of the spray drying process than the inlet temperature are responsible for the changes in the crystalline structure of the drug.

It should be noted that the DSC analysis was carried out immediately after collecting, therefore it is assumed that the effect of quick recrystallisation of the amorphous material at room temperature due to the very low glass transition temperature is avoided. Thermogravimetric analysis was conducted in order to evaluate ethanol/moisture residues in the spray dried materials. It showed between 1.7% and 3.2% weight loss in the 25-100°C region, which could be attributed to loosely bounded solvents adsorbed to the surface. Compared with the starting material this represents a 2-4-fold increase. On all TGA traces there was a drastic slope change starting at ~150°C, indicating that salbutamol base decomposes during melting.

XRD analysis demonstrated that the degree of crystallinity of the spray dried salbutamol base systems was greatly reduced (Figure 3.2), as previously indicated by the recrystallisation exotherms seen on the DSC curves (Figure 3.1). It has to be said, however, that the percentage crystallinity of the spray dried samples should be regarded as relative values, as it is known that the limit of amorphous phase detection by XRD is 5-10% (Giron *et al.*, 1997), but even this approximation gives an indication of how various spray drying parameters affect the crystallinity of salbutamol base.

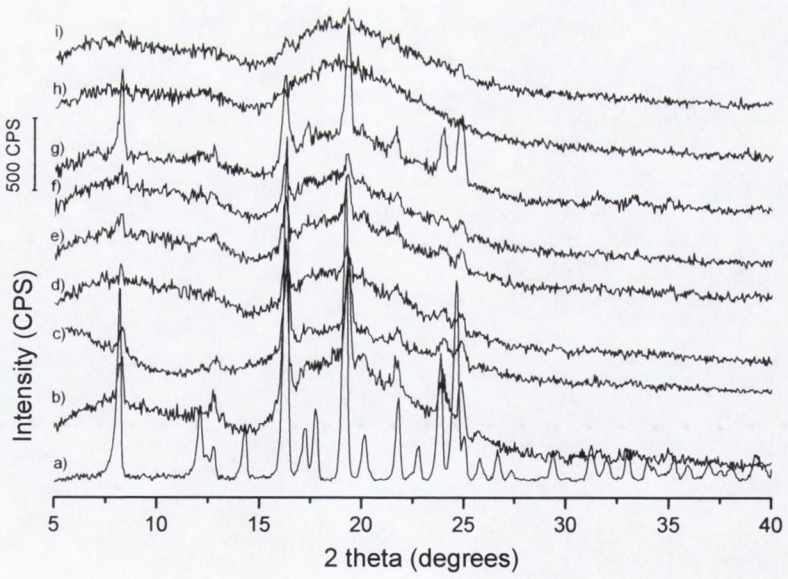

Figure 3.2 XRD diffraction patterns of the (a) crystalline salbutamol base and its spray dried samples: (b) SB1, (c) SB2, (d) SB3, (e) SB4, (f) SB5, (g) SB6, (h) SB7 and (i) SB8.

Table 3.3 gives the percentage content of the crystalline form calculated by XRD. The combined area under the peaks placed between 15.50 and 16.65 2 theta degrees and 18.55-19.55 2 theta degrees was taken for calculation. The crystallinity of unprocessed salbutamol was assumed to be 100%. Figure 3.2 and Table 3.3 demonstrate that one of the samples (SB7) was shown to be

completely XRD amorphous. The rest of the spray dried powders can be regarded as predominantly amorphous.

Table 3.3 Content of the crystalline fraction for salbutamol base spray dried calculated from the XRD data.

System	% crystallinity
SB1	25
SB2	7
SB3	9
SB4	10
SB5	8
SB6	19
SB7	0
SB8	5

The infrared spectra of the crystalline and spray dried salbutamol base are shown in Figure 3.3.

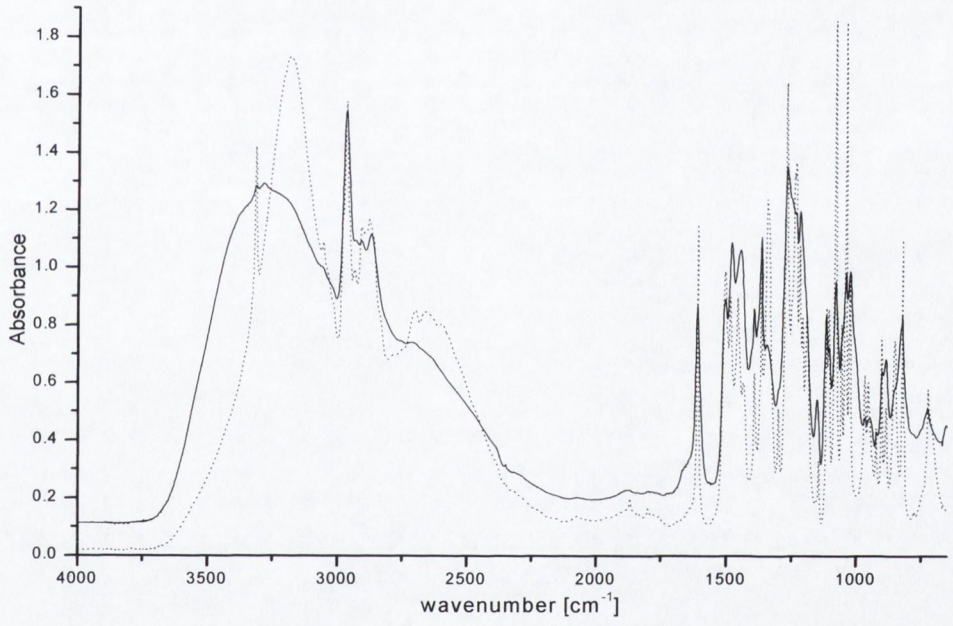

Figure 3.3 Infrared spectra of crystalline salbutamol base (dotted line) and the spray dried material (solid line).

Although the IR spectra are similar in the band positions in the fingerprint regions, a number of differences are apparent in the 2500-4000 cm^{-1} region. Spray dried drug gave a "smoother" spectrum than its crystalline counterpart. This phenomenon is well known and often occurs for polymers (Meyers, 2000) indicating a lack of the crystal lattice which causes band splitting. This is further confirmation of the fact that spray drying significantly reduced crystallinity of the starting material. Due to the fact that the molecule of salbutamol base contains three OH groups (Chapter 1.6.2) and one NH group, their stretching frequencies occur in the same spectral range and band assignments appearing in 2500-4000 cm^{-1} cannot be performed precisely. According to the Handbook of Infrared Frequencies (Socrates, 2001) the free OH vibration occurs as a sharp band at

around 3600 cm^{-1}, while for the majority of condensed phase samples this OH band is broadened and shifted to 3500-2500 cm^{-1} due to various types of hydrogen bonds formation. The NH stretching band appears in the same range and therefore the band at ~3315 cm^{-1} observed as a peak in the salbutamol base unprocessed material spectrum could be due to either OH vibration or secondary amino stretching, free or weakly hydrogen bonded. A broad peak with the maximum at 3179 cm^{-1} corresponds to the hydrogen bonded OH groups. The 2400-2800 cm^{-1} fragment is of special interest, as a series of bands appearing there can imply the presence of so called chelation intramolecular hydrogen bonds. The chelation type hydrogen bonding is formed when the OH group is involved in a molecular resonance structure while the OH group is on the β carbon of a C=C conjugated with an electron acceptor moiety (Socrates, 2001). It is possible that this type of hydrogen bonds can be created in a molecule of salbutamol base as one of the OH groups is attached directly to the benzene ring in very close proximity to the primary OH on the flexible CH_2 link. Looking at the spectrum of the spray dried drug (Figure 3.3), compared to the starting material, one can notice an upward shift and broadening of the peak initially located between 3000 and 3200 cm^{-1}. This newly formed band overlaps with a very sharp peak at 3315 cm^{-1}, which did not change its position when compared to its location in the crystalline drug spectrum. We can thus conclude that the hydrogen bonding structure underwent a change towards weakening of the bonds. The bands in the 2400-2800 cm^{-1} region also weakened indicating perhaps a disruption of the intramolecular hydrogen bonds.

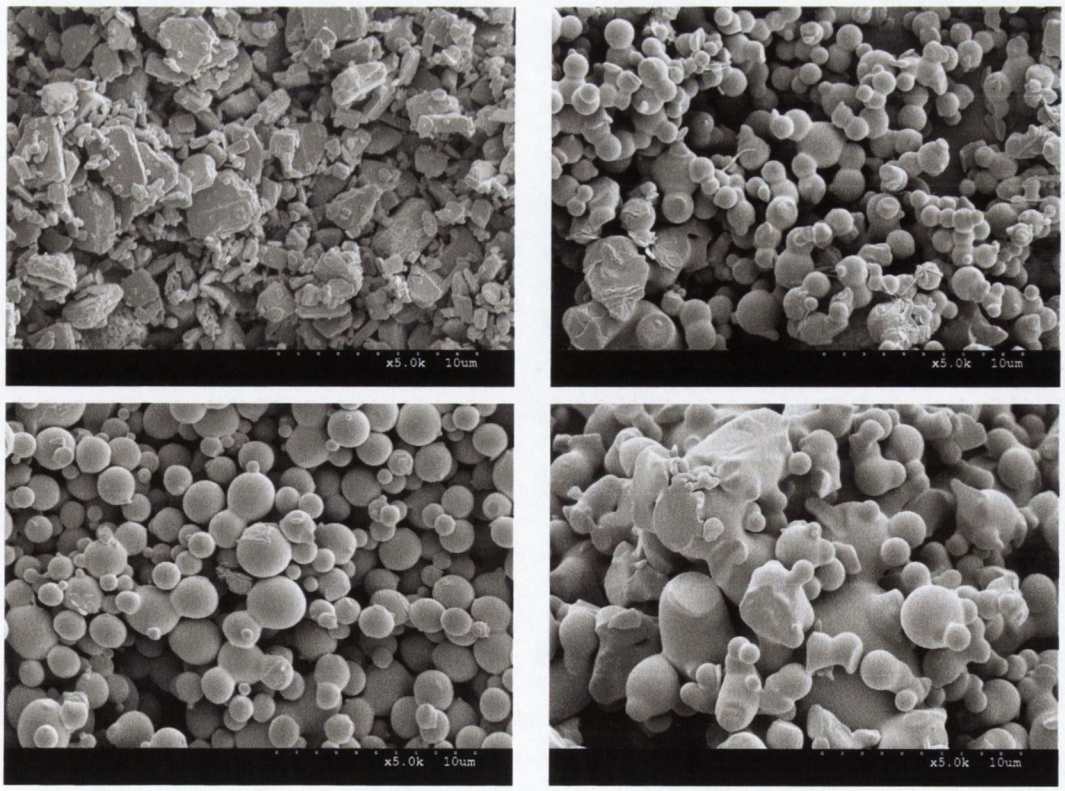

Figure 3.4 SEM photographs of the crystalline salbutamol base (top left), SB2 (top right), SB4 (bottom left) and SB7 (bottom left).

SEM micrographs (Figure 3.4) disclosed that the milled, crystalline drug had small, irregular and plate-like particles as opposed to the processed powders that had clearly spherical, but fused particles.

3.2.2 Influence of the spray drying conditions on crystallinity of salbutamol base

Analysis of variance (ANOVA) was performed on the numerical data collected from the XRD analysis (Table 3.3). As the runs were not replicated, estimation of the experimental error was based on a fractional mathematical model and it was assessed on all the main effects and their interactions that were not statistically significant.

Out of all the terms investigated only two appeared to have an impact ($p<0.05$) on the degree of crystallinity of salbutamol base. They were the pump feed speed and the interaction aspirator-airflow (Figure 3.5). The level of amorphicity of salbutamol base can be greatly increased using higher pump flow and greater aspiration suction together with lower air consumption.

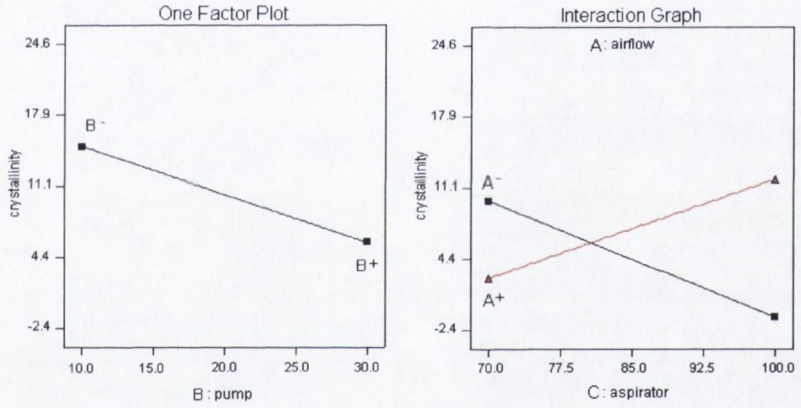

Figure 3.5 Graphical representation of the main effect of pump (left) and interaction aspirator-airflow (right) on the crystallinity of spray dried salbutamol base. The red line on the interaction plot represents the lowest settings of the airflow, the black line – the highest. The interaction plot shows the values of crystallinity when the pump is at its highest speed.

The studies of Prinn *et al.* (2002) pointed at increasing liquid feed rate as one the major factors causing a decrease in the outlet temperature. When more liquid is sprayed, more heat is removed by the vaporisation process decreasing the outlet temperature. As salbutamol free base has quite a low T_g, lower outlet temperatures would sustain the disordered phase and prevent excessive *in situ* recrystallisation. However, when the degree of crystallinity (by XRD) was correlated with the resulting outlet temperature observed at each process, no apparent relationship was discerned and the points were randomly spread (Figure 3.6). This implies that the crystallinity of the systems is affected not only by the outlet temperature.

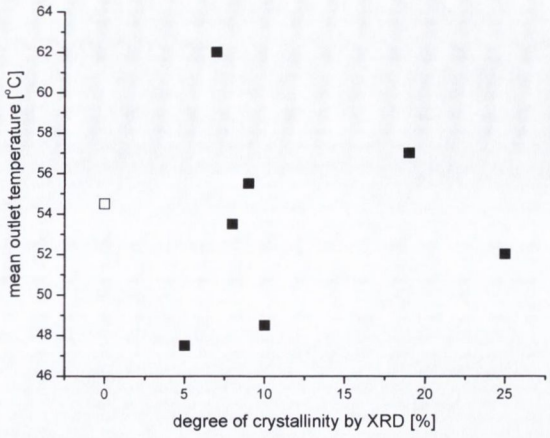

Figure 3.6 Relationship between the degree of crystallinity as determined by XRD analysis and the mean outlet temperature. The empty square denotes the completely amorphous sample (SB7).

As regards the effect of the aspirator it is dual and higher air suction used throughout the spray drying process ensures higher atomisation energy and shorter residence time in the device (Büchi B-191 technical specification). The effect of the airflow settings is not clear, however it can be hypothesised that because low flow rates of the drying medium produce larger particles, the cores of these particles may retain more amorphous product as they are not exposed to high temperatures in the collecting vessel.

An interesting relationship between the feed flow rate and crystallinity of spray dried hydrogenated soybean phospholipids-mannitol mixtures has been observed by Alves and Santana (2004). More amorphous structures were obtained at low and high feed rates, whereas moderate feed rates gave greater contents of the crystalline material.

3.3 Salbutamol base co-spray dried composites

3.3.1 Introduction

In the experiments on spray drying of salbutamol free base, the yield did not exceed 20% and some part of the product stuck to the walls of the drying chamber and cyclone separator. On the basis of the DSC and SEM analyses it was concluded that fusion of salbutamol base particles and their stickiness to the apparatus walls during spray drying was related to the relatively low T_g (~ 40°C) of the drug. The problem of stickiness caused by low T_gs has been reported in the food technology field (Masters, 1980; Papadakis and Bahu, 1992; Bhandari *et al.*, 1997). Excipients known to have much higher T_gs have been used, e.g. maltodextrins (Adhikari *et al.*, 2004), to reduce the adhesiveness of such substances to the spray dryer walls and to result in disaggregated particles. Since salbutamol base behaves in the same way as a sticky foodstuff, it was thought that the addition of sugars with higher T_gs (lactose, trehalose or maltodextrin) would increase the T_g of the resulting mixtures and prevent particles stickiness.

However, technological difficulties during preparation of solutions for spray drying were noticed, caused by low dissolution of sugars in ethanol. The second problem encountered was a possible Maillard-type reaction (Fayle and Gerrard, 2002) occurring between -NH- moiety of salbutamol and the carbonyl group of a reducing sugar (e.g. lactose and maltodextrin) resulting in a yellow tint in the sprayed solution. All the above issues resulted in trials of spray drying salbutamol base with PVP.

3.3.2 Co-spray dried salbutamol base and lactose monohydrate

Two systems of salbutamol base with lactose monohydrate were spray dried, where lactose monohydrate constituted 10% and 50% by weight of solids. The solvent used for spray drying of the composite containing 10% (w/w) of lactose monohydrate was 65% (v/v) ethanol and the solvent used for spray drying of the composite containing 50% (w/w) of lactose monohydrate was 69% (v/v) ethanol. The processing conditions are given in Appendix I.

The thermograms of lactose monohydrate had two endotherms peaking at ~150°C and ~220°C (Figure 3.7). The first peak was interpreted as dehydration and the second as melting of the anhydrous α-lactose (Corrigan *et al.*, 2002). Salbutamol base crystalline material showed only one peak, namely a melting endotherm at ~160°C (Section 3.2.1). The melting of the drug was accompanied by thermal decomposition as indicated by TG analysis (Figure 3.8). A very weak indication of the lactose monohydrate presence was found on the DSC trace of the mechanical mix containing 10% (w/w) of this sugar and a dehydration endotherm of the excipient was observed at a higher magnification (Figure 3.7d). The weight loss in the 25-100°C range was only ~0.3% compared with the mass loss for crystalline salbutamol base of ~0.8% in the same temperature range (Figure 3.8).

In the thermogram of the 1:1 physical mixture of the drug and sugar (Figure 3.7) one can observe a small, broad endotherm at ~152°C perhaps due to the dehydration of lactose and broadening of the melting endotherms of salbutamol and lactose with the latter moved greatly towards lower temperatures. This alteration of the melting point may indicate the presence of solid-state interactions between the drug and lactose. The thermogram of the co-spray dried composite at 10% of lactose (Figure 3.7) had an exotherm peaking at ~90°C evidencing recrystallisation of the amorphous material produced on processing. No T_g was found to confirm this. The reason for this could be that it was overlapped by a weak peak of adsorbed solvent liberation at 25-80°C. TGA revealed ~3.5% weight loss in the 25-100°C region. This exotherm was followed by an endotherm peaking at ~151°C. The same thermal events were recorded for the 1:1 composite with the difference that the exotherm was shifted and peaked at ~104°C and the endotherm occurred at ~148°C.

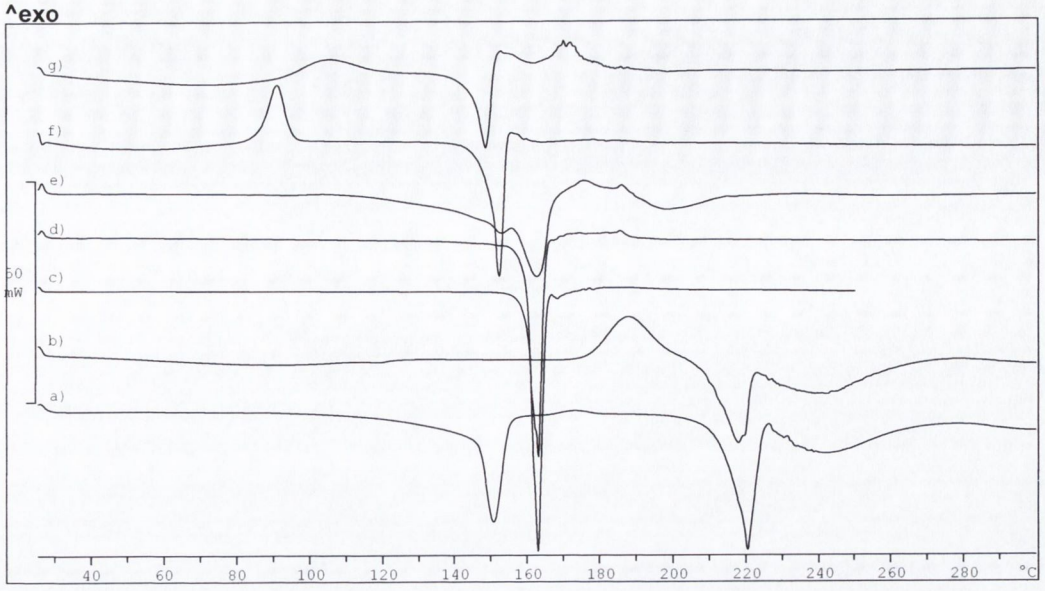

Figure 3.7 DSC scans of (a) lactose monohydrate crystalline commercial product, (b) spray dried lactose monohydrate, (c) crystalline salbutamol base, (d) physical mixture of salbutamol base and lactose monohydrate 10% (w/w), (e) physical mixture of salbutamol base and lactose monohydrate 50% (w/w), (f) co-spray dried salbutamol base and lactose monohydrate 10% (w/w) and (g) co-spray dried salbutamol base and lactose monohydrate 50% (w/w).

The position and temperature occurrence of the peaks would suggest that the component undergoing the recrystallisation is predominantly salbutamol free base. Spray dried lactose underwent recrystallisation at a much higher temperature (the peak temperature was ~188°C) and this was followed by its melting at ~217°C. In all spray dried composites the melting endotherm was shifted towards lower temperatures with respect to the drug on its own, implying that there may be a eutectic or a solid-solution formation between the drug and sugar. Looking at the DSC curve of the 1:1 composite a weak and jagged exotherm at ~175°C can be spotted. It may be indicative of recrystallisation of the excess of amorphous lactose with thermal decomposition underlying this process or could also indicate the latter process only. Perhaps temperature controlled XRD could elucidate what is occuring, as recrystallisation is not accompanied by mass loss and TG analysis would not show any dissimilarity.

The co-spray dried powders had more solvent residues than the corresponding physical mixtures. Weight losses in the 25-100°C region were ~3.5% and ~4% for the 10% and 50% (w/w) sugar content, respectively (Figure 3.8).

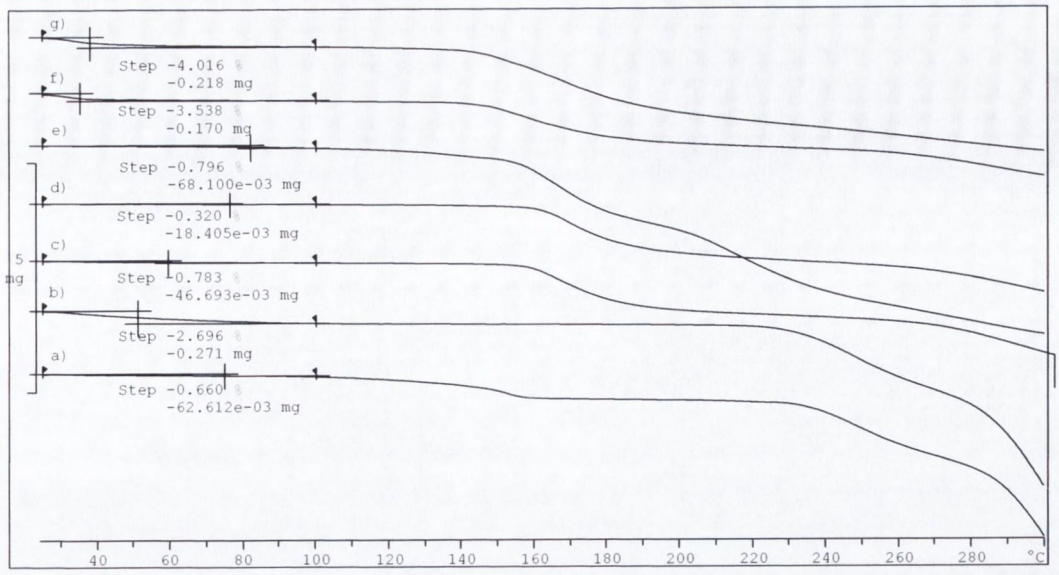

Figure 3.8 TGA scans of (a) lactose monohydrate crystalline commercial product, (b) spray dried lactose monohydrate, (c) crystalline salbutamol base, (d) physical mixture of salbutamol base and lactose monohydrate 10% (w/w), (e) physical mixture of salbutamol base and lactose monohydrate 50% (w/w), (f) co-spray dried salbutamol base and lactose monohydrate 10% (w/w) and (g) co-spray dried salbutamol base and lactose monohydrate 50% (w/w).

XRD confirmed that both of the co-spray dried composites were amorphous, i.e. the drug and sugar were in the disordered state (Figure 3.9). They contrasted with the corresponding physical mixtures, which were XRD crystalline (Figure 3.9). The peaks were easily attributable to those of salbutamol base (black arrows) and lactose monohydrate (blue arrows).

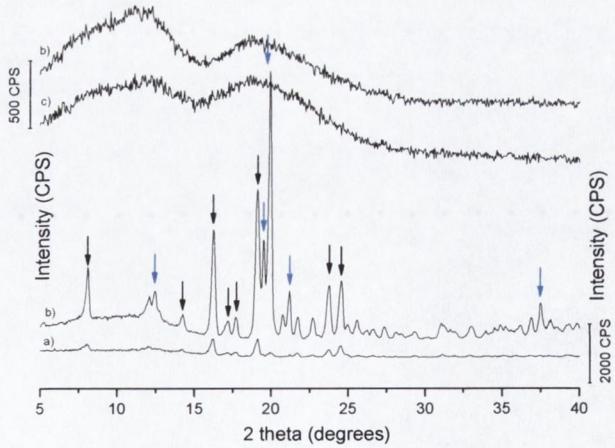

Figure 3.9 XRD diffractograms of (a) physical mixture of salbutamol base and lactose monohydrate 10% (w/w), (b) physical mixture of salbutamol base and lactose monohydrate 50% (w/w), (c) co-spray dried salbutamol base and lactose monohydrate 10% (w/w) and (d) co-spray dried salbutamol base and lactose monohydrate 50% (w/w). Black arrows indicate the peaks of salbutamol free base and the blue arrows the peaks of lactose monohydrate. The left hand side scale applies to the curves (c) and (d) and the right hand side scale applies to the curves (a) and (b).

SEM micrographs (Figure 3.10) of the co-spray dried salbutamol base-lactose mixtures are shown in Figure 3.10. The particles of the 10% (w/w) containing composite were mainly fused but consisted of distinguishable spheres contrasting with the nearly separated and round particles of the 50% (w/w) sample.

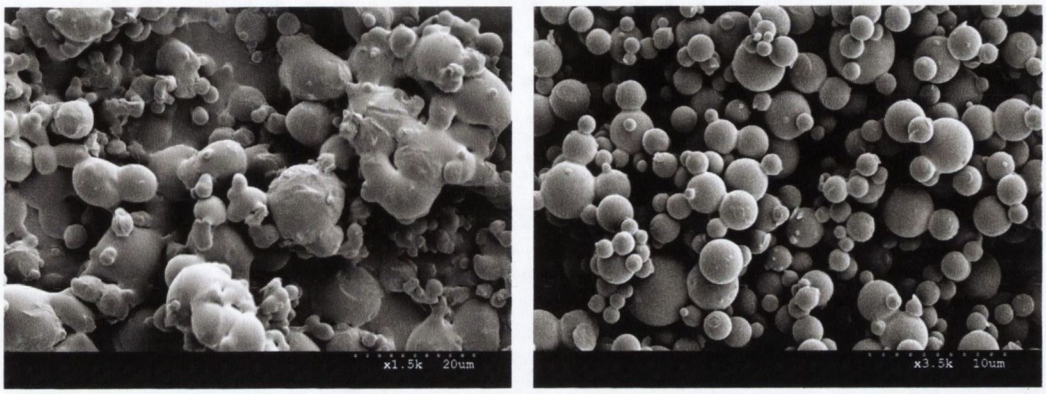

Figure 3.10 SEM micrographs of co-spray dried salbutamol base and lactose monohydrate 10% (w/w) (left) and co-spray dried salbutamol base and lactose monohydrate 50% (w/w) (right).

3.3.3 Co-spray dried salbutamol base and trehalose dihydrate

Two systems of salbutamol base with trehalose dihydrate were spray dried, where trehalose dihydrate constituted 10% and 50% by weight of solids. The solvent used for spray drying of the composite containing 10% (w/w) of trehalose dihydrate was 75% (v/v) ethanol and the solvent used for spray drying of the composite containing 50% (w/w) of trehalose dihydrate was 68% (v/v) ethanol. The processing conditions are given in Appendix I.

The trehalose dihydrate commercial product presented three endotherms (Figure 3.11), one at ~100°C, a small dip at ~143°C and another large peak at ~212°C assigned to the dehydration process, melting of the α-form of the sugar produced on dehydration and the melting of the β-form stable crystals, respectively (Sussich *et al.*, 2002). The dehydration and melting points of the components in the mechanical mixes showed signs of broadening, but changes in their positions were negligible. This may imply that no strong interactions, if any, take place between the substances. In the case of the solid dispersions similar DSC curves (Figure 3.11) were recorded as for the salbutamol base-lactose composites. Only two thermal events appeared irrespective of the sugar content: a recrystallisation exotherm peaking at ~92°C and at ~105°C and an endotherm at ~154°C and at ~153°C for the 10% and 50% (w/w) trehalose concentration, respectively. Comparing with the temperature depression of the peaks observed with those for the co-spray dried salbutamol-lactose powders, trehalose seems to interact less with the drug molecules. Taking into consideration that amorphous trehalose does not recrystallise on heating, though it exhibits a T_g at ~120°C , both of the peaks by DSC can be ascribed to the amorphous-crystalline transition of salbutamol. The melt of the drug does not seem to depress the melting point of trehalose and assuming no considerable interactions between the crystalline components as stated earlier, the amorphous form of the sugar appears to interact with the disordered state of salbutamol by, first of

all, shifting the exotherm to higher temperatures and secondly, depressing the melting of the recrystallised drug. A similar phenomenon of interaction in the liquid but not in the crystalline state was observed by Weuts *et al.* (2004) for the PVP/fragment 1 of loperamide solid dispersions.

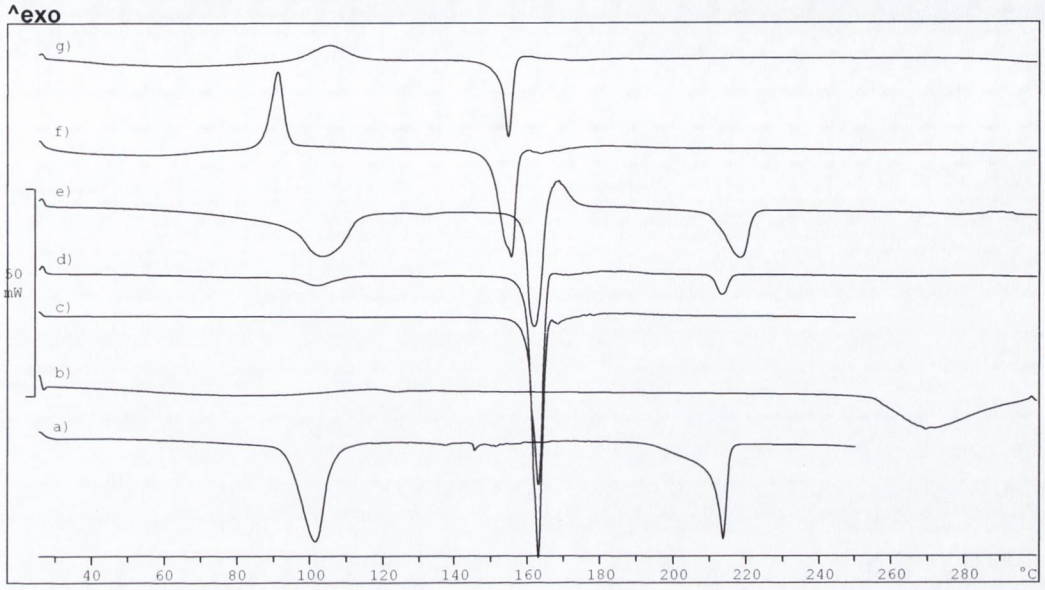

Figure 3.11 DSC scans of (a) trehalose dihydrate crystalline commercial product, (b) spray dried trehalose dihydrate, (c) crystalline salbutamol base, (d) physical mixture of salbutamol base and trehalose dihydrate 10% (w/w), (e) physical mixture of salbutamol base and trehalose dihydrate 50% (w/w), (f) co-spray dried salbutamol base and trehalose dihydrate 10% (w/w) and (g) co-spray dried salbutamol base and trehalose dihydrate 50% (w/w).

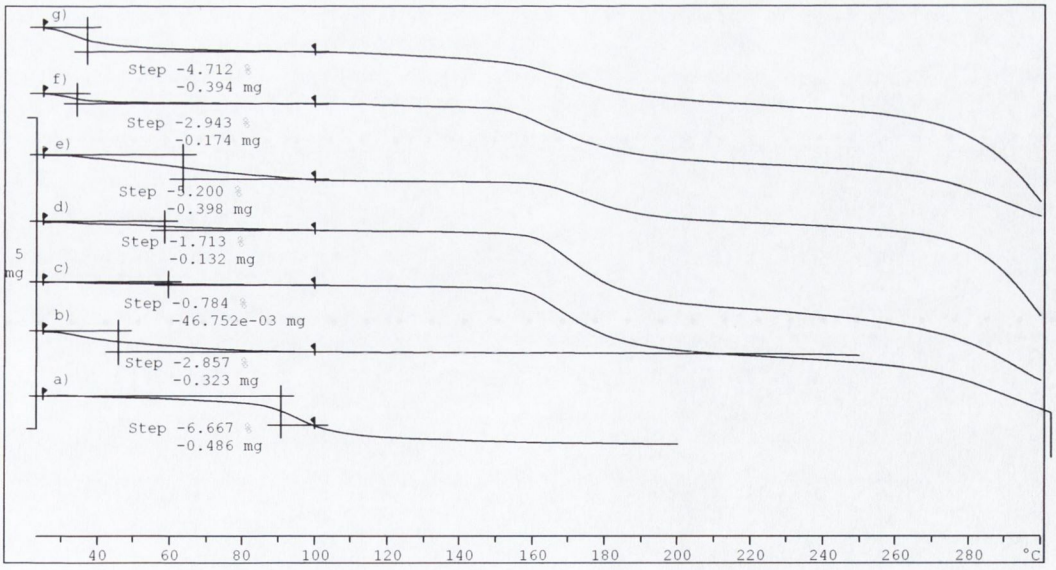

Figure 3.12 TGA scans of (a) trehalose dihydrate crystalline commercial product, (b) spray dried trehalose dihydrate, (c) crystalline salbutamol base, (d) physical mixture of salbutamol base and trehalose dihydrate 10% (w/w), (e) physical mixture of salbutamol base and trehalose dihydrate 50% (w/w), (f) co-spray dried salbutamol base and trehalose dihydrate 10% (w/w) and (g) co-spray dried salbutamol base and trehalose dihydrate 50% (w/w).

The processed composites retained quite a large amount of residual moisture and the weight loss in the 25-100°C region was ~3% and ~4.7% for the 10% and 50% sugar containing mixtures, respectively. The equivalent physical blends displayed ~1.7% and ~5.2% mass loss in the same temperature range (Figure 3.12).

X-ray diffraction studies showed amorphous forms of the drug and sugar to be present in both of the solid dispersions (Figure 3.13) as indicated by broad "halos". The diffraction spectra of the equivalent physical mixtures presented peaks of salbutamol as well as trehalose in the crystalline structures and the black and blue arrows point to peaks of the drug and sugar, respectively (Figure 3.13).

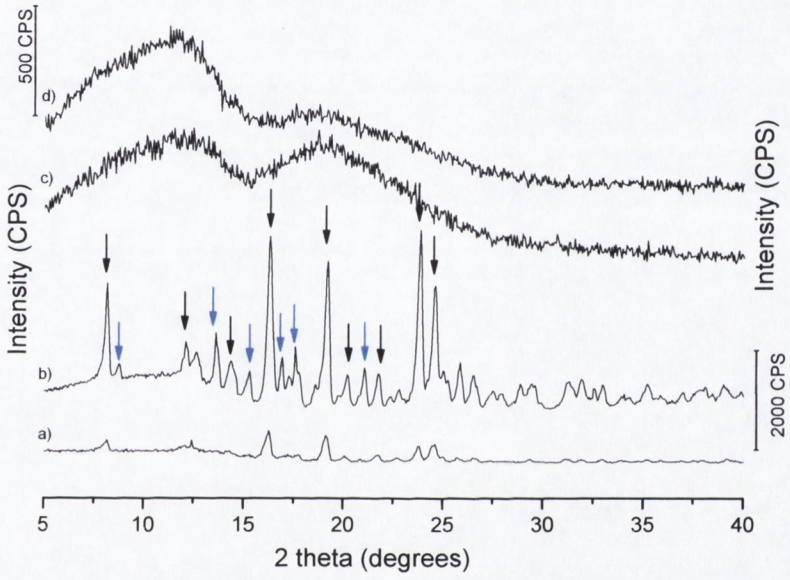

Figure 3.13 XRD diffractograms of (a) physical mixture of salbutamol base and trehalose dihydrate 10% (w/w), (b) physical mixture of salbutamol base and trehalose dihydrate 50% (w/w), (c) co-spray dried salbutamol base and trehalose dihydrate 10% (w/w) and (d) co-spray dried salbutamol base and trehalose dihydrate 50% (w/w). Black arrows indicate the peaks of salbutamol free base and the blue arrows the peaks of lactose monohydrate. The left hand side scale applies to the curves (c) and (d) and the right hand side scale applies to the curves (a) and (b).

Co-spray drying with trehalose appeared to be less efficient in terms of separation of the fused particles than when lactose was used and more interparticulate bridges can be seen when comparing the particle morphologies of the 1:1 composites. Still, the powders consist of more or less spherical particles with a very high degree of fusion for the salbutamol base-trehalose 10% (w/w) co-spray dried sample (Figure 3.14).

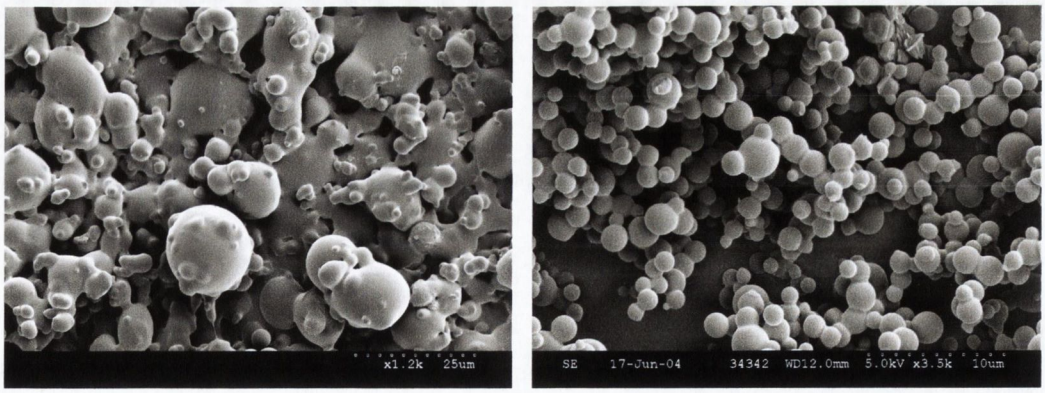

Figure 3.14 SEM micrographs of co-spray dried salbutamol base and trehalose dihydrate 10% (w/w) (left) and co-spray dried salbutamol base and trehalose dihydrate 50% (w/w) (right).

3.3.4 Co-spray dried salbutamol base and maltodextrin

Due to the very low ethanolic solubility of maltodextrin, spray drying of the composites was limited to only one containing 10% (w/w) of the sugar. The solvent used for spray drying of this composite was 46% (v/v) ethanol. The spray drying conditions are given in Appendix I.

Maltodextrin starting material was DSC (Figure 3.15) and XRD amorphous (Figure 3.16) as evidenced by a lack of either recrystallisation exotherm or melting endotherm as well as by the presence of a broad "halo" on the X-ray diffractogram. No indication of any kind of interaction between the crystalline drug and amorphous excipients was discerned by DSC. On the other hand, similarly to the lactose and trehalose solid dispersions, a slight depression in the salbutamol melting point was observed for the co-spray dried powder. Miscibility of the two components appears to exist only in the liquid state, as was observed for trehalose. DSC showed that in the solid dispersion salbutamol recrystallised at ~88°C and melted at ~157°C, indicating the weakest interactions created among the sugars used.

XRD analysis revealed the composite was predominantly amorphous but a few low intensity peaks were evident. These peaks, when contrasted with those of the corresponding physical mixture, matched the crystalline salbutamol. The peaks of the drug are marked by black arrows (Figure 3.16).

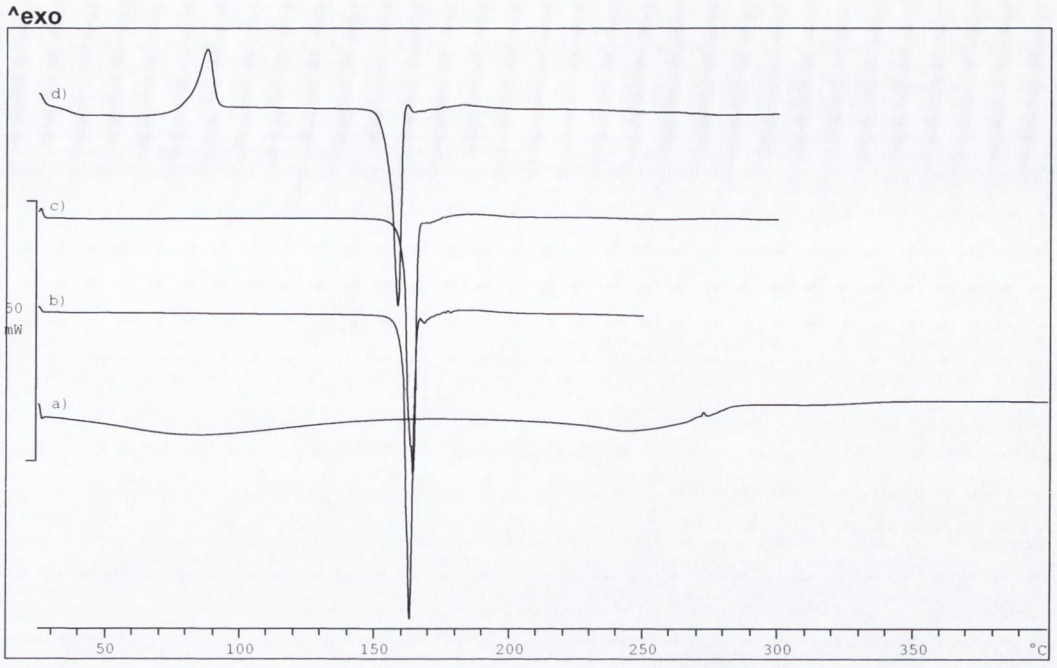

Figure 3.15 DSC scans of (a) maltodextrin raw material powder, (b) crystalline salbutamol base, (c) physical mixture of salbutamol base and maltodextrin 10% (w/w) and (d) co-spray dried salbutamol base and maltodextrin 10% (w/w).

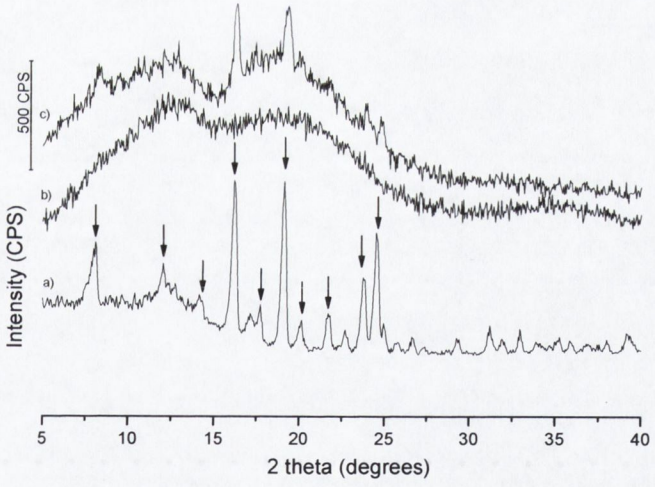

Figure 3.16 XRD diffractograms of (a) physical mixture of salbutamol base and maltodextrin 10% (w/w), (b) maltodextrin raw material powder and (c) co-spray dried salbutamol base and maltodextrin 10% (w/w). Arrows indicate the peaks of salbutamol free base.

Surprisingly, taking into account the low miscibility of the composite constituents, maltodextrin even at the 10% level succeeded in separation of the particles, although they were quite large (Figure 3.17). Their surfaces were rough as opposed to the smooth exteriors of the 10%-containg lactose and trehalose co-spray dried powders (Figure 3.10 and Figure 3.14).

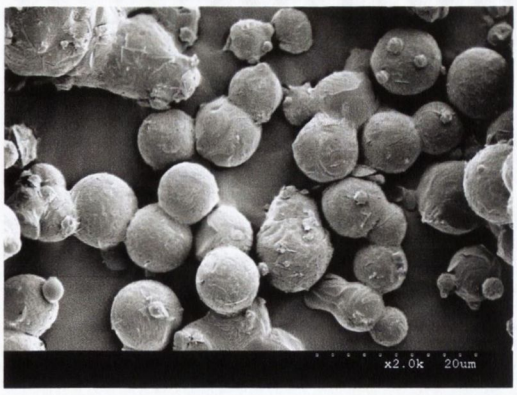

Figure 3.17 SEM micrograph of co-spray dried salbutamol base and maltodextrin 10% (w/w).

3.3.5 Co-spray dried salbutamol base and PVP

No difficulties were encountered in the preparation of ethanolic solutions of salbutamol base-PVP intended for spray drying as PVP is known to be very soluble in ethanol. Therefore a range of five composites comprising 10%, 30%, 50%, 70% and 90% (w/w) PVP were prepared and Appendix I gives the processing details. The solvent used for the preparation of these systems was 95% (v/v) ethanol.

The results of the DSC analysis (Figure 3.18) on the solid dispersions show a gradual disappearance of the melting peak of salbutamol base and at the 50% level and above no such endotherm is seen. Furthermore, on the DSC curve for the sample containing only 10% of the polymer this peak is split and shifted towards lower temperatures. The powder with 30% content of PVP showed two separate endotherms, broad and small in magnitude, that vanished completely at 50% of the polymer content, indicating a complete miscibility of the components above the 30% polymer concentration. This also indicates that the drug is no longer present as a crystalline material when its concentration does not exceed 50%, but is converted into the amorphous state. A weak deflection in the baseline below 120°C (preceding the endotherm if it exist) for all DSC curves was seen at high magnification and this was attributed to the glass transition temperatures of the dispersions.

XRD demonstrated that dispersions containing more that 10% of PVP were amorphous as only broad "halos" were observed (Figure 3.20). The co-spray dried salbutamol base-PVP 10% composite was primarily amorphous but the peak around 7.0 2θ corresponded to one of the peaks of crystalline drug as indicated by the black arrows. Several diffraction peaks attributable to salbutamol base could be detected in the physical mixture with PVP when the concentration of the drug was 90% (w/w) (Figure 3.20).

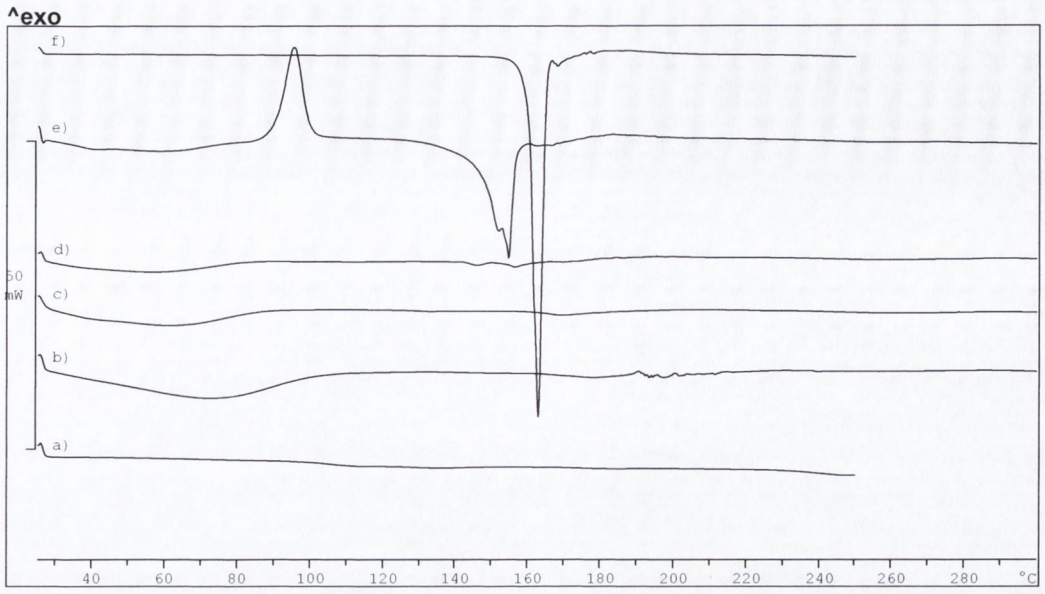

Figure 3.18 DSC traces of (a) co-spray dried salbutamol base and PVP 90% (w/w), (b) co-spray dried salbutamol base and PVP 70% (w/w), (c) co-spray dried salbutamol base and PVP 50% (w/w), (d) co-spray dried salbutamol base and PVP 30% (w/w), (e) co-spray dried salbutamol base and PVP 10% (w/w) and (f) crystalline salbutamol base.

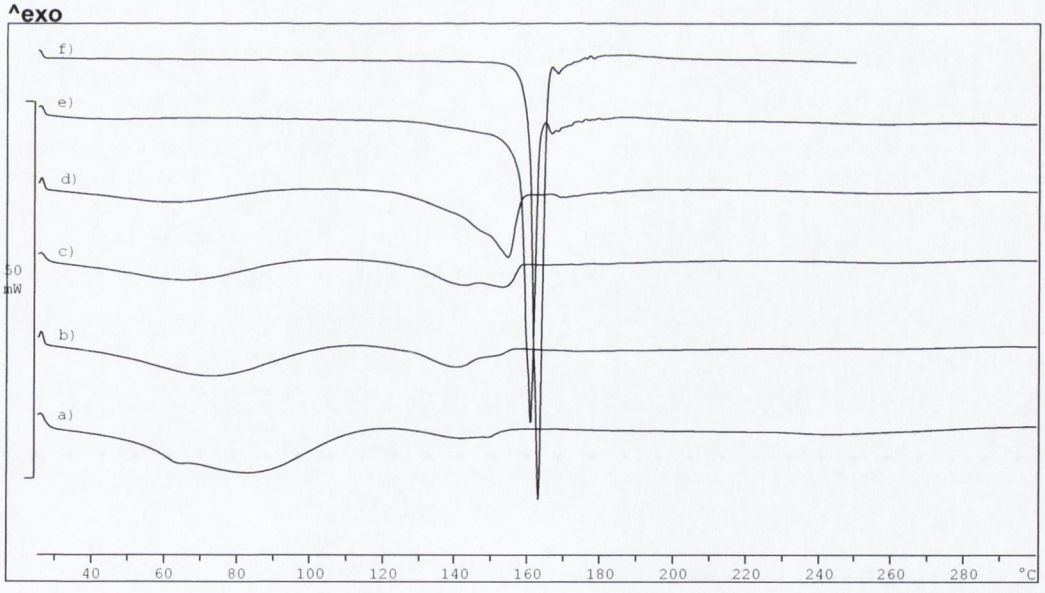

Figure 3.19 DSC traces of (a) co-spray dried salbutamol base and PVP 90% (w/w), (b) co-spray dried salbutamol base and PVP 70% (w/w), (c) co-spray dried salbutamol base and PVP 50% (w/w), (d) co-spray dried salbutamol base and PVP 30% (w/w), (e) co-spray dried salbutamol base and PVP 10% (w/w) and (f) crystalline salbutamol base.

To investigate further the interactions between the polymer and salbutamol base, equivalent physical mixtures were prepared and analysed by DSC and XRD. As the polymer content increases, the endotherm of the drug melting broadens and its onset and peak are depressed (Figure 3.19). A second endotherm becomes more apparent at the 50% PVP level and peaks at ~143°C. Its position, despite the width changes, seems to be more or less constant and it is located between ~150°C and ~140°C for various PVP concentrations.

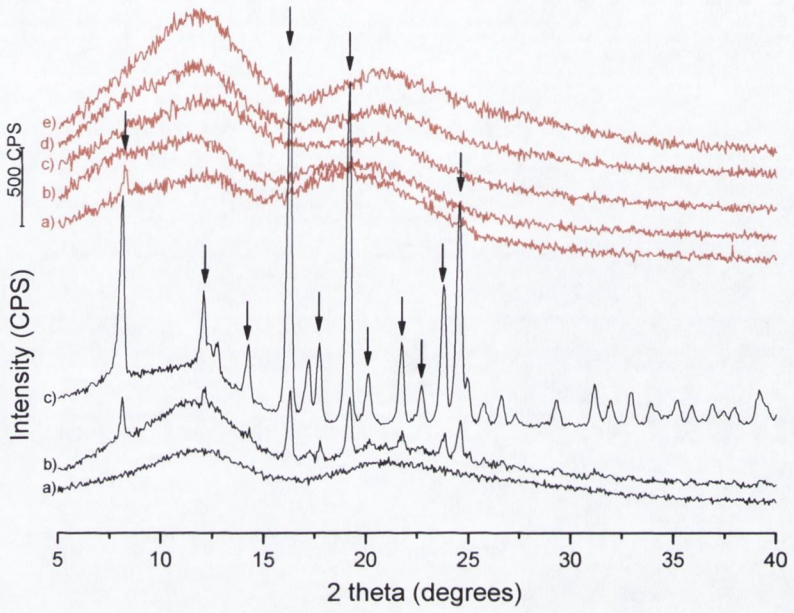

Figure 3.20 XRD diffractograms of PVP raw material powder (black a), physical mixture of salbutamol base and PVP 90% (w/w) (black b), physical mixture of salbutamol base and PVP 10% (w/w) (black c), co-spray dried salbutamol base and PVP 10% (w/w) (red a), co-spray dried salbutamol base and PVP 30% (w/w) (red b), co-spray dried salbutamol base and PVP 50% (w/w) (red c), co-spray dried salbutamol base and PVP 70% (w/w) (red d), co-spray dried salbutamol base and PVP 90% (w/w) (red e).

The sequence of SEM micrographs in Figure 3.21 presents changes in particle morphology due to the presence of PVP. It can be observed that 70% of the polymer content sufficed to produce individual, spherical particles in the 1-6 μm size. Lower concentrations were not that efficient and the lower the PVP concentration the greater the degree of fusion detected.

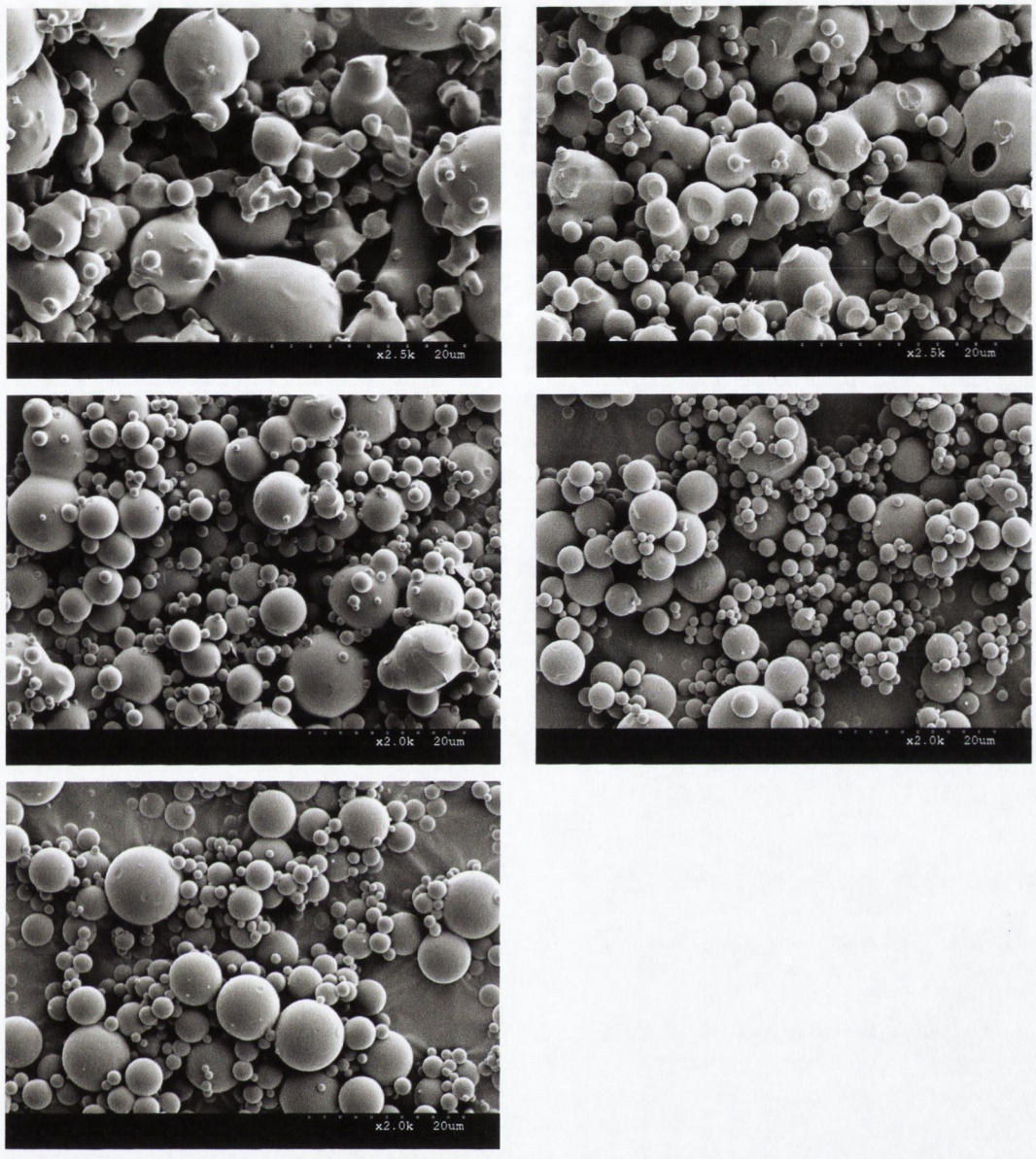

Figure 3.21 SEM micrographs of the co-spray dried salbutamol base and PVP 10% (w/w) (top left), co-spray dried salbutamol base and PVP 30% (w/w) (top right), co-spray dried salbutamol base and PVP 50% (w/w) (middle left), co-spray dried salbutamol base and PVP 70% (w/w) (middle right), co-spray dried salbutamol base and PVP 90% (w/w) (bottom).

3.4 Conclusions

The rationale for spray drying of salbutamol free base originated from very limited information on processing of this substance. Spray drying of salbutamol base alone from ethanolic solutions resulted in predominantly amorphous powdered products and the degree of amorphicity depends on the spray drying conditions. The drug has shown difficulties in processing due to its low glass transition temperatures (~45˚C) and according to the work of Corrigan *et al.* (2004), the formation and physical stability of amorphous composites prepared by spray drying is dependant on the T_g of the mixture. The problems in spray drying of salbutamol base manifested in low yields obtained

and production of highly fused particulate agglomerates. To reduce the stickiness, preliminary studies on co-spray drying of salbutamol free base with various sugars and PVP were conducted and composite particles produced demonstrated a lesser degree of particle fusion. The higher the excipients content, the more separated the particles became.

Also other excipients e.g. chitosan, that is believed to be a potential candidate for carrying biotherapeutic compounds to the lung (Williams *et al.*, 1998), could be used in future investigations on co-spray drying of salbutamol base. On the other hand, instead of using the above excipients, a different solvent could be used e.g. methanol and chloroform to produce milder manufacturing conditions and thereby reduce the likeliness of forming agglomerates. This was not feasible at the time of planning the experiments as the methanol and chloroform vapours are highly toxic and in order to use them, another model of spray dryer ensuring safety of the process must have been used. For instance, a new model of Mini Spray Dryer Büchi B-290 offers this advantage.

FACTORIAL DESIGN STUDY OF CO-SPRAY DRIED BUDESONIDE-FORMOTEROL FUMARATE DIHYDRATE 100:6

4.1 Introduction

Effective control of asthma symptoms and maintenance of optimal lung function are critical for the long-term management of patients with persistent asthma. In patients receiving inhaled glucocorticosteroids whose asthma is not fully controlled, national and international guidelines recommend a step-wise approach (Zetterström *et al.*, 2001). Increasing the dose of inhaled glucocorticosteroid or, alternatively, the addition of a long-acting β2-agonist to low-dose inhaled glucocorticosteroids are two therapeutic options. In 2001 evidence was found that the addition of a long-acting β2-agonist to inhaled glucocorticosteroids may be more beneficial in terms of asthma control than increasing the dose of corticosteroids alone (Zetterström *et al.*, 2001). A more recent study has established that budesonide/formoterol inhaled twice-daily was significantly more effective than an equivalent or higher daily dose of budesonide alone or high-dose fluticasone propionate alone at improving peak expiratory flow in adults with predominantly moderate persistent asthma (Goldsmith and Keating, 2004). The synergistic effect of using budesonide and formoterol together has recently been explained on a molecular basis; β_2–agonists are capable of activating the glucocorticoid receptor, and combined low doses of formoterol and budesonide show antiproliferative effects on bronchial smooth muscle cells by synchronizing cell-cycle control (Roth *et al.*, 2002).

The first commercial inhaler containing budesonide and formoterol was Symbicort® using the Turbohaler® device produced by AstraZeneca. It contains an inhalation powder, which is a mixture of the active ingredients, budesonide and formoterol fumarate dihydrate. The other ingredient is lactose (Symbicort®, product leaflet). Because Symbicort® consists of a physical mixture of the active ingredients that may not always ensure a uniform dose of the drugs inhaled, a co-spray drying process could be more suitable method of producing inhalable powders since each particle will contain the components at a fixed ratio.

On the other hand, as spray drying is a complex technological procedure offering an adjustment of up to six different parameters (inlet temperature, feed concentration, aspirator performance, pump rate, airflow and nozzle diameter), great dependence of the machinery settings on the resulting product has been demonstrated (Chawla *et al.*, 1994; Billon *et al.*, 2000). As stated in the previous chapter, statistical factorial designs can be of help when investigating complex systems and the effects of more than one factor are investigated simultaneously in all their possible combinations. Therefore, it was decided that this approach would be also used in this study as it saves time and reduces costs.

4.2 Design study - structure

The choice of an experimental design depends on the objectives of the experiment and the number of factors to be investigated. A 2^{5-1} factorial design study was commenced to assess the effect of spray drying processing variables on particle characteristics for a 100/6 combination of budesonide and formoterol fumarate dihydrate, spray dried from 95% (v/v) ethanol solution. This is an expanded version of a statistical study on this combination of drugs undertaken by Corrigan (2002) when only two parameters (airflow rate and pump rate) were investigated. The processing variables that were studied using the Büchi 191 Mini Spray Dryer were: (A) inlet temperature, (B) spray drier airflow rate, (C) pump rate/setting, (D) aspirator setting and (E) feed concentration. Each factor was studied at two levels as listed in Table 4.1.

Table 4.1 Processing variables used in the factorial study.

Parameter	Low (-)	High (+)	Units
A (inlet temperature)	78	84	°C
B (airflow)	400	800	L/hr
C (pump setting)	10	40	%
D (aspirator setting)	70	100	%
E (feed concentration)	1	1.75	%

All runs of the experiment were performed in a randomised manner to eliminate any unknown possible sources of bias. The design matrix for the experiment is shown in Table 4.2.

Table 4.2 The design matrix consisting of one half fraction of the 2^5 design.

Run	Inlet temperature A	Airflow rate B	Pump setting C	Aspirator setting D	Feed concentration E	Sample ID
1	-	-	-	-	+	8AB
2	+	-	-	-	-	14AB
3	-	+	-	-	-	5AB
4	+	+	-	-	+	9AB
5	-	-	+	-	-	17AB
6	+	-	+	-	+	6AB
7	-	+	+	-	+	11AB
8	+	+	+	-	-	16AB
9	-	-	-	+	-	3AB
10	+	-	-	+	+	10AB
11	-	+	-	+	+	13AB
12	+	+	-	+	-	15AB
13	-	-	+	+	+	2AB
14	+	-	+	+	-	4AB
15	-	+	+	+	-	7AB
16	+	+	+	+	+	12AB

Each system was prepared in duplicate. The response variables that were analysed by the factorial experiment were: percentage yield, Carr's compressibility index, median particle size obtained from Sympatec laser diffraction particle size measurements and the *in vitro* respirable fraction obtained by twin stage impinger deposition studies. The statistical analysis was carried out with the assistance of the Minitab™ software (version 13.32) due to the complexity of calculations. The full statistical factorial analysis of the density response was not possible due to large variability of the replicate values. Table 4.3 shows the data used in the statistical analysis to estimate the most important factors that influenced the spray dying process for different responses.

Table 4.3 Table summarising the data collected from the analyses and used in the statistical factorial design.

System	Percentage yield (%)	Carr's index (%)	Median particle size (μm)	Average *in vitro* respirable fraction (%)	True density (g/cm^3)
2AB Run 1	31.9	52.4	3.64	0.80	1.257
Run 2	32.5	53.5	3.81		1.254
3AB Run 1	57.2	42.4	2.93	2.29	1.262
Run 2	48.2	47.2	2.78		1.214
4AB Run 1	26.6	35.8	3.59	2.24	1.240
Run 2	23.0	37.5	3.59		1.263
5AB Run 1	35.0	25.0	1.77	1.57	1.201
Run 2	41.7	31.3	2.11		1.250
6AB Run 1	26.0	37.1	4.57	1.12	1.231
Run 2	21.9	38.9	5.15		1.237
7AB Run 1	58.2	44.1	1.97	0.74	1.226
Run 2	58.5	40.5	1.96		1.210
8AB Run 1	41.6	45.6	4.99	1.17	1.218
Run 2	41.6	51.1	5.08		1.234
9AB Run 1	62.0	48.7	2.06	0.89	1.214
Run 2	53.3	50.0	2.12		1.198
10AB Run 1	49.2	60.0	4.06	1.30	1.220
Run 2	53.8	60.0	4.12		1.200
11AB Run 1	56.8	48.8	2.52	0.59	1.210
Run 2	59.9	46.5	2.44		1.211
12AB Run 1	64.3	47.5	2.23	0.93	1.222
Run 2	60.2	47.5	2.16		1.228
13AB Run 1	69.1	47.7	1.74	1.52	1.212
Run 2	52.7	44.4	1.77		1.207
14AB Run 1	41.1	43.3	4.76	4.64	1.214
Run 2	41.5	43.8	4.48		1.209
15AB Run 1	58.5	45.2	1.94	1.13	1.215
Run 2	57.3	41.9	1.87		1.199
16AB Run 1	56.9	45.5	2.14	1.19	1.222
Run 2	65.8	45.7	2.18		1.231
17AB Run 1	22.6	42.4	4.46	1.94	1.215
Run 2	20.6	47.1	4.37		1.227

4.3 The statistical analysis of the 2^{5-1} factorial design

4.3.1 Experimental design: response "percentage yield"

The weights of the powder collected after every spray dryer run were expressed as the per cent of the initial amount of the solids taken for solution preparation. Table 4.3 shows the values obtained. The lowest yield achieved was for sample 17AB (around 22% of the starting dose) and the greatest was for 12AB (~62%) (Table 4.3). A major difficulty during collection of the powders was associated with a static charge built-up and an antistatic "gun" was used to reduce this effect. Static charge production on the surface of budesonide particles has been reported for both MDIs (Barry and O'Callaghan, 1995) and DPIs (Byron *et al.*, 1997).

Firstly, a cube plot was created to show the relationship between parameters and to visualise the design. The plot below (Figure 4.1) illustrates a five-factor cube plot for the "percentage yield" data and the values in red are the real response data.

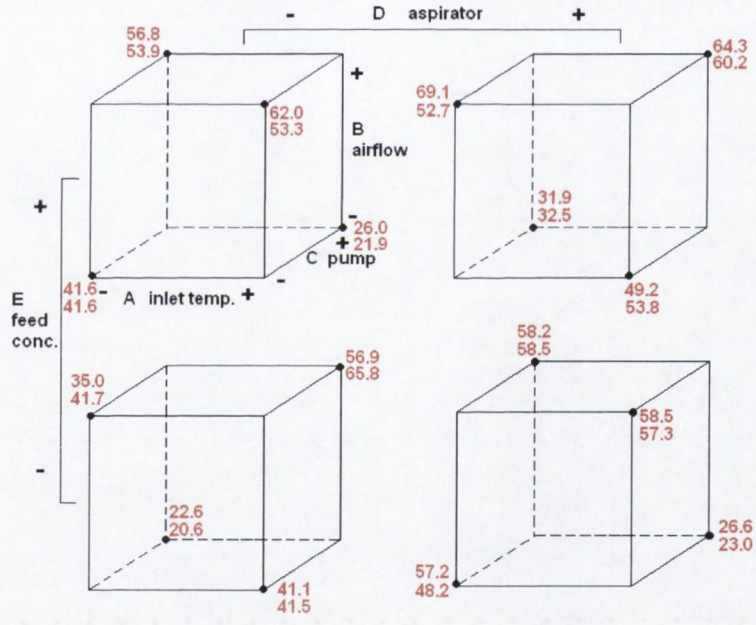

Figure 4.1 The cube plot for the response "percentage yield".

From Figure 4.1 it can be seen that generally smaller values of yields were obtained when the aspirator was set at minimum.

To see if any trends or anomalies appear, the data were plotted in several ways. The distribution of the response is given below (Figure 4.2):

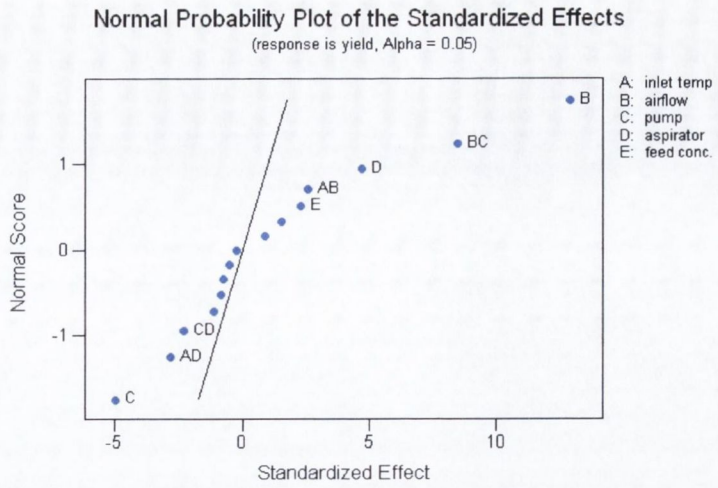

Figure 4.2 Normal probability plot of effects.

The straight line is the fitted normal distribution. The statistical term "effect" used in the normal probability plot is defined as the change in average response when a factor goes from its lower level to the higher level. The expression "standardised" means that each mean for an effect was divided by its standard deviation.

In the normal plot of the effects, points that do not fall near the line usually signal important effects. Important effects are larger and farther from the fitted line than unimportant effects, thus in our case, we can conclude that main effects: B, C, D, E and interactions: AB, BC, AD, and CD will have a significant effect on the spray drying process of budesonide-formoterol fumarate dihydrate 100:6. Further statistical analysis was performed to decide which effects and at which confidence levels can be considered as significant. For further considerations the analysis of variance, ANOVA, was performed. Only main effects and 2-factor interactions were considered as the most likely to influence the response and only they constituted the theoretical model. The higher interaction terms were used to estimate the experimental error. This is mainly due to the fact that such complex interactions are rarely significant and they are very difficult to interpret. The first ANOVA model had a good R^2 value (correlation coefficient) equal to 0.952 and was in reasonable agreement with the R^2 adjusted (R^2 value adjusted downwards by the sample size and number of parameters in the factorial design) value of 0.907. The difference between these two R^2 values implied that there were some insignificant terms in the model. Generally, in the case of the R^2 parameters, a number close to one is preferred and a smaller difference between an R^2 and an R^2 adjusted indicates a better fit. Excluding from the model all terms (except the main effect A which was involved in interactions and must be included in calculations) with p-value under 0.05 and refitting gave the following ANOVA table (Table 4.4).

Table 4.4 Analysis of variance output for the response "percentage yield" after removing insignificant terms.

Source of variation	Sum of squares	DF	Mean square	F-value	p-value	
Model	6198.98	9	688.78	39.47	<0.0001	Significant **
A	48.27	1	48.27	2.77	0.1105	
B	3298.75	1	3298.75	189.03	<0.0001	Significant **
C	481.28	1	481.28	27.58	<0.0001	Significant **
D	441.79	1	441.79	25.32	<0.0001	Significant **
E	105.49	1	105.49	6.04	0.0223	Significant *
AB	134.07	1	134.07	7.68	0.0111	Significant *
AD	153.56	1	153.56	8.80	0.0071	Significant **
BC	1432.46	1	1432.46	82.09	<0.0001	Significant **
CD	103.32	1	103.32	5.92	0.0235	Significant *
Error	383.92	22	17.45			
Total	6582.90	31				

*-significant at the 95% level
**-significant at the 99% level

The F-value for the final statistical interaction model was 39.47, indicating that the model was significant. The following factors: B, C, D, and BC are significant model terms at the 99% level and E, AB, AD, CD are significant model terms at the 95% level. The R^2 of 0.9417 is in good agreement with the adjusted R^2 of 0.9178 and gives a lower difference between them indicating a better fit than the previous model.

Before accepting the mathematical model, the residuals (the differences between the experimental values and the corresponding predictions) were examined for normality of distribution and independence from the run order and the processing variables (i.e. factors). The residuals exhibited an approximate normal distribution and a lack of a pattern to the residuals demonstrating no violation of the statistical model assumptions (the graphs are not shown).

Finally, the fitted equation (Equation 4.1) describing the dependence of the percentage yield achieved on the spray dryer settings was computed:

$$\text{Yield (weight\%)} = 46.36+1.23A+10.15B-3.88C+3.72D+1.82E +2.05AB-2.19AD+6.69BC-1.80CD \quad \text{(Equation 4.1)}$$

The equation coefficients were calculated using the coded values, thus the various terms can be compared directly regardless of their magnitude. The coding used throughout the statistical analysis denotes that -1 was taken instead of the actual value for the factor on its lower level and +1 for the upper level. Therefore, a positive parameter coefficient indicates that the output increases with increasing variable level and a negative coefficient that the output increases with decreasing variable level.

Among the main effects four are positive i.e. inlet temperature, airflow, aspirator and feed concentration and one negative – pump performance as showed in Equation 4.1. The main effect of the inlet temperature was determined to be not significant (Table 4.4). The greatest influence on the spray drying process was the airflow through the apparatus due to the greatest F value equal to

189.03 (Table 4.4). In the case of the feed concentration the p-value of 0.0223 in the analysis of variance indicates its importance at the 95% level only. The works of Chawla *et al.* (1994) and Prinn *et al.* (2002) stated that the feed solution concentration was the most significant factor affecting the efficiency of the spray drying process. However, the feed concentrations used by Chawla *et al.* (1994) were 10% and 20% (w/w) for the minimum and maximum values, respectively and the strengths of bovine serum albumin solutions employed by Prinn *et al.* (2002) differed by 50-fold. In this study the difference between the lower and upper levels for the feed concentration is only 0.75% as this was limited by the solubility of budesonide and this may be the cause for the lesser significance of this variable.

All main effects, except feed concentration (E), influenced one another (i.e. there was an interaction between them) and this means that the effect of one factor was dependent upon a second factor. The strongest interaction observed was between airflow and pump rate (BC) with the p-value lower that 0.0001. The F-value for this term was 82.09, being 10-fold and over greater than the F-values of the rest of interactions. The other 2-way interactions were comparable with regard to the ability to influence the yield as indicated by the close values of F- and p-values. Figure 4.3 shows graphically the B-C interaction.

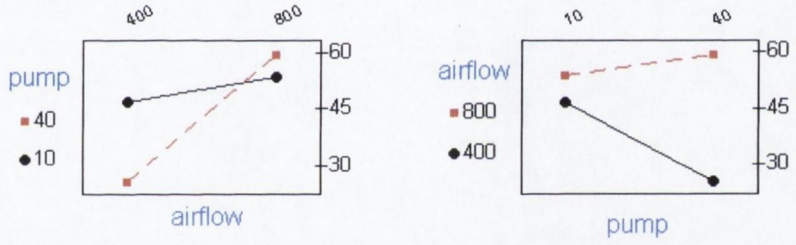

Figure 4.3 Airflow-pump interaction (BC). The black and red lines indicate the magnitude of response (% yield) when the parameter given on the left-hand side of the graph is on its lower and higher levels, respectively.

Figure 4.3 shows that better yield can be obtained if both airflow and pump are on higher levels and the greatest effect on the percentage yield is pump rate especially when set on a higher level. This interaction overrides the meaning of the pump alone, as Equation 4.1 suggests that greater yield values can be obtained when the pump is set at a lower level.

The same interaction and effect of alteration of pump and airflow rates on the yield achieved was determined by Corrigan (2002). This also confirms reproducibility and validity of the spray drying process despite a different operator and time frame employed, which is very important when consistency of the product is needed.

Airflow is known to affect the particle size and higher airflow results in smaller particles but higher pump rates have the opposite effect on the particle size (Masters, 1985). A correlation between the yield and the mean particle size was carried out and is depicted in Figure 4.4. It can be seen that

greater yields were achieved with smaller particles and this may be due to their greater adhesiveness and cohesiveness.

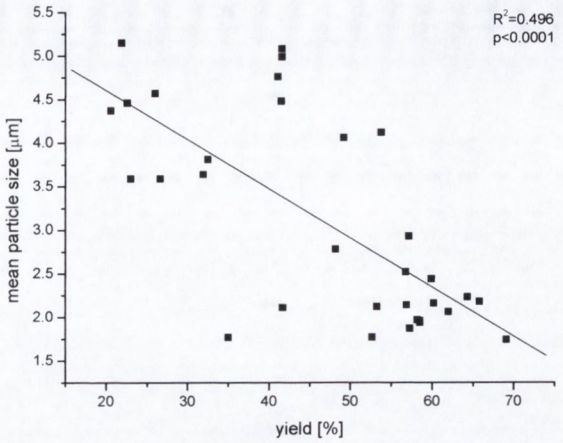

Figure 4.4 Correlation between the yield and mean particle size.

Overall, to optimise yield, taking into consideration all factors studied, all parameters of the apparatus have to be maintained at high levels.

4.3.2 Experimental design: response "median particle size"

The median particle size was in the range 1.7-5.2 µm (Table 4.3) which lies within the range of 0.5-8 µm for the ideal particle size of the powders intended for inhalation purposes as set by Davies *et al.*, (1976). The particle size distributions were monomodal in all cases.

To assess the influence of various spray dryer parameters the same sequence of statistical analyses as for the response "yield" was applied.

Figure 4.5 presents the data obtained from laser diffraction measurements as a cube plot. The powder particles seem to be smaller in size when the drying air flow is high and this is in agreement with the technical specification of the apparatus (Büchi B-191 technical specification).

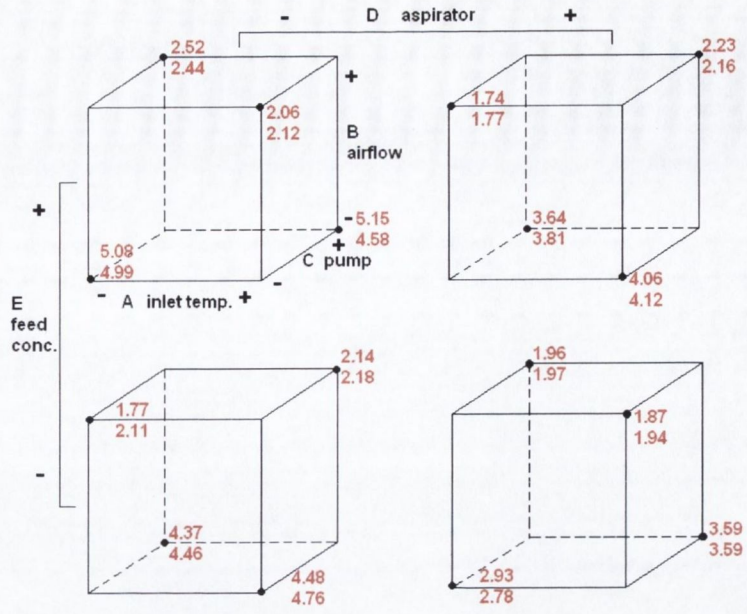

Figure 4.5 The cube plot for the response "median particle size".

The nature of the distribution of the response is shown in Figure 4.6. The points lying the farthest away from the straight line of normal distribution are B, D and BD and thus they will have the greatest impact on the particle size.

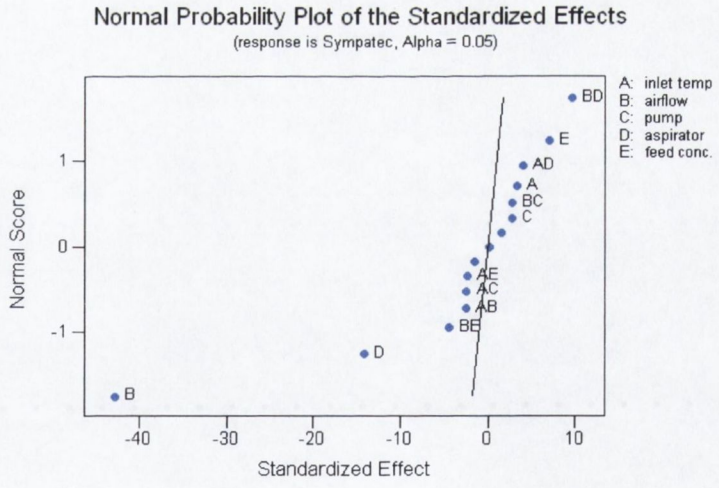

Figure 4.6 Normal probability plot of effects.

For further consideration the analysis of variance, ANOVA, was performed. While the mathematical model had very good R^2 values close to 1, the test for normality and independence of the residuals showed that they had a rather poor normal distribution (graphs not shown). It was concluded that the chosen model, i.e. of normal distribution, was inappropriate without mathematical transformation of the data.

It is well known and believed that the size distribution for particulates obtained by industrial processes e.g. milling, spray drying can be well represented by the Log-Normal model. It has also

been used to represent the particle size distributions of aerosols (Dunbar and Hickey, 2000). Thus, the modification of the origin model includes the logarithmic transformation of the response data. The resulting ANOVA table (after excluding statistically insignificant terms) is as follows:

Table 4.5 Analysis of variance output for the response "median particle size" after removing insignificant terms.

Source of variation	Sum of squares	DF	Mean Square	F value	p-value	
Model	0.84	10	0.084	198.73	<0.0001	Significant **
A	5.091E-3	1	5.091E-003	12.07	0.0023	Significant **
B	0.72	1	0.72	1702.42	<0.0001	Significant **
C	8.257E-3	1	8.257E-003	19.57	0.0002	Significant **
D	0.058	1	0.058	137.26	<0.0001	Significant **
E	0.016	1	0.016	37.87	<0.0001	Significant **
AC	3.814E-003	1	3.814E-003	9.04	0.0067	Significant **
AD	7.565E-003	1	7.565E-003	17.93	0.0004	Significant **
BC	5.486E-003	1	5.486E-003	13.00	0.0017	Significant **
BD	0.013	1	0.013	31.91	<0.0001	Significant **
BE	2.619E-003	1	2.619E-003	6.21	0.0212	Significant *
Error	0.1	21	0.00047			
Total	0.85	31				

*-significant at the 95% level
**-significant at the 99% level

A very large number of terms: A, B, C, D, E and AC, AD, BC and BD were significant at the 99% level and BE was a significant model term at the 95% level, which implies that the particle size is very sensitive to the process variable changes. For the new model the R^2 value was equal to 0.9895 and R^2 adjusted was 0.9846. The very small difference between these values shows an excellent fit. The tests for normality and independence were of the residuals repeated and now they were acceptable (graphs not shown).

The fitted Equation 4.2 relates the particle size to the process variables:

$$\log\text{Median particle size}(\mu m) = 0.46+0.013A-0.15B+0.016C-0.043D+0.022E-0.011AC+0.015AD+0.013BC+0.021BD-0.009BE \quad \text{(Equation 4.2)}$$

Three of the main effects are positive i.e. inlet temperature, pump and feed concentration and two are negative i.e airflow and aspirator (Equation 4.2). The effects which have the greatest influence on the spray drying process are airflow through the apparatus and the aspirator value with F-values 1702.42 and 137.26, respectively as seen in Table 4.5. The higher atomisation flow needed for the production of smaller particles is associated with more energy supplied for breaking down the liquid droplets (Masters, 1985). Whereas this trend is commonly known and observed (Chawla *et al.*, 1994; Ståhl *et al.*, 2002), the importance of the aspirator is not that obvious and may also be connected with a higher degree of aerosolisation of the solution caused by the suction forces produced by the aspiration. Importance of the feed concentration is often reported e.g. works of

Chawla *et al.* (1994) and Prinn *et al.* (2002) related larger particle sizes to more concentrated solutions used. It can be assumed that if more extreme concentrations of the liquids had been used, this effect would have had larger importance.

All the main effects are involved in interactions and analysis of variance revealed 5 relationships, four at the 99% level: inlet temperature and pump (AC), inlet temperature and aspirator (AD), airflow and pump (BC), airflow and aspirator (BD) and one at the 95% level - airflow and feed concentration (BE). The strongest interaction appears to be between airflow and aspirator (BD) which is not surprising judging by the very high F-values (Table 4.5) of the parameters on their own. Figure 4.7 shows graphically this interrelation.

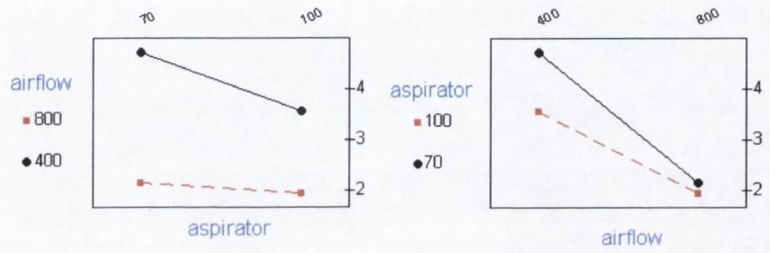

Figure 4.7 Airflow - aspirator interaction (BD). The black and red lines indicate the magnitude of response (median particle size) when the parameter given on the left-hand side of the graph is on its lower and higher levels, respectively.

Figure 4.7 shows that the smaller median particle size can be obtained if both airflow and aspirator are on higher levels and the F-value equal to 31.91 shows that this interaction plays the main role.

To minimise the median particle size taking into consideration all factors, we should use the inlet temperature, pump and feed concentration at low levels and the airflow and aspirator must be set at high levels.

4.3.3 Experimental design: response: "Carr's compressibility index"

Micronised drug particles may be very adhesive and cohesive, which is reflected in poor flow properties (Hickey *et al.*, 1994). In the design of the dry powder inhalations it is important to consider how to obtain a good outflow from capsules and devices. Therefore the evaluation of the flow and packing properties of the inhalable powders is necessary. A few studies have been reported on the assessment of the aforementioned mechanical characteristics and focusing on the carrier-based powder mixtures (Iida *et al.*, 2001; Kawashima *et al.*, 1998b).

The principles of evaluation of flowability as well as their mathematical correlations were first explained by Carr (1965). The estimation of flowability involves the use of properties that can be measured by the following methods: angle of repose, compressibility, angle of spatula and cohesion (Carr, 1965). Detailed accounts regarding these methods can be found in literature and automated powder flowability analysers are available on the market. Thus, out of the four above

methods only compressibility was deemed to be feasible to carry out. The results were called the Carr's compressibility indices in contrast to Carr's indices involving a use of all of the methods of flowability estimation. Lower values of the index are desirable as they indicate better flow (Carr, 1965). Table 4.3 lists the Carr's compressibility indices calculated from the bulk and tap densities according to Equation 4.3.

Carr's compressibility index = [(tap density – bulk density)/tap density] x 100 (Equation 4.3)

The lowest value of 25% was measured for the sample 5ABI and the greatest equal to 60% for 10AB, but generally the values oscillated around 40% (Table 4.3).

Figure 4.8 presents the data for the response "Carr's compressibility index" as the cube plot to visualise the results achieved.

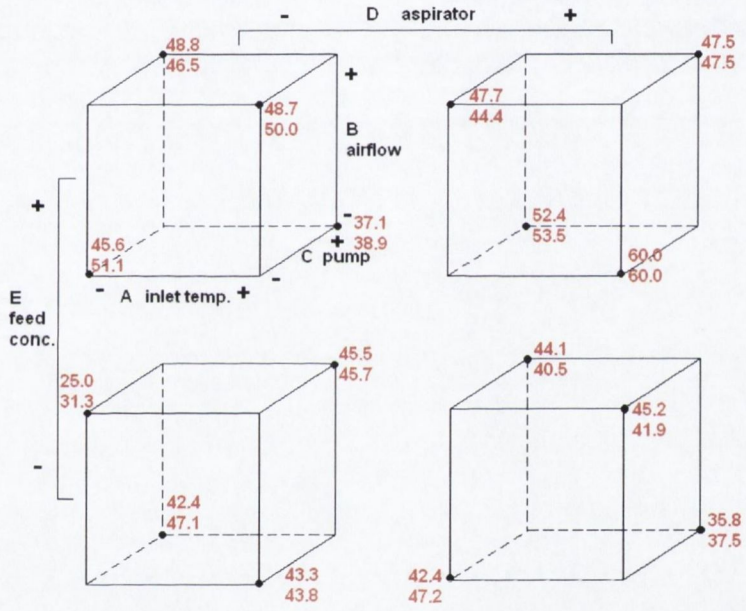

Figure 4.8 The cube plot for the response "Carr's index".

As the only assumption that could be drawn from Figure 4.8 was that lower feed concentrations gives lower Carr's compressibility values, an additional mathematical treatment of the data was needed.

The nature of the distribution of the response is shown in Figure 4.9.

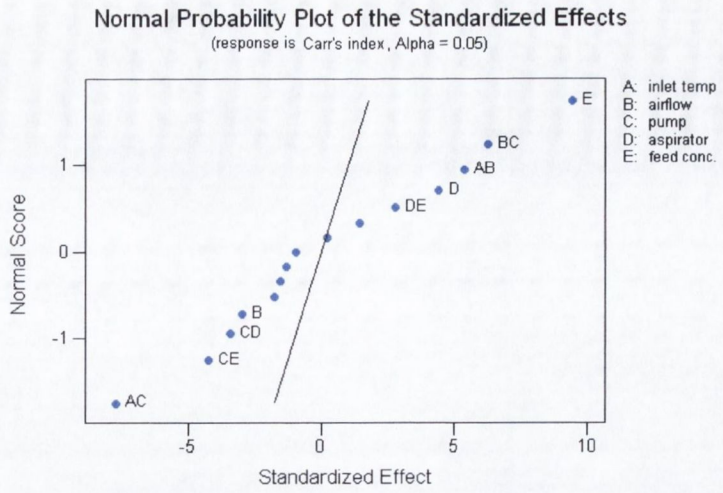

Figure 4.9 Normal probability plot of effects.

Looking at the normal probability plot of effects, all the outliers from a straight line will significantly affect the spray drying process. In this response: B, D, E, AB, AC, BC, CD, CE and DE might influence Carr's index of the resulting product.

For further considerations the analysis of variance, ANOVA, was carried out, however despite the model R^2 value equal to 0.9483 and close to 1, it seemed to be too far from R^2 adjusted (0.8999). Excluding from the model all terms (except main effects A and C involving in interactions) with p-values under 0.05 and refitting, the following ANOVA table (Table 4.6) was computed.

Table 4.6 Analysis of variance output for the response "Carr's compressibility index" after removing insignificant terms.

Source of variation	Sum of squares	DF	Mean square	F-value	p-value	
Model	1466.43	11	133.31	23.58	<0.0001	Significant **
A	10.70	1	10.70	1.89	0.1842	
B	44.89	1	44.89	7.94	0.0106	Significant *
C	8.72	1	8.72	1.54	0.2288	
D	101.18	1	101.18	17.89	0.0004	Significant **
E	458.29	1	458.29	81.05	<0.0001	Significant **
AB	149.21	1	149.21	26.39	<0.0001	Significant **
AC	300.74	1	300.74	53.19	<0.0001	Significant **
BC	203.52	1	203.52	35.99	<0.0001	Significant **
CD	58.59	1	58.59	10.36	0.0043	Significant **
CE	90.79	1	90.79	16.06	0.0007	Significant **
DE	39.83	1	39.83	7.04	0.0152	Significant *
Error	113.09	20	5.65			
Total	1579.52	31				

*-significant at the 95% level
**-significant at the 99% level

The Model F-value of 23.58 evidenced that the model was significant, additionally confirmed by the p-value lower than 0.0001. The terms: D, E and AB, AC, BC, CD, CE were significant at the 99% level and B and DE were important model terms at the 95% level. By eliminating the

insignificant elements from the model, the difference between the total and adjusted R^2 values decreased to about 0.04. The residuals were normally distributed and after analysis of plots of the residuals versus the run order and factor it was concluded that no pattern appeared for the residuals, which validated the model (graphs not shown).

The dependence of the Carr's compressibility index on the spray dryer settings using the coded values can be described by the following equation (Equation 4.4):

Carr's compressibility index (%) = 44.95+0.58A-1.18B-0.52C+1.78D+3.78E+ 2.16AB-3.07AC+2.52BC-1.35CD-1.68CE+1.12DE (Equation 4.4)

The factor having the greatest impact on this response will be feed concentration of the spraying solution with the F-value of 81.05 according to Table 4.6. It is also connected to two interactions: pump-feed concentration (CE) and aspirator-feed concentration (DE). This term is positive as indicated by the sign "+" in Equation 4.4 and it means that the greater the concentration of spray drying solution, the greater the Carr's compressibility index. Goula and Adamopoulos (2004) investigating the spray drying of tomato pulp observed that an increase in the feed concentration caused a decrease in bulk density of the resulting powder. Perhaps the same effect may be responsible for the changes in the Carr's compressibility index of the powders as the values are dependant on the bulk density.

This response has as many as five interactions with statistical significance at the 99% level. The most significant seem to be three relationships: inlet temperature and airflow (AB), inlet temperature and pump (AC) and airflow and pump (BC) with the greatest F-values (Table 4.6) and coefficients (Equation 4.4).

Figure 4.10-Figure 4.12 show the above relationships graphically:

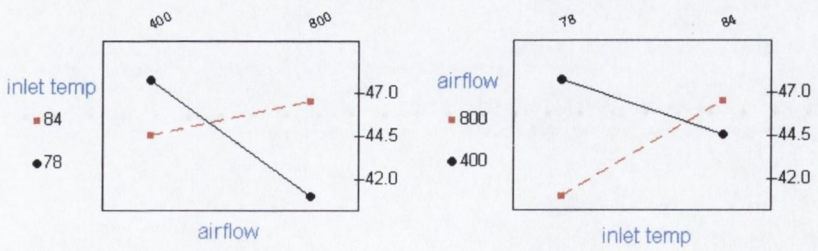

Figure 4.10 Inlet temperature-airflow interaction (AB). The black and red lines indicate the magnitude of response (Carr's compressibility index) when the parameter given on the left-hand side of the graph is on its lower and higher levels, respectively.

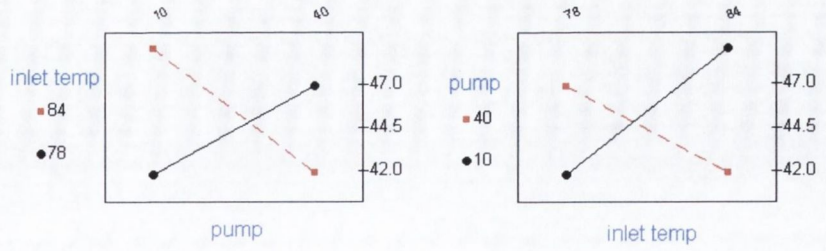

Figure 4.11 Inlet temperature-pump interaction (AC). The black and red lines indicate the magnitude of response (Carr's compressibility index) when the parameter given on the left-hand side of the graph is on its lower and higher levels, respectively.

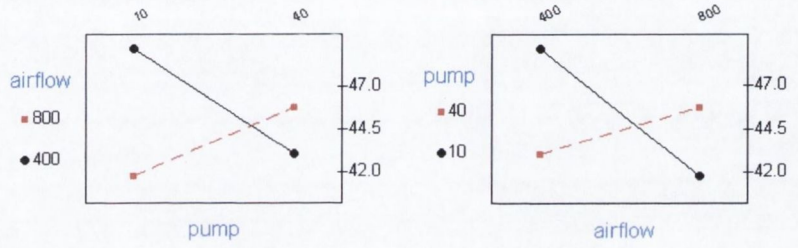

Figure 4.12 Airflow-pump interaction (BC). The black and red lines indicate the magnitude of response (Carr's compressibility index) when the parameter given on the left-hand side of the graph is on its lower and higher levels, respectively.

From the above plots we can conclude that between these 3 factors exists some kind of 3-way relationship. In this response the aim is to minimise Carr's index in order to achieve better flowability. Thus, maintaining the inlet temperature and airflow at lower and higher values, respectively, the response can be reduced. If we then include the pump setting and keep it at a low level we are able to minimise the Carr's compressibility index. Taking into consideration the influence coming from feed concentration and aspirator, we can say that the following settings: inlet temperature, pump, aspirator and feed concentration at lower levels and maximised airflow make it possible to minimise the Carr's index.

4.3.4 Experimental design: response "*in vitro* respirable fraction"

It was not possible to carry out separate analysis of each replicate sample due to an insufficient amount of material being available. Therefore sample blends were prepared by mixing for 15 min in a Turbula mixer equal weights of the 2 replicates and these blends were used for loading the capsules used in the twin stage impinger analysis. All analysis was carried out 5 times for each blended sample. Results were compared to the results for the physical mix of budesonide and formoterol fumarate dihydrate mixed in the ratio 100:6. The Rotahaler® device was chosen due to its simple construction allowing comparison of the dispersibility of loaded powders. The quantities of both, budesonide and formoterol fumarate were determined (the HPLC method used is described

in Chapter 2) and the fraction of the total dose of the drugs retained in each part of the twin impinger and the device was expressed as a percent.

Results of the twin impinger analysis of the above samples are graphically shown in Figure 4.13

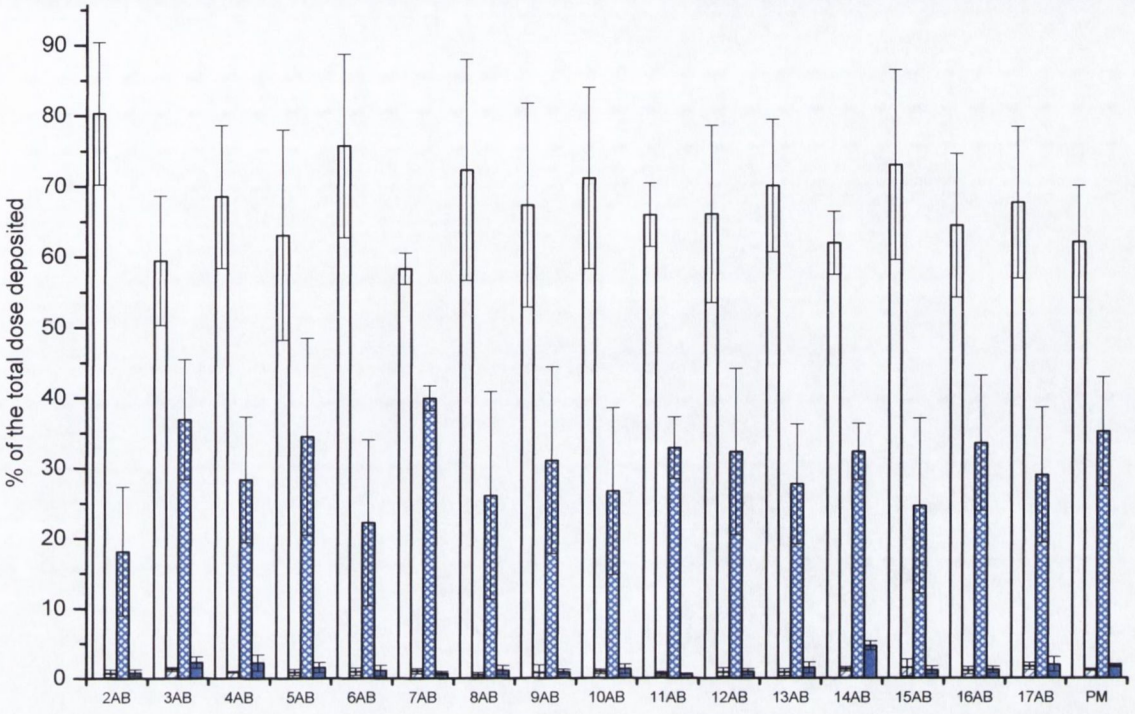

Figure 4.13 Twin impinger analysis of the samples employed in the 2^{5-1} factorial design compared to the corresponding physical mixture (PM). The white, blue diagonal, blue grid and full blue filled bars indicate the percentage retained in the capsule and device, mouthpiece, stage 1 and stage 2 on the twin stage impinger, respectively.

Figure 4.13 clearly indicates that the great majority of the spray dried samples was retained in the device and deposited in the upper stage of the impinger. The physical blend is not different in this respect. This is the second indication of poor flowability as implied earlier by the high Carr's compressibility indices. Taking into consideration the mean dose released from the device only, the lowest value of 19.67% was obtained for 2AB and the highest value of 41.7% was obtained with sample 7AB.

The ratio between budesonide and formoterol fumarate in the lower stage for all spray dried samples as measured by HPLC analysis was 100 to 6. Due to the fact that the content of budesonide was taken as a constant and related to 100 in the total 106 parts in the mixture, the deviation of content was calculated only for formoterol fumarate and was for all samples taken together ± 3%. For the physical mix the mean ratio of budesonide:formoterol fumarate for this fraction was 100 to 7.5 with ± 30% deviation of content for formoterol fumarate. This is a remarkable finding, as with the development of novel DPIs based on binary mixtures of micronised actives, the discrepancy between the dose stated and that delivered can be significant, affecting the efficiency of therapy. A considerable number of publication have been devoted to the clinical

comparisons of such mixtures (Zetterström *et al.*, 2001; Palmqvist *et al.*, 2001) but none to our knowledge assess the actual quantities of drugs reaching the lungs.

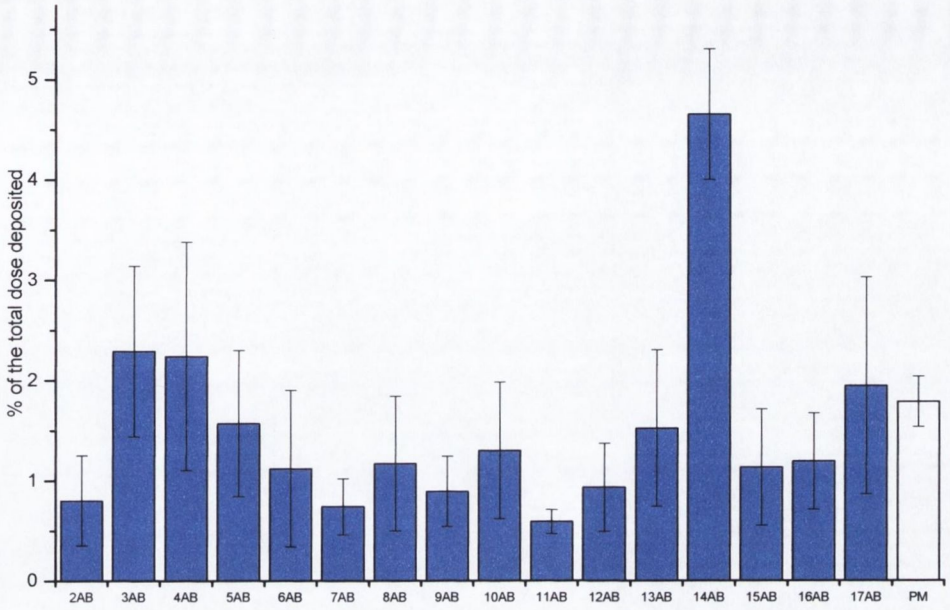

Figure 4.14 The respirable fractions (i.e. deposited on stage 2 of twin impinger) of budesonide/formoterol fumarate dihydrate (100/6) samples spray dried in different conditions. The physical mixture is also included.

The respirable fraction (the lower stage) varied from about 0.6 to 4.6 % only and sample 14AB showed the greatest deposition in the lower stage (Figure 4.14). For the physical mixture there was 1.78±0.25% deposition in the lower stage of the impinger. The material which reaches stage 2 is considered to be respirable, as the theoretical cut-off is 6.4 μm with 60 l/min air stream (Hallworth and Westmoreland, 1987) and SEM as well as laser diffraction particle size analysis showed that the diameter of at least 60% particles is less than the cut-off diameter. Because the respirable fractions are much lower than 60% it is obvious that the influence of cohesive and adhesive forces is very strong. The possibility of a charge build-up arising was signalised earlier.

The sample with the greatest respirable fraction (14AB) was spray dried at the higher inlet temperature (84°C) from 1% (w/v) solution and all other parameters of the spray drier were maintained at their lower settings (airflow 400 Nl/h, pump 10%, aspirator 70%). This resulted in relatively large particles (median 4.6 μm according to the laser diffraction measurements) with a low content of solvents in the material (about 1% mass loss in the range 25-100°C by TGA).

Owing to the complexity of factors influencing the deposition of material in the lower stage of the impinger, a statistical analysis was employed in order to elucidate which parameters of the spray drying process may have an important effect on the magnitude of respirable fractions. The details of the statistical design were the same as described earlier in the text with the exception that 16 observations with 5 replicates without random order of the runs were used. The data for the analysis are presented in Table 4.3.

Briefly, Table 4.7 summarises the final ANOVA.

Table 4.7 Analysis of variance ANOVA for the response "respirable fraction"

Source of variation	Sum of squares	DF	Mean Square	F value	p-value	
Model	65.12	9	7.24	14.84	<0.0001	Significant **
A	2.48	1	2.48	5.09	0.0272	Significant *
B	15.04	1	15.04	30.84	<0.0001	Significant **
C	7.82	1	7.82	16.03	0.0002	Significant **
D	1.46	1	1.46	3.00	0.0879	
E	17.10	1	17.10	35.07	<0.0001	Significant **
AB	3.59	1	3.59	7.36	0.0084	Significant **
AE	1.96	1	1.96	4.02	0.0487	Significant *
BE	11.35	1	11.35	23.27	<0.0001	Significant **
DE	4.31	1	4.31	8.84	0.0040	Significant **
Error	34.14	70	0.49			
Total	99.26	79				

*-significant at the 95% level
**-significant at the 99% level

The equation fitted to the model using the coded values of variables is as follows:

Respirable fraction(%) = 1.50+0.18A-0.43B-0.31C-0.14D-0.46E-0.21AB-0.16AE+ 0.38BE+0.23DE (Equation 4.5)

The following terms: B, C, E, AB, BE and DE were significant at the 99% level and A, AE were significant model terms at the 95% level. The same diagnostics of the normality of the residuals and their independence from the run order and the processing factors as for the response "yield" were carried out, but no unusual patterns were noticed. The normal probability plot of residuals showed an approximate normal distribution (the graph is not shown).

From Equation 4.5 one can say that only the inlet temperature effect is positive and all others negative. Furthermore, they fully correspond with the settings of the spray drier used for processing of sample 14AB, which, as mentioned earlier, is the sample with the greatest respirable fraction.

The factors having the largest coefficients in Equation 4.5, thereby most affecting the respirable fractions are the feed concentration and airflow. Moreover, they are involved in an interaction emphasising their significance. The negative coefficients indicate that a low drying gas flow and concentration has to be used to obtain high respirable doses.

The significance of the feed concentration was shown for the response "Carr's compressibility index" and the same is observed here, for the respirable fraction. The trend is identical, i.e. in both cases lower solution concentrations are needed to optimise the response. It would suggest that indeed, the bulk density of an inhalable powder can be a measure of its flowability (French *et al.*, 1996; Steckel and Brandes, 2004). But the manner in which the respirable fraction is affected by the airflow is puzzling and one would expect that lower particle sizes are desirable. It implies that cohesive attraction also has a great impact on the respirable fractions achieved and it is known that

a powder inhaler containing a significant proportion of particles below 5 μm has poor dispersibility (Hickey *et al.*, 1994). The cohesion between the particles by contact surfaces is proportional to the specific surface area, hence the particle size (Chew *et al.*, 2000). Particle radius also appears in the expressions on the Van der Waals and electrostatic cohesion forces (Hickey *et al.*, 1994). Thus, by increasing the size of particles, the cohesiveness can be reduced and better dispersibility attained. Several authors report on low respirable *in vitro* doses obtained linked to the strong interparticulate forces (Bosquillon *et al.*, 2001b; Voss and Finlay, 2002).

4.3.5 Statistical analysis of the true density values

For this response the statistical factorial analysis was not feasible due to a large variability between different runs of the same sample e.g. 3ABI versus 3ABII and the low magnitude of the response, making accurate statistical interpretation of the data impossible (Table 4.3). Generally, for the majority of samples there is no statistically important difference in true density (e.g. 12ABI – 15ABII), but in some cases a statistically significant difference does exist e.g. between 5ABI and 5ABII. The large variability of the response is associated with a 0.1 cm^3 cup used for the pycnometric studies, as very the low quantities of the available powders did not permit the use of a larger size cup. Furthermore, the studies of Viana *et al.* (2002) presented that the variation in pycnometric density due to operating parameters can affect the accuracy of the result to the nearest 0.01 g/cm^3.

Figure 4.15 shows the average true density for the combined sample (i.e. duplicate runs and taking the overall average density) in comparison with the true density of the corresponding physical mix of budesonide and formoterol fumarate dihydrate in the ratio 6:100. The 2-sample t-test analysis for the difference between two population means for each pair: a sample and the physical mix was carried out. On the basis of the input from t-test analysis we can conclude that there is no statistical difference between the true densities of samples: 2AB, 3AB, 4AB, 5AB and the true density of the physical mix. All other spray dried samples have a true density which is statistically significantly different from that of the physical mix.

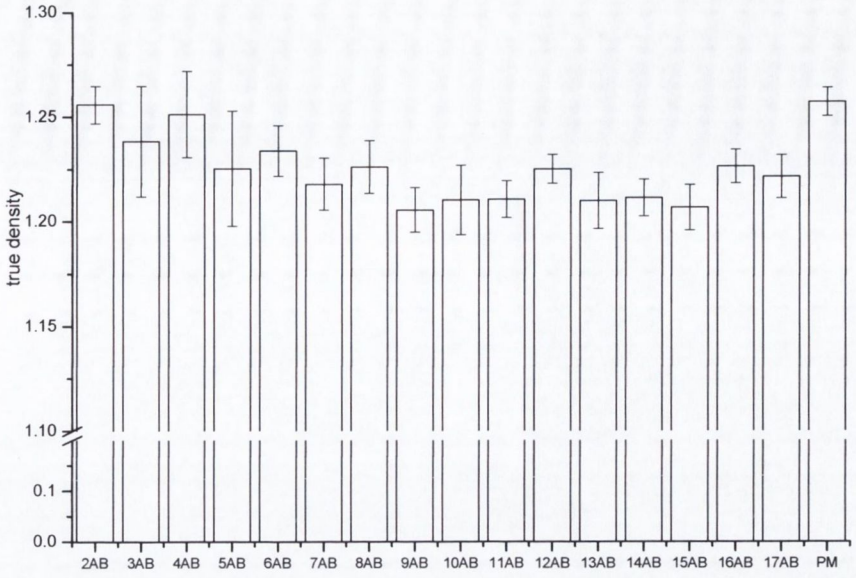

Figure 4.15 The bar plot of true density for the spray dried sample and the physical mix. The axis break is aimed at emphasising the difference between the samples. The sample size for each group was 4.

An independent t-test on the average densities for the spray dried samples versus physical mix was also performed and showed that at the 0.05 level, the two means were significantly different and the true density of the processed samples was lower than that of the physical blend. It is known that the density of an amorphous form of the substance compared to that of its crystalline phase is lower and furthermore, true density may be used for a determination of the crystallinity content (Saleki-Gerhardt *et al.*, 1994).

4.4 Physicochemical characterisation

4.4.1 Formoterol fumarate

Formoterol fumarate dihydrate "as supplied" crystalline material was very well characterised by Corrigan (2002), but no data has so far been published about spray drying of this drug alone. Spray drying was employed in the production of hollow porous particles called PulmoSpheres™, but the content of formoterol fumarate in the final powder was only 1.8% (w/w) (Dellamary *et al.*, 2000). Other constituents used in this work were lactose monohydrate and calcium chloride as well as perfluorooctyl ethane as the blowing agent. No physicochemical characterisation except SEM, TEM and density was carried out. The spray drying conditions of formoterol fumarate dihydrate are presented in Appendix I. Spray drying resulted in an amorphous form of the drug as shown by a diffused "halo" in the XRD pattern (Figure 4.16). The starting powdered material of formoterol fumarate was crystalline with a well-defined peak pattern corresponding to that recorded by Apperley *et al.* (2003).

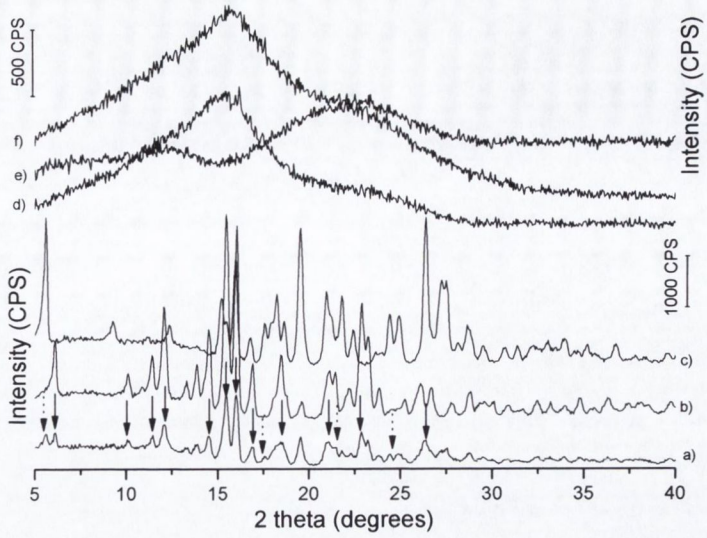

Figure 4.16 XRD diffraction patterns of (a) physical mixture of budesonide-formoterol fumarate dihydrate 100:6, (b) crystalline budesonide, (c) crystalline formoterol fumarate dihydrate, (d) spray dried budesonide, (e) spray dried formoterol fumarate dihydrate and (f) 14ABI. The dotted arrows indicate the peaks of formoterol fumarate dihydrate and the black arrows indicate the peaks of budesonide. The scale on the left hand side applies to curves d-f and the scale on the right hand side applies to curves a-c.

Three endothermic peaks on the DSC scan of the pure formoterol fumarate dihydrate raw material sample were recorded (Figure 4.17). The first, which was also the largest, appeared at ~122°C and this was followed by the second endotherm at ~140°C. The last endotherm was the smallest and peaked at ~155°C. Above this temperature, a thermal decomposition of the material was seen in the form of a jagged baseline. TGA (Figure 4.18) helped in differentiation of the peaks, and a 5.4% mass loss in one step occurred in the 25-120°C range, out of which 4.3% is associated with the release of two water molecules (as 4.3% corresponds to the two water molecules in the molecule of formoterol fumarate dihydrate) and 1.1% account for some surface moisture. Therefore the peak at ~140°C was ascribed to dehydration (Corrigan, 2002). The other endotherms correspond to melting of the two racemates of formoterol fumarate and the endotherm at ~140°C is consistent with melting of the enantiomer A (the literature value 138-140°C) and the endotherm at ~155°C corresponds to melting of the enantiomer B (the literature value 154-155°C) (Murakami *et al.*, 1973).

A recrystallisation exotherm was evident in the DSC of the amorphous sample (Figure 4.17), with a peak at ~106°C and this was followed by a melting endotherm with a peak at ~160°C (both of the peaks were visible at a higher magnification). The temperature of the melting endotherm does not correspond to any of those of the crystalline enantiomers. Crystalline formoterol fumarate dihydrate is claimed to exist as a racemic mixture (Gao *et al.*, 2001). The exotherm was preceded by and overlapped with a broad endotherm which could be due to residual solvent liberation. Thermogravimetry demonstrated ~3% weight loss for the spray dried material occurring from 25 to 100°C (Figure 4.18).

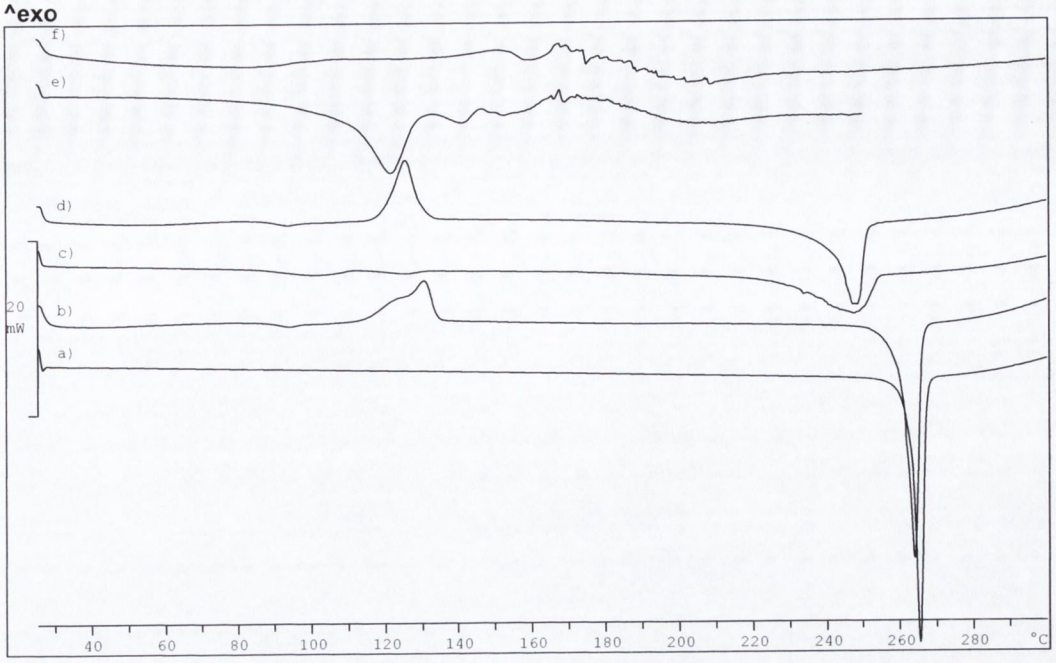

Figure 4.17 DSC analysis of the (a) crystalline budesonide, (b) spray dried budesonide, (c) physical mixture of budesonide/formoterol fumarate dihydrate 100:6, (d) 14ABI (spray dried composite budesonide/formoterol fumarate dihydrate 100:6) , (e) crystalline formoterol fumarate dihydrate and (f) spray dried formoterol fumarate dihydrate.

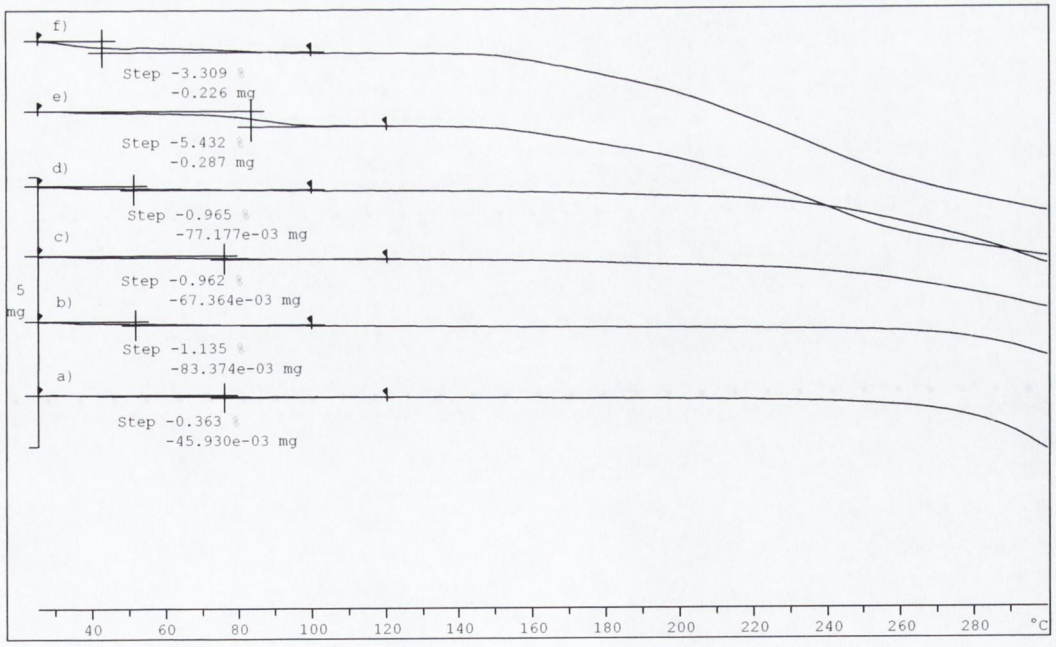

Figure 4.18 TGA analysis of the (a) crystalline budesonide, (b) spray dried budesonide, (c) physical mixture of budesonide-formoterol fumarate dihydrate 100:6, (d) 14ABI (spray dried composite budesonide/formoterol fumarate dihydrate 100:6), (e) crystalline formoterol fumarate dihydrate and (f) spray dried formoterol fumarate dihydrate.

FTIR scans for spray dried and crystalline drug were similar and the peaks were more distinct and sharper for the latter sample (Figure 4.19). Processing led to a disappearance or shift of the band at 3484 cm^{-1}. According to the literature data (Socrates, 2001), the OH stretch vibration of water with hydrogen bonding to other molecules appears at 3500 cm^{-1}. It is thus reasonable that the peak at 3484 cm^{-1} is assigned to the stretch vibration of the crystalline water molecules in the hydrate. A similar phenomenon was reported by Akao *et al.* (2001) for crystalline trehalose dihydrate. The disappearance of this peak indicates the lack of crystalline water in the spray dried sample. A second change in the FTIR spectra of the drug was a shift of the C=O stretching band, called also the Amide I group (Socrates, 2001), of the formamide group from 1690 cm^{-1} for the crystal to 1675 cm^{-1} for the amorphous counterpart. This may be a sign of the formation of hydrogen bonds between the drug molecules as the carbonyl stretching band tends to change its position when involved in hydrogen bonding (Socrates, 2001).

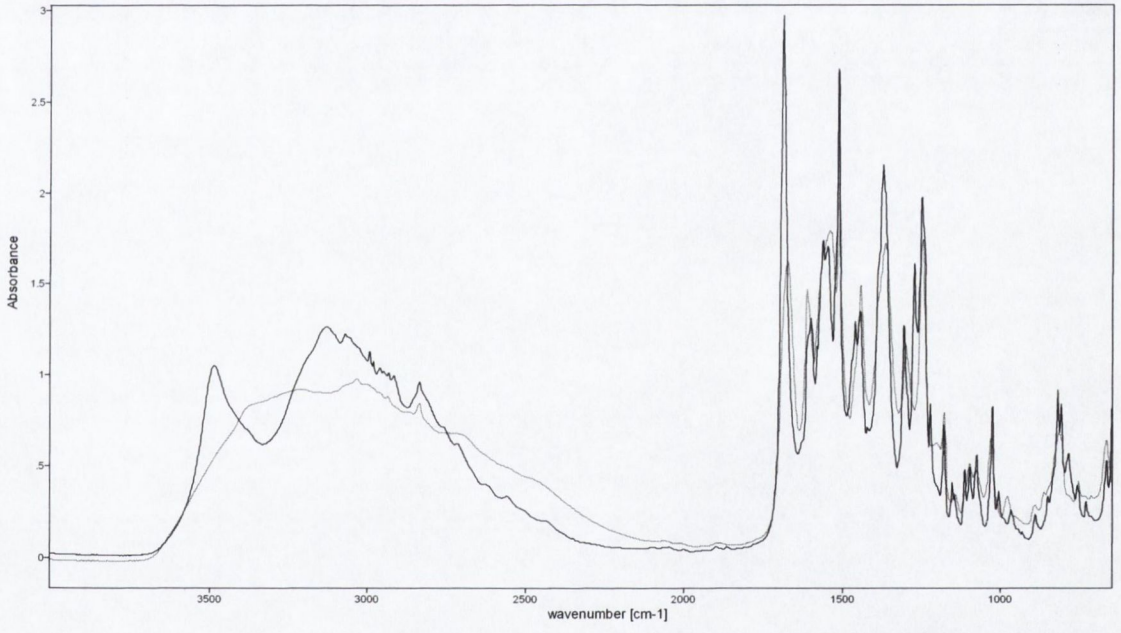

Figure 4.19 FTIR spectra of the crystalline formoterol fumarate dihydrate (solid line) and spray dried formoterol fumarate dihydrate (dotted line).

Small spheres, typical of amorphous material were observed by SEM in contrast to irregular and rough particles of the unprocessed sample (Figure 4.20).

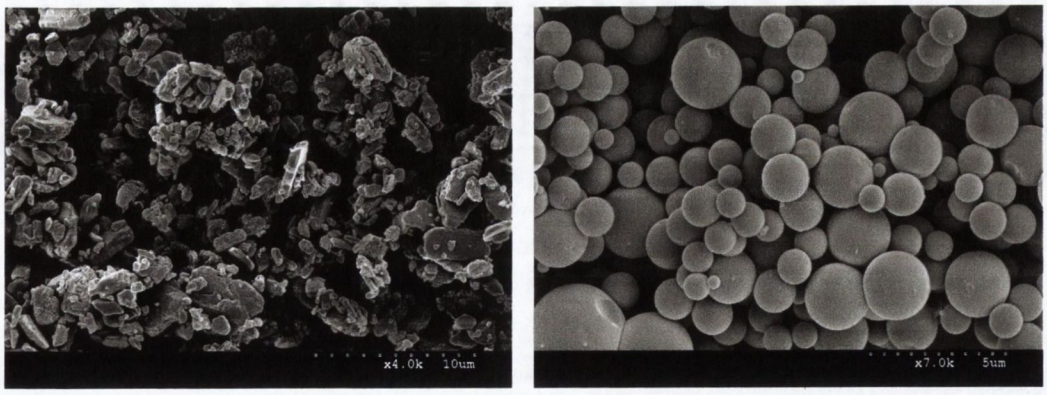

Figure 4.20 SEM micrographs of the crystalline formoterol fumarate dihydrate (left) and spray dried formoterol fumarate dihydrate (right).

The median particle size was 1.98 μm and 1.88 μm for the raw particulate material and spray dried sample, respectively as measured by a Sympatec and Malvern Mastersizer 2000 laser diffraction particle size analyser, respectively.

4.4.2 Budesonide

Budesonide was supplied as a micronised material with a median particle size of 1.4 μm as determined by the laser diffraction particle size analysis. The particle size distribution was monomodal and all particles were below 6 μm (as determined by Malvern Mastersizer 2000). The XRD pattern (Figure 4.16) of the drug was typical of a crystalline material and the peak positions and their relative intensities were consistent with the XRD spectra presented by Pham and Wiedmann (2001). DSC analysis presented in Figure 4.17 confirmed the crystalline nature of the starting material powder as only one endotherm peaking at 263.5°C was observed. The onset was at 261.7°C, which is in good agreement with the observation of Velaga *et al.* (2002) who stated that the melting point of crystalline budesonide is 258.7°C.

Other workers have demonstrated that budesonide may be processed by supercritical carbon dioxide (Steckel *et al.*, 1997) but neither changes in the crystalline structure nor morphology of the particles before and after the process were observed. Spray drying of the drug has also been reported, but in this case lipid-coated microcrystals from emulsion based stock were produced (Tarara *et al.*, 2004).

An amorphous form of budesonide was produced on spray drying from a 95% (v/v) ethanolic solution by Corrigan (2002). The same type of spray dryer was used in the present work but the conditions under which the drug was processed differed. The differences between the processing parameters were that the pump rate used by Corrigan (2002) was 30% and the aspirator speed was 100%. Even when other manufacturing parameters were used (listed in Appendix I), the powder was amorphous as evidenced by DSC (Figure 4.17) and XRD (Figure 4.16). A recrystallisation exotherm was evidenced in the DSC, with a peak at ~130°C and this was followed by a melting

endotherm with a peak at ~262°C. The exotherm was preceded by a glass transition with the midpoint at ~89.5°C. There was a small endotherm between 25°C and 80°C due to desolvation of residual water and/or ethanol. TGA showed approximately a 1% weight loss between 25 and 100°C probably due to solvent desorption, which compared with the TGA results of the crystalline sample is nearly a four-fold increase (Figure 4.18). XRD showed a pattern typical of amorphous material with no distinct peaks (Figure 4.16). Small, spherical particles with generally smooth surfaces were observed by SEM (Figure 4.22) and the laser diffraction particle size analysis revealed that the median particle size was 4.5 μm and all particles were below 9 μm. The particle size distribution was, again, monomodal, but much narrower when compared with the unprocessed sample. The FTIR spectrum of budesonide showed carbonyl stretching bands at 1723 cm^{-1} and 1667 cm^{-1} (Figure 4.21). The first carbonyl stretch peak was assigned as belonging to the nonconjugated acetyl C=O vibrations and the second peak to the conjugated dihydrobenzenoquinone C=O (Tarara *et al.*, 2004). Spray drying resulted in a material demonstrating a similar spectrum, but the peaks were more diffuse. Moreover, a shift in the conjugated C=O stretching band from 1667 cm^{-1} to ~1658 cm^{-1} was observed, suggesting a possible change in the environment of the conjugated C=O group of budesonide (Tarara *et al.*, 2004). Also the OH bands appearing as a broad peak located in the 3300-3700 cm^{-1} region changed shape with broadening of the peak and a shift in the peak maximum from 3491 cm^{-1} to 3448 cm^{-1}.

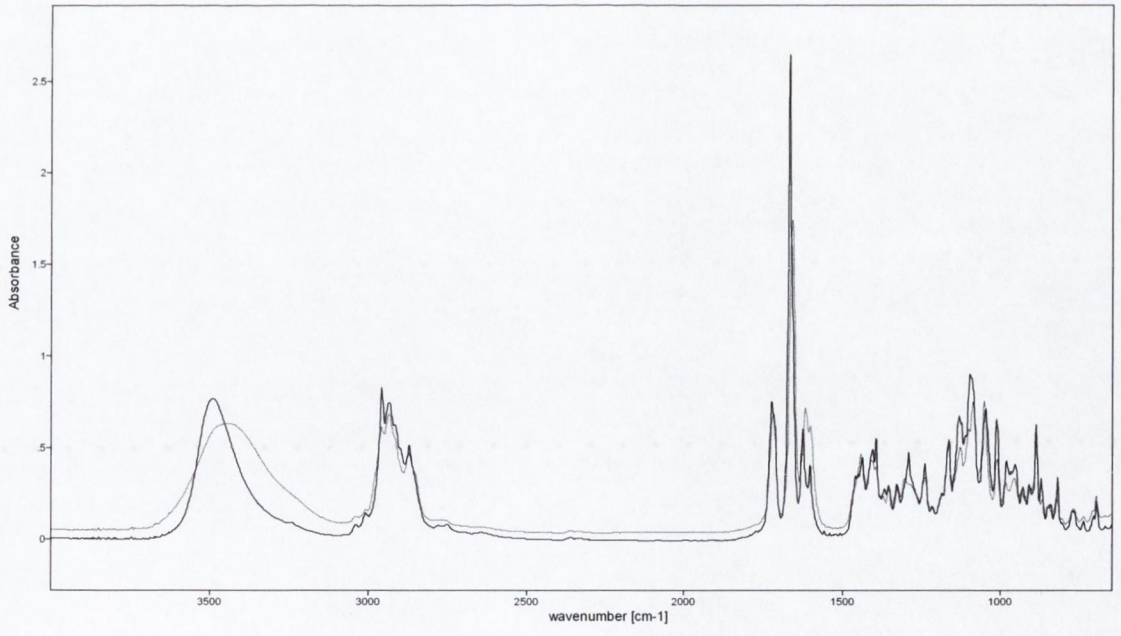

Figure 4.21 FTIR spectra of the crystalline budesonide (solid line) and spray dried budesonide (dotted line).

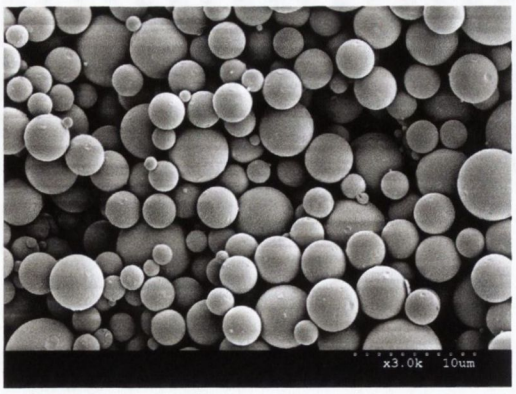

Figure 4.22 SEM micrographs of the spray dried budesonide.

4.4.3 Budesonide/formoterol fumarate dihydrate 100:6

The physical blend of budesonide and formoterol fumarate dihydrate 100:6 was crystalline by XRD, as expected. The peaks of both substances, as seen in Figure 4.16, were visible despite the low level of formoterol present in the mixture. DSC measurements revealed the existence of three endothermic peaks at ~102°C, ~140°C (visible at a higher magnification) and ~245°C, ascribed to dehydration and melting of formoterol fumarate dihydrate and melting of budesonide, respectively. The endotherms of formoterol were shifted towards lower temperatures, which may suggest some degree of interaction/miscibility between the two components. The melting peak of budesonide was broadened and asymmetric, most likely due to the presence of the thermal decomposition products of formoterol fumarate dihydrate.

A recrystallisation exotherm was evident in the DSC of all spray dried samples with a peak between 122 and 131°C, this was followed by a melting endotherm which had a peak between 245°C and 249°C. There appears to be a glass transition with a midpoint between 90.2°C and 93.1°C for all samples. The variations in the T_g were probably caused by a different residual solvent content that fluctuated between 1% and 2% in the 25-100°C region as determined by TGA (Figure 4.18). Water frequently acts as a potent plasticiser and this plasticization effect is ascribed to its very low T_g equal to 135K (Hancock and Zografi, 1994). Ethanol has even lower T_g (90K or 95K as stated by Angell (1997)) and it may be expected that it will depress the glass transition temperature more significantly than water. The physical mixture in the 25-120°C region exhibited a ~1% weight loss (Figure 4.18). All the spray dried powders showed XRD patterns typical of an amorphous material with no distinct peaks. Figure 4.16 illustrates a representative spectrum of 14ABI where only a broad "halo" can be seen. FTIR scans of the physical mixture and spray dried samples resemble those of budesonide and two arrows in Figure 4.23 point to peaks of formoterol fumarate dihydrate. Neither differences in the peaks positions in the FTIR spectra nor additional bands were detected in the processed blends, indicating no differences in chemical structure, but when compared to the mechanical mix, broadening of the bands in the 3200-3600 cm^{-1} region was seen.

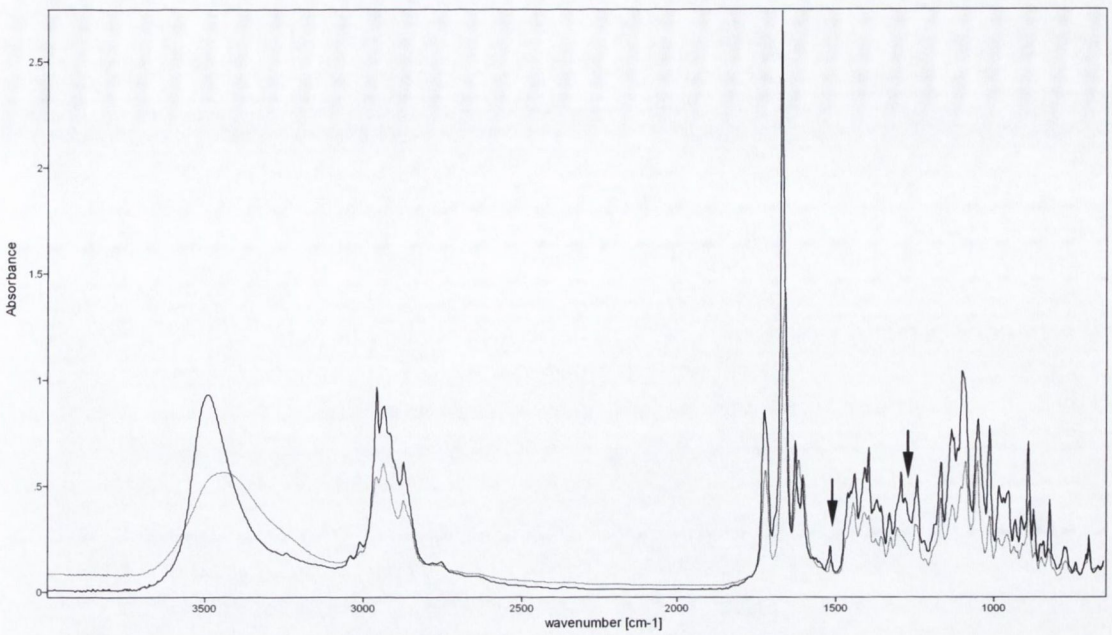

Figure 4.23 FTIR spectra of the physical mixture of budesonide and formoterol fumarate dihydrate 100:6 (solid line) and 14ABI (dotted line). The arrows indicate the bands of formoterol fumarate dihydrate.

Small spherical particles, typical of amorphous material, were observed by SEM (Figure 4.24). Particle surfaces were generally smooth with sizes determined by laser diffraction particle size analysis and given in Table 4.3. The largest particles were obtained for sample 6AB (spray dried with inlet temperature, pump and feed concentration on the highest levels) and the smallest for 3AB and 15AB (aspirator on the highest level and inlet temp., airflow rate and aspirator on the highest levels, respectively). An interesting observation for some systems was the presence of apparently hollow particles (Figure 4.24). This was observed for systems 6AB, 8AB, 10AB, 13AB and 14AB.

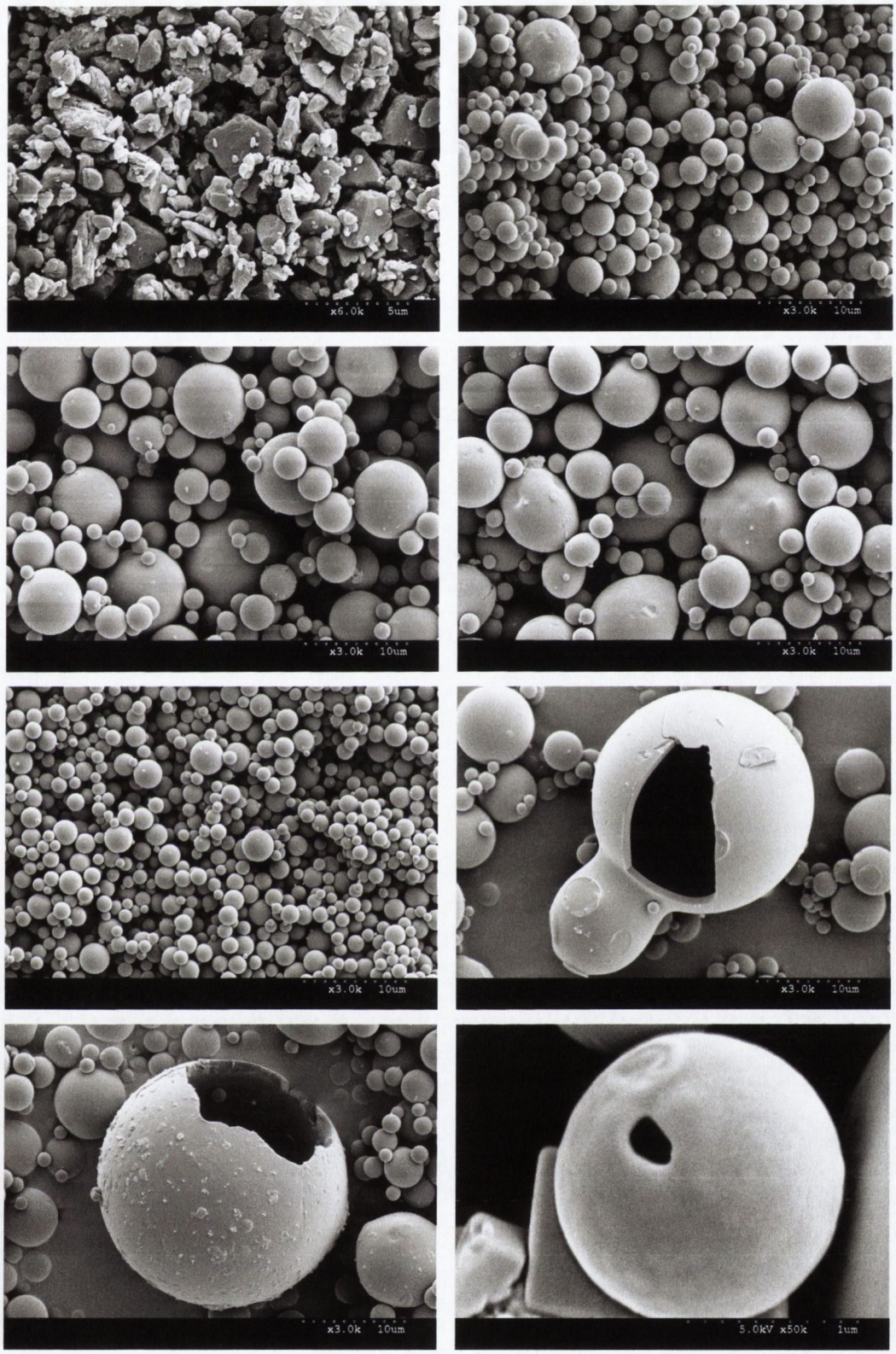

Figure 4.24 SEM micrographs of the physical mixture of budesonide-formoterol fumarate dihydrate 100:6 (first row, left), 3ABII (first row, right), 8ABI (second row, left), 14ABI (second row, right), 15ABII (third row, left), 6ABI (third row, right), 8ABII (fourth row, left), 14ABI (fourth row, left).

Not only the largest spheres were hollow, but as shown in the last SEM micrograph in Figure 4.24, also particles as small as 1μm had blowholes implying hollowness. To check if all small particles

had nonsolid structures, transmission electron microscopy (TEM) was used, but did not verify this (Figure 4.25). Substantial difficulties were encountered during the performance of TEM measurements as the particles tended to soften and melt at the temperature created by the energy of electron beams used. This could lead to collapse of the spheres and production of liquid droplets indistinguishable from the solid particles in the conditions of the experiment. As an alternative to TEM, confocal microscopy may be utilised in future work as it has been shown to allow the detection of voids in inhalable, spray dried particles (Chew and Chan, 2001).

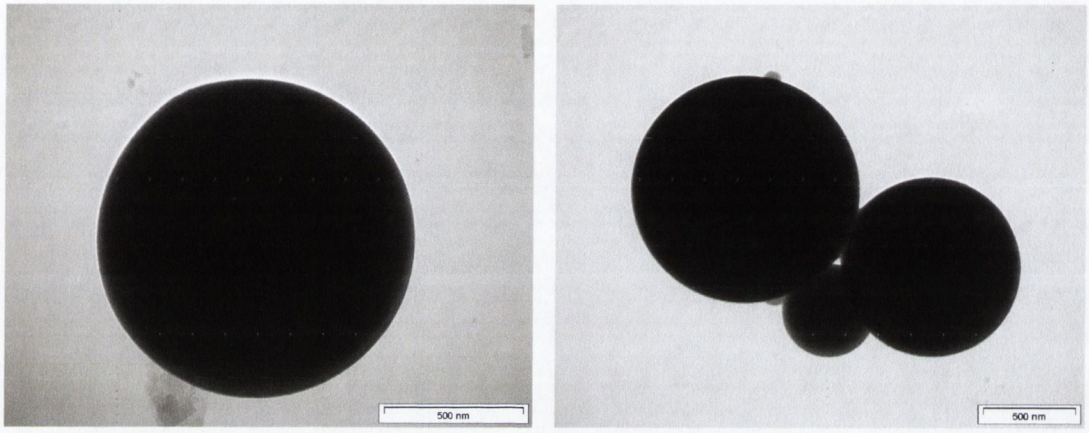

Figure 4.25 TEM micrographs of spray dried budesonide-formoterol fumarate dihydrate 100 :6.

SEM and TEM micrographs suggested that the processed powders may be mixtures of solid and non-solid spheres. A hollow interior can arise from expansion of gas in the droplets with a vapour-impervious film or from air entrained in the liquid feed (Elversson *et al.*, 2003). In particles where the drying film is impermeable to vapour, an overpressure is created and blowholes or exploded particles may occur (Crosby and Marshall, 1958). Therefore, it is likely that some hollow spheres may be created on spray drying as budesonide is a hydrophobic material. Furthermore, the shell thickness increases with concentration of the feed solution (Elversson *et al.*, 2003) and it is reasonable to assume that larger particles would have thinner shells. This may translate into the better *in vitro* respirable fraction of 14AB (having large mean particle size and spray dried from low concentration solution) as hollow particles are known to have advantageous lung deposition (French *et al.*, 1996) due to the small aerodynamic diameters.

4.5 Conclusions

The effect of five variables (air inlet temperature, airflow, pump feed rate, aspirator capacity and feed concentration) on the flowability and physicochemical properties of co-spray dried budesonide-formoterol fumarate dihydrate 100:6 were evaluated by a 2^{5-1} factorial experimental design. Amorphous particulate powders were formed in each case and the particles were in the inhalable range. The drugs when spray dried alone were obtained in amorphous phases. In the mixtures, both of the components were transformed into disordered states, as no peaks of this drug

were seen on the XRD patterns of all spray dried samples in contrast to the physical mixture. It was shown that alterations of the production conditions affected the yield obtained and also the physicochemical properties.

Overall, the parameter that had the greatest influence on each response investigated was:

- Yield – airflow (higher airflow gives greater yields)
- Median particle size – airflow (higher airflow gives smaller particle sizes)
- Carr's index – feed concentration (lower feed concentration gives smaller Carr's indices)
- *In vitro* respirable fraction - feed concentration (lower feed concentration gives greater respirable fractions)

Attempts have been made to correlate either the Carr's compressibility index, median particle size and the respirable fractions obtained from the twin impinger studies, but no obvious trends were discerned indicating that these measures do not interrelate in a simple way (Figure 4.26).

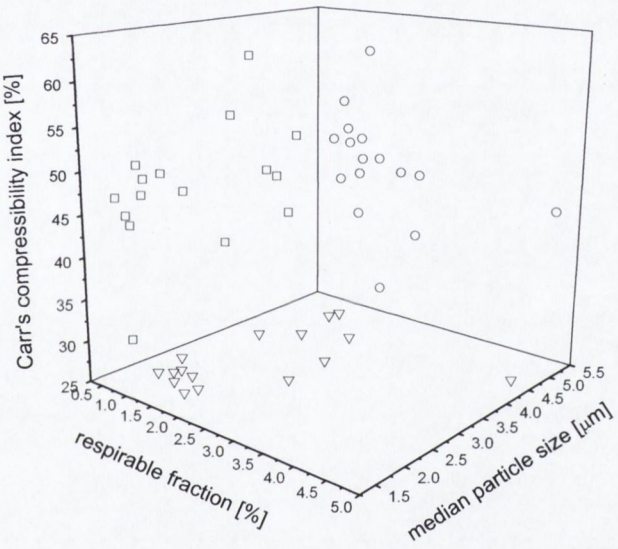

Figure 4.26 3-D correlation graph indicating a relationship between: the median particle size and respirable fractions (empty triangles), the median particle size and Carr's compressibility index (empty squares) and the respirable fraction and Carr's compressibility index (empty circles).

One of the processed specimens (14AB) gave a 2.6-fold increase in the powder deposition in the lower stage of the twin stage impinger, which is considered to be a trap for respirable material only. The sample was spray dried at the higher inlet temperature (84°C) from 1% (w/v) solution and all other parameters of the spray drier were maintained at their lower settings (airflow 400 Nl/h, pump 10%, aspirator 70%). It has been hypothesised, having observed hollow interiors of some of the particles, that the manufacturing conditions and material properties may facilitate formation of such non-solid spheres, causing better flowability and dispersibility of sample 14AB. Larger particles, in this case, are more desirable due to high cohesive forces and charge build-up on the surfaces of the smaller particles. Lower true density values of the powder compared with the equivalent physical blend may imply hollowness of the particles, but the density measurements are burdened with some

level of error. Summarising, statistical factorial designs can be of significant benefit in development of inhalable powders, as they allow us to optimise the product. In our case, taking into consideration both yield and the *in vitro* fine particle dose, the statistical prediction showed that high inlet temperature has to be used, whereas the rest of the parameters have to be set at lower levels.

The twin impinger studies presented that the ratio in which the mechanical binary mixture of actives was prepared did not result in the same ratio being attained in the second stage of the apparatus. Spray dried powders are a superior alternative in this regard as every particle contains the blend of drugs at a permanent ratio.

CO-SPRAY DRIED FORMOTEROL FUMARATE DIHYDRATE/EXCIPIENT COMPOSITES FOR USE IN DPIs

5.1 Introduction

For the treatment of asthma, formoterol is usually administered by the inhalation route by means of dry powder inhalers (DPIs). Currently marketed dry powder formoterol formulations e.g. Foradil® or Oxis® are storable under normal ambient conditions. Nevertheless, the stability of formoterol salts and water absorption are the major problems encountered in the formulation of formoterol for therapeutic use (Lewis *et al.*, 2001). There are two salts of formoterol that have been of a particular interest: fumarate and tartarate. As regards stability, it was found that, although little degradation occurs in dry lactose formulations, upon the addition of 5% water and storage at 60°C/75% RH for one month, a 5:4 mixture of formoterol salt and lactose showed 95% recovery of formoterol from racemic (R,R/S,S in a ratio 1:1) formoterol fumarate dihydrate (commercial salt of formoterol), 81% from R,R formoterol L-tartarate and only 0.3% from R,R formoterol hemifumarate (Gao *et al.*, 2001). S,R-formoterol stored in similar conditions (a 1:4 mixture of formoterol and lactose, 5% water, 60°C/75% RH) had, after one month, only 3.2% of the initial potency (Jerussi and Senanayake, 2001). To facilitate powder filling and dispersion, the drug particles can be formulated with additional excipients, usually lactose monohydrate (Prime *et al.*, 1997). All the above mentioned formoterol formulations contain lactose as the carrier particles, thereby the presence of this excipient poses a potential threat of the long-term stability for the drug, especially if inappropriately stored. The chemical instability of formoterol in mixtures with lactose results from a chemical reaction occurring between the drug molecule and the aldehyde group of lactose molecule. Formulation of formoterol into MDIs based on the chlorofluorocarbon-free propellants might be an alternative, but it is known that those aerosol formulations consisting just of propellant and formoterol fumarate without additional excipient(s) sometimes encounter problems such as caking on manufacturing equipment, high deposition in the vial or valve of inhalers and valve sticking (Oliver *et al.*, 2000).

In Chapter 4 it was shown that the spray drying technique offers a better alternative for production of inhalable powders than milling of the active. This is mainly due to ability to change the spray dryer's settings allowing for a wide range manipulation of the manufacturing conditions thus the particulate characteristics can be controlled.

In order to avoid formulation of formoterol into MDIs and also to overcome the problems associated with the use of lactose as a carrier, it was considered that systems resulting from co-spray drying of the drug with an excipient other than lactose might have appropriate performance characteristics to be used in a carrier-free DPI. Also it was of interest to compare and assess the powders in respect of dispersibility by comparison with a commercially obtainable, micronised sample of formoterol fumarate dihydrate.

5.2 Formoterol fumarate dihydrate and PEG 20000 systems

Polyethylene glycols (PEGs) are polymers consisting of ethylene oxide units with a molecular weight in the range 200-300000. For the manufacture of solid dispersions PEGs with molecular weights of 1500-20000 are usually employed (Leuner and Dressman, 2000). Different composites utilising PEGs as an additive were successfully produced by spray drying with lactose (Corrigan *et al.*, 2002), bendroflumethiazide (Corrigan *et al.*, 2003) and salbutamol sulphate (Corrigan *et al.*, 2004). Co-spray dried lactose/PEG 3000 or PEG 6000 particles have recently been shown to be promising carriers for use in DPIs (Gilani *et al.*, 2004). Chiou and Riegelman (1969) were able to achieve a noticeable increase in the release rate of griseofulvin from solid dispersions in PEG 4000, 6000 and 20000. The result of research with PEG-griseofulvin combinations is the marketed product, Gris-PEG®.

There are a few toxicity concerns associated with the use of PEGs and the low molecular weight compounds tend to show greater toxicity (Wade and Weller, 1994). A soft, difficult to formulate into a satisfactory dosage form solid dispersion may be produced if a PEG with too low molecular weight is used (Shah *et al.*, 1995). Keeping these potential problems in mind, PEG with a molecular weight of 20000 was selected for the production of formoterol fumarate solid dispersions.

5.2.1 Spray dried PEG 20000

Corrigan (2002) attempted the spray drying of PEG 20000 as a 1% (w/v) solution from 95% (v/v) ethanol. A Büchi 191 spray dryer was used with an inlet temperature of 78°C which, together with the rest of the settings, gave an outlet temperature of 47-48°C. No amorphous material was produced and DSC and XRD analyses showed even a slight increase in crystallinity. This was a surprise, as a lower grade of PEG with molecular weight of 4000 has been demonstrated to produce a spray dried material with the degree of crystallinity reduced by 10-15% (Corrigan *et al.*, 2002).

In this study, dichloromethane instead of 95% (v/v) ethanol was employed. Consequently, a lower inlet temperature of 45°C was used, which together with the other settings of the apparatus resulted in an outlet temperature in the range of 35-36°C. The details of the spray drying conditions are given in Appendix I.

Figure 5.1 presents the DSC scans of the raw material sample of PEG 20000 and its spray dried counterpart. The melting onset temperature was nearly the same for both samples and was ~62°C, but the endotherms had slightly different maxima, with a shift of 1°C towards lower temperatures for the processed sample. This could be due to the formation of amorphous material and/or changes in conformation of PEG molecules. The enthalpy of melting was reduced for the spray dried PEG and was ~165 J/g when compared to ~189 J/g for the unprocessed sample. Assuming 100% crystallinity of the starting material, the change in enthalpy by DSC implies over a 10% fall in

crystallinity. However, no T_g was detected, which would confirm the formation of a disordered phase. A conventional DSC was used for thermal analysis, but modulated temperature DSC systems have been shown to be superior over standard equipment in detecting glass transition temperatures of solids and it has been demonstrated for PEG 4000 that while a peak at around -80°C was seen on the MTDSC, the conventional DSC recorded only a baseline (Craig, 1995). TG analysis revealed that the weight loss between 25°C and 100°C was approximately 0.9% and 0.5% for the unprocessed and spray dried PEG, respectively, which perhaps is associated with adsorbed moisture and/or residual solvent liberation. This slight reduction may be due to the use of organic solvent for the spray drying process thus limiting moisture availability in the drying medium.

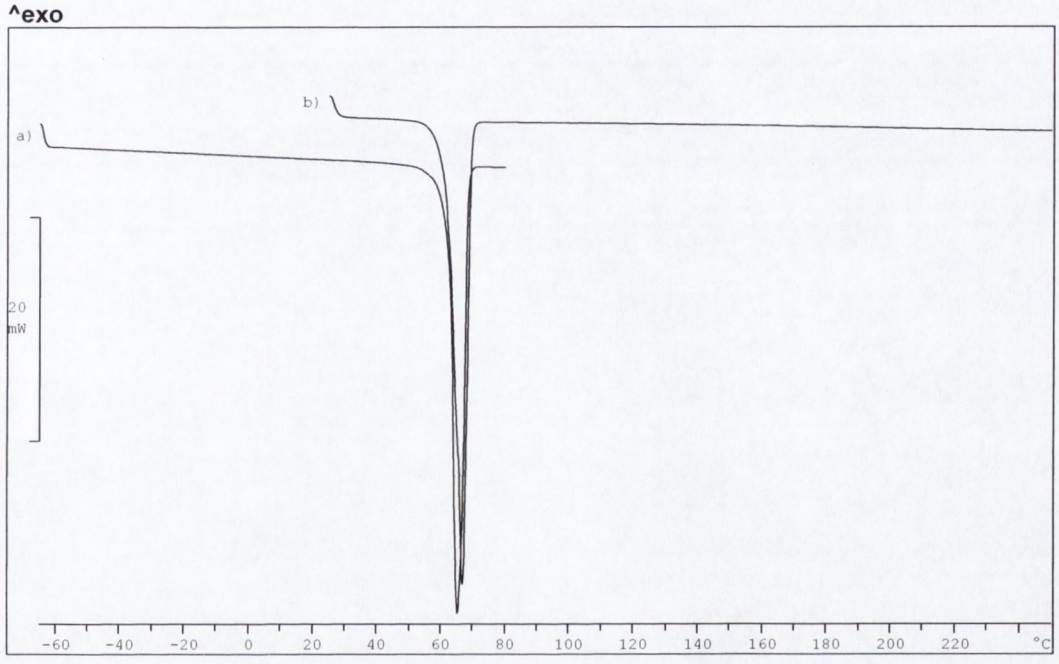

Figure 5.1 DSC scans of (a) spray dried PEG 20000 and (b) unprocessed PEG 20000.

XRD diffraction patterns are presented in Figure 5.2 and are typical of crystalline materials. However, the intensity of the peaks of the spray dried PEG was greatly reduced compared to the starting material. The reduction in crystallinity by XRD was calculated to be ~45% comparing the total sum of intensities of the peaks at 19.2 2θ and 23.4 2θ, taking unprocessed PEG to be fully crystalline.

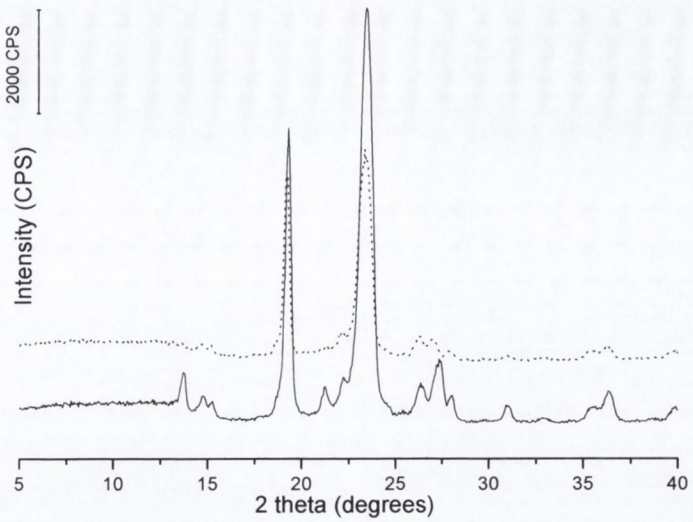

Figure 5.2 XRD diffractograms of the unprocessed PEG 20000 (solid line) and spray dried PEG 20000 (dotted line).

Spray drying induced only marginal changes in the FTIR spectrum of the PEG 20000 sample as seen in Figure 5.3. Ford *et al.* (1986) attributed these changes to a modification in the crystallinity of the polymer. The most significant changes took place in the bands at 947 and 962 cm^{-1} (CH_2 rocking, CH_2 twisting), the decrease in the intensity of the peak at 947 cm^{-1} with respect to that at 962 cm^{-1} indicating an decrease in the crystalline fraction. The modification of the band at 842 cm^{-1} is related to the crystallinity too, a decrease in intensity being associated with an increase in the amorphous fraction (Anguiano-Igea *et al.*, 1995). The ratio between intensity of the bands at 947 and 962 cm^{-1} was 0.85 for the starting material compared with 0.58 for the processed sample, which suggests over a 30% decrease in crystallinity. The band at 842 cm^{-1} also reduced its intensity when compared to the band at 962 cm^{-1} or 2890 cm^{-1} (CH_2 stretching).

Spray drying of PEG 20000 also led to a shift of the band located initially at 3300-3650 cm^{-1} and ascribed to OH hydrogen bonded groups. This broad band shifted towards lower wavenumbers indicating, probably, strengthening of the hydrogen bonds caused by processing.

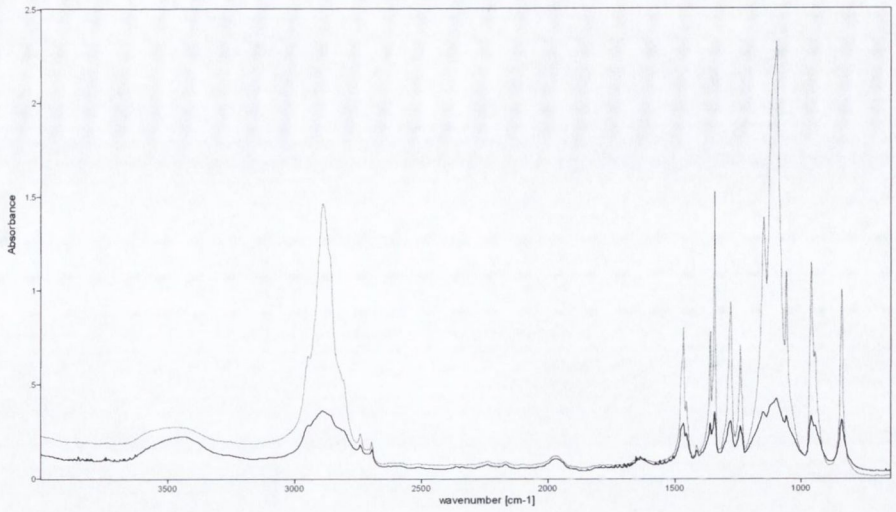

Figure 5.3 FTIR scans of the unprocessed PEG 20000 (solid line) and spray dried PEG 20000 (dotted line).

SEM micrographs presented in Figure 5.4 showed that the spray dried material consisted of spherical particles but merged into aggregates. The surfaces were rough with cracks when observed at high magnification (Figure 5.4, top right). The starting PEG material comprised of large, semitransparent plates, contrasting with the processed particles, however the surfaces of these plates were also rough as observed at a higher magnification (Figure 5.4). Laser diffraction particle size analysis using the Malvern Mastersizer 2000 revealed that the distribution of the spray dried particles was nearly monomodal with a minor "tail" of very small particles having size of ~1 μm. The median particle size was equal to 15 μm.

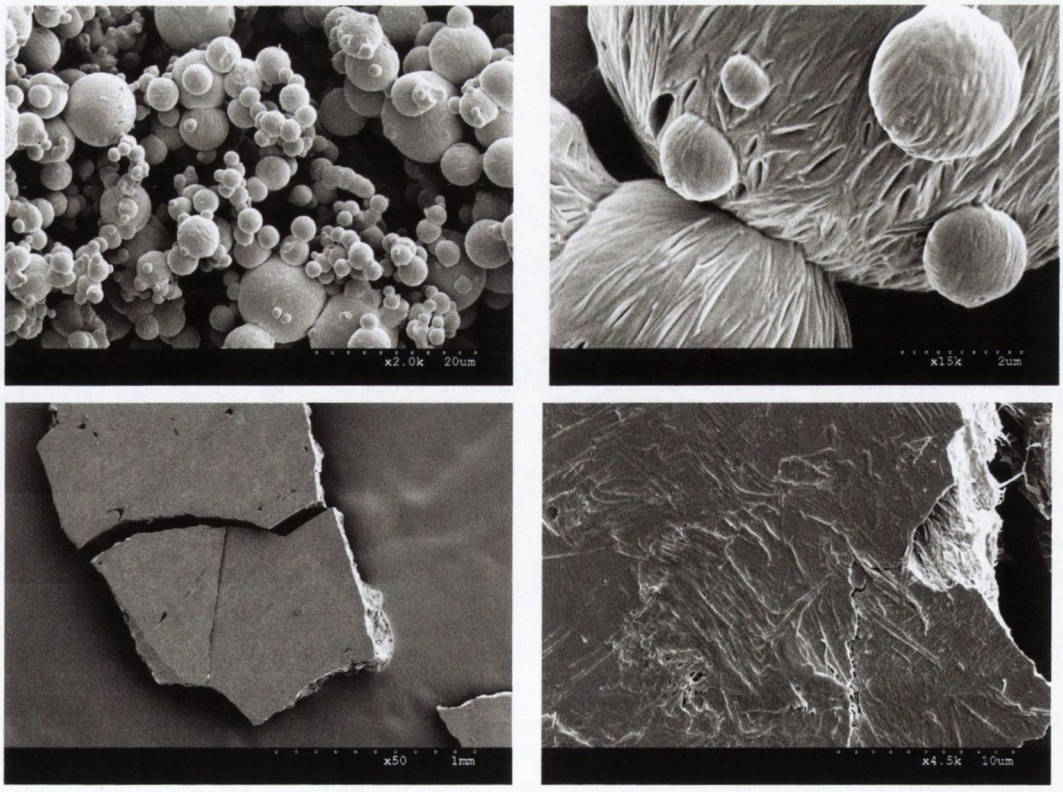

Figure 5.4 SEM micrographs of the spray dried PEG 20000 (top) and unprocessed PEG 20000 (bottom). Note the different magnifications of the micrographs.

Summarising, PEG 2000 was found to form an amorphous phase on spray drying from dichloromethane, but different analytical techniques indicated a differing degree of crystallinity. PEG molecules have a helical conformation but on melting this structure is lost and a liquid containing random coils is obtained (Craig, 1995). PEGs can also show different conformations in solutions. Solutions prepared with chloroform and dichloromethane contain random coils, whereas PEGs in aqueous solutions retain the helical configuration. This behaviour in solution may explain the large content of the amorphous material resulting from spray drying from dichloromethane, as the random coils had not enough time to convert into the stable helical structure. It can also be reasoned, as neither the inlet nor outlet temperatures of the process exceeded the melting point of PEG 20000, that the very mild manufacturing conditions prevented the recrystallisation of the amorphous material.

5.2.2 Co-spray dried formoterol fumarate/PEG 20000

Two systems of formoterol fumarate dihydrate with PEG 20000 (constituting 10% or 30% by weight of solids) were spray dried from 98% (v/v) ethanol. Spray drying conditions are given in Appendix I.

Spray drying of the mixture containing 10% of the polymer resulted in a powdered product that was recovered from the collecting vessel. However, the system containing 30% of PEG melted in the spray drier and only a small amount of material, which subsequently hardened, was scraped out of the apparatus for characterisation.

A broad endotherm overlapping with an exotherm was observed by DSC for the co-spray dried system containing 10% PEG (Figure 5.5). The endotherm peaked at ~62°C, which could be due to the residual solvent release and/or PEG melting, as spray dried PEG melts with an endothermic peak at 64°C. The recrystallisation exotherm was very weak and visible at a higher magnification only. It peaked at 90°C and was followed by a second melting endotherm which was observed to occur at ~160°C. The equivalent physical mix gave three endotherms and no exothermic peak, with the endotherms peaking at 64°C, 120°C and 139°C indicating melting of PEG, dehydration of the drug and melting of one of its enantiomers, respectively (Figure 5.5). The melting of the second enantiomer was overlapped with a jagged baseline indicative of thermal decomposition and could not be integrated. The onset of PEG melting was slightly depressed and appeared at 60.7°C. Also the endotherms of formoterol fumarate were somewhat shifted towards lower temperatures.

On the DSC scan (Figure 5.5) of the 30% PEG-containing composite an endotherm was observed at 65°C, corresponding to PEG melting. A second endotherm at ~164°C corresponded to formoterol fumarate melting. No distinct exothermic peak was observed. The mechanical mixture gave a DSC trace similar to the mix containing 10% PEG (Figure 5.5) and the peaks occurred at lower temperatures, but the presence of PEG did not noticeably reduce the temperature of formoterol fumarate melting. This absence of obvious alterations in the peak positions indicates negligible

interactions between the constituents in the solid state. A similar behaviour for naproxen/PEG 20000 mixtures was reported by (Mura *et al.*, 1996).

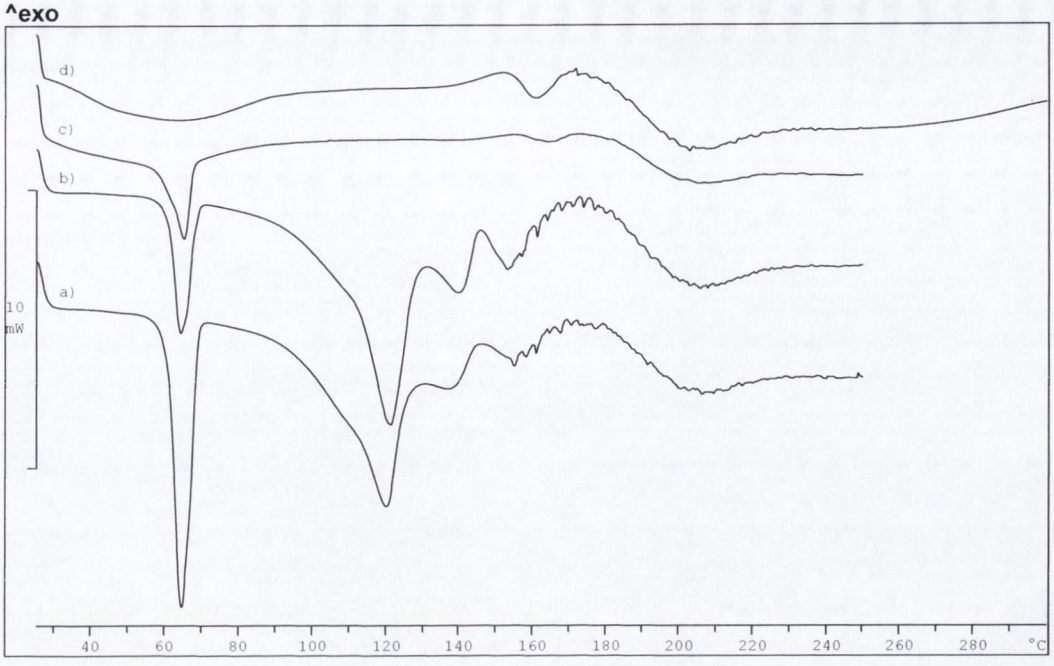

Figure 5.5 DSC scans of (a) physical mixture of formoterol fumarate dihydrate and PEG 20000 30% (w/w), (b) physical mixture of formoterol fumarate dihydrate and PEG 20000 10% (w/w), (c) co-spray dried formoterol fumarate dihydrate and PEG 20000 30% (w/w) and (d) co-spray dried formoterol fumarate dihydrate and PEG 20000 10% (w/w).

There was approximately 3% and 2% weight loss by TGA for the co-spray dried 10% PEG and 30% PEG sample, respectively, occurring between ~25 and 100°C. The shape of TGA trace was different for the physical mixtures and the co-spray dried counterparts, being a one step process for all of them, but the greatest weight loss occurred between 25 and 60°C for the spray dried composites and between 80 and 110°C for the mechanical mixes.

The XRD diffractogram of the 10% PEG system showed a pattern typical of amorphous material with no distinct peaks (Figure 5.6). The equivalent physical mixture presented peaks of both components. This indicates that XRD can detect this concentration of the polymer and suggests that both components were in disordered phases in the co-spray dried sample. Co-spray dried formoterol fumarate dihydrate and PEG 30% was predominantly amorphous and only two weak peaks of PEG were recorded. This indicates that in this mixture the drug was in an amorphous state but the polymer was crystalline. The intensity of the peak at 23.4 2θ was greatly reduced compared to that of the equivalent physical mixture, demonstrating that only a fraction of PEG was crystalline.

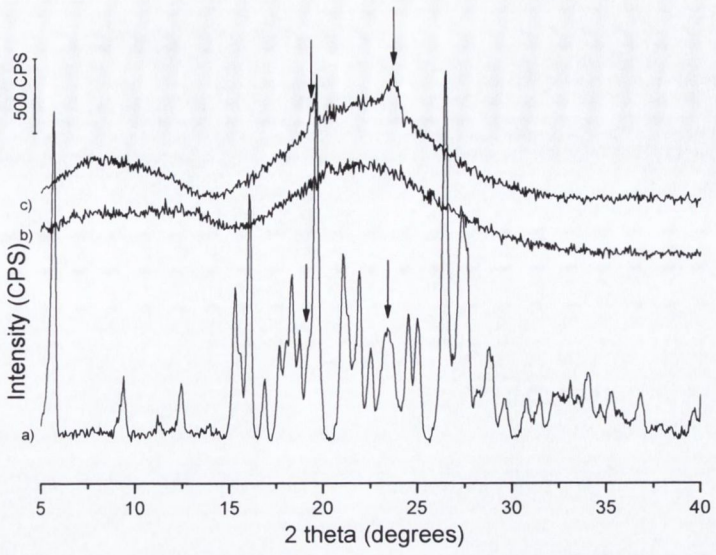

Figure 5.6 XRD diffractograms of (a) physical mixture of formoterol fumarate dihydrate and PEG 20000 10% (w/w), (b) co-spray dried formoterol fumarate dihydrate and PEG 20000 10% (w/w) and (c) co-spray dried formoterol fumarate dihydrate and PEG 20000 30% (w/w). The arrows indicate peaks of crystalline PEG 20000.

The FTIR spectra of the spray dried composites (Figure 5.7) were similar in shape to that of spray dried formoterol fumarate (Chapter 4). A shift of the formoterol C=O stretching band initially located at 1675 cm^{-1} for the processed drug alone was observed. The peak position was found to be at 1676 cm^{-1} and 1677 cm^{-1} for the 10% and 30% PEG-containing sample, respectively. The direction of the shift would indicate destabilisation of the formoterol fumarate hydrogen bonds towards weakening and/or an involvement in newly formed hydrogen bonds with PEG. The latter possibility was assumed as an explanation for a shift of the C=O groups of naproxen in PEG solid dispersions (Mura *et al.*, 1996). Most of dissimilarities were discerned in the 900-1200 cm^{-1} region where PEG has very strong bands. The infrared spectra of the equivalent mechanical mixtures (not shown) were almost superimposable with the spectrum of the crystalline drug. There was almost no indication of the PEG presence except a few minor peaks. Also no shift of formoterol fumarate C=O at 1689 cm^{-1} was noted.

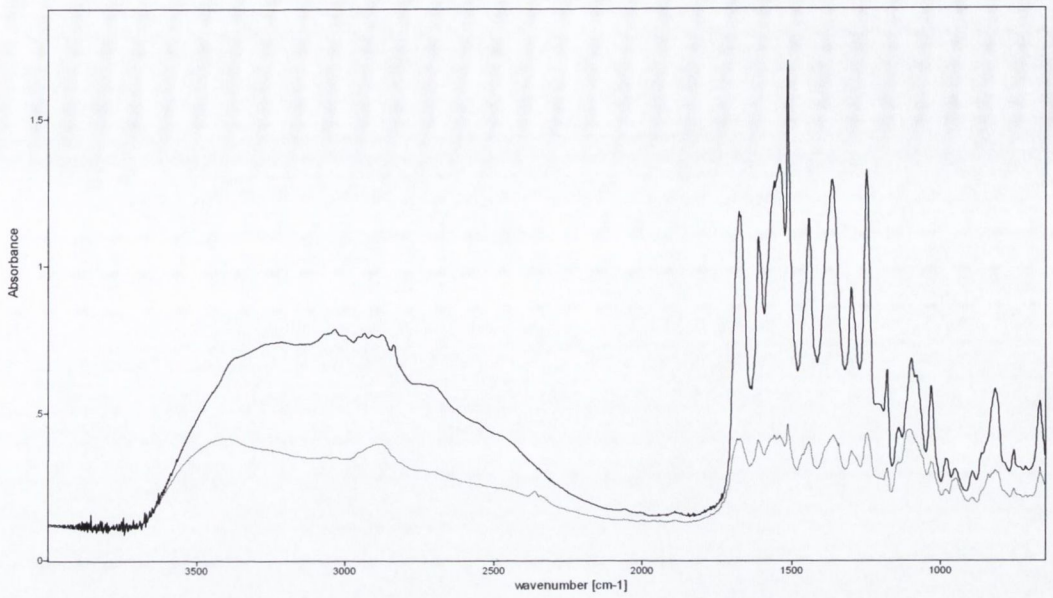

Figure 5.7 FTIR spectra of co-spray dried formoterol fumarate dihydrate and PEG 20000 10% (w/w) (solid line) and co-spray dried formoterol fumarate dihydrate and PEG 20000 30% (w/w) (dotted line).

Spherical particles with various degrees of aggregation were observed by SEM (Figure 5.8). The 30% PEG-containing solid dispersion had a strong tendency to aggregate and appeared as a merged mass of particles. Particle surfaces were smooth. Despite SEM suggesting quite large particle dimensions of the co-spray dried formoterol fumarate dihydrate/PEG 10%, the laser diffraction particle size analysis by Sympatec showed that the median particle size was 2.3 µm. No particle size analysis was carried out for the 30% PEG containing sample, as it failed to produce a particulate system.



Figure 5.8 SEM micrographs of the co-spray dried formoterol fumarate dihydrate and PEG 20000 10% (w/w) (left) and co-spray dried formoterol fumarate dihydrate and PEG 20000 30% (w/w) (right). Note the lower magnification of the left micrograph.

5.3 Co-spray dried formoterol fumarate dihydrate and PVP 10000 systems

Polyvinylpyrrolidone compounds have been widely used in the pharmaceutical sector since the 1940s (Leuner and Dressman, 2000). They are resultants of polymerisation of vinylpyrrolidone units with molecular weights ranging from 2500 to 3000000. Due to their good solubility in a wide variety of organic solvents (Wade and Weller, 1994), they are particularly suitable for the preparation of solid dispersions by the solvent method. PVP is commonly used to form solid dispersions and it has been reported that over 60 drugs have been dispersed in this polymer (Ford, 1986). The main advantage of PVP over other polymers is its ablility to inhibit crystallisation in both solution (Simonelli *et al.*, 1969) and amorphous solid dispersion (Yoshioka *et al.*, 1995). Polyvinylpyrrolidone also forms covalent adducts with drugs containing nucleophilic functional groups which enable preparation of PVP-based polymer-drug conjugates having greater plasma half-lifes than the drugs alone. PVPs, when given orally, are regarded as being non-toxic, partly because they have too high molecular weights to be absorbed from the gastrointestinal tract. Reports of side effects are restricted to the formation of granulomas after intramuscular injection (Nair, 1998). All of the above may make PVP compounds an attractive alternative to the use of sugars in DPIs.

Two systems of formoterol fumarate dihydrate with PVP 10000 (constituting 10% or 30% by weight of solids) were spray dried from 98% (v/v) ethanol. Spray drying conditions are given in Appendix I. PVP was also spray dried from an ethanolic solution for comparison purposes and the process settings are included in Appendix I.

Thermal analysis scans of various PVP/formoterol fumarate systems are shown in Figure 5.9. DSC of the composite containing 10% PVP presented a broad endotherm with a peak at ~60˚C, which was followed by a broad, but weak exotherm with a peak at 110˚C. The endotherm is probably due to desolvation of the material caused by the presence of hygroscopic PVP. A similar broad endotherm peaking at ~80˚C was seen in the DSC of pure PVP raw material and the spray dried specimen, corresponding to PVP dehydration. It was consisted with the TG analysis, which showed ~6% and 5.6% weight losses up to 100˚C, for the unprocessed and spray dried sample, respectively. The exotherm observed in the DSC for this system was perhaps due to formoterol recrystallisation. A second endotherm, due to formoterol melting, was observed to peak at 163˚C. The 30% PVP-containing co-spray dried system had similar thermal characteristics as recorded by DSC, but the exotherm was narrower, more pronounced and peaked at ~109˚C. Also the second endotherm was shifted to higher temperatures and was observed to peak at 166˚C. Thermal decomposition was observed above 180˚C and was manifested as an irregular and rough baseline.

The equivalent physical mixtures exhibited broad endotherms peaking at ~60˚C with the 30% PVP system having a broader and more distinct peak which is consistent with the higher polymer content. In both cases the endotherm was followed by another endothermic peak of formoterol

fumarate dehydration. No significant alteration of the peak position in comparison with the drug alone was seen and was 122°C, 120°C and 121°C for the crystalline formoterol fumarate dihydrate, 10% PVP and 30% PVP sample, respectively. Two additional endothermic peaks were recorded for the physically mixed drug with 10% PVP consistent with melting of formoterol fumarate.

No glass transition temperature of PVP was detected on the DSC scans of the mechanical mixes as it was covered by the drug dehydration endotherm. The T_g of the PVP untreated sample was determined to be ~120°C.

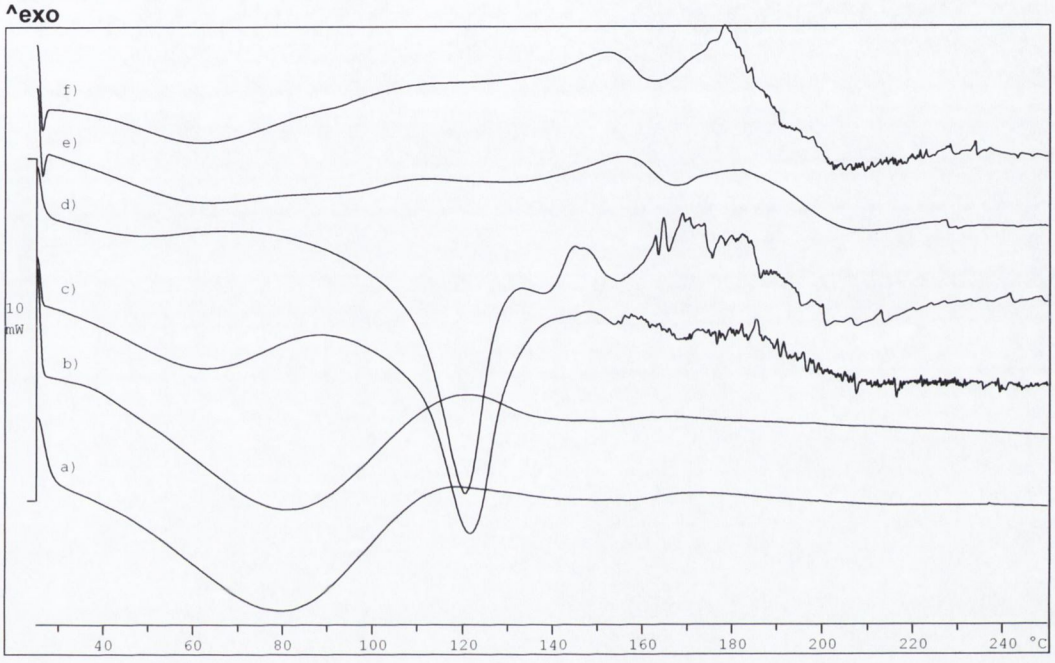

Figure 5.9 DSC scans of (a) unprocessed PVP 10000, (b) spray dried PVP 10000, (c) physical mixture of formoterol fumarate dihydrate and PVP 10000 30% (w/w), (d) physical mixture of formoterol fumarate dihydrate and PVP 10000 10% (w/w), (e) co-spray dried formoterol fumarate dihydrate and PVP 10000 30% (w/w) and (f) co-spray dried formoterol fumarate dihydrate and PVP 10000 10% (w/w).

The PVP co-spray dried composites retained more solvent residues than the PEG-based systems. There was 3.4% and 4.3% weight loss by TGA between 25 and 100°C for the 10% and 30% PVP-containing dispersions, respectively.

The formoterol fumarate-PVP systems were confirmed to be amorphous as X-ray diffraction showed patterns with no distinct peaks (Figure 5.10). Amorphous "halos" were also registered for the starting and spray dried PVP powders which was expected, as PVP is an inherently amorphous substance.

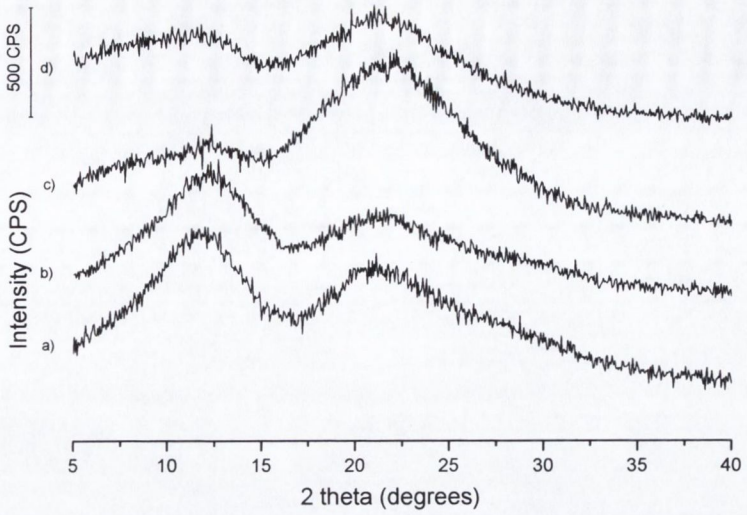

Figure 5.10 XRD diffractograms of (a) PVP 10000 starting material, (b) spray dried PVP 10000, (c) co-spray dried formoterol fumarate dihydrate and PVP 10000 10% (w/w) and (d) co-spray dried formoterol fumarate dihydrate and PVP 10000 30% (w/w).

Although DSC analysis demonstrated no evidence of interactions between the components, infrared spectroscopy was shown to be a more suitable tool in detecting possible intermolecular interactions present in the co-spray dried material. Firstly, a shift of the band assigned to the carbonyl stretching of the formoterol formamide group was discerned and it can be observed in Figure 5.11. The greater the polymer content the more pronounced the shift towards lower wavenumbers that was observed. The band position was recorded to occur at 1675, 1672 and 1668 cm^{-1} for the 0%, 10% and 30% PVP content, respectively. This trend suggests an interaction taking place and specifically the possibility of hydrogen bonds formation between the species. This can be substantiated by the fact that the pattern of vibrations between 3100 and 3500 cm^{-1} was also different and a broad band located at 3211 cm^{-1} for the spray dried formoterol fumarate alone moved to 3213 and 3258 cm^{-1} for the 10% and 30% PVP composite, respectively. A minor alteration of the relative intensities of the peaks occurring in the 1520-1580 cm^{-1} region was discerned and these bands arose probably from the N-H bending vibrations. The fingerprint region resembled that of processed drug and only very weak peaks of PVP were observed. The infrared spectra of physical mixtures were nearly identical with the spectrum of the crystalline active and neither shift of the C=O peak nor in the hydrogen bonds region was evident (spectra not shown).

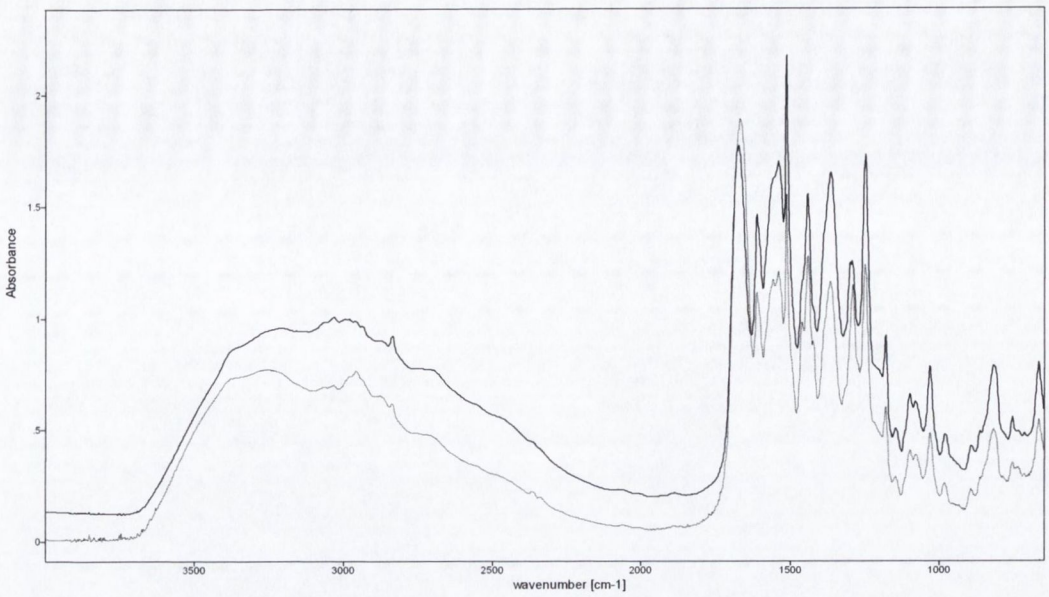

Figure 5.11 FTIR spectra of co-spray dried formoterol fumarate dihydrate and PVP 10000 10% (w/w) (solid line) and co-spray dried formoterol fumarate dihydrate and PVP 10000 30% (w/w) (dotted line).

SEM revealed that the polymer alone (raw material) comprised of roughly spherical particles, either with folded or inflated surfaces (Figure 5.12, top micrographs). The median particle size as measured by Malvern Mastersizer 2000 laser diffraction particle sizer was 26 μm. Spray drying of PVP allowed for a seven-fold decrease in the median particle size (the median particle size of spray dried PVP was 3.7 μm) as well as narrowing of the particle size distribution. All particles resembled "deflated balloons".

Small spherical particles, typical of amorphous material were observed by SEM for the spray dried composites (Figure 5.12, bottom micrographs). Particle diameters by SEM were similar and generally were less than ~5μm. An occasional particle as large as ~6-7 μm was observed for the composite containing 30% PVP. The laser particle size analysis by Sympatec revealed that the median particle size was 2.4 μm and 2.5 μm for the co-spray dried drug/PVP 10% and 30% system, respectively.

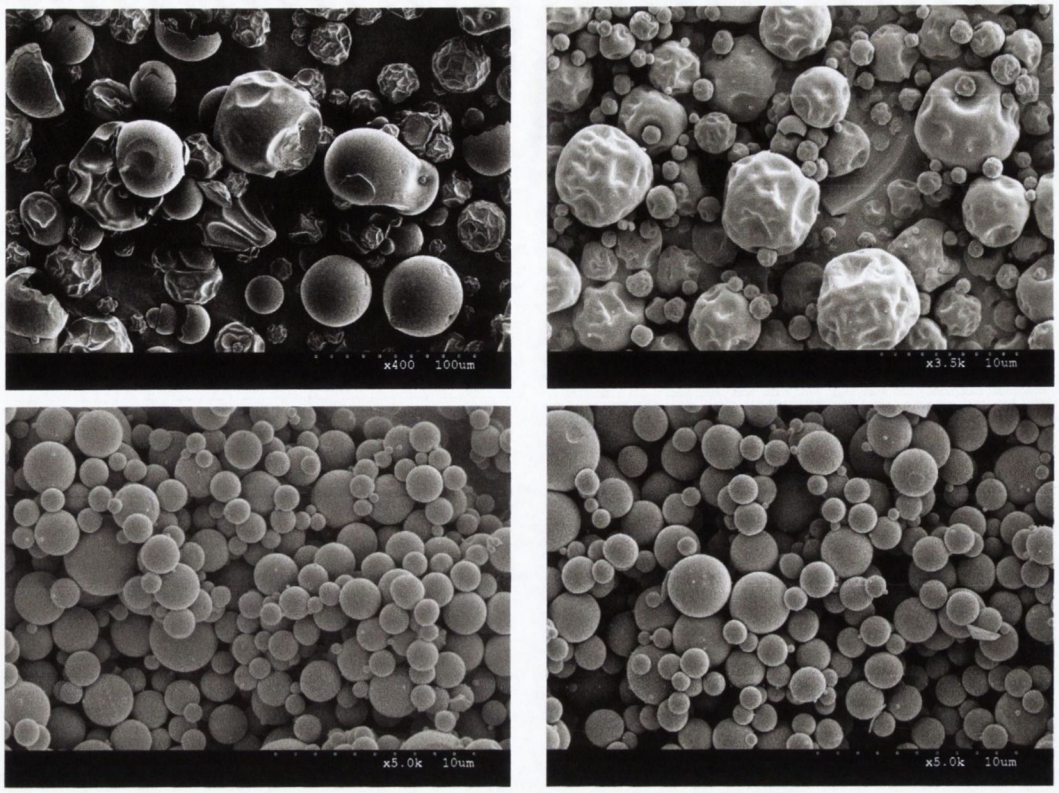

Figure 5.12 SEM micrographs of the PVP 10000 starting material (top left), spray dried PVP 10000 (top right), co-spray dried formoterol fumarate dihydrate and PVP 10000 10% (w/w) (bottom left) and co-spray dried formoterol fumarate dihydrate and PVP 10000 30% (w/w) (bottom right). Note the lower magnification of the top micrographs.

5.4 Co-spray dried formoterol fumarate dihydrate and trehalose dihydrate systems

Trehalose is a non-reducing sugar in contrast to lactose. Trehalose confers to certain plant and animal cells the ability to survive dehydration and to restore activity after rehydration (Patist and Zoerb, 2005). This sugar may have opportunities as an ingredient for dried and processed food as well as a non-toxic cryoprotectant of vaccines and organs for surgical transplants (Colaço *et al.*, 1992). The potential of trehalose as an excipient that may be used in pulmonary delivery has been indicated by Naini *et al.* (1998).

Two systems of formoterol fumarate dihydrate with trehalose dihydrate (constituting 10% or 30% by weight of solids) were spray dried from 98% (v/v) ethanol. Spray drying conditions are given in Appendix I.

The co-spray dried composites were XRD amorphous and showed no diffraction peaks as demonstrated in Figure 5.13. The equivalent mechanically mixed blends were, as expected, crystalline. The diffraction pattern of the 10% trehalose physical mixture consisted of the formoterol fumarate dihydrate peaks, with two additional peaks, at 13.8 2θ and 23.9 2θ degrees, of trehalose dihydrate. In the 30% sugar mix the trehalose peaks were more pronounced.

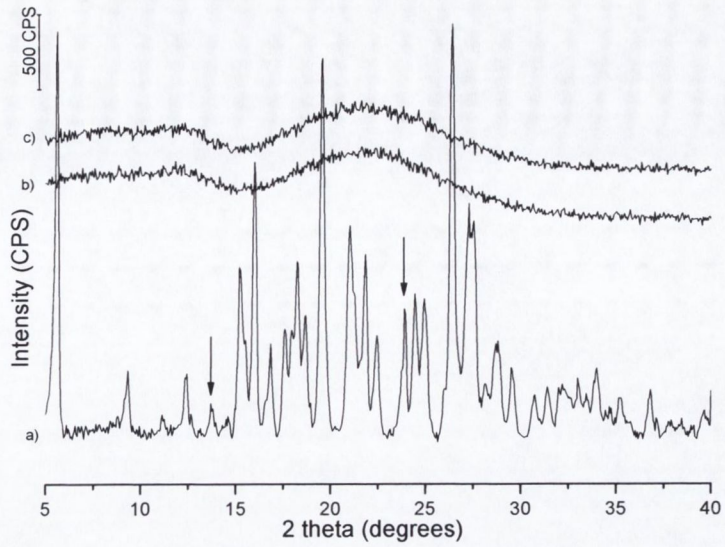

Figure 5.13 XRD diffractograms of (a) physical mixture of formoterol fumarate dihydrate and trehalose dihydrate 10% (w/w), (b) co-spray dried formoterol fumarate dihydrate and trehalose dihydrate 10% (w/w) and (c) co-spray dried formoterol fumarate dihydrate and trehalose dihydrate 30% (w/w). The arrows indicate peaks of crystalline trehalose dihydrate.

The lack of a crystalline phase as demonstrated by XRD in the co-spray dried samples is consistent with their DSC scans shown in Figure 5.14. A broad endotherm (with a peak at ~70˚C) overlapping with a broad exotherm (with a peak at 109 and 114˚C for the 10% and 30% trehalose system, respectively) was observed by DSC. Due to the possibility of residual solvents being retained, the endotherm is probably due to their liberation. TGA showed a 3.4% and 4.7% weight loss in the 25-100˚C region for the formoterol/trehalose 10% and 30% system, respectively. A second exotherm was present in the DSC scan of the co-spray dried mix containing 10% trehalose, which peaked at ~155˚C indicating perhaps the beginning of thermal decomposition, as a considerable weight loss was recorded by TGA in the same temperature range. The endotherm corresponding to melting of recrystallised formoterol occurring at ~160˚C was minor and rapidly followed by evidence of degradation. In the 30% trehalose/drug composite this endotherm was distinct and peaked at 165˚C. The thermal transitions of both the sugar and drug appeared on the DSC scans of the mechanical mixtures (Figure 5.14). Regardless of the concentration, dehydration and melting processes of trehalose were visible at ~100˚C and ~210˚C, respectively. Also dehydration of the active compound was seen on the scans at ~122˚C. Comparing the peak temperatures of the constituents in the mixtures with those in pure substances, no differences were noticed. Two other endothermic peaks in the 10% trehalose-based mixture were recorded, corresponding to melting of the formoterol enantiomers.

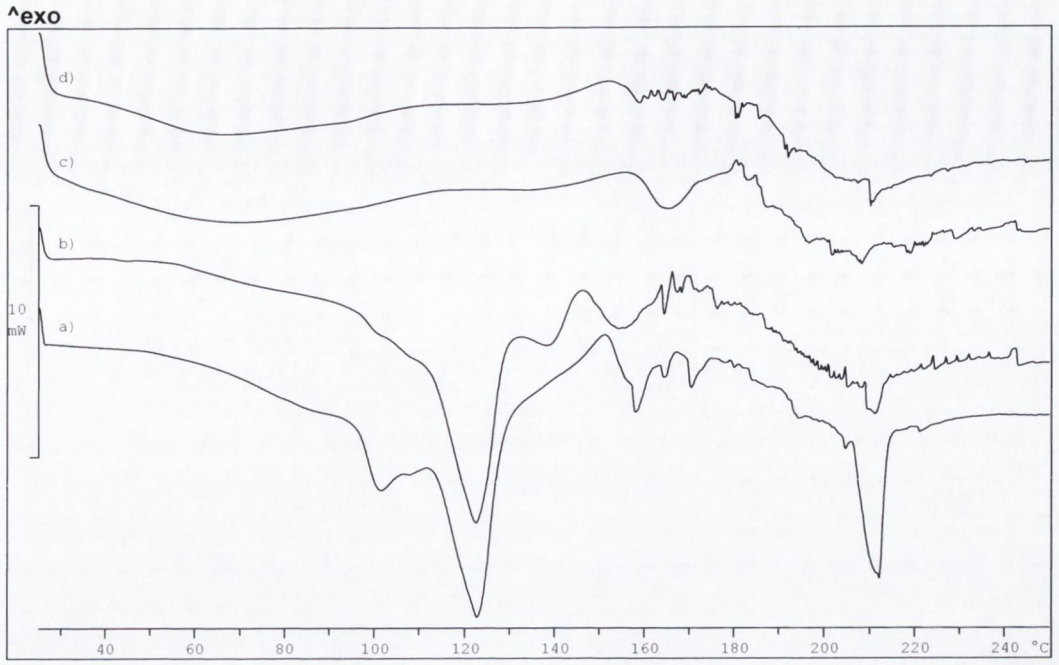

Figure 5.14 DSC scans of (a) physical mixture of formoterol fumarate dihydrate and trehalose dihydrate 30% (w/w), (b) physical mixture of formoterol fumarate dihydrate and trehalose dihydrate 10% (w/w), (c) co-spray dried formoterol fumarate dihydrate and trehalose dihydrate 30% (w/w) and (d) co-spray dried formoterol fumarate dihydrate and trehalose dihydrate 10% (w/w).

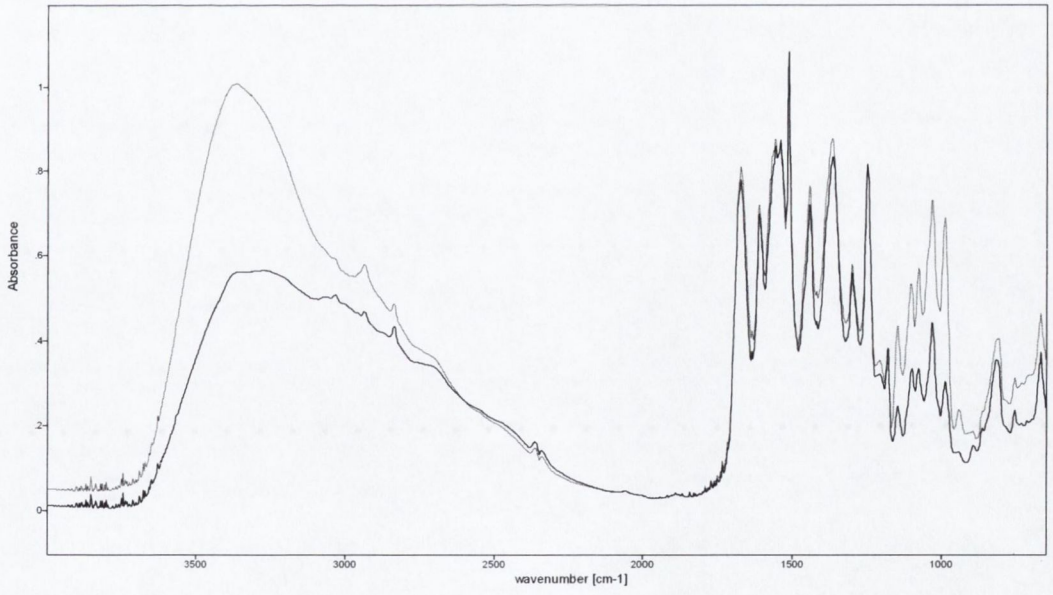

Figure 5.15 FTIR spectra of co-spray dried formoterol fumarate dihydrate and trehalose dihydrate 10% (w/w) (solid line) and co-spray dried formoterol fumarate dihydrate and trehalose dihydrate 30% (w/w) (dotted line).

FTIR confirmed a lack of interactions between the sugar and drug in the co-processed systems. No shift of the carbonyl stretching band of the formoterol formamide group was noticed and its position remained unchanged at 1675 cm^{-1} (Figure 5.15). There were differences in the 3000-3500 cm^{-1} vibration modes associated with hydrogen bonding rearrangements. They may have arisen due

to a disruption in the intermolecular bonds among the drug molecules caused by the presence of trehalose. The presence of the sugar was manifested in extra peaks in the 900-1200 cm^{-1} region that were of the α-(1↔1) glycosidic bonds (Akao *et al.*, 2001).

Figure 5.16 shows that small spherical particles with generally smooth surfaces were observed by SEM for both of the co-spray dried systems. An occasional non-spherical particle or particle fragment was also seen. Additionally, surface indentations were apparent for some of the particles of the 10% trehalose containing composite. In the case of the 30% trehalose sample, rougher surface texture and fused aggregates were noticeable for a small number of particles. The median particle size as determined by Sympatec laser particle sizer was 2.5 μm and 2.1 μm for the 10% and 30% trehalose systems, respectively.

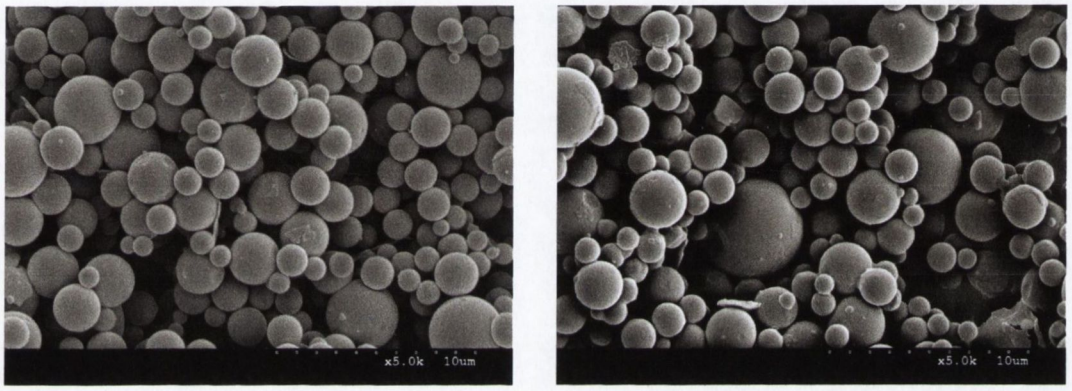

Figure 5.16 SEM micrographs of the co-spray dried formoterol fumarate dihydrate and trehalose dihydrate 10% (w/w) (left) and co-spray dried formoterol fumarate dihydrate and trehalose dihydrate 30% (w/w) (right).

5.5 Co-spray dried formoterol fumarate dihydrate and raffinose pentahydrate systems

Raffinose is a non-reducing trisacharride the molecule of which constitutes of D-galactose, D-glucose and D-fructose. Due to its non-reducing properties it may be used instead of reactive lactose in formoterol DPI formulations. Saleki-Gerhardt *et al.* (1995) have presented that anhydrous raffinose can accommodate a significant amount of water to form a stable pentahydrate and would appear as a potentially useful water scavenger in certain types of dosage form. Raffinose has been considered as one of the candidate excipients to be used as a carrier in DPIs (Hancock and Shamblin, 1998).

Two systems of formoterol fumarate dihydrate with raffinose pentahydrate (constituting 10% or 30% by weight of solids) were spray dried from 98% (v/v) ethanol. Spray drying conditions are given in Appendix I. Raffinose pentahydrate was also processed and due to its low ethanolic solubility an aqueous solution was prepared and spray dried. The spray dryer settings are presented in Appendix I.

The XRD diffraction pattern of the sugar "as received" presented in Figure 5.18 was compared to those of different hydrate pseudopolymorphs of raffinose in order to ensure that the initial product was pentahydrate. The X-ray diffractograms of the raffinose penta-, tetra- and trihydrate were published by Kajiwara *et al.* (1999) and allowed the identification of the starting material as either penta- or tetrahydrate. DSC of the sample (Figure 5.17) showed an endotherm with a peak at 88°C and another broad and jagged endothermic process with the onset at ~120°C. To substantiate the dehydration and melting of the sugar, TG analysis was also carried out. The scan presented that around 15% weight was lost up to 120°C and this corresponds to five water molecules being removed during heating. Therefore the first endotherm by DSC is the raffinose dehydration and the second endothermic process is related to melting of the sugar, corresponding to the literature value which was found to be ~84°C (Kajiwara *et al.*, 1999). The purchased sample was recognised as pentahydrate.

The spray dried raffinose was amorphous as evidenced by a broad "halo" on the X-ray diffractogram (Figure 5.18). A broad endotherm due to residual moisture removal with the peak at about 95°C followed by the glass transition at ~118°C was observed by DSC (Figure 5.17). Another endotherm was observed to begin at ~220°C and corresponded to thermal degradation of the material, confirmed additionally by a weight loss starting at this temperature by TGA. No distinct recrystallisation exotherm was observed by DSC.

SEM micrographs (Figure 5.20, top micrographs) demonstrated that spherical particles were produced on spray drying. Particle surfaces were generally smooth and some of the particles were dimpled. Their morphology contrasted with large, rough and elongated crystals of raffinose starting material. The particle size distribution of the processed raffinose was monomodal with the median particle size of 3.8 μm as measured by Malvern Mastersizer 2000 particle sizer.

Very similar scans for both of the co-spray dried samples were recorded by DSC and demonstrated in Figure 5.17. A broad endotherm due to the release of the remaining solvents peaked first at ~70°C. A second endothermic process of formoterol fumarate melting peaked at ~162°C and ~164°C for the samples with the 10% and 30% raffinose, respectively. This was preceded by an exotherm of the amorphous phase recrystallisation with the maximum at 110°C and 115°C for the 10% and 30% sugar containing composite, respectively. Beyond ~170°C an evidence of the thermal decomposition was seen manifesting itself as a very irregular and rough baseline. Both composites held ~3% of residual solvents as quantified by TGA in the 25-100°C temperature range. They were XRD amorphous and the diffractograms presented only diffuse "halos" (Figure 5.18).

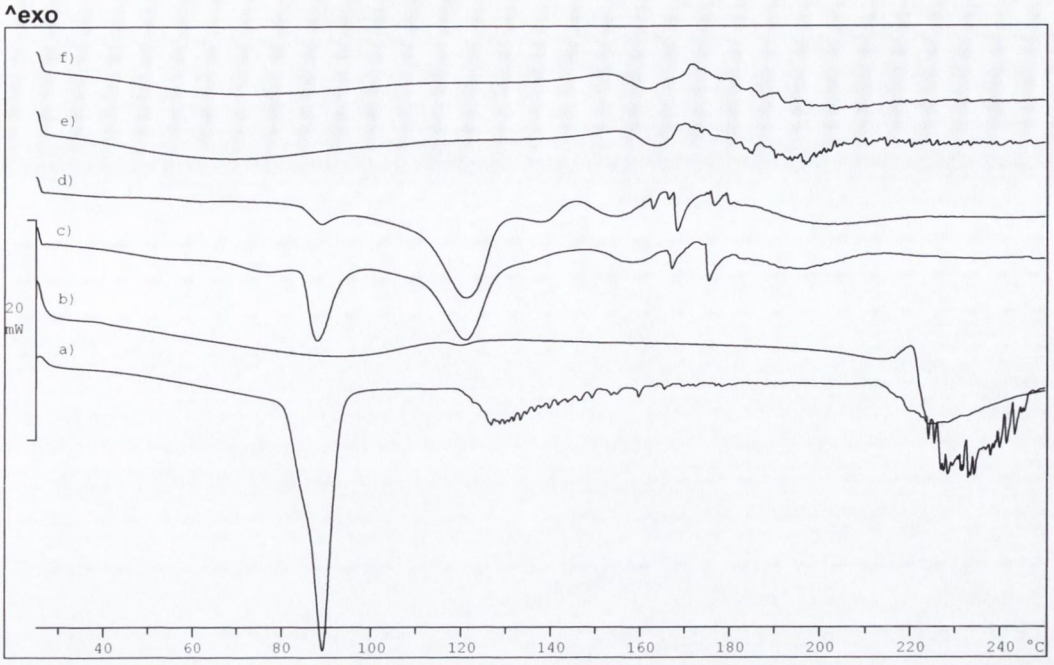

Figure 5.17 DSC scans of (a) unprocessed raffinose pentahydrate, (b) spray dried raffinose pentahydrate, (c) physical mixture of formoterol fumarate dihydrate and raffinose pentahydrate 30% (w/w), (d) physical mixture of formoterol fumarate dihydrate and raffinose pentahydrate 10% (w/w), (e) co-spray dried formoterol fumarate dihydrate and raffinose pentahydrate 30% (w/w) and (f) co-spray dried formoterol fumarate dihydrate and raffinose pentahydrate 10% (w/w).

The physical mixtures were, in turn, crystalline by XRD (Figure 5.18) and in the mixture comprising 10% raffinose two peaks, at 14.2 2θ and 20.6 2θ degrees, were assigned as those from the sugar. The rest of the peaks were of the drug. Since XRD was able to detect the crystalline sugar at this concentration and no peaks were visible in the diffractograms of the processed mixes, it is evidence that both of the constituents in the composites were amorphous. DSC (shown in Figure 5.17) was also capable of detecting the compounds in the equivalent physical mixtures and peaks of sugar dehydration, drug dehydration and drug enantiomers melting endotherms occurred at ~88°C, ~121°C, ~138°C and ~155°C, respectively. No major shifts in the peak positions were noticed. However, one and two extra endotherms were observed to appear at ~60°C as well as at ~53°C and ~76°C for the mechanically mixed formoterol fumarate dihydrate with 10% and 30% of sugar, respectively. This may mean that the presence of the active caused the dehydration of raffinose to occur earlier and in steps.

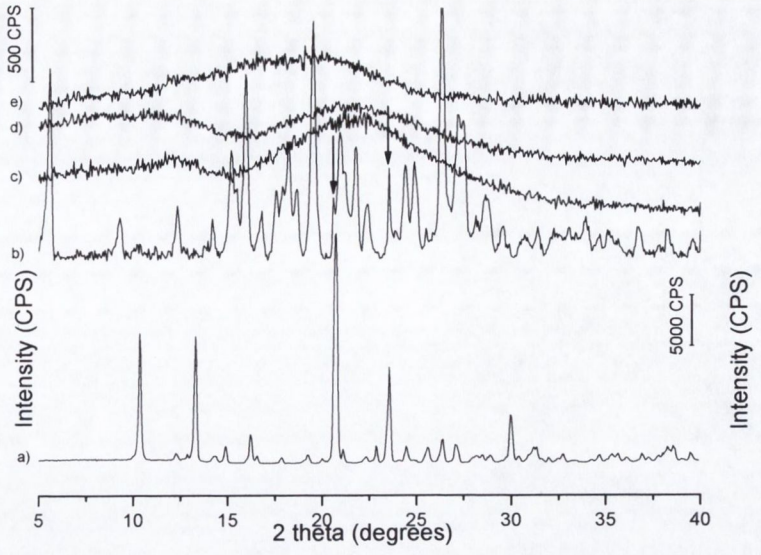

Figure 5.18 XRD diffractograms of (a) raffinose pentahydrate starting material, (b) physical mixture of formoterol fumarate dihydrate and raffinose pentahydrate 10% (w/w), (c) co-spray dried formoterol fumarate dihydrate and raffinose pentahydrate 10% (w/w), (d) co-spray dried formoterol fumarate dihydrate and trehalose dihydrate 30% (w/w) and (e) spray dried raffinose pentahydrate. The arrows indicate peaks of crystalline raffinose pentahydrate. Dotted lines indicate raffinose pentahydrate alone in contrast to its mixtures (solid lines).

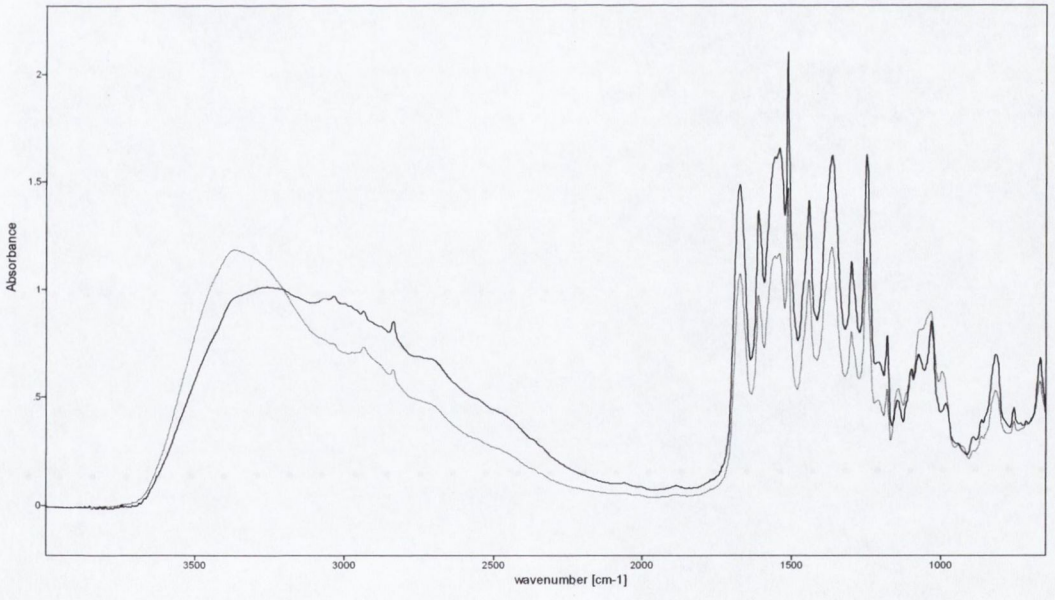

Figure 5.19 FTIR spectra of co-spray dried formoterol fumarate dihydrate and raffinose pentahydrate 10% (w/w) (solid line) and co-spray dried formoterol fumarate dihydrate and raffinose pentahydrate 30% (w/w) (dotted line).

Similarly, as for the trehalose/formoterol fumarate composites, the position of the C=O stretching band of the formamide group of formoterol remains unchanged at 1675 cm^{-1} as seen in Figure 5.19. The raffinose presence was marked in the 900-1200 cm^{-1} region by the glycosidic linkage and C-O-H bending vibration modes (Kacuráková and Mathlouthi, 1996). Some major changes were

detected in the hydrogen bonding region and the broad band at ~3360 cm^{-1} became narrower for the 30% raffinose composite.

Spray drying of formoterol and raffinose mixtures gave spherical and smooth particles as displayed in Figure 5.20 (bottom micrographs), but they were smaller in size than those of spray dried raffinose and their median particle size, as measured using the Sympatec laser diffraction particle sizer, was 2.4 and 2.8 μm for the 10% and 30% raffinose-containing composite, respectively.

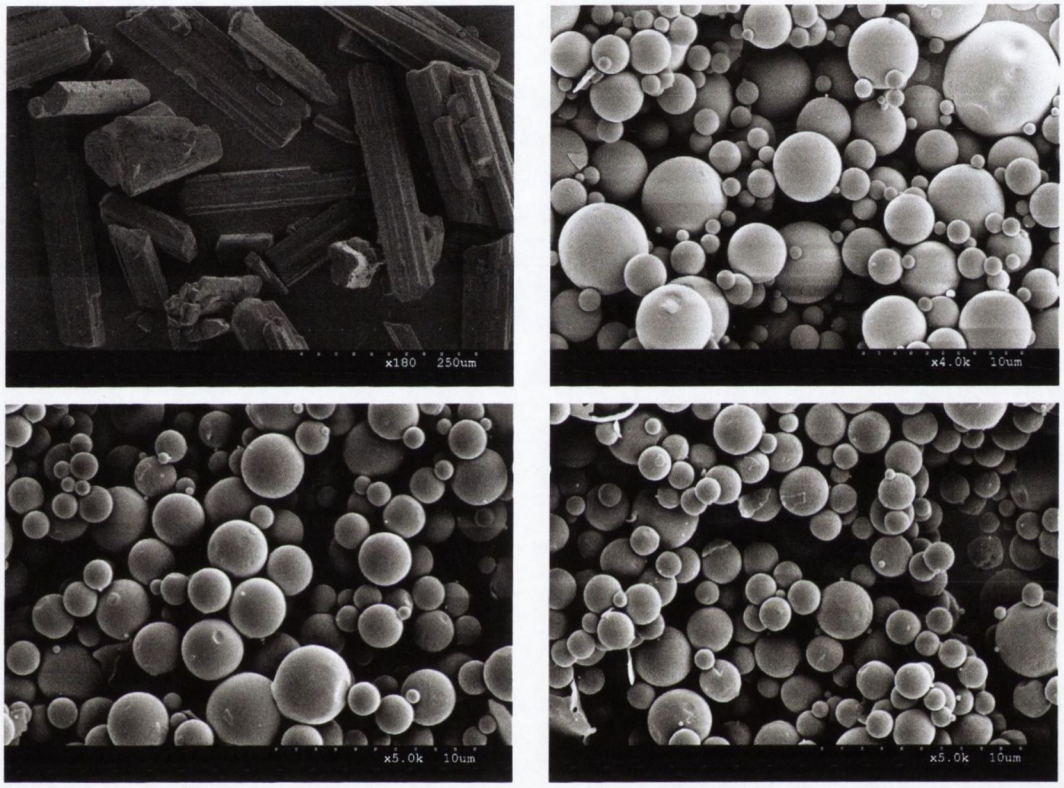

Figure 5.20 SEM micrographs of the raffinose pentahydrate starting material (top left), spray dried raffinose pentahydrate (top right), co-spray dried formoterol fumarate dihydrate and raffinose pentahydrate 10% (w/w) (bottom left) and co-spray dried formoterol fumarate dihydrate and raffinose pentahydrate 30% (w/w) (bottom right). Note the lower magnification of the top micrographs.

5.6 Co-spray dried formoterol fumarate dihydrate and hydroxypropyl-β-cyclodextrin systems

Cyclodextrins may be potential excipients in inhalation powders e.g. to increase drug stability, dissolution rate and bioavailability. They may also be employed to decrease local irritation of an inhaled drug (Kinnarinen *et al.*, 2003). Studies of Cabral Marques *et al.* (1991) on the absorption and pharmacokinetics of β-CD, DM-β-CD and HP-β-CD following intratracheal instillation in rabbits revealed that the absolute bioavailabilities were considerably higher than cyclodextrin absorption following other nonparenteral routes. Wall *et al.* (1994) showed that even a compound which associates strongly with HP-β-CD did not demonstrate reduced rates of pulmonary absorption after administration *in vivo*. The naturally occurring cyclodextrins such as α-CD and β-

CD cause severe nephrotoxicity and are unsafe for parenteral use (Rajewski and Stella, 1996). In vivo toxicity studies on γ-CD have shown that this compound after injection into rats did not significantly increase the blood urea nitrogen and urinary creatinine and additionally there was no change in the rate of haemolysis in the tests on human red blood cells (Srichana *et al.*, 2001). As regards *in vitro* deposition studies, the formulation of a freeze-dried salbutamol-γ-CD complex mixed with lactose carrier was found to have much greater drug delivery to the lower stage of twin stage impinger than the control formulation, prepared by mechanical mixing of micronised salbutamol with carrier (Srichana *et al.*, 2001).

For the investigations in this thesis hydroxypropyl-β-cyclodextrin (HP-β-CYC), a chemically modified β-CD, was chosen due to its low parenteral toxicity (Rajewski and Stella, 1996). Two systems of formoterol fumarate dihydrate with hydroxypropyl-β-cyclodextrin (constituting 10% or 30% by weight of solids) were spray dried from 98% (v/v) ethanol. Spray drying conditions are given in Appendix I.

An amorphous XRD pattern (Figure 5.23) lacking crystalline peaks was observed for the cyclodextrin "as supplied" and no obvious sign of melting was detected by DSC (Figure 5.21). A broad endotherm peaking at ~70°C and a baseline deflection at ~200°C were seen. The peak was ascribed to water desorption as it is known that cyclodextrins can retain water molecules inside the cavities (Giordano *et al.*, 2001). The sample lost approximately 4.8 % of its weight between 25 and 100°C as assessed by TGA. The second thermal event may be attributed either to a T_g or other thermal transformation of HP-β-CYC in the solid state (Giordano *et al.*, 2001).

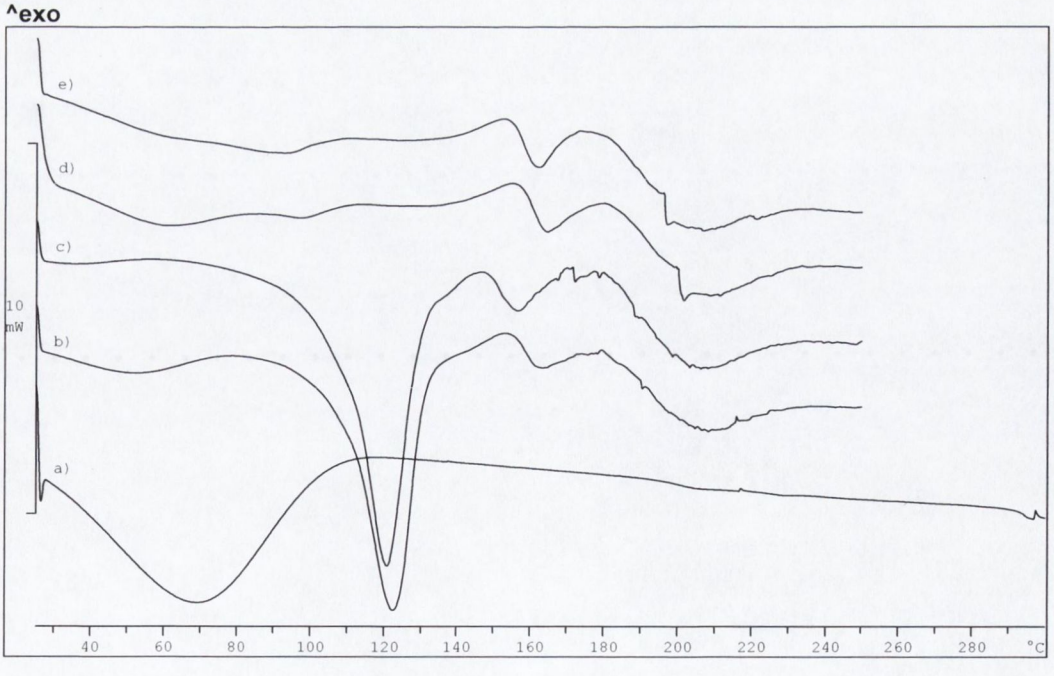

Figure 5.21 DSC scans of (a) unprocessed HP-β-CYC, (b) physical mixture of formoterol fumarate dihydrate and HP-β-CYC 30% (w/w), (c) physical mixture of formoterol fumarate dihydrate and HP-β-CYC 10% (w/w), (d) co-spray dried formoterol fumarate dihydrate and HP-β-CYC 30% (w/w) and (e) co-spray dried formoterol fumarate dihydrate and HP-β-CYC 10% (w/w).

The XRD diffractograms of the physical mixtures (not shown) showed peaks of each of the pure components, but the intensities of these peaks were reduced. The co-spray dried mixtures were, in turn, completely XRD amorphous (Figure 5.23). Figure 5.21 presents DSC traces of the composites. They are nearly identical with the endothermic desolvation peak followed by an exotherm and another endotherm, perhaps of drug melting, peaking at ~163°C. The recrystallisation exotherms differed in the onset temperature, which was at 95°C for the 10% cyclodextrin sample being 95°C and 100°C for the 30% cyclodextrin sample. This trend of shifting in the recrystallisation temperature may suggest antiplasticising properties of cyclodextrin. The traces of the equivalent physical mixtures were dominated by the dehydration endothermic event followed by melting of the drug at ~160°C. No endotherm of the earliest melting enantiomer was found. This may be an evidence of mixing occurring between the different species. For instance, a 1:1 inclusion complex of salbutamol with β-CYC has been shown to exist and the same work presented that the ability of a guest molecule to penetrate the cyclodextrin host is determined by its size, stereochemistry and polarity (Cabral Marques *et al.*, 1990).

To evaluate the possibility of an inclusion complex formation between the active and HP-β-CYC, visualisation software Sculpt 3.0 (MDL) was employed to examine the formoterol and cyclodextrin conformations and obtain approximate dimensions of the molecules. The 3D optimisation algorithm allows the planar (2D) structure from ISIS/Draw to be translated into a realistic 3-dimensional structure. The program utilises a simple molecular mechanics optimisation algorithm. The molecules were optimised until the minimum energy, taking into consideration only van der Waals interactions, was reached. For the sake of simplicity, a molecule of β-CYC instead of HP-β-CYC was constructed as it has been shown that substituted cyclodextrins, such as HP-β-CYC retain the complexing properties of the parent cyclodextrins (Williams and Liu, 1999). Although imprecise, this simple experiment allowed us to visualise that because of the conformation, formoterol is unlikely to form an inclusion complex with HP-β-CYC. The molecule is large, with a distance around 4Å and 4.8Å between the aromatic rings and the oxygens of the aldehyde and hydroxyl moieties attached to one of the phenyl groups, respectively (Figure 5.22, left). The diameter of the void was estimated to be 5.5Å (Figure 5.22, right), which is in fairly good agreement with the literature value of 6.0-6.5Å for β-CYC (Giordano *et al.*, 2001). The formoterol molecule can be regarded as hydrophilic having aldehyde and OH moieties and therefore it may be repulsed by the low polarity interior of the cyclodextrin.

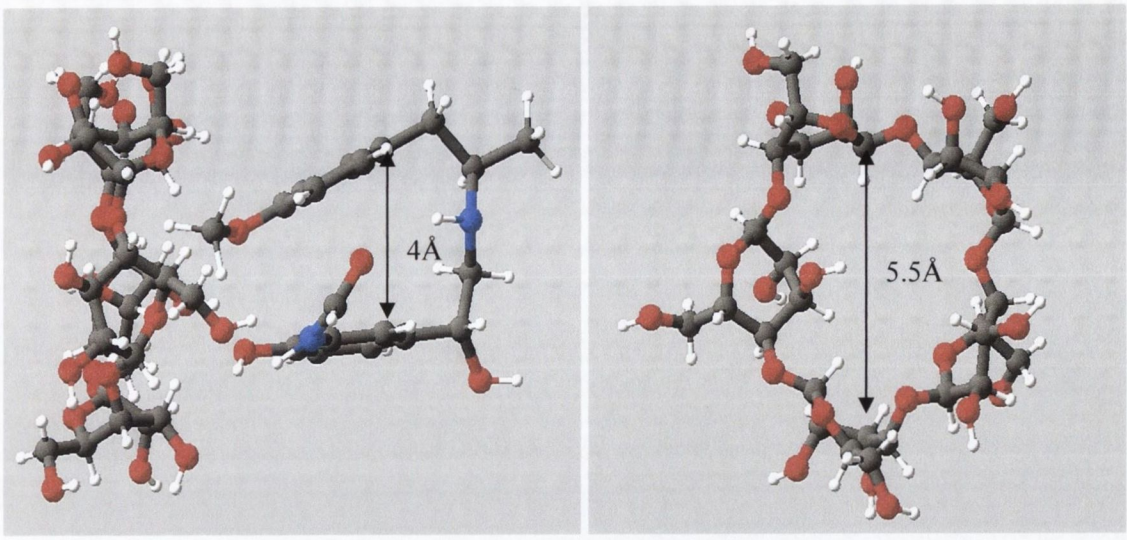

Figure 5.22 Comparison of the sizes of formoterol and β-CYC molecules at minimum van der Waals energy. The left picture presents the side view of the cyclodextrin, the right – face view. The molecule containing blue balls is formoterol. Key: red atoms – oxygen, grey – carbon, blue – nitrogen and white – hydrogen.

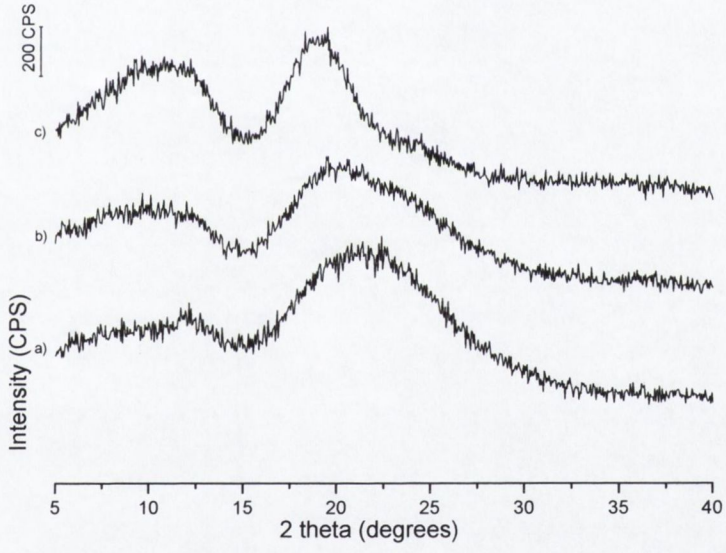

Figure 5.23 XRD diffractograms of (a) co-spray dried formoterol fumarate dihydrate and hydroxypropyl-β-cyclodextrin 10% (w/w) and (b) co-spray dried formoterol fumarate dihydrate and hydroxypropyl-β-cyclodextrin 30% (w/w) and (c) hydroxypropyl-β-cyclodextrin starting material.

Figure 5.24 shows the FTIR spectra of the solid dispersions of formoterol fumarate and HP-β-CYC. The peak position resulting from the absorption band of the carbonyl group of the drug was not altered in the mixtures and appeared at 1657 cm^{-1}, which is exactly the same position as for the drug spray dried alone. The hydrogen bonding region (3000-3600 cm^{-1}) was slightly changed and so were some of the vibration bands occurring between 1000-1200 cm^{-1}, but this originated from overlapping of the cyclodextrin and formoterol fumarate peaks. As a result, the infrared

spectroscopy investigations showed not only the absence of an inclusion complex, but also the lack of any interactions arising between the components at the 10% and 30% cyclodextrin content.

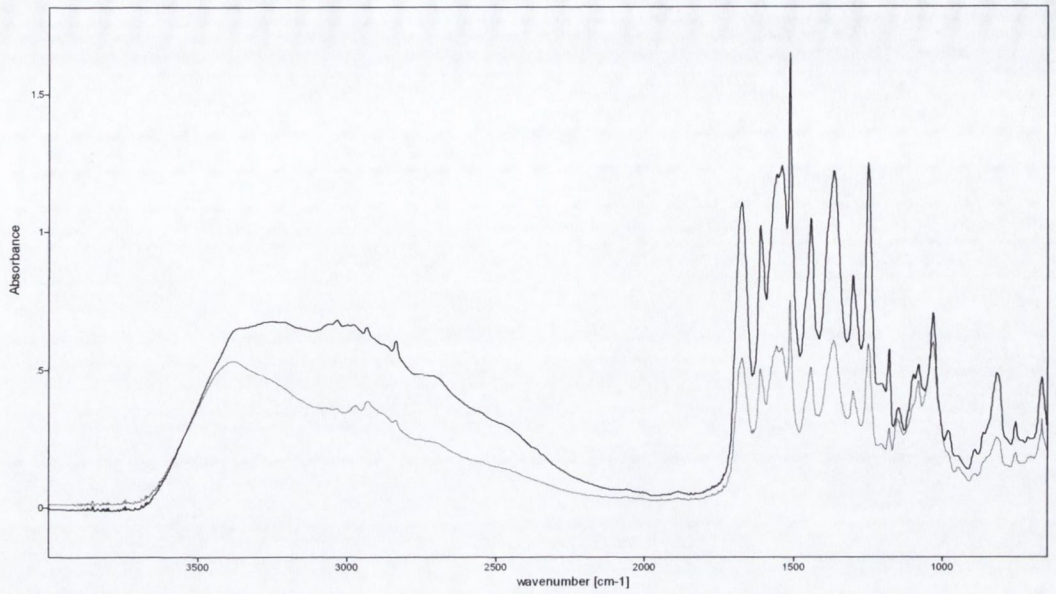

Figure 5.24 FTIR spectra of the co-spray dried formoterol fumarate dihydrate and hydroxypropyl-β-cyclodextrin 10% (w/w) (solid line) and co-spray dried formoterol fumarate dihydrate and hydroxypropyl-β-cyclodextrin 30% (w/w) (dotted line).

The particles of HP-β-CYC were large with signs of surface indentation (Figure 5.25, bottom). The majority of them were hollow. The composite having 10% excipient had small, spherical particles with smooth surfaces (Figure 5.25, top left) and the median size was ~2.6 μm as measured by Sympatec laser diffraction particle sizer. The particles of the co-spray dried 30% cyclodextrin system were not as spherical or uniform in shape as the former sample (Figure 5.25, top right) and the median particle size was 2.3 μm by the same method.

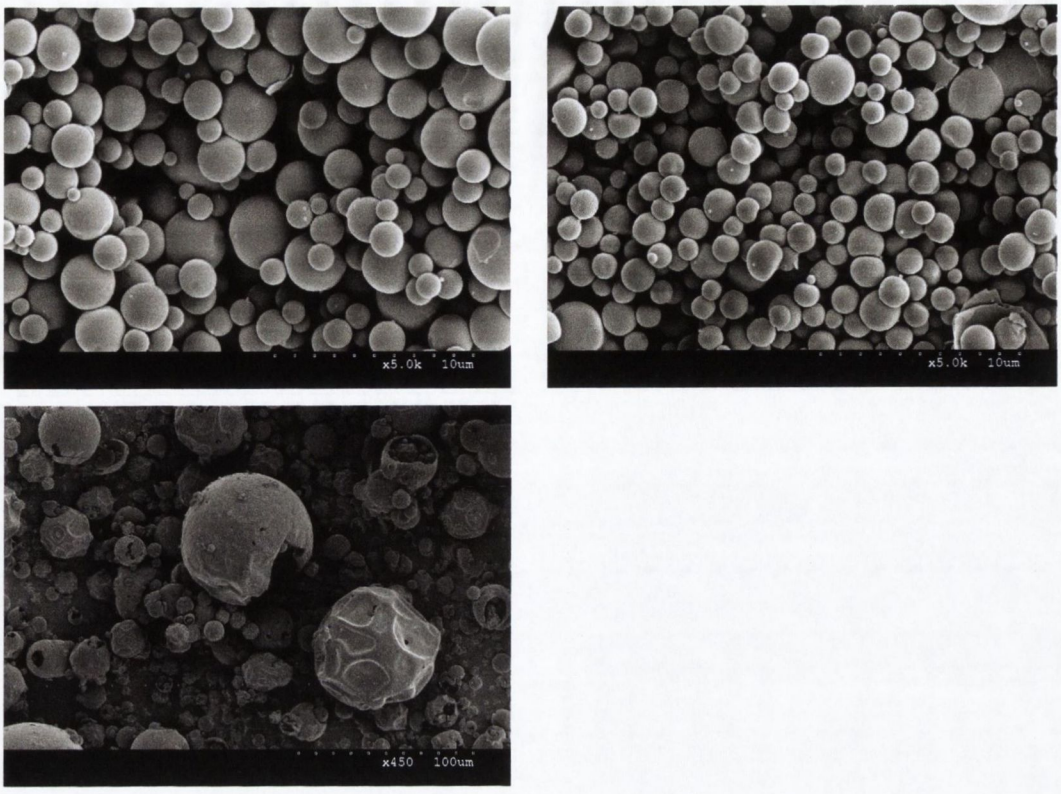

Figure 5.25 SEM micrographs of the co-spray dried formoterol fumarate dihydrate and hydroxypropyl-β-cyclodextrin 10% (w/w) (top left) and co-spray dried formoterol fumarate dihydrate and hydroxypropyl-β-cyclodextrin 30% (w/w) (top right) and hydroxypropyl-β-cyclodextrin starting material (bottom). Note the lower magnification of the bottom micrograph.

5.7 Co-spray dried formoterol fumarate dihydrate and Brij 58 systems

Brij 58 is polyoxyethylene palmityl ether, a non-ionic surfactant. Brij compounds may be used as emulsifying, solubilising and lubricant additives in pharmaceutical formulations. For instance Sjökvist *et al.* (1992), by the introduction of small quantities of Brij 35 into a 10% (w/w) dispersion of griseofulvin in PEG 3000, a substantial increase in both rate and extent of dissolution was achieved. Williams and Liu (1998) attempted to utilise Brij 97 and 98 in the production of co-lyophilised bovine serum albumine systems intended for use in pressurised metered dose inhalers. The similarity of Brij 58 to PEG compounds regarding the chemical structure and additionally the solid state properties at room temperature renders it a potentially useful excipient which may be used in the spray drying procedure to obtain solid dispersions for DPIs.

Two systems of formoterol fumarate dihydrate with Brij 58 (constituting 0.5% or 2% by weight of solids) were spray dried from 98% (v/v) ethanol. Spray drying conditions are given in Appendix I.

No traces of Brij 58 were detected by XRD in the equivalent physical mixtures. Figure 5.26 presents the diffractogram of the formoterol fumarate dihydrate/Brij 58 2%, but all the peaks were of the drug. The excipient content was too low to be measured by XRD even at the 2% level. And it

cannot be determined whether both of the substances were converted into amorphous phases or not. The composites were amorphous, though, as confirmed by broad "halos" on the diffractograms.

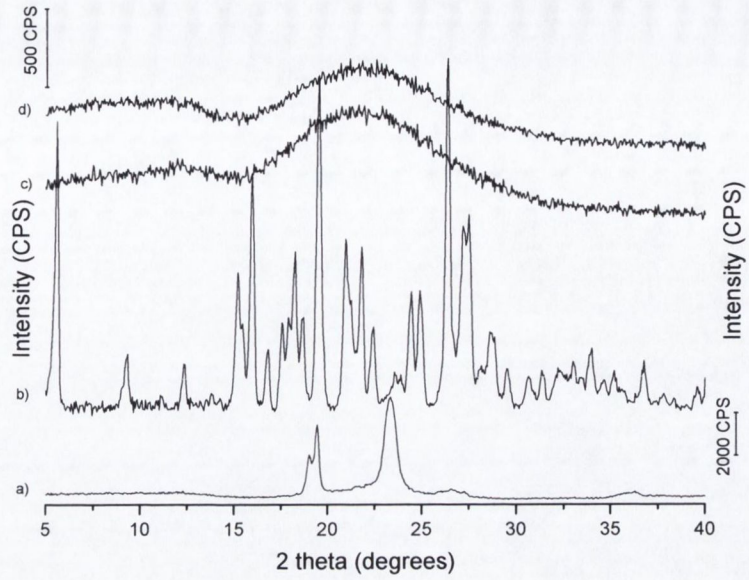

Figure 5.26 XRD diffractograms of (a) Brij 58 starting material, (b) physical mixture of formoterol fumarate dihydrate and Brij 58 2% (w/w), (c) co-spray dried formoterol fumarate dihydrate and Brij 58 0.5% (w/w) and (d) co-spray dried formoterol fumarate dihydrate and Brij 58 2% (w/w). The scale of the left hand side applies to the curve (a) and scale of the right hand side applies to curves (b), (c) and (d).

DSC was a more sensitive tool in exposing Brij 58 in the mechanical mixtures and a small endothermic peak (visible at a higher magnification) appeared at ~40°C on the traces regardless of the excipient content. The DSC thermograms are shown in Figure 5.27. Pure Brij 58 melted at ~44°C. As usual, the dehydration peak of formoterol fumarate together with melting of the enantiomer at ~141°C was recorded as well. Irregular peaks evidencing thermal decomposition arose above ~150°C, overlapping with melting of the second enantiomer.

Both of the composites exhibited a recrystallisation exotherm peaking at ~105°C and ~97°C for the 0.5% and 2% Brij 58 level, respectively. Also formoterol fumarate melting apparent on the scans was shifted to lower temperatures and peaked at 159°C and 157°C for the 0.5% and 2% surfactant-containing samples, respectively. This alteration in the recrystallisation and melting processes can be related to plasticising properties of Brij 58, which was the opposite of the effect which cyclodextrin had on the amorphous formoterol fumarate.

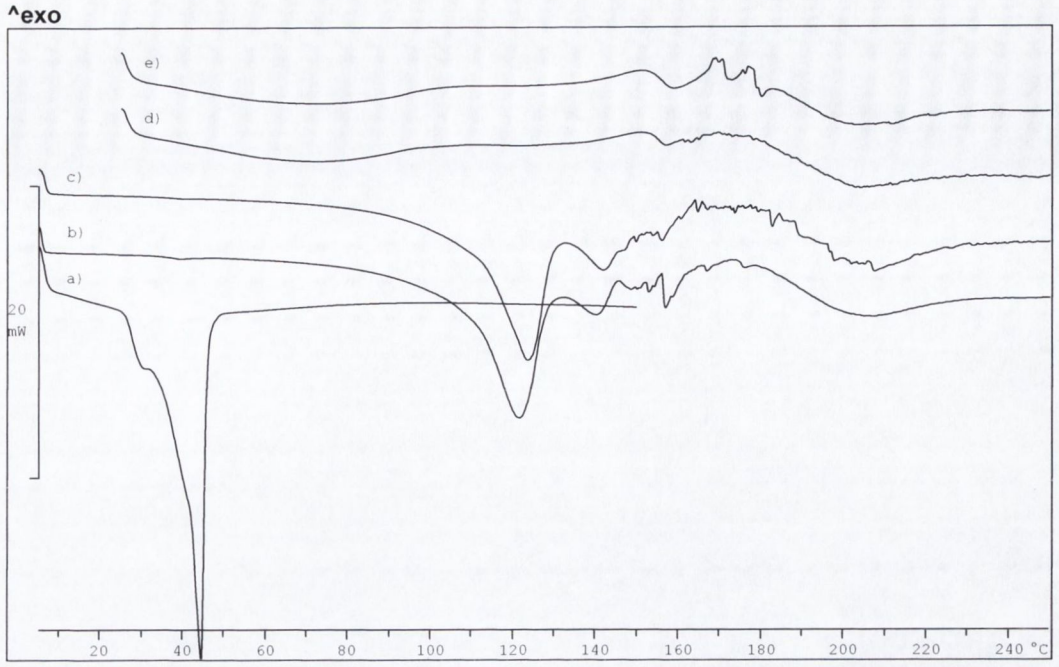

Figure 5.27 DSC scans of (a) unprocessed Brij 58, (b) physical mixture of formoterol fumarate dihydrate and Brij 58 2% (w/w), (c) physical mixture of formoterol fumarate dihydrate and Brij 58 0.5% (w/w), (d) co-spray dried formoterol fumarate dihydrate and Brij 58 2% (w/w) and (e) co-spray dried formoterol fumarate dihydrate and Brij 58 0.5% (w/w).

Infrared spectra of the co-spray dried systems are not shown, but were identical to that of amorphous formoterol fumarate and no band shifts were found except for a broad peak located initially at 3211 cm^{-1} for the processed drug, which moved to 3203 cm^{-1} and 3205 cm^{-1} for the sample containing 0.5% and 2% Brij 58, respectively. This was the only manifestation of Brij 58 presence in the mixtures.

The co-spray dried formoterol fumarate/Brij 58 0.5% system was composed of small, spherical particles with some of them fused by bridges formed between the surfaces (Figure 5.28). The particles of the sample having 2% Brij 58 appeared to be smaller but more aggregated due to the greater surfactant content. The laser diffraction particle size analysis by Sympatec reflected this behaviour in the greater median size of the particles of the 2% Brij composite being 3 μm in contrast to the 0.5% surfactant content system having 2.6 μm.

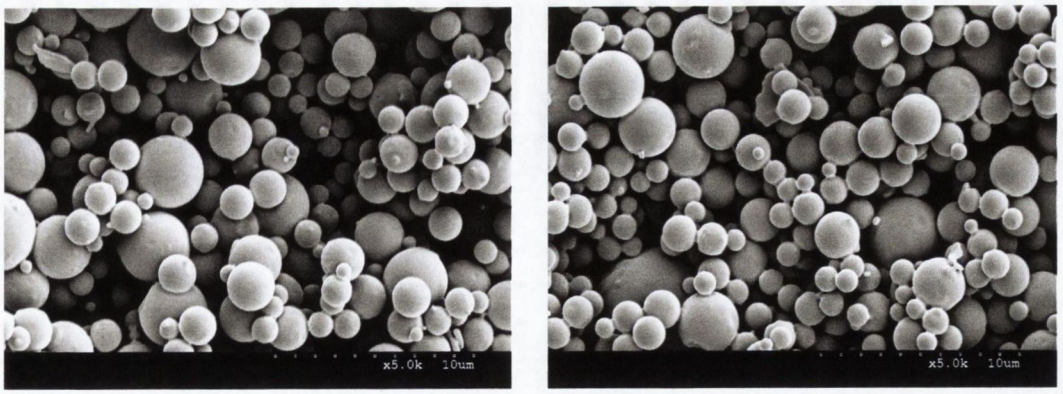

Figure 5.28 SEM micrographs of the co-spray dried formoterol fumarate dihydrate and Brij 58 0.5% (w/w) (left) and co-spray dried formoterol fumarate dihydrate and Brij 58 2% (w/w) (right).

5.8 Co-spray dried formoterol fumarate dihydrate and Myrj 59 systems

Myrj 59 is polyoxyethylene stearate ester, a non-ionic surfactant, similar to Brij 58. It is based on a long chain containing 100 polyoxyethylene units compared to only 20 for Brij 58. Its use in pharmaceutical formulations is analogous to Brijs. Ahmed (2001) reported that Myrj surfactants were successful in increasing the apparent solubility of meclizine.

Two systems of formoterol fumarate dihydrate with Myrj 59 (constituting 0.5% or 2% by weight of solids) were spray dried from 98% (v/v) ethanol. Spray drying conditions are given in Appendix I.

Spray drying of the formoterol fumarate dihydrate with Myrj 59 rendered the mixtures amorphous as shown on the XRD diffractograms in Figure 5.29. Like the Brij systems, XRD was unable to detect the surfactant at such low levels and no peaks of Myrj 59 were found in the equivalent physical mixtures. The surfactant itself was crystalline as presented in Figure 5.29.

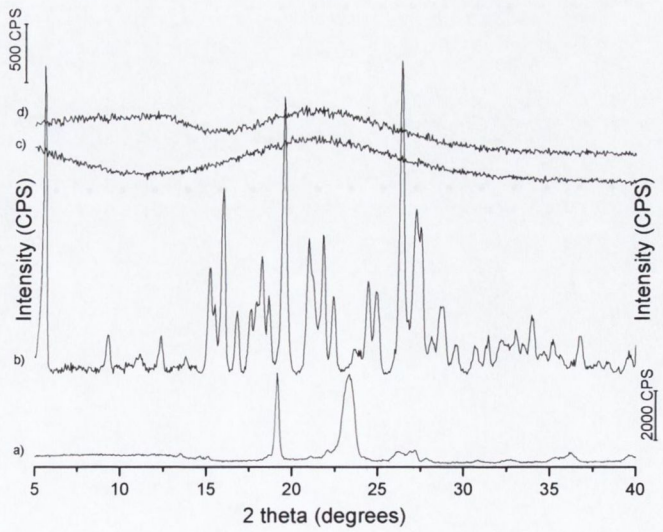

Figure 5.29 XRD diffractograms of (a) Myrj 59 starting material, (b) physical mixture of formoterol fumarate dihydrate and Myrj 59 2% (w/w), (c) co-spray dried formoterol fumarate dihydrate and Myrj 59 0.5% (w/w) and (d) co-spray dried formoterol fumarate dihydrate and Myrj 59 2% (w/w). The scale of the left hand side applies to the curve (a) and scale of the right hand side applies to the curves (b), (c) and (d).

DSC scans (Figure 5.30) of the unprocessed mixtures demonstrated peaks of both of the constituents, with Myrj 59 melting first at ~55°C. The remaining endotherms were of dehydration and melting of the drug with melting of the second enantiomer overlapped by thermal decomposition peaks. Pure surfactant had only one endotherm of melting at ~57°C.

The composites displayed broad desolvation endotherms peaking at ~70°C and, as substantiated by TGA, corresponding to 3.7% and 3.3% weight losses in the 25-100°C region for the 0.5% and 2% Myrj 59-containg sample, respectively. The next thermal event occurring on the DSC traces was the recrystallisation exotherm peaking at ~105°C and ~104°C followed by the drug melting process at ~159°C and ~158°C for the 0.5% and 2% Myrj 59 content, respectively. By decreasing the temperature of the recrystallisation and melting processes, Myrj 59 appears to possess plasticising properties, like Brij 58.

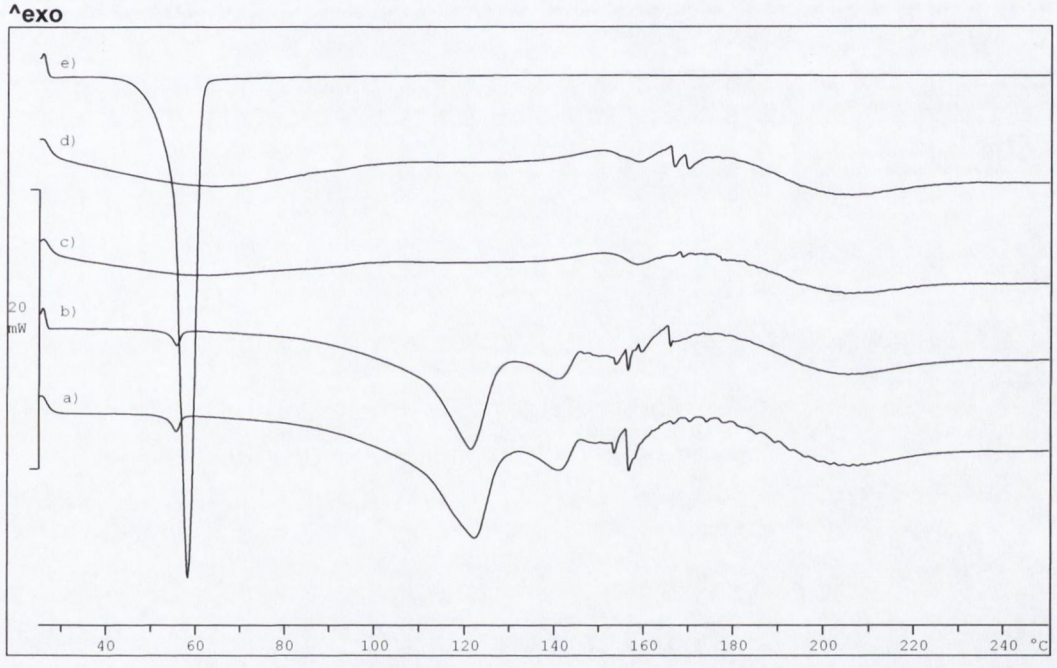

Figure 5.30 DSC scans of (a) physical mixture of formoterol fumarate dihydrate and Myrj 59 2% (w/w), (b) physical mixture of formoterol fumarate dihydrate and Myrj 59 0.5% (w/w), (c) co-spray dried formoterol fumarate dihydrate and Myrj 59 2% (w/w), (d) co-spray dried formoterol fumarate dihydrate and Myrj 59 0.5% (w/w) and (e) unprocessed Myrj 59.

Infrared analysis, similarly to XRD, failed to detect any traces of Myrj 59 manifesting as vibration bands in the fingerprint region. The scans were superimposable with that of spray dried formoterol fumarate dihydrate alone and only small modifications of the band at 3211 cm^{-1} were seen. For the 0.5% Myrj 59 composite the peak appeared at 3204 cm^{-1} and for the 2% surfactant sample the band was shifted even more and occurred at 3199 cm^{-1}. The spectra are not shown.

SEM micrographs presented in Figure 5.31 demonstrate morphology of the co-spray dried composites. Small, spherical particles can be observed and some of them were merged into

agglomerates by interparticulate bridges. The median particle size was determined by the Sympatec particle sizer and was 2.5 μm and 2.7 μm for the 0.5% and 2% Myrj 59 content, respectively.

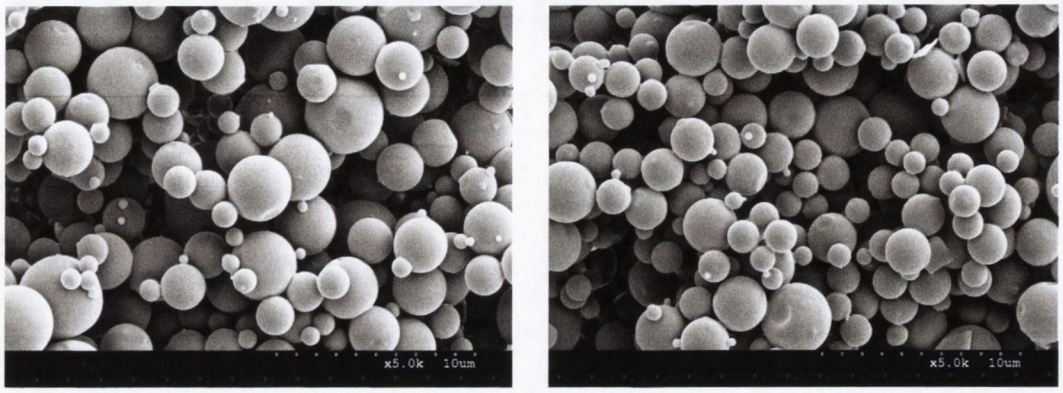

Figure 5.31 SEM micrographs of the co-spray dried formoterol fumarate dihydrate and Myrj 59 0.5% (w/w) (left) and co-spray dried formoterol fumarate dihydrate and Myrj 59 2% (w/w) (right).

5.9 *In vitro* respirable fractions assessment by twin stage impinger

The twin impinger analysis was done in triplicate for each sample. For comparison purposes the same analysis was performed for formoterol fumarate spray dried material and the drug was taken straight from the container. For these samples twin impinger analysis was carried out 5 times for each sample. The results of twin impinger analysis are presented in Figure 5.32.

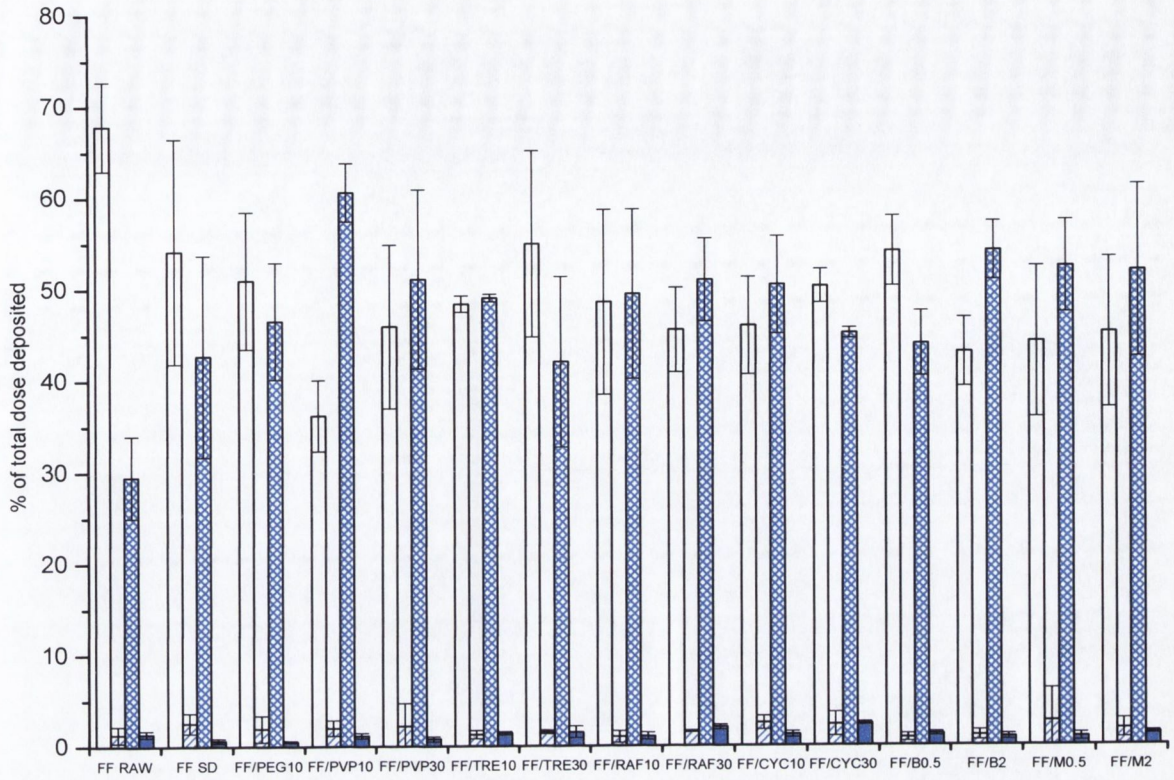

Figure 5.32 Twin impinger analysis of the unprocessed and spray dried formoterol fumarate dihydrate as well as co-spray dried formoterol fumarate dihydrate/excipient samples. The white, blue diagonal, blue grid and full blue filled bars indicate the percentage retained in the capsule and device, mouthpiece, stage 1 and stage 2 on the twin stage impinger, respectively. Key – RAW – unprocessed, SD – spray dried, FF – formoterol fumarate, TRE – trehalose, RAF – raffinose, CYC – HP-β-CYC, B – Brij 58 and M – Myrj 59. The number indicates the percentage content of the excipient.

Figure 5.32 indicates that the percentage of the non-respirable dose is very high, however there is a difference in the ratio of dose retained in the device to that deposited in the upper stage of the impinger. The greatest ratio is for formoterol fumarate dihydrate raw material and is 2.3 (67.82% device/29.52% stage I) and the lowest is for co-spray dried formoterol fumarate dihydrate/PVP 10% and is 0.6 (36.21% device/60.59% stage I). To investigate the emitted doses further, a statistical analysis using ANOVA with Tukey's pairwise comparison was carried out to assess if processing had any impact on the emission of the particles. Emitted dose was defined as the total quantity of drug recovered from upper and lower stages of the impinger and expressed as a percent of the total dose loaded into the capsule. Table 5.1 shows the statistical data contrasting the percent of emitted doses acquired with the crystalline formoterol fumarate dihydrate and the spray dried drug as well as co-spray dried composites.

Table 5.1 ANOVA comparing the emitted fractions of the unprocessed and spray dried formoterol fumarate dihydrate as well as co-spray dried formoterol fumarate dihydrate/excipient samples. Key – as Figure 5.32.

				Individual 95% Confidential Intervals For Mean Based on Pooled StDev
Level	N	Mean	StDev	----+---------+---------+---------+--
FF RAW	5	32.178	4.877	(---*----)
FF SD	5	45.840	12.289	(----*---)
FF/PEG10	3	49.030	7.466	(-----*----)
FF/PVP10	3	63.787	3.869	(-----*----)
FF/PVP30	3	54.097	8.922	(-----*-----)
FF/TRE10	3	51.660	0.894	(----*-----)
FF/TRE30	3	45.083	10.160	(-----*-----)
FF/RAF10	3	51.473	10.091	(----*-----)
FF/RAF30	3	54.507	4.604	(----*-----)
FF/CYC10	3	54.090	5.308	(-----*-----)
FF/CYC30	3	49.790	1.843	(-----*-----)
FF/BR0.5	3	45.990	3.815	(-----*----)
FF/BR2	3	56.027	3.782	(----*-----)
FF/MR0.5	3	55.887	8.225	(-----*-----)
FF/MR2	3	54.900	8.211	(-----*----)
				----+---------+---------+---------+--
Pooled StDev =		7.366		30 45 60 75

Processing by spray drying improved significantly the emitted fraction in all cases comparing the means and the co-spray dried formoterol with PVP 10000 at 10% level emptied the best. Tukey's comparison analysis revealed that 10% and 30% PVP, 10% raffinose, 30% HP-β-CYC, 2% Brij as well as 0.5% and 2% Myrj 59 were considerably better than micronised, crystalline formoterol fumarate dihydrate (significant at 0.05 level). There was no dissimilarity among the spray dried samples including processed formoterol fumarate. In the case of the Myrj surfactant even 0.5% of the additive was able to improve the released dose, when compared with that of the crystalline drug, in such noticeable manner.

Figure 5.33 shows the percentage of dose deposited in stage 2 of the twin impinger i.e. respirable fractions.

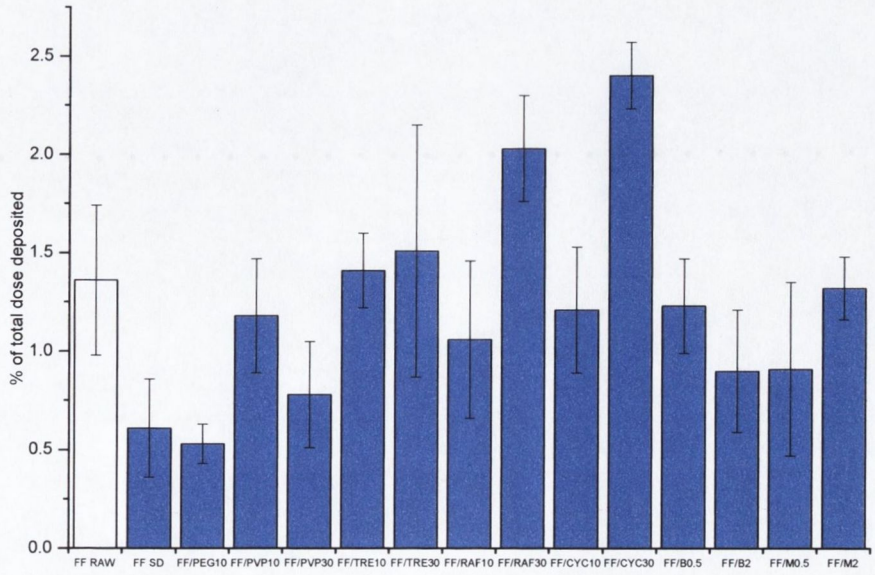

Figure 5.33 The respirable fractions (i.e. deposited on stage 2 of twin impinger) of the unprocessed and spray dried formoterol fumarate dihydrate as well as co-spray dried formoterol fumarate dihydrate/excipient samples. Key – as Figure 5.32.

In order to compare the respirable fractions and find any important differences between them, an analysis of variance ANOVA was carried out. Table 5.2 presents the output from Minitab™ software.

Table 5.2 ANOVA comparing the respirable fractions of the unprocessed and spray dried formoterol fumarate dihydrate as well as co-spray dried formoterol fumarate dihydrate/excipient samples. Key – as Figure 5.32.

				Individual 95% Confidential Intervals For Mean Based on Pooled StDev
Level	N	Mean	StDev	---------+---------+---------+-------
FF RAW	5	1.3580	0.3797	(---*---)
FF SD	5	0.6100	0.2503	(---*--)
FF/PEG10	3	0.5300	0.0985	(----*---)
FF/PVP10	3	1.1767	0.2950	(----*---)
FF/PVP30	3	0.7733	0.2730	(----*---)
FF/TRE10	3	1.4067	0.1850	(----*---)
FF/TRE30	3	1.5067	0.6422	(----*----)
FF/RAF10	3	1.0633	0.4000	(---*----)
FF/RAF30	3	2.0300	0.2762	(---*----)
FF/CYC10	3	1.2033	0.3182	(----*----)
FF/CYC30	3	2.4033	0.1665	(----*----)
FF/B0.5	3	1.2300	0.2364	(---*----)
FF/B2	3	0.9033	0.3017	(---*----)
FF/M0.5	3	0.9133	0.4400	(---*----)
FF/M2	3	1.3233	0.1570	(----*---)
				---------+---------+---------+-------
Pooled StDev =		0.3219		0.80 1.60 2.40

A significant difference was found between the respirable fractions of unprocessed formoterol fumarate dihydrate and the spray dried counterpart, with the unprocessed sample showing a greater respirable fraction. The sample with the best deposition on stage 2 of twin impinger was co-spray dried formoterol fumarate dihydrate and HP-β-CYC at 30% level. The fraction of this sample on stage 2 of the impinger was significantly greater than that of formoterol fumarate dihydrate raw material indicated in the ANOVA by the non-overlapping confidence intervals. The improvement in the respirable fraction in DPIs using the spray drying of a drug with different types of cyclodextrins has been reported earlier in this chapter and has also been found elsewhere (Ramalhete *et al.*, 2002). ANOVA revealed also a significant difference between co-spray dried formoterol fumarate dihydrate/HP-β-cyclodextrin 10% and the sample with HP-β-cyclodextrin content 30% as well as co-spray dried formoterol fumarate dihydrate/raffinose 10% and the system with 30% raffinose.

An attempt has been made to find a correlation between either emitted dose or the fraction deposited in the stage 2 of twin impinger and the median particle size. Figure 5.34 shows the results and there was no obvious relationship between the particle size and respirable fraction, indicating that differences in respirable fractions obtained with these powders were due to other factors. In contrast to this, a good correlation was discovered between the fraction released from the device and the median particle size of the powered being aerosolised, with larger particles

giving better device emptying. It would indicate that the particle diameter had a significant impact, at least partly, on the ability to separate from the rest of the particles in the capsule. As the smaller particles disperse less well, the trend may suggest a large contribution of adhesive and cohesive forces preventing the satisfactory dispersibility of the formoterol fumarate powders. Large static effects were also blamed for the poor respirable fractions of the co-spray dried budesonide/formoterol fumarate systems, as presented in Chapter 4.

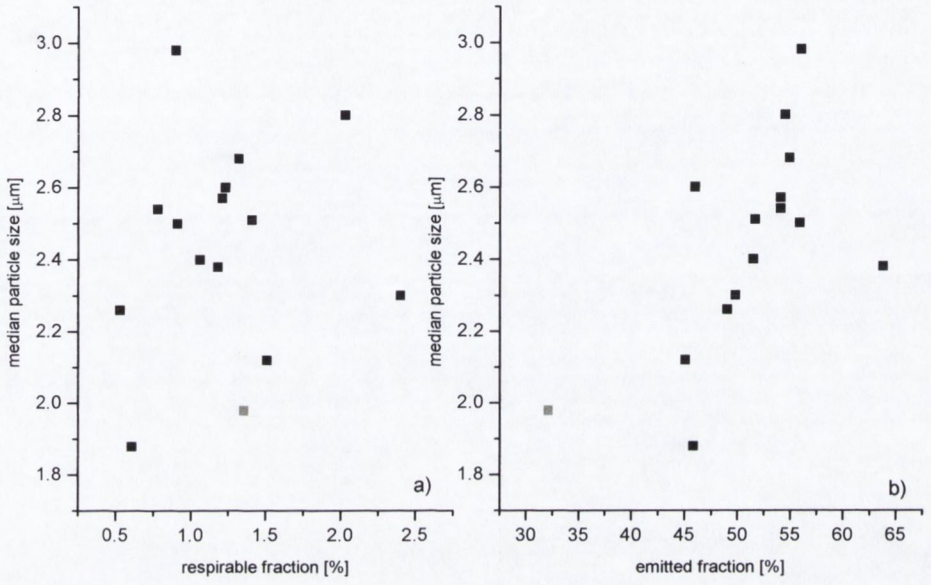

Figure 5.34 Correlation between the median particle size of the unprocessed and spray dried formoterol fumarate dihydrate as well as co-spray dried formoterol fumarate dihydrate/excipient samples and (a) respirable fraction (b) emitted fraction. The grey square indicates unprocessed formoterol fumarate dihydrate.

5.10 Conclusions

Co-spray drying of formoterol fumarate dihydrate with various polymers, sugars and surfactants resulted in XRD amorphous systems, except for the drug/PEG 20000 30% sample, which was predominantly amorphous with weak peaks of the crystalline polymer. PEG 20000 when processed alone gave material with a reduced degree of crystallinity by at least 10%. The formation of an amorphous phase of the polymer was observed by DSC, XRD and FTIR and these methods were employed to estimate the level of crystallinity of the powder.

All entirely amorphous systems exhibited a weak and broad recrystallisation exotherm, the peak temperature of which depended on the excipient used. The highest temperature exotherm was measured for the co-processed formoterol fumarate dihydrate with 30% raffinose pentahydrate. Unfortunately, no T_gs were detected as they were overlapped with the diffused endotherms of the residual solvent liberation.

Specific drug-carrier interactions were established using the FTIR analysis in the co-spray dried systems with PEG 20000 and PVP 10000, although the way in which the formamide group of

formoterol interacted with each of them was different. A hypsochromic effect (a shift to higher wavenumbers) was observed when the drug was co-processed with PEG, but the exact opposite shift was noticed for the PVP solid dispersions. The former phenomenon indicates wakening of the intermolecular hydrogen bondings, caused by the introduction of the long chains of PEG. Moreover, each PEG molecule has only two OH groups available for hydrogen bonding.

The bathochromic shift created by PVP signifies strengthening of the hydrogen bonds as probably new bonds were formed by the interacting molecules of formoterol and the polymer units. Both the formamide group and PVP subunit possess hydrogen bonding donor-acceptor moieties, therefore it is not clear which of them contributes to the interaction. Hydrogen bonded association may shift all of the absorptions. The most often examined interactions of PVP in solid dispersions arise from the carbonyl group of the polymer (Taylor and Zografi, 1997; Taylor and Zografi, 1998a; Weuts *et al.*, 2004). No interactions were detected for the rest of the excipients used in co-spray drying, at least at the concentrations investigated.

The spray drying procedure converted the mixtures into powdered systems consisting of particles suitable for administered to the lungs, because the median particle size of the samples varied from 2.1 to 3.0 μm. For this reason, to assess the aerolisation properties, the *in vitro* twin stage impinger studies were carried out and revealed that the sample with the best deposition on stage 2 of twin impinger, i.e respirable fraction, was co-spray dried formoterol fumarate dihydrate and HP-β-CYC at 30% level. As regards the emitted dose, the best performance was discerned for the processed mixture of formoterol fumarate dihydrate and PVP 10000 10%, which was superior to both the commercial powder and spray dried drug alone. The other co-processed dispersions markedly eased emptying from the capsule and device. A good correlation was established between the fraction released from the device and the median particle size of the powered being aerosolised with larger particles giving better emitted fractions.

CO-SPRAY DRIED BUDESONIDE/EXCIPIENT(S) SYSTEMS FOR USE IN DPIs

6.1 Introduction

As already signalled in Chapter 4, budesonide exhibits strong electrostatic surface charge, which greatly diminishes the respirable fractions obtained from dry powder inhalers. Particle agglomeration in pharmaceutical powders has led to problems in attaining satisfactory drug content uniformity and, in dry powder inhalers, to an unwanted decrease in respirable fraction. Electrostatic forces have been identified as playing a major role in cohesion/adhesion processes. Triboelectrification or contact charging has been shown to be influenced by several factors including particle size and shape, contact area, surface purity and atmospheric conditions (Carter *et al.*, 1992; Rowley, 2001).

Previous investigations (Cassidy *et al.*, 1996) indicated that the electrostatic charging tendency of particulate systems could be altered by modifying the surface of the particles. Ilari and Graindorge (2001) found that the addition of a glidant or surfactant to casein and dry egg powder could neutralize the surface charge. European patent application number 0239798A1 (Chiesi and Pavesi, 1987) discloses the use of a suitable lubricant such as sodium benzoate, magnesium stearate, colloidal silica etc. in inhalable conglomerates prepared by a granulation technique. The improvement of emitted doses of formoterol fumarate by the inclusion of a low level of a surfactant such as Brij 58 or Myrj 59 was shown in Chapter 5.

In the light of the above information it seemed that spray drying of budesonide with glidants or lubricants might improve the fraction of inhalable particles. A range of excipients was selected including stearic acid, ascorbyl palmitate, Aerosil 200 Pharma as a commercial product of colloidal silica, microcrystalline cellulose and magnesium stearate. Due to polymorphic properties of the latter, a comparison of three different products available was carried out.

In addition to co-spray drying with lubricant or glidant compounds, trials in processing budesonide with either raffinose or hydroxypropyl-β-cyclodextrin were undertaken owing to the enhancement in respirable fractions which was observed when formoterol fumarate was co-spray dried with any of these excipients as presented in Chapter 5.

6.2 Co-spray dried budesonide and raffinose pentahydrate 30% system

On the basis of the studies on formoterol fumarate/excipient systems described in Chapter 5, raffinose pentahydrate at the 30% level was chosen for the spray drying experiments with budesonide. The sample was spray dried as a solution from 70% (v/v) ethanol, where raffinose pentahydrate constituted 30% by weight of solids. This ethanol concentration used was due to the low ethanolic solubility of the sugar. Spray drying conditions are given in Appendix I.

The DSC thermogram of the co-spray dried budesonide and raffinose pentahydrate 30% is shown in Figure 6.1. The broad endothermic peak observed at ~60°C is attributed to liberation of the residual solvents remaining after spray drying. TG analysis showed ~2.6% weight loss in the 25-100°C region. This endotherm is followed by a deflection in the baseline at 91.5°C indicating perhaps the T_g of the mixture. The T_gs of amorphous budesonide and raffinose were determined to be ~89.5°C (see Chapter 4) and ~118°C (see Chapter 5), respectively. The T_g of the co-spray dried sample observed here is an intermediate value of both of the T_gs of the individual components suggesting their miscibility in the amorphous state. A double exotherm can also be seen beginning at ~108°C and having two maxima, at ~113°C and ~123°C. The origin of the peak splitting is not clear but it may suggest the formation of two phases, one containing an amorphous budesonide/raffinose complex and the second – amorphous budesonide. The picture is more complicated by the fact that double exotherms were also observed for one component systems - spray dried salbutamol base (Chapter 3). Another endotherm was seen in the DSC trace (Figure 6.1) beginning at ~211°C and a similar event was observed for crystalline and spray dried raffinose (Chapter 5) and ascribed to thermal decomposition. The endotherm was accompanied by an abrupt weight loss as observed on the TGA curve of the composite. The last event in the DSC was also an endotherm, peaking at ~256°C and linked to melting of budesonide. Its appearance at a lower temperature compared to that of spray dried budesonide (at ~262°C) may be indicative of mixing of the constituents.

The equivalent physical blend of raffinose pentahydrate with budesonide showed the DSC trace due to both crystalline components. The first endotherm was of raffinose dehydration and its peak temperature was the same as of the crystalline sugar on its own (Chapter 5), and two remaining endothermic peaks at ~225°C and ~260°C were of thermal decomposition and budesonide melting, respectively.

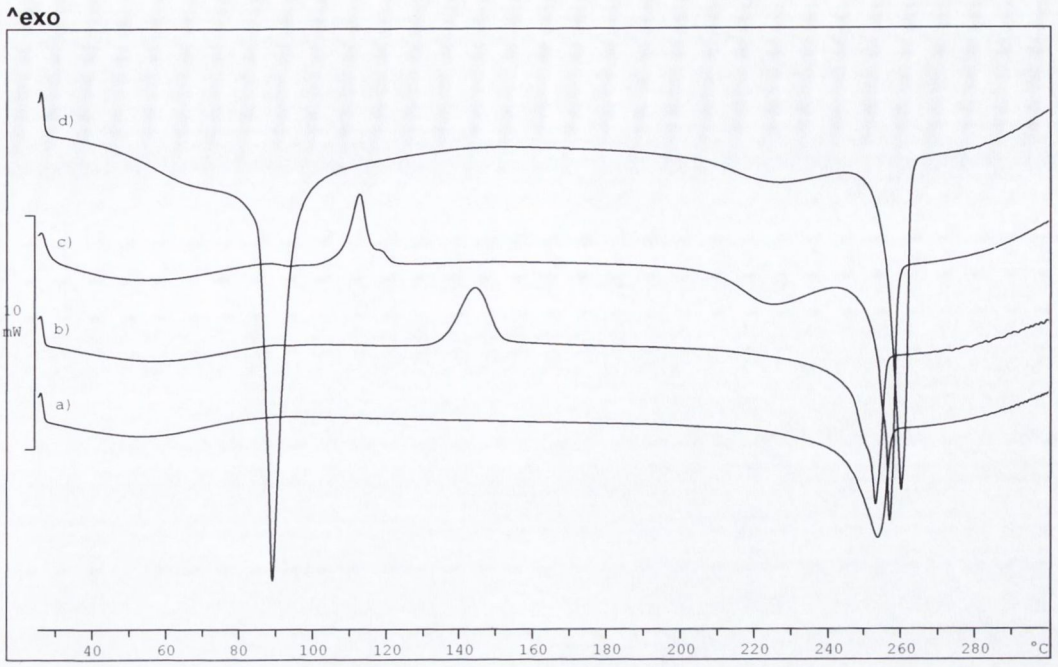

Figure 6.1 DSC scans of (a) physical mixture of budesonide and HP-β-cyclodextrin 30%, (b) co-spray dried budesonide/HP-β-cyclodextrin 30%, (c) co-spray dried budesonide with 30% raffinose pentahydrate and (d) physical mixture of budesonide with 30% raffinose pentahydrate.

X-ray diffraction analysis, shown in Figure 6.2, confirmed the amorphous nature of the co-spray dried composite.

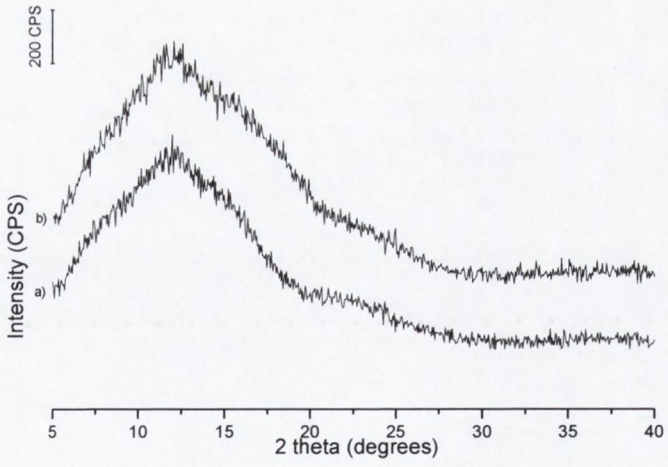

Figure 6.2 XRD diffractograms of (a) co-spray dried budesonide with 30% raffinose pentahydrate, (b) co-spray dried budesonide/HP-β-cyclodextrin 30%.

The particles of the system were generally spherical with rough surfaces. Some of them had visible holes and broken particles were also present, exposing hollow interiors. A number of particles were fused. The particle size distribution was symmetrical and monomodal with a median size of 2.2 μm as determined by Malvern Mastersizer 2000.



Figure 6.3 SEM micrograph of co-spray dried budesonide with 30% raffinose pentahydrate.

6.3 Co-spray dried budesonide/hydroxypropyl-β-cyclodextrin 30%

In Chapter 5 it was shown that the co-spray dried sample of formoterol fumarate with 30% (w/w) HP-β-cyclodextrin gave the greatest respirable fraction in the *in vitro* twin stage impinger studies. Therefore the same concentration of the excipient was selected for the spray drying experiments with budesonide. The sample was spray dried from 95% (v/v) ethanol as a solution and the spray drying conditions are given in Appendix I.

The thermograms of the binary systems of budesonide with HP-β-cyclodextrin are presented in Figure 6.1. For the spray dried system, a broad endothermic process of the surface solvents release was observed to peak at ~60°C. An exotherm indicative of an amorphous phase recrystallisation peaked at 144°C and was followed by budesonide melting with a maximum at 252°C. The DSC trace of the mechanical mixture showed a minimum at ~60°C due to the release of the moisture adsorbed on the cyclodextrin powder. The budesonide melting endotherm was found at 253°C, which is nearly the same as that of the processed composite.

The X-ray diffraction pattern of the spray dried specimen was completely diffuse, revealing the amorphous nature of the powder (Figure 6.2).

The sample was composed of roughly spherical, but dimpled or collapsed particles which, in contrast to those of the previous system with raffinose, had smooth surfaces. The sample morphology is presented in Figure 6.4. The particle size distribution was monomodal with the median particle size of 2.5 μm as experimentally determined by the Malvern Mastersizer 2000 laser diffraction particle sizer.

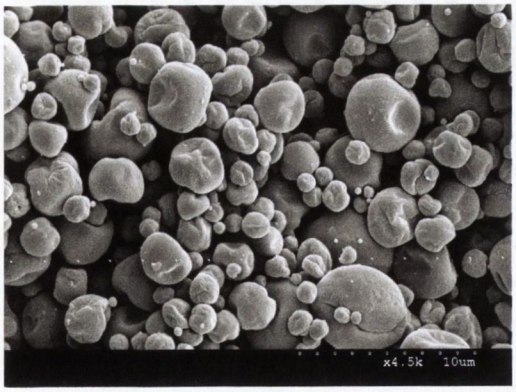

Figure 6.4 SEM micrograph of co-spray dried budesonide/HP-β-cyclodextrin 30%.

6.4 Budesonide/stearic acid systems

Four systems of budesonide with stearic acid were spray dried as solutions from 95% (v/v) ethanol, where stearic acid constituted 1, 2, 5 and 10% by weight of solids. Spray drying conditions are given in Appendix I.

The DSC scans of the co-spray dried powders are shown in Figure 6.5 and it can be seen that all exhibit an endothermic peak appearing between 250°C and 260°C depending on the stearic acid content. A systematic decrease in the onset and peak temperature of the endotherm was observed when the concentration of stearic acid in a sample increased and the peak occurred at 261.7, 261.6, 260.1 and 253.4°C, for the 1, 2, 5 and 10% of stearic acid, respectively.

A small recrystallisation exotherm was evidenced in the DSC of the budesonide/stearic acid 1% system (Figure 6.5) with a peak at ~105°C, most likely due to the budesonide recrystallisation, which for the pure, spray dried drug occurred at ~130°C. For the 2% stearic acid-containing sample only one thermal event seemed to appear on the DSC curve - the budesonide melting. However, when the trace was magnified, another endotherm with a very small magnitude was found at ~59°C. It is possible that this peak is of stearic acid melting, although depressed by the presence of budesonide. Melting of the crystalline stearic acid occurred at ~71°C as shown in Figure 6.9.

A small endotherm (with a peak at ~68°C and ~70°C) overlapping with an exotherm (with a peak at ~81°C and ~74°C) was registered by DSC for the 5% and 10% stearic acid co-spray dried system, respectively. The endotherm is probably due to stearic acid melting and the exotherm could be due to budesonide recrystallisation during heating. The gradual move of the latter to lower temperatures indicates greater physical instability of the budesonide systems containing stearic acid at higher levels. Also, the mutual ability for decreasing the melting point suggests an interaction between the components.

A partial miscibility of stearic acid and budesonide was additionally demonstrated by running a DSC analysis of the mechanical mixture of budesonide and stearic acid 10% (w/w). The thermogram is presented in Figure 6.5. The normalised heats of the stearic acid melting obtained for the co-spray dried and mechanically mixed samples containing 10% stearic acid were then compared and showed that the value of the former was equal to ~11 J/g and the latter was ~24 J/g.

The heats of budesonide fusion did not vary considerably and were ~69 J/g and ~72 J/g for the processed and physical mix, respectively. The similar values of the heats of budesonide melting may be caused by the thermal decomposition of stearic acid upon heating in the DSC furnace. The content of stearic acid diminished when the temperature rose, as TGA revealed that stearic acid started to degrade at ~140°C and evaporated completely before ~260°C.

TGA showed less than 1% weight loss between 25 and 100°C probably due to solvent desorption.

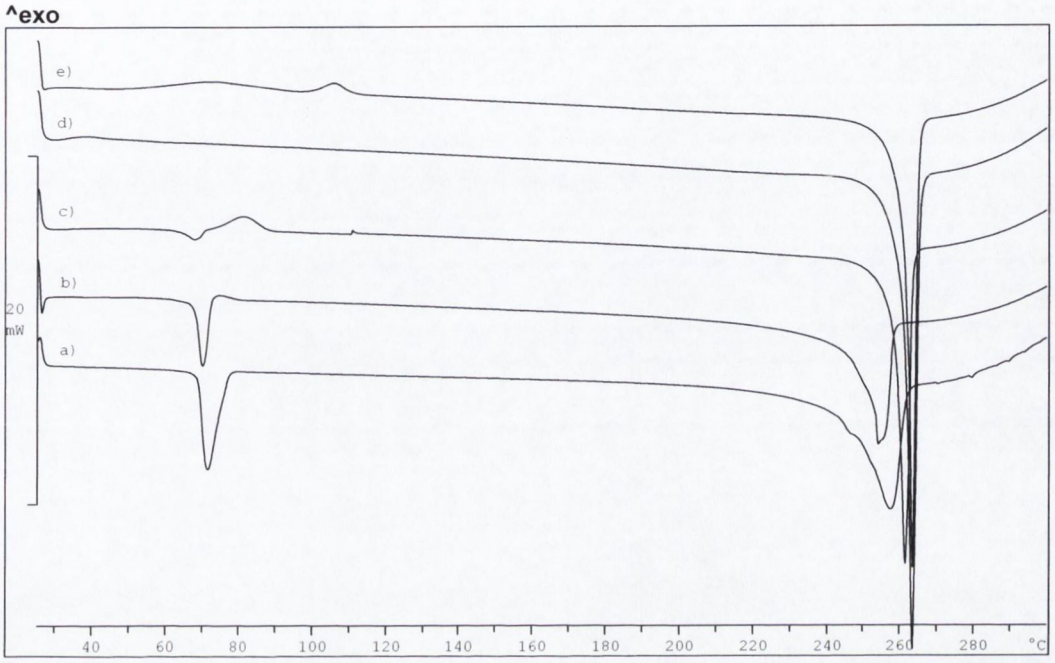

Figure 6.5 DSC scans of (a) physical mixture of budesonide and stearic acid 10%, (b) co-spray dried budesonide/stearic acid 10%, (c) co-spray dried budesonide/stearic acid 5%, (d) co-spray dried budesonide/stearic acid 2% and (e) co-spray dried budesonide/stearic acid 1%.

In the case of all co-spray dried systems XRD showed peak patterns characteristic of crystalline budesonide as seen in Figure 6.6. The intensity of the peaks, however, was reduced to around 1/3 in comparison to the budesonide raw material powder. There was no evidence of the presence of stearic acid for the 1% and 2% excipient-containing materials probably due to its low content in the samples. However, for the budesonide/stearic acid 5 and 10% samples the presence of stearic acid was demonstrated by an increase in intensity of the peak at ~21.5 2θ and indicated by the arrows in Figure 6.6. The diffractogram of stearic acid is presented in Figure 6.10. The physical blend of budesonide and 10% stearic acid showed, again, a diffractogram characteristic of crystalline budesonide with two peaks identified as being of stearic acid, at 6.6 and ~21.5 2θ. The intensity of the latter was greater than that of the spray dried system implying possible miscibility of stearic acid in budesonide or partial amorphousness of the former substance.

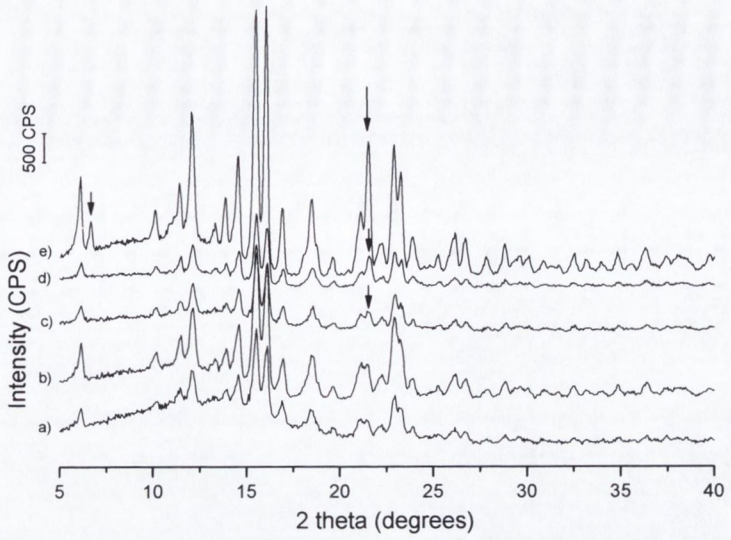

Figure 6.6 XRD diffractograms of (a) co-spray dried budesonide/stearic acid 1%, (b) co-spray dried budesonide/stearic acid 2%, (c) co-spray dried budesonide/stearic acid 5%, (d) co-spray dried budesonide/stearic acid 10% and (e) physical mixture of budesonide/stearic acid 10%. The arrows indicate peaks of stearic acid.

The infrared spectra of the co-spray dried systems were similar in shape and were representative of crystalline budesonide rather than the amorphous form. The presence of stearic acid was manifested by a change in intensities of the C-H stretching bands in the 2800-3000 cm^{-1} region. Moreover, the peaks of the carbonyl (C=O) moieties stretching located for the crystalline budesonide at 1667 and 1723 cm^{-1} (their assignment is described in Chapter 4) slightly changed their positions by 1-3 cm^{-1} to lower wavenumbers depending on the stearic acid concentration.

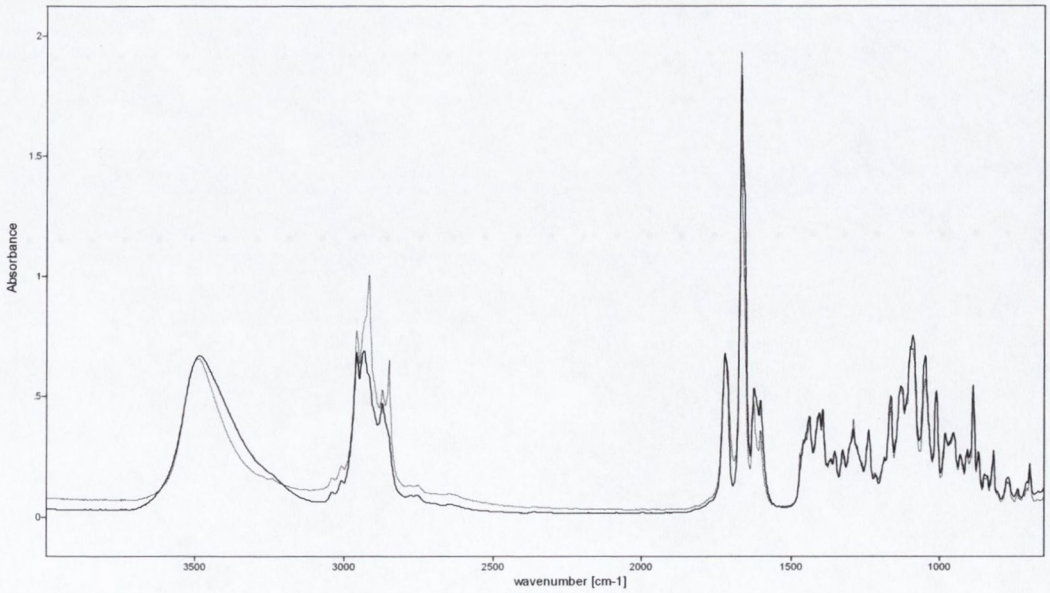

Figure 6.7 FTIR spectra of co-spray dried budesonide/stearic acid 1% (solid line) and co-spray dried budesonide/stearic acid 10% (dotted line).

Small, spherical particles were observed by SEM (Figure 6.8). Some of the particles had small holes and occasional particle fragments and fractured particles were also observed. The surface roughness increased with the increased content of stearic acid. Fusion of particles was seen for the sample containing 10% excipient and this could be attributed to the low melting temperature of stearic acid. The median particle size of all the co-spray dried samples was measured by Malvern Mastersizer 2000 and was 2.9, 2.9, 2.7 and 3.2 μm for the 1%, 2%, 5% and 10% stearic acid level, respectively. The particle size distribution (by volume) was approximately monomodal with a small fraction of submicron sized particles.

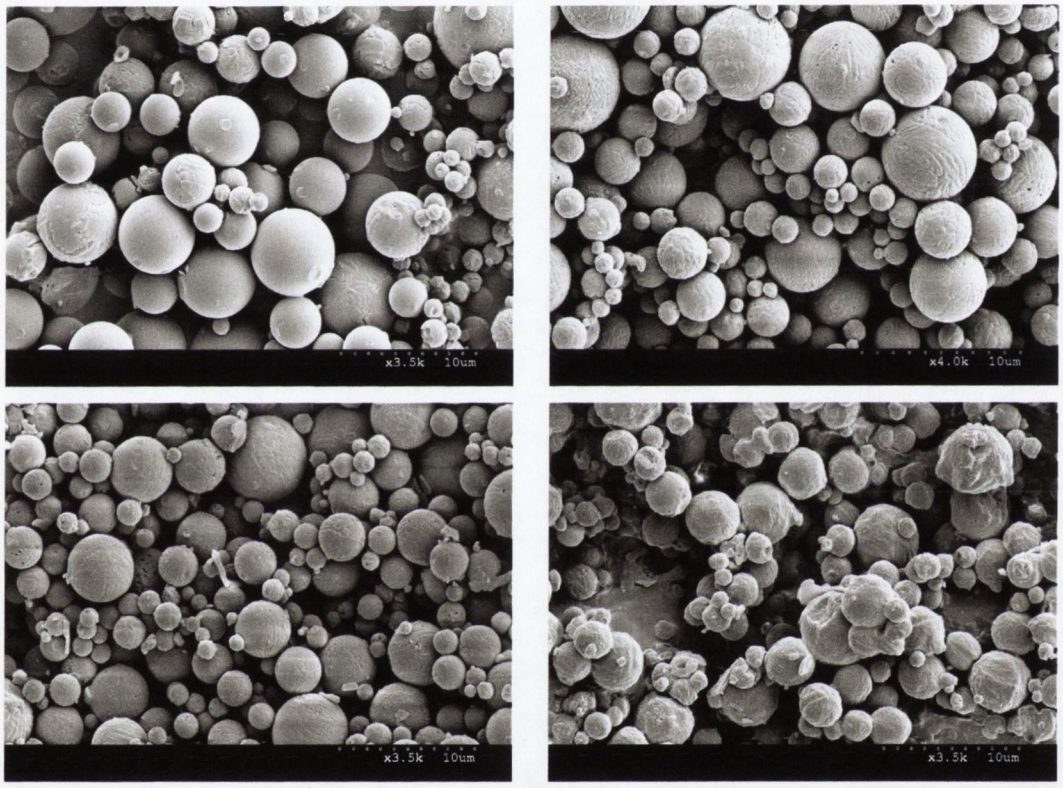

Figure 6.8 SEM micrographs of co-spray dried budesonide/stearic acid 1% (top left), co-spray dried budesonide/stearic acid 2% (top right), co-spray dried budesonide/stearic acid 5% (bottom left), co-spray dried budesonide/stearic acid 10% (bottom right). Note a different magnification of the top right micrograph.

6.4.1 Budesonide co-spray dried with PVP 10000 and stearic acid

Co-spray drying of budesonide with stearic acid resulted in powdered systems that were mainly crystalline in nature. PVP is known to stabilise amorphous phases of drugs as shown by Corrigan *et al.* (1984). Moreover, having observed the ability of PVP 10000 to enhance the emitted dose of formoterol fumarate, when the drug was co-spray dried with the polymer at 10% level (data presented in Chapter 5), it was deemed interesting to test the properties of a spray dried ternary system containing budesonide, PVP and stearic acid. The sample was spray dried from 95% (v/v) ethanol as a solution, where PVP and stearic acid constituted 10% and 5% by weight of solids, respectively. Spray drying conditions are given in Appendix I.

A recrystallisation exotherm was evident in the DSC thermogram presented in Figure 6.9 with a peak at ~106°C. This peak was more distinct and occurred at a higher temperature than those of the budesonide/stearic acid powders. No stearic acid melting was visible, but there appeared to be a glass transition (observed at a higher magnification) with a midpoint at ~65°C. The exotherm was followed by the budesonide melting endotherm, which had a peak at ~257°C.

On the DSC trace of the equivalent physical mixture (Figure 6.9) both of the melting processes, of stearic acid and drug, were observed. The endotherm of the excipient was found at ~71°C and neither onset nor peak temperatures were different to those of unprocessed stearic acid. As the budesonide endotherm was broad and peaked at ~256°C and the position of the stearic acid peak remained unaltered, this suggests that PVP interacting with budesonide is responsible for the decrease in its melting temperature.

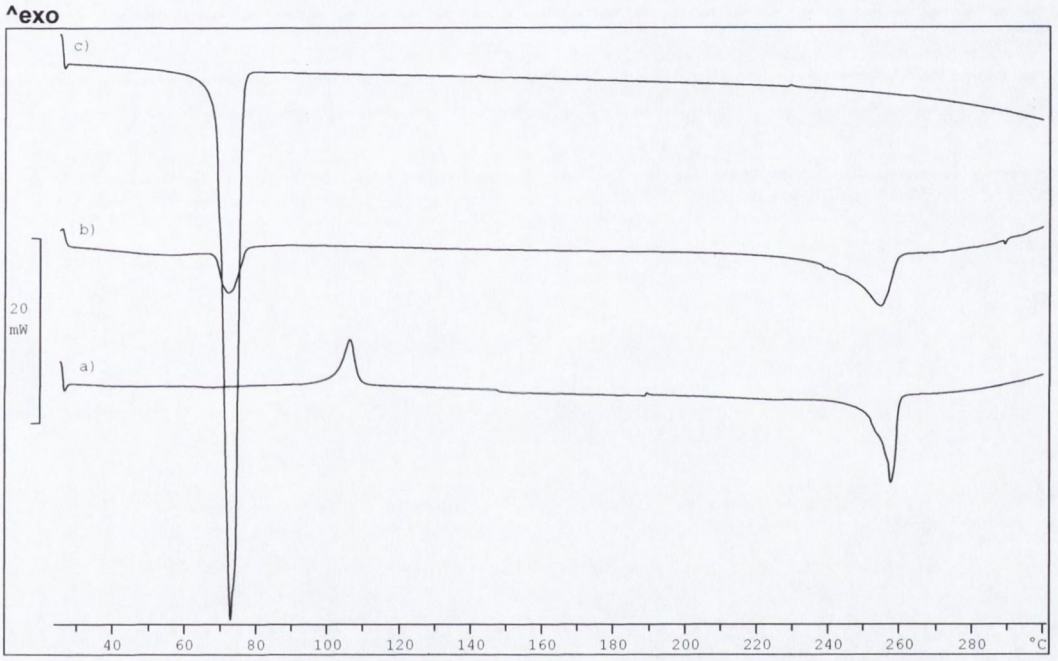

Figure 6.9 DSC scans of (a) co-spray dried budesonide/PVP 10000 10%/stearic acid 5%, (b) physical mixture of budesonide and PVP 10000 10% and stearic acid 5% and (c) unprocessed stearic acid.

XRD showed a pattern of amorphous material with weak peaks of crystalline budesonide (Figure 6.10). The sample showed a greater amorphous content than the other spray dried budesonide/stearic acid samples. This evidences that the addition of PVP to budesonide and stearic acid is able to increase the amorphous fraction of the drug and perhaps even that of stearic acid. No peaks of the excipient were present in the diffractogram of the processed sample but they were clearly apparent in the XRD trace of the physical blend as indicated by the arrows. The diffractograms of the above samples together with the scan of the untreated stearic acid are presented in Figure 6.10.

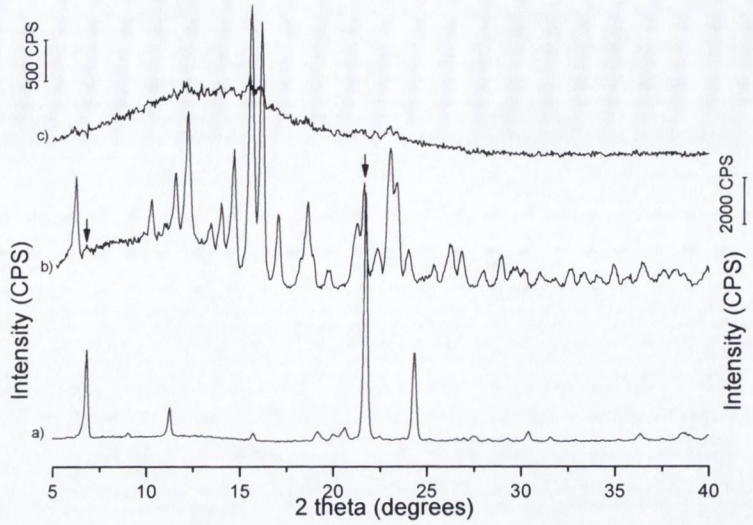

Figure 6.10 XRD diffractograms of (a) unprocessed stearic acid, (b) co-spray dried budesonide/PVP 10000 10%/strearic acid 5% and (c) physical mixture of budesonide/PVP 10000 10%/strearic acid 5%. The arrows indicate peaks of stearic acid. The right-hand side scale applies to the curve (a).

The infrared spectrum of the processed sample resembled that of spray dried budesonide confirming the amorphous nature of the powder. The spectrum was slightly altered by the vibration bands of PVP.

Small, generally spherical-shaped particles were observed by SEM (Figure 6.11). Particle surfaces were smooth unlike the co-spray dried budesonide/stearic acid systems. The only similarity between the latter and the PVP-containing samples lay in the presence of visible holes in the surface. Occasional particle fragments and particles with rough surfaces were noticed. The majority of the particles were deformed in contrast to the spheres of the formoterol fumarate/PVP powders as presented in Chapter 5. The median particle size was 3.2 μm as determined by Malvern Mastersizer 2000.

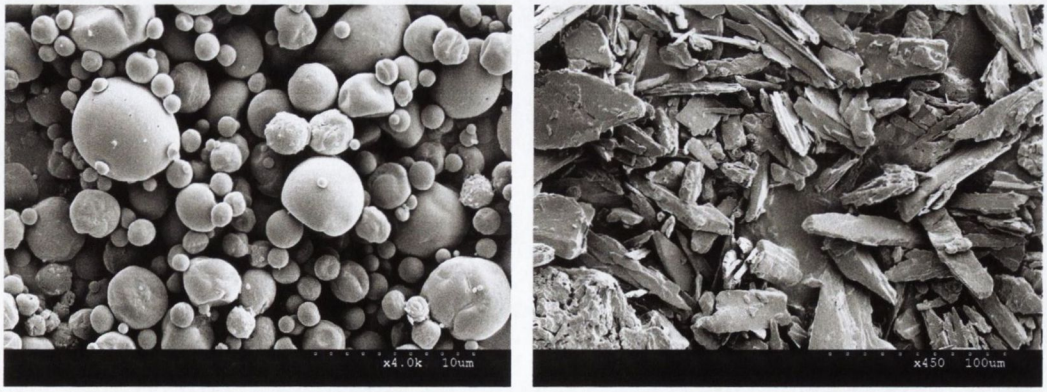

Figure 6.11 SEM micrographs of co-spray dried budesonide/PVP 10000 10%/strearic acid 5% (left) and unprocessed stearic acid (right). Note the different magnifications of the micrographs.

6.5 Budesonide/ascorbyl palmitate systems

Two systems of budesonide with ascorbyl palmitate were spray dried as solutions from 95% (v/v) ethanol, where ascorbyl palmitate constituted 5% and 10% by weight of solids. Spray drying conditions are given in Appendix I.

A small endotherm (with a peak at 81°C) overlapping with an exotherm (with a peak at ~104°C) was observed by DSC for the spray dried sample containing 5% excipient. The endotherm perhaps is a glass transition of the material and the exotherm could be budesonide and ascorbyl palmitate recrystallisation. The exotherm was followed by a second endotherm at ~258°C due to budesonide melting. The 10% ascorbyl palmitate-containing sample gave a similar DSC thermogram and a recrystallisation exotherm peaked at ~100°C, followed by two melting endotherms: the first with a very low magnitude peaking at ~124°C and the second at ~253°C corresponding to melting of budesonide. The exotherm was preceded by a glass transition with the midpoint at ~72°C. DSC of ascorbyl palmitate unprocessed material showed four thermal events: a broad endotherm at ~62°C probably due to free palmitic acid melting, a second, sharp endotherm peaking at ~117°C due to melting of ascorbyl palmitate, a third, very small unidentified endotherm at ~160°C and broad exotherm with onset at ~210°C due to thermal decomposition as substantiated by TGA. The thermogram of the budesonide mechanically mixed with 10% ascorbyl palmitate showed no exotherm, but two melting processes of the excipient and drug. They occurred at lower temperatures comparing to the melting endotherms of the crystalline substances run separately implying a possible interaction or miscibility. The DSC scans are presented in Figure 6.12.

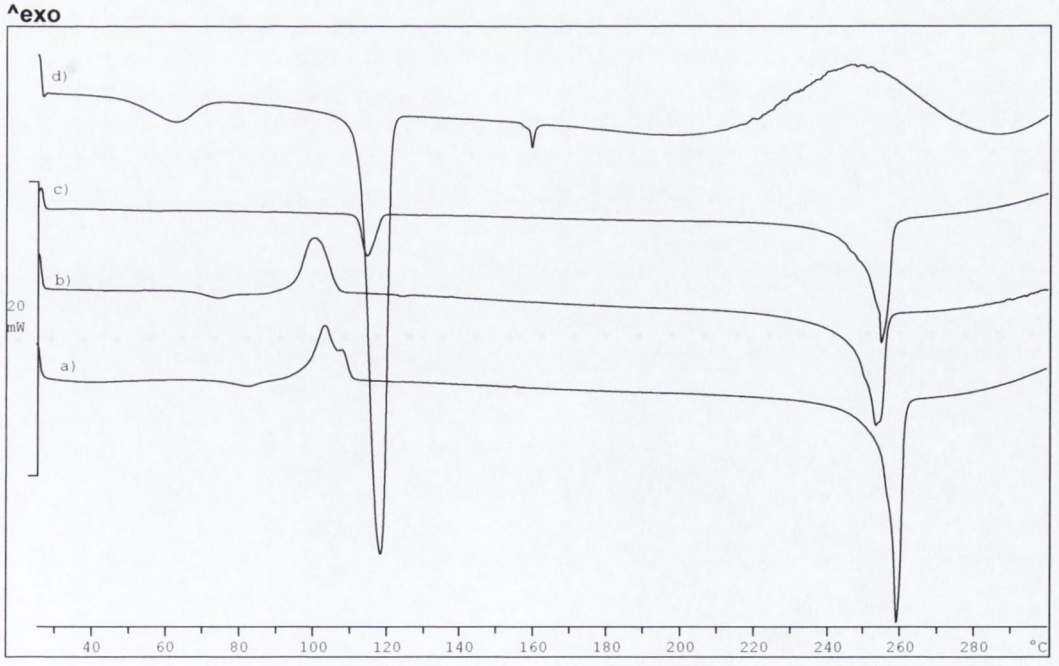

Figure 6.12 DSC scans of (a) co-spray dried budesonide/ascorbyl palmitate 5%, (b) co-spray dried budesonide/ascorbyl palmitate 10%, (c) physical mixture of budesonide and ascorbyl palmitate 10% and (d) unprocessed ascorbyl palmitate.

XRD traces of the co-spray dried powders showed patterns typical of amorphous material with no distinct peaks (Figure 6.13). Ascorbyl palmitate in the equivalent physical mixtures was detectable at the 10% level only. Nevertheless, the absence of the excipient peaks in the diffractogram of the spray dried budesonide/ascorbyl palmitate 10% composite suggests an amorphous transformation of ascorbyl palmitate.

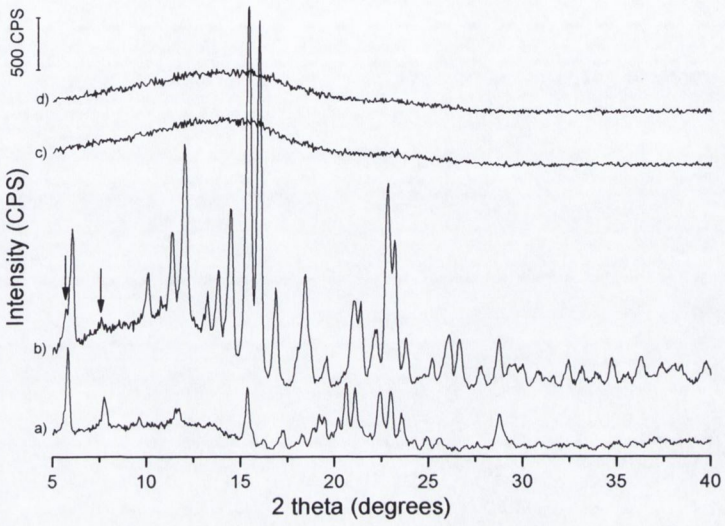

Figure 6.13 XRD diffractograms of (a) unprocessed ascorbyl palmitate, (b) physical mixture of budesonide and ascorbyl palmitate 10%, (c) co-spray dried budesonide/ascorbyl palmitate 5% and (d) co-spray dried budesonide/ascorbyl palmitate 10%. The arrows indicate peaks of ascorbyl palmitate.

The FTIR spectra of the processed mixtures were good matches to that of amorphous budesonide. An additional peak of ascorbyl palmitate at 1757 cm^{-1} for the unprocessed mixture was also visible but shifted to around 1766 cm^{-1} in the spectra of the spray dried mixtures.

Spherical particles were observed by SEM as seen in Figure 6.14. Occasional particle fragments were noticed. The particle surfaces were generally smooth, although a few particles were seen to have surface indentations. The median particle size was 3.1 μm for both of the samples as determined by Malvern Mastersizer 2000.

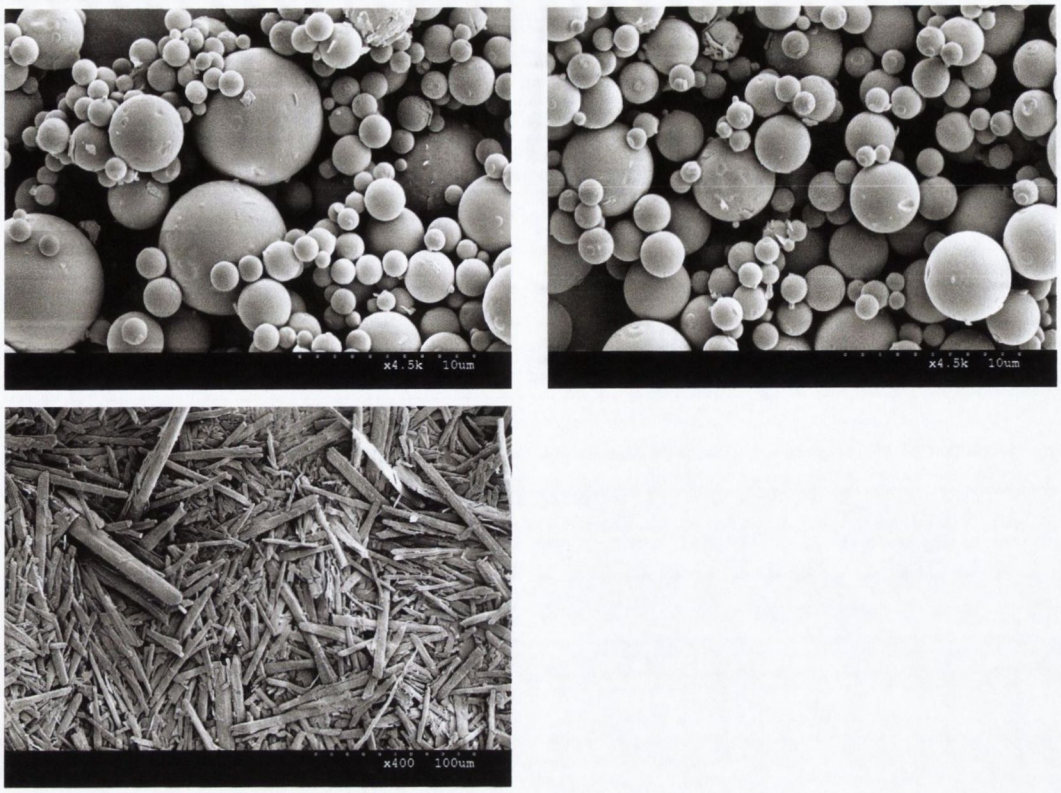

Figure 6.14 SEM micrographs of co-spray dried budesonide/ascorbyl palmitate 5% (top left), co-spray dried budesonide/ascorbyl palmitate 10% (top right) and unprocessed ascorbyl palmitate (bottom). Note the different magnification of the bottom micrograph.

6.6 Budesonide/Aerosil 200 Pharma systems

A new method aimed at improving the inhalation efficiency of hydrophobic cohesive particles by surface modification was proposed by Kawashima *et al.* (1998a). Hydrophobic colloidal silica Aerosil was used to change the surface morphology of pranlukast hydrate and various manufacturing processes, including spray drying, were employed. More recent work of Steckel and Bolzen (2004) has shown that 2% of Aerosil can improve the inhalation efficiency of budesonide when mechanically mixed with different sugar carriers.

Two systems of budesonide with colloidal silica acquired under a commercial name Aerosil 200 Pharma were spray dried as suspensions from 95% (v/v) ethanol, where colloidal silica constituted 5% and 10% by weight of solids. The suspensions were prepared by dissolving budesonide in the solvent and then adding Aerosil which constituted the dispersed phase. Constant stirring by a means of a magnetic stirrer was provided during the process. Spray drying conditions are given in Appendix I.

The DSC profiles of the samples are shown in Figure 6.15. When the physical mixture of budesonide containing 10% Aerosil was heated, only an endothermic peak due to the drug melting was detected by DSC at around 265°C. When compared with melting of crystalline budesonide (262°C, Chapter 4) the peak occurred at higher temperature.

The co-spray dried samples, in contrast, showed additional endothermic and exothermic processes at ~91°C and ~92°C as well as ~120°C and ~116°C for the 5% and 10% of Aerosil, respectively.

The thermal events were ascribed to the glass transition and recrystallisation, respectively. This increase in the T_g of budesonide (the T_g of amorphous budesonide is ~89.5°C as stated in Chapter 4) indicates a stabilisation of the amorphous phase upon Aerosil addition.

The budesonide melting endotherm peaked at ~263°C for both of the systems. DSC of Aerosil 200 Pharma raw material did not reveal any significant thermal event but a very broad endotherm with a very low magnitude due to dehydration/desolvation was observed.

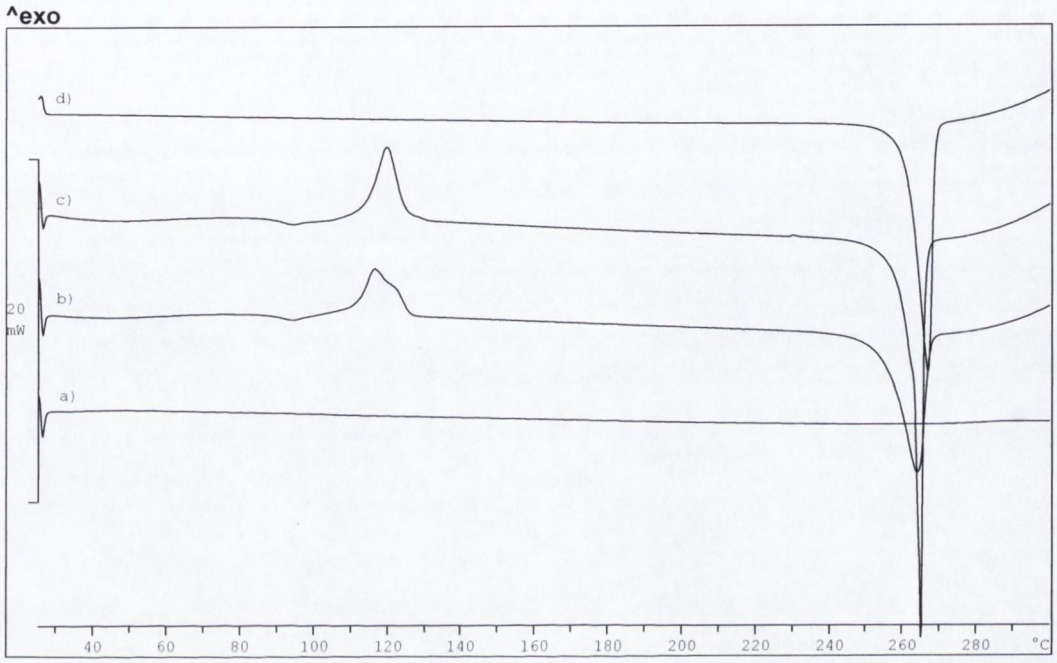

Figure 6.15 DSC scans of (a) unprocessed Aerosil, (b) co-spray dried budesonide/Aerosil 5%, (c) co-spray dried budesonide/Aerosil 10% and (d) physical mixture of budesonide and Aerosil 10%.

The X-ray powder diffractograms of the co-spray dried dispersions presented in Figure 6.16 did not show any of the peaks of crystalline budesonide. Also Aerosil, as being intrinsically amorphous, presented only a diffused "halo".

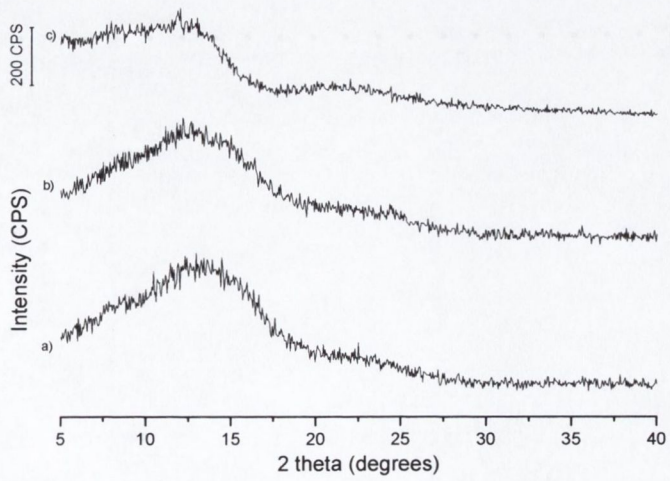

Figure 6.16 XRD diffractograms of (a) co-spray dried budesonide/Aerosil 5% and (b) co-spray dried budesonide/Aerosil 10% and (c) unprocessed Aerosil.

The FTIR spectra of the co-spray dried mixtures corresponded with the spectrum of amorphous budesonide, although the peak intensities appearing between 1000 and 1300 cm^{-1} were greater compared to those of the spray dried drug due to overlapping with a strong band of Si-O vibrations form the Aerosil.

Small, generally spherical particles with were observed by SEM. The particle surfaces were very rough with perforations. Many larger particles of the 10% Aerosil system had a distinct "sponge-like" appearance. The median particle size was 2.3 μm for the 5% Aerosil system and 2.7 μm for the 10% Aerosil sample measured by Malvern Mastersizer 2000.

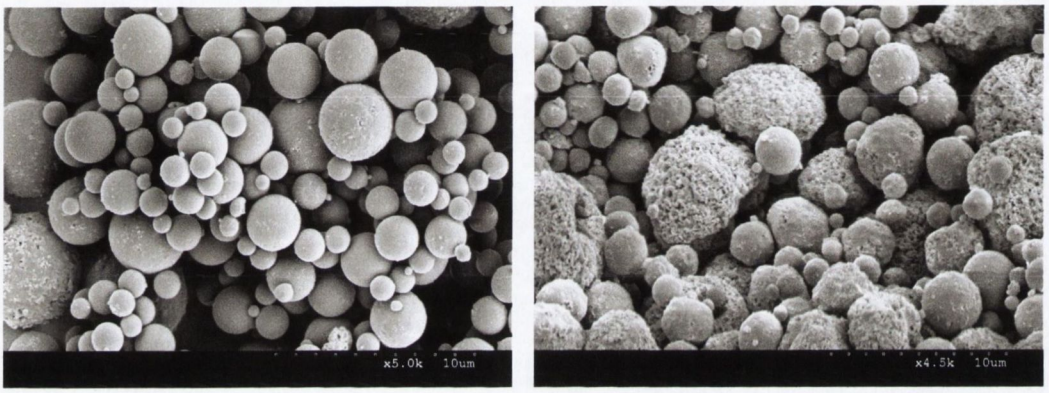

Figure 6.17 SEM micrographs of co-spray dried budesonide/Aerosil 5% (left) and co-spray dried budesonide/Aerosil 10% (right). Note the different magnifications of the micrographs.

6.7 Budesonide/microcrystalline cellulose systems

Two systems of budesonide with microcrystalline cellulose were spray dried from 95% (v/v) ethanol as suspensions, where the excipient constituted 5% and 10% by weight of solids. The suspensions were prepared in a similar manner as the suspensions of budesonide and Aerosil (Chapter 6.6). Constant stirring by a means of a magnetic stirrer was provided during the process. Spray drying conditions are given in Appendix I.

The DSC results are presented in Figure 6.18. DSC of microcrystalline cellulose unprocessed material showed three thermal events: a broad endotherm at ~70°C probably due to water/solvents desorption, a second, very broad endotherm at ~200°C represented as a baseline slope change, probably due to the glass transition of the material and a broad exotherm with onset at ~290°C due to thermal degradation. The onset of the exotherm coincides with a rapid weight loss by TGA.

DSC thermograms of the solid dispersions exhibited a small endotherm with a peak at 93°C and an exotherm with a peak at ~119°C. The first thermal event is probably the glass transition of the material and the exotherm could be budesonide recrystallisation. In both cases the exotherm was followed by a second, sharp endothermic process at ~258°C due to budesonide melting.

The mechanically mixed budesonide with 10% microcrystalline cellulose showed only melting of budesonide at ~259°C. The small decrease in the peak melting temperature of the drug in mixtures may be evidence of weak interactions between the constituents, but is interesting that the peak

temperatures of neither of the thermal events were altered by a different concentration of the excipient used, in contrast to what has been observed so far for other budesonide systems.

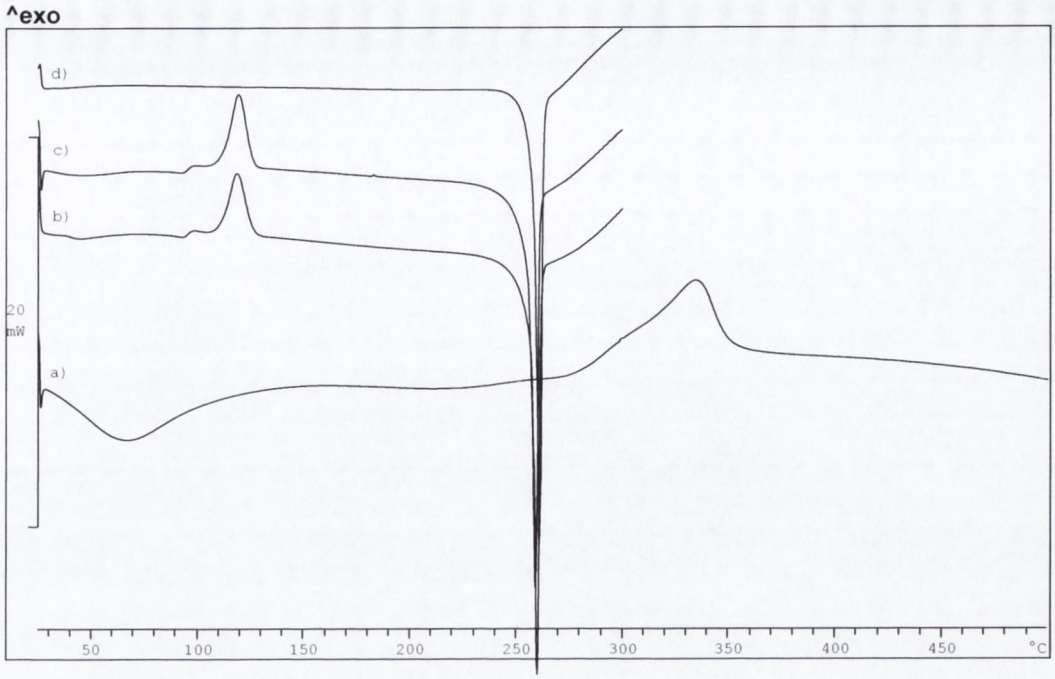

Figure 6.18 DSC scans of (a) unprocessed microcrystalline cellulose, (b) co-spray dried budesonide/microcrystalline cellulose 5%, (c) co-spray dried budesonide/microcrystalline cellulose 10% and (d) physical mixture of budesonide and microcrystalline cellulose 10%.

XRD scan of microcrystalline cellulose displayed one major peak at 22.7 2θ and a few other, broad peaks (Figure 6.19). No peaks attributable to the excipient were found in the physical mixtures, even when the concentration of microcrystalline cellulose was 10%. The 5% excipient-containing solid dispersion showed a pattern typical of amorphous material with no distinct peaks. The co-spray dried budesonide/microcrystalline cellulose 10% also presented an amorphous "halo" but a broad, jagged peak from the crystalline fraction of microcrystalline cellulose between 20-24 2θ degrees was apparent as indicated by the arrow in Figure 6.19.

The infrared spectra of the solid dispersions were superimposable with that of spray dried budesonide and no perceptible peak shifts were discerned.

Spherical particles of the solid dispersions were observed by SEM and sample micrographs are shown in Figure 6.20. Occasional particle fragments were also noticed. The particle surfaces were generally smooth, although some of the particles of the 10% excipient system had rough surfaces. The median particle size (by Malvern Mastersizer 2000) of the untreated microcrystalline cellulose was 30.6 μm, but surprisingly the values for the 5% and 10% excipient-containing dispersions were only 3.1 and 3.6 μm, respectively.

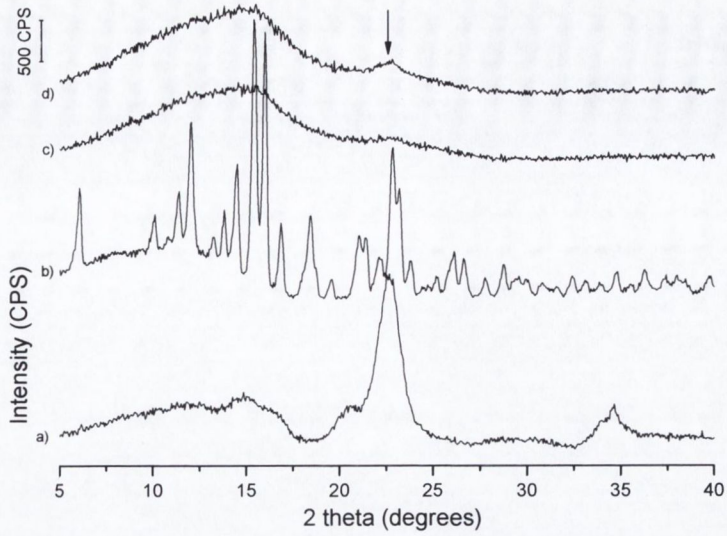

Figure 6.19 XRD diffractograms of (a) unprocessed microcrystalline cellulose, (b) physical mixture of budesonide and microcrystalline cellulose 10%, (c) co-spray dried budesonide/microcrystalline cellulose 5% and (d) co-spray dried budesonide/microcrystalline cellulose 10%. The arrows indicate peaks of ascorbyl palmitate.

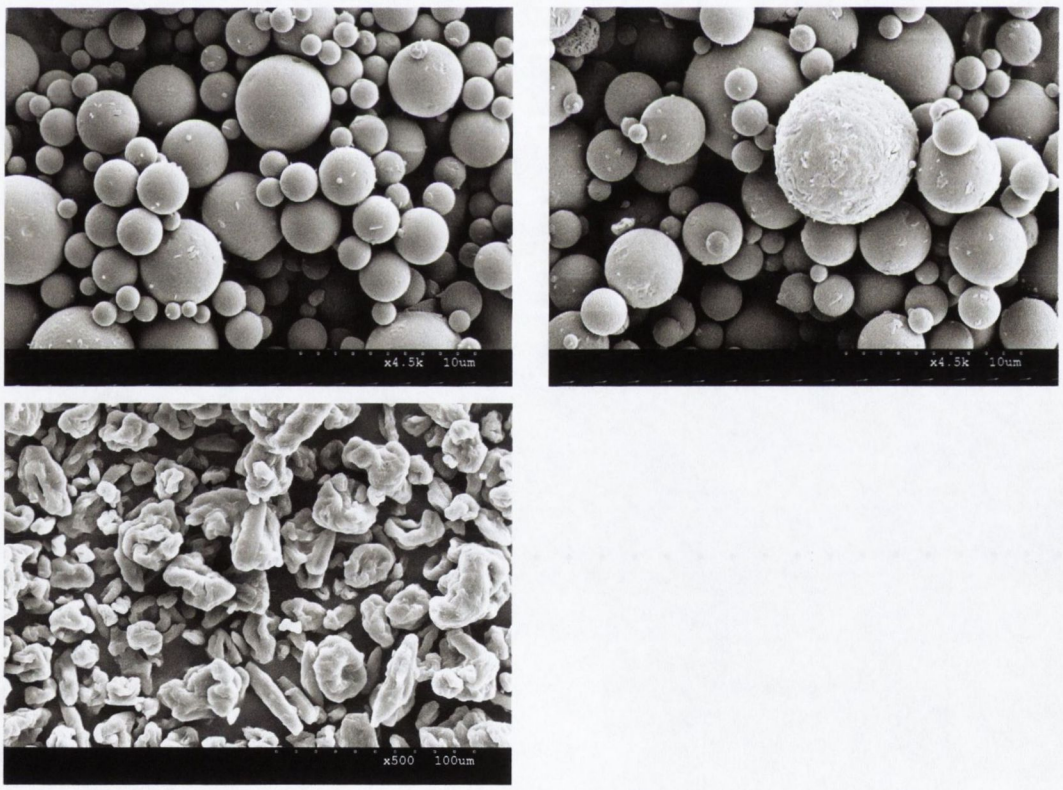

Figure 6.20 SEM micrographs of co-spray dried budesonide/microcrystalline cellulose 5% (top left) and co-spray dried budesonide/ microcrystalline cellulose 10% (top right) and microcrystalline cellulose starting material (bottom). Note the different magnification of the bottom micrograph.

6.8 Evaluation of *in vitro* respirable fractions of the co-spray dried budesonide systems by twin stage impinger

The twin impinger analysis was carried out on the spray dried budesonide and the co-spray dried budesonide/excipient samples. The analysis was done in triplicate for each sample except spray dried budesonide and unprocessed budesonide for which the twin impinger analysis was performed 5 times. The results of twin impinger analysis are presented in Figure 6.21.

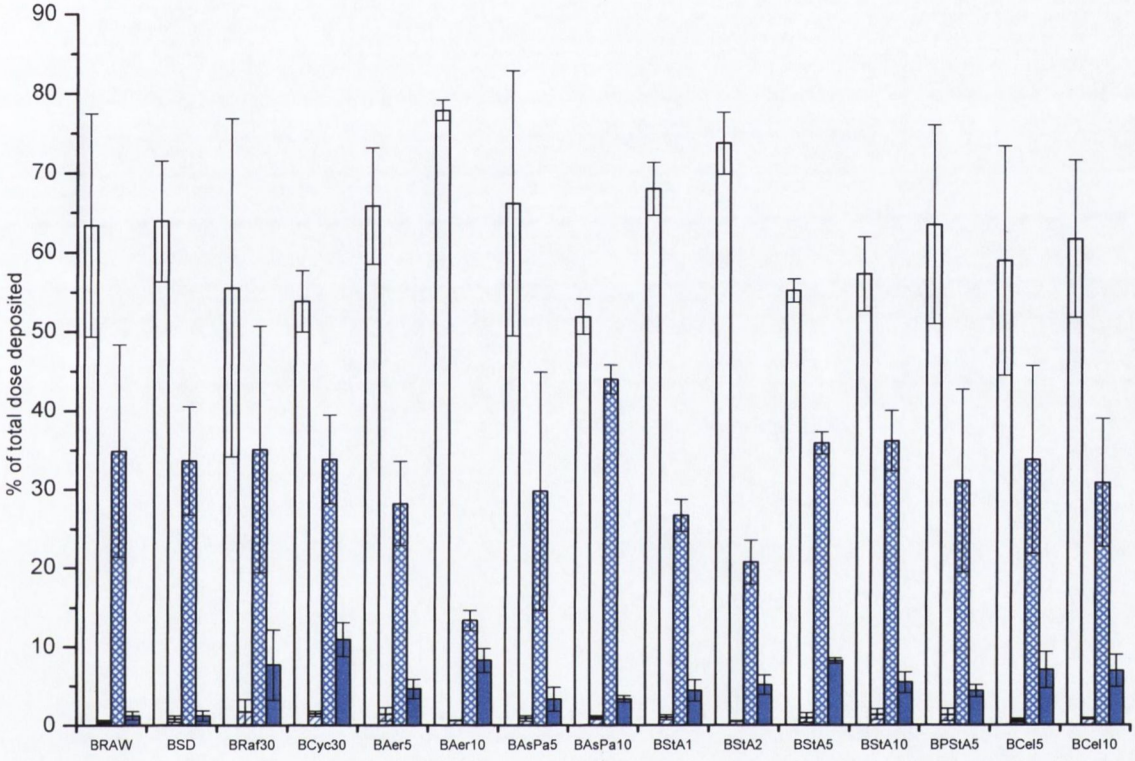

Figure 6.21 Twin impinger analysis of spray dried and unprocessed budesonide and the budesonide/excipient co-spray dried samples. The white, blue diagonal, blue grid and full blue filled bars indicate the percentage retained in the capsule and device, mouthpiece, stage 1 and stage 2 on the twin stage impinger, respectively. Key: RAW – unprocessed, SD – spray dried, B – budesonide, Raf – raffinose, Cyc – HP-β-CYC, Aer – Aerosil, AsPa – ascorbyl palmitate, StA- stearic acid, P – PVP 10000 10% and Cel – microcrystalline cellulose. The number indicates the percentage content of the excipient.

Figure 6.21 indicates that the percentage of the non-respirable dose is varied and depends on the excipient used. Also the content of the excipient is influential. There is a difference in the ratio of dose retained in the device and capsule to that emitted. The greatest ratio is for co-spray dried budesonide/Aerosil 200 10% and is 3.5 (77.83% device/22.17% emitted) and the lowest is for co-spray dried budesonide/ascorbyl palmitate 10% and is 1.1 (51.82% device/48.18% emitted). The fractions emitted from the device were calculated and compared using the ANOVA test, but no striking differences among them were observed. The particles of the micronised, untreated budesonide and spray dried drug gave the same emitted fractions of 36%. The large error bars for the co-spray dried budesonide and raffinose pentahydrate 30% as well as budesonide/ascorbyl

palmitate 5% indicate large standard deviations and inconsistency of the dosing. This may eliminate them from being used in inhalation formulations.

The respirable fractions (i.e. retained on the stage 2 of the twin stage impinger) are showed graphically as a bar plot in Figure 6.22. They were contrasted and statistically analysed by ANOVA, which results are summarised in Table 6.1.

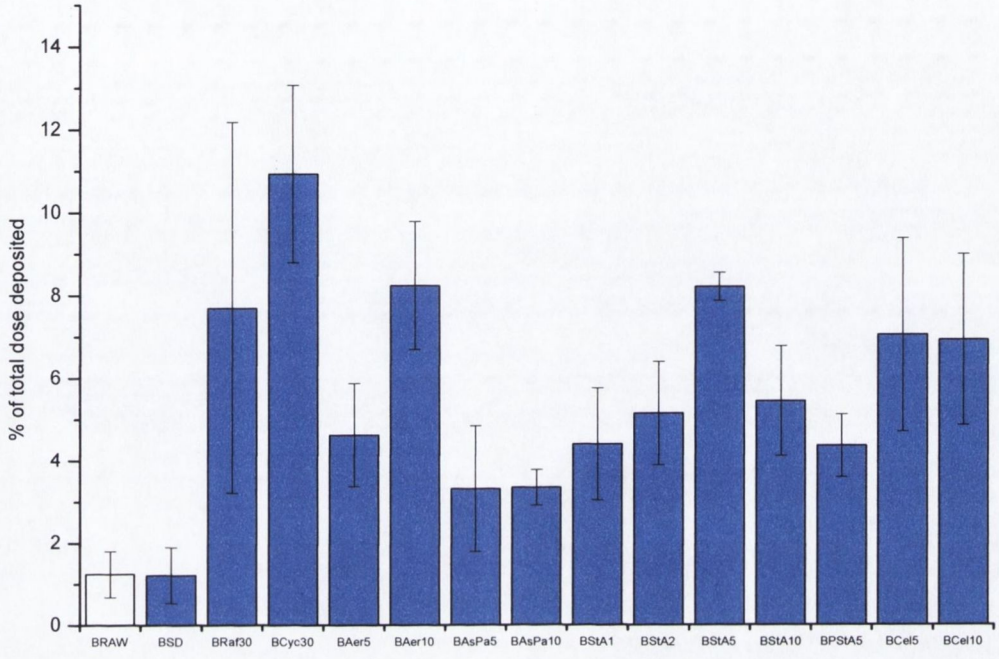

Figure 6.22 The respirable fractions (i.e. deposited on stage 2 of twin impinger) of spray dried and unprocessed budesonide and the budesonide/excipient co-spray dried samples. Key – as Figure 6.21.

Table 6.1 ANOVA comparing the respirable fractions for the spray dried and unprocessed budesonide and budesonide/excipient samples. Key – as Figure 6.21.

			Individual 95% Confidential Intervals For Mean Based on Pooled StDev
Level	N	Mean	StDev -+---------+---------+---------+-----
BRAW	5	1.640	0.685 (---*---)
BSD	5	1.236	0.554 (---*---)
BRaf30	3	7.690	4.475 (----*----)
BCyc30	3	10.923	2.139 (----*----)
BAer5	3	4.617	1.250 (----*---)
BAer10	3	8.230	1.536 (----*----)
BAsPa5	3	3.310	1.534 (----*----)
BAsPa10	3	3.337	0.430 (----*----)
BStA1	3	4.390	1.358 (----*----)
BStA2	3	5.137	1.251 (----*----)
BStA5	3	8.187	0.338 (---*----)
BStA10	3	5.427	1.335 (----*----)
BCel5	3	7.023	2.330 (----*---)
BCel10	3	6.903	2.055 (----*----)
BPStA5	3	4.337	0.761 (----*----)
			-+---------+---------+---------+-----
Pooled StDev =		1.683	0.0 4.0 8.0 12.0

Although from Figure 6.22 it may seem that all co-processed powders are better than the drug alone, the results of ANOVA showed a slightly different picture. This statistical analysis tests

whether or not two or more data sets have the same means and assures constant variance. Consequently, ANOVA uses a pooled standard deviation in sample comparisons.

The mean respirable fraction obtained with the original particles of budesonide was very low, around 1.6% of the total dose loaded into the capsules. In addition, spray drying of the drug alone did not improve the fine particle fraction, as seen in Table 6.1. The stage 2 fractions were significantly increased by formulating budesonide with a modifier. A significant difference was found between the respirable fractions of either spray dried or raw budesonide with the composites containing raffinose, HP-β-cyclodextrin, 10% Aerosil, 5% stearic acid and 5% and 10% microcrystalline cellulose indicated in the ANOVA table by the non-overlapping confidence intervals. The sample with the best deposition on stage 2 of twin impinger was co-spray dried budesonide and HP-β-cyclodextrin 30%. The fraction of this sample on stage 2 of the impinger was significantly greater than that for the other samples except budesonide processed with raffinose, Aerosil 10% and stearic acid 5%. The statistical studies revealed also a significant difference between co-spray dried budesonide/Aerosil 200 5% and the system with 10% Aerosil.

The particles of the systems showing an enhancement of the fine particle fraction were generally composed of deformed spheres with rough exteriors with the exception of the microcrystalline cellulose systems consisting of smooth spheres with a small admixture of particles having "fluffy" surfaces. HP-β-cyclodextrin at 30% level was shown in Chapter 5 to be superior in terms of the formoterol fumarate fraction lodged on the stage 2 of twin impinger. The quite good performance of the budesonide/Aerosil 10% sample may be attributed to the presence of porous, "sponge"-like particles that are known to flow better than the non-porous ones due to the lower aerodynamic diameters (Ben-Jebria *et al.*, 1999).

The $d_{50\%}$ (median particle size) values for the above systems lay between 2.2 and 3.6 μm, which is in the inhalable range, whereas the particle sizes of the budesonide starting material powder and its spray dried equivalent were 1.4 and 2.7 μm, respectively. As the differences are not large, the surface alteration may primarily account for the inhalation performance of the various modified budesonide samples.

6.9 Budesonide/magnesium stearate systems

6.9.1 Introduction

Magnesium stearate is most widely used as a lubricant in the tableting process due to its ability to reduce friction (Wada and Matsubara, 1992). According to the European Pharmacopoeia (2004), magnesium stearate is a mixture of magnesium salts of different fatty acids composed mainly of stearic and palmitic acids. Moreover, magnesium stearate can exist as four different pseudopolymorphs: anhydrous, mono-, di- and trihydrate (Rajala and Laine, 1995). The dihydrate has been shown to be the best lubricant (Miller and York, 1988). Due to the variability in chemical

and physical character, commercially available batches may have unpredictable effect on formulations (Rajala and Laine, 1995).

It has been reported by Ganderton *et al.* (1995) that the respirable fraction of a drug can be increased by the addition of ternary components, such as magnesium stearate, to binary mixtures of the drug and carrier. Zeng *et al.* (1998) prepared and investigated ternary powder formulations containing salbutamol sulphate, lactose carrier and magnesium stearate at concentration of 1.5% (w/w). Magnesium stearate was found to increase significantly the fine particle fraction of the drug. Also the invention disclosed in the US Patent 6645466B1 (Keller and Müller-Weltz, 2003) aimed at improving the moisture resistance of dry powder formulations for inhalation which contain a carrier, active and magnesium stearate. The authors claimed that a high respirable dose can be maintained under relatively extreme temperature and humidity conditions.

Unfortunately, the toxicological implications of the chronic pulmonary delivery of magnesium stearate are unknown and require further investigations.

6.9.2 Physicochemical characterisation of the "as received" and spray dried magnesium stearate samples

Three samples of magnesium were obtained – two were purchased from commercial traders: Aldrich and Riedel de Haën, further referred to as magnesium stearate Aldrich and magnesium stearate RDH, respectively and one sample was acquired from the Élan research laboratories and named magnesium stearate Élan. The specimens were spray dried on their own from 95% (v/v) ethanol as 0.5% (w/v) suspensions. Constant stirring by a means of a magnetic stirrer was provided during the process. Spray drying conditions are given in Appendix I.

DSC results for the unprocessed and spray dried magnesium stearate Élan are shown in Figure 6.23. A baseline change or small endotherm was observed at ~50°C for the untreated sample that corresponded to around 0.6% weight loss by TGA. This was followed by an endotherm peaking at ~120°C which, in turn, was related to a ~3.1% mass loss as recorded by TGA. The literature value for the melting point of magnesium stearate is quoted to be between 111°C and 115°C (Ahmed *et al.*., 1994), therefore this endothermic peaks may by of dehydration and melting simultaneously. A small exotherm occurred at ~143°C, and was associated probably with reacting impurities (Wada and Matsubara, 1992). This was followed by another small endotherm peaking at ~204°C that has been attributed to the end of melting by Wada and Matsubara (1992). The total weight loss between 25°C and 120°C was ~3.7%. The two-stage mass loss suggests that the moisture was held in two different ways: loosely absorbed and bound water as previously observed for magnesium stearate 'sample B' (Rajala and Laine, 1995).

Spray drying caused splitting of the endotherm previously peaking at ~120°C into two endothermic events. The first now occurred at ~113°C and is of dehydration of the powder and the second peaks at 127°C and is most likely due to melting. The appearance and positions of the rest of the peaks

remained unchanged. Moisture was lost in two stages similarly as for the untreated sample and totalled ~4% in the 25°C-120°C temperature range.

The magnesium stearate Aldrich starting material showed one exothermic and four endothermic events when analysed by DSC (Figure 6.23). They occurred at ~140°C, 58°C, ~90°C, ~116°C and ~150°C, respectively. The first two endothermic peaks are perhaps of dehydration as they incurred a ~5.2% weight loss by TGA. The endotherm at ~116°C was asymmetrical suggesting that it was responsible for two processes, dehydration and melting and corresponded to a ~0.4% weight loss. The small exotherm is perhaps of impurities but the origin of the minor peak appearing at ~150°C is unknown. The overall mass loss recorded by TGA was ~5.6%, which is comparable to that of 5.8% obtained by Rajala and Laine (1995) for 'sample C' and classified as dihydrate.

The material collected after the spray drying process gave a slightly different DSC curve (shown in Figure 6.23) and again, splitting of the endotherm previously emerging at ~116°C is observed. Therefore, the peak appearing at ~110°C is attributed to dehydration and the endotherm at 116°C may be related to melting of the material. No shifts were observed for the other thermal events. The moisture content was estimated by TGA and was ~5.3% between 25°C and 120°C. The water released stepwise in four stages.

The same four-stage solvent liberation was discerned for the unprocessed magnesium stearate RDH and it accounted for an about 4.1% weight loss when heated up to 120°C. The DSC scan presented in Figure 6.23 shows two small endotherms occurring at ~60°C and ~90°C linked to moisture removal as they represented ~3.2% weight loss (TGA). In addition to these two thermal processes, another major endotherm was seen at ~117°C. It had a shoulder on the high-temperature side implying two processes combined into one and, as it was observed for the previous batches of magnesium stearate, it was assigned to dehydration and melting of the material. The weight loss up to 120°C associated with this peak was ~0.9%. In the case of spray dried magnesium stearate RDH, the small peak at ~60°C disappeared and the shoulder appearing on the endotherm occurring at ~117°C separated, and together with the parent peak formed a broad endotherm with two maxima, at 116°C and ~125°C, indicative of dehydration and melting, respectively. The moisture content in the spray dried sample was ~4.3% as shown by TG analysis.

Generally, for all spray dried samples differences in the hydration, when compared with the unprocessed counterparts, were noticed, resulting in differences in the DSC thermograms and caused perhaps by the processing conditions as well as organic solvent used for suspension preparation. However, the water content did not change substantially.

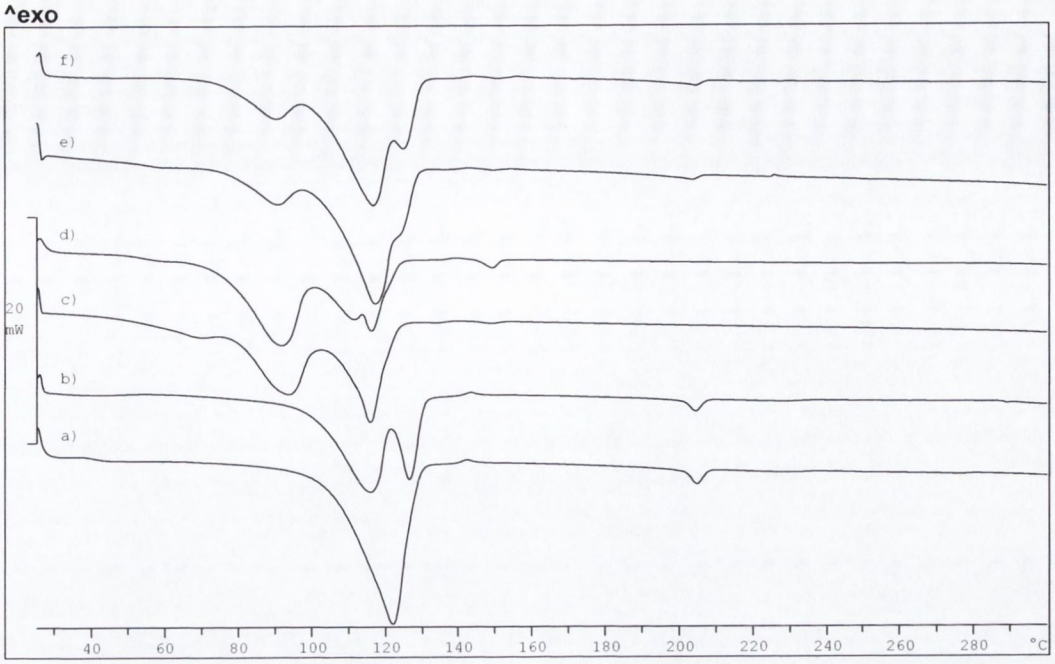

Figure 6.23 DSC scans of (a) unprocessed magnesium stearate Élan, (b) spray dried magnesium stearate Élan, (c) unprocessed magnesium stearate Aldrich, (d) spray dried magnesium stearate Aldrich, (e) unprocessed magnesium stearate RDH and (f) spray dried magnesium stearate RDH.

Figure 6.24 shows X-ray powder diffractograms of the unprocessed and spray dried magnesium stearate samples. The patterns were similar in shape and peak positions, but some changes were clearly discernible and are summarised in Table 6.2.

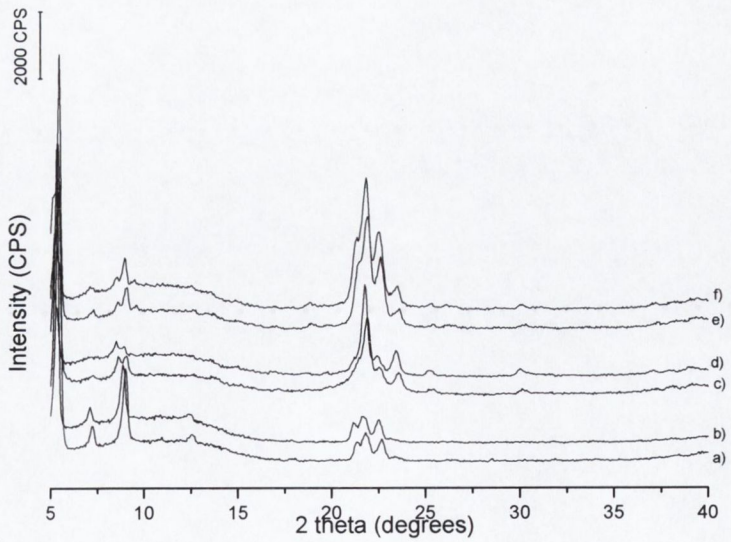

Figure 6.24 XRD diffractograms of (a) unprocessed magnesium stearate Élan, (b) spray dried magnesium stearate Élan, (c) unprocessed magnesium stearate Aldrich, (d) spray dried magnesium stearate Aldrich, (e) unprocessed magnesium stearate RDH and (f) spray dried magnesium stearate RDH.

Table 6.2 Peak positions (2θ) and their relative intensities (r. int.) of the unprocessed and spray dried samples of magnesium stearate. SD – spray dried, raw – unprocessed.

Magnesium stearate Élan raw		Magnesium stearate Élan SD		Magnesium stearate Aldrich raw		Magnesium stearate Aldrich SD		Magnesium stearate RDH raw		Magnesium stearate RDH SD	
2θ	r. int.	2θ	r. int.	2θ	r. int.	2θ	r. int.	2θ	r. int.	2θ	r. int.
				5.30	100	5.10	100	5.25	26	5.20	48
5.50	100	5.30	100					5.50	100	5.45	69
7.25	10	7.10	13	7.25	6			7.30	18	7.25	18
				8.60	11	8.65	36	8.60	8	8.50	21
9.00	23	8.90	27	9.05	11	8.90	31	9.00	32	9.00	29
12.55	8										
21.35	6	21.15	8			21.20	22	21.35	49	21.30	58
21.80	8	21.70	10	21.90	49	21.75	85	21.90	79	21.85	100
22.65	6	22.50	9	22.50	19	22.40	23	22.60	52	22.50	61
				23.55	17	23.40	27	23.60	18	23.60	21
						25.20	9				
						30.00	11				

There was nearly no impact of the processing on the magnesium stearate Élan batch, as the relative intensities of the peaks remained practically unchanged (Table 6.2). The slight alteration in the peak positions for all the samples may result from a different location of the supporting mount inside the diffractometer. Spray drying of magnesium stearate Aldrich resulted in previously unseen small intensity peaks indicating a change in the crystallographic form. A small amount of water was lost upon processing as described earlier, so these changes may account for dehydration of the powder. Generally, no extra peaks were observed to appear on the diffractogram of processed magnesium stearate RDH, but minor alterations in peak intensities may also suggest modification of the crystalline structure (Table 6.2).

Due to the different origin, animal-derived or vegetable, of the fatty acids used for production of magnesium stearate and, as indicated earlier, chemical constitution of various batches of magnesium stearate, the analysis of elements comprising the samples of magnesium stearate was carried out. The energy dispersive X-ray analysis (EDXA) method described in detail in Chapter 2 and the spectra are presented in Appendix III.

In all cases, the main peaks were of carbon and magnesium, which is expectable considering the chemical structure of magnesium stearate. The samples were contaminated with calcium and the Aldrich and RDH specimens also had aluminium traces. This would mean that the most likely both of the samples are of vegetable origin. Magnesium stearate Élan was somewhat different, as sodium and sulphur were evident on the scan indicating an animal source of the fatty acids.

Infrared spectra of the unprocessed samples are shown in Figure 6.25. All the samples have strong bands in the region 2800-3000 cm^{-1} of C-H stretching vibrations of the CH_2 and CH_3 groups constituting the hydrocarbon chain of stearic acid. A common feature is the band at ~1570 cm^{-1}

ascribed to Mg-carboxylate anion stretching vibrations. Also the band at ~1540 cm^{-1} is of the same assignment, but it is seen only on the spectra of magnesium stearate Aldrich and RDH. The appearance of this band may be associated with the hydration state of the samples as the intensity of the band increases when the water content increases. It is reasonable to say that, as being the only hydrophilic part of the molecule, the carboxylate anion can be the binding spot for the crystalline water. The ~1540 cm^{-1} and ~1570 cm^{-1} were reported to be present in a spectrum of magnesium stearate by Wada and Matsubara (1992) but no assignment was presented. The confirmation of the assignment was based on the work of Deamer *et al.* (1967).

The bands around ~1465 cm^{-1} are perhaps C-H bending peaks. The samples demonstrated different shapes of the broad band composed of a few peaks overlapping one another and located in the 3000-3600 cm^{-1}. Since, as the magnesium stearate molecule does not have OH moieties, they can be only of the crystalline water OH stretching vibrations. The band is the strongest for the magnesium stearate Aldrich.

The infrared spectra of the spray dried powders (not shown) were nearly identical with those of the "as supplied" materials, indicating that processing did not alter their chemical structures.

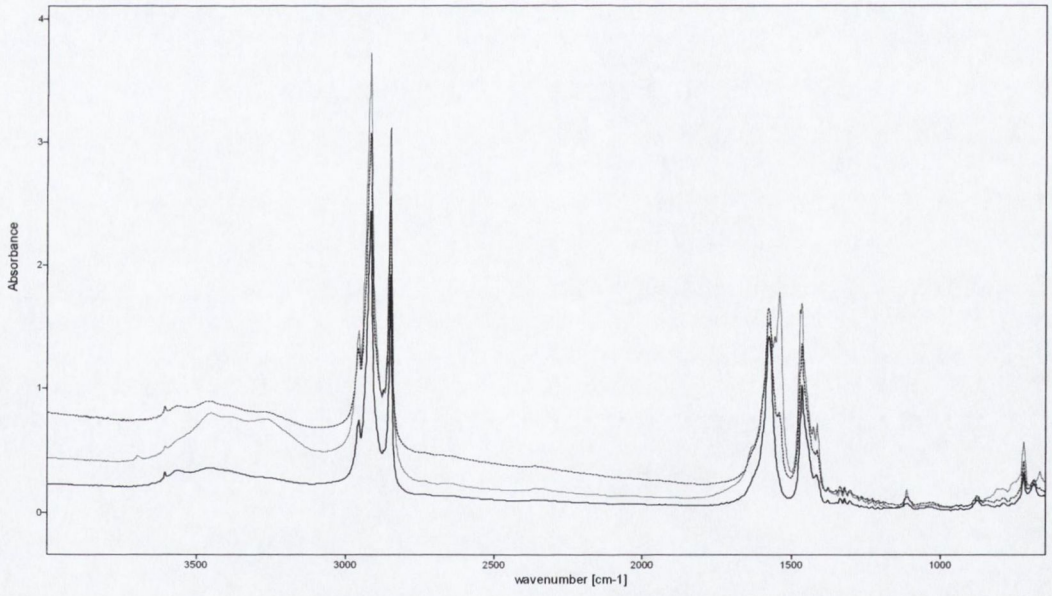

Figure 6.25 FTIR spectra of unprocessed magnesium stearate Élan (solid line), unprocessed magnesium stearate Aldrich (dotted line) and unprocessed magnesium stearate RDH (dashed line).

The samples of magnesium stearate were observed by SEM (Figure 6.26). Particles of all of them were plate-shaped with the magnesium stearate Élan having slightly larger particles. The median particle sizes were measured by Malvern Mastersizer 2000 and they were 7.0, 4.8 and 4.6 μm for the unprocessed magnesium stearate Élan, Aldrich and RDH, respectively. Spray drying did not induce considerable changes in particle size and the median sizes were as follows: 6.6, 5.0 and 4.6 μm for the spray dried magnesium stearate Élan, Aldrich and RDH, respectively.

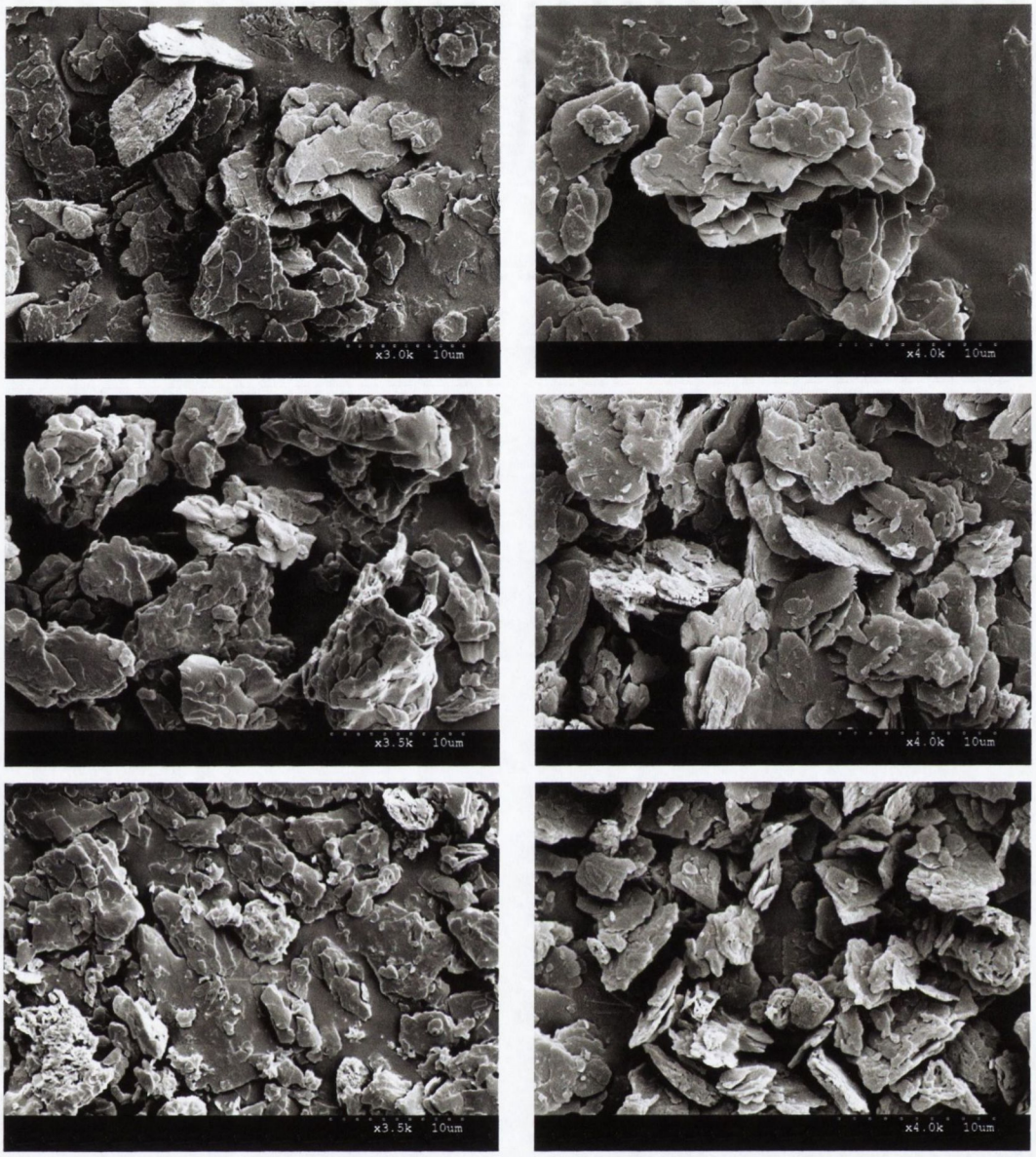

Figure 6.26 SEM micrographs of unprocessed magnesium stearate Élan (top left), spray dried magnesium stearate Élan (top right), unprocessed magnesium stearate Aldrich (middle left), spray dried magnesium stearate Aldrich (middle right), unprocessed magnesium stearate RDH (bottom left) and spray dried magnesium stearate RDH (bottom right). Note the different magnifications of the micrographs.

6.9.3 Budesonide/magnesium stearate Élan systems

6.9.3.1 Co-spray dried budesonide/magnesium stearate Élan

Three systems of budesonide with magnesium stearate Élan were spray dried from 95% (v/v) ethanol as suspensions, where the excipient constituted 1, 2 and 5% by weight of solids. The suspensions were prepared in a similar manner as the suspensions of budesonide and Aerosil (Chapter 6.6). Constant stirring by a means of a magnetic stirrer was provided during the process and the spray drying conditions are given in Appendix I.

Figure 6.27 shows the DSC thermograms obtained for the co-spray dried powders. Regardless of the magnesium stearate concentration, a small endotherm with a peak at ~88°C (1 and 2%

excipient) or ~89°C (5% excipient) was clearly discernible by DSC. Its magnitude increased with increasing content of magnesium stearate implying that it could by of the additive. The assignment cannot be precise, as the T_g of budesonide appears in the same temperature range. The endotherm was followed by an exothermic peak at ~119°C (1% excipient) or ~118°C (2 and 5% excipient) due to drug recrystallisation during heating, as magnesium stearate was shown to be crystalline after spray drying. The exotherm was followed by the budesonide melting endotherm. The peak and onset temperatures of the last process were gradually reduced as the level of the additive increased and the peak values were ~255, ~250 and ~242°C for the 1, 2 and 5% magnesium stearate concentration, respectively.

With regard to the budesonide/magnesium stearate 5% physical mixture, the DSC curve (Figure 6.27) showed three endothermic peaks. The first and second peaks reflect perhaps dehydration and melting of magnesium stearate, while the third is acknowledged as melting of budesonide. Although only one major endotherm at ~120°C (Figure 6.23) was observed and assigned as to of both dehydration and melting of the unprocessed excipient, it cannot be ruled out that the presence of the active may have caused separation of this endotherm and for the mechanical mix two thermal events are seen, at 93 and 129°C. The budesonide melting occurred at ~240°C, which is at a temperature considerably lower than the crystalline compound and in addition the shape of the endotherm was irregular.

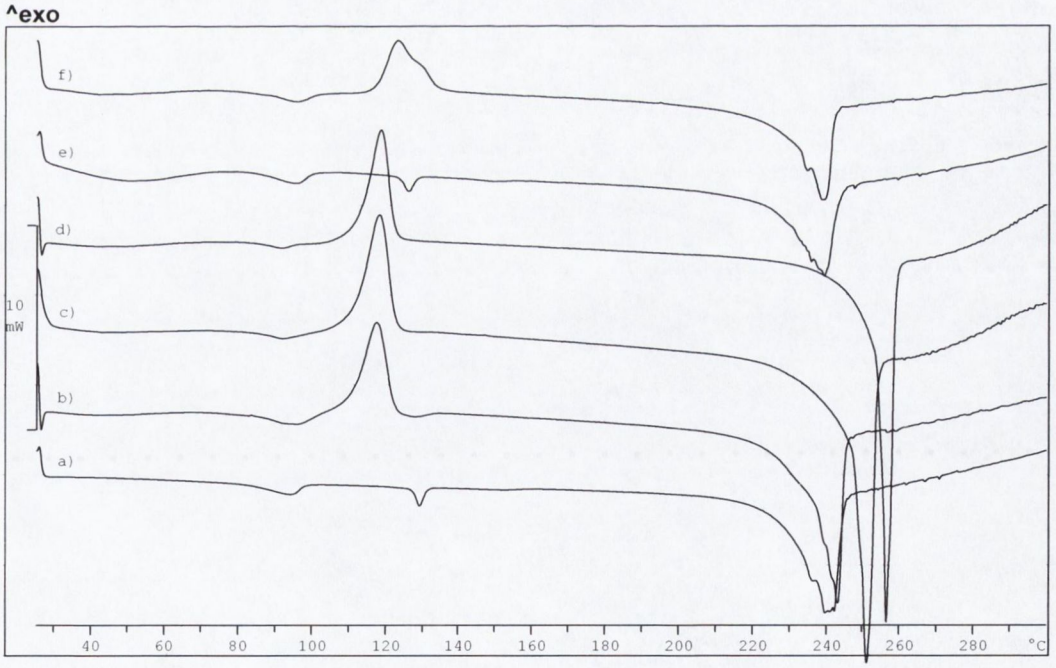

Figure 6.27 DSC scans of (a) physical mixture of budesonide and magnesium stearate Élan 5%, (b) co-spray dried budesonide/magnesium stearate Élan 5%, (c) co-spray dried budesonide/magnesium stearate Élan 2%, (d) co-spray dried budesonide/magnesium stearate Élan 1%, (e) physical mixture of budesonide, PVP 10000 10% and magnesium stearate Élan 5% and (f) co-spray dried budesonide/PVP 10000 10%/magnesium stearate Élan 5%.

Three peaks of crystalline magnesium stearate were found in the XRD pattern of the mechanically mixed budesonide with 5% magnesium stearate. The diffractogram is shown in Figure 6.28 and the excipient peaks are indicated by arrows. The X-ray patterns of the dispersions generally showed diffractograms typical of amorphous materials. However, at ~5.5 2θ degrees a single peak of small magnitude was observed, which is indicative of crystalline magnesium stearate. For the 1% magnesium stearate sample this peak was barely distinguishable from the background. With exception of this sample, other evidence of the presence of magnesium stearate was observed between 21 and 24 2θ. The X-ray diffraction traces are presented in Figure 6.28 and the arrows indicate the peaks of magnesium stearate.

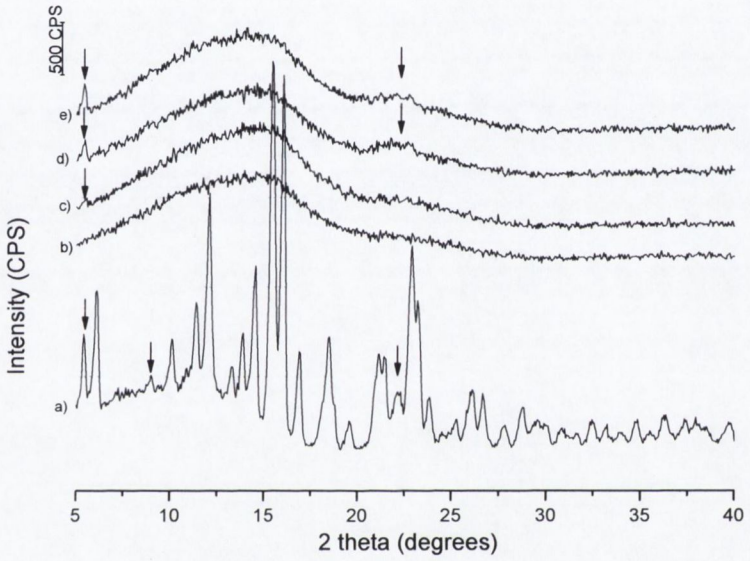

Figure 6.28 XRD diffractograms of (a) physical mixture of budesonide and magnesium stearate Élan 5%, (b) co-spray dried budesonide/magnesium stearate Élan 1%, (c) co-spray dried budesonide/magnesium stearate Élan 2%, (d) co-spray dried budesonide/magnesium stearate Élan 5% and (e) co-spray dried budesonide/PVP 10000 10%/magnesium stearate Élan 5%.

The infrared spectra of the budesonide/magnesium stearate dispersions corresponded to the pattern of spray dried budesonide confirming the amorphous nature of the drug. The only alteration of the peaks due to magnesium stearate was a different shape of the C-H stretching bands between 2800 and 3000 cm^{-1} wavenumbers caused by overlapping of the constituents' peaks in this region.

Generally, spherical, but sometimes slightly deformed particles were observed by SEM for the co-spray dried systems and sample micrographs are presented in Figure 6.29. The powders seem to be mixtures of small, even spheres and large particles with rough exteriors. The median particle size measured by Malvern Mastersizer 2000 was 3.3, 3.5 and 3.9 μm for the 1, 2 and 5% magnesium stearate-containing budesonide systems, respectively.

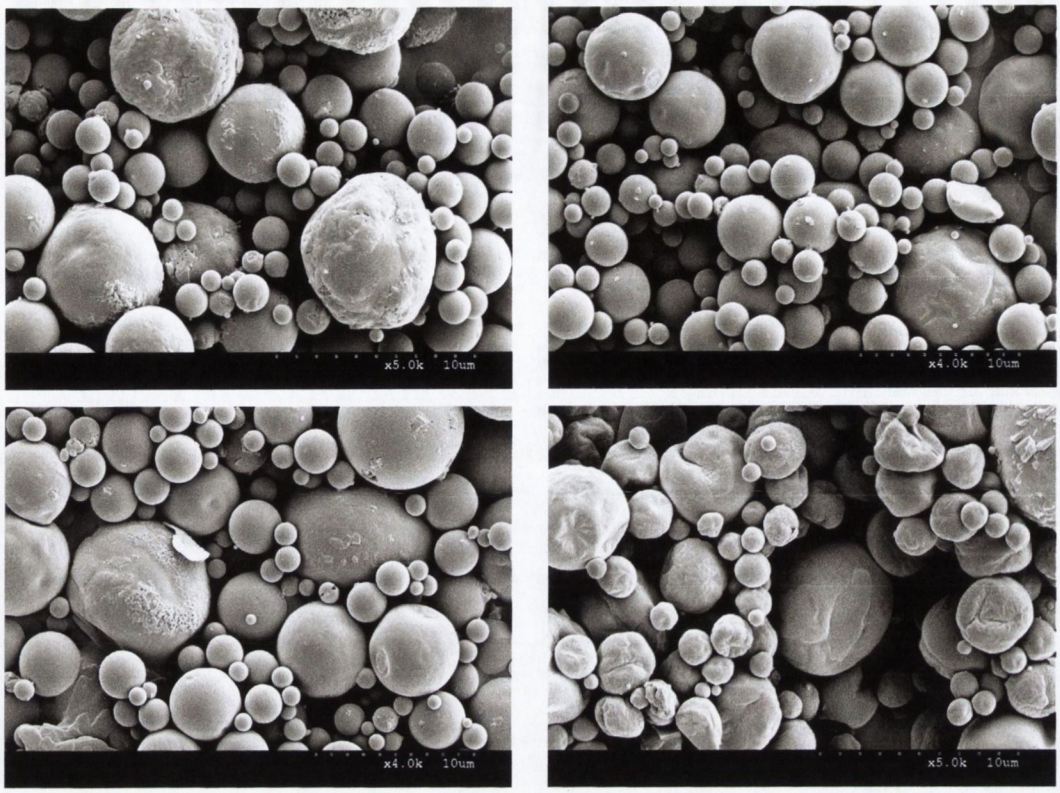

Figure 6.29 SEM micrographs of co-spray dried budesonide/magnesium stearate Élan 1% (top left), co-spray dried budesonide/magnesium stearate Élan 2% (top right), co-spray dried budesonide/magnesium stearate Élan 5% (bottom left) and co-spray dried budesonide/PVP 10000 10%/magnesium stearate Élan 5% (bottom right). Note the different magnifications of the micrographs.

6.9.3.2 Co-spray dried budesonide, PVP 10000 and magnesium stearate Élan

Only one system of budesonide with PVP 10000 and magnesium stearate Élan was spray dried. The content of PVP was chosen on the basis of the experiments on the co-spray drying of formoterol fumarate/excipient systems described in Chapter 5. PVP at 10% level succeeded best in improving the emitted fraction and also increased the fine particle dose of formoterol fumarate. Therefore the polymer content was set to be 10% (w/w). The concentration of magnesium stearate was chosen to be 5% (w/w) as this showed greatest respirable dose obtained in the twin stage impinger studies on the co-spray dried budesonide/magnesium stearate Élan described later in this chapter. The solvent used was 95% (v/v) ethanol. Firstly, a solution of budesonide and PVP was prepared and then magnesium stearate was added to formulate the suspension. Constant stirring by a means of a magnetic stirrer was provided during the process and the spray drying conditions are given in Appendix I.

The thermograms of co-spray dried and physically mixed blends of budesonide, PVP 10000 10% and magnesium stearate Élan 5% are presented in Figure 6.27. For the processed mixture, the recrystallisation phenomenon was found to occur at a higher temperature (~123°C) than the exotherms of the co-spray dried binary budesonide/magnesium stearate Élan mixtures (118-119°C). As the excipients do not recrystallise, the peak denotes the budesonide recrystallisation process. The increase in the exotherm peak temperature suggests that the amorphous phase of the drug was

stabilised by PVP and the ternary sample is more likely to exhibit extended physical stability (Van den Mooter *et al.*, 2001). The exotherm process was followed by a melting endotherm, which appears to split into two different signals (at ~233°C and ~239°C). Similar splitting of the melting peak occurred for salbutamol base co-spray dried with the same polymer, also at 10% level (Chapter 3). It seems that PVP (at least a fraction of it) dissolved in the drug and formed a complex that melts at a different temperature than the active alone. For this system, a small endotherm was seen. It was classified as a glass transition with a midpoint at ~86°C.

The thermogram of the equivalent mechanical blend exhibited three endothermic processes at ~94°C, ~126°C and ~240°C, which assignment is the same as for the previously described binary physical mix of budesonide/magnesium stearate Élan 5%.

X-ray diffraction studies showed an amorphous form of the drug to be present in the processed sample. The scan is shown in Figure 6.28. Generally, the pattern was identical with the diffractogram of the budesonide/Mg stearate Élan 5% system. The lubricant was crystalline as confirmed by a peak at 5.5 2θ characteristic of magnesium stearate and an additional "bump" on the scan between 21.0 and 24.0 2θ.

The infrared spectrum of the dispersion was similar in shape to those of the binary co-spray dried systems of budesonide and magnesium stearate Élan, with additional minor changes of the peak appearance affected by the presence of polymer. Characteristic broadening of the band at 3100-3700 cm^{-1} implied rearrangements of the hydrogen bonding.

Small, generally spherical-shaped "shrunken" particles were observed by SEM (Figure 6.29). Similar shape of particles were seen for the co-spray dried budesonide/PVP 10000 10%/stearic acid 5% system (Figure 6.11), so it seems that the presence of the polymer causes the deformation. Despite the distortions, the particle surfaces were smooth, although occasional particle fragments and particles with rough surfaces were noticed. The median particle size by Malvern Mastersizer 2000 was 3.8 μm.

6.9.4 Co-spray dried budesonide/magnesium stearate Aldrich systems

6.9.4.1 Co-spray dried budesonide/magnesium stearate Aldrich

One system of budesonide with magnesium stearate Aldrich was spray dried from 95% (v/v) ethanol as a suspension, where the excipient constituted 5% by weight of solids. The suspension was prepared in a similar manner as the suspensions of budesonide and Aerosil (Chapter 6.6). Constant stirring by a means of a magnetic stirrer was provided during the process and the spray drying conditions are given in Appendix I.

The thermogram is demonstrated in Figure 6.30 and the first process registered was a broad endotherm of the adsorbed solvent residues release found at ~55°C. The second peak was an endotherm resembling a T_g, therefore it was evaluated as a glass transition process and its midpoint was determined to be at ~75°C. This was followed by another endothermic phenomenon peaking at ~92°C ascribed to the crystalline water release from magnesium stearate (by TGA). The assignment

was based on the fact that this batch of the lubricant investigated contained the greatest fraction of the crystalline moisture. Budesonide recrystallised at ~128°C and the exotherm had two peaks, with the minor process occurring as a shoulder on the low-temperature side of the main exothermic peak. Also melting of the recrystallised drug was split with the first peak found just below 240°C and the second at ~242°C.

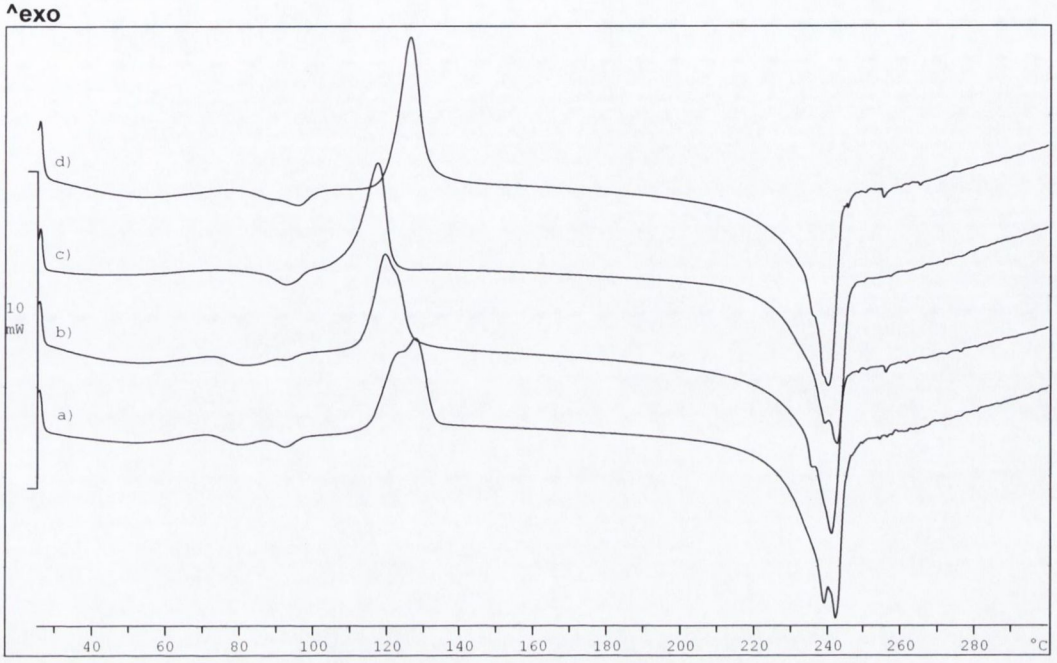

Figure 6.30 DSC scans of (a) co-spray dried budesonide/magnesium stearate Aldrich 5%, (b) co-spray dried budesonide/PVP 10000 10%/magnesium stearate Aldrich 5%, (c) co-spray dried budesonide/magnesium stearate RDH 5% and (d) co-spray dried budesonide/PVP 10000 10%/magnesium stearate RDH 5%.

The powder diffraction pattern of the dispersion did not show peaks corresponding to budesonide indicating that the drug was in an amorphous form. Magnesium stearate was crystalline, as expected, and one characteristic peak of this excipient was observed at 21.8 2θ. The diffractogram is presented in Figure 6.31 with the arrow pointing at the peak of magnesium stearate.

An infrared vibration band of magnesium stearate Aldrich at 1540 cm^{-1} was the only feature differing the FTIR spectrum of the system from that of spray dried budesonide.

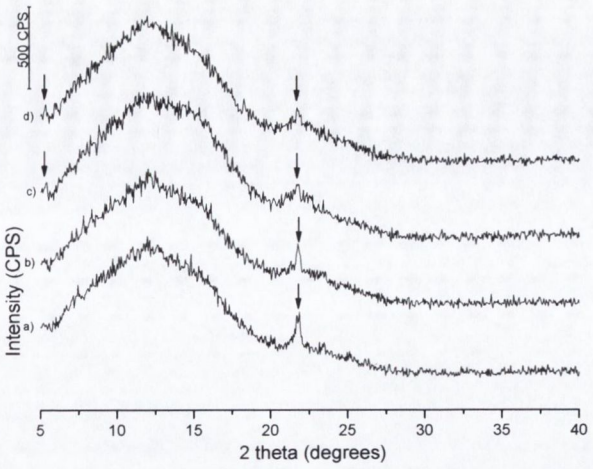

Figure 6.31 XRD diffractograms of (a) co-spray dried budesonide/magnesium stearate Aldrich 5%, (b) co-spray dried budesonide/PVP 10000 10%/magnesium stearate Aldrich 5%, (c) co-spray dried budesonide/magnesium stearate RDH 5% and (d) co-spray dried budesonide/PVP 10000 10%/magnesium stearate RDH 5%. The arrows indicate peaks of magnesium stearate.

A sample SEM micrograph displayed in Figure 6.32 showed that the system was composed of spherical and smooth particles. A small amount of particulate fragments can additionally be observed. The median particle size by Malvern Mastersizer 2000 was 2.8 μm.

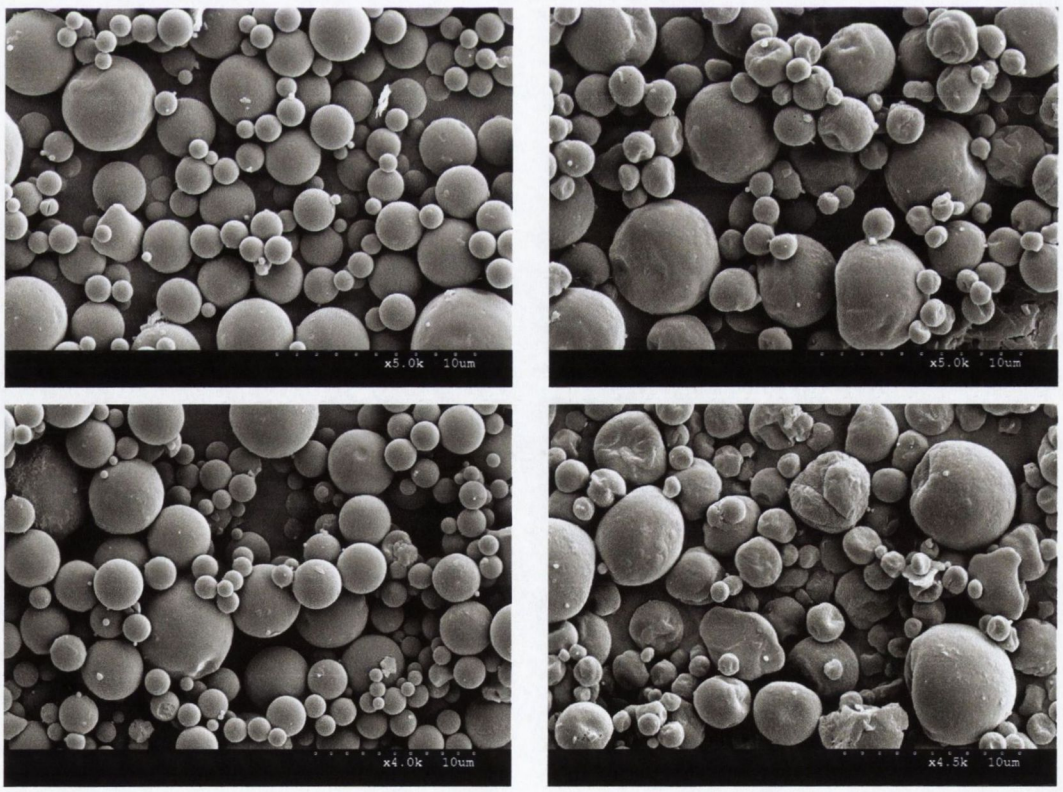

Figure 6.32 SEM micrographs of co-spray dried budesonide/magnesium stearate Aldrich 5% (top left), co-spray dried budesonide/PVP 10000 10%/magnesium stearate Aldrich 5% (top right), co-spray dried budesonide/magnesium stearate RDH 5% (bottom left) and co-spray dried budesonide/PVP 10000 10%/magnesium stearate RDH 5% (bottom right). Note the different magnifications of the micrographs.

6.9.4.2 Co-spray dried budesonide, PVP 10000 and magnesium stearate Aldrich

One system of budesonide with PVP 10000 10% and magnesium stearate Aldrich was spray dried from 95% (v/v) ethanol as a suspension, where the excipient constituted 5% by weight of solids. The suspension was prepared in a similar manner as the suspension of budesonide PVP and magnesium stearate Élan (Chapter 6.9.3.2). Constant stirring by a means of a magnetic stirrer was provided during the process and the spray drying conditions are given in Appendix I.

A DSC trace showed in Figure 6.30 is basically similar to that previously observed for budesonide/magnesium stearate Aldrich formulated without PVP. The T_g was shifted by 1°C in comparison with the binary system to higher temperatures and occurred at ~77°C. The recrystallisation exotherm was asymmetric and actually peaked at ~119°C, which is considerably lower than the sample containing no polymer. The higher Tg suggests an improvement in the physical stability of the ternary mixture when compared to the sample having no PVP and it is consistent with the antiplasticising properties of the polymer (Zhang and Zografi, 2001). Nevertheless, the sample recrystallised at a lower temperature implying otherwise. This unusual behaviour of PVP may perhaps be explained by the moisture interchange taking place between magnesium stearate and the drug/polymer mixture as the polymer is known to be hygroscopic.

The XRD pattern was identical with that of the sample lacking PVP and indicated amorphous budesonide. The diffractogram is presented in Figure 6.31 and a peak (indicated by an arrow) of the excipient can also be seen.

Similar alterations of the FTIR spectrum to those observed for the ternary mixture of budesonide, PVP and magnesium stearate Élan were discerned together with broadening of the hydrogen bonding region.

The particles constituting the powder were deformed sphere-shaped. The sample SEM micrograph is presented in Figure 6.32 and depicts particle shapes. The median particle size was the same as for the binary budesonide/magnesium stearate Aldrich specimen and was 2.8 μm as determined by the laser diffraction technique with a use of Malvern Mastersizer 2000.

6.9.5 Co-spray dried budesonide/magnesium stearate Riedel de Haën systems

6.9.5.1 Co-spray dried budesonide/magnesium stearate Riedel de Haën

One system of budesonide with magnesium stearate RDH was spray dried from 95% (v/v) ethanol as a suspension, where the excipient constituted 5% by weight of solids. The suspension was prepared in a similar manner as the suspensions of budesonide and Aerosil (Chapter 6.6). Constant stirring by a means of a magnetic stirrer was provided during the process and the spray drying conditions are given in Appendix I.

A small endotherm (with a peak at ~93°C) followed by a single exotherm (with a peak at ~118°C) was observed by DSC (Figure 6.30). The endotherm may be either a glass transition of the material or a weak peak of the excipient, whereas the exotherm is probably budesonide recrystallisation.

The DSC curve resembles those previously seen for the processed budesonide/magnesium stearate Élan powders, but the endotherm was weaker. The budesonide melting endotherm peaked at ~241°C and showed signs of splitting.

The powder was predominantly amorphous and, as only two weak peaks of the excipient were found at 5.40 and 21.65 2θ in the XRD diffractogram, it can be said that budesonide was completely amorphous. The XRD pattern is shown in Figure 6.31 with the arrows indicating the peaks of crystalline magnesium stearate.

The infrared spectrum was nearly superimposable with that of amorphous budesonide with two additional absorptions found in the C-H stretching region at 2851 and 2918 cm^{-1}.

The median particle size was 2.6 μm (determined by Malvern Mastersizer 2000) and the powder was composed of small, generally smooth spheres possessing minor surface indentations or occasionally having rough exteriors (Figure 6.32).

6.9.5.2 Co-spray dried budesonide, PVP 10000 and magnesium stearate Riedel de Haën

One system of budesonide with PVP 10000 10% and magnesium stearate RDH was spray dried from 95% (v/v) ethanol as a suspension, where the excipient constituted 5% by weight of solids. The suspension was prepared in a similar manner the suspension of budesonide PVP and magnesium stearate Élan (Chapter 6.9.3.2). Constant stirring by a means of a magnetic stirrer was provided during the process and the spray drying conditions are given in Appendix I.

The DSC thermogram is in principle similar to that of the binary, no PVP containing system as showed in Figure 6.30. An additional, endotherm which was small in magnitude peaked at ~85°C and it may be of magnesium stearate. The recrystallisation exotherm was sharper and more distinct occurring at ~126°C. The peak melting of budesonide was depressed when compared o the crystalline substance and split into two signals with the main endotherm at ~240°C.

The XRD pattern (Figure 6.31) was the same as of the previous system with two small peaks of magnesium stearate and amorphous "halo" of budesonide.

Amongst the differences in the infrared spectra of the system and amorphous budesonide are weak peaks of PVP which were obviously not present in the system of budesonide alone. There is also slight broadening in the hydrogen bonding absorptions between 3100 and 3700 cm^{-1}.

Particles of this powder were in the main spherical but distorted with wrinkled surfaces. The sample micrograph is presented in Figure 6.32. The median particle size was estimated by Malvern Mastersizer 2000 to be 2.7 μm.

6.10 Evaluation of *in vitro* respirable fractions of the co-spray dried budesonide/magnesium stearate systems by twin stage impinger

The twin stage impinger studies were carried out in triplicate for each budesonide sample modified with magnesium stearate and/or PVP. Their performance was compared to that of budesonide starting material and spray dried powders. Each portion of the powder retained in different parts of the inhalation device and stages of the testing apparatus was expressed as the percent of the total dose loaded into the capsules and presented as a bar plot in Figure 6.33.

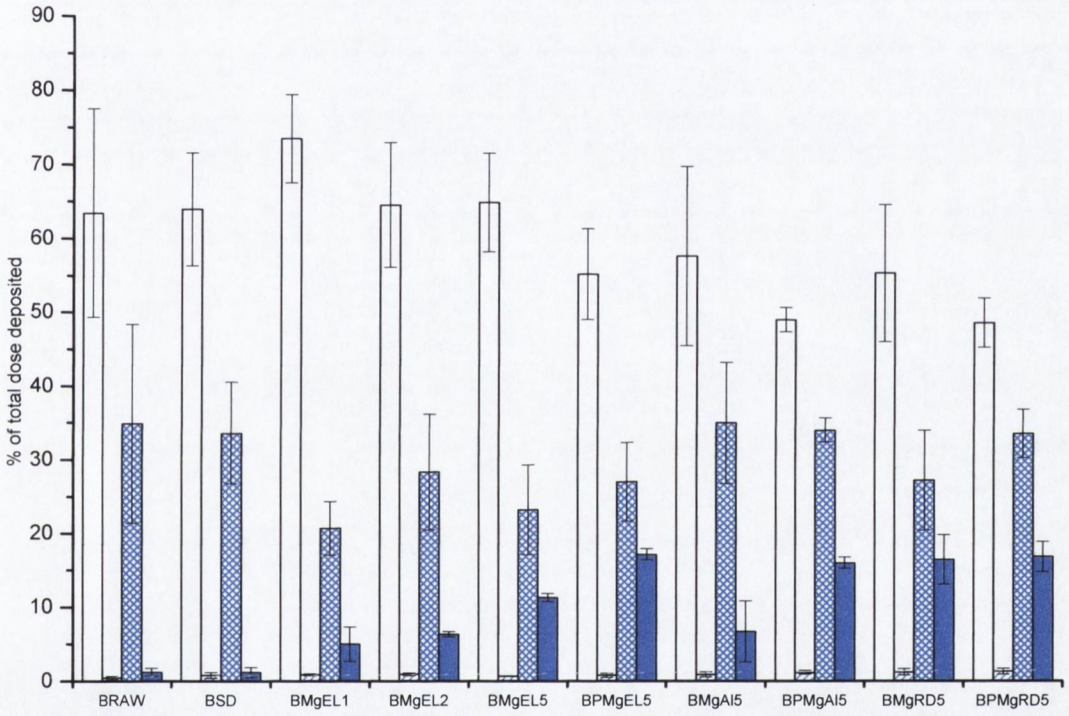

Figure 6.33 Twin impinger analysis of spray dried and unprocessed budesonide and the budesonide/magnesium stearate co-spray dried samples. The white, blue diagonal, blue grid and full blue filled bars indicate the percentage retained in the capsule and device, mouthpiece, stage 1 and stage 2 on the twin stage impinger, respectively. Key: RAW – unprocessed, SD – spray dried, B – budesonide, MgEL – magnesium stearate Élan, MgAl – magnesium stearate Aldrich, MgRD – magnesium stearate RDH and P – PVP 10000 10%. The number indicates the percentage content of the excipient.

ANOVA results (not presented) indicated that none of the samples investigated emptied from the device better than any of the single drug systems, nevertheless co-spray dried budesonide/PVP/magnesium stearate Aldrich and budesonide/PVP/magnesium stearate RDH had superior emitted fractions than the binary processed blend of budesonide/magnesium stearate Élan 5%. The greatest ratio of dose retained in the device to that emitted is for co-spray dried budesonide/magnesium stearate Élan 1% and is 2.8 (73.39% device/26.61% emitted) and the

lowest is for co-spray dried budesonide/PVP 10%/magnesium stearate RDH 5% and is 0.9 (48.47% device/51.53% emitted).

The percentage of total dose deposited in stage 2 of the twin impinger i.e. respirable fractions is shown in Figure 6.34 and the output from the statistical analysis by ANOVA is presented in Table 6.3.

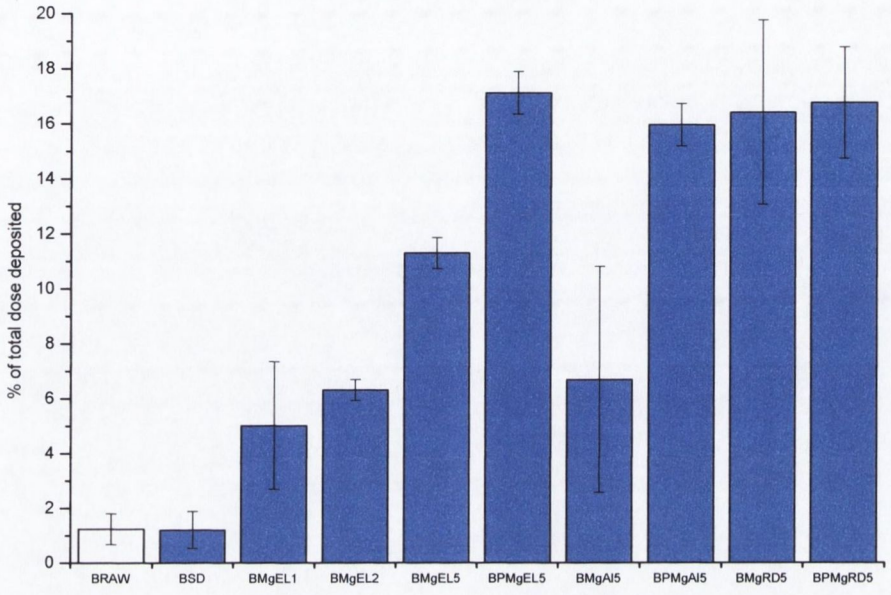

Figure 6.34 The respirable fractions (i.e. deposited on stage 2 of twin impinger) of spray dried and unprocessed budesonide and the budesonide/magnesium stearate co-spray dried samples. Key – as Figure 6.33.

Table 6.3 ANOVA comparing the respirable fractions for the spray dried and unprocessed budesonide and budesonide/magnesium stearate samples. Key – as Figure 6.33.

				Individual 95% Confidential Intervals For Mean Based on Pooled StDev
Level	N	Mean	StDev	-+---------+---------+---------+-----
BRAW	5	1.640	0.685	(--*--)
BSD	5	1.236	0.554	(--*--)
BMgEL1	3	5.017	2.329	(--*---)
BMgEL2	3	6.320	0.382	(---*--)
BMgEL5	3	11.300	0.566	(---*---)
BPMgEL5	3	17.123	0.784	(---*--)
BMgAl5	3	6.687	4.127	(---*---)
BPMgAl5	3	15.960	0.767	(---*--)
BMgRD5	3	16.410	3.355	(--*---)
BPMgRD5	3	16.763	2.024	(---*---)
				-+---------+---------+---------+-----
Pooled StDev =		1.849		0.0 6.0 12.0 18.0

The effect of magnesium stearate concentration on the respirable fractions of the binary systems was determined by examining the results for the three budesonide/magnesium stearate Élan systems. The average respirable fraction increased with an increase in the lubricant content, with significant differences between the 5% magnesium stearate sample and both 1 and 2% excipient-containing systems. As seen in Table 6.3, the 1 and 2% dispersions were not shown to be different.

Among the binary systems processed with various sources of the lubricant the best was the mixture with magnesium stearate RDH and the mean respirable fraction attained was well over 2-fold greater than that of the budesonide/magnesium stearate Aldrich powder and nearly 1.5-fold greater than that of the sample containing 5% magnesium stearate Élan. The dihydrate form is that of the best lubricant properties (Rajala and Laine, 1995) and the batch of the Aldrich excipient was recognised as being dihydrate before spray drying. The other samples contained less water before and after spray drying, thus they may be considered as having lesser lubricant efficiency. It is therefore unexpected to find that actually the dihydrate form produced the worst fine particle fraction. Furthermore, if the determinant of the respirable fraction was to be the particle size of the composites, the system with magnesium stearate Aldrich would have intermediate aerolisation properties. It is likely that other factors e.g. particle morphology influences the inhalation characteristics of the binary budesonide/magnesium stearate systems. It may be speculated that the lubricant properties of magnesium stearate in co-spray dried systems will depend on whether this excipient is located on the surface or is rather embedded inside the particles.

The co-spray dried ternary systems were comparable as regards the fine particle fractions. Regardless of the magnesium stearate batch these systems achieved superior respirable doses. It was previously presented in Chapter 5 that PVP improved the emitted fractions, but it seems that the polymer, when in a mixture with magnesium stearate, can also significantly enhance the fine particle fractions.

Generally, a significant difference was found between the respirable fractions of all co-spray dried binary and ternary mixtures and unprocessed budesonide except the system containing 1% magnesium stearate Élan.

6.11 Production and characterisation of budesonide porous particles

To date, all marketed dry powder inhaler products rely on jet-milled, micronised drugs (Steckel and Brandes, 2004). The micronisation process leads to small and irregular particles having high surface energies causing adhesion and cohesion of the particles, thereby showing poor flow properties. A high degree of micronisation can also be attained by spray drying. Obtained in this way particles are often rendered spherical, as showed in the previous chapters, which consequently results in lowering of the area of contact between particles leading to a higher respirable fraction than mechanically micronised active (Chew and Chan, 1999).

The manufacture of porous particles which have low densities and are aerodynamically suitable for inhalation purposes presents an opportunity to optimise the lung delivery. It has been demonstrated by many authors that those particles disperse well from both DPIs (Vanbever *et al.*, 1999; Steckel and Brandes, 2004) and MDIs (Dellamary *et al.*, 2000; Hirst *et al.*, 2002). A number of preparation techniques have been employed, for instance solvent extraction or evaporation (Steckel and Brandes, 2004). The spray drying method has also been used and porous particles were shown to be

produced from emulsions containing a fluorocarbon compound as the blowing agent and a surfactant (Dellamary *et al.*, 2000; Steckel and Brandes, 2004).

However, the preparation of porous particles by spray drying from a simple solution containing an active and dissolved blowing agent has not yet been reported. In this novel method, ammonium carbonate was employed as the pore-making substance and 80% (v/v) ethanol was used as the solvent. Ammonium carbonate constituted 10% (w/w) of the solids dissolved. The influence on the inlet temperature settings on the physicochemical and aerolisation properties of the resultant powders was additionally investigated and two different temperatures were chosen: 78 and 85°C. The rest of the spray drying conditions is given in Appendix I.

The results from thermal analysis are shown in Figure 6.35. From the DSC curve of the ammonium carbonate "as supplied" powder it can be seen that the melting point peak of the blowing agent was around 97°C. Another endotherm peaked at ~124°C and it was attributed to thermal decomposition. TGA registered a steady weight loss starting at 25°C and complete sample evaporation occurred just before 140°C.

Infrared analysis was carried out on all co-spray dried samples to confirm if all ammonium carbonate was removed during drying. All spectra perfectly matched the absorption spectrum of spray dried budesonide alone and even minor changes in either peak positions or shapes were absent.

The DSC trace of the sample processed at the inlet temperature of 78°C is presented in Figure 6.35. A small endotherm assigned to the T_g of budesonide was observed and the midpoint determined was ~91°C. This temperature corresponds well to that of the T_g of amorphous budesonide, estimated to be ~89.5°C (Chapter 4). The budesonide main recrystallisation exotherm occurred at ~116°C and just prior to this a second, low in magnitude exotherm peaked at ~102°C. The melting endotherm was sharp with a peak of ~262°C and arose at exactly the same temperature as that of spray dried budesonide.

The thermogram of the budesonide system spray dried at the higher temperature (Figure 6.35) resembled that of amorphous budesonide prepared without additives. The T_g was detected at ~91°C and this was followed by the budesonide recrystallisation exotherm peaking at ~128°C, which for spray dried drug appeared at ~130°C. Also the sharp melting endothermic peak was recorded to occur at ~262°C, indicating no differences with amorphous budesonide.

No thermal events of ammonium carbonate were seen for both co-spray dried systems and therefore, as supported by the FTIR analysis, it can be concluded that the powders were composed solely of amorphous budesonide.



Figure 6.35 DSC scans of (a) spray dried budesonide, (b) co-spray dried budesonide/ammonium carbonate 10% at the inlet temperature 78°C, (c) co-spray dried budesonide/ammonium carbonate 10% at the inlet temperature 85°C and (d) crystalline ammonium carbonate.

The amorphous nature of the powders was confirmed by a diffused "halo" appearing on both of the diffractograms. The XRD patterns are shown in Figure 6.36.

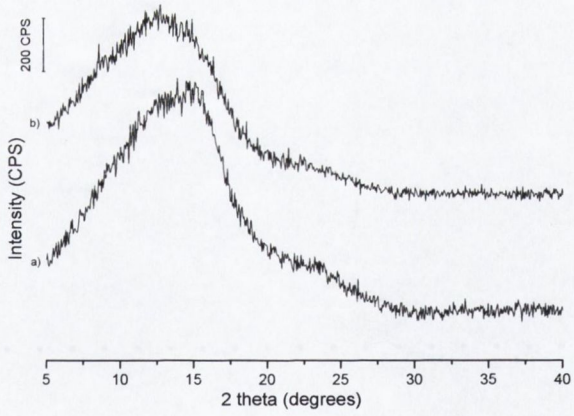

Figure 6.36 XRD diffractograms of (a) co-spray dried budesonide/ammonium carbonate 10% at the inlet temperature 78°C and (b) co-spray dried budesonide/ammonium carbonate 10% at the inlet temperature 85°C.

Sample SEM micrographs of the budesonide co-spray dried with ammonium carbonate systems are shown in Figure 6.37. The sample processed at 78°C consisted exclusively of spheroidal porous particles (top left). The top right micrograph shows the topology of one of the particles at a higher magnification and presents the non-solid structure of the particle. The bottom pictures present the particles of the sample spray dried at 85°C and a mixture of porous and "wrinkled", corrugated particles having rough surfaces can be discerned.

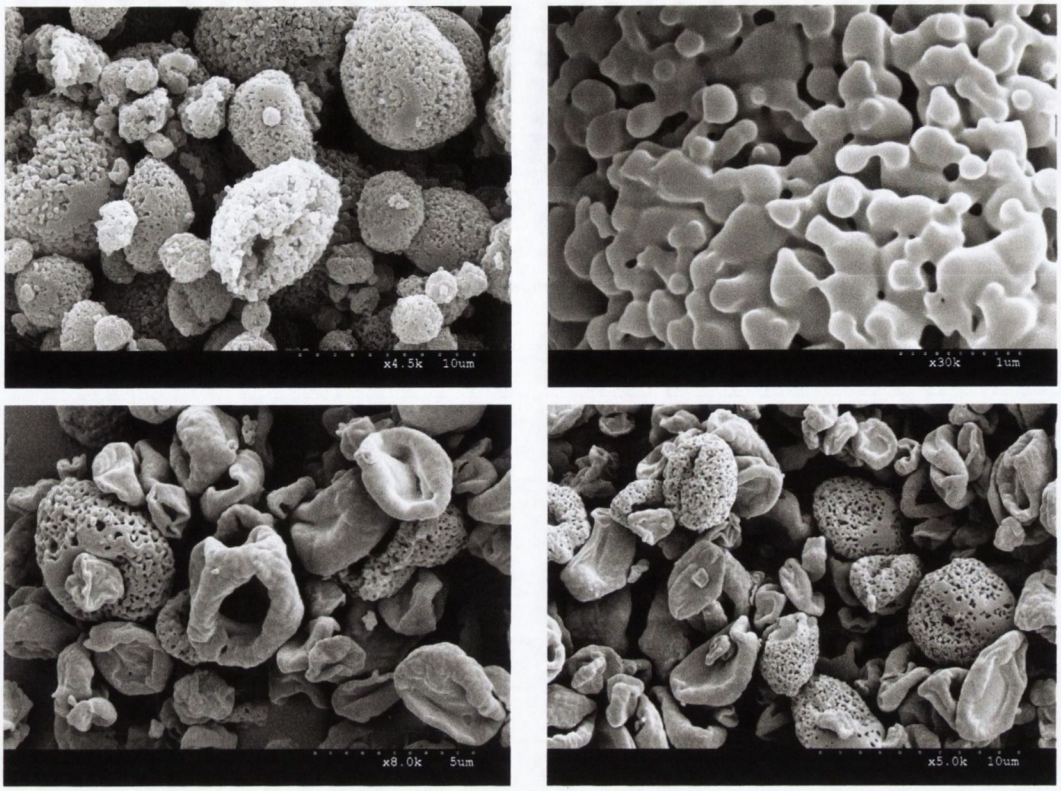

Figure 6.37 SEM micrographs of porous particle of budesonide spray dried at the inlet temperature 78°C (top) and porous particle of budesonide spray dried at the inlet temperature 85°C (bottom). Note the different magnifications of the micrographs.

The particle size distribution profiles of the two porous systems were different, as presented in Figure 6.38. The sample spray dried at 85°C showed a narrower particle size distribution. The system processed at the lower inlet temperature exhibited a fraction of submicron sized particles. This may be due to their fragile nature and perhaps some of them may have fragmented in the compressed air during the analysis. Similar values of the median particle size were determined by Malvern Mastersizer 2000 and they were 2.9 and 2.6 μm for the system spray dried at 78 and 85°C, respectively.

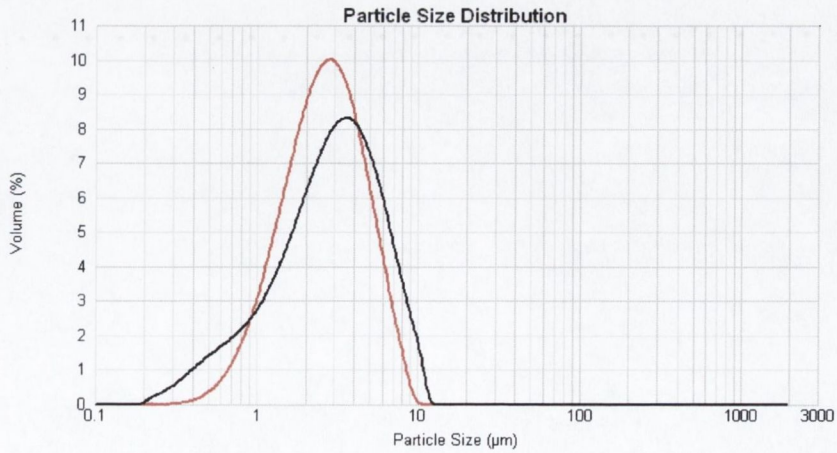

Figure 6.38 Particle size distribution profile of porous particle of budesonide spray dried at the inlet temperature 78°C (black) and porous particle of budesonide spray dried at the inlet temperature 85°C (red).

The mechanism of formation of the porous particles is not clear. It has been found in the literature (Wakisaka *et al.*, 2001) that for ethanol/water mixtures the formation of alcohol self-aggregating clusters was observed when the molar fraction of ethanol was ~0.2 and above. Therefore, it can be hypothesised that, as ammonium carbonate is insoluble in ethanol and on the other hand budesonide is insoluble in water, a microemulsion-like mixture comprising of the aqueous solution of ammonium carbonate and ethanolic solution of budesonide is formed. During drying, ammonium carbonate decomposes into volatile ammonia and water and together with the ethanol vapour the expanding gases are removed with the drying medium leaving a porous particle. As seen from the SEM micrographs the manufacturing process depends on the temperature inside the drying chamber. Perhaps, when the vapours are more rapidly eliminated, the porous structure is not given enough time to be developed or maybe the fine organisation of the liquid mixture is being destroyed.

Appendix IV presents the SEM micrographs of porous particles composed of compounds other than budesonide. These systems were produced as the results of similar studies on other materials in an attempt to produce porous particles. The studies on porous particles are being continued in our laboratory.

6.11.1 Twin stage impinger studies

The twin stage impinger studies were performed in triplicate for each porous budesonide samples. For comparison purposes, their performance was contrasted with those of systems showing the best aerolisation properties achieved in the two previous sections of this chapter – co-spray dried budesonide/HP-β-cyclodextrin and budesonide/PVP 10000 10%/magnesium stearate Élan 5%. They were also compared to the budesonide starting material and spray dried powders. Each portion of the powder retained in different parts of the inhalation device and stages of the testing apparatus was expressed as the percent of the total dose loaded into the capsules and presented as a bar plot in Figure 6.39.

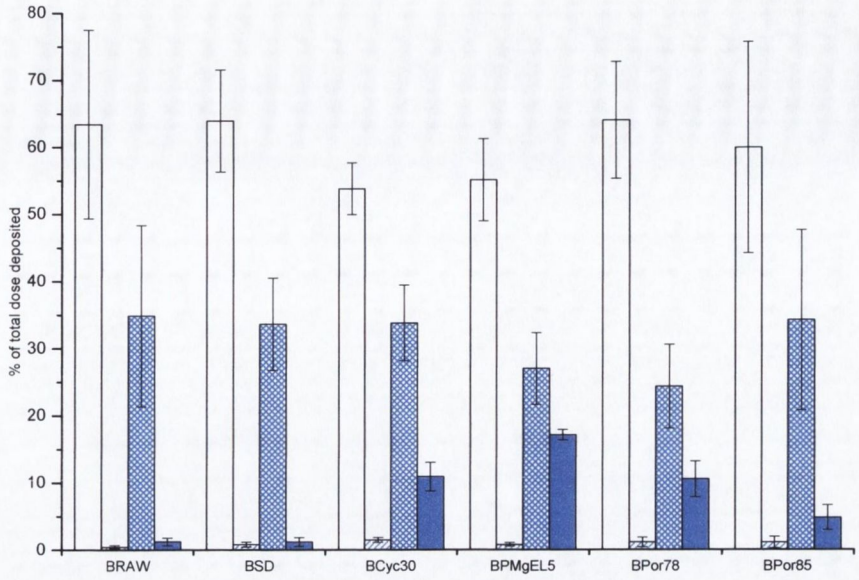

Figure 6.39 Twin impinger analysis of spray dried and unprocessed budesonide, co-spray dried budesonide/HP-β-cyclodextrin 30%, co-spray dried budesonide/PVP 10000 10%/magnesium stearate Élan 5% and porous budesonide samples. The white, blue diagonal, blue grid and full blue filled bars indicate the percentage retained in the capsule and device, mouthpiece, stage 1 and stage 2 on the twin stage impinger, respectively. Key: RAW – unprocessed, SD – spray dried, B – budesonide, Cyc – HP-β-cyclodextrin 30%, MgRD – magnesium stearate RDH 5%, P – PVP 10000 10%, Por – ammonium carbonate 10%, 78 and 85 – inlet temperature of 78 and 85°C, respectively.

The porous particles did not show an improvement of the emitted dose fractions for both of the porous budesonide samples when statistically (using ANOVA, results not shown) compared to those of non-porous systems. The confidence intervals overlapped in all cases indicating no significant variations.

The results for the stage 2 deposition of the twin impinger are depicted in Figure 6.40. The fine particle fractions of the two porous budesonide batches appeared to differ and a considerably lower portion of the powder spray dried at the higher temperature was lodged in the lower stage of impinger. To substantiate this observation, a one-way ANOVA was carried out and the data are presented in Table 6.4.

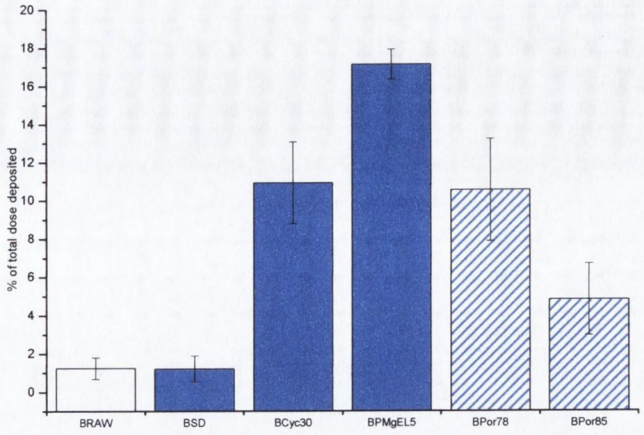

Figure 6.40 The respirable fractions (i.e. deposited on stage 2 of twin impinger) of spray dried and unprocessed budesonide, co-spray dried budesonide/HP-β-cyclodextrin 30%, co-spray dried budesonide/PVP 10000 10%/magnesium stearate RDH 5% and porous budesonide samples. Key – as Figure 6.39.

Table 6.4 ANOVA comparing the respirable fractions of spray dried and unprocessed budesonide, co-spray dried budesonide/HP-β-cyclodextrin 30%, co-spray dried budesonide/PVP 10000 10%/magnesium stearate RDH 5% and porous budesonide samples. Key – as Figure 6.39.

			Individual 95% Confidential Intervals For Mean Based on Pooled StDev				
Level	N	Mean	StDev	-+---------+---------+---------+-----			
BRAW	5	1.640	0.685	(--*-)			
BSD	5	1.236	0.554	(-*-)			
BCyc30	3	10.923	2.139			(--*--)	
BPMgEL5	3	17.123	0.784				(--*--)
BPor78	3	10.540	2.667			(--*--)	
BPor85	3	4.813	1.864		(--*--)		
				-+---------+---------+---------+-----			
Pooled StDev =		1.472		0.0	6.0	12.0	18.0

From Table 6.4 it can be seen that the respirable fractions achieved from the two powders consisting of porous budesonide particles were significantly different with better performance of the sample processed at 78˚C. The fine particle fraction obtained with this material was comparable to that of co-spray dried budesonide/HP-β-cyclodextrin, but in turn it was not superior to that of the spray dried ternary mixture of the active with PVP and magnesium stearate.

All fine particle fractions attained with the porous particles of budesonide were significantly greater than the doses acquired with either micronised, crystalline budesonide or the active spray dried alone. The improvement in the respirable fraction was striking, especially for the sample produced at the inlet temperature of 78˚C, and over a 6-fold and nearly a 3-fold increase in the fine particle fraction was accomplished with the sample spray dried at 78 and 85˚C, respectively, when compared to that of the budesonide starting powder.

Due to the low bulk density (the precise studies were not performed) of the powders quantities of only 35±2 mg were loaded into capsules (see Chapter 2 Materials and methods). Since respirable fractions calculated on the basis of percentage of total dose are reliant on the amount of powder

filled into the capsules (Vanbever *et al.*, 1999), the fine particle fractions were also determined based on the emitted doses are presented graphically in Figure 6.41.

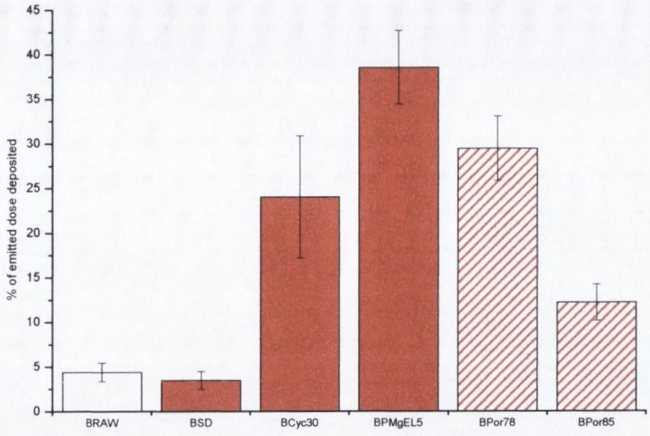

Figure 6.41 The respirable fractions (i.e. deposited on stage 2 of twin impinger) of spray dried and unprocessed budesonide, co-spray dried budesonide/HP-β-cyclodextrin 30%, co-spray dried budesonide/PVP 10000 10%/magnesium stearate RDH 5% and porous budesonide samples calculated on the basis of the emitted dose only. Key – as Figure 6.39.

As much as 38% of the dose released from the device was deposited in the lower stage of impinger. The best sample among the systems comprising of porous particles gave nearly a 30% deposition, whereas the percentage of the particles of unprocessed and spray dried budesonide reaching the stage 2 was only 4.4 and 3.4%, respectively.

Bearing in mind that no toxicological studies on magnesium stearate have been done yet to date and that the safety of HP-β-cyclodextrin in pulmonary delivery has not been fully established to date, the particles composed only of the active present advantages over the powders containing these additives.

6.12 Crystallinity of co-spray dried budesonide systems by FTIR and XRD.

A variety of different methods have been applied to quantify crystallinity and the X-ray powder diffraction (XRD) technique remains one of the most widely used procedure (Black and Lovering, 1977). FT-Raman has also been used in the quantification of the amorphous content of indomethacin by Taylor and Zografi (1998) and near-infrared (NIR) spectroscopy has recently been introduced by Hogan and Buckton (2001a) as an alternative method for quantification of amorphous and crystalline forms of lactose.

Generally, the spectroscopic methods have the advantage that the analysis can be very rapid and often no sample preparation is required (Taylor and Zografi, 1998b). The application of Fourier Transform Infrared (FTIR) spectroscopic techniques to assess polymer crystallinity has been done

for many years (Wu *et al.*, 2001), but little information on the use of the FTIR method to determine crystallinity of pharmaceutical systems has been found (Black and Lovering, 1977).

For the quantitative analysis of crystallinity of a system, it is necessary to identify peaks characteristic of each, amorphous and crystalline, form (Taylor and Zografi, 1998b). Consequently, having observed the differences in the positions of the carbonyl stretching bonds of budesonide, these peaks were chosen as potential candidates for the quantitative analysis. The greatest shift was identified for the conjugated dihydrobenzenoquinone C=O and both amorphous and crystalline forms had easy to determine maxima at 1657.5 and 1667.0 cm^{-1}, respectively. Therefore only this peak was used for further investigations. It was noticed that the carbonyl absorption of untreated budesonide was broad probably as a consequence of a small amount of an amorphous phase being present in the sample. It may be due to milling of the crystalline material. The contribution of the amorphous peak to the crystalline peak intensity was also taken into account. Curve fitting (using Origin software) of the recorded scans in the 1640-1690 cm^{-1} range was utilised and up to three Gaussian peaks provided an adequate fit for all the systems studied. Not all the co-spray dried systems were subjected to the mathematical spectrum deconvolution and the samples containing an excipient, which infrared spectrum exhibited strong band(s) in the given above wavenumbers range were not included.

As mentioned above, the measured infrared spectra were subjected to the deconvolution procedure i.e. separation of the overlapping peaks. The maximum of the crystalline band was taken as 1667 cm^{-1} and the amorphous as 1657.5 cm^{-1}. These values were held constant throughout the fitting procedure, as was the position of the peak at 1653 cm^{-1}. The latter was observed for all investigated systems that were XRD crystalline, but its assignment, unfortunately, remains unidentified.

As the spectra were not normalised, the ratio of the areas of the crystalline and amorphous separated peaks was chosen to represent the crystallinity index and therefore to eliminate the effect of sample concentration. For instance, Black and Lovering (1977) instead of separation of the bands utilised the ratios of various peak heights. The determined areas of the peaks and the computed crystallinity indices are summarised in Table 6.5.

Table 6.5 The areas of the separated crystalline (C) and amorphous (A) budesonide C=O peaks, crystallinity indices and the degree of budesonide crystallinity by XRD for various samples.

System	area of the crystalline peak at 1667 cm^{-1} (C)	area of the amorphous peak at 1657.5 cm^{-1} (A)	area of the peak at 1653 cm^{-1}	crystallinity index	degree of crystallinity by XRD (%)
BRAW	26.44	1.97	5.44	13.42	100
BSD	3.10	28.37	0	0.11	0
BAer5	3.50	28.74	0	0.12	0
BAer10	2.33	20.87	0	0.11	0
BStA1	18.27	3.66	1.68	4.99	40
BStA2	25.44	2.52	4.54	10.10	74
BStA5	19.46	3.52	6.44	5.53	31
BStA10	18.91	4.84	2.59	3.91	31
BCel5	3.37	24.67	0	0.14	0
BCel10	4.32	29.81	0	0.14	0
BMgEL1	2.34	30.26	0	0.08	0
BMgEL2	2.34	30.68	0	0.08	0
BMgEL5	3.24	31.48	0	0.10	0
BMgAl5	1.82	27.16	0	0.07	0
BMgRD5	1.69	24.23	0	0.07	0
BPor78	2.79	26.79	0	0.10	0

The crystallinity indices for the XRD amorphous samples were below 0.15 in all cases and for the systems demonstrating peaks on X-ray diffractograms the ratios were much greater.

An attempt to correlate the crystallinity indices with the degree of crystallinity determined by X-ray diffraction analysis for the budesonide dispersions was made. For the XRDs the combined area under the strongest peaks placed between 14.90 and 16.50 2θ i.e. exhibiting maxima at 15.50 and 16.10 2θ was taken for calculations. The crystallinity of unprocessed budesonide was assumed to be 100%. Table 6.5 gives the percentage content of the crystalline form calculated by XRD.

Figure 6.42 shows a correlation plot relating the percentage of the remaining crystalline form of the drug in different systems with the corresponding values of the crystallinity index estimated on the basis of the FTIR analysis.

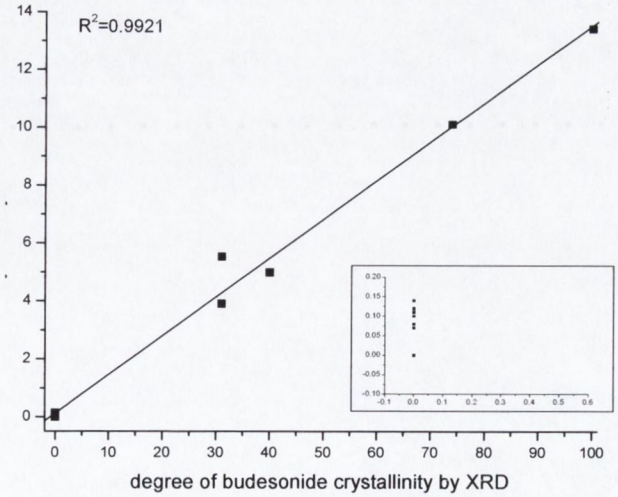

Figure 6.42 Correlation of the degree of budesonide crystallinity determined by XRD with the crystallinity indices calculated for the infrared analysis. The smaller graph is a magnified part of the main graph presenting the overlapping points lying close to the point of origin. R^2 – the correlation coefficient.

The plot was fitted by least squares analysis to a straight line which has a correlation coefficient of 0.9921, indicating a very good fit. One point did not fall on the fitted line signalling a deviation from the general trend. The data point belongs to the co-spray dried budesonide/stearic acid 5% system. Previous studies have found a good agreement between the degree of crystallinity measured by infrared spectroscopy and the X-ray diffraction method (Black and Lovering, 1977). But according to Meyers (2000) XRD assesses long-range order whereas infrared measures short-range order of the molecules. Therefore, these analytical techniques may not necessarily measure the same crystallinity. It is more likely that FTIR is able to detect small sized crystallites dispersed in the amorphous matrix, thereby overestimating the degree of crystallinity when compared with the XRD results. This phenomenon might be the cause for the point found to be an outlier in the correlation plot (Figure 6.42).

6.13 Conclusions

The particle sizing analysis revealed that all particles of the co-spray dried systems were in the inhalable range, but no correlation of the particle size with either emitted or respirable fractions were discerned, as presented in Figure 6.43. Hence, it can be assumed that the surface modification defines the aerolisation properties of these systems.

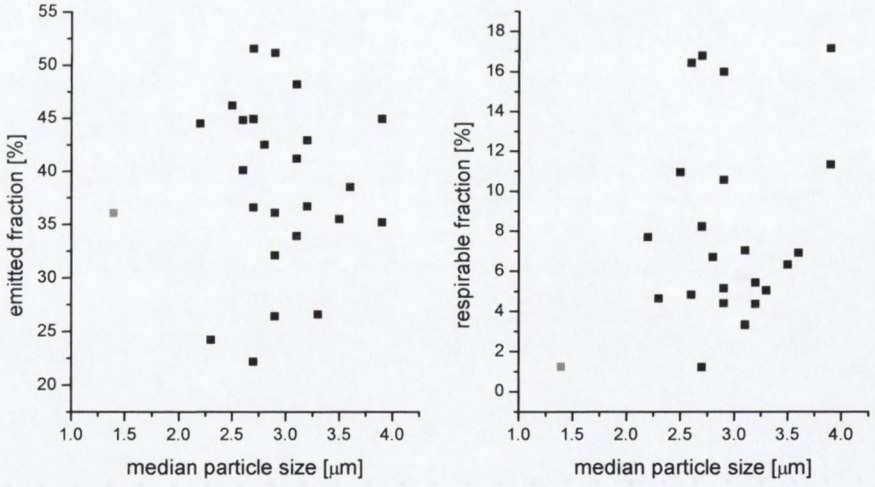

Figure 6.43 Correlation between the median particle size of the unprocessed and spray dried budesonide as well as co-spray dried budesonide/excipient samples and (a) emitted fraction (b) respirable fraction. The grey square indicates unprocessed budesonide.

Not all spray dried systems were amorphous, which was apparent from the DSC and XRD traces. The series of budesonide/stearic acid systems was partially crystalline with the highest degree of crystallinity for the 2% stearic acid sample and the melting endotherm of stearic acid was observed for 2, 5 and 10% content of this excipient in co-spray dried composites. Also the system containing budesonide, stearic acid and PVP contained remnants of the crystalline active, but a considerable increase in the amorphous phase content was observed.

Budesonide in all magnesium stearate specimens was amorphous, but the lubricant processed either alone or with the drug was crystalline. No reduction in the degree of magnesium stearate crystallinity was shown upon addition of PVP into the binary systems. All other co-spray dried systems were XRD amorphous.

The twin stage impinger analysis of the budesonide powders comprising an excipient other than magnesium stearate revealed that the sample with the best deposition on the stage 2 of twin impinger was co-spray dried budesonide and HP-β-cyclodextrin 30%. The quite good aerolisation properties of the budesonide/Aerosil 10% powder was attributed to the presence of porous, "sponge"-like particles. Among the system spray dried with magnesium stearate the ternary systems having the lubricant and PVP achieved the superior respirable doses. The effect of magnesium stearate concentration on the respirable fractions of the binary systems was also examined with the 5% magnesium stearate sample performing better that those containing the excipient at lower levels.

A novel method of preparation of porous particles made solely of budesonide by spray drying from a solution containing an active and dissolved blowing agent was presented. The manufactured powders differed in the morphology of the particles, which was dependent on the inlet temperature employed in spray drying. Also the aerolisation behaviour was found to be dissimilar with the completely porous system giving an over 6-fold increase in the fine particle fraction compared to that of the budesonide starting powder.

A good correlation was obtained between the percentage of the remaining crystalline form of the drug in different systems and the corresponding values of the crystallinity index estimated on the basis of the FTIR analysis.

CO-SPRAY DRIED FORMOTEROL FUMARATE DIHYDRATE/EXCIPIENT COMPOSITES FOR USE IN DPIs

7.1 Introduction

Apart from the patent literature little has been published concerning the stability of formoterol fumarate and its formulation into MDIs. Formoterol and its derivative have proven difficult to formulate in conventional aerosols. Such formulations have exhibited short shelf-lives and require refrigeration (Lewis *et al.,* 2001). Therefore, there is a need for aerosol formulations for such β-agonist drugs that remain chemically and physically stable during storage at ambient conditions of temperature and humidity (Blondino *et al.,* 2002). Besides storage at low temperatures, the stability problem of active ingredients in solutions may also be solved by a conventional technology adopted in the pharmaceutical field, based on reservoir container systems designed for the reconstitution of solution immediately before use, wherein a liquid component (solvent) and a solid component (soluble material) are placed in separate compartments. Two basic problems are met if this technology is considered for formoterol fumarate formulations for inhalatory use. The first is that it may not be possible to dose the required quantity of active ingredient with sufficient precision as the standard dose of formoterol is usually about 12 microgram. Another problem encountered is that the excipients have to be chosen only among those approved for respiratory use, with demonstrated tolerability on the respiratory tract (Meoli *et al.,* 2004).

On the other hand, aerosol formulations consisting of propellant and formoterol fumarate without additional excipients sometimes exhibit problems such as caking on manufacturing equipment, high deposition in the vial or valve of inhalers and valve sticking (Oliver *et al.,* 2000). Water absorption is the second major problem encountered in formulating formoterol for therapeutic use (Gao *et al.,* 2001). In addition, aerosol compositions consisting of formoterol fumarate, hydrofluoroalkane (HFA-134a) and ethanol have proven to be extremely sensitive to ethanol concentrations. Ethanol concentrations of 3.5% (w/w) may cause unacceptable crystal growth, however its presence assists in the stability, the general performance and in the manufacture of the formulation (Oliver *et al.,* 2000).

In spite of the fact that formoterol as the fumarate dihydrate has been demonstrated to be stable on long-term storage, even at high temperatures and high relative humidities, its chemical structure makes the molecule prone to chemical degradation when in contact with e.g. a reactive species like an aldehyde (lactose) or under stress conditions (Trofast, 2000). Due to the higher polarity of the HFA propellants with respect to CFC (chlorofluorocarbon) vehicles, HFA solution formulations may suffer to a greater extent from chemical stability problems with respect to the corresponding CFC formulations. The higher polarity of the vehicle may accelerate the rate of the formamide (a functional group of formoterol) solvolysis reaction and affect the chemical stability of formoterol fumarate. The chemical stability may be improved by the proper and combined selection of the canister type and apparent environmental pH (pH') (Lewis *et al.,* 2001). It was found that the pH' of the drug dissolved in propellant can be adjusted with strong mineral acids such as hydrochloric or phosphoric and that formoterol is most stable if the apparent pH is between 3.0 and 3.5. The addition of a low volatility component with a reduced polarity with respect to the co-solvent, such

as an ester, may allow either the amount of acid to be added for adjusting pH to be reduced or the polarity of the medium to be diminished so limiting the possible uptake of environmental water (Lewis *et al.*, 2001). The physical stability of formulations can be improved when mixtures of HFA-134a and HFA-227 are used which density match with the drug. Stable suspensions may be obtained by the incorporation of a micronised bulking agent which will slowly sediment in the propellant e.g. lactose, DL-alanine (Oliver *et al.*, 2000).

The aim of the present study was to achieve, first of all, the best chemical stabilisation of the formoterol fumarate dihydrate but also to maximise the physical performance of a dispersion of the drug in propellant. Unfortunately, there is little information available in literature about the chemical stability of formoterol fumarate. Akapo and Asif (2003) reported poor hydrolytic stability of the drug in a low pH aqueous environment (pH<4). They also published limited data regarding the forced degradation of formoterol fumarate in 0.1M HCl and NaOH. Information on the solid state chemical stability of formoterol fumarate dihydrate alone and in mixtures with lactose was presented in Chapter 5.

7.2 Chemical stability of formoterol fumarate in solutions

7.2.1 Order of reaction

Three different types of buffer were used in order to assess the impact of pH on the degradation rates of formoterol fumarate. They were: the Britton-Robinson, phosphate and citrate buffer. The preparation and composition of each of these buffers is described in Chapter 2. In the case of the Britton-Robinson buffered solutions the stability studies were carried out at two temperatures: 40°C and 25°C. The analysis at 40°C was aimed at screening the buffered solutions of formoterol fumarate with a wide pH range between 2.05 and 9.60 in order to choose three or four pH values at which the drug degradation rates were the slowest. The phosphate and citrate buffers were chosen as they are physiologically compatible. Furthermore, the salts constituting their solutions are not volatile and further stability studies of formoterol fumarate in the solid state can be carried out (see Section 7.4).

Generally, the pH values of all the buffered reaction mixtures did not vary by more than 0.1 pH unit during the incubation period.

Previous work of Mälkki and Tammilehto (1990) on the stability of salbutamol demonstrated that the degradation kinetics of the drug were generally first-order. Here, formoterol fumarate dissolved in Britton-Robinson buffer solutions exhibited similar behaviour and the kinetics of the chemical degradation process were also of first-order. The degradation processes in some of the phosphate and citrate buffers as well as deionised water showed sigmoidal degradation kinetics. These results suggest that the decomposition of the drug followed a complicated kinetic mechanism (Carstensen, 1995). An analogous phenomenon was observed by Teraoka *et al.* (1993) for ranitidine hydrochloride in acetate buffer.

The rate constants (k_{obs}) were calculated assuming first-order reaction kinetics (Equation 7.1):

$$\ln c = \ln c_0 - k_{obs} \cdot t \qquad \text{(Equation 7.1)}$$

where c and c_0 are the time dependent and the initial concentrations of formoterol fumarate at the times: t>0 and t=0, respectively and k_{obs} is the observed rate constant of the first-order reaction of degradation.

The k_{obs} coefficients were determined from the slopes of the plots of the natural logarithm of the remaining formoterol fumarate concentration versus time. The method of least squares fit was used to determine the slope. The half-lifes were calculated from Equation 7.2:

$$t_{1/2} = \frac{0.693}{k_{obs}} \qquad \text{(Equation 7.2)}$$

and shelf-lifes from Equation 7.3:

$$t_{10} = \frac{0.105}{k_{obs}} \qquad \text{(Equation 7.3)}$$

7.2.2 HPLC assay and degradation products of formoterol

The stability indicating HPLC assay of formoterol fumarate is described in Chapter 2. This method was developed and validated by IVAX Pharmaceuticals and only a few minor changes were introduced to adjust it to the current HPLC system. The original IVAX technique used an electrochemical amperometric detector DECADE and because this type of detector was not available to us, UV detection was utilised instead. The wavelength was set to 242 or 280 nm as in the method of HPLC assay for formoterol fumarate developed by Akapo and Asif (2003). It was also found that the phosphate buffer:acetonitrile ratio 78:22 used by IVAX caused tailing of the formoterol peak, therefore this was optimised and set to 83:17.

Information about the possible decomposition products was also supplied by IVAX Pharmaceuticals. Their names and relative retention times are presented in Table 7.1.

Table 7.1 Potential degradation products of formoterol fumarate and their relative retention times reported in the original specification of the HPLC method supplied by IVAX.

Compound name	Relative retention time
Diastereoisomer of formoterol fumarate (FF isomer)	0.99
Formoterol fumarate desformyl analog [a)] (FFD)	0.88
Formoterol fumarate acetamide analog [a)] (FFA)	1.05
2-hydroxy-5-formyl formanilide (A-4)	0.62

[a)] also reported by Akapo and Asif (2003)

HPLC analysis revealed that different degradation compounds were formed depending on the pH of the buffer solutions. Table 1 in Appendix V lists the position and retention times of the peaks detected. It contains also detailed peak assignment. The retention times and relative retention times differ slightly from the original HPLC assay due to the changes introduced (described above).
It appears that the compound FFD is the main decomposition product at pH<8.20. Above this value formoterol fumarate degraded into many unknown chemical entities without any major product. The FFA compound is formed at nearly neutral (pH=6.70) and alkaline pH only. It is noteworthy that in the whole pH range additional peaks with retention times between 2.00 and 5.00 min were detected, suggesting the formation of decomposition products with low molecular weights. These were not analysed as they were overlapped by the buffer peaks.

7.2.3 pH-rate degradation profile

7.2.3.1 Britton-Robinson buffer at 40°C

The pH-rate degradation profile of formoterol fumarate at 40°C is shown in Figure 7.1. It was constructed from the observed decomposition rates presented in Table 7.2.

Table 7.2 Decomposition rates (k_{obs}), half-lives ($t_{1/2}$) and shelf-lives (t_{10}) for formoterol fumarate in the Britton-Robinson buffer at 40°C. Number of data points taken for the calculations: pH of 2.05 and 8.20 – 16 data points, pH of 3.00, 8.70 and 9.60 – 19 data points, pH of 3.90 and 6.10 – 21 data points, pH of 6.70 – 23 data points and pH of 5.00 – 37 data points.

pH	$10^3 \times k_{obs}$ [day^{-1}] S.D.	$t_{1/2}$ [day]	t_{10} [day]	R^2
2.05	359.86 ± 0.66	1.93	0.29	0.9993
3.00	45.22 ± 0.21	15.33	2.32	0.9921
3.90	8.94 ± 0.41	77.52	11.74	0.9511
5.00	2.58 ± 0.10	268.60	40.70	0.8638
6.10	6.06 ± 0.09	114.45	17.34	0.9266
6.70	14.64 ± 0.46	47.35	7.17	0.9705
8.20	98.51 ± 0.98	7.04	1.07	0.9834
8.70	103.37 ± 0.27	6.70	1.02	0.9976
9.60	80.80 ± 0.41	8.58	1.30	0.9970

The rate constants were not corrected for zero buffer concentration (k_0) as the ionic strength of the Britton-Robinson buffer solutions was low (μ=0.1). The points represent the experimental data, while the line through the data points corresponds to the fit of the data to the mathematical model developed as an aid to understanding the degradation kinetics of formoterol.

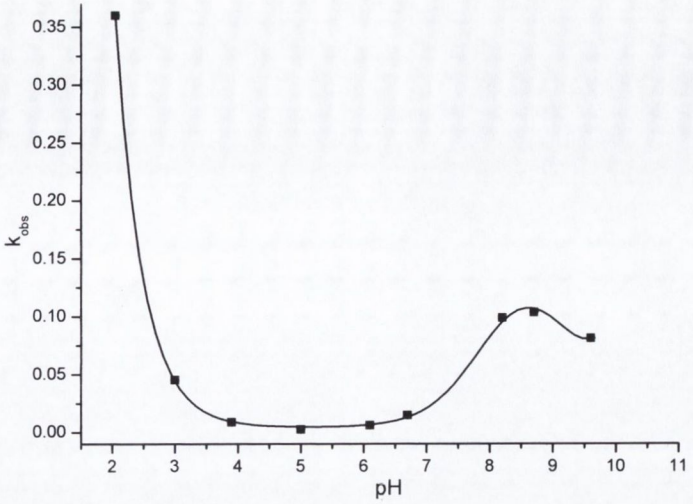

Figure 7.1 The pH-rate profile for the degradation of formoterol fumarate in the Britton-Robinson buffer at 40°C.

In aqueous solution, formoterol can exist as the cationic (FH^+), unionised (F) and anionic (F^-) species depending on the pH of the solution. The dissociation constants for this compound have been determined by Ochsner *et al.* (1999) and reported as being 7.88 for the secondary amino group (pKa_1) and 9.33 for the phenolic group (pKa_2). The amide group of formoterol is considered as neutral because it does not dissociate (Wade, 1991). Thus, one can predict from the Henderson-Hasselbach equation (Equation 7.4) that practically the sole presence of only one type of the above species exists at a pH lower or higher than pKa±1.

$$pH = pK_a + \log \frac{basic \quad species}{acidic \quad species} \qquad \text{(Equation 7.4)}$$

Figure 7.2 presents the same pH-rate profile of degradation of formoterol fumarate as shown in Figure 7.1 but with a graphical illustration of the dissociation process of the drug.

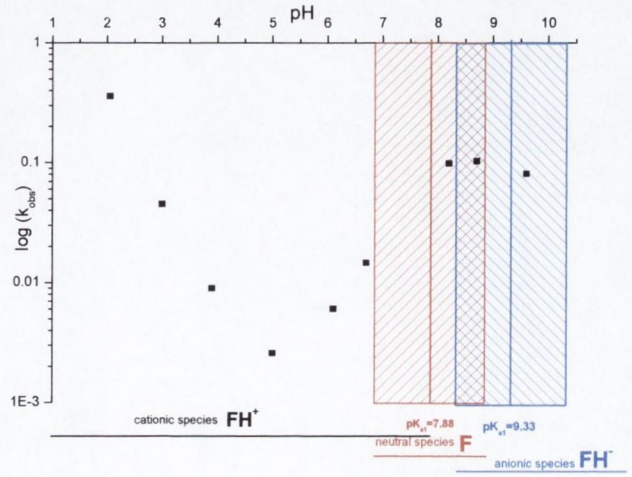

Figure 7.2 Dissociation of formoterol and its pH-rate degradation profile in Britton-Robinson buffer at 40°C.

The observed rate in the pH-rate profile is a summation of a series of rates of catalytic reaction by the hydrogen and hydroxyl ions and water molecules. The degradation of formoterol is rapid in the acidic region indicating specific hydrogen-ion catalysis. The reaction reaches its minimum around pH=5, then accelerates again and levels off around pH=8. Thus, the overall velocity of decomposition of the drug is equal to the total sum of the microscopic rates of degradation of different formoterol species driven by H^+, OH^- and H_2O. Against this background, one can write all possible reactions occurring between the ions and formoterol species in aqueous solution (Table 7.3):

Table 7.3 Possible reactions and their rate constants of the cationic, neutral and anionic fractions of formoterol in aqueous solution.

Reaction	Rate constant
$FH^+ + H^+ \xrightarrow{H_2O} products$	k_1
$FH^+ \xrightarrow{H_2O} products$	k_2
$FH^+ + OH^- \xrightarrow{H_2O} products$	k_3
$F \xrightarrow{H_2O} products$	k_4
$F + OH^- \xrightarrow{H_2O} products$	k_5
$F^- \xrightarrow{H_2O} products$	k_6
$F^- + OH^- \xrightarrow{H_2O} products$	k_7

Therefore:

$$v = -d[F]/dt =$$
$$k_{obs}[F] = k_1[FH^+][H^+] + k_2[FH^+] + k_3[FH^+][OH^-] + k_4[F] \quad \text{(Equation 7.5)}$$
$$+ k_5[F][OH^-] + k_6[F^-] + k_7[F^-][OH^-]$$

where v is the velocity of the reaction, $[FH^+]$, $[F]$, $[F^-]$ are the concentrations of the cationic, neutral and anionic species of formoterol, respectively and k_1-k_7 are the macroscopic rate constants for the various reactions.

The fraction of each individual species can be calculated as a function of pH and the ionisation constants (K_{a1} and K_{a2}) of formoterol by using the following equations:

$$K_{a1} = \frac{[H^+][F]}{[FH^+]} \quad \text{(Equation 7.6)}$$

$$K_{a2} = \frac{[H^+][F^-]}{[F]} \quad \text{(Equation 7.7)}$$

and

$$f_{FH^+} = \frac{[FH^+]}{[FH^+]+[F]+[F^-]} \quad \text{(Equation 7.8)}$$

$$f_{F} = \frac{[F]}{[FH^+]+[F]+[F^-]} \quad \text{(Equation 7.9)}$$

$$f_{F^-} = \frac{[F^-]}{[FH^+]+[F]+[F^-]} \quad \text{(Equation 7.10)}$$

The equations 7.11-7.13 enable us to calculate the fractions of species of formoterol knowing only its dissociation constants:

$$f_{FH^+} = \frac{[H^+]^2}{[H^+]^2 + [H^+]\cdot K_{a1} + K_{a1}\cdot K_{a2}} \quad \text{(Equation 7.11)}$$

$$f_{F} = \frac{[H^+]\cdot K_{a1}}{[H^+]^2 + [H^+]\cdot K_{a1} + K_{a1}\cdot K_{a2}} \quad \text{(Equation 7.12)}$$

$$f_{F^-} = \frac{K_{a2}\cdot K_{a1}}{[H^+]^2 + [H^+]\cdot K_{a1} + K_{a1}\cdot K_{a2}} \quad \text{(Equation 7.13)}$$

Consequently, Equation 7.5 for the macroscopic rate of degradation of formoterol reduces to the following:

$$k_{obs} = (k_1[H^+]^3 + k_2[H^+]^2 + k_3[H^+]\cdot K_w + k_4[H^+]\cdot K_{a1} + k_5\cdot K_{a1}\cdot K_w + k_6\cdot K_{a1}\cdot K_{a2} + \frac{+k_7\cdot K_{a1}\cdot K_{a2}\cdot K_w}{[H^+]}) / ([H^+]^2 + [H^+]\cdot K_{a1} + K_{a1}\cdot K_{a2}) \quad \text{(Equation 7.14)}$$

where K_w is the autoprotolysis constant of water at 40°C equal to 13.5 (Perrin and Dempsey, 1974). Equation 7.14 was fitted to the experimental pH-rate profile by the least-squares method. It allowed for the removal of some of the terms (due to their very low values, which did not change the goodness of the fit) and the simplified model is shown below:

$$k_{obs} = (k_1[H^+]^3 + k_2[H^+]^2 + k_4[H^+]\cdot K_{a1} + \frac{k_7\cdot K_{a1}\cdot K_{a2}\cdot K_w}{[H^+]}) / ([H^+]^2 + [H^+]\cdot K_{a1} + K_{a1}\cdot K_{a2}) \quad \text{(Equation 7.15)}$$

The microscopic rate constants obtained from this model are presented in Table 7.4.

Table 7.4 Microscopic rate constants obtained from non-linear regression using kinetic model at 40°C. [b)]

k_1 (l/mol per h)	k_2 (h^{-1})	k_4 (h^{-1})	k_7 (l/mol per h)
39.91 (0.31)	$4.25*10^{-2}$ ($1.15*10^{-2}$)	$1.46*10^{-1}$ ($2.60*10^{-2}$)	401.79 (35.25)

[b)] standard errors of parameters are given in parentheses, R^2=0.9997

Figure 7.3 presents once more the pH-k_{obs} profile with the fitted curve and its deconvolution.

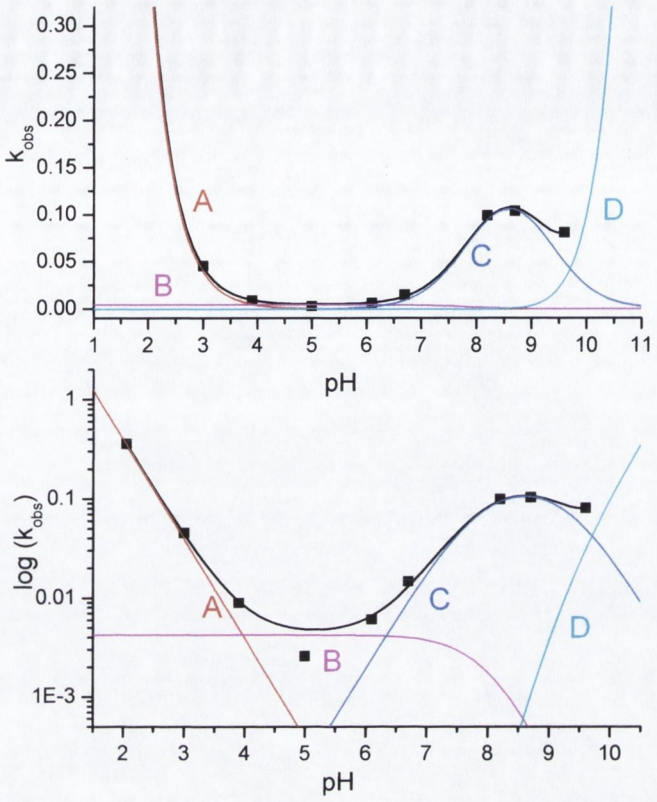

Figure 7.3 pH-rate profile in two different scales: normal (top) and logarithmic (bottom) of the degradation of formoterol fumarate in the Britton-Robinson buffer at 40°C. The points are experimental values and the lines are theoretical curves. A – (k_1) hydrogen-ion catalysed degradation of cationic species, B – (k_2) water catalysed degradation of cationic species, C – (k_4) water catalysed degradation of neutral species and D – (k_7) hydroxide-ion catalysed degradation of anionic species.

First of all, the model shows a lack of contribution of hydroxide ion catalysis on the cationic and neutral species of formoterol. As one may expect, acid catalysis of formoterol dominates in the pH region from 2 to 5. This is due to an amide group of formoterol which is not ionised in these conditions and is easily available to an H^+ attack. With increasing pH the ability of the buffer to fragment the amide bond decreases and the reaction slows down. However, it can be seen from the top Figure 7.3 that a parallel reaction to the acid catalysis occurs in this environment – solvent driven hydrolysis process of the amide and positively charged secondary amine moiety (cationic species), which leads to breaking up of the molecule. This process ends at pH around 8. The decomposition compounds can be easily monitored by HPLC analysis (Table 1, Appendix IV) and indeed, the higher the pH the more compounds elute. Between pH values 7 and 8 the hydrolysis of formoterol continues with oxidation of the alcohol group in the chain at higher pH values (indicated by the presence of compound A-4 on the chromatograms). Finally, at extremely basic pH values, the degradation of the drug increases again, as the amide group and phenolate anion are susceptible to electrophilic substitution in the presence of OH^- ions.

7.2.3.2 Britton-Robinson buffer at 25°C

Four solutions with pH values ranging from 4.00 to 6.95 were employed in the decomposition study at 25°C. Table 7.5 shows the data calculated for these samples.

Table 7.5 Decomposition rates (k_{obs}), half-lives ($t_{1/2}$) and shelf-lives (t_{10}) for formoterol fumarate in the Britton-Robinson buffer at 25°C. Number of data points taken for the calculations was 28 in all cases. * indicates the extrapolated value.

pH	10^3 x k_{obs} [day^{-1}] S.D.	$t_{1/2}$ [day]	t_{10} [day]	R^2
4.00	2.78 ± 0.06	249.73 *	37.84	0.9757
5.20	0.62 ± 0.01	1118.64 *	169.49	0.7955
6.20	1.28 ± 0.01	543.53 *	82.35	0.9320
6.95	3.94 ± 0.13	176.11	26.68	0.9871

A pH-degradation rate profile was built similarly as for the reaction temperature of 40 °C (Section 7.2.3.1) and is shown in Figure 7.4.

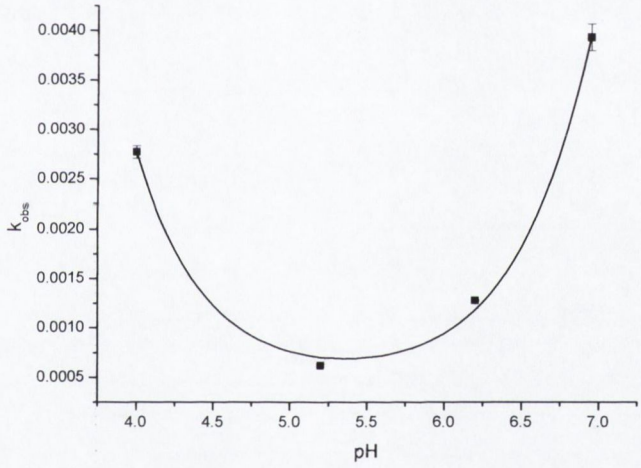

Figure 7.4 The pH-rate profile for the degradation of formoterol fumarate in the Britton-Robinson buffer at 25°C.

The same mathematical model developed previously was applied to estimate the microscopic rates of degradation at the lower temperature. Since only four points in a quite narrow range of pH values (4-7) are available, one can assume that the part of Equation 7.15 for hydroxyl ion catalysis may be excluded. In fact, there was no significant impact on k_1, k_2 and k_4 parameters when k_7 was eliminated. The following equation was then used:

$$k_{obs} = (k_1[H^+]^3 + k_2[H^+]^2 + k_4[H^+] \cdot K_{a1}) / ([H^+]^2 + [H^+] \cdot K_{a1} + K_{a1} \cdot K_{a2}) \quad \text{(Equation 7.16)}$$

Table 7.6 presents the microscopic rate constants obtained by the least squares fit of the Equation 7.16 to the measured data:

Table 7.6 Microscopic rate constants obtained from non-linear regression using kinetic model at 25°C. [c)]

k_1 (l/mol per h)	k_2 (h^{-1})	k_4 (h^{-1})
22.75 (1.71)	$4.9*10^{-4}$ ($1.1*10^{-4}$)	$3.34*10^{-2}$ ($1.61*10^{-3}$)

[c)] standard errors of parameters are given in parentheses, R^2=0.9975

All of the estimated values are lower than those given for the buffer at 40 °C. This may mean that the kinetics of degradation processes of formoterol fumarate adhere to the Arrhenius equation (Equation 7.17) (Carstensen, 1995):

$$k = A \cdot \exp^{(-E_a / RT)} \qquad \text{(Equation 7.17)}$$

where k, A, E_a, R and T are the rate constant, frequency factor, activation energy, gas constant and temperature in Kelvins, respectively.

Figure 7.5 presents the pH-k_{obs} profile together with the fitted curve and its deconvolution.

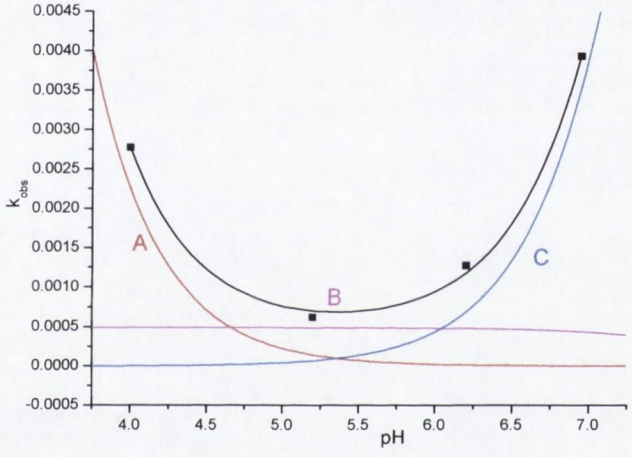

Figure 7.5 The pH-rate profile of the degradation of formoterol fumarate in the Britton-Robinson buffer at 25°C. The points are experimental values and the lines are theoretical curves. The letters have the same meaning as in Figure 7.3.

7.2.3.3 0.1 M solution of HCl at 25°C

To allow for comparison with the data on formoterol fumarate degradation provided by IVAX Pharmaceuticals UK., a decomposition study of the drug in 0.1M HCl at 25°C was carried out. The HPLC analysis was performed using the method described in Chapter 2, but the wavelength used was 280 nm due to negative peaks of the HCl solution on the HPLC chromatogram. The k_{obs} was equal to 1.93 day^{-1}, which means that 90% of the sample was left intact in the solution after 1.3 hours, whereas the $t_{½}$ was 8.6 hours. The data on the acid hydrolysis of formoterol fumarate in 0.1M HCl provided by IVAX allowed us to calculate the degradation rate, which in this case was equal to 0.99 day^{-1}. The kinetics data are shown graphically in Figure 7.6.

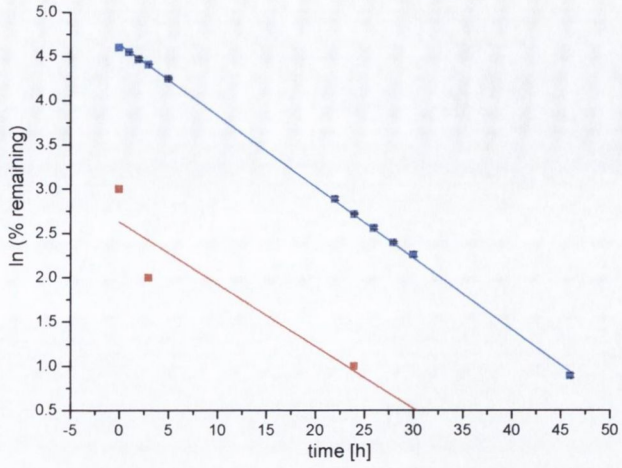

Figure 7.6 The first order reaction of decomposition of formoterol fumarate in 0.1M HCl at 25°C (blue squares) compared with the decomposition rate of the drug in the same solution as found by IVAX (red squares). The lines through the points represent linear fits.

Different conditions of storage i.e. a broad term "room temperature" instead of a specific reaction temperature used by IVAX could explain the difference between these two values.

7.2.3.4 Phosphate buffer at 25 °C

Seven solutions of phosphate buffer with pH values ranging from 4.75 to 6.25 were chosen. They covered the pH region of the best stability of formoterol fumarate as indicated by the stability study in the Britton-Robinson buffer at 25°C (Section 7.2.3.2). The ionic strength of the buffer solutions was constant and kept at 0.1. Table 7.7 shows the data calculated for these samples.

Table 7.7 Decomposition rates (k_{obs}), half-lives ($t_{1/2}$) and shelf-lives (t_{10}) for formoterol fumarate in the phosphate buffer at 25°C. Number of data points taken for the calculations was 18 in all cases. * indicates the extrapolated value.

pH	$10^3 \times k_{obs}$ [day^{-1}] S.D.	$t_{1/2}$ [day]	t_{10} [day]	R^2
4.75	1.43 ± 0.05	486.32 *	73.68	0.9489
4.90	1.35 ± 0.09	515.24 *	78.07	0.9460
5.10	1.20 ± 0.14	577.50 *	87.50	0.9395
5.40	2.67 ± 0.16	259.55 *	39.33	0.8247
5.65	2.95 ± 0.19	235.31 *	35.65	0.9399
5.95	4.89 ± 0.02	141.86	21.49	0.9160
6.25	2.55 ± 0.02	272.30 *	41.26	0.9685

A pH-degradation rate profile was constructed (Figure 7.7) and it can be noticed that it is not as smooth as the profile depicted in Figure 7.5.

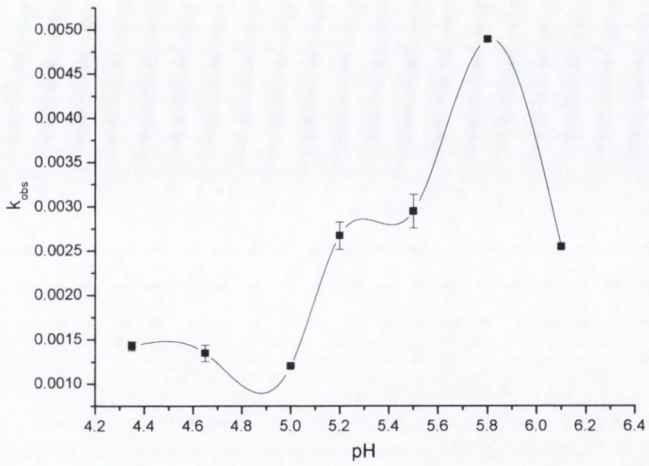

Figure 7.7 The pH-rate profile of the degradation of formoterol fumarate in the phosphate buffer at 25°C. The points are experimental values and the line through the points is for the sake of simplicity only.

Due to complexity and the very narrow range of pH investigated, no attempts were made to fit the points to Equation 7.15. The pH of maximum of stability for formoterol fumarate in the phosphate buffer was found to be at pH=5.0.

7.2.3.5 Citrate buffer at 25 °C

The stability study of formoterol fumarate in the citrate buffer at pH values below 5.0 was not possible to carry out, as the HPLC analysis showed splitting of the peak of the drug. An ion interchange could be responsible for this phenomenon and it was not investigated further. Thus, only five buffered solutions with pH ranging from 5.00 to 6.10 were explored. Similarly as for the phosphate buffered solution, the ionic strength was maintained at 0.1.The results are shown in Table 7.8.

Table 7.8 Decomposition rates (k_{obs}), half-lives ($t_{1/2}$) and shelf-lives (t_{10}) for formoterol fumarate in the citrate buffer at 25°C. Number of data points taken for the calculations was 10 in all cases. * indicates the extrapolated value.

pH	$10^4 \times k_{obs}$ [day^{-1}] S.D.	$t_{1/2}$ [day]	t_{10} [day]	R^2
5.00	5.85 ± 0.52	1184.62 *	179.49	0.9046
5.20	4.04 ± 0.71	1715.35 *	259.90	0.8266
5.50	4.87 ± 0.86	1424.46 *	215.83	0.8346
5.80	4.84 ± 1.68	1431.82 *	216.94	0.8831
6.10	6.61 ± 0.62	1048.41 *	158.85	0.9374

The k_{obs}-pH dependence plot for citrate buffer is presented in Figure 7.8.

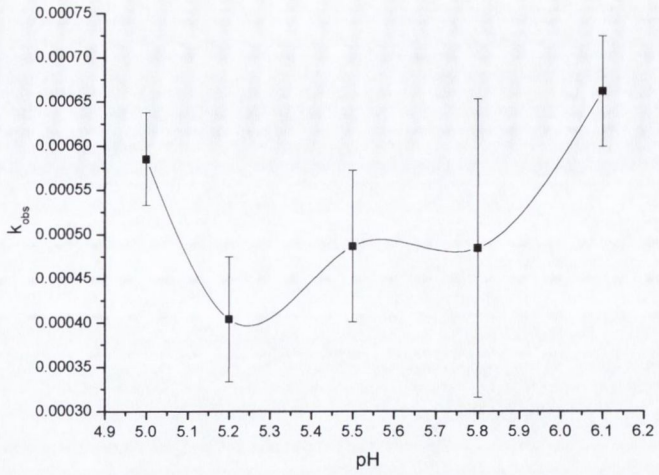

Figure 7.8 The pH-rate profile of the degradation of formoterol fumarate in the citrate buffer at 25°C. The points are experimental values and the line through the points is for the sake of simplicity only.

It can be seen that the chemical degradation of formoterol fumarate in this set of buffered solutions was slowest at pH=5.2.

7.2.4 Buffer catalysis

7.2.4.1 Phosphate buffer

The effect of phosphate buffer concentration at two different pH values on the rate of degradation of formoterol fumarate is given in Table 7.9.

Table 7.9 Decomposition rates k_{obs}, half-lives ($t_{1/2}$) and shelf-lives (t_{10}) for the decomposition of formoterol fumarate in various concentrations of phosphate buffer at pH values 5.1 and 5.7 at 25°C. Number of data points taken for the calculations was 18 in the case of the 0.05M concentration of citrate buffer and for the rest of samples it was 5. * indicates the extrapolated value.

pH	Buffer concentration [M]	10^3 x k_{obs} [day^{-1}] S.D.	$t_{1/2}$ [day]	t_{10} [day]	R^2
5.1	0.05	2.67 ± 0.16	259.55 *	39.33	0.9395
	0.10	1.19 ± 0.01	582.35 *	88.24	0.9717
	0.23	2.61 ± 0.03	265.52 *	40.23	0.9999
	0.44	4.64 ± 0.13	149.35 *	22.63	0.9969
5.7	0.05	4.89 ± 0.02	141.86 *	21.49	0.9399
	0.09	1.54 ± 0.05	451.47 *	68.40	0.9969
	0.20	2.94 ± 0.16	236.12 *	35.78	0.9983
	0.36	4.60 ± 0.34	150.65 *	22.83	0.9994

The concentration versus k_{obs} plots are presented in Figure 7.9.

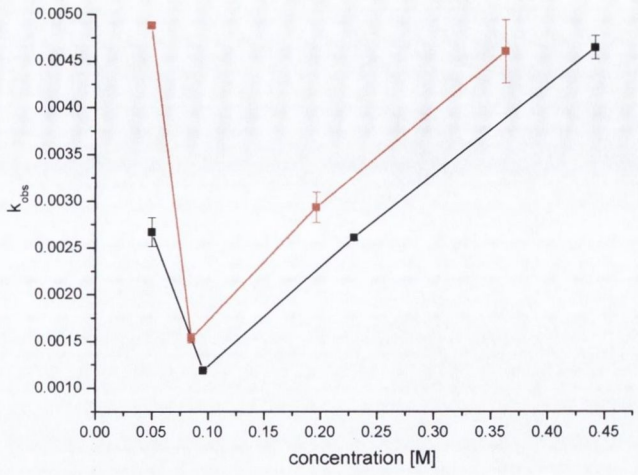

Figure 7.9 Plots of observed rate constants versus the phosphate buffer concentrations at pH=5.1 (black) and pH=5.7 (red) at 25°C.

It can be seen that these relationships are not linear, in contrast to trends that have been observed for phosphate buffer solutions for cefepime by Fubara and Notari (1998) or for cefaclor by Dimitrovska *et al.* (1995). The lowest concentration used in our case (0.05 M) gave k_{obs} coefficients over two and three-fold greater than the rate constants for the 0.1 M concentration for the pH values of 5.1 and 5.7, respectively. This may be an indication of the very poor buffer capacity at these pH points. Looking at the pK_a values of the phosphate buffer which are equal to 2.15, 7.20 and 12.33 (Carstensen, 1995), it can be expected that, in the pH region investigated, the buffer should have little buffer ability as the maximum is to be realised within ±1 unit around a pK_a (Carstensen, 1995).

The catalytic effect of a buffer (k_{buffer}) can be estimated from Equation 7.18:

$$k_{obs} = k_0 + k_{buffer} \cdot c_{buffer} \qquad \text{(Equation 7.18)}$$

where k_0 is the rate constant at zero buffer concentration and c_{buffer} represents total buffer concentration. The k_0 and k_{buffer} values were calculated excluding the k_{obs} values at the lowest buffer concentration and are as follows: 0.00027 (k_0), 0.00992 (k_{buffer}) and 0.00067 (k_0), 0.01094 (k_{buffer}) for pH=5.1 and pH=5.7, respectively.

It is known that different buffer species contribute to different catalytic effect at particular pH values. In the pH region 4-6 only one phosphate buffer species was found to be catalytic – $H_2PO_4^-$ (Pinsuwan *et al.*, 1999).

7.2.4.2 Citrate buffer

The effect of the citrate buffer concentration at two different pH values on the rate of degradation of formoterol fumarate is given in Table 7.10.

Table 7.10 Decomposition rates k_{obs}, half-lives ($t_{1/2}$) and shelf-lives (t_{10}) for the decomposition of formoterol fumarate in various concentrations of citrate buffer at pH values 5.2 and 5.8 at 25°C. Number of data points taken for the calculations was 10 and 13 in the case of the 0.01M and 0.05M concentrations of citrate buffer, respectively and for the rest of samples it was 5. * indicates the extrapolated value.

pH	Buffer concentration [M]	$10^4 \times k_{obs}$ [day^{-1}] S.D.	$t_{1/2}$ [day]	t_{10} [day]	R^2
5.2	0.01	4.04 ± 0.71	1715.35 *	259.90	0.9046
	0.02	6.12 ± 0.30	1133.28 *	171.71 *	0.9626
	0.05	9.30 ± 0.77	745.56 *	112.96	0.8624
	0.09	10.90 ± 0.94	636.07 *	96.37	0.9617
5.8	0.01	4.84 ± 1.68	1431.82 *	216.94	0.8831
	0.02	5.25 ± 0.46	1321.26 *	200.19 *	0.8842
	0.05	8.42 ± 0.08	823.53 *	124.78	0.8861
	0.08	8.70 ± 0.14	796.55 *	120.69 *	0.9684

The concentration versus k_{obs} plots are presented in Figure 7.10.

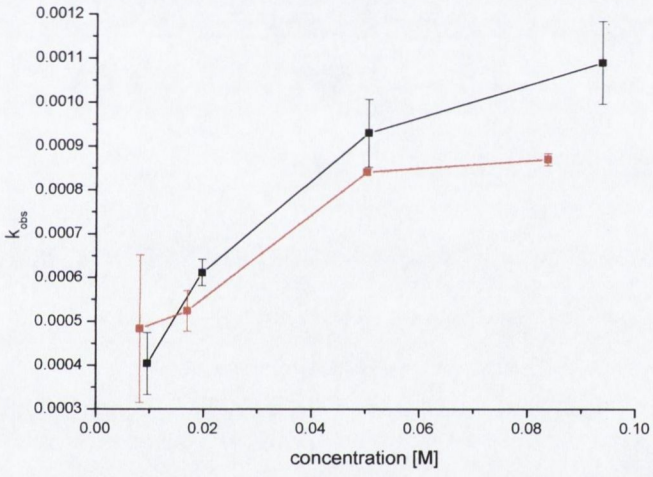

Figure 7.10 Plots of observed rate constants versus the citrate buffer concentrations at pH=5.2 (black) and pH=5.8 (red) at 25°C.

An increase in the buffer concentration accelerated the decomposition of formoterol fumarate, but at high buffer concentrations the relationship between k_{obs} and the concentration deviated from linearity and levelled off. An analogous process has been observed for salbutamol sulphate when the same buffer was used (Mälkki *et al.*, 1995).

The catalytic buffer effect was estimated using Equation 7.18. At pH=5.2 the k_0 and k_{buffer} values were 0.00042 and 0.00778, respectively, and at pH=5.8 they were equal to 0.00046 and 0.00556, respectively. These data suggest that the most catalytic species in the case of citrate buffer is H_2Cit^-. A comparison of the k_{buffer} coefficients of the phosphate and citrate buffers indicates that the latter has a lower catalytic potential.

7.2.5 Stability study in ethanol-water mixtures

The reformulation of CFC products as HFA equivalents presents considerable difficulties, as HFA and CFC propellants possess quite different physical and chemical properties. One of the major issues is the higher vapour pressures of the HFA compounds (Vervaet and Byron, 1999). High vapour pressure will provide small droplets due to rapid propellant evaporation but the velocity of plume discharge can result in a large percentage of the emitted dose being lost by impaction in the oro-pharynx (McDonald and Martin, 2000). Because there is no 'low pressure' HFA alternative to CFCs, only ethanol or presently untested additives can be used to reduce the vapour pressures in new MDIs (Vervaet and Byron, 1999). The second reason supporting the use of ethanol in the new formulations is that "inhalation-approved" (oleic acid, Span 85) surfactants can only be used effectively in propellant blends containing co-solvents like anhydrous ethanol which enable their dissolution (Purewal and Greenleaf, 1995). However, the presence of ethanol in the propellant also has disadvantages such as increased water sorption caused by leakage of valves (Butz *et al.*, 2002) which can lead to a decrease in chemical and physical stability of the active substance (Williams *et al.*, 1997). In light of the above information it seemed appropriate to investigate the influence of different ethanol concentrations on the decomposition rate of formoterol fumarate.

It has been established that the use of a non-aqueous medium or its mixtures with water can retard the degradation of a substance (Hartmann *et al.*, 1977) or, in some cases, accelerate that decomposition (Sanyude *et al.*, 1991). Generally, the influence of a solvent on the rate of reaction can be related to the solvation of the compound participating in that reaction (Laidler, 1987). That selective solvation of the molecule depends on the dielectric constant of the solvent, which in turn represents the capacity of the medium to reorient permanent and induced dipoles to achieve electrostatic stabilisation of a solute (Li *et al.*, 2000). Another physical constant is used to describe the contribution of induced dipoles only – polarizability (α_s). It is a function of the refractive index (η) of the medium and can be calculated using the Clausius-Mossotti equation (Laidler, 1987):

$$\alpha_s = \frac{(\eta^2 - 1)}{(\eta^2 + 2)} \qquad \text{(Equation 7.19)}$$

Summarising, one can say that the rate of decomposition of a compound can be correlated with the dielectric constant and/or polarizability of the reaction solvent.

There are some papers published about the influence of these constants on the rate of degradation or transformation of drugs. Laskar and Ayres (1977), for instance, have found proportionality between the apparent degradation rates of carmustine and the macroscopic dielectric constants of ethanol or propylene glycol-water mixtures. Desai *et al.* (2001) have established that the rate of photoisomerisation of sorivudine increased with increasing polarizability of the n-alcohol solvent.

An attempt was made to establish if the decomposition of formoterol fumarate dihydrate in ethanolic solutions depends on the dielectric constant and/or polarizabity of the reaction media. Table 7.11 details the decomposition rate constants of the drug in four different ethanolic solutions.

Table 7.11 Degradation rate constants of formoterol fumarate dihydrate in ethanol-water mixtures at 25°C. The values of dielectric constant were taken from Akhadov (1981), refractive indices from CRC Handbook of Chemistry and Physics (1994) and the polarizability of the medium used were calculated using Equation 7.19.

Concentration of ethanol [%]	$10^4 \times k_{obs}$ [day^{-1}] S.D.	Dielectric constant	Refractive index (η)	Polarizability
50	8.20 ± 0.52	53.57	1.3590	0.220147
80	12.00 ± 1.36	35.77	1.3652	0.223556
95	11.32 ± 0.66	27.04	1.3646	0.223227
99.5	8.81 ± 0.16	24.58	1.3614	0.221469

Presenting the values graphically, it can be discerned that there is no proportionality between either concentration of ethanol or dielectric constant of the mixtures and the degradation rates (Figure 7.11).

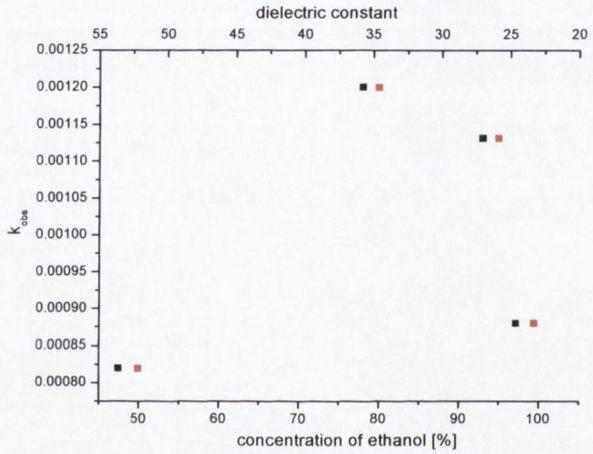

Figure 7.11 Dependence of the ethanol concentration (red squares) and dielectric constant of ethanol-water mixtures (black squares) on the degradation rate of formoterol fumarate dihydrate at 25°C.

The lack of correlation between the dielectric constant and the rates of degradation can be explained by more complex interactions between the solute and solvent. Since, as the dielectric constant is responsible for both induced and permanent dipoles and reflects the total thermodynamics of the molecule, there is a possibility that higher dielectric constant values can unfavourably change the conformation of the molecule and break it up.

A different situation is observed when the rates of degradation of formoterol fumarate were compared with the values of polarizability of ethanol solutions (Figure 7.12).

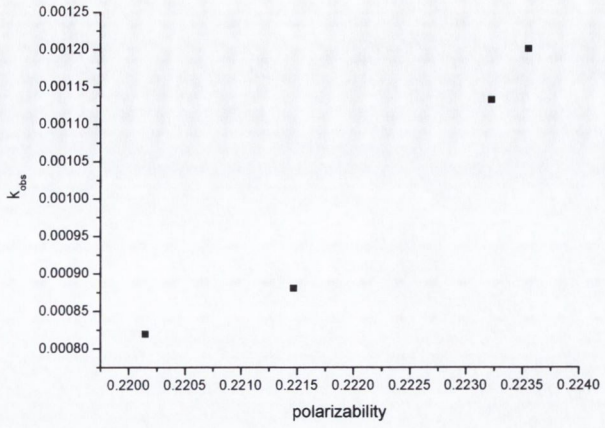

Figure 7.12 Dependence of the polarizability values of ethanol-water mixtures on the degradation rate of formoterol fumarate dihydrate at 25°C.

The effect of polarizability of the chemical stability of formoterol fumarate is understandable considering the fact that polarizability is responsible only for inducing of dipoles. When the concentration of the ethanol increases, there is less water and ion particles able to generate the conformational changes leading to the hydrolysis of the molecules.

The apparent pH values measured for the ethanolic solutions of formoterol fumarate were 6.45-6.57, 7.22-7.23, 7.44-7.50 and 7.38-7.43 for 50% (v/v), 80% (v/v), 95% (v/v) and 99.5% (v/v) ethanol concentrations, respectively.

7.2.6 The effect of drug concentration

The effect of the formoterol fumarate concentration on its decomposition in deionised water was investigated in view of a similar study carried out for salbutamol by Mälkki and Tammilehto, (1990). They have observed that the decomposition of salbutamol appeared to proceed faster in concentrated solutions than in dilute ones.

A different relationship between the concentration and degradation rate constants has been ascertained for formoterol fumarate. Table 7.12 shows the degradation characteristics of formoterol fumarate in deionised water.

Table 7.12 Degradation rate constants of formoterol fumarate dihydrate in deionised water at 25°C and 40°C. Number of data points taken for the calculations was 13 and 6 in the case of the samples stored at 25°C and 40°C, respectively. * indicates the extrapolated value.

Temperature [°C]	Concentration [%]	$10^3 \times k_{obs}$ [day^{-1}] S.D.	$t_{1/2}$ [day]	t_{10} [day]	R^2
25	0.02	2.04 ± 0.31	339.71 *	51.47	0.9619
40	0.02	3.22 ± 0.38	215.55 *	32.66	0.9064
40	0.1	2.30 ± 0.16	301.83 *	45.73	0.9152

It can be seen that the drug in 0.1% (w/v) solution degraded slower than the diluted sample (0.02% (w/v)). This, however, cannot be explained by pH changes on storage. The pH values measured for both of the concentrations at the beginning of the experiment were nearly identical and were 5.91-5.99. After 6 months of storage at 40°C these values changed into 4.92-5.07 and 4.56-4.65 for the 0.02% and 0.1% formoterol fumarate concentrations, respectively. Provided that the optimum stability pH is around 5.00, the lower drug concentrations should degrade slower. Perhaps other mechanisms are responsible for the prolonged stability of the drug in the concentrated solution.

7.3 Spray drying of excipients and formoterol fumarate-excipient(s) systems

7.3.1 Introduction

The objective of this part of the research was to produce and characterise particles of co-spray dried formoterol fumarate with various excipients including sugars, polymers and buffers. The rationale for these studies was to protect the drug by the presence of an excipient and the addition of buffer salts aimed at improving the chemical stability of the drug. It was indended to formulate the spray dried particles in pressurised metered dose inhalers. The second aim of these investigations was to examine the dispersibility and stability of the formulated MDIs. One of the most important requirements was the particle size of the powder to be produced. The goal was to produce powders in which 95% of particles should be smaller than 5 μm and all of particles should be below 10 μm size. Because lactose monohydrate, the most frequently used carrier in aerosols (Steckel and Bolzen, 2004), has proven to be not compatible with formoterol fumarate (Gao *et al.*, 2001), other additives were selected. They were:

- Macrogol 6000 (PEG 6000)
- Mannitol
- Xylitol
- Hydroxypropylmethylcellulose grade E5 (HPMC)
- Polyvinylpyrrolidone 40000 (PVP)

Mannitol and xylitol are polyols, compounds that recently have become more important in pharmaceutical applications due to their suitability for use by diabetics and their non-carriogenic properties (Talja and Roos, 2001) as well as their possible application as alternative carriers in DPIs (Steckel and Bolzen, 2004). PVP and PEG are well established as excipients used for a variety of purposes and also have the ability to produce drug conjugates (Greenwald, 2001; Kaneda *et al.*, 2004) which can improve drugs' plasma half-lifes. All chosen excipients are hydrophilic substances and may additionally offer bioavailability enhancement when formulated as solid dispersions (Serajuddin, 1999) with formoterol fumarate, which is known to be poorly soluble in

water (J. P., 2003). First of all, a literature survey was undertaken to assess the feasibility of the spray drying process to fulfil the requirements as regards the drug MDI formulations (particle size). Table 7.13Table 7.13 summarises the physicochemical characteristics of the excipients, relevant to the technological process, i.e. melting temperature, glass transition temperature and solubility.

Table 7.13 Physicochemical characteristics of the chosen excipients (Wade and Weller, 1994).

	Melting temperature (°C)	Temperature of glass transition (°C)	Solubility
PEG 6000	55-63	-50[a]	Soluble in water, ethanol, methanol, dichloromethane
Mannitol	166-168	12.6[b]	Water 1 in 5.5 Ethanol 1in 83
Xylitol	92-95	-23[c]	Water 1 in 1.6 Ethanol 1in 80 Methanol 1 in 16.7
HPMC E5	190-200	170-180	Soluble in cold water, practically insoluble in ethanol 95% and chloroform
PVP K-30	-----	Softens at 150	Freely soluble in water, ethanol methanol and chloroform

[a] – from Ford, (1987)
[b] – fromYu *et al.*, (1998a)
[c] – from Roos, (1995)

After reviewing the available information about the physicochemical properties of all of the excipients, Macrogol 6000 was excluded from further study due to problems in processing. It has been shown that by spray drying of Macrogol 20000 (Chapter 5), a particulate product can be obtained when the inlet temperature was set to 45°C and dichloromethane was used as the solvent. Moreover, the majority of the particles were fused. Work previously performed by Corrigan (2002) demonstrated that spray drying of PEG 4000 from water was unsuccessful. Sphere-like particles were produced when ethanol 95% (v/v) was used and the outlet temperature was 45-46°C, and these were quite large, approximately 50-70 μm in diameter. PEG 6000 is expected to behave similarly as it melts at ~59°C, which is intermediate between the melting temperatures of PEG 4000 (~54°C) and PEG 20000 (~61°C).

Initially therefore, mannitol, xylitol, HPMC and PVP 40000 were spray dried alone to assess the feasibility of producing of a particulate powder having suitable particle size as outlined above.

7.3.2 Mannitol

The starting conditions for spray drying of mannitol are given in Appendix I (under sample code Mannitol I).

DSC (Figure 7.13) and TGA were initially carried out on the raw material powder prior to spray drying. One endothermic peak was visible on investigation by DSC with the onset at ~166°C. This is indicative of the melting temperature, as the substance was XRD crystalline (Figure 7.14). After

spray drying only one peak was again observed (Figure 7.13) and the melting point was almost the same (~165°C) as the raw material sample signifying that no changes detectable by DSC took place in the crystalline structure of mannitol during the process. Examination of mannitol raw material by TG resulted in only 0.8% weight loss up to the beginning of melting at ~167°C and this was probably due to desorption of loosely bound moisture. Similar results were seen when the powder was examined after spray drying with 0.77% weight loss up to 167°C, suggesting a similar degree of hygroscopicity compared to the crystalline form.

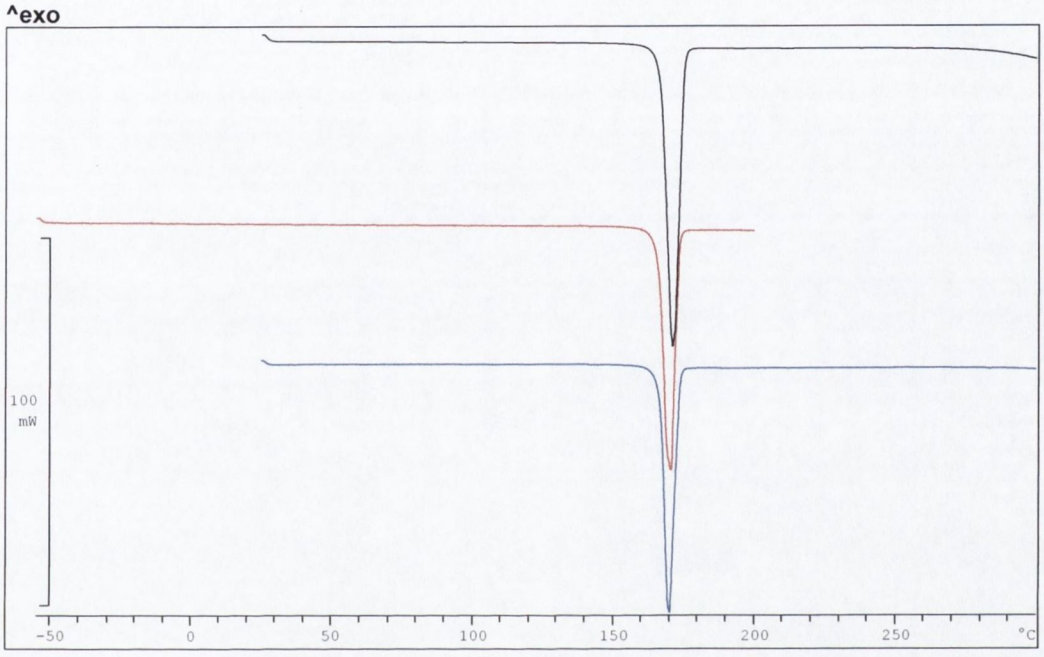

Figure 7.13 DSC scans of mannitol starting material powder (black), Mannitol I (red) and Mannitol II (blue).

As mentioned above, the XRD diffraction patterns (Figure 7.14) obtained for mannitol raw material suggest that it was a crystalline substance. The peak positions and intensities were compared with the mannitol scans from the Powder Diffraction File (PDF) crystallographic database available in the Physics Department, TCD (Figure 7.15). On this basis they were attributed to the β-form of D-mannitol. The XRD of spray dried mannitol confirmed that it remained crystalline after the spray drying process, however the degree of crystallinity compared with the unprocessed material was lower as indicated by the reduction in peak intensities (Figure 7.14). Again, the XRD pattern of this sample was recognised as being predominantly of the β-form, although some discrepancies between the two scans can be discerned. The arrows in Figure 7.14 show the peak position changes with regard to the untreated mannitol.

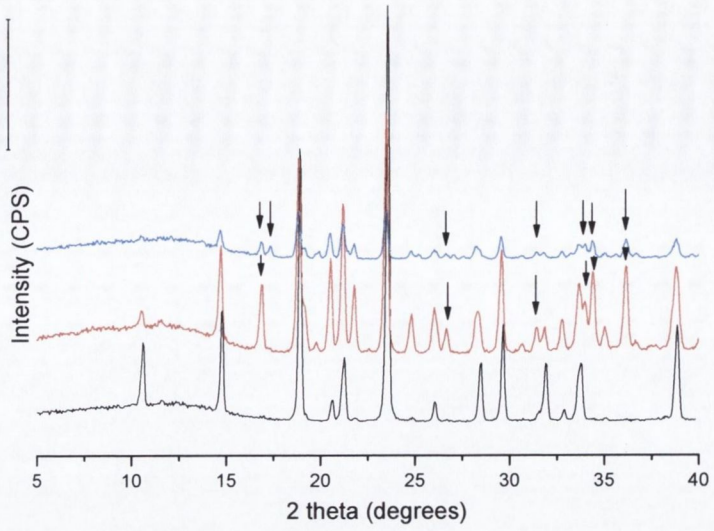

Figure 7.14 XRD patterns of mannitol starting material powder (black), Mannitol I (red) and Mannitol II (blue). Arrows indicate additional peaks not found in the diffractogram of the mannitol starting material powder.

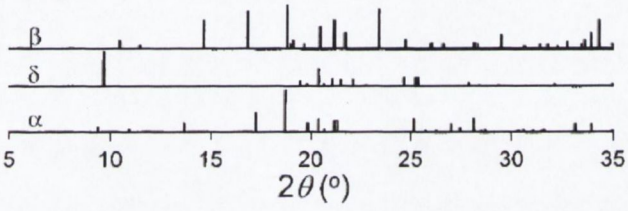

Figure 7.15 XRD profiles of crystalline α-mannitol (bottom trace), β- mannitol (top trace) and δ-mannitol (middle trace).

Spray drying of mannitol as a carrier or active substance which can be used in aerosols was reported by (Chew and Chan, 1999). They also noticed a reduced crystallinity of the processed samples but no detectable (by XRD) changes in the crystallographic form of mannitol.

After spray drying, the mannitol particles were roughly spherical (Figure 7.16). Some of them appeared to be hollow, had one hole or more and had a rough surface. For comparison purposes Figure 7.16 shows the morphology of unprocessed mannitol, where large, elongated and coarse particles can be viewed.

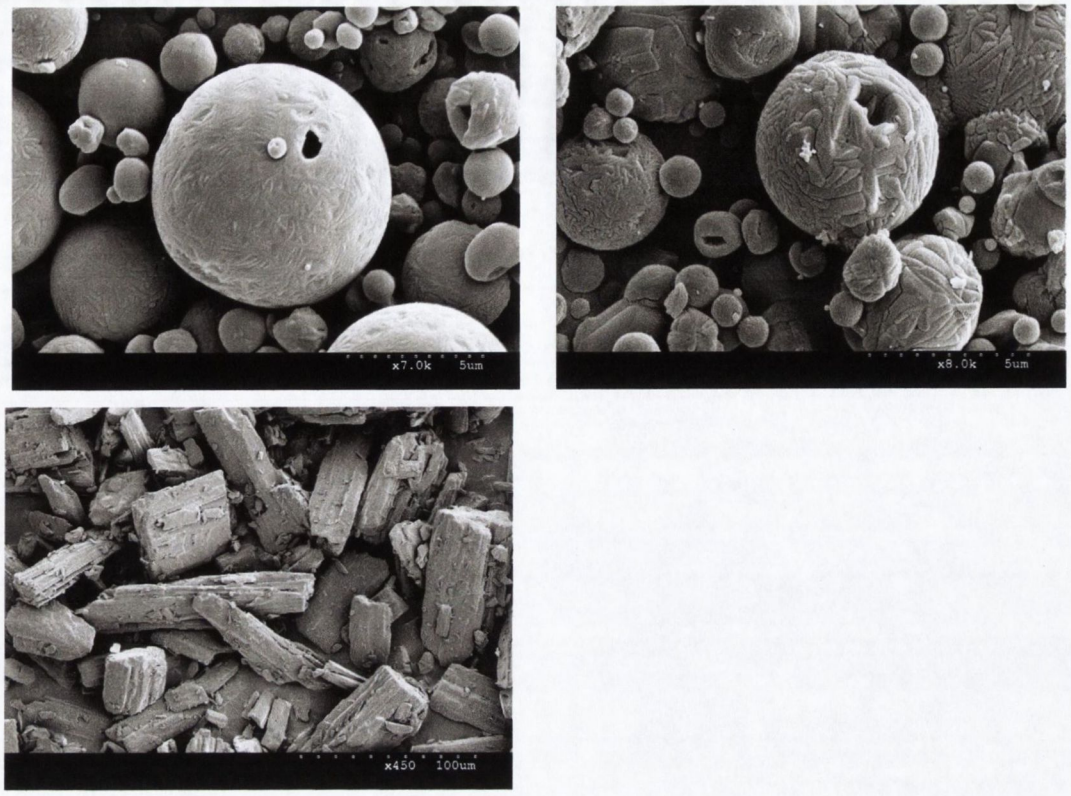

Figure 7.16 SEM images of mannitol starting material powder (bottom), Mannitol I (top left) and Mannitol II (top right). Note different magnifications of the micrographs.

Laser diffraction particle size analysis (result presented in Figure 7.17) revealed that 71.1% (by volume) of particles were below 5 μm and nearly 99% were below 10 μm. The particle size distribution was clearly bi-modal with a small fraction of the volume distribution of very small particles ranging between 0.2-1 μm. Contrasting with the starting material (Figure 7.17), a significant degree of micronisation was attained.

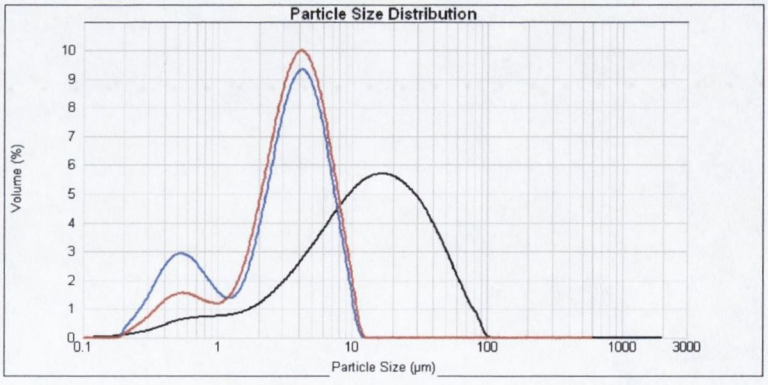

Figure 7.17 Laser diffraction particle size distribution profiles (obtained by the Malvern Mastersizer 2000) of mannitol starting material powder (black), Mannitol I (red) and Mannitol II (blue).

In order to decrease the particle size a change in the spray drying conditions was necessary. The statistical analysis of 2^{5-1} fractional factorial design study of formoterol fumarate dihydrate spray dried with budesonide (6:100) described in the Chapter 4 revealed that airflow rate and aspirator suction had the greatest influence on particle size. Setting these two parameters at the higher levels would result in the production of a finer powder. The other major factor, which was found to have a similar impact on the particle size, was the concentration of solution, with lower solution concentrations giving smaller particles. Also an increase in inlet temperature may supposedly change the surface tension of the solution being spray dried, thus decreasing the particle size (Masters, 1985).

Taking into consideration all the above, mannitol was spray dried at new conditions (Appendix I, sample code Mannitol II).

Once again, the resulting powder was XRD crystalline but with a high content of an amorphous material (Figure 7.14) showing a broad "halo" at low 2θ angles. Yoshinari *et al.* (2003) reported a polymorphic conversion of mannitol during a wet-granulation procedure. The high level of amorphous compound achieved after spray drying indicates a potential risk of forming other polymorphs, which may hardly be detectable by the XRD method. On examination of the diffractograms of the spray dried powders, some changes in the peak positions and intensities are evident. An additional peak at 17.7 2θ for Mannitol II and changes in the ratio of intensities between two peaks at 19.2 and 19.5 2θ with the lowest ratio being again for Mannitol II (Figure 7.14) were observed. This may be indicative of the α-form of mannitol being present in all of the spray dried samples with the greatest content of this polymorph in Mannitol II.

Burger *et al.* (2000) have presented important physicochemical properties of different modifications of mannitol with selected FTIR bands characteristic of individual polymorphs. Table 7.14 details those peak positions compared with the measured peak values for the raw material mannitol sample, Mannitol I and Mannitol II.

Table 7.14 Comparison of the FTIR peak positions of the mannitol starting material and processed samples with the data taken from Burger et al. (2000).

Wavelength [cm^{-1}]					
Burger *et al.*(2000)			Mannitol crystalline	Mannitol I	Mannitol II
α	β	δ			
1196	1210	1193	1210	1210	1209
1085	1081	1088	1080	1080	1080
1020	1019	1025	1020	1020	1020
953	959	968	959	958	953 (broad peak)
927	930	932	929	930	929

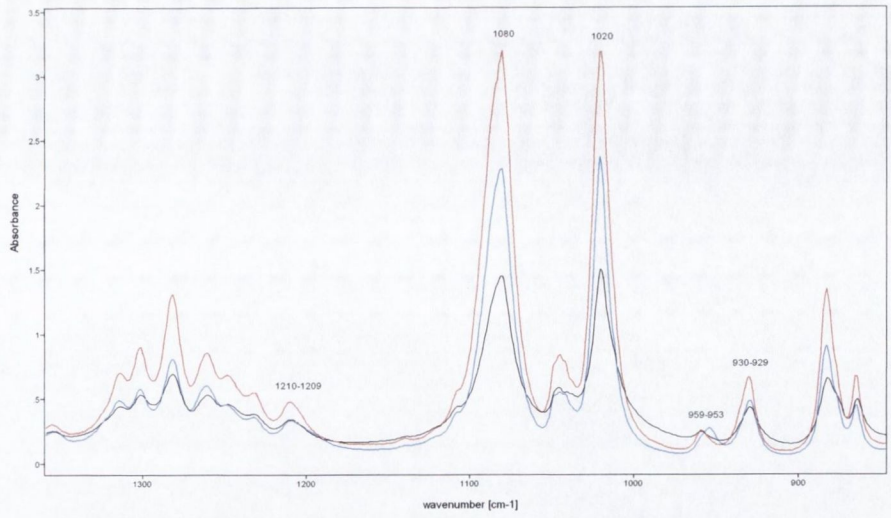

Figure 7.18 Infrared spectra of mannitol starting material powder (black), Mannitol I (red) and Mannitol II (blue). Only the wavenumber range 950-1350 cm^{-1} is shown.

The infrared analysis (Figure 7.18) confirmed the hypothesis that all the mannitol samples were essentially in the β-form. Nevertheless, there is an indication that the starting material could contain a small amount of the α modification as an admixture as suggested by the XRD and the position of peaks at 1020 and 929 cm^{-1} by FTIR. Additionally, there is an indication that the spray drying process induced a polymorphic transformation in Mannitol II converting it further into the α form (existence of a broad peak at 953 cm^{-1}, Table 7.14).

One endothermic peak was visible on investigation of Mannitol II by DSC with the onset at ~166°C (Figure 7.13). Examination of this sample by TG analysis showed 1.2% weight loss up to 167°C indicating that the material adsorbed more solvent during spray drying than the previous batch. This moisture might have been retained by the amorphous fraction of mannitol despite the higher inlet temperature used compared with the previous sample. Similarly, after spray drying, the mannitol particles were generally spherical (Figure 7.16) and the majority had a rough surface. Particle size analysis (Figure 7.17) revealed that 74.71% of particles were below 5 μm and more than 99% were below 10 μm. The particle size distribution was bi-modal and the small particles fraction was even more pronounced than that of the first sample of spray dried mannitol.

In spite of the fact that mannitol appeared to be suitable for manufacture by spray drying, it was decided that further changes in the processing conditions are unlikely to affect the particle size greatly as the airflow and aspirator rates were set at the maximum value possible in the Büchi 191 and a further increase in the inlet temperature could cause melting of mannitol.

7.3.3 Xylitol

Xylitol was spray dried from aqueous solution under the conditions given in Appendix I.

There was a melting endotherm visible on examination of xylitol raw material by DSC (Figure 7.19). The onset temperature of melting was ~93.6°C.

In the spray dried sample, apart from a melting endotherm peaking at ~95°C and beginning at ~93°C, a small endotherm was seen at -9.4°C (at higher magnification) representing the temperature of glass transition (Figure 7.19). This indicates that the spray dried material was partially amorphous. The onset of T_g of xylitol is regarded to be -24 °C (Talja and Roos, 2001), thus the glass transition temperature observed here was higher than expected, possibly due to the crystalline content of the sample. The heat of fusion associated with the melting of spray dried xylitol was 232 J/g as compared to 245 J/g for the untreated material, providing further evidence that some amorphous xylitol was formed.

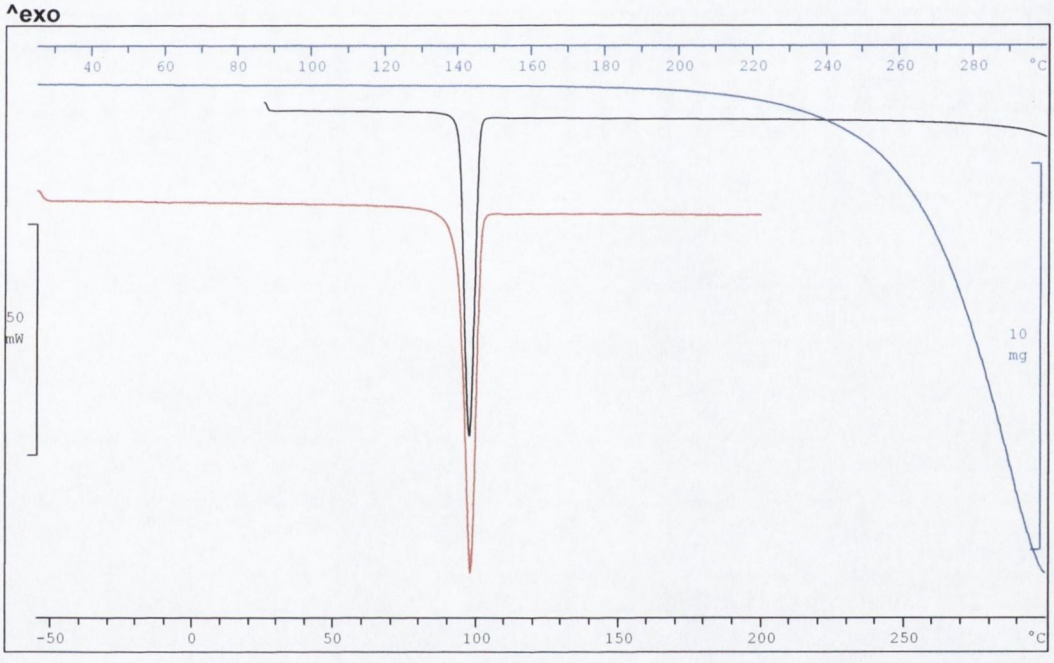

Figure 7.19 DSC (black) and TGA (blue) scans of xylitol starting material powder and DSC scan of spray dried xylitol (red).

There was only 0.2% weight loss due to water desorption from the xylitol raw material up to 95°C when examined by TG (Figure 7.19). XRD of xylitol raw material illustrated that it was not 100% crystalline (Figure 7.20). It was partially amorphous as represented by the initial background "halo".

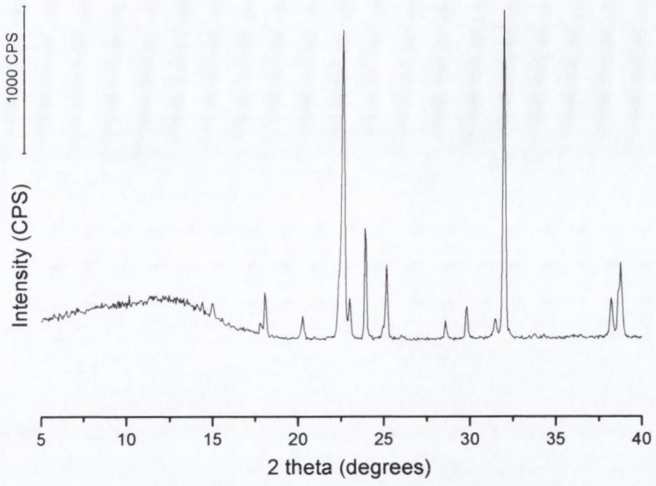

Figure 7.20 XRD pattern of xylitol starting material powder.

The use of the above processing conditions resulted in a soft, glassy substance, which stuck to the walls of the cyclone and collecting vessel. This made extraction of even a small quantity of spray dried xylitol impossible (only a few milligrams was extracted for the DSC analysis). While a decrease in inlet temperature might be expected to result in powdered product rather than the tacky substance produced, it is not feasible to spray dry from water at a lower temperature as high moisture content in the processed material is likely to result. Modification of the process to use a different solvent is unlikely to be successful due to the very low solubility of xylitol in ethanol and lack of solubility in apolar solvents. Therefore, it is reasonable to conclude that xylitol is not suited to the spray drying process.

7.3.4 Hydroxypropylmethylcellulose grade (HPMC) E5

The spray drying conditions for HPMC are given in Appendix I.

DSC analysis of the raw material powder revealed a broad endothermic peak due to dehydration, a change in the slope of the baseline at ~152°C corresponding to the temperature of glass transition and another endothermic peak possibly denoting the melting of HPMC (Figure 7.21). The T_g detected was close to that reported by Cilurzo *et al.*(2002) and equal to 162°C despite the lower molecular weight grade used in this study. The DSC (Figure 7.21) of the spray dried sample was similar in nature to the raw material powder in relation to the first two thermal events i.e. dehydration and the glass transition. The third peak at ~170°C, which is exothermic, is probably due to recrystallisation of the amorphous material formed on spray drying.

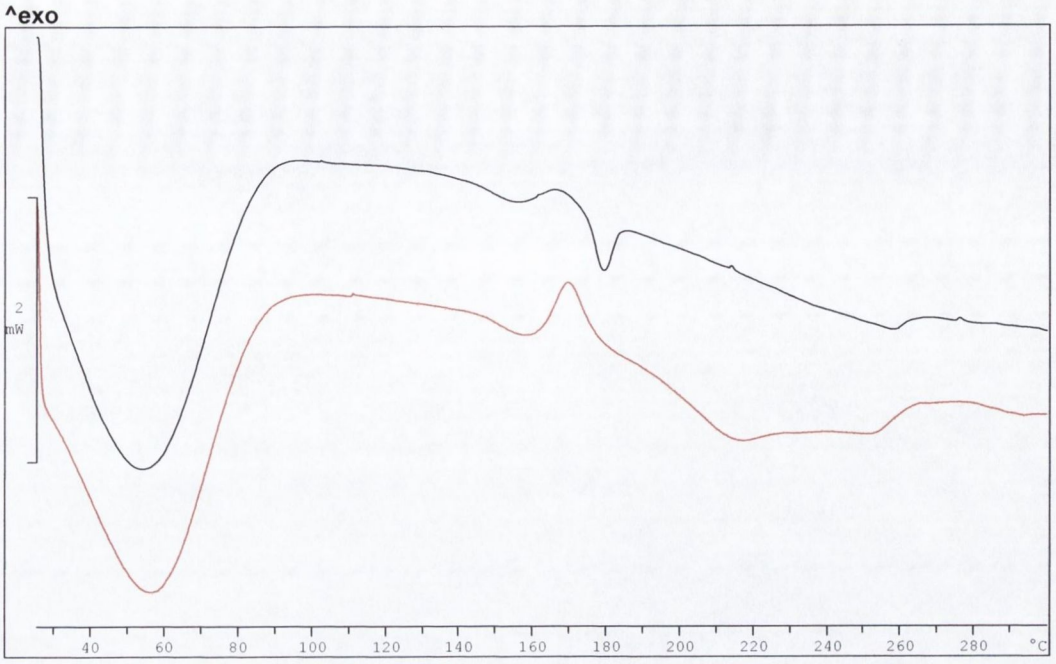

Figure 7.21 DSC scans of HPMC starting material powder (black) and the spray dried sample (red).

Thermogravimetric analysis of the raw material sample showed a weight loss of just under 2% up to 100°C. This was probably due to water desorption. The spray dried sample similarly underwent a weight loss of 2.3%.

Examination of the XRD patterns of both unprocessed and spray dried HPMC confirms that they are amorphous in nature (Figure 7.22). The occurrence of a peak in both samples could be explained by the presence of a small fraction of the crystalline material. Cilurzo *et al.* (2002) and Verreck *et al.* (2003) also observed a peak at around 32 2θ degrees for Methocel E50 and HPMC 2910 5mPa·s grades, respectively, so it appears that this is a characteristic feature of XRD patterns of hydroxypropylmethylcellulose irrespective of the grade. The magnitude of the peak is lower in the spray dried sample confirming the DSC findings of amorphous transformation.

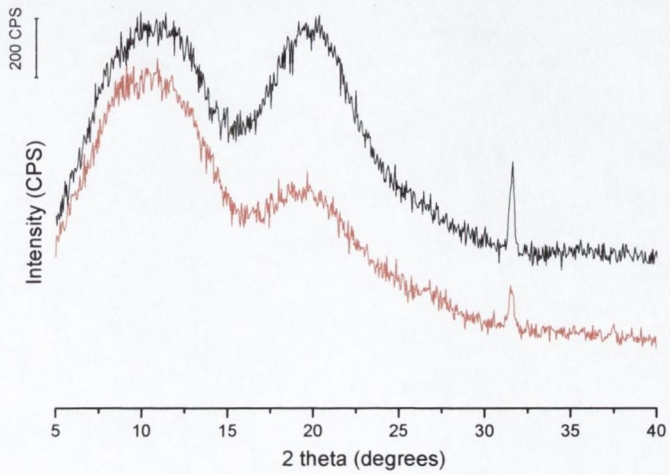

Figure 7.22 XRD patterns of HPMC starting material powder (black) and the spray dried sample (red).

Spray drying resulted in a fluffy powder with folded particles resembling those of spray dried PVP (Figure 7.23). HPMC-tolbutamide 5:1 solid dispersion particles were spray dried by Chen *et al.* (2004) and had similar shapes. The particle surfaces were smooth (Figure 7.23).

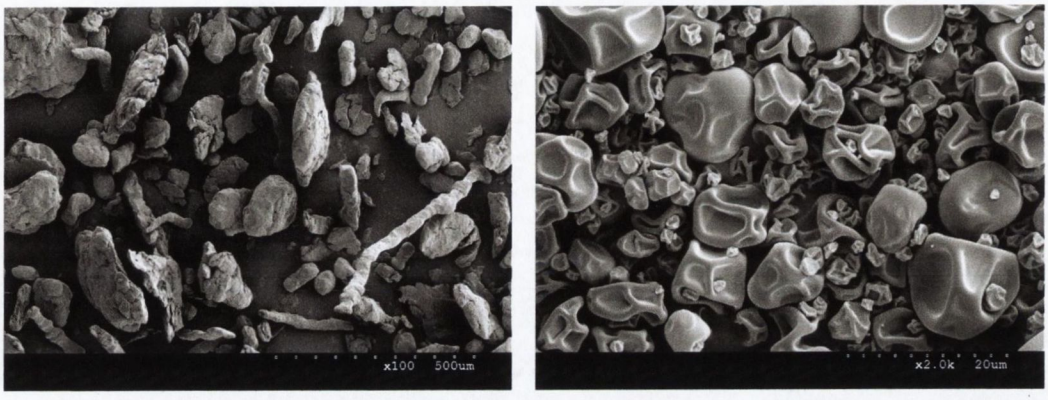

Figure 7.23 SEM images of HPMC starting material powder (left) and the spray dried sample (right). Note different magnifications of the micrographs.

The particle size distribution (Figure 7.24) was tri-modal with a large particle fraction with sizes between 100-600 μm. Only about 19% of particles were ≤ 5 μm and 47% were smaller than 10 μm. It can be concluded that spray drying decreased the particle size of HPMC but the goal set previously (i.e. 95% of particles smaller than 5 μm and all of particles below 10 μm) had not been met.

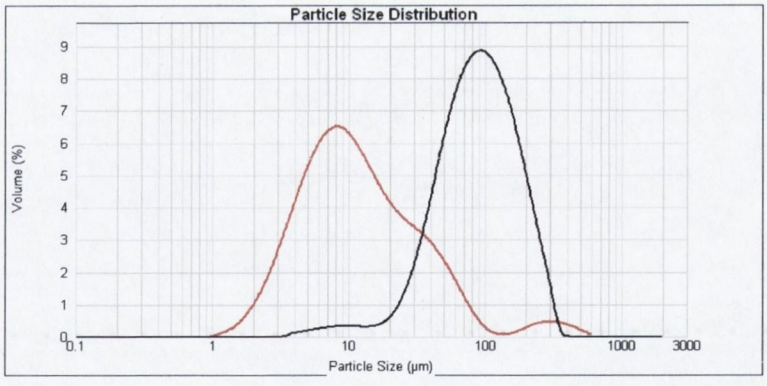

Figure 7.24 Laser diffraction particle size distribution profiles (obtained by the Malvern Mastersizer 2000) of HPMC starting material powder (black) and the spray dried sample (red).

It was concluded that a significant change in the particle size of HPMC would not be expected to result by changing the spray drying conditions alone. Even when the spray drying conditions for mannitol were changed (as described in Chapter 7.3.2), this resulted in only ~10% decrease in particle size (based on the $d_{50\%}$ value – median particle size). Moreover, due to the insolubility of HPMC in e.g. ethanol, a further alteration in the particle size by the spray drying method seems unfeasible.

7.3.5 PVP

The PVP grade chosen for spray drying was PVP with an average molecular weight of 40,000 and K value of 30. The spray drying conditions are specified in Appendix I as PVP I.

DSC (Figure 7.25) revealed a broad endothermic peak in the raw material and spray dried samples due to water desorption from the surface of the powders, as PVP is hygroscopic. The temperatures of glass transition observed were ~167°C and ~169°C for the starting and spray dried materials, respectively. PVP is a stable amorphous substance and therefore, neither recrystallisation nor melting was seen on examination of the raw material and spray dried samples.

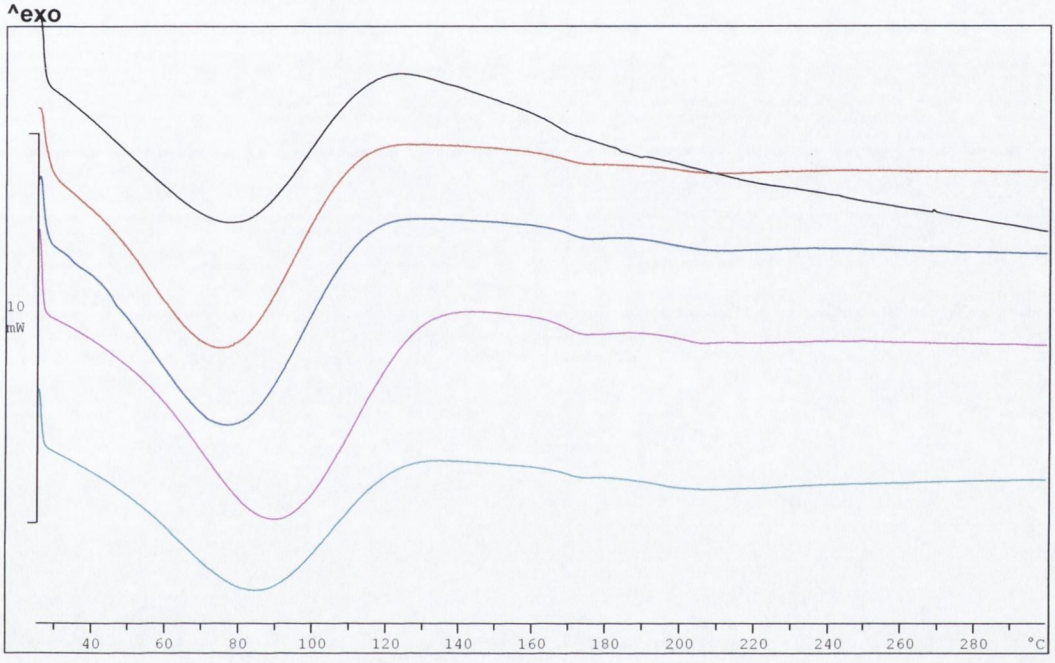

Figure 7.25 DSC scans of PVP starting material powder (black), PVP I (red), PVP II (blue), PVP III (magenta) and PVP IV (cyan).

There was ~7% weight loss from the raw material powder up to 100°C compared with a weight loss of ~5.2% in the same region for the spray dried sample on analysis by TGA. This weight loss was related to surface moisture liberation and a reduction in the amount of water in the processed sample was observed. XRD (Figure 7.26) revealed that both the unprocessed and spray dried PVP were amorphous.

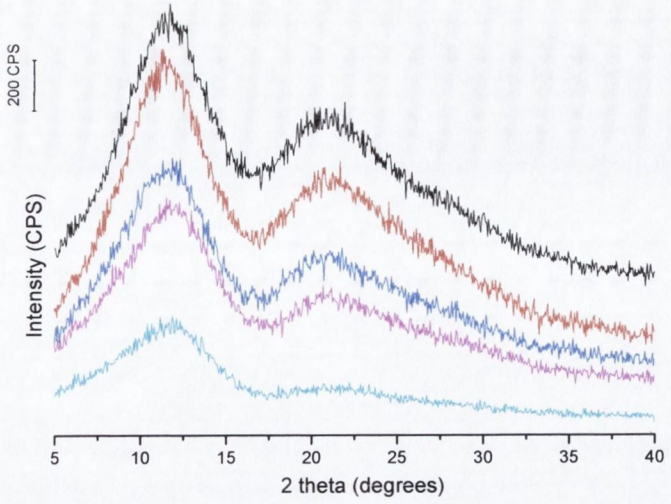

Figure 7.26 XRD patterns of PVP starting material powder (black), PVP I (red), PVP II (blue), PVP III (magenta) and PVP IV (cyan).

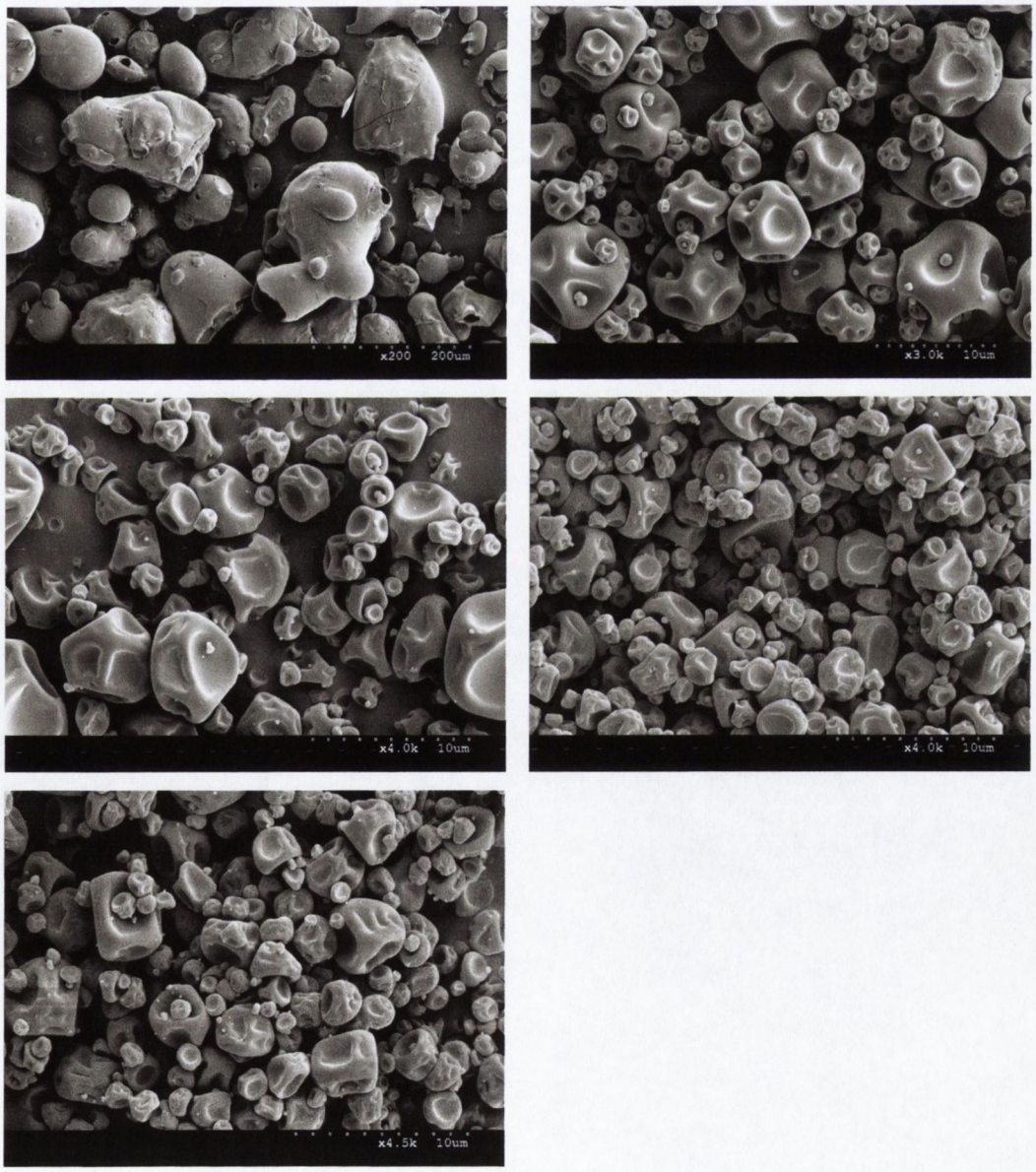

Figure 7.27 SEM images of PVP starting material powder (top left), PVP I (top right), PVP II (middle left), PVP III (middle right) and PVP IV (bottom). Note different magnifications of the micrographs.

SEM showed that the spray dried particles had folded but smooth surfaces (Figure 7.27). A reduction in particle size due to spray drying was seen.

The particle size distribution (Figure 7.28) can be regarded as mono-modal, but there was a "tail" towards smaller sizes indicating a small fraction of particles having diameters between 0.3-1 μm. Around 47% of particles were 5 μm and smaller and 88.7% were below 10 μm. These values however did not fulfil the requirements previously set for the ideally sized inhalable particles (see Section 7.3.1).

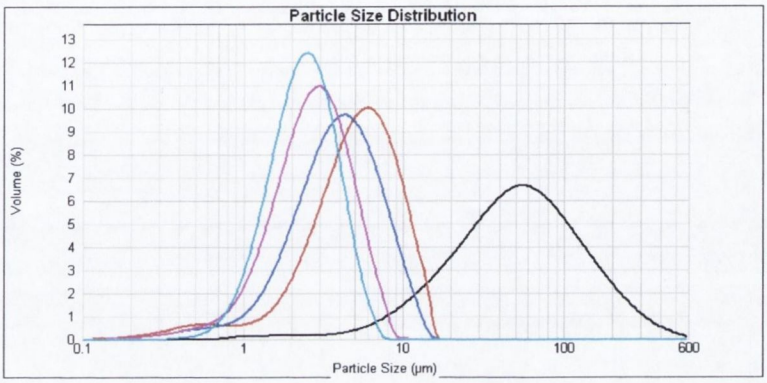

Figure 7.28 Laser diffraction particle size distribution profiles (obtained by the Malvern Mastersizer 2000) of PVP starting material powder (black), PVP I (red), PVP II (blue), PVP III (magenta) and PVP IV (cyan).

It was thought that using ethanol as the solvent with a lower surface tension than that of water could result in the production of smaller particles by spray drying. A second batch of PVP particles was produced using the processing conditions described in Appendix I as PVP II, but the solution was prepared on 95% (v/v) ethanol instead of deionised water.

DSC (Figure 7.25) revealed a broad endothermic peak due to water desorption and the temperature of glass transition was observed at around 170°C. There was ~6.5% weight loss up to 100° by TGA and the sample was XRD amorphous (Figure 7.26).

The particles' appearance was the same as when PVP was spray dried from water (Figure 7.27) but they seemed to be more "collapsed". The particle size distribution (Figure 7.28) was mono-modal and 64.7% of particles were 5 μm or smaller and 95.6% were below 10 μm, which was closer to the specification. Thus, using 95% (v/v) ethanol instead of deionised water caused a significant change in the particle size. It was decided to continue further experiments utilising ethanolic solutions only and adjusting the spray drying conditions to obtain PVP particles of the desired size.

For the next sample, the influence of airflow through the spray dryer as the factor having the greatest impact on the particle size (see Section 7.3.2) was investigated. The conditions for spray drying were as quoted in Appendix I as PVP III.

The DSC (Figure 7.25) trace resembled that of the previously manufactured batch of PVP. There was ~7% weight loss up to 100° by TGA and again no differences in the crystalline structure were seen as the sample was XRD amorphous (Figure 7.26). The particles' appearance was the same as previously (Figure 7.27). The particle size distribution (Figure 7.28) was mono-modal and 87.7%

of particles were 5 μm or smaller and 100% were below 10 μm indicating that one of the specifications with regard to particle size was finally met.

The last sample was spray dried with the airflow set at the highest level and using a lower concentration of solution, conditions which according to the results of the factorial design study described in Chapter 4, should result in a reduced particle size. The inlet temperature used was higher than previously in order to decrease the surface tension of the solution. The full specification of the conditions used is given in Appendix I as PVP IV.

Once again, DSC analysis (Figure 7.25) revealed a broad, endothermic peak due to water desorption and the temperature of glass transition was observed at around 170.4°C.

There was ~6% weight loss up to 100°C by TGA. When the weight loss of the samples spray dried from ethanol was compared to that obtained from aqueous solution it was determined that the former batches contained more volatile substances which were being released up to 100°C and this may be evidence of residual ethanol being trapped in the PVP.

The sample was XRD amorphous (Figure 7.26). The particles' appearance was the same as previously (Figure 7.27). Particle size analysis (Figure 7.28) revealed that in this case 95% of particles were below 5 μm and 100% were below 8 μm. The particle size distribution was mono-modal.

To summarise, in terms of a spray drying process that might result in a product with the required characteristics as regards the particle size, one can say that the most promising excipients, which were used in the next phases of this work were:

- PVP, which resulted in spray dried particles of the ideal size according to the requirements set in Section 7.3.1.
- Mannitol, which gave particles close to the desired size (74.71% of particles were below 5 μm and more than 99% were below 10 μm).

7.3.6 Dispersibility study of the spray dried excipients in HFA-134a

To assess the feasibility of dispersing the candidate excipients in propellant, small portions of the spray dried powders were hand-filled into glass canisters, crimped with valves and filled with HFA-134a propellant as described in Chapter 2. Some of the suspensions were prepared with a small quantity of ethanol (99.9% by (v/v)) and/or a surfactant. Initially, solubility studies of surfactants were carried out to select the most suitable compounds.

7.3.6.1 Solubility study of surfactants in HFA-134a

Hydrophobic surfactants such as lecithin, sorbitol trioleate or oleic acid, which are easily dissolved in CFC propellants used in previous generation medicinal pressurised inhalers, have proven insoluble and inefficient in the novel HFA-based MDIs (Vervaet and Byron, 1999). Such surfactants were included in formulations mainly due to their lubricant properties improving

reproducibility of the dosage delivered from the valve and also to aid in the dispersibility of the suspended particles. However, as a result of technical developments, it is now possible to purchase valves able to function even without these oily lubricants. Therefore, the use of surfactants in HFA MDIs may have a different rationale. While in solution formulations they still can be utilised to overcome valve stickiness or to increase drug solubility, in suspension-based MDIs they may be included to prevent caking or reduce adhesion of the suspension particles to the container walls. Another application includes retardation of separation between the solid and liquid phases (Vervaet and Byron, 1999).

In order to improve dispersion, a surfactant should be soluble in the propellant (Williams and Liu, 1998). For this reason, to find candidates for the solubility studies and then select some of them to be used in formoterol MDI formulations, a literature survey was first conducted.

Williams and Liu (1998) determined that lecithin, Span 80 and Span 85 were not soluble in HFA 134a, regardless of the ethanol content in the propellant. Insolubility of the above surfactants as well as oleic acid was confirmed by Vervaet and Byron (1999). On this basis, these compounds were excluded from our solubility studies as they were established to be unsuitable.

It has been reported (Byron and Blondino, 1996) that polar surfactants with higher HLB (hydrophilic lipophilic balance) values have higher solubilities in HFA 134a due to the hydrophilic properties of the propellant. Examples of such surfactants are polyoxyethylene alkyl ethers (Brij) and polyoxyethylene esters (Myrj). Some of these compounds were selected for further investigations. One anionic surfactant, Aerosol OT (dioctyl sodium sulphosuccinate), and a propylene glycol derivative, Capmul PG-12 (propylene glycol monolaurate), were also examined.

The method of preparation of vials for solubility studies is described in Chapter 2. Solubility of a surfactant was determined visually (Williams and Liu, 1998). The observation of phase separation or cloudiness indicated that the surfactant was not dissolved completely in the propellant, and a clear solution showed that the surfactant was dissolved in HFA-134a. Additionally, the solubility of some of the surfactants was determined with and without ethanol. Table 7.15 summarises the results of solubility studies of selected compounds.

Table 7.15 Solubility determinations of surfactants in HFA 134a propellant.

Surfactant	HLB	Apparent solubility [%(w/w)]	Amount of ethanol [%(w/w)]	Observation
PEG 300	20 *	1.05	0.00	clear solution
		2.06	0.00	clear solution
		5.05	0.00	not soluble
		4.99	0.52	clear solution
PEG 1000		0.50	0.00	soluble
		1.00	0.00	soluble
		2.00	0.00	soluble
		5.00	0.00	cloudy
		4.73	0.49	soluble
		4.76	0.96	soluble
PEG 4000		0.51	0.00	insoluble
		0.50	0.50	insoluble
		0.49	1.00	insoluble
		0.50	2.04	insoluble
		0.49	4.94	soluble
		0.99	2.06	insoluble
		0.98	4.85	soluble
PEG 6000		0.50	0.00	insoluble
		0.50	1.98	insoluble
		0.99	1.96	insoluble
Myrj 59	18.8 **	0.50	0.00	insoluble
		0.51	0.49	insoluble
Myrj 53	17.9 **	0.47	0.00	slightly cloudy
		0.51	0.49	slightly cloudy
Brij 58	15.7 **	0.50	0.00	soluble
		1.00	0.00	soluble
		2.02	0.00	slightly cloudy
		1.94	0.50	slightly cloudy
		2.00	0.95	slightly cloudy
		4.74	0.94	cloudy
		4.78	1.97	slightly cloudy
Brij 35	16.9 **	0.50	0.00	soluble
		0.97	0.00	soluble
		2.04	0.00	slightly cloudy
Brij 97	12.4 **	1.01	0.00	insoluble
Capmul PG-12	4.5 ***	0.50	0.00	soluble
		0.98	0.00	soluble
		1.96	0.00	slightly cloudy
		4.98	0.00	cloudy
Aerosol OT		0.51	0.00	insoluble
Precirol ATO 5	2.0 ***	4.80	0.00	insoluble
Gelucire 50/13	13.0 ***	0.50	0.00	insoluble
Labrasol	14.0 ***	0.50	0.00	cloudy
Tween 20	16.7 **	0.49	0.00	cloudy
Tween 80	15.0 **	0.49	0.00	cloudy

* - from Vervaet and Byron (1999)
** - from Wade and Weller (1994)
*** - product information leaflets (Gattefossé)

No dependence of solubility on HLB number was determined. For instance, Brij 35 and Tween 20 having almost the same HLB gave different results, with the former compound dissolving

completely in HFA-134a. Dickinson *et al.* (2000) aimed to correlate the solubility of different solutes in HFA propellant with two physical measures – Fedors solubility parameters and clogP values but no or weak (with clogP) relationships were found. The chemical structure is more likely to determine the solubility of surfactants in the propellant and, as mentioned earlier, compounds with more hydrophilic groups dissolve better.

In the case of the series of Brij surfactants the two which were completely soluble in HFA-134a without the presence of ethanol were Brij 58 and Brij 35. The numbers of ethylene oxide groups that these compounds contain are 20 and 35, respectively, indicating that Brij 35 is the more hydrophilic. Brij 97, containing only 10 ethylene oxide moieties, did not result in a clear solution and was classified as insoluble in this set of conditions (Table 7.15).

The Myrj class, despite the high HLB numbers of 17.9 and 18.8 for Myrj 53 and 59, respectively, were not soluble in the propellant even at a 0.5% (w/w) level. The addition of 0.5% (w/w) ethanol did not improve their solubility. The reason for this behaviour may be due to the presence of stearic acid chains, which are highly hydrophobic and contribute to the poor dissolution properties of Myrj surfactants. Similarly, hydrophobic properties of the fatty acid residues constituting glycerides were responsible for producing two-phased systems: a cloudy mixture in the case of Labrasol and a suspension-like blend in the case of Gelucire 50/13.

Propylene glycol monolaurate (Capmul PG-12) has a HLB value of about 4.5 indicating its high hydrophobicity but it was miscible with the propellant at concentrations up to 2% (w/w). This is a further example which proves that the choice of surfactant for a MDI formulation should not be based on the HLB number alone. Vervaet and Byron (1999) investigated propoxylated polyethylene glycol with the HLB equal to 4.0 and found that even 3.6% (w/w) resulted in a transparent solution.

Low molecular weight, liquid polyoxyethylene glycols 300 and 1000 dissolved in HFA-134a producing clear solutions for up to 2% (w/w). When formulated with 0.5% (w/w) ethanol, they gave cloudless solutions even at a level of 5% (w/w). The lower solubility of solid PEG 4000 and PEG 6000 may be a consequence of their crystallinity. A large quantity of ethanol was required in order to completely dissolve PEG 4000 (Table 7.15).

Summarising, the following five surfactants were selected to be used in formoterol fumarate suspension MDIs based on their solubility in HFA-134a propellant: PEG 300, PEG 1000, Brij 58, Brij 35 and Capmul PG-12. A further two compounds: Myrj 97 and Myrj 53 were considered to be potentially useful for formulations containing ethanol.

7.3.6.2 Spray dried Mannitol II

The dispersibility studies of the spray dried mannitol were carried out. Only the sample that gave the smallest particles was examined (Mannitol II). Various surfactants, as selected in Section 7.3.6.1, were employed with and without the addition of ethanol. The results of the dispersibility investigations are summarised in Table 7.16.

Table 7.16 Dispersibility studies of spray dried mannitol (sample code Mannitol II). 'A. s. time' indicates approximate sedimentation time.

Sample	Additive (content w/w)	A.s. time	Suspension quality
Mannitol II	0% EtOH	~2 min	flocculation
	0.1% EtOH	~2 min	flocculation
	1% EtOH	~2 min	flocs but good dispersion
	2% EtOH	~4 min	flocculation
	5% EtOH	~30 sec	flocculation
Mannitol II	1% PEG 300	~1 min	flocculation
	1% PEG 1000	~2 min	flocculation
	1% Capmul PG-12	~1 min	significant flocculation
	1% Brij 35	~1 min	flocculation
	1% Brij 58	~1 min	flocculation
Mannitol II	1% EtOH and 1% PEG 300	~1 min	flocculation
	1% EtOH and 1% PEG 1000	~1 min	flocculation
	1% EtOH and 1% Capmul PG-12	~1 min	good dispersion
	1% EtOH and 1% Brij 35	~1 min	flocculation
	1% EtOH and 1% Brij 58	~1 min	flocculation
Mannitol II	2% EtOH and 1% PEG 300	~2 min	significant flocculation
	2% EtOH and 1% PEG 1000	~2 min	significant flocculation
	2% EtOH and 1% Capmul PG-12	~2 min	good dispersion
	2% EtOH and 1% Brij 35	~2 min	significant flocculation
	2% EtOH and 1% Brij 58	~2 min	significant flocculation
Mannitol II	1% EtOH and 1% Brij 97	~1 min	good dispersion
	2% EtOH and 1% Brij 97	~1 min	good dispersion
	1% EtOH and 1% Myrj 53	~1 min	good dispersion
	2% EtOH and 1% Myrj 53	~1 min	good dispersion

Appendix VI presents a comparison of the samples after mixing (top) and 2 minutes later (bottom), illustrating differences in the extent of sedimentation for mannitol.

7.3.6.3 Spray dried PVP IV

The dispersibility studies of the spray dried PVP were also carried out. The sample that gave the smallest particles was examined (PVP IV). Various surfactants, as selected in Section 7.3.6.1, were employed with and without the addition of ethanol. The results of the dispersibility investigations are summarised in Table 7.17.

Table 7.17 Dispersibility studies of spray dried PVP (sample code PVP IV). 'A. s. time' indicates approximate sedimentation time.

Sample	Additive (content w/w)	A. s. time	Suspension quality
PVP IV	0% EtOH	~2 min	flocculation
	0.1% EtOH		caking and clumping
	1% EtOH		very stable suspension
	2% EtOH		very stable suspension
	5% EtOH		clear solution
PVP IV	1% PEG 300		clear solution
	1% PEG 1000		clear solution
	1% Brij 58	~1 min	caking and flocculation
	1% Capmul PG-12		clear solution
	1% Brij 35	~2 min	flocculation

The observations from the dispersibility studies of PVP in mixtures of propellant with ethanol lead to the conclusion that no ethanol can be used in formulations of PVP in HFA-134a, since it either causes stickiness or dissolves the particles. Furthermore, if PVP is able to dissolve in the propellant containing ethanol, it ceases to have protective properties and exposes formoterol fumarate to detrimental effects of the propellant.

Appendix VI presents a comparison of the samples after mixing (top) and 2 minutes later (bottom), illustrating differences in the extent of sedimentation for mannitol.

7.3.6.4 Spray dried Mannitol II in propellant containing PVP

Having observed the good solubility of PVP in the ethanol-propellant system, it was decided to check its surfactant/suspension stabilising ability, as some polymers are good suspension aids (Martin, 1993). The results of the dispersibility investigations of mannitol sample II are summarised in Table 7.18.

Table 7.18 Dispersibility studies of spray dried mannitol (sample code Mannitol II) suspended in propellant with the addition of ethanol and PVP. 'A. s. time' indicates approximate sedimentation time.

Sample	Additive (content w/w)	A. s. time	Suspension quality
Mannitol II	2% EtOH and 0.2% PVP		polymer did not dissolve, stickiness of mannitol
	2% EtOH and 0.1% PVP	~5 min	flocculation
	2% EtOH and 0.05% PVP	~4 min	flocculation
Mannitol II	5% EtOH and 0.2% PVP	~25 min	good and stable dispersion
	5% EtOH and 0.1% PVP	~25 min	good and stable dispersion
	5% EtOH and 0.05% PVP	~25 min	good and stable dispersion

The mechanism of PVP surfactant action is not clear, but it may be hypothesised that, when dissolved in a mixture of propellant and ethanol, it increases the viscosity of propellant.

Appendix VI presents a comparison of the samples after mixing (top) and 5 and 10 minutes later (bottom) for the 2% and 5% ethanol content, respectively, illustrating differences in the extent of sedimentation for mannitol.

7.3.6.5 Conclusions from the dispersibility studies of single spray dried excipients

The dispersibility studies of single spray dried excipients in HFA-134a allowed us to draw some conclusions about the suitability of the excipients as carriers for formoterol fumarate in CFC-free MDIs. Mannitol was demonstrated to be successful in terms of producing good quality dispersions, but PVP exhibited stickiness or dissolved in the presence of ethanol. Nevertheless, this polymer can still be used in HFA-134a formulations in the role of a suspension stabilising agent as it was able to slow down the sedimentation of mannitol particles. Pictures have not been shown but spray dried HPMC also gave stable and uniform suspensions. However the particles were too large for inhalation purposes (Section 7.3.4), therefore it was deemed reasonable to co-spray dry HPMC with mannitol with the aim of decreasing the particle size. Co-spray drying mannitol and PVP was aimed at achieving a combined effect of good dispersion, as obtained with mannitol and deceleration of sedimentation as observed with PVP.

7.3.7 Co-spray dried mannitol/HPMC

An aqueous solution of mannitol and HPMC was prepared for spray drying. The final product contained 30% (w/w) of the polymer. The processing conditions are given in Appendix I.

DSC analysis (Figure 7.29) of the co-spray dried powder revealed an endothermic peak at ~55°C probably due to the T_g of the mixture. This peak accompanying the glass transition is generated as a consequence of enthalpy recovery (Christensen *et al.*, 2002). The second thermal event recorded by DSC for the spray dried sample was an exotherm assigned to recrystallisation of the amorphous material and another endothermic peak beginning at ~163°C due to mannitol melting. The equivalent physical mixture did not demonstrate an exothermic peak and furthermore, the onset of mannitol melting occurred at ~165°C. The comparison of the heats of mannitol fusion of the mechanical mix (204 J/g) to the processed specimen (167 J/g) revealed that the latter was lower by 37 J/g indicating either miscibility of the two components or the fact that some amorphous material was formed but did not recrystallise (Weuts *et al.*, 2005).

Thermogravimetric analysis (Figure 7.29) of the processed batch showed a weight loss of ~1.8% up to 100°C compared to only ~0.6% weight loss of the physical mix. This may indicate greater moisture adsorption of the former.

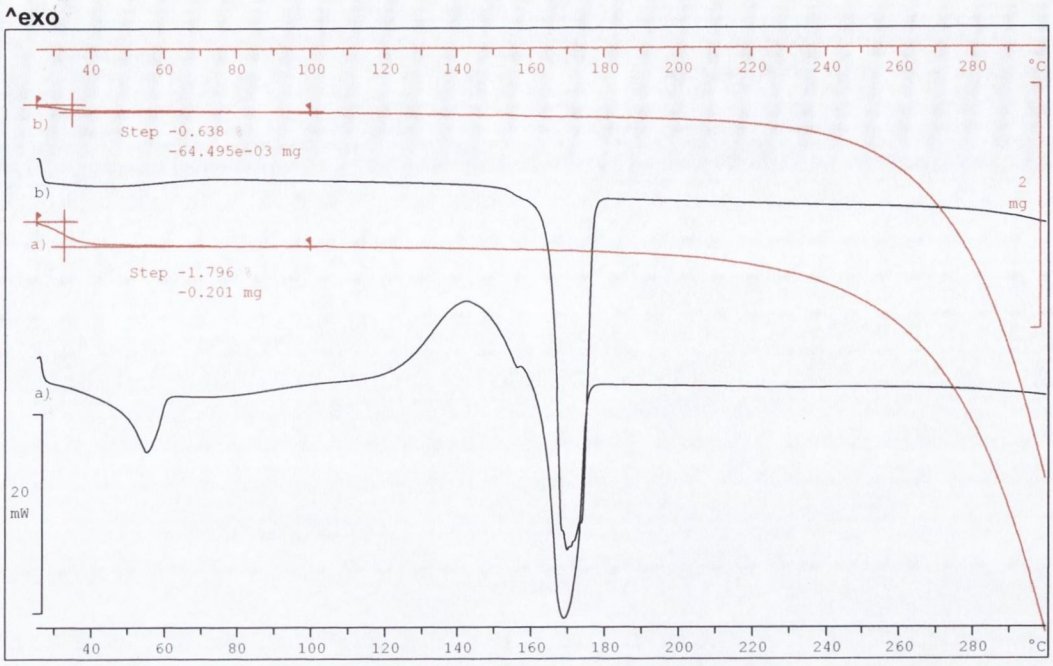

Figure 7.29 DSC traces of mannitol/HPMC 30%: co-spray dried (black a), physical mixture (black b) and TGA traces of mannitol/HPMC 30%: co-spray dried (red a), physical mixture (red b).

In the XRD pattern of the spray dried mixture the characteristic peaks of crystalline mannitol which were still present in the physical mixture disappeared and the X-ray diffraction pattern of the co-spray dried sample was typical of the XRD spectrum of an amorphous substance (Figure 7.30).

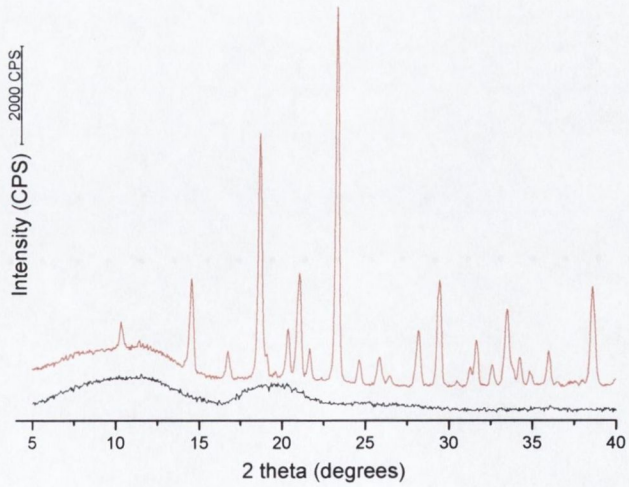

Figure 7.30 XRD diffraction patterns of mannitol/HPMC 30%: co-spray dried (black) and physical mixture (red).

SEM pictures analysis (Figure 7.31) demonstrates that the sample consisted of folded, collapsed particles resembling those of the HPMC spray dried alone (Figure 7.23).

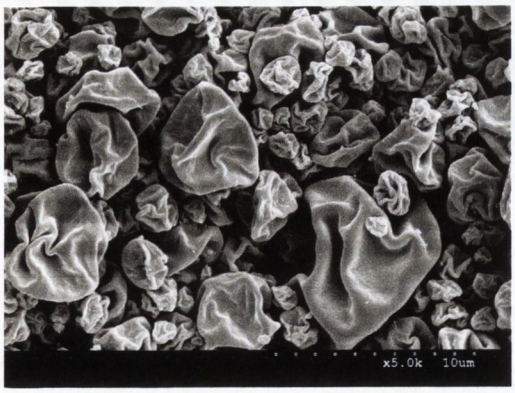

Figure 7.31 SEM photograph of spray dried mannitol/HPMC 30%.

Laser diffraction particle size analysis revealed that the particle size distribution was nearly mono-modal with a "tail" towards smaller sizes indicating a small fraction of particles having diameters between 0.3-1μm. Around 80% (by volume) of particles were 5 μm and smaller and all were below 10 μm.

HPMC has been reported to prevent the formation of a monotropic mezophase of itraconazole during melt extrusion and thus forms an amorphous solid dispersion (Verreck *et al.*, 2003). It also exhibited amorphisation abilities on tolbutamide (Chen *et al.*, 2004) as well as tacrolimus (Yamashita *et al.*, 2003). In the case of these previous studies it was observed that at least 50% (w/w) content of HPMC was needed in order to convert a crystalline drug into its amorphous counterpart. Our studies demonstrated that, in the case of mannitol, only 30% (w/w) HPMC sufficed to transfer the crystalline form of the sugar on spray drying into the disordered state.

7.3.8 Co-spray dried mannitol/PVP

The conditions for spray drying composites of mannitol and PVP 40000 are given in Appendix I.

The first spray dried mixture of mannitol and PVP was that containing 50% (w/w) of the polymer. A soft, glassy substance, which stuck to the walls of the cyclone resulted on spray drying and only a few milligrams was extracted from the collecting vessel. This was enough to carry out the DSC analysis, which revealed three thermal events, namely: the glass transition occurring at ~33°C, recrystallisation exotherm at ~90°C and mannitol melting endotherm beginning at ~141°C (Figure 7.32). Due to the very low T_g the sample recrystallised very quickly at room temperature and this was evidenced in a decrease in the normalised heat of recrystallisation (from 53 J/g immediately after recovering from the apparatus to 9 J/g after 1h of storage in room temperature) observed in the second DSC run.

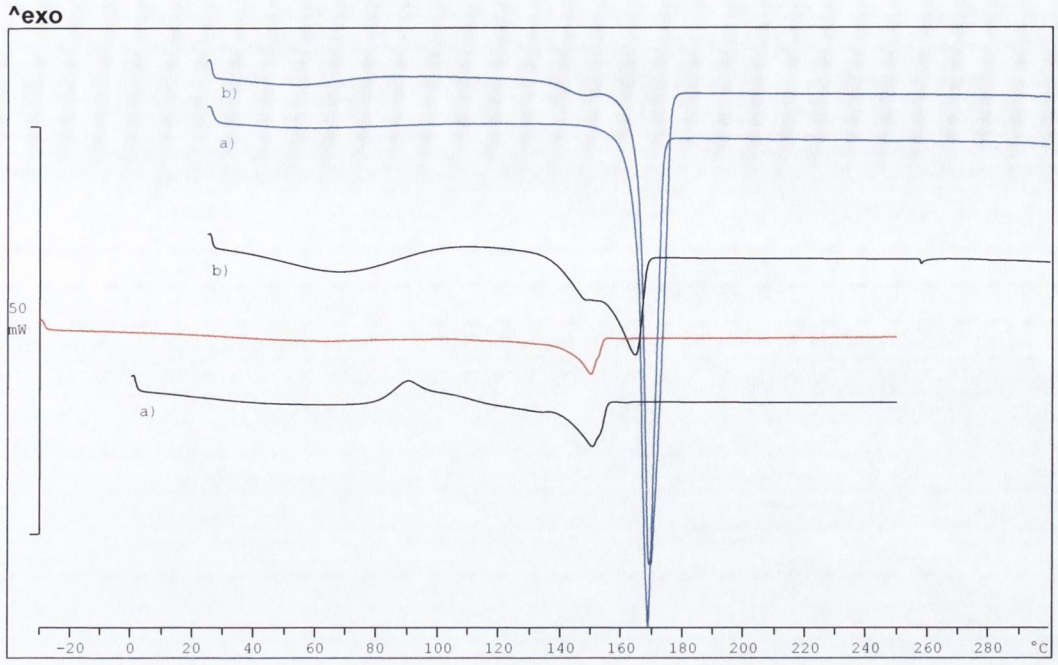

Figure 7.32 DSC traces of: spray dried mannitol/PVP 50% run immediately after recovering (black a), spray dried mannitol/PVP 50% run after 1 hour on storage in room temperature (red), physical mix of mannitol/PVP 50% (black b), spray dried mannitol/PVP 10% (blue a) and physical mix of mannitol/PVP 10% (blue b).

The melting endotherm of the spray dried sample was very broad and its maximum corresponded to the first peak of the double endotherm of the equivalent mechanical mix. Similarly, as for the mannitol/HPMC 30% spray dried composite, mannitol/PVP 50% exhibited a decrease in the heat of melting when compared to its physical mix. It was reduced by 94 J/g due to likely miscibility of the two components on melting.

Since a powdered sample was required as a carrier, another batch of mannitol-PVP composite was spray dried, this time containing only 10% (w/w) of PVP.

DSC of the spray dried composite revealed a single endothermic peak with the onset at ~164°C due to melting of mannitol Figure 7.32. There was ~1.2% weight loss from the powder by TGA up to 100°C related to water desorption compared with ~0.9% mass loss for the mechanical mix.

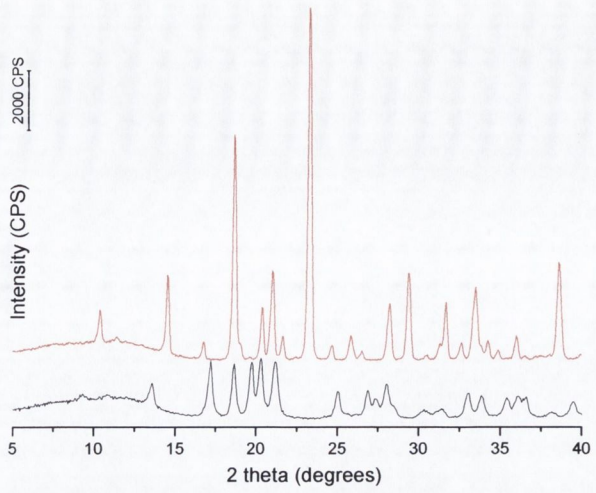

Figure 7.33 XRD diffractograms of co-spray dried mannitol/PVP 10% (black) and the equivalent physical mixture (red).

The XRD diffraction pattern obtained for this sample suggested that it was crystalline but the presence of a broad "halo demonstrates that the sample contains some amorphous material. The mannitol in this composite was predominantly in the α form. Recently, Cavatur *et al.* (2002) reported a complete inhibition of mannitol crystallisation by PVP in solutions intended for freeze-drying and our study on spray drying of mannitol-PVP systems have shown that the degree of sugar amorphicity depends on the PVP content.

The shape of the spray dried particles can be observed in Figure 7.34, which reveals that they were spherical but fused. Particle size analysis revealed that ~30% of particles (by volume) were below 5 μm and about 63% were below 10 μm. The particle size distribution was bi-modal with a small particles fraction with sizes 0.2-1 μm.

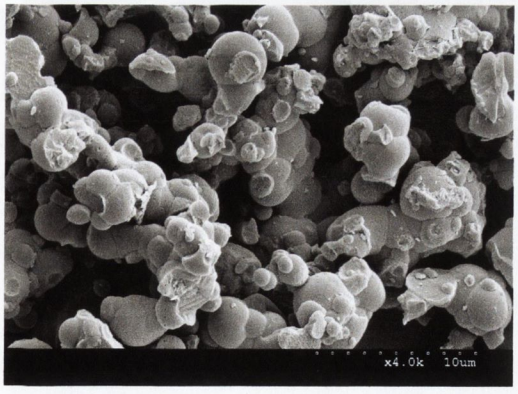

Figure 7.34 SEM microphotograph of the spray dried mannitol/PVP 10% composite.

7.3.9 Co-spray dried mannitol/formoterol fumarate dihydrate

Co-spray during of mannitol with 50% PVP 40000 resulted in larger particles than those of Mannitol II, whereas particles of the spray dried mixture of mannitol and HPMC 30% were similar in size to the sizes of particles of Mannitol II. Therefore it may be concluded that no significant decrease in the particle size for the binary systems was observed. It was then decided that for the simplicity of preparation of solutions for spray drying and to avoid unwanted stability issues associated with the amorphous state of the mannitol/HPMC 30% system, further co-spray dying studies with formoterol fumarate would be based only on mannitol.

Three mannitol/formoterol fumarate blends were spray dried from aqueous solutions containing either 10%, 20% or 30% of formoterol fumarate as dihydrate. The processing conditions are given in Appendix I. DSC analysis of the co-spray dried powders revealed only a single endothermic peak at 165-166°C regardless of the drug concentration, which was probably due to mannitol melting (Figure 7.35). This peak showed a minor shift towards lower temperatures with increasing content of formoterol fumarate and the onsets were at 164.2°C, 163.6°C and 163.1°C for 10%, 20% and 30% (w/w) drug content, respectively. The depression in the mannitol melting point was caused by the presence of the drug, as was also observed for the BFMT/PEG physical mixtures (Corrigan *et al.*, 2003). No apparent thermal event indicating the presence of the drug either in crystalline or amorphous form could be seen. When the heats of fusions were compared with the calculated ones assuming that the heat of melting of mannitol is 290 J/g, reductions in the energy by 9 J/g, 15 J/g and 19 J/g for the 10%, 20% and 30% drug-containing composites were detected. The explanation for this phenomenon may be due to similar mechanisms of interaction between the substances as was the case for the mannitol/HPMC 30% (w/w) system (Section 7.3.8).

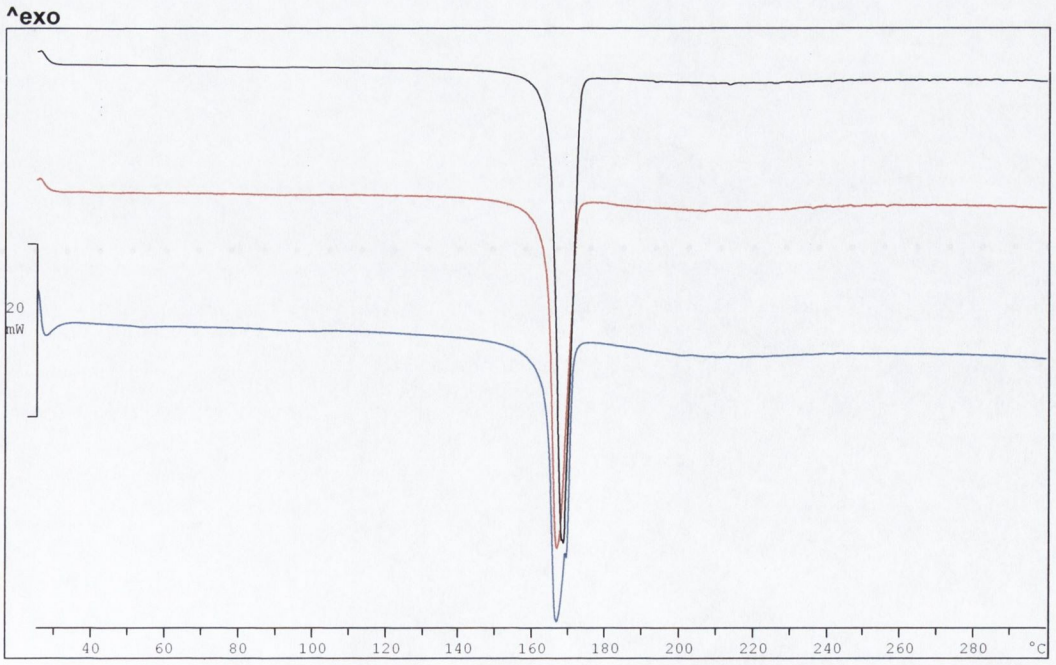

Figure 7.35 DSC traces of the mannitol/formoterol fumarate 10% (black), mannitol/formoterol fumarate 20% (red) and mannitol/formoterol fumarate 30% (blue) spray dried systems.

Thermogravimetric analysis of the samples showed a weight loss of ~0.8-0.9% up to 100°C, which was ascribed to moisture desorption. Examination of the XRD results of the mannitol/formoterol fumarate co-spray dried mixtures presented in Figure 7.36 confirmed that they were crystalline in nature, but broad "halos" of amorphous fractions were also apparent.

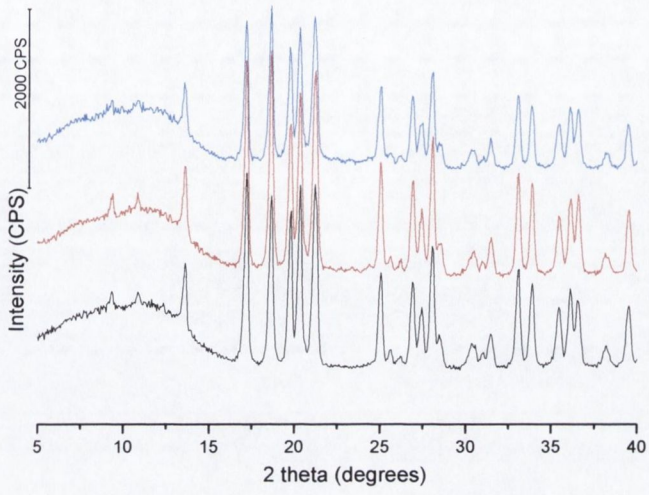

Figure 7.36 XRD diffractograms of the mannitol/formoterol fumarate 10% (black), mannitol/formoterol fumarate 20% (red) and mannitol/formoterol fumarate 30% (blue) spray dried systems.

They were no peaks of crystalline formoterol fumarate, and furthermore, the diffractograms were ascribed to the α-form of mannitol. The drug spray dried alone gave an amorphous phase (Chapter 4). This means that the co-spray drying of mannitol with the drug caused a polymorphic transition of the excipient. A similar phenomenon was described by Todo *et al.* (2004) for spray dried insulin-mannitol powders. The lack of formoterol fumarate peaks by XRD and no traces of the crystalline drug recorded by DSC indicates that the drug may be embedded inside the crystalline matrix of mannitol which would be a desirable outcome. It means that the drug may be protected by mannitol as only the excipient will be exposed to propellant. Such formulations may prolong the chemical stability of formoterol provided that the drug is isolated from the detrimental external environment. To confirm this hypothesis the samples were subjected to prolonged and accelerated stability studies, the results of which are described in further sections of this chapter.

SEM pictures revealed (Figure 7.37) that the samples consisted of spherical, but fused particles with some of the particles having rough surfaces. On visual examination of the photographs it appeared that the greater the drug content the more fused the particles were. The morphology of these particles was different to that of spray dried mannitol on its own, where the majority of the particles had one or more holes and rougher surfaces (Figure 7.16).

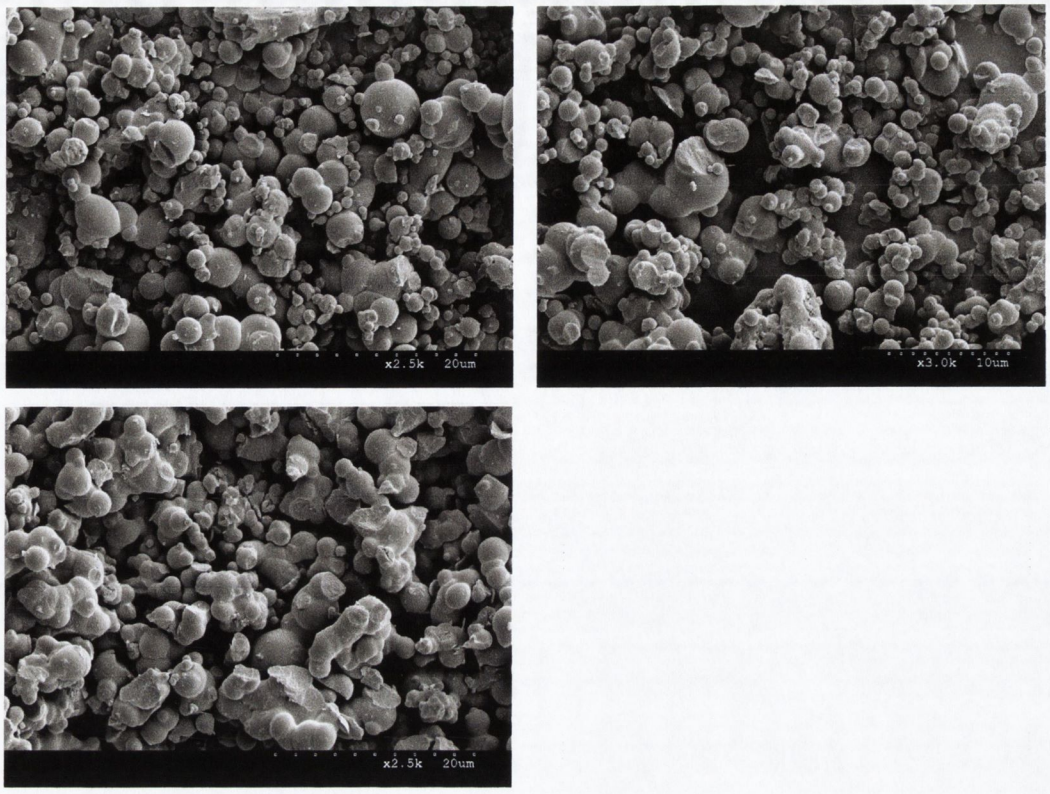

Figure 7.37 SEM pictures of the mannitol/formoterol fumarate 10% (top left), mannitol/formoterol fumarate 20% (top right) and mannitol/formoterol fumarate 30% (bottom) spray dried systems. Note a different magnification of the top right micrograph.

Laser diffraction particle size analysis (Figure 7.38) revealed that the particle size distributions were clearly tri-modal (10% of formoterol) or tetra-modal (20% and 30% of the drug content). Around 60%, 55% and 52% of particles were 5 μm and smaller and over 90%, 85% and 84% were below 10 μm, for the spray dried mannitol/formoterol fumarate 10%, 20% and 30% (w/w), respectively.

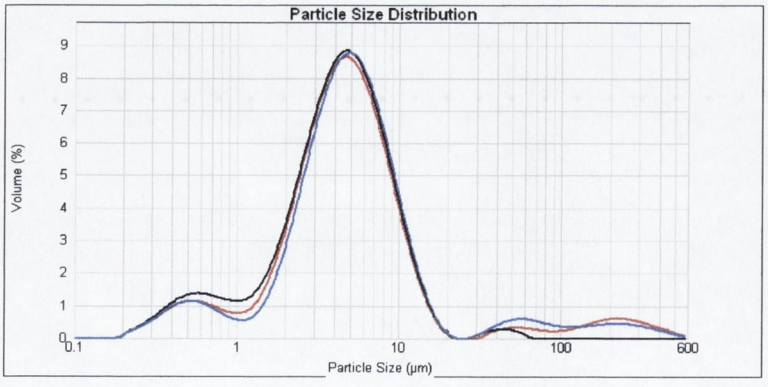

Figure 7.38 Laser diffraction particle size distribution profiles (obtained by the Malvern Mastersizer 2000) of the mannitol/formoterol fumarate 10% (top left), mannitol/formoterol fumarate 20% (top right) and mannitol/formoterol fumarate 30% (bottom) spray dried systems.

7.3.10 Solid state pH modification of formoterol fumarate

7.3.10.1 Introduction

The objective of these studies was to determine if co-spray drying formoterol fumarate with excipients and buffers is able to improve the chemical stability of the drug.

Assessing the role of effective pH in solid state reactions is complicated by the fact that pH technically is defined only in aqueous solution (Song *et al.*, 2001). Practically, by this definition, there should be no pH phenomenon observed for the solid state. But on the other hand, it is well known that chemical reactions are influenced by the presence of water (Duckworth, 1975) and it has been evidenced that the sorbed moisture layer has solvent properties (Carstensen, 1995). Therefore, if the soluble components can dissolve in the residual moisture, they are able to control the pH of the system which is a critical factor for determining product shelf-life. Knowing that a compound is more stable at a given pH, one can use an acid or base to adjust the microenvironment pH to its optimum value. To complicate the stability study in the solid state, there has been no generally accepted method of measuring hydrogen ion activity in solids (Song *et al.*, 2001). One of the approaches adopted in many chemical stability studies defines the "effective pH" of the solid as the pH measured in aqueous solution prior to the process or following reconstitution of the solid (Strickley and Anderson, 1996; Bell and Labuza, 1994). This is not always a valid approach as the solution created by moisture sorption could be of a pH value which is displaced from that observed in solution (Carstensen, 1995) and, for instance Nikfar *et al.* (1990) have demonstrated the existence of a "solid pH-profile", which was parallel to the theoretical pH-profiles of the drug in solution. The solid state pH-profile was displaced by 1.4 pH units and this may be attributed to the kinetic salt effect. A much worse scenario was demonstrated by Gerhard and Carstensen (1989) for phenobarbital and in this case it was necessary to shift the profile by 6 pH units to superimpose it with the pH-profile determined for solutions.

The 2003 ICH guidelines on stability studies (ICH, 2003) specify a minimum set of testing conditions and define that the long term testing should be carried out at 25°C±2°C and 60% RH±5% and the accelerated testing at 40°C±2°C and 75% RH±5%.

7.3.11 Introductory experiments-pH of concentrated and diluted buffer solutions

The stability study of formoterol fumarate in buffered solution indicated that the maximum stability can be achieved when phosphate buffer at pH=5.0 or citrate buffer at pH=5.2 was used. The buffers used in this study were well diluted with water, thus the above pH values may not reflect the microenvironment pH existing in the solid state. The water available to create such microenvironment pH can be delivered from the suspended powder (monitored here by TG analysis), air during storage of the formulation and finally from the inhaler propellant. Moreover, high water content in the formulation may lead to clumping/flocculation of the suspended particles.

Determination of water content in HFA-134a by Karl Fisher titration (method described in Chapter 2) revealed that the average water content was 171 ppm ± 9 ppm. This was below the maximum moisture content determined by the manufacturer of the propellant, which equals to 193 ppm.

As the purpose of this work was to achieve the greatest chemical stabilisation of formoterol fumarate in buffered spray dried composites, it was deemed necessary to explore if the pH of diluted buffers is the same as the concentrated solutions.

For this reason, a set of saturated buffer solutions was prepared and their pH was measured. Appropriate quantities of salts were mixed in simple binary proportions (the amounts of the substances taken were corrected for the crystalline water) then 10 ml of water was added to each blend and thoroughly mixed until a cloudy mixture was obtained. This aimed to recreate as closely as possible the condition in a propellant driven inhaler when only a limited amount of moisture is available and the buffer salts are not fully dissolved. The pH values were measured at two chosen temperatures, at 25°C and 40°C.

Table 7.19 and Table 7.20 present the results of the experiment for phosphate and citrate buffer, respectively.

Table 7.19 The average pH values of concentrated phosphate buffer solutions at 25°C and 40°C.

sodium dihydrogen phosphate [g]	di-sodium hydrogen phosphate [g]	pH at 25°C	pH at 40°C
0.0	10.0	8.90	8.75
1.0	9.0	7.21	7.37
2.0	8.0	6.88	6.90
3.0	7.0	6.58	6.54
4.0	6.0	6.23	6.21
5.0	5.0	5.88	5.87
6.0	4.0	5.53	5.48
7.0	3.0	5.13	5.08
8.0	2.0	4.71	4.60
9.0	1.0	4.07	3.99
10.0	0.0	3.31	3.18

Table 7.20 The average pH values of concentrated citrate buffer solutions at 25°C and 40°C.

citric acid [g]	tri-sodium citrate [g]	pH at 25°C	pH at 40°C
0.0	10.0	8.23	8.19
1.0	9.0	5.38	5.35
1.5	8.5	5.05	5.06
2.0	8.0	4.90	4.85
3.0	7.0	4.44	4.34
4.0	6.0	4.10	3.97
5.0	5.0	3.70	3.61
6.0	4.0	3.29	3.11
7.0	3.0	2.80	2.62
8.0	2.0	2.35	2.17
9.0	1.0	1.76	1.57
10.0	0.0	0.69	0.45

Generally, all the pH values measured at 40°C were lower than those at 25°C. The reasons for this are different hydrogen ion activities at these temperatures as well as solubilities of the salts. The pH values of maximum stability of the drug in phosphate and citrate buffers were 5.00 and 5.20, respectively (Chapter 7.2.3.4 and Chapter 7.2.3.5), but these solutions were diluted (0.05M for the phosphate buffer and 0.01M for the citrate buffer). In the nearly saturated state, the compositions of the phosphate and citrate buffers giving approximately the same optimum values of pH are sodium dihydrogen phosphate:di-sodium hydrogen phosphate in the ratio 7:3 and citric acid:tri-sodium citrate in the ratio 1.5:8.5, respectively.

However, it is known that the pH of a buffer changes with its concentration, thus the effect of dilution on the pH of the buffers was evaluated. Figure 7.39 shows this graphically.

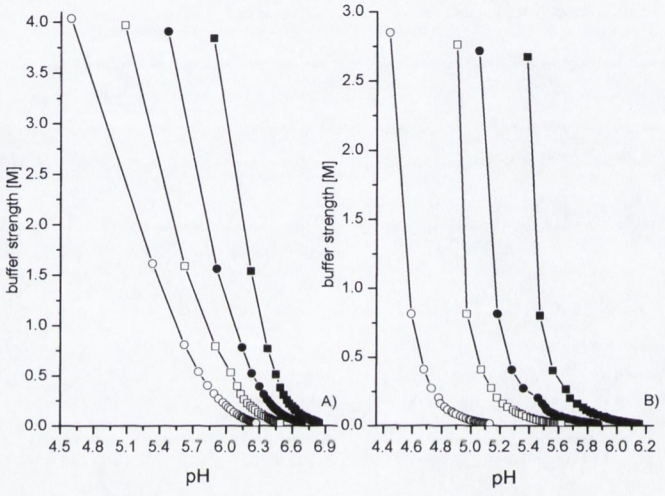

Figure 7.39 Effect of dilution on the pH values of A) phosphate buffer composed of sodium dihydrogen phosphate and di-sodium hydrogen phosphate (amounts corrected for the crystalline water) in the ratio 5:5 (full squares), 6:4 (full circles), 7:3 (open squares) and 8:2 (open circles), B) citrate buffer consisted of citric acid and tri-sodium citrate (corrected for the crystalline water) in the ratio 1:9 (full squares), 1.5:8.5 (full circles), 2:8 (open squares) and 3:7 (open circles).

A significant difference between the pH values for the saturated and diluted buffers can be noticed. It varies between 1 and 1.7 units for the phosphate and around 0.7-0.8 for the citrate buffers depending on the composition, with the lowest pH values being for the concentrated solutions. This observation is consistent with the study of Bell and Labuza (1994) on phosphate buffer solutions, when the actual pH of reduced moisture systems containing this buffer appeared to be lower than in dilute solution. This result means also that changes in hydration of the buffer salts will have greater influence on phosphate than the citrate buffer.

Summarising, appropriate adjustments to the buffer compositions respecting the pH differences in the diluted and concentrated states were made before spray drying. The ratio 7:3 for sodium dihydrogen phosphate:di-sodium hydrogen phosphate was chosen to correspond to around pH=5.0 of the diluted phosphate buffer and the ratio 1.5:8.5 for citric acid:tri-sodium citrate was taken as the pH=5.2 of the diluted citrate buffer.

7.3.12 Co-spray drying of mannitol/formoterol fumarate dihydrate/ buffer salts composites

The addition of citrate and phosphate buffer salts aimed at combining the chemical stability studies in buffered solutions (Chapter 7.2 and Chapter 7.3.11) and studies on co-spray drying mannitol with formoterol fumarate (Chapter 7.3.9). As indicated by Lewis *et al.* (2001), modification of the environmental apparent pH may improve chemical stability of formoterol fumarate.

7.3.12.1 Mannitol/formoterol fumarate dihydrate 10%/citrate buffer (citric acid:tri-sodium citrate 1.5:8.5) 1% (w/w)

The DSC analysis registered only one asymmetric endothermic peak at 162 °C (Figure 7.40) ascribed as melting of mannitol. However the onset of this peak was depressed and began at ~130 °C. This can be caused by the presence of citric acid, which is known to have plasticising properties (Wan *et al.*, 1993).

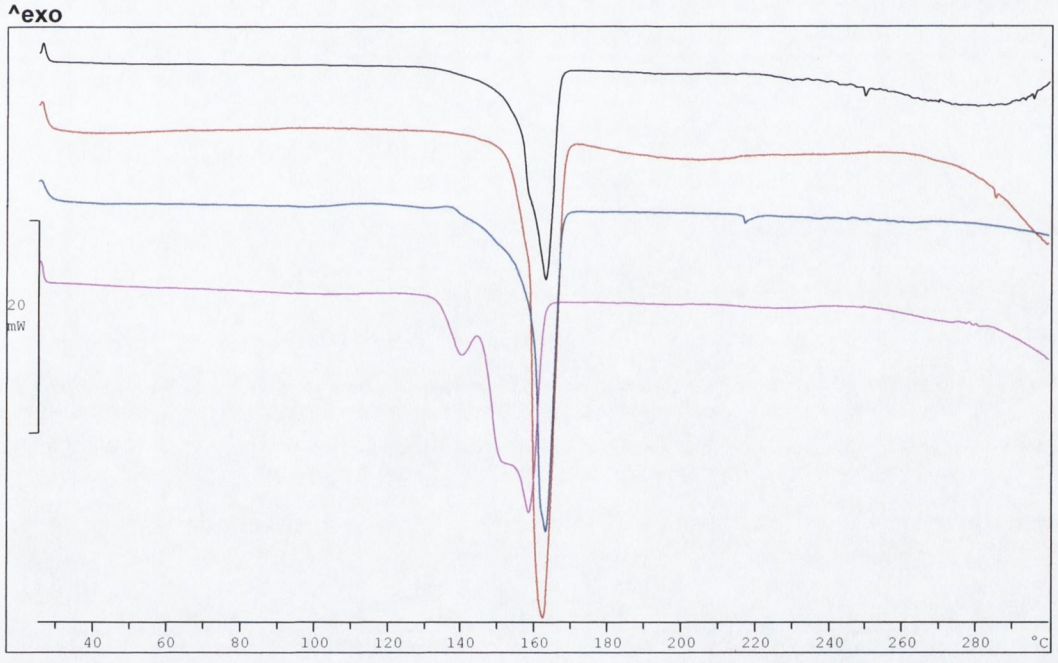

Figure 7.40 DSC traces of co-spray dried: mannitol/formoterol fumarate 10%/citrate buffer salts 1% (w/w) (black), mannitol/formoterol fumarate 10%/phosphate buffer salts 1% (w/w) (red), mannitol/formoterol fumarate 10%/calcium chloride 5% (w/w) (blue) and mannitol/formoterol fumarate 10%/calcium chloride 5%/citrate buffer salts 1% (w/w) (magenta).

TG examination of the powder showed ~1.2% weight loss for up to 100 °C, most likely associated with water liberation from the sample.

The powder was crystalline by XRD as shown in Figure 7.41 and all peaks but one were ascribed to the α polymorph of mannitol. The peak at 24 2θ was characteristic of the β-form. XRD analysis

confirmed that all other constituents were either rendered amorphous or their crystalline content was below the detection level of XRD (in the case of the buffer).

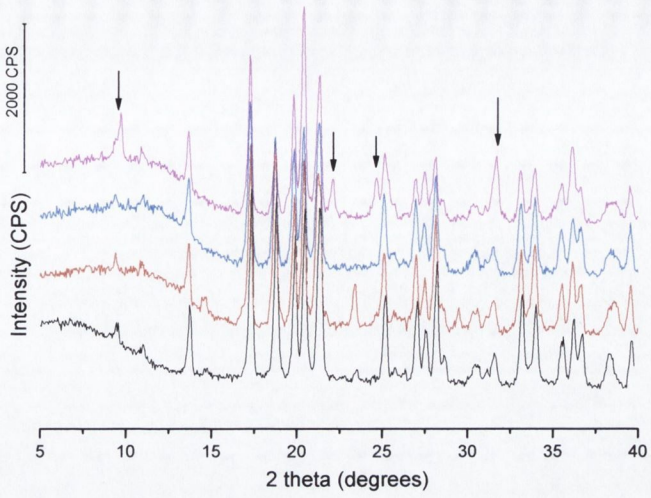

Figure 7.41 XRD diffractograms of co-spray dried: mannitol/formoterol fumarate 10%/citrate buffer salts 1% (w/w) (black), mannitol/formoterol fumarate 10%/phosphate buffer salts 1% (w/w) (red), mannitol/formoterol fumarate 10%/calcium chloride 5% (w/w) (blue) and mannitol/formoterol fumarate 10%/calcium chloride 5%/citrate buffer salts 1% (w/w) (magenta). The arrows indicate peaks characteristic of the β polymorph of mannitol.

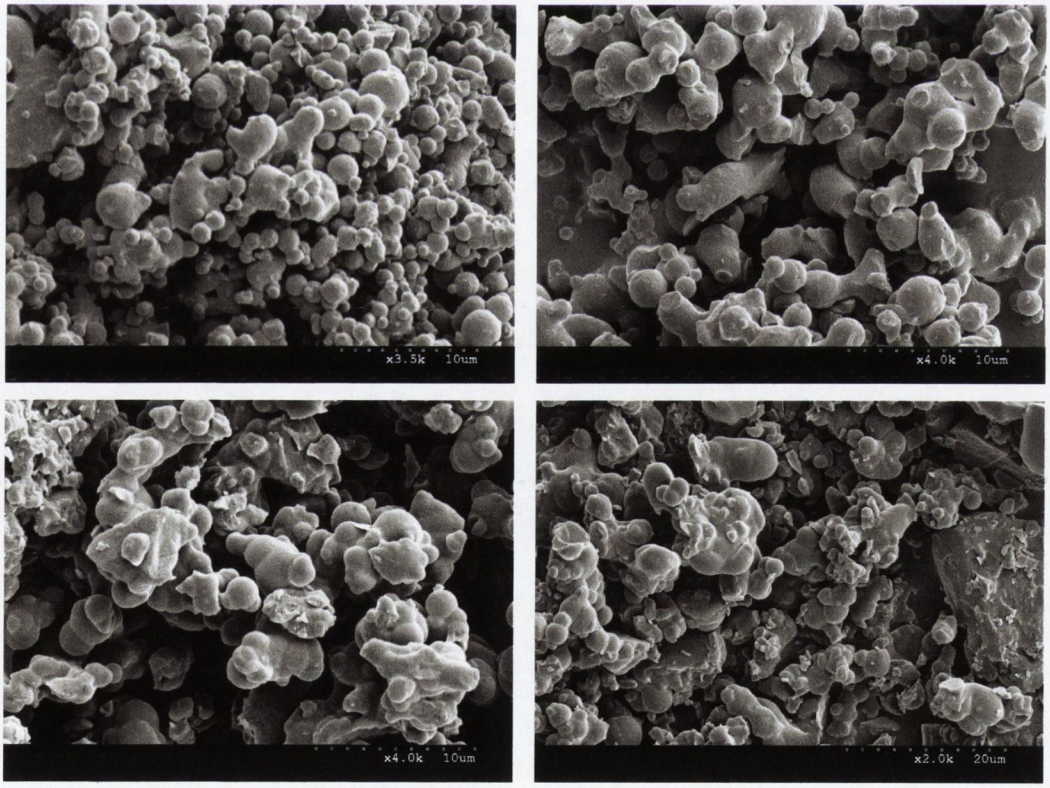

Figure 7.42 SEM photographs of co-spray dried: mannitol/formoterol fumarate 10%/citrate buffer salts 1% (w/w) (black), mannitol/formoterol fumarate 10%/phosphate buffer salts 1% (w/w) (red), mannitol/formoterol fumarate 10%/calcium chloride 5% (w/w) (blue) and mannitol/formoterol fumarate 10%/calcium chloride 5%/citrate buffer salts 1% (w/w) (magenta). Note different magnifications of the micrographs.

The particles were round but fused as observed by SEM (Figure 7.42). At higher magnification their exteriors were rough.

Particle size analysis demonstrated that the particle size distribution was essentially mono-modal with a "tail" of a fraction of smaller particles (Figure 7.43). Over 75% of particles were below 5 μm and nearly all were below 10 μm.

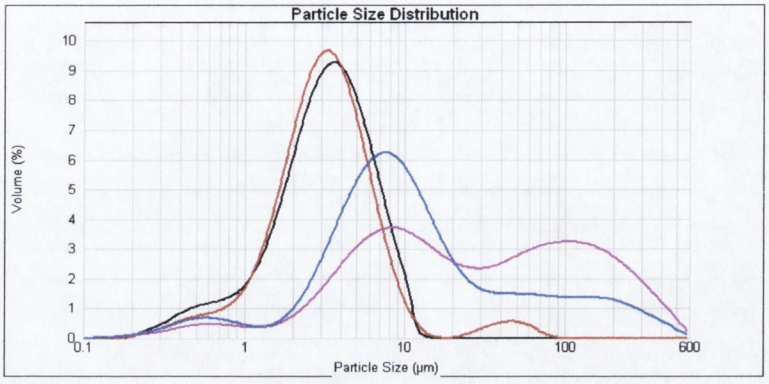

Figure 7.43 Laser diffraction particle size distribution profiles (obtained by the Malvern Mastersizer 2000) of co-spray dried: mannitol/formoterol fumarate 10%/citrate buffer salts 1% (w/w) (black), mannitol/formoterol fumarate 10%/phosphate buffer salts 1% (w/w) (red), mannitol/formoterol fumarate 10%/calcium chloride 5% (w/w) (blue) and mannitol/formoterol fumarate 10%/calcium chloride 5%/citrate buffer salts 1% (w/w) (magenta).

7.3.12.2 Mannitol/formoterol fumarate dihydrate 10%/phosphate buffer (sodium dihydrogen phosphate: di-sodium hydrogen phosphate 7:3) 1% (w/w)

Similarly, as in the case of the previous samples, only one, fairly symmetrical endotherm was seen on the DSC curve (Figure 7.40). It peaked at ~160°C and was narrower than the mannitol melting peak observed for the mannitol/formoterol fumarate 10%/citrate buffer 1% (w/w). Phosphate buffers have been demonstrated to increase the T_gs of trehalose and sucrose (Ohtake *et al.*, 2004), thus no plasticising effect should be seen. TG analysis showed ~1.2% weight loss between 25-100°C, most probably associated with dehydration of adsorbed moisture.

The XRD pattern evidenced that the mannitol transformed to the α-form but the presence of the β polymorph was apparent as demonstrated in Figure 7.41. Similarly, as for the composite spray dried with citrate buffer, all remaining constituents were amorphous or had a crystalline content below the detection limit of the XRD apparatus. SEM photographs demonstrated that the particles were generally round, but fused with dented and perforated-like surfaces (Figure 7.42). The particle size distribution (Figure 7.43) was bimodal with a small percentage (by volume) of particles sized between 20-80 μm. Around 77% of particles were below 5 μm and over 95% were below 10 μm.

7.3.13 Co-spray drying of mannitol/formoterol fumarate dihydrate/ calcium chloride dihydrate composites

The use of calcium chloride was aimed at an examination of its desiccant properties and therefore potential improvement of chemical stability of the drug.

7.3.13.1 Mannitol/ formoterol fumarate dihydrate 10%/Calcium chloride dihydrate 5% (w/w)

DSC analysis demonstrated an exotherm at ~115°C (weak in magnitude and more apparent at a higher magnification) followed by an endothermic peak at ~162°C due to melting of mannitol (Figure 7.40). The appearance of the exothermic peak could indicate that a fraction of the composite was amorphous and recrystallised on heating. Undoubtedly, it is due to the presence of the calcium salt, as it was not observed for either of the binary co-spray dried mannitol/formoterol fumarate systems or for the ternary buffered composites. There was ~1.4 % weight loss for up to 100 °C ascribed to the water desorption as detected by TGA. Only peaks of the α polymorph of mannitol were recorded by XRD (Figure 7.41) suggesting that the drug and calcium chloride were amorphous. The particles were round with a high degree of fusion as observed by SEM (Figure 7.42). Their exteriors were rough. Laser diffraction particle size analysis showed that the particle size distribution profile was irregular with the main mode between 1 and 20 μm (Figure 7.43). Only 25% of particles were below 5 μm and around 52% were below 10 μm.

7.3.13.2 Mannitol/ Formoterol fumarate dihydrate 10%/ Calcium chloride dihydrate 5%/Citrate buffer (citric acid:tri-sodium citrate 1.5:8.5) 1% (w/w)

There were three overlapped endothermic peaks as detected by DSC (Figure 7.40). The first peaked at ~140°C followed by an endotherm seen as a "bump" on the left-hand sided slope of the main endothermic peak at ~157°C. Splitting of the mannitol melting peak can be caused by formation of a eutectic mixture between the constituents as observed for the mannitol/PVP co-spray dried systems (Section 7.3.8). Alternatively, there is a possibility of an ion exchange between the citrate buffer salts and calcium chloride leading to the formation of calcium citrate. The melting behaviour of this specimen is not clear as, for instance, the sodium salt of citric acid is able to increase the T_g of sucrose freeze-dried mixtures (Kets *et al.*, 2004). On the other hand, sugars have been reported to form complexes with calcium ions (Lu *et al.*, 2003), so potentially this can also occur during spray drying. There was ~1.2% weight loss from the powder up to 100°C by TGA related to water desorption. Mannitol was crystalline by XRD and present as a mixture of the α and β polymorphic forms with the former prevailing (Figure 7.41). SEM photographs showed aggregates of fused particles with smooth surfaces in contrast to the sample containing $CaCl_2$ alone (Figure 7.42). Laser diffraction particle size analysis established that around 16% of particles were below 5 μm and over 32% were below 10 μm. The particle size distribution (Figure 7.43) can be described as trimodal

with two fractions of particles ranging from 1 μm to hundreds of microns and one with submicron sized spheres.

7.3.14 Dispersibility study of formoterol fumarate dihydrate and co-spray dried systems in HFA134a

7.3.14.1 Binary co-spray dried mannitol/excipient mixtures

The dispersibility studies of the co-spray dried mannitol with HPMC and PVP were carried out. The samples were examined suspended in propellant alone and in ethanol/propellant mixtures. The results of the dispersibility investigations are summarised in Table 7.21.

Table 7.21 Dispersibility studies of co-spray dried mannitol/HPMC 30% and co-spray dried mannitol/PVP 10%. 'A. s. time' indicates approximate sedimentation time.

Sample	Additive (content w/w)	A. s. time	Suspension quality
Co-spray dried mannitol/HPMC 30%	0% EtOH	~30 sec	significant flocculation
	1% EtOH		caking and clumping
Co-spray dried mannitol/PVP 10%	0% EtOH	~10 min	good and stable dispersion
	0.1% EtOH	~10 min	good and stable dispersion
	1% EtOH	~10 min	good and stable dispersion
	2% EtOH	~10 min	good and stable dispersion
	5% EtOH	~10 min	good and stable dispersion

A good dispersibility with no flocs was achieved for the co-spray dried mannitol/PVP 10% sample. The settling times (approx. 10 min, Table 7.21) were longer than that of spray dried mannitol alone but shorter than those of mannitol dispersed in the PVP/5% (w/w) ethanol/propellant system (Chapter 7.3.6). Appendix VI presents a comparison of the samples after mixing (top) and 1 and 5 minutes later (bottom) for the co-spray dried mannitol/HPMC 30% and co-spray dried mannitol/PVP 10% samples, respectively, illustrating differences in the extent of sedimentation for mannitol.

7.3.14.2 Formoterol fumarate dihydrate starting material and its co-spray dried systems

The dispersibility studies of the formoterol fumarate dihydrate starting material powder and its co-spray dried systems were carried out. Various surfactants, as selected in Section 7.3.6.1, were employed with and without the addition of ethanol. Also PVP/ethanol/propellant mixtures were utilised as the dispersant media. In the experiments with the formoterol fumarate "as received" powder oleic acid was also used, as low levels of oleic acid (0.005-0.5%) have been shown surprisingly to impart a flocculant effect to produce a stable dispersion (Oliver *et al.*, 2000). The results of the dispersibility investigations are summarised in Table 7.22.

Table 7.22 Dispersibility studies of the formoterol fumarate dihydrate (FF) starting material powder and the co-spray dried drug/excipient(s) systems. 'A. s. time' indicates approximate sedimentation time.

Sample	Additive (content w/w)	A. s. time	Suspension quality
FF starting material	0% EtOH	~2 min	flocculation
	1% EtOH	~2 min	flocculation
	0.5% oleic acid		caking and clumping
	1% EtOH and 0.5% oleic acid		caking and clumping
	5% EtOH and 0.2% PVP	~20 min	good dispersion
	1% EtOH and 0.01% PVP	~2 min	flocculation
Mannitol/FF 10%	0% EtOH	~20 min	good dispersion, small flocs
	1% EtOH	~20 min	good dispersion, small flocs
	1% PEG 1000	~10 min	flocculation
	1% Brij 35	~10 min	flocculation
	5% EtOH and 0.2% PVP	~1 min	significant flocculation
	1% EtOH and 0.01% PVP	~20 min	good dispersion
Mannitol/FF 20%	0% EtOH	~20 min	good dispersion
	1% EtOH	~20 min	good dispersion
	1% PEG 1000	~5 min	flocculation
Mannitol/FF 30%	0% EtOH	~20 min	good dispersion
	1% EtOH	~20 min	good dispersion
Mannitol/FF 10%/citrate buffer salts 1%	0% EtOH	~15 min	good dispersion
	1% EtOH	~10 min	good dispersion, small flocs
	5% EtOH	~2 min	flocculation
Mannitol/FF 10%/phosphate buffer salts 1%	0% EtOH	~15 min	good dispersion
	1% EtOH	~10 min	good dispersion, small flocs
	5% EtOH	~4 min	flocculation
Mannitol/FF 10%/calclium chloride 5%	0% EtOH	~10 min	good dispersion
	1% EtOH	~10 min	good dispersion
	1% PEG 1000	~2 min	large flocs
	1% Brij 35	~2 min	large flocs
	5% EtOH and 0.2% PVP	~1 min	large flocs
	1% EtOH and 0.01% PVP	~25 min	good dispersion
Mannitol/FF 10%/calclium chloride 5%/citrate buffer salts 1%	0% EtOH	~10 min	good dispersion
	1% EtOH	~10 min	good dispersion
	1% PEG 1000	~2 min	large flocs
	1% Brij 35	~2 min	large flocs
	5% EtOH and 0.2% PVP	~1 min	large flocs
	1% EtOH and 0.01% PVP	~15 min	good dispersion

The dispersions of formoterol fumarate dihydrate starting material were prepared for comparison purposes. No visual difference was observed in the size of the flocs or the floc settling rate obtained with the three co-spray dried binary mixtures of formoterol fumarate/mannitol. Since this part of the work was accomplished before spray drying of the mannitol-drug-buffer and mannitol-drug-calcium chloride systems it was decided to use drug at the 10% (w/w) level only for further studies.

Appendix VI presents a comparison of the samples after mixing (top) and 2 minutes later (bottom) for the crystalline formoterol fumarate dihydrate and co-spray dried samples, respectively, illustrating differences in the extent of sedimentation for the investigated systems.

7.3.14.3 Conclusions from the dispersibility studies of formoterol fumarate dihydrate and co-spray dried composites

The dispersibility study of formoterol fumarate dihydrate and different co-spray dried blends showed that formoterol fumarate dihydrate raw material powder gave the best suspension when the 0.2% (w/w) PVP-5% (w/w) ethanol-propellant medium was employed. The majority of particles of this suspension settled to the bottom after over 20 min. There was no visual difference observed in the size of the flocs or the floc settling rates obtained with the three co-spray dried mannitol/formoterol fumarate dihydrate composites containing 10%, 20% and 30% of the drug. In the case of co-spray dried mannitol/formoterol fumarate dihydrate 10%/calcium chloride dihydrate 5% (w/w) and mannitol/formoterol fumarate dihydrate 10%/calcium chloride dihydrate 5% citrate buffer salts 1% (w/w) composites, the most uniform and slowly sedimenting dispersion was obtained with the use of the 0.01% (w/w) PVP-1% (w/w) ethanol-propellant medium. The majority of particles of the first sample sedimented in 25 min and the second settled to the bottom of the vial in around 15 min.

In general, the optimum medium for physical stability in terms of suspension settling rates of the suspension inhaler formulations investigated appears to be a HFA 134a-ethanol-PVP combination.

7.4 Solid state stability study of formoterol fumarate dihydrate and its co-spray dried composites

7.4.1 Stability study of formoterol fumarate composites at 25°C and 60% relative humidity

The preparation and characterisation of the mannitol-formoterol fumarate spray dried mixtures are described previously (Section 7.3.9, 7.3.12 and 7.3.13). The rationale for these studies was to examine whether formoterol fumarate co-sprayed with mannitol and mannitol/buffer salts have enhanced chemical stability compared to the crystalline drug alone. Therefore the formoterol fumarate dihydrate starting, crystalline material was taken as the reference. The data obtained is limited (see Table 7.23) but initial values imply that the kinetics of degradation reaction in the solid state is first order. A summary of the stability analysis carried out at 25°C and 60 % RH is shown in Table 7.23.

Table 7.23 Decomposition rates k_{obs}, half-lives ($t_{1/2}$) and shelf-lives (t_{10}) for the chemical degradation of the formoterol fumarate dihydrate starting material and its composites at 25°C and 60% RH. Number of data points taken for the calculations was 3 with the exception of the binary mannitol/drug mixtures for which 4 points were taken. * indicates extrapolated value.

System	$10^4 \times k_{obs}$ [day^{-1}]	$t_{1/2}$ [day] *	t_{10} [day]
FF crystalline	1.98	3501.77	530.57 *
M-FF 10%	4.64	1492.57	226.15 *
M-FF 20%	0.78	8930.41	1353.09 *
M-FF 30%	0.24	28401.64	4303.28 *
M-FF 10%-cit buf 1%	7.30	949.45	143.86 *
M-FF 10%-ph buf 1%	15.92	435.41	65.97
M-FF 10%-CaCl2 5%	0.89	7777.78	1178.45 *
M-FF 10%-CaCl2 5%-cit buf 1%	2.20	3150.00	477.27 *

All the samples studied were initially white, but on storage they turned off-white. The discoloration was more evident for the samples having poorer chemical stability.

One can see that the presence of mannitol has a protective effect on formoterol but the relationship between the polyol sugar content and stability of the drug is somewhat atypical. This means that lower concentrations of mannitol stabilise formoterol fumarate better. Also the mannitol-formoterol fumarate 10%-$CaCl_2$ 5% composite had a lower decomposition rate than the formoterol fumarate on its own. The presence of buffers had a profound effect on the drug chemical stability. The citrate buffer appeared to accelerate the degradation of formoterol by over three-fold and it was even more pronounced for phosphate buffer when an eight-fold increase in degradation was observed when compared to crystalline formoterol fumarate. This may be attributed to a completely different microenvironmental pH reached in the solid state despite the correction for dilution employed for the composites. It could also be related to the augmented moisture sorption.

7.4.2 Stability study of formoterol fumarate composites at 40°C and 75% relative humidity

The same set of samples was stored at 40°C and 75% RH in order to determine if accelerated stability study conditions can change the degradation profiles. The data collected are presented in Table 7.24.

Table 7.24 Decomposition rates k_{obs}, half-lives ($t_{1/2}$) and shelf-lives (t_{10}) for the chemical degradation of the formoterol fumarate dihydrate starting material and its composites at 40°C and 75% RH. Number of data points taken for the calculations was 3 with the exception of the binary mannitol/drug mixtures for which 4 points were taken. * indicates extrapolated value.

System	$10^4 \times k_{obs}$ [day^{-1}]	$t_{1/2}$ [day] *	t_{10} [day]
FF crystalline	3.24	2142.19	324.57 *
M-FF 10%	5.65	1226.33	185.81 *
M-FF 20%	14.74	470.15	71.23
M-FF 30%	10.01	692.52	104.93
M-FF 10%-cit buf 1%	15.12	458.33	69.44
M-FF 10%-ph buf 1%	35.28	196.46	29.77
M-FF 10%-CaCl2 5%	51.18	135.42	20.52
M-FF 10%-CaCl2 5%-cit buf 1%	17.13	404.53	61.29

The degradation rates are dramatically different to those obtained for the lower temperature and relative humidity conditions and none of the spray dried samples had superior stability than the drug starting material substance. Mannitol did not demonstrate any protective capabilities on the drug, as suggested previously at 25°C/60% RH. Again, the formulations containing a buffer were five- and ten-times more labile than formoterol fumarate, as ascertained for the citrate and phosphate buffer respectively. Furthermore, they turned brown and semi-solid after about a month of storage. The weakest drug stability was encountered for the mannitol-formoterol fumarate 10%-$CaCl_2$ 5% co-spray dried sample. This is somewhat surprising, as this formulation was one of the best in terms of stabilisation capabilities of the drug at 25°C/60% RH. However, as no peaks of the calcium salt were detected by XRD suggesting that this constituent was amorphous (Chapter 7.3.13) loosing its crystalline water, it can be expected that $CaCl_2$ recrystallised back to the dihydrate form. Indeed, small crystalline formations were observed in this sample after about a month on storage. These findings are consistent with the investigations of Kirsch *et al.* (2001) who studied the stability of co-lyophilised formulations of (R, R)-formoterol (L)-tartrate and mannitol, lactose and acetate buffer. They established that the solid state instability of the drug was highly dependent on the residual moisture and diluent type. The study proved that although the residual moistures in mannitol formulations were below 1%, the degradation rates were 1.3 to 20-fold greater than those observed for lactose formulations. Also, at high relative humidity, the presence of acetate buffer significantly increased the degradation rate.

Therefore, as the impact of moisture seems to be of a great importance, the effect of the relative and residual moistures on the stability of formoterol fumarate in the solid state should be included in any future work.

7.5 Chemical stability of formoterol fumarate in pMDI formulations

The solvency properties of HFA propellants differ significantly from the CFC predecessors. Their increased polarity is reflected in larger values of dipole moments and dielectric constants than those for CFC compounds and can lead to increased chemical instabilities of substances (Vervaet and Byron, 1999).

As there is no marketed formoterol fumarate HFA-134a based MDI formulation, no direct comparison studies were possible. Therefore, the formoterol fumarate dihydrate formulation in HFA-134a was considered as the control. The impact of the mannitol content on the chemical degradation of the drug was investigated by employing two concentrations of the sugar: at 90% and 70% (w/w). As it was suspected (Section 7.2.5) that the presence of ethanol could accelerate the drug decomposition, some of the formulations were made with HFA-134a containing 1% (w/w) ethanol. The mannitol-formoterol fumarate 10%-phosphate buffer 1% co-spray dried composite was not included as it demonstrated the greatest chemical decay of formoterol fumarate. Thus, the pMDI dispersions included in this study are listed below:

- Formoterol fumarate dihydrate crystalline milled material
- Formoterol fumarate dihydrate crystalline milled material and 1% (w/w) ethanol
- Co-spray dried mannitol-formoterol fumarate dihydrate 10%
- Co-spray dried mannitol-formoterol fumarate dihydrate 10% and 1% (w/w) ethanol
- Co-spray dried mannitol-formoterol fumarate dihydrate 30%
- Co-spray dried mannitol-formoterol fumarate dihydrate 10%-citrate buffer 1%
- Co-spray dried mannitol-formoterol fumarate dihydrate 10%-$CaCl_2$ 5%

The chemical degradation characteristics of the pMDI formulations over the storage period at 40°C/75% RH are shown in Table 7.25.

Table 7.25 Decomposition rates k_{obs}, half-lives ($t_{1/2}$) and shelf-lives (t_{10}) for the chemical degradation of the MDI formulations at 40°C and 75% RH. Number of data points taken for the calculations was 3 with the exception of the binary mannitol/drug mixtures for which 4 points were taken. * indicates extrapolated value and ** indicates that the values were calculated from the data given in the EP 1157689 A1 patent (Lewis *et al.*, 2001) using the Arrhenius equation (Equation 8.17).

System	$10^4 \times k_{obs}$ [day^{-1}]	$t_{1/2}$ [day]*	t_{10} [day]	t_{10} [month]
FF crystalline	5.60	1237.50	187.50*	6.25*
FF crystalline + EtOH 1%	3.40	2038.24	308.82*	10.29*
M-FF 10%	26.83	258.29	39.14	1.30
M-FF 10% + EtOH 1%	43.74	158.44	24.01	0.80
M-FF 30%	11.09	624.89	94.68	3.16
M-FF 10%-cit buf 1%	12.45	556.63	84.34	2.81
M-FF 10%-CaCl2 5%	15.64	443.09	67.14	2.14
formulation from the EP 1157689 A1 patent **	12.82	540.56	81.90	2.73

Formoterol fumarate was soluble to some extent in the propellant as evidenced by a brown ring of degraded drug on the inner surface of vials in the case of all formulations. It was evident that formoterol fumarate formulated in the co-spray dried complex with 90% mannitol and formulated with 1% (w/w) ethanol exhibited the most significant degree of degradation. The most chemically stable was formoterol fumarate dihydrate untreated material in HFA-134a containing 1% (w/w) of ethanol. The presence of ethanol seemed to retard or accelerate the degradation of the drug depending on the type of formulation of formoterol fumarate used when compared with counterpart aerosols containing no solvent. The content of mannitol also was of importance and the co-spray dried mannitol with formoterol fumarate dihydrate 30% composite degraded over two times slower than the composite containing only 10% of the drug.

Generally, the decomposition rate constants for degradation of the drug in HFA-134a were greater than those in the solid state at 40°C and 75% RH except for co-spray dried mannitol-formoterol fumarate dihydrate 10% with citric acid 1% or calcium chloride 5%. This may indicate limited water availability inside the HFA-134a formulations and reactions in which water is necessary as a reagent (microenvironmental pH for the citric buffer or moisture absorption for calcium chloride) can be decelerated.

Compared to the best formulation prepared by the inventors of EP 1157689 A1 (WO 01/89480 A1, Lewis *et al.*, 2001) patent a nearly four-fold increase in the stability of the drug was achieved for the formoterol fumarate crystalline sample formulated with HFA-134a containing 1% ethanol (w/w). Also formoterol fumarate unprocessed and co-spray dried mannitol-formoterol fumarate 30% and mannitol-formoterol fumarate 10%-citrate buffer 1% were better than the patented formulation. The main reason for this would appear to be that our samples were formulated as suspensions and not as solutions as claimed in the EP 1157689 A1 patent.

7.6 Conclusions

Buffered media can prolong the chemical stability of formoterol fumarate in aqueous solutions and the greatest improvement was notice for the Britton-Robinson buffer at pH=5.20, phosphate buffer 0.1M at pH=5.1 and citrate buffer 0.01M at pH=5.20 with over 3-fold, 1.5-fold and 5-fold increase in t_{10} at 25°C, respectively when compared with deionised water at the same temperature. Chemical degradation of the drug in the ethanol-water mixtures was dependent on the polarizability of the solutions used and was the slowest in 50% (v/v) ethanol.

Out of the excipients spray dried alone, the best dispersions with the longest settling times were achieved with the spray dried mannitol suspended in various PVP-5% (w/w) ethanol-propellant systems and the co-spray dried mannitol/PVP 10% in HFA-134a with and without ethanol. Formoterol fumarate dihydrate raw material powder gave the best suspension when the 0.2% (w/w) PVP-5% (w/w) ethanol-propellant medium was employed. The majority of particles of this suspension settled to the bottom after over 20 min. There was no visual difference observed in the

size of the flocs or the floc settling rates obtained with the three co-spray dried mannitol/formoterol fumarate composites containing 10%, 20% and 30% of the drug. In the case of co-spray dried mannitol/formoterol fumarate dihydrate 10%/calcium chloride dihydrate 5% (w/w) and mannitol/formoterol fumarate dihydrate 10%/calcium chloride dihydrate 5% citrate buffer salts 1% (w/w) composites, the most uniform and slowly sedimenting dispersion was obtained with the use of the 0.01% (w/w) PVP-1% (w/w) ethanol-propellant medium. The majority of particles of the first sample sedimented in 25 min and the second settled to the bottom of the vial in around 15 minutes.

In general, the optimum medium for physical stability in terms of suspension settling rates of the suspension inhaler formulations investigated appeared to be a HFA 134a-ethanol-PVP combination.

Solid state stability studies indicated protective properties of mannitol on formoterol fumarate at 25°C and 60% RH, but at the accelerated conditions of storage (40°C/75% RH) the opposite effect, i.e. acceleration of chemical degradation, was noticed.

The stability study of HFA-134a inhalers showed that the most chemically stable was formoterol fumarate dihydrate untreated material in HFA-134a containing 1% (w/w) of ethanol. The presence of ethanol and mannitol concentration improved the chemical stability of formoterol fumarate depending on formulation. The decomposition rate constants for degradation of the drug from co-spray dried mannitol and citric acid 1% or calcium chloride 5% composites were lower than those in the solid state at 40°C and 75% RH. Compared to the best formulation prepared by the inventors of EP 1157689 A1 patent (Lewis *et al.*, 2001) a nearly four-fold increase in the stability of the drug was achieved for the formoterol fumarate crystalline sample formulated with HFA-134a containing 1% ethanol (w/w). Also the formoterol fumarate "as supplied" and co-spray dried: mannitol-formoterol fumarate 30% and mannitol-formoterol fumarate 10%-citrate buffer 1% samples dispersed in HFA-134a were better than the patented formulation.

GLASS TRANSITION COMPOSITION RELATIONSHIPS OF AMORPHOUS DRUG/PVP COMPOSITES

8.1 Introduction

Processes involving solvent evaporation such as spray drying, often lead to the transformation of crystalline substances and their mixtures into their amorphous counterparts as was shown in the previous chapters. Such chaotically organised phases may have favourable biopharmaceutical properties e.g. enhanced dissolution capabilities (Ford, 1986). Each amorphous substance or composite may be characterised by a glass transition temperature (T_g), which is a critical physical property that can dramatically affect its physical stability. Despite a broad range of methods allowing the determination of the T_g of amorphous solids, the true physical nature of this phenomenon is still poorly understood (Debendetti, 2001). As the amorphous state is energetically unstable and transforms back to the crystalline phase, there is a need to develop methods to promote formation and stabilisation of the amorphous drug. The recrystallisation process can be retarded by storage at a temperature significantly below the T_g (Hancock, 2002) or by avoiding exposure to water vapour that it is known to depress the T_gs of amorphous substances (Oksanen and Zografi, 1993). However, for practical reasons, the above mentioned approaches may not be possible. Preparation of drug-polymer composites, using polymers such as polyethylene glycols (PEG) and polyvinylpyrrolidone (PVP), which have excellent water solubility and a wide range of molecular weights (Wade and Weller, 1994), is often employed. Many authors have reported that drugs dispersed at a molecular level in such polymeric carriers, on processing, result in amorphous dispersed drug, combining the benefits both of a disordered phase of the drug and improved stability due to the presence of the polymer (Ford, 1986).

Very often the addition of the excipient with a higher temperature of glass transition than the drug is required in order to retard the undesired crystalline conversion. In this regard PVP seems to be a very good additive being an amorphous polymer itself with a comparatively high T_g depending on the molecular weight. A number of studies on PVP as a stabilising agent for amorphous materials have been carried out (Corrigan and Holohan, 1984; Yoshioka *et al.*, 1995; Khougaz and Clas, 2000). PVP also has other advantageous properties such as the ability to: reduce the stickiness (fusion of particles during spray drying) of salbutamol base (Chapter 3), improve emitted fractions of processed formoterol fumarate dihydrate (Chapter 5), enhance respirable fractions of the budesonide/magnesium stearate spray dried blends (Chapter 6) and form, together with ethanol and propellant, an MDI medium able to prolong the suspension settling time (Chapter 7). Recent work suggests that the T_g is an important determinant of the stability of spray dried systems (Corrigan *et al.*, 2004), thus the ability to predict T_g seems to be crucial. A review of different approaches allowing the T_g of mixtures to be predicted is included in Section 8.2 later in the text.

The objective of the current study was to evaluate the thermal properties of various co-spray dried, PVP-containing systems. These include salbutamol base/PVP blends, which production and general physicochemical characterisation was described in Chapter 3 of this thesis, and thiazide diuretic/PVP systems that, in preliminary studies, demonstrated unusual dependence of their T_gs on

the PVP content. The effect of the polymer content on the glass transition temperatures of the systems and the use of different models to predict the T_gs of mixed systems are appraised.

8.2 Theoretical background

A number of relationships between the T_g and the phase composition of mixed amorphous systems have been proposed (Gordon and Taylor, 1952; Jenckel and Heusch, 1953; Fox, 1965; Couchman, 1978; Couchman and Karasz, 1978; Kwei, 1984; Kwei *et al.*, 1987; Brekner *et al.*, 1988; Schneider, 1989). The most widely known and used is the Gordon-Taylor equation (Gordon and Taylor, 1952).

These relationships can be divided into two major groups, based on the theoretical interpretation of the glass transition phenomenon. The first group of models considers the glass transition as an arrested, frozen-in metastable state of matter controlled by the free volume and based on a P-V-T equation of state. The models included in this group, and discussed below, are those of Gordon and Taylor (Gordon and Taylor, 1952), Fox (Fox, 1965), Kwei (Kwei, 1984; Kwei *et al.*, 1987) and Jenkel-Heusch (Jenckel and Heusch, 1953). As the glass transition observed experimentally exhibits a thermodynamic second order conversion, the second approach is to assume that this phase is a thermodynamic stable fourth state of matter characterised by a S-V-T equation of state and zero conformational entropy. The Couchman-Karasz (Couchman, 1978; Couchman and Karasz, 1978), Brekner (Brekner *et al.*, 1988) and Schneider (Schneider, 1989, Schneider, 1997) models are based on this approach. Both the free volume (group 1) and thermodynamic (group 2) model types were used originally to describe the composition dependence of the glass transition temperature of polymer mixtures, but have since been successfully applied to pharmaceutical drug-polymer systems (Taylor and Zografi, 1998; Crowley and Zografi, 2002). The exception to this is the Schneider equation, which has not previously been applied to drug-polymer systems.

The most commonly used and known equation for predicting the T_g of a two-component mixed composite, the Gordon-Taylor expression, was originally based on the volumes additivity rule (Gordon and Taylor, 1952):

$$T_g = \frac{w_1 \cdot T_{g_1} + K_{GT} \cdot w_2 \cdot T_{g_2}}{w_1 + K_{GT} \cdot w_2} \qquad \text{(Equation 8.1)} \quad \text{where} \quad K_{GT} = \frac{d_1 \cdot \Delta\alpha_2}{d_2 \cdot \Delta\alpha_1}$$

T_g, w, d and $\Delta\alpha$ are the glass transition temperature in degrees Kelvin, the weight fraction, density and expansion coefficients of the $_1$-first component, $_2$-second component and $_{(\text{no subscript})}$-mixture, respectively.

Frequently, due to difficulties in estimation of the expansion coefficient, the Simha-Boyer rule (Simha and Boyer, 1962) is used. It assumes that $\Delta\alpha \cdot T_g$ is equal to 0.113 (constant) and K_{GT} can be calculated as follows:

$$K_{GT} = \frac{d_1 \cdot T_{g_1}}{d_2 \cdot T_{g_2}}$$

When $d_1 \sim d_2$, then the value of the K_{GT} coefficient becomes unimportant and the Gordon-Taylor equation reduces to the Fox expression (Fox, 1965):

$$\frac{1}{T_g} = \frac{w_1}{T_{g_1}} + \frac{w_2}{T_{g_2}} \qquad \text{(Equation 8.2)}$$

To improve the fit of the experimental T_g data, second power equations have been proposed to account for the effect of interactions. One of these is the equation of Kwei (Kwei, 1984; Kwei *et al.*, 1987):

$$T_g = \frac{w_1 \cdot T_{g_1} + K_k \cdot w_2 \cdot T_{g_2}}{w_1 + K_k \cdot w_2} + q \cdot w_1 \cdot w_2 \qquad \text{(Equation 8.3)}$$

where K_k and q are fitted values to the experimental data.

The first term on the right-hand side of this equation is identical to the Gordon-Taylor equation and the second term represents the effect of the components interactions.

On the other hand Jenckel and Heusch proposed the following expression (Jenckel and Heusch, 1953) in order to account for decreases in the T_gs of polymers in mixtures with plasticisers:

$$T_g = w_1 \cdot T_{g_1} + w_2 \cdot T_{g_2} + b\left(T_{g_2} - T_{g_1}\right) w_1 \cdot w_2 \qquad \text{(Equation 8.4)}$$

where b characterises the solvent quality of the plasticizer.

A thermodynamic approach to the glass transition temperature of compatible polymer blends was proposed by Couchman-Karasz (Couchman, 1978; Couchman and Karasz, 1978), whose logarithmic expression utilises changes in the heat capacities at the T_gs (Δc_p) of the components:

$$\ln T_g = \frac{w_1 \cdot \Delta c_{p_1} \cdot \ln T_{g_1} + w_2 \cdot \Delta c_{p_2} \cdot \ln T_{g_2}}{w_1 \cdot \Delta c_{p_1} + w_2 \cdot \Delta c_{p_2}} \qquad \text{(Equation 8.5)}$$

It has also been shown that the Gordon-Taylor equation, in spite of the additivity volume origins, can also be obtained by applying the thermodynamic theory of the glass transition (Di Marzio, 1990). Brekner *et al.*'s approach (1988) using the Kanig's lattice theory (Kanig, 1963) suggests that the T_g of compatible polymer blends depends on both the free volume distribution and related conformational mobility, thus combining the two aforementioned approaches.

A second power equation created by Brekner *et al.* is as follows:

$$(T_g - T_{g_1})/(T_{g_2} - T_{g_1}) = (1 + K_{1B})\phi - K_{1B} \cdot \phi^2 \qquad \text{(Equation 8.6)}$$

where ϕ is the volume fraction of the component with the higher T_g and K_{1B} is the contact-specific enthalpic interaction. Unfortunately, the above second power equation assumes that the combinatorial entropy of mixing is negligible and thus can be ruled out from the thermodynamic condition of miscibility:

$$\Delta G_m = \Delta H_m - T \cdot \Delta S_m \qquad where \qquad \Delta G_m < 0 \qquad \text{(Equation 8.7)}$$

Zero entropy is generally true for the large polymer molecules having very limited mobility due to their sizes, but the entropic component cannot be excluded in a case of smaller molecules participating in a mixture.

To explain conformational reorganisations of molecules in the closest neighbourhood of their contact, accompanied by corresponding conformational entropy changes, a third power element was added to the Brekner equation. This equation was developed by Schneider (Schneider, 1989; Schneider, 1997) and is presented below:

$$(T_g - T_{g_1})/(T_{g_2} - T_{g_1}) = (1 + K_1)\phi - (K_1 + K_2)\phi^2 + K_2 \cdot \phi^3 \qquad \text{(Equation 8.8)}$$

where $\phi = \frac{K \cdot w_2}{w_1 + K \cdot w_2}$, K_1 and K_2 are parameters adjustable to the data by fitting and K (=K_{GT}) is taken from the Gordon-Taylor expression (Equation 8.1).

The Schneider K_1 coefficient depends mainly on the difference between interaction energies of hetero- (unlike molecules) and homo- (like molecules) contacts, but it includes also an entropic effect component making K_1 different in meaning to K_{1B}. The K_2 parameter considers only effects related to molecules rearrangement in the neighbourhood of the contact.

The parameters interrelate with each other and stronger interaction energies lead to a larger probability of conformation changes restricting mobility of the molecules at the contact site. As a consequence, both the conformational entropy and the free volume are diminished, resulting in an increase in the glass transition temperature of the mixture (Schneider, 1997).

When K_1 and K_2 are equal to zero, the equation reduces to the Gordon-Taylor equation written in the following form:

$$(T_g - T_{g_1})/(T_{g_2} - T_{g_1}) = \phi \qquad \text{(Equation 8.9)}$$

In spite of an advantage of the Schneider approach combining the free volume rule and the thermodynamic origins of the glass transition, K_1 and K_2 cannot be estimated by means other than fitting the experimental data.

The second law of thermodynamics (Equation 8.7) clearly specifies conditions to be fulfilled in order to obtain a miscible mixture of the constituents. This means that $\Delta S_m>0$ and $\Delta H_m\leq 0$ are needed to attain a negative free energy of mixing ensuring mutual solubility.

The enthalpy of mixing is in turn closely linked to the concept of solubility parameters and according to Hildebrand (van Krevelen, 1990) the enthalpy of mixing can be calculated by using the following equation:

$$\Delta H_m = \phi_1 \cdot \phi_2 (\delta_1 - \delta_2)^2 \cdot V_m \qquad \text{(Equation 8.10)}$$

where δ and V_m are the solubility parameter and the molar volume of the mixture respectively. When $\delta_1=\delta_2$, then $\Delta H_m=0$ leaving the free energy of mixing to be dependent solely on the entropy of the system. The above equation assumes that no specific forces between the molecules are involved and if both substances contain polar groups and/or groups able to create hydrogen bonds, solubility may be promoted (van Krevelen, 1990). For these reasons a more developed interpretation of the solubility parameters considers using three parameters constituting a total solubility parameter. This approach is known as the Hansen's solubility parameters and the corresponding equation allowing estimation of the subsequent parameters is:

$$\delta_t^{\,2} = \delta_d^{\,2} + \delta_p^{\,2} + \delta_h^{\,2} \qquad \text{(Equation 8.11)}$$

where δ_t is the total solubility parameter and δ_d, δ_p, δ_h correspond to the contribution of dispersion forces, polar forces and hydrogen bonding respectively (van Krevelen, 1990).

The usefulness of solubility parameters as the descriptors of many physical properties of pharmaceutical materials have been suggested by many authors (Rowe, 1988; Greenhalgh *et al.*, 1999). The latter have demonstrated that the difference in total solubility parameters can be helpful in estimating the degree of miscibility between constituents in the preparation of solid dispersions.

The group contribution method of van Krevelen and Hoftyzer (van Krevelen, 1990) was used to estimate the solubility parameters of the compounds. The molar volumes (V_m) were calculated according to (Equation 8.12).

$$V_m = \frac{M_w}{d} \qquad \text{(Equation 8.12)}$$

where M_w and d are molecular weight and true density, respectively. The densities values of the amorphous substances were determined by helium pycnometry and were: 1.17 g/cm^3 for PVP 10000, 1.16 g/cm^3 for salbutamol base, 1.49 g/cm^3 for bendroflumethiazide, 1.75 g/cm^3 for hydroflumethiazide and 1.74 g/cm^3 for hydrochlorothiazide. The experimental values of molar volumes were used as not all of the constants for the chemical groups constituting the drug molecules were included in the method of Fedors (van Krevelen, 1990). This approach has also been used previously (van Krevelen, 1990). The solubility parameters of PVP were taken from the work of Rowe (1988).

8.3 Salbutamol base/PVP composites

8.3.1 Thermal analysis

In Chapter 3 it was reported that deflections in the baselines below 120°C for all salbutamol base/PVP dispersions were detected on the DSC curves and they were assigned as the glass transition processes. As they were very weak and overlapped with the desolvation endotherms, all samples were subjected to a residual solvent removal procedure by heating up to 90°C in the DSC furnace and cooling down to 25°C. Thermal analysis on samples pre-prepared in this way revealed more distinct T_gs than those measured for the untreated specimens. Moreover, the thermal history of the samples could be standarised (Hancock *et al.*, 1995).

The thermal characteristics of the components are summarised in Table 8.1.

Table 8.1 The thermal characteristics of the individual components.

	Melting point [K] (°C)	Glass transition temperature [K] (°C)	Heat of fusion ΔH [J/g]	Δc_p [J/(g·K)]	Tg/Tm
PVP 10000	-	402 (129)	-	0.215	-
Salbutamol base	429 (156)	318 (45)	204	1.30	0.74

One, single T_g was observed for all dispersions, indicating miscibility between the drug and polymer (Timko and Lordi, 1984). The difference in the total solubility parameters of salbutamol base and PVP is equal to 4.8 (Table 8.2). The Greenhalgh *et al.*'s classification of solid dispersions in terms of solubility (Greenhalgh *et al.*, 1999) indicates that $\Delta\delta_t$ around 1.6 suggests complete miscibility of components in the liquid state with complex formation and $\Delta\delta_t$ of 2.0 and above-a possibility of separation of constituents. The latter was demonstrated for the 10% PVP content system, when both the drug recrystallisation and melting processes were observed on the DSC trace. Also a gradual disappearance of the melting peak of salbutamol base was seen as the PVP content was increased and at the 50% level and above no such endotherm was recorded (Chapter 3). This indicates that the solubility parameters are able to predict the degree of miscibility of substances but this is dependent on the ratio in which the constituents are mixed.

Table 8.2 The Hansen's solubility parameters of salbutamol (calculated) and PVP (Rowe, 1988).

	δ_t ($MPa^{1/2}$)	δ_d ($MPa^{1/2}$)	δ_p ($MPa^{1/2}$)	δ_h ($MPa^{1/2}$)	$\Delta\delta_t$ ($MPa^{1/2}$)
PVP 10000	21.2	15.5	11.7	8.6	-
Salbutamol base	26.0	18.8	4.4	17.5	4.8

The dependence of the experimentally determined T_g values on the polymer content is shown in Figure 8.1. These data points were contrasted with those predicted by the Fox (Equation 8.2), Gordon-Taylor (Equation 8.1), Couchman-Karasz (Equation 8.5), Kwei (Equation 8.3) and Schneider (Equation 8.8) equations and the calculated values are presented as lines in Figure 8.1.

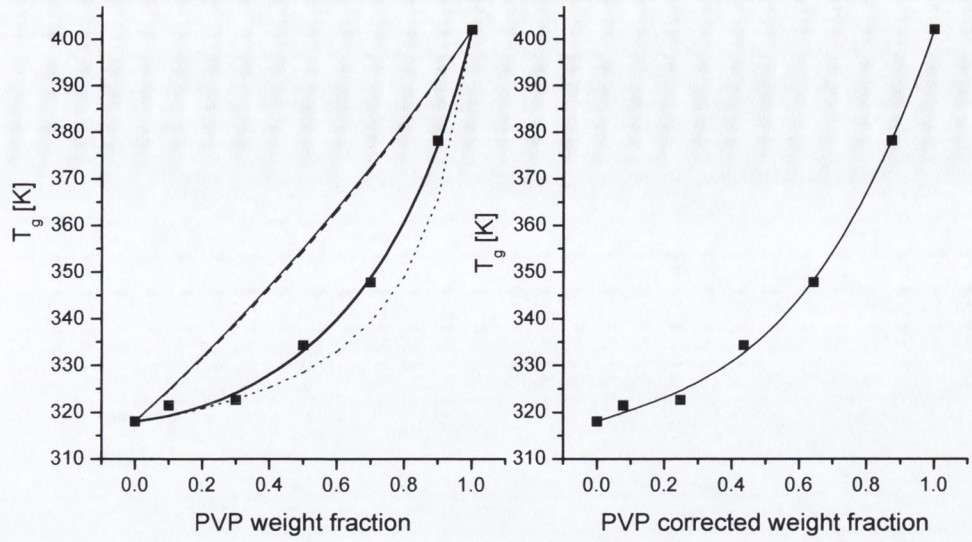

Figure 8.1 Glass transition temperatures of spray dried salbutamol base/PVP systems as a function of PVP content. The solid, dashed, dotted, and thick solid lines on the left-hand side graph represent the predictions based on the Fox, Gordon-Taylor, Couchman-Karasz and Kwei equations, respectively and the solid line on the right-hand side graph represents the line fitted using the Schneider equation.

The experimental data points shown in Figure 8.1 demonstrate negative deviations from the T_gs predicted with the Fox and Gordon-Taylor equations. These two equations predicted very similar T_g values and the lines overlap. A substantial amount of water present in ketoconazole/PVP dispersions was found to account for discrepancies between the experimental T_gs and those predicted by the Gordon-Taylor equation (Van den Mooter *et al.* 2001). However, this explanation is doubtful in this case, as the residual water or ethanol which may act as plasticisers were removed during the pretreatment procedure. As a result, only the presence of salbutamol base itself can account for the plasticising effect observed and negative deviations from the Gordon-Taylor equation. Similar negative departures from the volume additivity rule were reported for solid dispersions of indomethacin/PVP (Taylor and Zografi, 1997) and binary colyophilised mixtures of sucrose and PVP (Shamblin *et al.*, 1998). In these cases interactions between the molecules were found to be responsible for decreasing the glass transition temperatures. For the indomethacin dispersions the formation of new hydrogen bonds with PVP occurred at the cost of disruption of the drug dimers. The hydrogen bonds formed between sucrose and PVP were created at the expense of hydrogen bonds within sucrose. Generally, in the above cases the interactions between the molecules of same kind were much stronger than the new network of bonding.

The Couchman-Karasz relationship predicted the T_g values quite well, although most points were slightly underestimated (Figure 8.1). Only one glass transition temperature value, for the 30% polymer system, is consistent with the calculations. As seen in Table 8.1, the Δc_p of salbutamol base is quite large when compared to those of thiazide diuretics (Table 8.4). It may be due to the measurement errors, as the detection of the Δc_p was accomplished with the use of a conventional DSC. A modulated temperature instrument would have allowed for a separation of the total signal

into reversible and non-reversible components, thus isolate the glass transition process from other thermal events (Craig *et al.,* 2000). For this reason the predictions made on the basis of the Couchman-Karasz equation should be treated cautiously. No literature value for Δc_p of salbutamol base has been found, thus it cannot be verified.

All approaches utilising the fitting procedures (the Kwei and Schneider equations) presented very similar results and provided the best predictions as seen in Figure 8.1. The models very closely reflect the experimental points and the goodness of the fits in both cases is equal to 0.9985 (Table 8.3).

Table 8.3 The Gordon-Taylor K_{GT} parameter and the fitting coefficients obtained by using the Kwei and Schneider equations.

	Gordon-Taylor equation	Kwei equation (R^2)		Schneider equation (R^2)		
Salbutamol base/PVP	K_{GT}=1.30	K_k=3.43 q=-15.15	(R^2=0.9985)	K=0.77 K_1=-0.71 K_2=0.81	K_1-K_2=-1.52	(R^2=0.9985)

As mentioned previously, K_1 and K_2 in the Schneider equation (Equation 8.8) account for enthalpic and entropic effects occurring in a system. Schneider (1997) also introduced another parameter, namely the difference between these parameters: K_1 - K_2. It has a similar meaning to K_1 with the only difference being that K_1 is estimated from the volume fraction of the compound with the higher T_g whereas K_1 - K_2 accounts for a situation when the second constituent of the mixture is taken as the operative variable. Thus, one can say that K_1 reflects the influence of a drug molecule substitution by the PVP in the drug environment, whereas K_1 - K_2 describes the opposite substitution (Schneider, 1997).

Taking into account the values of K_1 and the difference of the K_1 - K_2 parameters, Schneider (1997) divided various compatible polymer blends into five major classes on the basis of different shapes of the T_g versus composition curves. When both the K_1 and K_1-K_2 parameters are negative, as in the case of the salbutamol base/PVP mixtures, the experimental T_gs should show negative deviations from additivity and this is observed in Figure 8.1.

8.3.2 FTIR analysis

The possibility of interactions existing between salbutamol base and PVP in the solid dispersions was investigated by infrared spectroscopy. For comparison purposes, equivalent physical mixtures composed of amorphous salbutamol base spray dried alone mixed with spray dried PVP were prepared. No specific interactions occurring between the constituents in these mixes were assumed. The assignment of some of the infrared bands of salbutamol base was presented in Chapter 3.

Typical infrared spectra of the salbutamol base/PVP 50% solid dispersion and the corresponding physical mixture are shown in Figure 8.2.

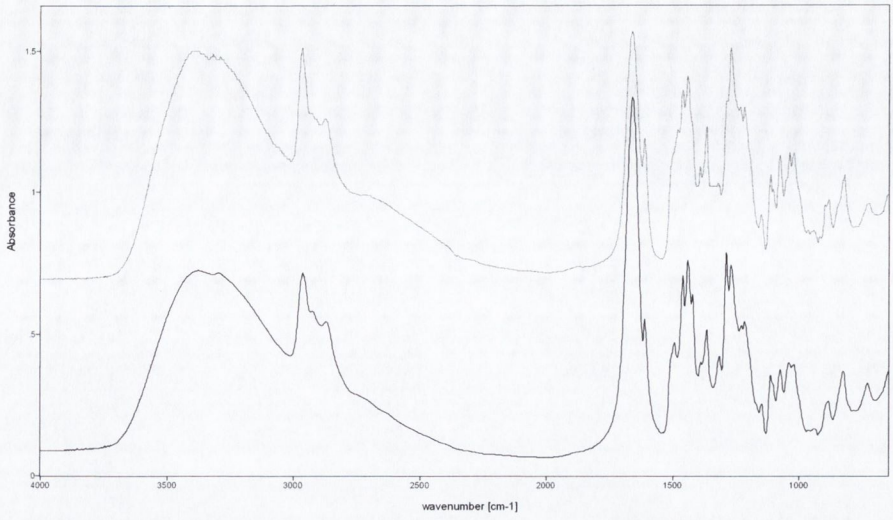

Figure 8.2 FTIR spectra of the salbutamol base/PVP 50% solid dispersion (solid line) and physical mix of amorphous salbutamol base with 50% PVP (dotted line).

The molecule of the drug contains only hydrogen donor groups (three hydroxyl and one secondary amine functions), whereas PVP can act as a hydrogen acceptor due to the carbonyl moiety having two lone pairs of electrons. Hence, if there is hydrogen bonding present in the solid dispersions that involves the above groups, evidence of this phenomenon may be expected to be found in the hydroxyl, amine and carbonyl band absorption ranges. The major dissimilarities between the spectra were observed in the fingerprint region (1800-600 cm^{-1}) as is seen in Figure 8.2. The physical mixture shows the presence of bands occurring in the same positions as expected for the infrared spectra of spray dried drug and PVP alone. No obvious changes in the position of the bands located in the 3000-3500 cm^{-1} range were discerned for the solid dispersions except for a slight broadening when compared to those of the physical mixtures. Thus, there is no conclusive evidence of the participation of OH and NH groups in interactions. Also the location of the carbonyl function band of the polymer remained unchanged in the solid dispersions regardless of the PVP content.

It has been reported that hydrogen bond formation is responsible for an increase in the intensity of the carbonyl band of PVP (Khougaz and Clas, 2000). To examine this, the ratios between the intensities of the PVP carbonyl (at ~1660 cm^{-1}) and salbutamol aromatic (at ~1611 cm^{-1}) vibration bands were calculated for the solid dispersions and physical blends. The latter band was chosen as the reference as it does not overlap with the other peaks and the mathematical procedure aimed at elimination of the bias due to sample concentration variations. The bands were well separated exhibiting individual maxima for up to 0.7 PVP weight fraction and merged into one broad peak at higher polymer contents. The comparison of the ratios obtained for the solid dispersions (black squares) and physical blends of amorphous salbutamol base with PVP (empty squares) is graphically presented in Figure 8.3.

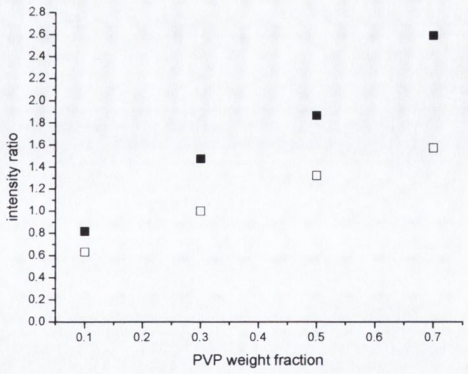

Figure 8.3 The calculated ratios of intensities of the PVP carbonyl (at ~1660 cm^{-1}) and salbutamol base aromatic (at ~1611 cm^{-1}) bands for solid dispersions (black squares) and physical mixtures of amorphous salbutamol base and PVP (empty squares).

The points presented in Figure 8.3 do not overlap as would be expected if the strength of interactions between the species was the same for both the physical mixes and solid dispersions. The smallest difference between the points is for the 10% PVP systems, indicating the weakest interactions. The greater the PVP content, the larger the departure between the points, suggesting an increase in the number of newly formed bonds and/or strength of the interactions. As a result of the infrared investigations it can be assumed that the species constituting the solid dispersions do interact by means of hydrogen bonding formation. Nevertheless, the magnitude of the interactions is weak and perhaps, as supported by the results of the thermal analysis, newly created bonds are weaker than the interactions connecting the molecules of salbutamol base. Therefore the overall strength of the hydrogen bonds is diminished resulting in lower T_gs than those predicted.

The FTIR conclusions may be supported by the XRD data presented earlier in Chapter 3, where minor, but apparent changes in the shapes of the diffuse X-ray reflections of the salbutamol/PVP co-spray dried systems were observed. Their shapes did not correlate with those additive XRD patterns constructed by combining the diffractograms of the components spray died alone. Porubcan *et al.*, (1978) demonstrated changes in the XRD patterns of montmorillonite interacted with tetracycline that were dependent on the pH of solution used for preparation of the complexes.

8.4 Thiazide diuretics/PVP composites

The drugs of choice for further investigations of PVP/drug combinations were bendroflumethiazide (BFMT), hydroflumethiazide (HFMT) and hydrochlorothiazide (HCT) as they have been shown to be amorphous on spray drying (Corrigan and Holohan, 1984; Corrigan *et al.*, 1984). The dissolution enhancement and amorphous properties of various thiazide diuretics/PVP solid dispersions have been extensively investigated (Corrigan and Timoney, 1975; Corrigan *et al.*, 1976; Corrigan and Holohan, 1984), but little research on the physical stability and thermal behaviour of these systems has been reported (Corrigan and Holohan, 1984).

The preparation of the systems was as follows. Appropriate amounts of a drug and/or PVP were dissolved in an ethanolic solvent with a composition of 95% v/v ethanol, 5% v/v water. The inlet temperature, airflow, aspirator and feed rates at which the spray dryer was operated were kept at 78°C, 600Nl/h, 100% and 20%, respectively. The only variable was the solution concentration and was 5% (w/w) or 2.5% (w/w) for BFMT and BFMT-PVP, 1% (w/w) for HFMT and HFMT-PVP and 0.5% (w/w) for HCT and HCT-PVP systems. Production of melts was described in Chapter 2.

8.4.1 Thermal analysis

All the diuretics studied, in their unprocessed forms, were crystalline as confirmed by XRD (Figure 8.4).

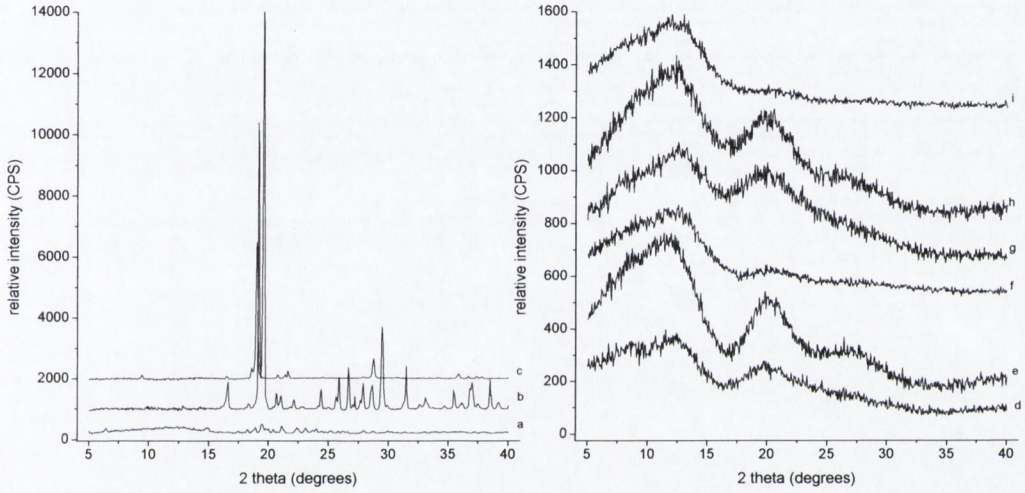

Figure 8.4 XRD patterns of (a) unprocessed BFMT, (b) unprocessed HFMT, (c) unprocessed HCT, (d) spray dried BFMT, (e) spray dried HFMT, (f) spray dried HCT, (g) co-spray dried BFMT and PVP in the ratio 1:1, (h) co-spray dried HFMT and PVP in the ratio 1:1 and (i) co-spray dried HCT and PVP in the ratio 1:1.

DSC analysis also confirmed crystallinity of the drug samples, giving only one endotherm, associated with the melting process (Figure 8.5). The lowest melting temperature was obtained for pure BFMT (Table 8.4).

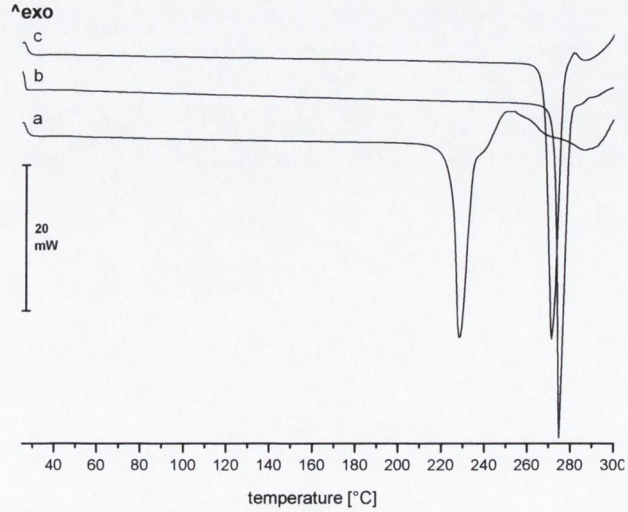

Figure 8.5 DSC traces of unprocessed materials (a) BFMT, (b) HFMT and (c) HCT.

Table 8.4 The thermal characteristics of the individual components.

	Melting point [K] (°C)	Glass transition temperature [K] (°C)	Heat of fusion ΔH [J/g]	Δc_p [J/(g·K)]	Tg/Tm
PVP	-	402 (129)	-	0.215	-
BFMT	498.9 (225.9)	392 (119)	107.8	0.17	0.79
HFMT	545.7 (272.7)	368.5 (95.5)	128.8	0.39	0.67
HCT	540.7 (267.7)	342 (69)	121.1	0.42	0.63

All the spray dried samples were XRD amorphous (Figure 8.4). This is consistent with the previously reported highly disordered state of the thiazide diuretics prepared by spray drying (Corrigan *et al.*, 1984; Corrigan *et al.*, 2003).

DSC of all of the processed drugs revealed an exotherm ascribed to the recrystallisation of the amorphous material followed by an endothermic peak, indicative of a melting process (Figure 8.6).

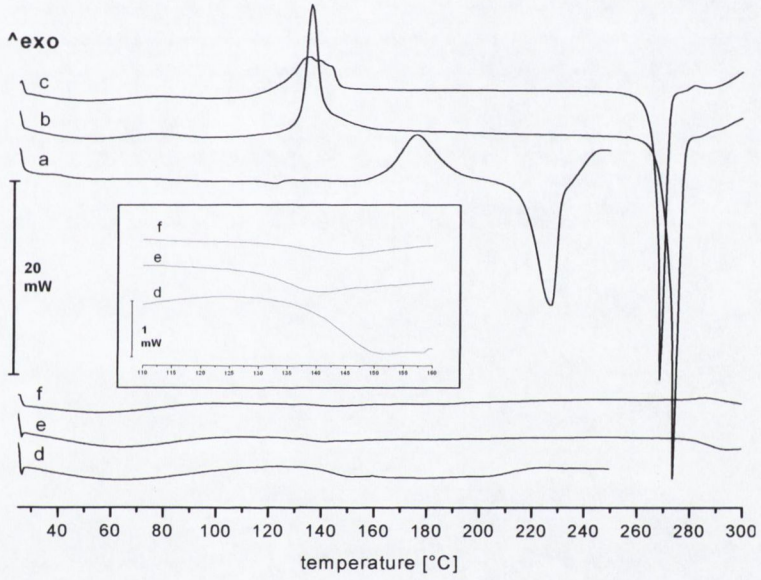

Figure 8.6 DSC traces of (a) spray dried BFMT, (b) spray dried HFMT, (c) spray dried HCT, (d) co-spray dried BFMT and PVP in the ratio 1:1, (e) co-spray dried HFMT and PVP in the ratio 1:1 and (f) co-spray dried HCT and PVP in the ratio 1:1.

On analysis of the mixtures, a single T_g was detected, consistent with complete miscibility of the two components (Figure 8.6) (Timko and Lordi, 1984). Neither recrystallisation exotherm, nor melting endotherm, observed earlier for spray dried BFMT, was detected for the BFMT/PVP composites. In the case of HFMT/PVP and HCT/PVP systems no additional peaks, except T_gs, were registered for up to 60% and 70% content of the drug, respectively. Above those concentrations, an exothermic and endothermic peak appeared. As PVP does not recrystallise during heating, these can only be from the thiazides. The phase separation manifesting in an exotherm and endotherm for HFMT/PVP co-spray dried systems was also noted previously by Corrigan and Holohan (1984). These workers suggested that in spray dried systems of low PVP weight fraction HFMT can be present as an amorphous drug phase and also dissolved in PVP. This concept is in good agreement with the use of Hansen's solubility parameters to predict the mutual

solubility of the mixture constituents. The excellent miscibility of the BFMT/PVP composites is consistent with the small difference between the solubility parameters of BFMT and PVP (equal to 1.4), whereas for the HFMT/PVP and HCT/PVP that dissimilarity is much greater (Table 8.5) as was the case for the salbutamol base/PVP systems.

Table 8.5 The Hansen's solubility parameters of the thiazide diuretics (calculated) and PVP (Rowe, 1988).

	δ_t ($MPa^{1/2}$)	δ_d ($MPa^{1/2}$)	δ_p ($MPa^{1/2}$)	δ_h ($MPa^{1/2}$)	$\Delta\delta_t$ ($MPa^{1/2}$)
PVP	21.2	15.5	11.7	8.6	-
BFMT	22.6	20.2	3.1	9.7	1.4
HFMT	25.6	22.2	4.5	11.9	4.4
HCT	26.9	23.2	5.8	12.4	5.7

Figure 8.7 shows the dependence of the glass transition temperature of the composites on the weight fraction of PVP. The trends are rather unusual and rarely reported for pharmaceutical composites. To our knowledge, the only examples of similar thermal behaviour have been presented by Timko and Lordi (1984) for glass systems of some sulphonamides with citric acid or dextrose and Crowley and Zografi (2002) for indapamide dispersed in K90 PVP.

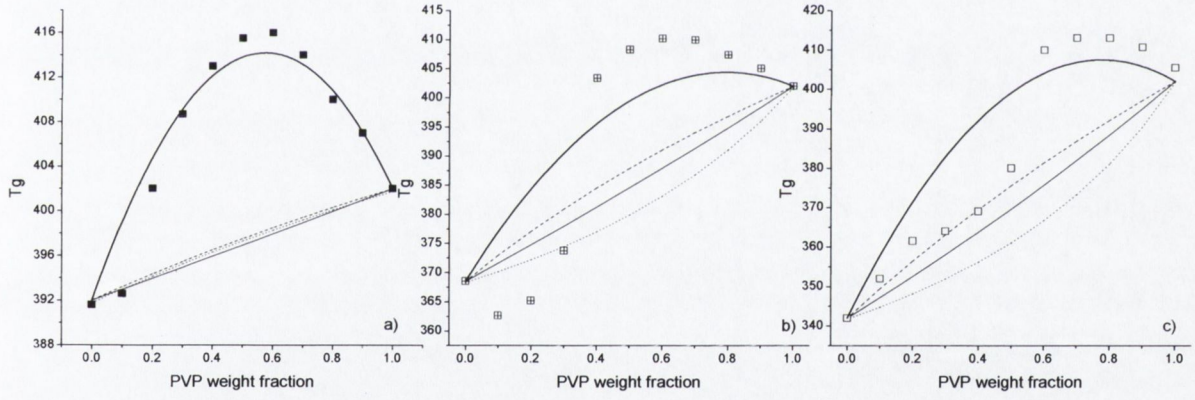

Figure 8.7 Glass transition temperatures of: a) spray dried BFMT/PVP and b) spray dried HFMT/PVP and c) spray dried HCT/PVP systems as a function of PVP content. The solid, dashed, dotted, and thick solid lines represent the predictions based on the Fox, Gordon-Taylor, Couchman-Karasz and Kwei equations, respectively.

In order to substantiate the T_gs of the spray dried composites determined by DSC, equivalent melts were prepared (data not shown). The glass transition temperatures were close to those obtained for the co-spray dried systems, however the accuracy of T_g determination is less reliable as the diuretics show degradation during melting, as observed by thermogravimetric analysis. Corrigan *at al.* (2003) reported 64 times increase in TFSA (5-trifluoromethyl-2,4-disulphamoylaniline, the main degradation product of BFMT) in a melt of BFMT/PEG with a weight ratio of 10:90 compared with the equivalent spray dried system. The temperature used for preparation of this melt was 80°C and it can be expected that melts obtained by heating up to 220°C might contain enough of the degradation products to influence the T_gs of the drug/PVP melts. Thermogravimetric analysis

of the polymer revealed a 4% weight loss between the T_g and 220°C and this could also be connected with a thermal decomposition. In the present work chemical degradation of the spray dried samples was not determined as the inlet temperature used in the spray drying process did not exceed either the melting point of any of the drugs or the Tg of PVP.

All the blends exhibited positive deviations from additivity, but the overall shape was dictated by the drug used (Figure 8.7). The T_gs of BFMT/PVP, HFMT/PVP and HCT/PVP co-spray dried systems were compared to those predicted by the Gordon-Taylor (Equation 8.1), Fox (Equation 8.2) and Couchman-Karasz (Equation 8.5) expressions.

In the case of BFMT/PVP mixtures, only one point (BFMT/PVP 10%) is consistent with the anticipated value (Figure 8.7a). The rest of the values are well above their calculated T_gs with a maximum reached at ~0.6 PVP weight fraction (5.7 mole of PVP pyrrolidone units : 1 mole of BFMT). It was thought that a better fit could be obtained if a second power equation was used e.g. the Kwei equation (Equation 8.3). The result is depicted on Fig. 5 and indeed, the composition dependence of the T_gs could be reflected more closely than when the Gordon-Taylor, Fox and Couchman-Karasz relationships were used. Finally, the third power Schneider equation (Equation 8.8) was applied (Figure 8.8a). It offered a better fit, when comparing the R^2 values, but the point representing the T_g of the BFMT/PVP 10% is well below the modelled curve (the fitting parameters for all the systems are given in Table 8.6).

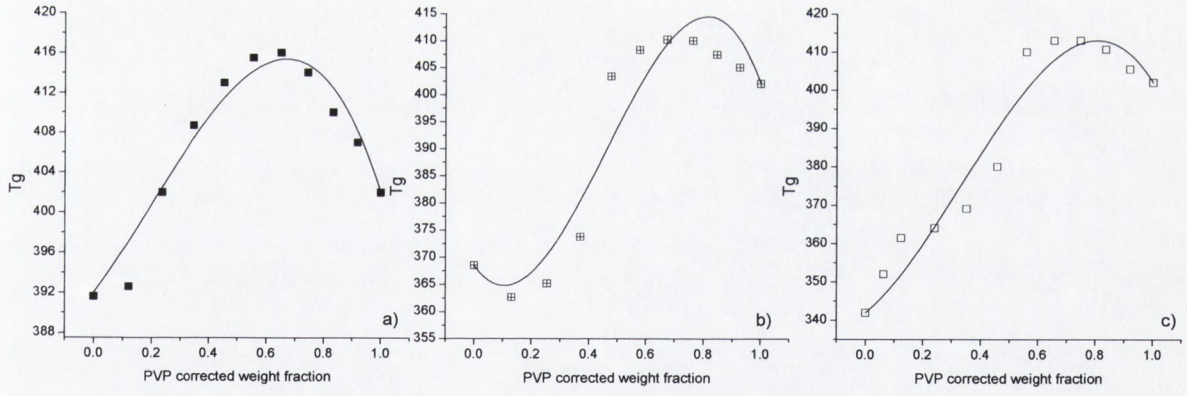

Figure 8.8 Glass transition temperatures of: a) spray dried BFMT/PVP and b) spray dried HFMT/PVP and c) spray dried HCT/PVP systems as a function of PVP content. The solid lines represent the lines fitted using the Schneider equation.

Table 8.6 The Gordon-Taylor K_{GT} parameter and the fitting coefficients obtained by using the Kwei and Schneider equations.

	Gordon-Taylor equation	Kwei equation (R^2)		Schneider equation (R^2)		
BFMT/PVP	K_{GT}=0.81	K_k=1 q=67.31	(R^2=0.9219)	K=1.24 K_1=2.86 K_2=-6.99	K_1-K_2=9.85	(R^2=0.9524)
HFMT/PVP	K_{GT}=0.73	K_k=1 q=56.88	(R^2=0.7262)	K=1.37 K_1=-3.19 K_2=-8.44	K_1-K_2=5.25	(R^2=0.9134)
HCT/PVP	K_{GT}=0.79	K_k=1 q =108.85	(R^2=0.9158)	K=1.265 K_1=0.00 K_2=-3.00	K_1-K_2=3.00	(R^2=0.9416)

The T_gs of the HFMT/PVP co-spray dried samples create an S-shaped curve (Figure 8.7b). It can be divided into 2 regions. Between 0 and 30% of PVP the T_g values are smaller than the theoretical ones predicted by the Fox and Gordon-Taylor equations and only HFMT/PVP 30% is consistent with the point given by Couchman-Karasz expression. We can say that HFMT in this concentration region behaves as a typical plasticizer, having the ability to effectively decrease the glass transition temperature. The T_gs of the samples consisting of at least 40% of PVP (more than 2 moles of PVP pyrrolidone units per 1 mole of the drug) have values much greater than those estimated by the Equation 8.1, Equation 8.2 and Equation 8.5. Again, the maximum increase in the glass transition temperature was achieved at 0.6 PVP weight fraction (4.5 mole of PVP pyrrolidone units : 1 mole of HFMT). The Kwei equation gave a slightly better fit, but not satisfactory (R^2=0.7262). The best in predicting the T_g values was the Schneider equation (R^2=0.9134), but it under- or overestimated some of the points (Figure 8.8b).

The dependence of the T_gs of HCT/PVP composites versus PVP weight fraction is shown in Figure 8.7c. The region between 0% and 30% PVP weight fraction forms a "hill" on the curve upward trend. These T_g values are the closest to the Gordon-Taylor prediction, but generally all the conventionally used expressions gave poor estimations. Again, when PVP comprises 40% and more, the T_g values are greater than anticipated. The maximum is reached for PVP weight fraction of 0.6-0.7 (4-6.1 mole of PVP pyrrolidone units : 1 mole of HCT). The Kwei equation gave an accurate prediction for a few points only and the fit obtained by the Schneider expression (Figure 8.8c) was only slightly better (R^2=0.9416 compared with the Kwei R^2=0.9158).

As has been shown so far, the Schneider equation gave the best agreement with the experimental data, but it is still not ideal. All the traditionally used relationships (Fox, Gordon-Taylor and Couchman-Karasz) failed to accurately predict the T_gs of the systems. They usually work well with systems where interactions between components are negligible (Schneider, 1997). Therefore, for these large deviations of the T_gs of the samples, an interaction may be responsible.

According to the Schneider's classification of the polymer blends mentioned previously, when $K_1 - K_2 > 0$ or $K_1 - K_2 < 0$ then a positive or negative deviation from the Gordon-Taylor equation, respectively, in the high concentration range of the component with higher T_g (PVP) appears.

Additionally, if $K_1<0$ or $K_1>0$, than a negative or positive departure, respectively, in the high concentration range of the component with the lower T_g (drug) can be observed.

It is known that stronger interaction energies can diminish the entropy of a system. Furthermore conformational transformations cause entropic changes, which influence the interaction energies leading to changes in the free volume. The latter are able to increase the glass transition of the sample (Schneider, 1997). Therefore, the fitting parameters of the Schneider equation may be useful in predicting which of the factors dominates. Estimation of K_2 coefficient gave negative values for all the systems investigated suggesting that the entropic interactions of the component are predominant (Schneider, 1997) (Table 8.6). In contrast the K_1 - K_2 values are positive implying changes in interaction energies caused by entropic changes especially in the high PVP concentration region (a PVP molecule/unit substitution by the drug molecule in the PVP environment). This indicates that a PVP-drug interaction is stronger than any PVP-PVP and drug-drug interaction and a change in thermal energy is involved.

8.4.2 FTIR analysis

8.4.2.1 Crystalline compounds

The spectra of the three crystalline drugs are shown in Figure 8.9.

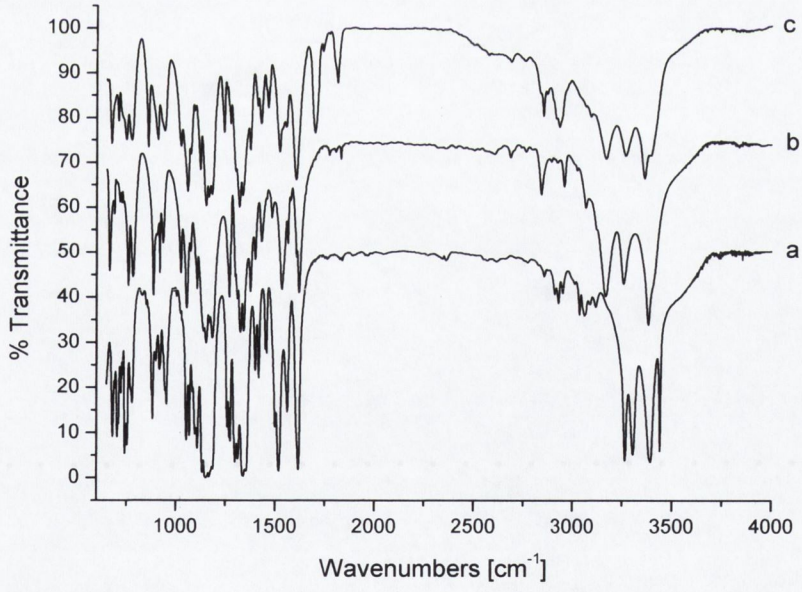

Figure 8.9 The FTIR spectra of unprocessed (a) BFMT, (b) HFMT and (c) HCT.

Differences in the peak positions are evident, particularly in the 3000-3400 cm^{-1} region. As the molecules do not contain hydroxyl groups, peaks were assigned to amine stretching vibrations. The peaks of BFMT are sharper, narrower and generally shifted towards higher wavenumbers when compared with HFMT and HCT. This could be due to low strength hydrogen bonding linking the molecules in the crystalline state and is consistent with the lower melting temperature of BFMT.

In the solid state sulphonamides have strong bands due to their N-H stretching vibrations in the region 3390-3245 cm^{-1} (Socrates, 2001). Primary sulphonamides give two bands in this region because they have two protons (asymmetric and symmetric stretching vibrations) and secondary compounds give only one peak. Thiazide diuretics contain one more N-H group - a secondary amine, which will vibrate at 3500-3300 cm^{-1}. Moreover, hydrogen bonds produced by N-H moieties can shift the band positions towards lower wavenumbers (Socrates, 2001). As the rules for crystal structures of small organic molecules state that after formation of intramolecular hydrogen bonds, the best hydrogen donor will bond to the best hydrogen-bond acceptor present and because hydrogen-bond donating abilities of similar functional groups correlate roughly with acidities, one can assume that more acidic protons in sulphonamides are better donors than less acidic amino protons (Adsmond and Grant, 2001). Against this background an attempt was made to assign all of the N-H stretching bands. The band at the highest frequency was assigned to the secondary amine, practically free from hydrogen bonds due to its low proton donating function. The highest peak in the group was taken as an asymmetric N-H vibration band of the primary sulphonamide. The next peak was attributed to the secondary sulphonamide N-H stretching peak and the band at the lowest wavenumber – the symmetric N-H stretch of the primary sulphonamide (Table 8.7). Unfortunately, confirmation of our peak assignments was not possible given the absence of crystallographic data enabling us to solve crystal structures of the thiazides.

Table 8.7 Infrared peak assignments for thiazide diuretics spectra in the crystalline and amorphous states.

Crystalline, wavenumber [cm^{-1}]			Amorphous, wavenumber [cm^{-1}]			Assignment
BFMT	HFTM	HCT	BFMT	HFTM	HCT	
3439	-[a]	3392	-	-	-	N-H stretch, secondary amine
3394	3382	3362	3378	3386	3380	Asymmetric N-H stretch, primary sulphonamide
3305	3258	3268	3266	3277	3265	N-H stretch, secondary sulphonamide
3265	3167	3169	3177	3176	3152	Symmetric N-H stretch, primary sulphonamide
1617	1619	1604	1616	1617	1600	Aromatic C=C ring stretch
-	1607	-	-	-	-	N-H scissoring vibration
1561	1563	1554	1563	1561	1553	N-H scissoring vibration
1518	1533	1521	1509	1524	1515	N-H scissoring vibration
1340	1324	1316	1346	1332	1325	Asymmetric SO_2 stretch
1152	1152	1152	1163	1161	1157	Symmetric SO_2 stretch
1069	1054	1059	1060	1026	1028	Aromatic C-H ring deformation

[a] - peak appears as a shoulder on the 3382 cm^{-1} band

8.4.2.2 Amorphous compounds

The spectra of the spray dried thiazides are to some extent different to those of the crystalline equivalents (Figure 8.10).

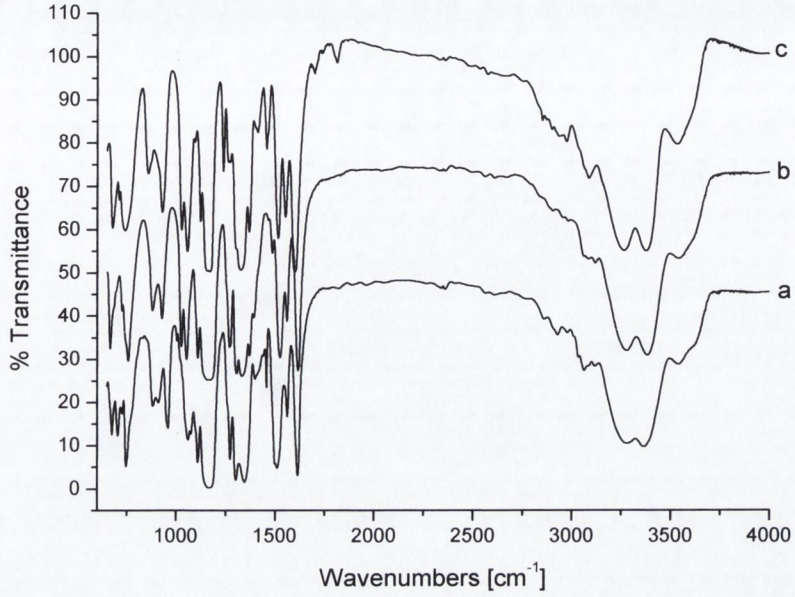

Figure 8.10 The FTIR spectra of spray dried (a) BFMT, (b) HFMT and (c) HCT.

The peaks are more diffuse, less sharp and furthermore, slightly shifted. For all of the compounds, two minor and broad bands appeared in the 3450-3650 cm^{-1} region and these were ascribed to a small fraction of free N-H groups. The greatest changes are also observed in the 3000-3500 cm^{-1} region. Surprisingly, in the amorphous state, the N-H peak positions are very similar for all the drugs (Table 8.7). The same phenomenon was reported by Tang *et al.* (2002b) for the amorphous state of dihydropiridine calcium channel blockers. It was explained by a uniform average of the hydrogen bonding strength. The greatest change in the band positions was observed for BFMT, suggesting the involvement of some of the previously idle groups in a hydrogen bonding network. The two bands at 1550-1500 cm^{-1} arising from N-H scissoring vibrations also became shifted, supporting our hypothesis about hydrogen bonding formation/rearrangements.

8.4.2.3 Co-spray dried composites

Absence of additional peaks on FTIR spectra of the PVP composites (Figure 8.11) suggests a lack of newly formed covalent bonds between the constituents. Thus, it was assumed that observed positive deviation in the T_gs was due to weaker interatomic interactions i.e. hydrogen bonding or other dipole-dipole forces. Similar behaviour, an increase of T_gs when contrasted with the calculated values, has been reported for many polymers and copolymers, e.g. mixtures of poly(vinylphenol) and poly(vinylpyrrolidone) (Kuo and Chang, 2001), blends of PMMA and Novolac resins (Kwei, 1984) and poly (acetoxystyrene-co-vinylpyrrolidone) copolymers (Kuo *et al.*, 2002).

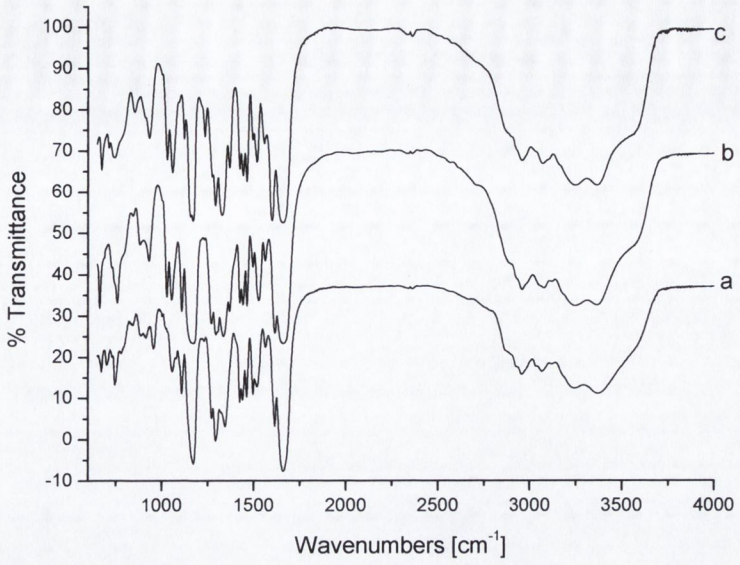

Figure 8.11 The FTIR spectra of (a) co-spray dried BFMT and PVP in the ratio 1:1, (b) co-spray dried HFMT and PVP in the ratio 1:1 and (c) co-spray dried HCT and PVP in the ratio 1:1.

The thiazide diuretics also have the possibility of intermolecular hydrogen bond formation. Each drug molecule contains four N-H moieties, which can act as hydrogen donors. On the other hand, the carbonyl group of PVP has often been reported as a hydrogen bond acceptor (Taylor and Zografi, 1998). Doherty and York (1987) described the possibility of hydrogen bond formation involving furosemide (containing one primary sulphonamide moiety) and PVP.

For this reason, it was our intention to examine if all of the N-H groups are bonded to the PVP carboxyl moiety and what was the order of the interaction. Consequently, all the spectra of spray dried samples were subjected to a peak deconvolution procedure, as the bands overlap one another. A multiple-Gaussian function was used with five peaks allowing for an accurate separation of the bands. Interactions between PVP and the drug results in a blue shift to the bands corresponding to the N-H stretching vibrations. Moreover, this causes the disappearance of the free N-H bands. Two of the N-H stretching peaks exhibit the same trend in the position change. They are the asymmetric and symmetric N-H primary sulphonamide stretches. The peak originally located at around 3380 cm^{-1}, moves towards lower wavenumbers by 16 cm^{-1}, 22 cm^{-1} and 12 cm^{-1} for BFMT, HFMT and HCT respectively with increasing PVP content and, at a certain polymer concentration, a red shift is evident (Figure 8.12). In the case of the symmetric N-H stretching vibration, the magnitude of the displacement is much smaller and the red shift more pronounced. The N-H secondary sulphonamide stretch demonstrates a steadier blue shift and changes its direction only when the PVP content is around 70% for all the drugs.

It was surprising that no shift in the PVP carbonyl stretching band engaged in hydrogen bonding was detected. The peak for the entire polymer concentration range used was at about 1660 cm^{-1}, a frequency which is reported to correspond to hydrogen bonded carbonyl group (Taylor and Zografi, 1998). This could be explained either by the presence of a small amount of moisture, not removed

even by drying of the samples, or by a complete saturation of this group by the hydrogen bonding network formed with the drug over the PVP concentration range. The second interpretation might be supported by shifting trends of the peaks assigned to the cyclic C-H PVP ring deformations.
In order to estimate the PVP weight fraction at which the hydrogen bonds, created by the NH_2 group, become the strongest two straight lines were fitted to both "arms" of the compositional dependence of the asymmetric primary sulphonamide N-H stretching peak position trend (shown in Figure 8.12).

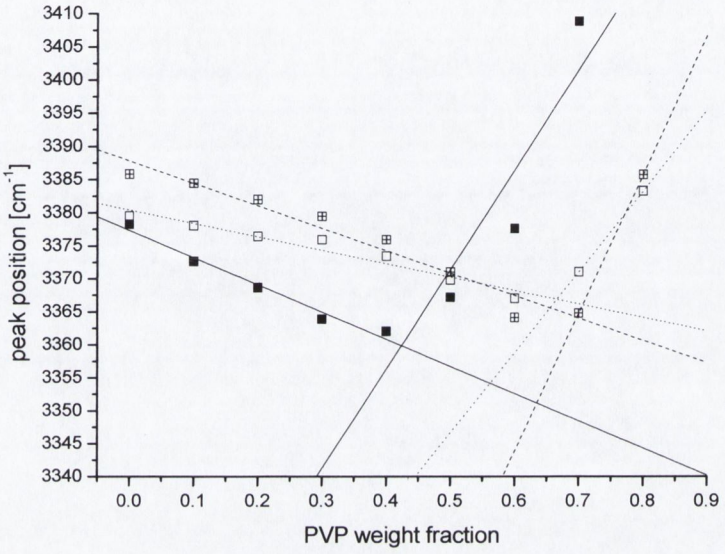

Figure 8.12 The shifting behaviour of the N-H primary sulphonamide asymmetric peak of: black squares – BFMT/PVP, crossed squares – HFMT/PVP and white squares – HCT/PVP co-spray dried systems. The solid, dashed and dotted lines represent the linear fits used to establish the maximum shift of the peak for BFMT/PVP, HFMT/PVP and HCT/PVP systems, respectively.

The intercept of the straight lines gives the maximum of the peaks blue shift. The data treatment gave a composition ratio of 2.6, 6.7 and 5.2 moles of PVP pyrrolidone units per 1 mole of BFMT, HFMT and HCT, respectively. The molar content of PVP and either HFMT or HCT estimated by FTIR is in agreement with the polymer content of the composite systems with the maximum T_g. This suggest that an increase in T_gs of HFMT/PVP and HCT/PVP systems is based on the hydrogen bonding network formed between N-H groups and the carbonyl moiety of the polymer.
The discrepancy for the BFMT/PVP co-spray dried systems (5.7 and 2.6 moles of PVP pyrrolidone units per 1 mole of BFMT given by DSC and FTIR, respectively) suggests an additional factor contributing to the augmented stability. It has been reported (Agha and Digenis, 1983) that polyvinylpyrrolidone can interact with the π-electron system of aromatic compounds and the complex is formed as the aromatic compound approaches the pyrrolidone ring from a site opposite to the negatively charged oxygen. Similar interaction is expected to appear in the BFMT/PVP dispersions because of the additional phenyl group in the BFMT molecule. The evidence for this is provided by the atypical, upward shift in the peak position recognised as aromatic C-H deformation at ~1060 cm^{-1}.

8.5 Conclusions

Glass transition composition behaviour for amorphous drug-PVP composites investigated deviated from the predictions of the commonly used Gordon-Taylor equation. For the salbutamol base/PVP systems negative deviations from the volume additivity rule were observed. The drug molecules exhibited plasticising behaviour and weak interactions between the polymer and salbutamol base molecules were discerned by FTIR.

Large positive deviations from theory may also be attributed to interactions between the constituents of the spray dried thiazide diuretics/PVP composites. The FTIR analysis suggest strong interactions between the two species of the mixed system - hydrogen bonding between the sulphonamide groups of the thiazide diuretics and the PVP molecule and, in the case of BFMT/PVP composites, an interaction between the phenyl group and polymer ring.

Of the various theoretical equations that may be used to attempt to fit the Tg-composition profiles, the Schneider equation proved to be the most promising. This equation is based on combining the free volume rule and the thermodynamic origins of the glass transition. The suitability of using the Schneider equation where other models are unsuccessful may be indicative of interactions between components of the co-spray dried systems.

GENERAL DISCUSSION

9.1 Introduction

The studies in this thesis explored the solid state and inhalation properties of various systems produced by the spray drying technique. The work focused primarily on the feasibility analysis of spray drying as a means of producing materials having properties suitable for pulmonary delivery. The chemical and physical stability of different processed systems have also been addressed. The physicochemical integrity of the spray dried materials will determine their long-term performance as dosage forms.

Three anti-asthmatic drugs: salbutamol base, formoterol fumarate dihydrate and budesonide as well as three thiazide diuretic drugs: bendroflumethiazide, hydroflumethiazide and hydrochlorothiazide drugs were selected as model actives for the spray drying investigations. They were spray dried alone and also formulated in binary or a higher degree of complexity mixtures utilising a range of sugars, polymers, buffer salts and other excipients.
In all cases the physicochemical characteristics were studied using thermal, spectroscopic and microscopic techniques. Also other methods essential in the determination of flowability and inhalation properties were used for the systems intended for deep lung delivery. Different aspects of stability studies were examined: the chemical stability assessment of formoterol fumarate formulations and physical stability of amorphous solids based on the glass transition temperature.

9.2 Morphology and aerolisation properties of systems for inhalation purposes

9.2.1 Dry powder inhalers

Chapters 3 to 6 of this thesis were dedicated to spray drying of materials for inhalations, particularly powders for dry powder inhalers. Chapter 3 focused on processing of salbutamol base and aimed at obtaining an amorphous form of the drug by manipulation of the apparatus settings and on reducing the stickiness of the particles, thereby improving yield and decreasing the degree of particle fusion. The production of an amorphous phase of the drug was successfully accomplished and the initial studies on reducing the stickiness tendency showed promising results. The aerolisation properties of the systems containing salbutamol either alone or with an additive have to be investigated to assess the impact of the alterations induced by spray drying. Systems composed of individual spherical particles should have superior respirable fractions delivered to the lungs than those obtained with fused particles.
Among over 50 spray dried systems presented in Chapters 4-6 all but one had satisfactory morphology and particle sizes for delivery to the lung and were therefore subjected to the *in vitro* twin stage impinger studies. The system that failed to produce a particulate system following spray

drying was the formoterol fumarate dihydrate processed with 30% PEG 20000. It melted in the apparatus and only a small amount of the material was removed.

Generally, the systems were spray dried from either solutions or suspensions. The suspensions were prepared by dissolving the active and to this solution a suitable amount of a substance being dispersed was added. In all cases the suspensions were constantly stirred during the process, ensuring a uniform composition of the sprayed droplets. The excipients that were insoluble in the solution medium were: Aerosil, microcrystalline cellulose and magnesium stearate and were spray dried from budesonide solutions as binary and ternary (with PVP 10000) mixtures.

Aerosil is a fine, white, light and amorphous powder consisting of particles about 12 to 16 nm in size (product leaflet). Co-spray dried budesonide with Aerosil at 5% and 10% of solid content resulted in systems which consisted of smooth and "sponge-like" particles. The rough, nearly porous appearance of the particles was also observed by Kawashima *et al.* (1998b) who spray dried pranlukast hydrate with Aerosil. The particles of that dispersion were not spherical, but elongated, however the surface roughness was visible. The very small size of Aerosil particles should not have influenced the particle size of the composite systems and the median particle size of the 10% Aerosil system was 2.7 μm while that of the of the 5% Aerosil sample was 2.3 μm. In contrast, the sizes of the particles of magnesium stearate/budesonide powders seemed to depend closely on the diameters of the lubricant particles. Figure 9.1 presents a comparison of the median particle sizes of the different batches of spray dried magnesium stearate contrasted with those determined for the budesonide/magnesium stearate 5% and budesonide/PVP 10%/magnesium stearate 5% systems.

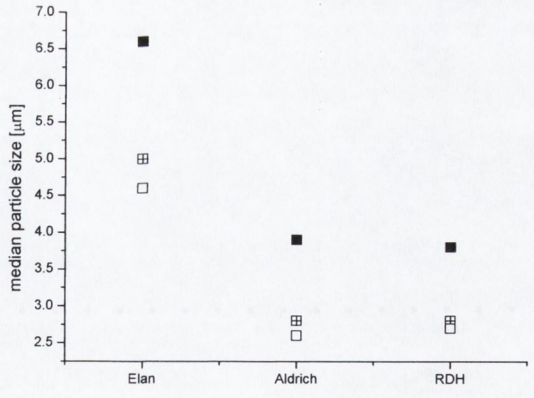

Figure 9.1 Comparison of the median particle sizes of spray dried magnesium stearate (black squares), budesonide/magnesium stearate 5% (empty squares) and budesonide/PVP 10000 10%/magnesium stearate 5% (crossed squares) systems.

From Figure 9.1 it can be seen that the samples of spray dried magnesium stearate had the larger median particles sizes when compared with those of the co-spray dried budesonide systems. A trend can be observed, as the median particle sizes of the co-spray dried powders are smaller by around 1.5-2.5 μm than those of the corresponding samples of magnesium stearate. Therefore, if the size of the excipient forming a suspension was to determine the particle size of the processed

powder then in the case of the spray dried budesonide/microcrystalline cellulose one might expect the creation of rather large particles. The median particle size of unprocessed cellulose was 30.6 μm, whereas the particles of the resultant budesonide composite powders had median sizes of only 3.1 and 3.6 μm for the 5 and 10% microcrystalline cellulose containing systems. Billon *et al.* (2000) investigated spray drying process of acetaminophen with microcrystalline cellulose Vivapur® PH101, where the mean particle diameter of the polymer was ~50 μm. The final product size followed a bimodal distribution indicating the presence of two populations of the particles, the larger corresponding to the cellulose initial particle size. Studies of Chidavaenzi *et al.* (1997) on spray drying lactose monohydrate from solutions and suspensions showed that the amount of amorphous sugar produced from the suspensions was much higher than would have been expected from the content of lactose present in solution. The possible explanation for this phenomenon was that the atomisation pressure in the spray nozzle had a milling effect on the suspended lactose. All particles of the budesonide/microcrystalline cellulose powders were below 13 μm (by volume) and it would imply that a similar process of milling of the excipient occurred during spray drying.

The median particle size of the systems spray dried from solutions fitted well within the range of respirable particles. The smallest median particle size was 1.8 μm for the co-spray dried budesonide with formoterol fumarate dihydrate 100:6 sample (code 13AB) and the largest median particle size was determined to be 5.0 μm for the same combination of drugs - sample 8AB.

It was of interest to examine whether the median particle size of the various produced samples correlates with the fractions retained in the lower stage of the twin stage impinger i.e. respirable fractions and the emitted portions of the total doses loaded into capsules. The values obtained presented in Figure 9.2. For comparison, the data on unprocessed materials are included and are represented as open squares.

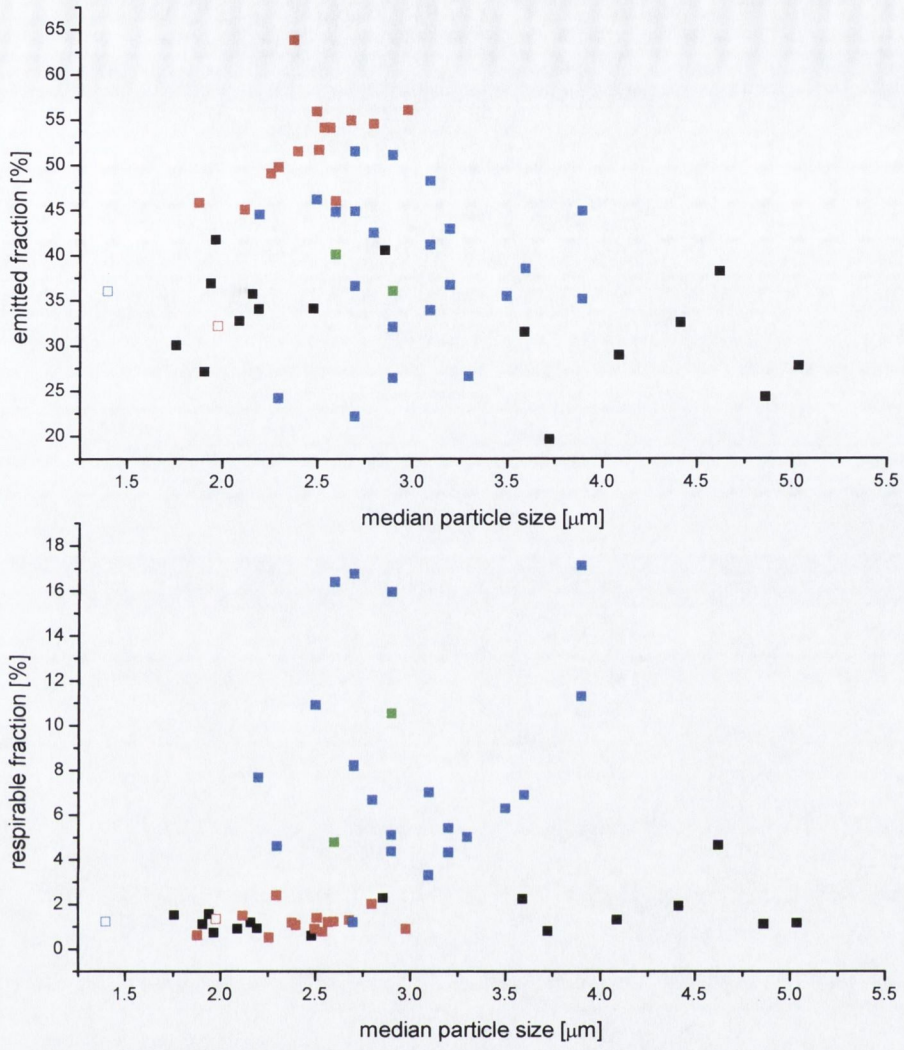

Figure 9.2 Relationship between the median particle size of the systems analysed by twin stage impinger and emitted fraction (top graph) respirable fraction (bottom graph). The open symbols indicate unprocessed materials and the full symbols present spray dried samples. Black symbols represent budesonide/formoterol fumarate 100:6, red symbols – formoterol fumarate, blue symbols – budesonide and green symbols – porous budesonide systems.

No apparent correlation was discerned from Figure 9.2, therefore it can be concluded that respirable or emitted doses were governed by factors other than the diameter of the particles. The statistical design studies on co-spray dried budesonide/formoterol fumarate dihydrate 100:6 dispersions described in Chapter 4 demonstrated that the respirable fractions (determined in *in vitro* twin stage impinger studies) of these powders were influenced by the feed concentration and airflow of the drying gas, with greater fine particle fractions obtained when both a lower solution concentration and lower airflow were used. Figure 9.3 graphically shows that no obvious trend existed between the feed concentrations employed in spray drying and the percentage of the respirable doses achieved in the twin stage analysis examinations. Similarly, no relationship

between the percentage of the dose retained in the lower impingement and the airflow through the spray dryer was seen. Hence, it is the most likely that the surface morphology and its alteration is responsible for the aerolisation properties of the co-spray dried systems produced.

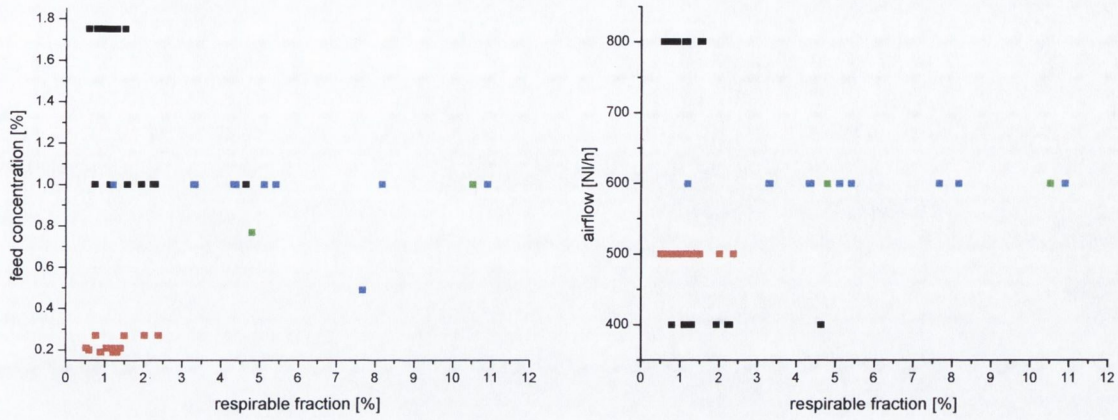

Figure 9.3 Graph showing respirable fractions versus feed concentration (left graph) and drying gas airflow (right graph) used during the spray drying of various systems. Key – as Figure 9.2.

The significance of surface phenomena such adhesion, cohesion and triboelectrification in relation to powders formulated in DPIs have been emphasised by many authors (Buckton, 1997; Kawashima *et al.*, 1998a; Podczeck, 1998). They are known to adversely affect the efficiency of DPIs. The degree of disorder caused by processing may influence the surface energy and hence modify interactions between the surfaces (Buckton, 1997). Spray dried formoterol fumarate alone achieved a worse respirable fraction compared to the unprocessed drug, but no significant difference was observed between the processed and unprocessed budesonide.

Among the co-processed systems of formoterol fumarate the sample with the best deposition on stage 2 of twin impinger was the system containing 30% HP-β-cyclodextrin which resulted in a nearly 2-fold greater respirable fraction than the starting material powder. The same excipient at a 30% level when co-spray dried with budesonide markedly improved the drug deposition in the lower impinger making it the best in terms of respirable fractions out of the budesonide powders comprising an excipient other than magnesium stearate (nearly a 7-fold increase over unprocessed drug). Budesonide/Aerosil 10% powder demonstrated quite good aerolisation properties attributed to the presence of porous, "sponge"-like particles. However superior respirable doses of budesonide were obtained with the ternary systems comprising of 5% magnesium stearate and 10% PVP 10000, where a greater than 10-fold improvement in the fine particle fraction was observed when compared with the budesonide "as received" sample. A trend between the particle surface smoothness and inhalation efficiency was observed. Particles which had rougher or corrugated surfaces had better deposition in the lower impinger. French *et al.* (1996) found that the inclusion of protein rhG-CSF with mannitol resulted in a less dense powder with surface indentations. This material had better inhalation performance than the mannitol alone. It has also been shown that by

designing therapeutic aerosol particles with porous morphology, relatively large particles can be successfully inspired into lungs (Vanbever *et al.*, 1999). More recent studies of Newhouse *et al.* (2003) on *in vivo* evaluation of the efficiency of pulmonary delivery of a tobramycin PulmoSphere formulation showed that the mean whole-lung deposition was nearly 7-fold greater than the commercially available nebulised tobramycin product. The novel method of preparation of porous particles made solely of budesonide using spray drying from a solution containing only an active and dissolved blowing agent was presented in Chapter 6. This manufacturing method does not require the spray dryer's nozzle modification as needed for the technique described by Steckel and Brandes (2004) and there is no emulsifier added as in the process developed by Dellamary *et al.* (2000). The best of the two budesonide porous systems produced gave a greater than 6-fold increase in the fine particle fraction compared to that of the budesonide starting powder. The porous drug powder composed exclusively of the active seems also a better alternative than the co-spray dried drug/excipient(s) samples as the pulmonary toxicity of some of the excipients is unclear. Only a few of them e.g. lactose or trehalose are GRAS (generally recognised as safe) listed. PVP has been used as a plasma expander up to relatively recently but it is known to cause intracellular depositions (Mohr and Endres-Klein, 2002). The fate of magnesium stearate following inhalation is unknown as no toxicological studies have been carried out to date. As regards HP-β-cyclodextrin, it has been used since 2000 in a commercial intravenous infusion, Sporanox® to solubilise itraconazole. Not only was the addition of an excipient shown to improve the aerolisation characteristics of a powder, but also the parameters of the spray drying process were demonstrated to yield materials with different inhalation qualities. This was presented in Chapter 4 using the example of co-spray drying of budesonide with formoterol fumarate dihydrate in the ratio 100:6. One sample was significantly better than the others as regards the *in vitro* respirable fraction and this was attributed to a formation of non-solid spheres, ensuring better flowability and dispersibility. The sample consisted of considerably large particles which result in lower strength of the interfacial forces and low aerodynamic compared to geometric diameters that in overall contributes to the good inhalation efficiency.

As regards uniformity of the dose released from the inhalation device containing a mix of two actives, spray dried powders were shown to be a superior alternative to physical mixtures as every composite particle contains the blend of drugs at a fixed ratio. The twin impinger studies demonstrated that the physical mix of budesonide and formoterol fumarate dihydrate 100:6 did not result in the same ratio being attained in the second stage of the twin stage impinger. This system exhibited greater variability than the co-spray dried samples. The deviation of the formoterol fumarate content was calculated to be ±3%, taking the amount of budesonide as 100. For the physical mix the mean ratio of budesonide to formoterol fumarate was around 100 to 7.5 (instead of the desired 100 to 6 ratio) with ± 30% deviation of the formoterol fumarate content.

The twin stage impinger analysis presented in this thesis was carried out on systems which had not been mixed with lactose carrier. It would be interesting to assess and contrast the *in vitro* lung

delivery properties of some of the powders as blends with such a carrier. Also the use of a different inhalation device would be of importance. Steckel and Müller (1997) compared the *in vitro* respirable fraction emitted from commonly used DPIs. The twin stage impinger was used and was operated at 60 l/min for 4 sec, which are similar conditions to those employed in this thesis. The fine particle fraction (i.e. respirable fraction) of budesonide discharged from a commercial Pulmicort™ Turbohaler™ formulation expressed as a percent of the total dose was 24.6%, whereas in our study the respirable fraction obtained was only 1.6%. Unfortunately, it was not possible to perform any comparison for formoterol fumarate due to the lack of literature data.

9.2.2 Metered dose inhalers

Chapter 7 focused on investigations of the MDIs formulations of formoterol fumarate dihydrate and its chemical stability.

As regards the stability studies of formoterol fumarate in buffered solutions, the pH at which the drug was the most stable was 5.00-5.20 depending on the temperature and buffer used. This is in good agreement with the optimum pH for formoterol fumarate aqueous solutions being in the range between 4.5 and 5.5. This pH range was disclosed in US Patent 6150418 (Hochrainer and Zierenberg, 2000) which presented an invention for the preparation of a formoterol solution or suspension concentrate suitable for storage intended for use in inhalers or nasal therapy. The most suitable buffered formulation of the drug presented in this thesis was based on a citrate buffer with a pH of 5.20 and ionic strength 0.1 M and stored at 25°C. The $t_{1/2}$ determined for this solution was around 57 months. Also lower concentrations of the drug were found to be more stable. Regarding the stability studies of the drug alone and co-spray dried mannitol systems containing formoterol fumarate, it was important whether the material exposed to various environmental conditions was in the powdered state or formulated into MDIs. Mannitol stabilised the drug in the dry state at low relative humidity and temperature values but the unprocessed drug dispersed in the propellant had the best chemical stability. The studies did not include the drug spray dried alone and this should be the subject of any future work.

Only one out of four excipients (mannitol, xylitol, PVP 40000 and HPMC E5) included in the initial investigations on the feasibility of spray drying to obtain particles of a suitable size fulfilled the requirements of the ideal diameter (95% below 5 μm and all below 10 μm). This was PVP 40000 processed from a 1.5% (w/v) ethanolic solution made of 95% (v/v) ethanol and 5% (v/v) water and spray dried at the inlet temperature 84°C with the pump set at 20%, aspirator at 100% and airflow at 800 Nl/h. The mannitol particles were larger when spray dried from similar conditions except when aqueous solution was used and subsequently a higher inlet temperature of 140°C was employed. In this case 99% particles (by volume) were below 10 μm. Furthermore, the polymorphic form of mannitol changed slightly on spray drying. Xylitol was found to be unsuitable

for the manufacture of a powdered material as only a tacky substance was recovered from the apparatus and HPMC generated large particles with irregular distribution of the size. No substantial decrease in the particle size was observed with mannitol processed with either HPMC or PVP as binary co-spray dried systems and the best among these was mannitol/HPMC 30% (w/w) for which ~80% (by volume) of particles were 5 μm and smaller and all were below 10 μm. Hence, only PVP and mannitol alone were regarded as appropriate excipients for producing suspension MDI formulations. PVP was found to be unsuitable for the production of stable suspensions in the propellant, especially when a mixture of ethanol and propellant was used, due to clumping or dissolving in these ethanolic mixtures. Therefore, the co-spray dried formoterol fumarate systems were based on mannitol. Upon addition of the drug, the particle size of the resulting co-spray dried powders increased and the formation of agglomerates was noticed. This was especially apparent in systems containing calcium chloride.

Stabilisation of a suspension MDI involves the same basic principles as an aqueous suspension and the Stoke's law (Equation 9.1) will also apply:

$$V = \frac{2r^2(d - d_0)g}{9\eta_0} \qquad \text{(Equation 9.1)}$$

where V is the sedimentation velocity, r is the radius of the dispersed phase, d and d_0 are the densities of the dispersed phase and dispersion medium, respectively, g is the gravitational acceleration constant and η_0 is the intrinsic viscosity of the dispersion medium (Martin, 1993).

Therefore, by using smaller particles, minimising the difference in the densities between the dispersed phase and dispersion medium or increasing viscosity of the dispersion medium the production of a suspension can be adjusted toward better quality dispersions. Moreover, small particles are also favourable in pulmonary delivery (Zeng *et al.*, 2001).

The particle size is determined by the processing conditions and this factor was optimised by using the spray dryer's settings allowing for manufacture of particles as small in size as possible. During the dispersibility examinations of the spray dried powder materials it was observed that the best dispersions and the longest settling times were achieved with a combination of PVP dissolved in the ethanol/propellant mixture. Two combinations were studied: 0.01% PVP-1% ethanol-HFA-134a and 0.2% PVP-5% ethanol-HFA-134a and, depending on the dispersed system, the optimal suspension was attained with the first or the second mixture. Steckel and Wehle (2004) were able to develop a technique of production of micro-fine suspension based MDI formulations by precipitation of the active out of a mixture of HP-β-cyclodextrin, PEG 300, ethanol and propellant HFA-227. Firstly, the test drug, budesonide, was dissolved in the investigated mixture of the polymers and ethanol, and after the addition of the propellant a milky suspension resulted which remained stable for 3 months. The very good quality of the suspension was explained by the cyclodextrin acting as a bulking agent. Budesonide and cyclodextrin formed a network-like structure perhaps by means of hydrogen bonds. In our method neither PVP nor drug precipitated

from the dispersion medium. The stability of the suspensions attained was thought to be attributed to the increased viscosity of the propellant solution.

Preliminary studies on the respirable fractions of some of the formoterol fumarate HFA-134a suspension inhalers were undertaken in our laboratory by Clarke (2005). The studies were aimed at the evaluation of the impact of excipients and other additives used on the inhalation performance of the formulated formoterol fumarate particles. An Andersen cascade impactor was employed and the respirable fraction was defined as the portion of a dose having particles below 4.7 μm. These experiments indicated around a 1.7-2-fold increase in respirable fractions when the 0.01% PVP-1% ethanol-HFA-134a medium was used compared to the formulations based solely on HFA-134a.

The porous budesonide particles that gave very good respirable fractions when formulated as DPIs were also prepared as suspension MDIs. Compared with the crystalline drug, less floc formation was observed and more even suspensions were produced. Budesonide spray dried alone formed larger particle agglomerates consisting of caked powder and visible flocs which sedimented the fastest. The sedimentation rate of unprocessed budesonide and porous budesonide spray dried at the inlet temperature of 78°C were comparable with the latter sedimenting slightly slower. This effect can be attributed to the lower bulk density of the porous sample because this material had a significantly greater median particle size (3.4 μm) than budesonide "as received" (1.4 μm) and yet sedimented more slowly. The photograph presented in Appendix VII shows the suspension quality of the budesonide MDIs prepared.

9.3 Crystallinity of spray dried systems

9.3.1 Systems spray dried alone

A number of drug substances, excipients and polymers were spray dried alone in the course of this thesis. The active substances include: salbutamol base, formoterol fumarate dihydrate, budesonide, bendroflumethiazide, hydroflumethiazide and hydrochlorothiazide. The polymer group encompasses PEG 20000, PVP 10000, PVP 40000, HPMC and the excipients processed were trehalose dihydrate, raffinose pentahydrate, mannitol, xylitol and magnesium stearate.

9.3.1.1 Drugs spray dried alone

Spray drying of all the drugs resulted in amorphous materials and in the case of salbutamol base it was dependent on the processing conditions. Formation of an amorphous phase of budesonide was reported previously by Corrigan (2002). Corrigan *et al.* (1984) spray dried bendroflumethiazide, hydroflumethiazide and hydrochlorothiazide from ethanolic solutions and amorphous phases also resulted. They found that the disordered phase of hydrochlorothiazide was unstable and the

exotherm detected by DSC had gone after 24 h, whereas the amorphous phases of BFMT and HFMT were still physically stable after 12 months.

The production of an amorphous formoterol fumarate is reported for the first time in the present work.

The degree of crystallinity of spray dried salbutamol base was dependent on the processing conditions and a completely amorphous material was obtained when the compound was spray dried from 1% (w/v) ethanolic solution (containing 95% (v/v) ethanol and 5% (v/v) water) at the inlet temperature of 78°C, airflow rate 400 Nl/h, pump rate 30% and aspirator setting 100%. The outcome of the processing conditions on the degree of crystallinity of the drug was explained by a combined effect of a low outlet temperature achieved due to the high speed of the pump feeding the solution used and high atomisation energy provided by a high aspiration rate. A few papers have been published regarding the impact of spray drying conditions on the physicochemical characteristics of single substances, nevertheless they mainly focus on the feed composition. Chidavaenzi *et al.* (1997) found that the concentration of feed material had a significant effect on the crystallinity of spray dried lactose. An increase in lactose concentration in the feed solution or suspension resulted in a decrease in amorphous lactose content. Harjunen *et al.* (2002) investigated the effect of the ethanol to water ratio in the feed solution on the physical properties of spray dried lactose. The sugar spray dried from pure ethanol was 100% crystalline, whereas when processed from water was 100% amorphous. The samples spray dried from ethanol/water mixtures had intermediate degrees of crystallinity. Ueno *et al.* (1998) prepared amorphous ursodeoxycholic acid (UDCA) by spray drying a solution of the compound from a mixture of ethanol and dichloromethane. It was observed that the resulting UDCA samples differed in crystallinity depending on the air inlet temperature employed and more amorphous materials were obtained when the inlet temperature was increased.

9.3.1.2 Polymers spray dried alone

Spray drying of both grades of PVP (10000 and 40000) resulted in the production of amorphous samples. This was expected, as PVP is an inherently disordered material and no changes in the molecular structures of these polymers were anticipated.

A reduction in crystallinity for spray dried PEG 20000 compared to the starting material was observed. Corrigan (2002) attempted the spray drying of PEG 20000 as an ethanolic solution, but no amorphous material was produced and DSC and XRD analyses showed even a slight increase in the crystallinity degree. In this work a different solvent was used, namely dichloromethane, and the spray dryer settings gave a lower outlet temperature than that obtained by Corrigan.

The unprocessed HPMC was predominantly amorphous as investigated by XRD with only one crystalline peak at around 32.0 2θ. Spray drying caused a decrease in intensity of this peak and a recrystallisation exotherm appeared on the DSC thermogram indicating that the processed powder had a greater degree of amorphous content than the starting material.

9.3.1.3 Excipients spray dried alone

The following excipients were spray dried from aqueous solutions: trehalose dihydrate, raffinose pentahydrate, mannitol and xylitol. Magnesium stearate was processed as a suspension prepared in a mixture of 95% (v/v) ethanol and 5% (v/v) water.

Trehalose dihydrate and raffinose pentahydrate produced completely amorphous phases. Spray drying of trehalose and its transformation into an amorphous form on processing was reported by Surana *et al.* (2004) and Maury *et al.*(2005), whereas Lechuga-Ballesteros *et al.* (2003) found that raffinose pentahydrate also forms an amorphous phase on spray drying.

Spray drying of mannitol induced the formation of an amorphous phase to some degree as was shown by a broad "halo" on the diffractogram but the resulting powder was predominantly XRD crystalline. Mannitol is a substance which exhibits polymorphism. To date, three different crystalline forms of the sugar have been identified: α, β and δ. The starting material was essentially in the β-form but processing induced a polymorphic transformation to the α polymorph, detected by XRD and FTIR analyses.

In the case of xylitol, the employed spray drying conditions resulted in a soft, glassy substance. Insufficient material was recovered to enable full analysis to be performed. Only DSC was performed and the diminished heat of fusion of the spray dried sample compared to that of the unprocessed xylitol implied that some amorphous xylitol was formed.

Magnesium stearate was processed as a suspension. All batches of the lubricant examined were crystalline before and following spray drying. Minor changes in the XRD and DSC patterns were discovered when compared to those of the starting powders. TGA showed that small amounts of water were lost upon processing, hence the differences were ascribed to slight modifications of the crystalline structures associated perhaps with a loss of fractions of the crystalline moisture.

A summary of the available information on the thermal properties of the active substances, polymers and excipients used in this work, either determined from the analyses performed for preparation of this thesis or various literature sources, are presented in Table 9.1.

Table 9.1 Thermal characteristics of the substances used in this thesis (empty fields mean that the information was not available, NA– not applicable, [a] – first enantiomer, [b] – based on the second endothermic peak on the DSC thermograms and regarded as melting of the anhydrous compound, [c] – temperature uncertain, [d] – from Miller and de Pablo, (2000), [e] – from Surana *et al.*, (2004), [f] – from Borde and Cesaro, (2001), [g] – from Kajiwara *et al.*, (1999), [h] – from Talja and Roos, (2001), [i] – from Watanabe *et al.*, (2001), [k] – from Suami *et al.*, (1973), [l] – from Roos and Karel, (1991), [m] – estimated from the rule $T_g = 0.7 \cdot T_m$,.

Material	Molecular weight	T_m [K]	ΔH [J/g]	T_g [K]	Δc_p at T_g [J/(g·K)]	Tg/Tm
Salbutamol base	239.3	431.6	204	318	1.3	0.74
Budesonide	430.5	534.6	87.1	362.5	0.17	0.68
Formoterol fumarate	828.9	407.6 [a]	8.3 [a]	352.4	0.69	0.86
BFMT	421.4	498.9	107.8	392	0.17	0.79
HFMT	331.3	545.7	128.8	368.5	0.39	0.67
HCT	297.7	540.7	121.1	342	0.42	0.63
Lactose	360.3	486.7 [b]	134.7 [b]	391.3	0.7 [d]	0.80
Trehalose	378.3	482.8 [b]	127 [b]	393.6	0.55 [e]	0.82
Maltodextrin	900-9000	NA	NA	461 [l]		NA
PVP 10000	1000	NA	NA	402	0.215	NA
PEG 20000	20000	335.4	187.8	234.8 [m]		0.7
Raffinose	594.5	404-409 [k]		391.2	1.31 [g]	
HP-β-cyclodextrin	1460	NA	NA	477 [c]	0.29	NA
Brij 58	1124	311.6	138	218.1 [m]		0.7
Myrj 59	4989.8	326.9	170	228.8 [m]		0.7
Stearic acid	284.5	341.4	213.4	239 [m]		0.7
Ascorbyl palmitate	414.5	385.3	131.6	269.7 [m]		0.7
Mannitol	182.2	438.9	289.7	287.5 [f]	1.23 [f]	0.66
HPMC E5	10000-1500000	447.5	2.3	423.9	0.17	0.95
Xylitol	152.2	366.6	245	249 [h]		0.68
PVP 40000	40000	NA	NA	439	0.34	NA
Aerosil 200	69	NA	NA	1473 [i]		NA
Microcrystalline cellulose	~36000					NA
Magnesium stearate	591.24	variable	variable			NA

9.3.2 Systems spray dried as mixtures

Corrigan *et al.*, (2004) have shown that the Gordon–Taylor equation can be useful in predicting the probability of the amorphous or crystalline nature of a two-composite on spray drying. This expression was also useful in predicting the physical stability of amorphous binary composites and predicted that even polymers with apparently low T_gs, such as PEGs, may be stabilised in an amorphous composite by a suitable additive having a sufficiently high T_g.

The Gordon-Taylor approach was applied here to investigate the thermal properties of the systems produced in the present work. Only binary systems spray dried from solutions were included in the

investigations as the miscibility of the constituents in the materials prepared from slurries, where one of the components was suspended, could not be guaranteed. The complete miscibility of the substances is one of the assumptions of the Gordon-Taylor approach.

Exhaustive analysis of the thermal properties of the salbutamol base, bendroflumethiazide, hydroflumethiazide and hydrochlorothiazide blends with PVP is described in Chapter 8. Only one system had a very weak peak on the diffractogram, which was indicative of a very small degree of drug crystallinity, namely the co-spray dried salbutamol base/PVP 10% system. The T_gs of the systems studied did not follow the Gordon-Taylor equation.

9.3.2.1 Formoterol fumarate systems

All co-spray dried formoterol fumarate/excipient systems described in Chapter 5 resulted in XRD amorphous powders, except for the drug/PEG 20000 30% sample. This was predominantly amorphous with weak peaks of the crystalline polymer. As the glass transition temperatures of the dispersions overlapped with the broad desolvation endotherms, the same DSC pre-treatment procedure as that applied to the salbutamol base/PVP systems described in Chapter 8 was used to release the volatile solvent residues. The predicted T_gs together with the experimentally measured values for all the systems are shown in Table 9.2. For calculations the density of PEG 20000 was taken as that of the spray dried sample. No literature values of the densities of Brij 58 and Myrj 59 were found, thus they were assumed to be equal to the density of PEG 20000 due to their similar chemical structures.

The T_gs predicted by the Gordon-Taylor equation for the amorphous systems were in good agreement with the experimental values and the differences did not exceed a few degrees (Table 9.2). The only exceptions were the samples co-spray dried with HP-β-cyclodextrin for which the equation predicted much larger values. It was discussed in Chapter 5 that formoterol is unlikely to form inclusion complexes with the cyclodextrin molecules, but undoubtedly they are interactions existing between the molecules. Fernandes *et al.*, (2002) also did not find convincing evidence on the formation of nicardipine/HP-β-cyclodextrin inclusion compound. Surface binding may also be responsible for the interactions detected.

The calculated T_gs of materials showing crystallinity were all below 34°C (Table 9.2). These include the mannitol/formoterol fumarate co-spray dried powders employed in the production of MDI formulations (Chapter 7) and the formoterol system comprising 30% PEG 2000. In all cases the XRD patterns of the mixtures showed that the peaks of the excipient and the drug were amorphous. Also PEG 20000 and mannitol when spray dried alone were crystalline. Corrigan *et al.*, (2004) used the Kauzmann temperatures to estimate the physical stability and crystallinity of spray dried blends at room temperature. The Kauzmann temperature (T_K) of an amorphous compound or mixture is the temperature below which the molecular motions can be considered as negligible (Hancock *et al.*, 1998). The molecular motions below the T_g are relatively slow but do exist and can still have a profound influence on the physical stability of a system. Hancock and Zografi,

(1997) stated that the Kauzmann temperature for a system can be estimated by subtracting 50K from the T_g value given in degrees Kelvin. More complicated methods of T_K calculation for a single substance are available e.g. Hancock *et al.*, (1998) derived an equation utilising knowledge of the melting point, heat of fusion and change of the heat capacity at the T_g.

Therefore, as the formoterol/mannitol and formoterol/PEG 20000 30% systems have T_Ks well below room temperature (Table 9.2) they will form only crystalline phases. The formoterol/PEG 20000 10% was amorphous after spray drying, but the T_K calculated for this system is only 291.4K (18.4°C) (Table 9.3) indicating that it probably will recrystallise on storage unless kept below 20°C. The rest of the formoterol blends should be physically stable, with the trehalose 30% sample having the greatest T_g (367.6 K = 94.6°C) and therefore T_K (317.6 K = 44.6°C). It should therefore be the best as regards physical stabilisation properties.

Table 9.2 The glass transition temperatures calculated from the Gordon-Taylor (G-T) equation, the Kauzmann temperatures calculated from the T_g-50K rule (for the amorphous systems the experimental T_gs were used, whereas the T_K of the crystalline samples was based on the T_gs predicted by G-T equation) and crystallinity for the formoterol fumarate systems (ND – not detected, C – peaks indicative of crystallinity, A – amorphous by XRD). Densities of the pure amorphous components: formoterol fumarate – 1.16 g/cm^3, PEG 20000 – 1.15 g/cm^3, PVP 10000 – 1.17 g/cm^3, raffinose – 1.51 g/cm^3, HP-β-cyclodextrin – 1.30 g/cm^3, Brij 58 – 1.15 g/cm^3 and Myrj 59 – 1.15 g/cm^3.

Additive and its content	T_g experimental	T_g predicted from G-T	T_K	Crystallinity
PEG 20000 10%	341.4 K (68.4°C)	341.3 K (68.3°C)	291.4 K (18.4°C)	A
PVP 10000 10%	361.8 K (88.8°C)	364.9 K (91.9°C)	311.8 K (38.8°C)	A
Trehalose 10%	364.0 K (91.0°C)	363.6 K (90.6°C)	314.0 K (41.0°C)	A
Raffinose 10%	363.7 K (90.7°C)	363.4 K (90.4°C)	363.7 K (40.7°C)	A
HP-β-CYC 10%	363.2 K (90.2°C)	369.1 K (96.1°C)	313.2 K (40.2°C)	A
PEG 20000 30%	ND	306.7 K (33.7°C)	306.7 K (-16.3°C)	C
PVP 10000 30%	364.4 K (91.4°C)	372.5 K (99.5°C)	314.4 K (41.4°C)	A
Trehalose 30%	367.6 K (94.6°C)	368.7 K (95.7°C)	317.6K (44.6°C)	A
Raffinose 30%	364.7 K (91.7°C)	368.2 K (95.2°C)	314.7 K (51.7°C)	A
HP-β-CYC 30%	366.2 K (93.2°C)	387.0 K (114.0°C)	316.2 K (43.2°C)	A
Brij 58 0.5%	360.9 K (87.9°C)	360.0 K (87.0°C)	310.9 K (37.9°C)	A
Myrj 59 0.5%	361.6 K (88.6°C)	360.2 K (87.2°C)	311.6 K (38.6°C)	A
Brij 58 2%	356.8 K (83.8°C)	356.2 K (83.2°C)	306.8 K (33.8°C)	A
Myrj 59 2%	358.9 K (85.9°C)	356.8 K (83.8°C)	308.9 K (35.9°C)	A
Mannitol 90%	ND	289.4 K (16.4°C)	289.4 K (-33.6°C)	C
Mannitol 80%	ND	296.9 K (23.9°C)	296.9 K (-26.1°C)	C
Mannitol 70%	ND	304.5 K (31.5°C)	304.5 K (-18.5°C)	C

9.3.2.2 Budesonide systems

Not all spray dried systems were amorphous, which was apparent from the DSC and XRD traces. The series of budesonide/stearic acid systems were partially crystalline with the highest degree of crystallinity for the 2% stearic acid sample. The melting endotherm of stearic acid was observed for 2, 5 and 10% content of this excipient in co-spray dried composites. Surprisingly, the drug was in the crystalline state even though budesonide when spray dried alone displayed amorphous character. In Chapter 5 it was observed that the compound with the lower T_g (PEG 20000) remained crystalline whereas the drug was in the amorphous phase. No literature data was found on co-spray drying of stearic acid with a drug and it can be hypothesised that stearic acid spray dried alone does not form an amorphous phase due to the low melting point (Table 9.1). Also the system containing budesonide, stearic acid and PVP contained remnants of the crystalline active, but a considerable increase in the amorphous phase content was observed.

Budesonide in all magnesium stearate specimens was amorphous, but the lubricant processed either alone or with the drug was crystalline. No reduction in the degree of magnesium stearate crystallinity was observed upon addition of PVP into the binary systems.

All other co-spray dried systems were XRD amorphous and the predicted (using the Gordon-Taylor equation) T_gs agree reasonably well with the experimental values (Table 9.3). The Kauzmann temperature calculated for the system with the lowest T_g (budesonide/ascorbyl palmitate 10%) was 295K (22.0°C). This suggests that it may be stable on storage if kept below this temperature.

Table 9.3 The glass transition temperatures calculated from the Gordon-Taylor (G-T) equation and crystallinity for the budesonide systems (ND – not detected, C – peaks indicative of crystallinity, A – amorphous by XRD). Densities of the pure amorphous components: budesonide – 1.21 g/cm^3, stearic acid – 1.52 g/cm^3 (Beilstein chemical database) and ascorbyl palmitate – 1.21 g/cm^3.

Additive and its content	Tg experimental	Tg predicted from G-T	Crystallinity
Formoterol fumarate 5.6%	363.2-366.1 K (90.2-93.1°C)	362.5 K (89.5°C)	A
Raffinose 30%	364.5 K (91.5°C)	369.4 K (96.4°C)	A
HP-β-CYC 30%	ND	389.2 K (116.2°C)	A
Stearic acid 1%	ND	361.4 K (88.4°C)	C
Stearic acid 2%	ND	358.0 K (85.0°C)	C
Stearic acid 5%	ND	351.6 K (78.6°C)	C
Stearic acid 10%	ND	341.5 K (68.4°C)	C
Ascorbyl palmitate 5%	354.0 K (81.0°C)	356.4 K (83.4°C)	A
Ascorbyl palmitate 10%	345.0 K (72.0°C)	350.5 K (77.5°C)	A

9.3.2.3 Mannitol systems

Mannitol was co-spray dried with PVP 40000 and HPMC in the course of preparation of powders suitable for MDIs (Chapter 7). The 10% PVP 40000 containing sample was XRD crystalline with peaks of mannitol, whereas upon addition of 50% of the polymer the resulting system was amorphous as evidenced by the recrystallisation exotherm obtained using DSC. Due to its low T_g (Table 9.4) this system recrystallised quickly at room temperature and no XRD analysis was done. There is a 44 degrees difference between the predicted and determined T_gs (Table 9.4), indicating that mannitol acts as a plasticiser and can effectively depress the glass transition temperature of the polymer. On the other hand, when HPMC at 30% level was co-spray dried with mannitol, the resulting powder was amorphous and exhibited a T_g which was greater by over 10 degrees than that predicted. This may imply additional stabilisation bonding formed between the constituents, as observed previously for the thiazide diuretics/PVP composites (Chapter 8). Despite this, the T_K for that system is only 278.0 K (5.0°C), which is insufficient to be stable at room temperature.

Table 9.4 The glass transition temperatures calculated from the Gordon-Taylor (G-T) equation and crystallinity for the mannitol systems (ND – not detected, * – by DSC, C – peaks indicative of crystallinity, A – amorphous by XRD). Densities of the pure amorphous components: mannitol – 1.50 g/cm^3 (from Chew and Chan, 1999), PVP 40000 – 1.26 g/cm^3 and HPMC – 1.33 g/cm^3 (from Wade, 1994).

Additive and its content	Tg experimental	Tg predicted from G-T	Crystallinity
PVP 40000 10%	ND	294.3 K (21.3°C)	C
PVP 40000 50%	306.0 K (33.0°C)	350.0 K (77.0°C)	A*
HPMC 30%	328.0 K (55.0°C)	316.6 K (43.6°C)	A

9.4 Interactions in co-spray dried polyvinylpyrrolidone (PVP) systems

A number of substances were co-spray dried with PVP in the course of this thesis. Binary mixtures with salbutamol base, formoterol fumarate, bendroflumethiazide, hydroflumethiazide, hydrochlorothiazide as well as mannitol were produced. Additionally, PVP was formulated into ternary systems with budesonide and magnesium stearate. Polyvinylpyrrolidone has extensively been used in the manufacture of solid dispersions due to its inhibitory effect on the crystallisation of drugs. The mechanisms of crystallisation retardation include the antiplasticising effect of PVP, thus the T_g of a mixture can be increased, with specific interactions occurring between the drug and PVP (Yoshioka *et al.*, 1995).

The Gordon-Taylor (G-T) equation has successfully been utilised in predicting the suitability of drug/polymer blends for melt extrusion (Forster *et al.*, 2001) and predicting the physical state of spray dried composites (Corrigan *et al.*, 2004). However, as presented in this work, the glass

transition temperatures of amorphous solid dispersions do not always adhere to this expression. Therefore, other approaches for the prediction of T_gs which are less commonly used in the pharmaceutical field were applied to describe the compositional dependence of the T_gs of drugs. These methods include the Fox (F), Couchman-Karasz (C-K), Kwei (K) and Schneider (S) equations. The last two expressions were applied for the first time to pharmaceutical systems.

A literature review showed that a substantial amount of work on the physicochemical characterisation of various PVP composites has been presented, including discussion of interactions present between the components. The main conclusions of the literature research are summarised in Table 9.5 and Table 9.6 and include the substance investigated, the grade of PVP used, models evaluated and the ability of the model to predict the measured values as well as interacting chemical groups.

All but one substance presented in Table 9.5 and Table 9.6 formed additional bonds with the carbonyl group of PVP. Only griseofulvin was found not to interact with the polymer. PVP is capable of forming a hydrogen bond either through the amide nitrogen or carbonyl group of the pyrrole ring. However steric hindrance prevents the involvement of the nitrogen atom in intermolecular interactions, hence making the carbonyl group more favourable for hydrogen bonding (Sekizaki *et al.*, 1995).

Hydrogen bonding is undoubtedly one of the factors, which influence the glass transition temperature (Taylor and Zografi, 1998a). It is noteworthy, that changes in T_g caused by the presence of PVP in a mixture are not unidirectional. For instance, Taylor and Zografi (1998a) commented on the tendency of hydrogen bonding to cause a decrease in the T_gs of sugar-polymer lyophilised samples. That behaviour was explained by a loss or weakening of hydrogen bonds in the self-associated sugar that were stronger than those formed between the sugar and PVP. Negative deviations between the measured and Gordon-Taylor predicted T_gs for the salbutamol base/PVP dispersions were observed in the present work. No conclusive evidence of the presence of hydrogen bonding between the drug and polymer was produced, however the discrepancies between the calculated and experimental T_gs may have arisen from the fact that the interactions between the salbutamol molecules are stronger than among molecules of different kinds.

A different phenomenon was investigated for the BFMT, HFMT and HCT solid dispersions, as a new hydrogen bonding network between the thiazide diuretic drug and polymer seemed to be much stronger than interactions in the amorphous active. This can be explained by the chemistry of the sulphonamide group. It is well known that compounds containing a sulphonamide group are more acidic than their amide counterparts (Patai and Rappaport, 1991). This is because the SO_2 group, a strong electron withdrawing group, is able to polarise the nitrogen atom positively, which in turn eases the release of the protons. Since each drug contains a sulphonamide group, mixing with PVP containing an amide moiety should yield a hydrogen bond, where the sulphonamide acts as a proton donor and the amide as a proton acceptor. The resulting hydrogen bond ought to be stronger than any thiazide-thiazide interaction. A confirmation of this interpretation was found in De

Groote's work on hydrogen bonding between polyamides and benzenosulphonamide compounds (De Groote *et al*. 2001).

Concluding, the glass transition temperature of a binary solid dispersion containing PVP seems to rely on the balance between inter and intramolecular interactions of molecules of the same kind and different species. Weaker self-aggregation of the substance molecules being mixed with PVP favours the formation of stronger bonds and an increase in the T_g may be expected. The ability to increase the T_g of a drug offers the possibility to stabilise an amorphous system according to the T_g-50K rule.

Table 9.5 Summary of interactions between the pharmaceutical actives and PVP in amorphous solid dispersions (empty fields mean that the information was not available, [a)] – from Khougaz and Clas, (2000), [b)] – from Di Martino *et al.*, (2004), [c)] – from Matsumoto and Zografi G., (1999), [d)] – from Weuts *et al.*, (2004), [e)] – from Van den Mooter *et al.*, (2001), [f)] – from Crowley and Zografi, (2002), [g)] – from Nair *et al.*, (2001). Abbreviations

Drug	PVP grade	Model	Comments	Interacting groups
Salbutamol base (this thesis)	10000 (K-15)	F G-T C-K K S	negative deviations negative deviations good prediction best prediction best prediction	hydroxyl, secondary amino with carbonyl PVP (unconfirmed, possible)
BFMT (this thesis)	10000 (K-15)	F G-T C-K K S	positive deviations positive deviations positive deviations good prediction best prediction	sulphonamide with carbonyl PVP aromatic with PVP
HFMT (this thesis)	10000 (K-15)	F G-T C-K K S	positive or negative deviations positive or negative deviations positive or negative deviations positive or negative deviations good prediction	sulphonamide with carbonyl PVP
HCT (this thesis)	10000 (K-15)	F G-T C-K K S	positive deviations positive deviations positive deviations good prediction best prediction	sulphonamide with carbonyl PVP
MK-0591 [a)]	K-90 K-30 K-17 K-12	G-T G-T G-T G-T	positive deviations positive deviations positive deviations positive deviations	COO^-Na^+ with carbonyl PVP
Ketoprofen [b)]	K-30	G-T	negative deviations	COOH with carbonyl PVP
Indomethacin [c)]	K-90 K-30 K-17 K-12	G-T G-T G-T G-T	negative deviations negative deviations negative deviations good prediction	COOH with carbonyl PVP
Loperamide [d)]	K-30	G-T	negative deviations	OH, amino with carbonyl PVP
Ketoconazole [e)]	K-25	G-T	good prediction	no interactions
Ursodeoxy-cholic acid [f)]	K-90	C-K	good prediction	
Indapamide [f)]	K-90	C-K	positive deviations	
Salicylamide [g)]	K-90	G-T	negative deviations	carbonyl PVP
Acetaminophen [g)]	K-90	G-T	negative deviations	carbonyl PVP
Carbamazepine [g)]	K-90	G-T	negative deviations	amino with carbonyl PVP
Naproxen [g)]	K-90	G-T	negative deviations	hydroxyl with carbonyl PVP
Propranolol HCl [g)]	K-90	G-T	negative deviations	carbonyl PVP
Griseofulvin [g)]	K-90	G-T	negative deviations	no interactions

Table 9.6 Summary of interactions between the pharmaceutical excipients and PVP in amorphous solid dispersions (empty fields mean that the information was not available, [a)] – from Nyamweya and Hoag, (2000), [b)] – from Feldstein, (2001), [c)] – from Taylor and Zografi, (1998a).

Excipient	PVP grade	Model	Comments	Interacting groups
HPMC K4M [a)]	K-30 (10000)	F	negative deviations	
		C-K	negative deviations	
PEG 400 [b)]	K-90	G-T	negative deviations	hydroxyl with carbonyl PVP
		F	negative deviations	
		C-K	good prediction	
sucrose [c)]	K-90	G-T	negative deviations	hydroxyl with carbonyl PVP
trehalose [c)]	K-90	G-T	negative deviations	hydroxyl with carbonyl PVP
raffinose [c)]	K-90	G-T	negative deviations	hydroxyl with carbonyl PVP

9.5 Main findings

- Spray drying can produce an amorphous phase of salbutamol base.
- The degree of crystallinity of a spray dried drug can be dependent on the processing parameters.
- Formoterol fumarate dihydrate produces an amorphous form on spray drying.
- Spray drying conditions can greatly influence the respirable fraction of powders.
- Co-spray drying offers a better alternative of uniform dosing over the equivalent physical mixtures of two active substances.
- Co-spray drying with raffinose pentahydrate and HP-β-cyclodextrin can improve the deep lung particle fractions.
- Polyvinylpyrrolidone (PVP) in connection with magnesium stearate can significantly improve *in vitro* respirable fractions of inhalable powders.
- Aerolisation properties can be improved by surface modification of particles accomplished by spray drying.
- A novel method of production of porous particles made of drugs was demonstrated. The systems have superior aerolisation properties over the unprocessed and spray dried drug alone.
- PVP-ethanol-HFA 134a mixture is a medium suitable for retarding sedimentation time for suspension-based MDIs.
- Formoterol fumarate formulated as a suspension has greater chemical stability over solution-based MDIs.
- Bendroflumethiazide, hydroflumethiazide and hydrochlorothiazide can be physically stabilised by PVP due to the formation of hydrogen bonds. Furthermore, depending on the PVP content, the glass transition temperature of the drug can be effectively increased.
- The Schneider and Kwei equations have successfully been used for the first time to describe the compositional dependence of the glass transition temperatures on the composition of pharmaceutical systems.
- Crystallinity of co-spray dried systems can be correlated with FTIR measurements.

9.6 Future work

- The *in vitro* twin impinger studies on the co-spray dried powders mixed with coarse lactose carrier particles may be performed to investigate whether greater respirable fractions could be obtained.
- It would be valuable to carry out toxicological studies on magnesium stearate involving cell cultures studies.
- Further work on the chemical and physical stability of the porous particles systems should be carried out. Also the studies may focus on elucidating the detailed mechanism of formation of pores. More advanced investigations should include spray drying of compounds other than drugs e.g excipients and mixtures e.g. drug/drug and drug/excipient.
- Further studies into the correlation of the Schneider equations with other physical parameters and measures, such as entropy, enthalpy, Hansen's solubility parameters should be undertaken.
- It would be of interest to include molecular modelling studies in the investigations of predictability of glass transition temperatures of mixtures as they provide information on the structure and energy of molecular bonds.

REFERENCES

Adhikari, B., Howes, T., Bhandari, B. R. and Troung, V., Effect of addition of maltodextrin on drying kinetics and stickiness of sugar and acid-rich foods during convective drying: experiments and modelling, J. Food Eng., 62 (2004) 53-68.

Adsmond, D. A. and Grant, D. J., Hydrogen bonding in sulfonamides, J. Pharm. Sci., 90 (2001) 2058-2077.

Agha, B. J. and Digenis, G. A., Studies on the interaction of PVP-related lactams with aromatic compounds using NMR spectroscopy. In: Proceedings of the International Symposium on Povidone, University of Kentucky, College of Pharmacy, April 17-20, USA, (1983).

Ahmed, M. O., Comparison of impact of the different hydrophilic carriers on the properties of piperazine-containing drug, Eur. J. Pharm. Biopharm., 51 (2001) 221-225.

Akao, K., Okubo, Y., Asakawa, N., Inoue, Y. and Sakurai, M., Infrared spectroscopic study on the properties of the anhydrous form II of trehalose. Implications for the functional mechanism of trehalose as a biostabilizer, Carbohydr. Res., 334 (2001) 233-241.

Akapo, S. O. and Asif, M., Validation of a RP-HPLC method for the assay of formoterol and its related substances in formoterol fumarate dihydrate drug substance, J. Pharm. Biomed. Anal., 33 (2003) 935-945.

Akhadov, Y. Y., Dielectric properties of binary solutions, Oxford, Pergamon, (1981).

Alexander, K. and King, C. J., Factors governing surface morphology of spray dried amorphous substances, Dry. Technol., 3 (1985) 321-348.

Allen, T., Particle size measurement, 5th ed., London, Chapman & Hall, (1997).

Alves, G. P. and Santana, M. H. A., Phospholipid dry powders produced by spray drying processing: structural, thermodynamic and physical properties, Powder Tech., 145 (2004) 139-148.

Angell, C. A., Entropy and fragility in supercooling liquids, J. Res. Natl. Inst. Stand. Technol., 102 (1997) 171-185.

Anguiano-Igea, S., Otero-Espinar, F. J., Vila-Jato, J. L. and Blanco-Mendez, J., The properties of solid dispersions of clofibrate in polyethylene glycols, Pharm. Acta Helv., 70 (1995) 57-66.

Apperley, D. C., Harris, R. K., Larsson, T. and Malmstrom, T., Quantitative nuclear magnetic resonance analysis of solid formoterol fumarate and its dihydrate, J. Pharm. Sci., 92 (2003) 2487-2494.

Barry, P. W. and O'Callaghan, C., The effect of delay, multiple actuations and spacer static charge on the in vitro delivery of budesonide from the Nebuhaler, Br. J. Clin. Pharmacol., 40 (1995) 76-78.

Bauer, J., Spanton, S., Henry, R., Quick, J., Dziki, W., Porter, W. and Morris, J., Ritonavir: an extraordinary example of conformational polymorphism, Pharm. Res., 18 (2001) 859-866.

Beddow, J. K., Philip, G. C., Vetter, A. F. and Nasta, M. D., On relating some particle profile characteristics to the profile Fourier coefficients, Powder Technol., 18 (1977) 19-25.

Bell, L. N. and Labuza, T. P., Influence of the low-moisture state on pH and its implication for reaction kinetics, J. Food Eng., 22 (1994) 291-312.

Bell, J. H., Hartley, P. S. and Cox, J. S., Dry powder aerosols. I. A new powder inhalation device, J. Pharm. Sci., 60 (1971) 1559-1564.

Ben-Jebria, A., Chen, D., Eskew, M. L., Vanbever, R., Langer, R. and Edwards, D. A., Large porous particles for sustained protection from carbachol-induced bronchoconstriction in guinea pigs, Pharm. Res., 16 (1999) 555-561.

Bhandari, B. R., Datta, N. and Howes, T., Problems associated with spray drying of sugar-rich foods, Dry. Technol., 15 (1997) 671-684.

Billon, A., Bataille, B., Cassanas, G. and Jacob, M., Development of spray-dried acetaminophen microparticles using experimental designs, Int. J. Pharm., 203 (2000) 159-168.

Black, D. B. and Lovering, E. G., Estimation of degree of crystallinity in digoxin by X-ray and infrared methods, J. Pharm. Pharmac., 29 (1977) 684-687.

Blackett, P. M. and Buckton, G., A microcalorimetric study of surfactant aggregation and surfactant drug-interaction in a model inhalation aerosol system, Int. J. Pharm., 125 (1995) 133-139.

Blondino, F. E., Brucato, M. and Buenafe, M., Pressurized metered dose inhalers and pharmaceutical aerosol formulations, United States Patent 6451285, (2002).

Borde, B. and Cesaro, A., A DSC study of hydrated sugar alcohols: isomalt, J. Therm. Anal. Calorim., 66 (2001) 179-195.

Bosquillon, C., Lombry, C., Préat, V. and Vanbever, R., Comparison of particle sizing techniques in the case of inhalation dry powders, J. Pharm. Sci., 90 (2001a) 2032-2041.

Bosquillon, C., Lombry, C., Préat, V. and Vanbever, R., Influence of formulation excipients and physical characteristics of inhalation dry powders on their aerosolization performance, J. Control. Release, 70 (2001b) 329-339.

Bot, A. I., Tarara, T. E., Smith, D. J., Bot, S. R., Woods, C. M. and Weers, J. G., Novel lipid-based hollow-porous microparticles as a platform for immunoglobulin delivery to the respiratory tract, Pharm. Res., 17 (2000) 275-283.

Brekner, M.-J., Schneider, H. A. and Cantow, H.-J., Approach to the composition dependence of the glass transition temperature of compatible polymer blends: 1. Polymer, 29 (1988) 78-85.

Briggner, L.-E., Buckton, G., Bystrom, K. and Darcy, P., The use of isothermal microcalorimetry in the study of changes in crystallinity induced during the processing of powders, Int. J. Pharm., 105 (1994) 125-135.

British Pharmacopoeia, The Stationery Office, Great Britain, (2004).

Brittain, H. G., Particle-size distribution, part I: Representations of particle shape, size, and distribution, Pharm. Tech., 25 (2001) 38-45.

Brittain, H. G., Polymorphism in pharmaceutical solids, Marcel Dekker, New York, (1999).

Broadhead, J., Rouan, S. K. E. and Rhodes, C. T., The spray drying of pharmaceuticals, Drug Dev. Ind. Pharm., 18 (1992) 1169-1206.

Buckton, G., Characterisation of small changes in the physical properties of powders of significance for dry powder inhaler formulations, Adv. Drug Deliv. Rev., 26 (1997) 17-27.

Buckton, G., Darcy, P., Greenleaf, D. and Holbrook, P., The use of isothermal microcalorimetry in the study of changes in crystallinity of spray-dried salbutamol Sulphate, Int. J. Pharm., 116 (1995) 113-118.

Buckton, G., Yonemochi, E., Hammond, J. and Moffat, A., The use of near infra-red spectroscopy to detect changes in the form of amorphous and crystalline lactose, Int. J. Pharm., 168 (1998) 231-241.

Burger, A., Henck, J. O., Hetz, S., Rollinger, J. M., Weissnicht, A. A. and Stöttner, H., Energy/temperature diagram and compression behavior of the polymorphs of D-mannitol, J. Pharm. Sci., 89 (2000) 457-468.

Butz, N., Porté, C., Courrier, H., Krafft, M. P. and Vandamme, T. F., Reverse water-in-fluorocarbon emulsions for use in pressurized metered-dose inhalers containing hydrofluoroalkane propellants, Int. J. Pharm., 238 (2002) 257-269.

Büchi B-191 technical specification, Büchi, Switzerland.

Byron, P. R. and Blondino, F., E., Metered dose inhaler formulations which include the ozone-friendly propellant HFC 134a and a pharmaceutically acceptable suspending, solubilizing, wetting, emulsifying or lubricating agent, United States Patent 5492688, (1996).

Byrn, S., Pfeiffer, R., Ganey, M., Hoiberg, C. and Poochikian, G., Pharmaceutical solids: a strategic approach to regulatory considerations, Pharm. Res., 12 (1995) 945-954.

Byron, P. R., Peart, J. and Staniforth, J. N., Aerosol electrostatics. I: Properties of fine powders before and after aerosolization by dry powder inhalers, Pharm. Res., 14 (1997) 698-705.

Cabral Marques, H. M., Hadgraft, J., Kellaway, I. W. and Taylor, G., Studies of cyclodextrin inclusion complexes. III. The pulmonary absorption of β-, DM-β- and HP-β-cyclodextrins in rabbits, Int. J. Pharm., 77 (1991) 297-302.

Cabral Marques, H. M., Hadgraft, J., Kellaway, I. W. and Taylor, G., Studies of cyclodextrin inclusion complexes. II. Molecular modelling and ^{1}H-NMR evidence for the salbutamol-β-cyclodextrin complex, Int. J. Pharm., 63 (1990) 267-274.

Caira, M. R., Easter, B., Honiball, S., Horne, A. and Nassimbeni, L. R., Structure and thermal stability of alprazolam and selected solvates, J. Pharm. Sci., 84 (1995) 1379-1384.

Carr, Jr., R. L., Classifying flow properties of solids, Chem. Eng., 72 (1965) 69-72.

Carstensen, J. T., Drug stability: principles and practices, New York, Marcel Dekker, (1995).

Carter, P. A., Rowley, G., Fletcher, E. J. and Hill, E. A., An experimental investigation of triboelectrification in cohesive and non-cohesive pharmaceutical powders, Drug Dev. Ind. Pharm., 18 (1992) 1505-1526.

Cassidy O., Rowley G. and Nguyen H., The effect of surface modification on electrostatic charge of a particulate solid, Eur. J. Pharm. Sci., 4 (1996) S65.

Cavatur, R. K., Vemuri, N. M., Pyne, A., Chrzan, Z., Toledo-Valasquez, D. and Suryanarayanan, R., Crystallization behavior of mannitol in frozen aqueous solutions, Pharm. Res., 19 (2002) 894-900.

Chao, R. S. and Vail, K. C., Polymorphism of 1,2-dihydro-6-neopentyl-2-oxonicotinic acid: characterization, interconversion, and quantitation, Pharm. Res., 4 (1987) 429-432.

Chawla, A., Taylor, K. M. G., Newton, J. M. and Johnson, M. C. R., Production of spray dried salbutamol sulphate for use in dry powder aerosol formulation, Int. J. Pharm., 108 (1994) 233-240.

Chen, R., Tagawa, M., Hoshi, N., Ogura, T., Okamoto, H. and Danjo, K., Improved dissolution of an insoluble drug using a 4-fluid nozzle spray-drying technique, Chem. Pharm. Bull., 52 (2004) 1066-1070.

Chen, X. M., Bates, S. and Morris, K. R., Quantifying amorphous content of lactose using parallel beam X-ray powder diffraction and whole pattern fitting, J. Pharm. Biomed. Anal., 26 (2001) 63-72.

Chew, N. Y. K. and Chan, H. K., Use of solid corrugated particles to enhance powder aerosol performance, Pharm. Res., 18 (2001) 1570-1577.

Chew, N. Y. K. and Chan, H. K., Influence of particle size, air flow, and inhaler device on the dispersion of mannitol powders as aerosols, Pharm. Res., 16 (1999) 1098-1103.

Chew, N. Y. K., Bagster, D. F. and Chan, H. K., Effect of particle size, air flow and inhaler device on the aerosolisation of disodium cromoglycate powders, Int. J. Pharm., 206 (2000) 75-83.

Chidavaenzi, O. C., Buckton, G., Koosha, F. and Pathak, R., The use of thermal techniques to assess the impact of feed concentration on the amorphous content and polymorphic forms present in spray dried lactose, Int. J. Pharm., 159 (1997) 67-74.

Chiesi, P. and Pavesi, L., New pharmaceutical compositions for inhalation, European Patent 0239798A1, (1987).

Chiou, W. L. and Riegelman, S., Pharmaceutical applications of solid dispersion systems, J. Pharm. Sci., 60 (1971) 1281-1302.

Chiou, W. L. and Riegelman, S., Preparation and dissolution characteristics of several fast-release solid dispersions of griseofulvin, J. Pharm. Sci., 58 (1969) 1505-1510.

Christensen, K. L., Pedersen, G. P. and Kristensen, H. G., Physical stability of redispersible dry emulsions containing amorphous sucrose, Eur. J. Pharm. Biopharm., 53 (2002) 147-153.

Cilurzo, F., Minghetti, P., Casiraghi, A. and Montanari, L., Characterization of nifedipine solid dispersions, Int. J. Pharm., 242 (2002) 313-317.

Clarke, G., "The use of the Andersen cascade impactor to evaluate the particle size distribution of metered dose inhalers", Senior Sophister project, School of Pharmacy, Trinity College, University of Dublin, (2005), unpublished data.

Colaço, C., Sen, S., Thangavelu, M., Pinder, S. and Roser, B., Extraordinary stability of enzymes dried in trehalose: simplified molecular biology, Biotechnology, 10 (1992) 1007-1011.

Corrigan, D. O., Preparation and evaluation of spray dried composites of pharmaceutical materials, Ph.D. Thesis, Trinity College, University of Dublin, (2002).

Corrigan, D. O., Corrigan, O. I. and Healy, A. M., Predicting the physical state of spray dried composites: salbutamol sulphate/lactose and salbutamol sulphate/polyethylene glycol co-spray dried systems, Int. J. Pharm., 273 (2004) 171-182.

Corrigan, D. O., Healy, A. M. and Corrigan, O. I., The effect of spray drying solutions of polyethylene glycol (PEG) and lactose/PEG on their physicochemical properties, Int. J. Pharm., 235 (2002) 193-205.

Corrigan, D. O., Healy, A. M. and Corrigan, O. I., The effect of spray drying solutions of bendroflumethiazide/polyethylene glycol on the physicochemical properties of the resultant materials, Int. J. Pharm., 262 (2003) 125-137.

Corrigan, O. I. and Holohan, E. M., Amorphous spray-dried hydroflumethiazide-polyvinylpyrrolidone systems: physiochemical properties, J. Pharm. Pharmacol., 36 (1984) 217-221.

Corrigan, O. I. and Timoney, R. F., The influence of polyvinylpyrrolidone on the dissolution properties of hydroflumethiazide, J. Pharm. Pharmacol., 27 (1975) 759-764.

Corrigan, O. I., Holohan, E. M. and Sabra, K., Amorphous forms of thiazide diuretics prepared by spray-drying, Int. J. Pharm., 18 (1984) 195-200.

Corrigan, O. I., Timoney, R. F. and Whelan, M. J., The influence of polyvinylpyrrolidone on the dissolution and bioavailability of hydrochlorothiazide. J. Pharm. Pharmacol., 28 (1976) 703-706.

Couchman, P. R., Compositional variation of glass-transition temperatures. 2. Application of thermodynamic theory to compatible polymer blends, Macromolecules, 11 (1978) 1156-1161.

Couchman, P. R. and Karasz, F. E., A classical thermodynamic discussion of the effect of composition on glass-transition temperatures, Macromolecules, 11 (1978) 117-119.

Craig, D. Q. M., A review of thermal methods used for the analysis of the crystal form, solution thermodynamics and glass transition behavior of polyethylene glycols, Thermochim. Acta, 248 (1995) 189-203.

Craig, D. Q. M., Barsnes, M., Royall, P. G. and Kett, V. L., An evaluation of the use of modulated temperature DSC as a means of assessing the relaxation behaviour of amorphous lactose, Pharm. Res., 17 (2000) 696-700.

CRC Handbook of Chemistry and Physics, editor in chief Lide, D. R., Boca Raton, CRC Press, (1994).

Crosby, E. J. and Marshall, Jr., W. R., Effects of drying conditions on properties of spray-dried particles, Chem, Eng. Prog., 54 (1958) 56-63.

Crowley, K. J. and Zografi, G., Water vapor absorption into amorphous hydrophobic drug/poly(vinylpyrrolidone) dispersions, J. Pharm. Sci., 91 (2002) 2150-2165.

Cullity, B. D., Elements of X-ray diffraction, 2nd Edition, London, Addison-Wesley, (1978).

Davies, P. J., Hanlon, G. W. and Molyneux, A. J., An investigation into the deposition of inhalation aerosol particles as a function of air flow rate in a modified 'Kirk Lung', J. Pharm. Pharmacol., 28 (1976) 908-911.

De Groote, P. H., Rouxhet, P. G., Devaux, J. and Godard, P., Infrared study of the hydrogen bonding association in polyamides plasticized by benzenesulfonamides. Part I: Self-association in amide and sulfonamide systems; Part II: Amide- sulfonamide interaction, Appl. Spectrosc., 55 (2001) 877-887.

Deamer, D. W., Meek, D. W. and Cornwell, D. G., Properties, composition, and structure of stearic acid-stearate monolayers on alkaline earth solutions, J. Lipid Res., 8 (1967) 255-263.

Debenedetti, P. G. and Stillinger, F. H., Supercooled liquids and the glass transition, Nature, 410 (2001) 259-267.

Dellamary, L. A., Tarara, T. E., Smith, D. J., Woelk, C. H., Adractas, A., Costello, M. L., Gill, H. and Weers, J. G., Hollow porous particles in metered dose inhalers, Pharm. Res., 17 (2000) 168-174.

Desai, D., Li, D., Janjikhel, R., Lang, B. and Jain, N., Effects of light intensity, n-alcohols, water-soluble colorants, and solution viscosity on photoisomerization of sorivudine, Pharm. Dev. Technol., 6 (2001) 99-106.

Di Martino, P., Joiris, E., Gobetto, R., Masic, A., Palmieri, G. F. and Martelli, S., Ketoprofen-poly(vinylpyrrolidone) physical interaction, J. Cryst. Growth, 265 (2004) 302-308.

Di Marzio, E. A., The glass temperature of polymer blends, Polymer, 31 (1990) 2294-2298.

Dickinson, P. A., Seville, P. C., McHale, H., Perkins, N. C. and Taylor, G., An investigation of the solubility of various compounds in the hydrofluoroalkane propellants and possible model liquid propellants, J. Aerosol Med.-Depos. Clear. Eff. Lung, 13 (2000) 179-186.

Dillen, K., Vandervoort, J., Van den Mooter, G., Verheyden, L. and Ludwig, A., Factorial design, physicochemical characterisation and activity of ciprofloxacin-PLGA nanoparticles, Int. J. Pharm., 275 (2004) 171-187.

Dimitrovska, A., Stojanoski, K. and Dorevski, K., Kinetics of degradation of cefaclor. I. Effects of temperature, phosphate buffer, pH and copper(II) ion on the rate of degradation, Int. J. Pharm., 115 (1995) 175-182.

Doherty, C. and York, P., Evidence for solid- and liquid-state interactions in a furosemide-polyvinylpyrrolidone solid dispersion, J. Pharm. Sci., 76 (1987) 731-737.

Drożdżewski, P. and Kordon, E., Isotopic studies of the metal-ligand vibrations in histamine complexes with copper(II), Spectroc. Acta Pt. A-Molec. Biomolec. Spectr., 56 (2000) 1299-1304.

Duckworth, R. Water relations of foods. Academic Press, New York, (1975).

Dunbar, C. A. and Hickey, A. J., Evaluation of probability density functions to approximate particle size distributions of representative pharmaceutical aerosols, J. Aerosol Sci., 31 (2000) 813-831.

Elversson, J., Millqvist-Fureby, A., Alderborn, G. and Elofsson, U., Droplet and particle size relationship and shell thickness of inhalable lactose particles during spray drying, J. Pharm. Sci., 92 (2003) 900-910.

Erden, N. and Celebi, N., Factors influencing release of salbutamol sulphate from poly(lactide-co-glycolide) microspheres prepared by water-in-oil-in-water emulsion technique, Int. J. Pharm., 137 (1996) 57-66.

European Pharmacopoeia, 5th Edition, (2004).

Fayle, S. E. and Gerrard, J. A., The Maillard reaction, Cambridge, Royal Society of Chemistry, (2002).

Feldstein, M. M., Peculiarities of glass transition temperature relation to the composition of poly(N-vinyl pyrrolidone) blends with short chain poly(ethylene glycol), Polymer, 42 (2001) 7719-7726.

Fernandes, C. M., Vieira, M. T. and Veiga, F. J. B., Physicochemical characterization and in vitro dissolution behavior of nicardipine-cyclodextrins inclusion compounds, Eur. J. Pharm. Sci., 15 (2002) 79-88.

Ford, J. L., Stewart, A. F. and Dubois, J.-L., The properties of solid dispersions of indomethacin or phenylbutazone in polyethylene glycol, Int. J. Pharm., 28 (1986) 11-22.

Ford, J. L., Pharmaceutical thermal analysis: techniques and applications, Chichester, Ellis Horwood, (1989).

Ford, J. L., The current status of solid dispersions, Pharm. Acta Helv., 61 (1986) 69-88.

Forster, A., Hempenstall, J., Tucker, I. and Rades, T., The potential of small-scale fusion experiments and the Gordon-Taylor equation to predict the suitability of drug/polymer blends for melt extrusion, Drug Dev. Ind. Pharm., 27 (2001) 549-560.

Fox, T. G., Influence of diluent and of copolymer composition on the glass temperature of a polymer system, Bull. Am. Phys. Soc., 1 (1956) 123.

French, D. L., Edwards, D. A. and Niven, R. W., The influence of formulation on emission, deaggregation and deposition of dry powders for inhalation, J. Aerosol Sci., 27 (1996) 769-783.

Fubara, J. O. and Notari, R. E., Influence of pH, temperature and buffers on cefepime degradation kinetics and stability predictions in aqueous solutions, J. Pharm. Sci., 87 (1998) 1572-1576.

Ganderton, D., Jone, T. and McGinity, J., (eds.) Advances in Pharmaceutical Sciences. London, Academic Press, (1995).

Gao, Y., Hett, R., Fang, K., Wald, S. A. and Senanayake, C. H., Formoterol process, United States Patent 6268533, (2001).

Gerhardt, A. and Carstensen, J. T., Influence of excipients on the solid state stability of a series of barbiturates in the presence of limited quantities of moisture, Pharm. Res., 6 (1989) S142.

Gibbs, J. H. and DiMarzio, E. A., Nature of glass transition and the glassy state, J. Chem. Phys., 28 (1958) 373-383.

Gilani, K., Rouholamini Najafabadi, A., Barghi, M. and Rafiee-Tehrani, M., Aerosolisation of beclomethasone dipropionate using spray dried lactose/polyethylene glycol carriers, Eur. J. Pharm. Biopharm., 58 (2004) 595-606.

Giordano, F., Novak, C. and Moyano, J. R., Thermal analysis of cyclodextrins and their inclusion compounds, Thermochim. Acta, 380 (2001) 123-151.

Giron, D., Contribution of thermal methods and related techniques to the rational development of pharmaceuticals-Part 1, Pharm. Sci. Technol., Today, 1 (1998) 191-199.

Giron, D., Remy, P., Thomas, S. and Vilette, E., Quantitation of amorphicity by microcalorimetry, J. Therm. Anal., 48 (1997) 465-472.

Goldsmith, D. R. and Keating, G. M., Budesonide/formoterol: a review of its use in asthma, Drugs, 64 (2004) 1597-1618.

Gombás, A., Antal, I., Szabó-Revész, P., Marton, S. and Erõs, I., Quantitative determination of crystallinity of alpha-lactose monohydrate by Near Infrared Spectroscopy (NIRS), Int. J. Pharm., 256 (2003) 25-32.

Gordon, M. and Taylor, J. S., Ideal copolymers and the second-order transitions of synthetic rubbers. 1. Non-crystalline copolymers, J. Appl. Chem., 2 (1952) 493-500.

Goula, A. M. and Adamopoulos, K. G., Spray drying of tomato pulp: effect of feed concentration, Dry. Technol., 22 (2004) 2309-2330.

Grant, D. J. W. and York, P., Entropy of processing: a new quantity for comparing the solid state disorder of pharmaceutical materials, Int. J. Pharm., 30 (1986) 161-180.

Greenhalgh, D. J., Williams, A. C., Timmins, P. and York, P., Solubility parameters as predictors of miscibility in solid dispersions, J. Pharm. Sci., 88 (1999) 1182-1190.

Greenwald, R. B., PEG drugs: an overview, J. Control. Release, 74 (2001) 159-171.

Groneberg, D. A., Witt, C., Wagner, U., Chung, K. F. and Fischer, A., Fundamentals of pulmonary drug delivery, Respir. Med., 97 (2003) 382-387.

Guinot, S. and Leveiller, F., The use of MTDSC to assess the amorphous phase content of a micronised drug substance, Int. J. Pharm., 192 (1999) 63-75.

Haleblian, J. and McCrone, W., Pharmaceutical applications of polymorphism, J. Pharm. Sci., 58 (1969) 911-929.

Hallworth, G. W. and Westmoreland, D. G., The twin impinger - a simple device for assessing the delivery of drugs from metered dose pressurized aerosolinhalers, J. Pharm. Pharmacol., 39 (1987) 966-972.

Hancock, B. C., Disordered drug delivery: destiny, dynamics and the Deborah number, J. Pharm. Pharmacol., 54 (2002) 737-746.

Hancock, B. C. and Shamblin, S. L., Water vapour sorption by pharmaceutical sugars, Pharm. Sci. Technol., Today, 1 (1998) 345-351.

Hancock, B. C. and Zografi, G., Characteristics and significance of the amorphous state in pharmaceutical systems, J. Pharm. Sci., 86 (1997) 1-12.

Hancock, B. C. and Zografi, G., The relationship between the glass transition temperature and the water content of amorphous pharmaceutical solids, Pharm. Res., 11 (1994) 471-477.

Hancock, B. C., Christensen, K. and Shamblin, S. L., Estimating the critical molecular mobility temperature (T_K) of amorphous pharmaceuticals, Pharm. Res., 15 (1998) 1649-1651.

Hancock, B. C., Shamblin, S. L. and Zografi, G., Molecular mobility of amorphous pharmaceutical solids below their glass transition temperatures, Pharm. Res., 12 (1995) 799-806.

Harjunen, P. I., Lehto, V. P., Välisaari, J., Lankinen, T., Paronen, P. and Järvinen, K., Effects of ethanol to water ratio in feed solution on the crystallinity of spray-dried lactose, Drug Dev. Ind. Pharm., 28 (2002a) 949-955.

Harjunen, P., Lehto, V.-P., Martimo, K., Suihko, E., Lankinen, T., Paronen, P. and Järvinen, K., Lactose modifications enhance its drug performance in the novel multiple dose Taifun® DPI, Eur. J. Pharm. Sci., 16 (2002b) 313-321.

Hartauer, K. J., Miller, E. S. and Guillory, J. K., Diffuse reflectance infrared Fourier transform spectroscopy for the quantitative analysis of mixtures of polymorphs, Int. J. Pharm., 85 (1992) 163-174.

Hartmann, V., Schnabel, G. and Ohlrich, H. J., Stability of liquid ergotalkaloid preparations as a function of the solvent polarity, Arzneimittel-Forschung, 27 (1977) 2276-2283.

Haynes, A., Shaik, M. S., Krarup, H. and Singh, M., Evaluation of the Malvern Spraytec® with inhalation cell for the measurement of particle size distribution from metered dose inhalers, J. Pharm. Sci., 93 (2004) 349-363.

Henwood, S. Q., Liebenberg, W., Tiedt, L. R., Lötter, A. P. and de Villiers, M. M., Characterization of the solubility and dissolution properties of several new rifampicin polymorphs, solvates, and hydrates, Drug Dev. Ind. Pharm., 27 (2001) 1017-1030.

Hickey, A. J. and Concessio, N. M., Descriptors of irregular particle morphology and powder properties, Adv. Drug Deliv. Rev., 26 (1997) 29-40.

Hickey, A. J., Concessio, N. M., Van Oort, M. M. and Platz, R. M., Factors influencing the dispersion of dry powders as aerosols, Pharm. Technol., 18 (1994) 58.

Hinds, W. C., Aerosol technology: properties, behavior, and measurement of airborne particles, 2nd ed., New York , Chichester, (1999).

Hirst, P. H., Pitcairn, G. R., Weers, J. G., Tarara, T. E., Clark, A. R., Dellamary, L. A., Hall, G., Shorr, J. and Newman, S. P., In vivo lung deposition of hollow porous particles from a pressurized metered dose inhaler, Pharm. Res., 19 (2002) 258-264.

Hochrainer, D. and Zierenberg, B., Active substance concentrate with formoterol, suitable for storage, United States Patent 6150418, (2000).

Hogan, S. E. and Buckton, G., The application of near infrared spectroscopy and dynamic vapor sorption to quantify low amorphous contents of crystalline lactose, Pharm. Res., 18 (2001a) 112-116.

Hogan, S. E. and Buckton, G., Water sorption/desorption-near IR and calorimetric study of crystalline and amorphous raffinose, Int. J. Pharm., 227 (2001b) 57-69.

Houzego, P., Deaggredation mechanisms in dry powder inhalers (DPIs), Drug Del. Systems & Sci., 2 (2002) 81-85.

ICH, (International Conference on Harmonisation) Guideline Specification Q1A(R2), Step 4, Draft, Stability testing of new drug substances and products, (2003).

ICH, (International Conference on Harmonisation) Guideline Specification Q6A, Step 3, Draft, Decision tree: investigating the need to set acceptance criteria for polymorphism in drug substances and drug products, (1997).

Iida, K., Hayakawa, Y., Okamoto, H., Danjo, K. and Leuenberger, H., Evaluation of flow properties of dry powder inhalation of salbutamol sulfate with lactose carrier, Chem. Pharm. Bull., 49 (2001) 1326-1330.

Ilari, J. L. and Graindogre, P., Study of interactions of particles in a binary mix of dairy and egg powders and glidants, First International Symposium on Spray Drying of Milk Products, Rennes, France, (2001).

Japanese Pharmacopoeia, Thirteenth Edition, (2003).

Jashnani, R. N. and Byron, P. R., Dry powder aerosol generation in different environments: performance comparisons of albuterol, albuterol sulfate, albuterol adipate and albuterol stearate, Int. J. Pharm., 130 (1996) 13-24.

Jashnani, R. N., Byron, P. R. and Dalby, R. N., Testing of dry powder aerosol formulations in different environmental conditions, Int. J. Pharm., 113 (1995) 123-130.

Jashnani, R. N., Dalby, R. N. and Byron, P. R., Preparation, characterization, and dissolution kinetics of two novel albuterol salts, J. Pharm. Sci., 82 (1993) 613-616.

Jenckel, E. and Heusch, R., Die Erniedrigung der Einfriertemperatur organischer Gläser durch Lösungsmittel, Kolloid Z., 130 (1953) 89-105.

Jerussi, T. P. and Senanayake, C., (S,R)-Formoterol methods and compositions, United States Patent 6303145, (2001).

Kacuráková, M. and Mathlouthi, M., FTIR and laser-Raman spectra of oligosaccharides in water: characterization of the glycosidic bond, Carbohydr. Res., 284 (1996) 145-157.

Kajiwara, K., Franks, F., Echlin, P. and Greer, A. L., Structural and dynamic properties of crystalline and amorphous phases in raffinose-water mixtures, Pharm. Res., 16 (1999) 1441-1448.

Kamat, M. S., Lodder, R. A. and DeLuca, P. P., Near-infrared spectroscopic determination of residual moisture in lyophilized sucrose through intact glass vials, Pharm. Res., 6 (1989) 961-965.

Kaneda, Y., Tsutsumi, Y., Yoshioka, Y., Kamada, H., Yamamoto, Y., Kodaira, H., Tsunoda, S., Okamoto, T., Mukai, Y., Shibata, H., Nakagawa, S. and Mayumi, T., The use of PVP as a polymeric carrier to improve the plasma half-life of drugs, Biomaterials, 25 (2004) 3259-3266.

Kanig, G., Zür Theorie der Glastemperatur von Polymerhomologen, Copolymeren und weichgemachten Polymeren, Kolloid Z. Z. Polym., 190 (1963) 1-16.

Katzung, B. G., Basic and clinical pharmacology, New York London, McGraw-Hill, (2001).

Kawashima, Y., Serigano, T., Hino, T., Yamamoto, H. and Takeuchi, H., Effect of surface morphology of carrier lactose on dry powder inhalation property of pranlukast hydrate, Int. J. Pharm., 172 (1998a) 179-188.

Kawashima, Y., Serigano, T., Hino, T., Yamamoto, H. and Takeuchi, H., Design of inhalation dry powder of pranlukast hydrate to improve dispersibility by the surface modification with light anhydrous silicic acid (AEROSIL 200), Int. J. Pharm., 173 (1998b) 243-251.

Keller, M. and Müller-Weltz, R., Dry powder for inhalation, United States Patent 6654566B1, (2003).

Kets, E. P. W., Ijpelaar, P. J., Hoekstra, F. A. and Vromans, H., Citrate increases glass transition temperature of vitrified sucrose preparations, Cryobiology, 48 (2004) 46-54.

Khougaz, K. and Clas, S. D., Crystallization inhibition in solid dispersions of MK-0591 and poly(vinylpyrrolidone) polymers, J. Pharm. Sci., 89 (2000) 1325-1334.

Kindratenko, V. V., Van Eespen, P. J. M., Treiger, B. A. and Van Grieken, R. E., Fractal dimensional classification of aerosol particles by computer-controlled scanning electron microscopy, Environ. Sci. Technol., 28 (1994) 2197-2202.

Kinnarinen, T., Jarho, P., Järvinen, K. and Järvinen, T., Pulmonary deposition of a budesonide/gamma-cyclodextrin complex in vitro, J. Control. Release., 90 (2003) 197-205.

Kirsch, L., Zhang, S., Muangsiri, W., Redmon, M., Luner, P. and Wurster, D., Development of a lyophilized formulation for (R,R)-formoterol (L)-tartrate, Drug Dev. Ind. Pharm., 27 (2001) 89-96.

Klug, H. P. and Alexander, L. E., X-ray diffraction procedures for polycrystalline and amorphous materials, Wiley Interscience, 2nd edition, (1974).

Kuo, S. W. and Chang, F. C., Studies of miscibility behavior and hydrogen bonding in blends of poly(vinylphenol) and poly(vinylpyrrolidone), Macromolecules, 34 (2001) 5224-5228.

Kuo, S.-W., Xu, H., Huang, C.-F. and Chang, F.-C., Significant glass-transition-temperature increase through hydrogen-bonded copolymers, J. Polym. Sci. Pol. Phys., 40 (2002) 2313-2323.

Kwei, T. K., The effect of hydrogen bonding on the glass transition temperatures of polymer mixtures, J. Polym. Sci. Pol. Lett., 22 (1984) 307-313.

Kwei, T. K., Pearce, E. M., Pennacchia, J. R. and Charton, M., Correlation between the glass transition temperature of polymer mixtures and intermolecular force parameters, Macromolecules, 20 (1987) 1174-1176.

Labiris, N. R. and Dolovich, M. B., Pulmonary drug delivery. Part I: Physiological factors affecting therapeutic effectiveness of aerosolized medications, Br. J. Clin. Pharmacol., 56 (2003a) 588-599.

Labiris, N. R. and Dolovich, M. B., Pulmonary drug delivery. Part II: The role of inhalant delivery devices and drug formulations in therapeutic effectiveness of aerosolized medications, Br. J. Clin. Pharmacol., 56 (2003b) 600-612.

Laidler, K. J (ed.), Chemical kinetics, Harper & Row, (1987).

Laskar, P. A. and Ayres, J. W., Degradation of carmustine in mixed solvent and nonaqueous media, J. Pharm. Sci., 66 (1977) 1076-1078.

Lechuga-Ballesteros, D., Bakri, A. and Miller, D. P., Microcalorimetric measurement of the interactions between water vapor and amorphous pharmaceutical solids, Pharm. Res., 20 (2003) 308-318.

Lee, S., Rao, S. P., Moon, M. H. and Giddings, J. C., Determination of mean diameter and particle size distribution of acrylate latex using flow field-flow fractionation, photon correlation spectroscopy, and electron microscopy, Anal. Chem., 68 (1996) 1545-1549.

Leuner, C. and Dressman, J., Improving drug solubility for oral delivery using solid dispersions, Eur. J. Pharm. Biopharm., 50 (2000) 47-60.

Lewis, D., Ganderton, D., Meakin, B., Brambilla, G. and Ferraris, A., Stable pharmaceutical solution formulations for pressurised metered dose inhalers, European Patent 1157689A1, (2001).

Li, R., D'Souza, A. J., Schowen, R. L., Borchardt, R. T., Topp, E. M. and Laird, B. B., Effects of solution polarity and viscosity on peptide deamidation, J. Pept. Res., 56 (2000) 326-334.

Lu, Y., Deng, G. C., Miao, F. M. and Li, Z. M., Sugar complexation with calcium ion. Crystal structure and FT-IR study of a hydrated calcium chloride complex of D-ribose, J. Inorg. Biochem., 96 (2003) 487-492.

Mälkki, L. and Tammilehto, S., Decomposition of salbutamol in aqueous solutions. I. The effect of pH, temperature and drug concentration, Int. J. Pharm., 63 (1990) 17-22.

Mälkki, L., Purra, K., Kähkönen, K. and Tammilehto, S., Decomposition of salbutamol in aqueous solutions. II. The effect of buffer species, pH, buffer concentration and antioxidants, Int. J. Pharm., 117 (1995) 189-195.

Martonen, T. B. and Katz, I. M., Deposition patterns of aerosolized drugs within human lungs: effects of ventilatory parameters, Pharm. Res., 10 (1993) 871-878.

Martin, A., Physical pharmacy, 4th edition, Lea & Febiger (1993).

Masters, K., Spray drying handbook, 4th edition, Bath, The Pitman Press, (1985).

Masters, K., Foodstuffs - Where spray drying plays a role, Chem. Eng. London, (1980) 145-148.

Matsumoto, T. and Zografi, G., Physical properties of solid molecular dispersions of indomethacin with poly(vinylpyrrolidone) and poly(vinylpyrrolidone-co-vinyl-acetate) in relation to indomethacin crystallization, Pharm. Res., 16 (1999) 1722-1728.

Maury, M., Murphy, K., Kumar, S., Shi, L. and Lee, G., Effects of process variables on the powder yield of spray-dried trehalose on a laboratory spray-dryer, Eur. J. Pharm. Biopharm., 59 (2005) 565-573.

McDonald, K. J. and Martin, G. P., Transition to CFC-free metered dose inhalers - into the new millennium, Int. J. Pharm., 201 (2000) 89-107.

McGregor, C., Saunders, M. H., Buckton, G. and Saklatvala, R. D., The use of high-speed differential scanning calorimetry (Hyper-DSC™) to study the thermal properties of carbamazepine polymorphs, Thermochim. Acta, 417 (2004) 231-237.

Meoli, A., Gagnoni, A. and Vanossi, S., Inhalatory compositions of formoterol, United States Patent 671994, (2004).

Meyers, R. A. (ed.), Encyclopaedia of analytical chemistry: applications, theory and instrumentation, Chichester, John Wiley, (2000).

Miller, D. P. and de Pablo, J. J., Calorimetric solution properties of simple saccharides and their significance for the stabilization of biological structure and function, J. Phys. Chem. B, 104 (2000) 8876-8883.

Miller, N. C., Marple, V. A., Schultz, R. K. and Poon, W. S., Assessment of the twin impinger for size measurement of metered-dose inhaler sprays, Pharm. Res., 9 (1992) 1123-1127.

Miller, T. A. and York, P., Pharmaceutical tablet lubrication, Int. J. Pharm., 41 (1988) 1-19.

Mohr, W. and Endres-Klein, R., Do polyvinylpyrrolidone (PVP) deposits still occur in internal organs at the turn of the millennium? Observations on three patients from the former USSR, Der Pathologie, 23 (2002) 386-388.

Mura, P., Manderioli, A., Bramanti, G. and Ceccarelli, L., Properties of solid dispersions of naproxen in various polyethylene glycols, Drug Dev. Ind. Pharm., 22 (1996) 909-916.

Murakami, M., Takahashi, K., Mase, T., Murase, K., Ida, H. and Urawa, S., α-Aminomethylbenzylalkoholderivate, German Patent 2305092, (1973).

Naini, V., Byron, P. R. and Phillips, E. M., Physicochemical stability of crystalline sugars and their spray-dried forms: dependence upon relative humidity and suitability for use in powder inhalers, Drug Dev. Ind. Pharm., 24 (1998) 895-909.

Nair, B., Final report on the safety assessment of polyvinylpyrrolidone (PVP), Int. J. Toxicol., 17 (1998) 95-130.

Nair, R., Nyamweya, N., Gönen, S., Martinez-Miranda, L. J. and Hoag, S. W., Influence of various drugs on the glass transition temperature of poly(vinylpyrrolidone): a thermodynamic and spectroscopic investigation, Int. J. Pharm., 225 (2001) 83-96.

Nernst, W. and Brunner, E., Theorie der Reaktionsgeschwindigkeit in heterogenen Systemen, A. Phys. Chem., 47 (1904) 56-102.

Newhouse, M. T., Hirst, P. H., Duddu, S. P., Walter, Y. H., Tarara, T. E., Clark, A. R. and Weers, J. G., Inhalation of a dry powder tobramycin PulmoSphere formulation in healthy volunteers, Chest, 124 (2003) 360-366.

Nikfar, F., Forbes, S. J., Mooney, K. G. and Carstensen, J. T., The effect of buffer hydrates on solid state decomposition in the presence of moisture. I. Decomposition of calcium D,L-leucovorin in the solid state in the presence of citrate buffers, Pharm. Res., 7 (1990) S182.

Nyamweya, N. and Hoag, S. W., Assessment of polymer-polymer interactions in blends of HPMC and film forming polymers by modulated temperature differential scanning calorimetry, Pharm. Res., 17 (2000) 625-631.

Nyqvist, H., Saturated salt solutions for maintaining specified relative humidities, Int. J. Pharm. Tech. & Prod. Mfr., 4 (1983) 47-48.

Oakley, D. E., Produce uniform particles by spray drying, Chem. Eng. Prog., 93 (1997) 48-54.

Ochsner, M., Jaekel, K., Mutz, M., Anderson, G. P. and John, E., Comparative biophysical analysis of the interaction of bronchodilating beta$_2$-adrenoceptor agonists with lipid membranes, Eur. J. Med. Chem., 34 (1999) 451-462.

Ohtake, S., Schebor, C., Palecek, S. P. and de Pablo, J. J., Effect of pH, counter ion, and phosphate concentration on the glass transition temperature of freeze-dried sugar-phosphate mixtures, Pharm. Res., 21 (2004) 1615-1621.

Oksanen, C. A. and Zografi, G., Molecular mobility in mixtures of absorbed water and solid poly(vinylpyrrolidone), Pharm. Res., 10 (1993) 791-799.

Oliver, M. J., Paling, S. G., Jinks, P. A. and Jaiswal, S. K., Medicinal aerosol formulations of formoterol, United States Patent 6054488, (2000).

Palmqvist, M., Arvidsson, P., Beckman, O., Peterson, S. and Lötvall, J., Onset of bronchodilation of budesonide/formoterol vs. salmeterol/fluticasone in single inhalers, Pulm. Pharmacol. Ther., 14 (2001) 29-34.

Papadakis, S. E. and Bahu, R. E., The sticky issues of drying, Dry.Technol., 10 (1992) 817-837.

Patai, S. and Rappaport, Z., The chemistry of sulphonic acids, esters and their derivatives, John Wiley & Sons, Chichester, (1991).

Patist, A. and Zoerb, H., Preservation mechanisms of trehalose in food and biosystems, Colloid Surf. B-Biointerfaces, 40 (2005) 107-113.

Patton, J. S., Mechanisms of macromolecule absorption by the lungs, Adv. Drug Deliv. Rev., 19 (1996) 3-36.

Perrin, D. D. and Dempsey, B. (eds.), Buffers for pH and metal ion control, London, Chapman and Hall, (1974).

Phadnis, N. V. and Suryanarayanan, R., Simultaneous quantification of an enantiomer and the racemic compound of ibuprofen by X-ray powder diffractometry, Pharm. Res., 14 (1997) 1176-1180.

Phadnis, N. V., Cavatur, R. K. and Suryanarayanan, R., Identification of drugs in pharmaceutical dosage forms by X-ray powder diffractometry, J. Pharm. Biomed. Anal., 15 (1997) 929-943.

Pham, S. and Wiedmann, T. S., Dissolution of aerosol particles of budesonide in Survanta™, a model lung surfactant, J. Pharm. Sci., 90 (2001) 98-104.

Phipps, M. A. and Mackin, L. A., Application of isothermal microcalorimetry in solid state drug development, Pharm. Sci. Technol. Today, 3 (2000) 9-17.

Pinsuwan, S., Alvarez-Núñez, F. A., Tabibi, E. S. and Yalkowsky, S. H., Degradation kinetics of 4-dedimethylamino sancycline, a new anti-tumor agent, in aqueous solutions, Int. J. Pharm., 181 (1999) 31-40.

Podczeck, F., Evaluation of the adhesion properties of salbutamol sulphate to inhaler materials, Pharm. Res., 15 (1998) 806-808.

Porubcan, L. S., Serna, C. J., White, J. L. and Hem, S. L., Mechanism of adsorption of clindamycin and tetracycline by montmorillonite, J. Pharm. Sci., 67 (1978) 1081-1087.

Prime, D., Atkins, P. J., Slater, A. and Sumby, B., Review of dry powder inhalers, Adv. Drug Deliv. Rev., 26 (1997) 51-58.

Prinn, K. B., Costantino, H. R. and Tracy, M., Statistical modelling of protein spray drying at the lab scale, AAPS PharmSciTech, 3 (2002) E4.

Purewal, T. S. and Greenleaf, D. J., Medicinal aerosol formulations, United States Patent 5605674, (1995).

Rajala, R. and Laine, E., The Effect of moisture on the structure of magnesium stearate, Thermochim. Acta, 248 (1995) 177-188.

Rajewski, R. A. and Stella, V. J., Pharmaceutical applications of cyclodextrins. 2. In vivo drug delivery, J. Pharm. Sci., 85 (1996) 1142-1169.

Ramalhete, N., Evaluation of freeze-drying and spray-drying as methods of preparing a salbutamol-HP-β-cyclodextrin complex for dry powder inhalation, 11th International Cyclodextrin Symposium, Reykjavik, Iceland (2002).

Roos, Y. H., Phase transitions in foods, Academic Press, (1995).

Roos, Y. H. and Karel, M., Phase transitions of mixtures of amorphous polysaccharides and sugars, Biotechnol. Prog., 7 (1991) 49-53.

Roth, M., Johnson, P. R. A., Rudiger, J. J., King, G. G., Ge, Q., Burgess, J. K., Anderson, G., Tamm, M. and Black, J. L., Interaction between glucocorticoids and β_2 agonists on bronchial airway smooth muscle cells through synchronised cellular signalling, Lancet, 360 (2002) 1293-1299.

Rowe, R. C., Binder-substrate interactions in tablets: a theoretical approach based on solubility parameters, Acta Pharm.Technol., 34 (1988) 144-146.

Rowley, G., Quantifying electrostatic interactions in pharmaceutical solid systems, Int. J. Pharm., 227 (2001) 47-55.

Saleki-Gerhardt, A., Ahlneck, C. and Zografi, G., Assessment of disorder in crystalline solids, Int. J. Pharm., 101 (1994) 237-247.

Saleki-Gerhardt, A., Stowell, J. G., Byrn, S. R. and Zografi, G., Hydration and dehydration of crystalline and amorphous forms of raffinose, J. Pharm. Sci., 84 (1995) 318-323.

Sanyude, S., Locock, R. A. and Pagliaro, L. A., Stability of aspartame in water-organic solvent mixtures with different dielectric constants, J. Pharm. Sci., 80 (1991) 674-676.

Saunders, M., Podluii, K., Shergill, S., Buckton, G. and Royall, P., The potential of high speed DSC (Hyper-DSC) for the detection and quantification of small amounts of amorphous content in predominantly crystalline samples, Int. J. Pharm., 274 (2004) 35-40.

Schneider, H. A., Conformational entropy contributions to the glass temperature of blends of miscible polymers, J. Res. Natl. Inst. Stand. Technol., 102 (1997) 229-248.

Schneider, H. A., Glass transition behaviour of compatible polymer blends, Polymer, 30 (1989) 771-779.

Serajuddin, A. T. M., Solid dispersion of poorly water-soluble drugs: early promises, subsequent problems, and recent breakthroughs, J. Pharm. Sci., 88 (1999) 1058-1066.

Sekizaki, H., Danjo, K., Eguchi, H., Yonezawa, Y., Sunada, H. and Otsuka, A., Solid-state interaction of ibuprofen with polyvinylpyrrolidone, Chem. Phar. Bull., 43 (1995) 988-993.

Shah, J. C., Chen, J. R. and Chow, D., Preformulation study of etoposide: II. Increased solubility and dissolution rate by solid-solid dispersions, Int. J. Pharm., 113 (1995) 103-111.

Shamblin, S. L., Taylor, L. S. and Zografi, G., Mixing behavior of colyophilized binary systems, J. Pharm. Sci., 87 (1998) 694-701.

Simha, R. and Boyer, R. F., On a general relation involving the glass temperature and coefficients of expansion of polymers, J. Chem. Phys., 37 (1962) 1003-1007.

Simonelli, A. P., Mehta, S. C. and Higuchi, W. I., Dissolution rates of high energy polyvinylpyrrolidone (PVP)-sulfathiazole coprecipitates, J. Pharm. Sci., 58 (1969) 538-549.

Sjökvist, E., Nyström, C., Aldén, M. and Caram-Lelham, N., Physicochemical aspects of drug release. XIV. The effects of some ionic and non-ionic surfactants on properties of a sparingly soluble drug in solid dispersions, Int. J. Pharm., 79 (1992) 123-133.

Smith, I. J., Developments in inhalation technology, Drug Dev. Systems & Sci., 2 (2002) 63-65.

Smyth, H. D. C. and Hickey, A. J., Multimodal particle size distributions emitted from HFA-134a solution pressurized metered-dose inhalers, AAPS PharmSciTech, 4 (2003) E38.

Socrates, G., Infrared and Raman characteristic group frequencies, Chichester, John Wiley & Sons, (2001).

Song, Y., Schowen, R. L., Borchardt, R. T. and Topp, E. M., Effect of 'pH' on the rate of asparagine deamidation in polymeric formulations: 'pH'-rate profile, J. Pharm. Sci., 90 (2001) 141-156.

Srichana, T., Suedee, R. and Reanmongkol, W., Cyclodextrin as a potential drug carrier in salbutamol dry powder aerosols: the in-vitro deposition and toxicity studies of the complexes, Respir. Med., 95 (2001) 513-519.

Ståhl, K., Claesson, M., Lilliehorn, P., Lindén, H. and Bäckström, K., The effect of process variables on the degradation and physical properties of spray dried insulin intended for inhalation, Int. J. Pharm., 233 (2002) 227-237.

Steckel, H. and Bolzen, N., Alternative sugars as potential carriers for dry powder inhalations, Int. J. Pharm., 270 (2004) 297-306.

Steckel, H. and Brandes, H. G., A novel spray-drying technique to produce low density particles for pulmonary delivery, Int. J. Pharm., 278 (2004) 187-195.

Steckel, H. and Müller, B. W., In vitro evaluation of dry powder inhalers. I. Drug deposition of commonly used devices, Int. J. Pharm., 154 (1997) 19-29.

Steckel, H. and Wehle, S., A novel formulation technique for metered dose inhaler (MDI) suspensions, Int. J. Pharm., 284 (2004) 75-82.

Steckel, H., Thies, J. and Müller, B. W., Micronizing of steroids for pulmonary delivery by supercritical carbon dioxide, Int. J. Pharm., 152 (1997) 99-110.

Stefely, J. S., Novel excipients for inhalation drug delivery: expanding the capability of the MDI, Drug Del. Technol., 6 (2002).

Strickley, R. G. and Anderson, B. D., Solid-state stability of human insulin. I. Mechanism and the effect of water on the kinetics of degradation in lyophiles from pH 2-5 solutions, Pharm. Res., 13 (1996) 1142-1153.

Suami, T., Otake, T., Nishimura, T. and Ikeda, T., Synthesis of raffinose and an isomer, Carbohydr. Res., 26 (1973) 234-239.

Surana, R., Pyne, A. and Suryanarayanan, R., Effect of preparation method on physical properties of amorphous trehalose, Pharm. Res., 21 (2004) 1167-1176.

Sussich, F., Bortoluzzi, S. and Cesàro, A., Trehalose dehydration under confined conditions, Thermochim. Acta, 391 (2002) 137-150.

Talja, R. A. and Roos, Y. H., Phase and state transition effects on dielectric, mechanical, and thermal properties of polyols, Thermochim. Acta, 380 (2001) 109-121.

Tang, X. C., Pikal, M. J. and Taylor, L. S., The effect of temperature on hydrogen bonding in crystalline and amorphous phases in dihydropyridine calcium channel blockers, Pharm. Res., 19 (2002a) 484-490.

Tang, X. C., Pikal, M. J. and Taylor, L. S., A spectroscopic investigation of hydrogen bond patterns in crystalline and amorphous phases in dihydropyridine calcium channel blockers, Pharm. Res., 19 (2002b) 477-483.

Tarara, T. E., Hartman, M. S., Gill, H., Kennedy, A. A. and Weers, J. G., Characterization of suspension-based metered dose inhaler formulations composed of spray-dried budesonide microcrystals dispersed in HFA-134a, Pharm. Res., 21 (2004) 1607-1614.

Taylor, L. S. and Zografi, G., Spectroscopic characterization of interactions between PVP and indomethacin in amorphous molecular dispersions, Pharm. Res., 14 (1997) 1691-1698.

Taylor, L. S. and Zografi, G., Sugar-polymer hydrogen bond interactions in lyophilized amorphous mixtures, J. Pharm. Sci., 87 (1998a) 1615-1621.

Taylor, L. S. and Zografi, G., The quantitative analysis of crystallinity using FT-Raman spectroscopy, Pharm. Res., 15 (1998b) 755-761.

Teraoka, R., Otsuka, M. and Matsuda, Y., Effects of temperature and relative humidity on the solid-state chemical stability of ranitidine hydrochloride, J. Pharm. Sci., 82 (1993) 601-604.

Timko, R. J. and Lordi, N. G., Thermal analysis studies of glass dispersion systems, Drug Dev. Ind. Pharm., 10 (1984) 425-451.

Timsina, M. P., Martin, G. P., Marriott, C., Ganderton, D. and Yianneskis, M., Drug delivery to the respiratory tract using dry powder inhalers, Int. J. Pharm., 101 (1994) 1-13.

Todo, H., Okamoto, H., Iida, K. and Danjo, K., Improvement of stability and absorbability of dry insulin powder for inhalation by powder-combination technique, Int. J. Pharm., 271 (2004) 41-52.

Trofast, E., Process of producing a stable pharmaceutical composition containing micronized formoterol, World Patent 0189491A1, (2001).

Ueno, Y., Yonemochi, E., Tozuka, Y., Yamamura, S., Oguchi, T. and Yamamoto, K., Characterization of amorphous ursodeoxycholic acid prepared by spray-drying, J. Pharm. Pharmacol., 50 (1998) 1213-1219.

United States Pharmacopeia 28, United States Pharmacopeial Convention, Rockville, Maryland (2005).

Usui, F., Maeda, K., Kusai, A., Nishimura, K. and Keiji, Y., Inhibitory effects of water-soluble polymers on precipitation of RS-8359, Int. J. Pharm., 154 (1997) 59-66.

Van den Mooter, G., Wuyts, M., Blaton, N., Busson, R., Grobet, P., Augustijns, P. and Kinget, R., Physical stabilisation of amorphous ketoconazole in solid dispersions with polyvinylpyrrolidone K25, Eur. J. Pharm. Sci., 12 (2001) 261-269.

van Krevelen, D. W., Properties of polymers: their correlation with chemical structure, their numerical estimation and prediction from additive group contribution, 3rd ed., Amsterdam, Elsevier, (1990).

Vanbever, R., Mintzes, J. D., Wang, J., Nice, J., Chen, D. H., Batycky, R., Langer, R. and Edwards, D. A., Formulation and physical characterization of large porous particles for inhalation, Pharm. Res., 16 (1999) 1735-1742.

Vaswani, S. K. and Creticos, P. S., Metered dose inhaler: past, present, and future, Ann. Allergy Asthma Immunol., 80 (1998) 11-19.

Velaga, S. P., Berger, R. and Carlfors, J., Supercritical fluids crystallization of budesonide and flunisolide, Pharm. Res., 19 (2002) 1564-1571.

Verreck, G., Six, K., Van den Mooter, G., Baert, L., Peeters, J. and Brewster, M. E., Characterization of solid dispersions of itraconazole and hydroxypropylmethylcellulose prepared by melt extrusion - part I, Int. J. Pharm., 251 (2003) 165-174.

Vervaet, C. and Byron, P. R., Drug-surfactant-propellant interactions in HFA-formulations, Int. J. Pharm., 186 (1999) 13-30.

Viana, M., Jouannin, P., Pontier, C. and Chulia, D., About pycnometric density measurements, Talanta, 57 (2002) 583-593.

Vidgren, M. T., Vidgren, P. A. and Paronen, T. P., Comparison of physical and inhalation properties of spray-dried and mechanically micronized disodium cromoglycate, Int. J. Pharm., 35 (1987) 139-144.

Voss, A. and Finlay, W. H., Deagglomeration of dry powder pharmaceutical aerosols, Int. J. Pharm., 248 (2002) 39-50.

Wada, Y. and Matsubara, T., Pseudopolymorphism and crystalline transition of magnesium stearate, Thermochim. Acta, 196 (1992) 63-84.

Wade, L. G., Organic chemistry, London, Prentice-Hall International, (1991).

Wade, A., Weller, P. J. (eds.), Handbook of pharmaceutical excipients, The Pharmaceutical Press, London, (1994).

Wakisaka, A., Komatsu, S. and Usui, Y., Solute-solvent and solvent-solvent interactions evaluated through clusters isolated from solutions: Preferential solvation in water-alcohol mixtures, J. Mol. Liq., 90 (2001) 175-184.

Wall, D. A., Marcello, J., Pierdomenico, D. and Farid, A., Administration as hydroxypropyl β-cyclodextrin complexes does not slow rates of pulmonary drug absorption in rat, S.T.P. Pharma Sciences, 4 (1994) 63-68.

Walther, M., Fischer, B. M. and Uhd Jepsen, P., Noncovalent intermolecular forces in polycrystalline and amorphous saccharides in the far infrared, Chem. Phys. 288 (2003) 261-268.

Wan, L. S. C., Heng, P. W. S. and Chia, C. G. H., Citric acid as a plasticizer for spray-dried microcapsules, J. Microencapsul., 10 (1993) 11-23.

Watanabe, T., Wakiyama, N., Usui, F., Ikeda, M., Isobe, T. and Senna, M., Stability of amorphous indomethacin compounded with silica, Int. J. Pharm., 226 (2001) 81-91.

Weuts, I., Kempen, D., Decorte, A., Verreck, G., Peeters, J., Brewster, M. and Van den Mooter, G., Phase behaviour analysis of solid dispersions of loperamide and two structurally related compounds with the polymers PVP-K30 and PVP-VA64, Eur. J. Pharm. Sci., 22 (2004) 375-385.

Weuts, I., Kempen, D., Verreck, G., Decorte, A., Heymans, K., Peeters, J., Brewster, M. and Van den Mooter, G., Study of the physicochemical properties and stability of solid dispersions of loperamide and PEG 6000 prepared by spray drying, Eur. J. Pharm. Sci., 59 (2005) 119-126.

Williams, R. O. and Liu, J., Formulation of a protein with propellant HFA 134a for aerosol delivery, Eur. J. Pharm. Sci., 7 (1998) 137-144.

Williams, R. O. and Liu, J., Influence of formulation technique for hydroxypropyl-β-cyclodextrin on the stability of aspirin in HFA 134a, Eur. J. Pharm. Biopharm., 47 (1999) 145-152.

Williams, R. O., Barron, M. K., Alonso, M. J. and Remuñán-López, C., Investigation of a pMDI system containing chitosan microspheres and P134a, Int. J. Pharm., 174 (1998) 209-222.

Williams, R. O., Liu, J. and Koleng, J. J., Influence of metering chamber volume and water level on the emitted dose of a suspension-based pMDI containing propellant 134a, Pharm. Res., 14 (1997) 438-443.

Wolkers, W. F., Oldenhof, H., Alberda, M. and Hoekstra, F. A., A Fourier transform infrared microspectroscopy study of sugar glasses: application to anhydrobiotic higher plant cells, Biochim. Biophys. Acta-Gen. Subj., 1379 (1998) 83-96.

Wolkers, W. F., Oliver, A. E., Tablin, F. and Crowe, J. H., A Fourier-transform infrared spectroscopy study of sugar glasses, Carbohydr. Res., 339 (2004) 1077-1085.

Wu, H. D., Wu, S. C., Wu, I. D. and Chang, F. C., Novel determination of the crystallinity of syndiotactic polystyrene using FTIR spectrum, Polymer, 42 (2001) 4719-4725.

Yamaguchi, T., Nishimura, M., Okamoto, R., Takeuchi, T. and Yamamoto, K., Glass formation of 4"-O-(4-methoxyphenyl) acetyltylosin and physicochemical stability of the amorphous solid, Int. J. Pharm., 85 (1992) 87-96.

Yamamura, S. and Rogers, J. A., Characterization and dissolution behavior of nifedipine and phosphatidylcholine binary systems, Int. J. Pharm., 130 (1996) 65-73.

Yamashita, K., Nakate, T., Okimoto, K., Ohike, A., Tokunaga, Y., Ibuki, R., Higaki, K. and Kimura, T., Establishment of new preparation method for solid dispersion formulation of tacrolimus, Int. J. Pharm., 267 (2003) 79-91.

Yoshinari, T., Forbes, R. T., York, P. and Kawashima, Y., The improved compaction properties of mannitol after a moisture-induced polymorphic transition, Int. J. Pharm., 258 (2003) 121-131.

Yoshioka, M., Hancock, B. C. and Zografi, G., Inhibition of indomethacin crystallization in poly(vinylpyrrolidone) coprecipitates, J. Pharm. Sci., 84 (1995) 983-986.

Yu, L., Amorphous pharmaceutical solids: preparation, characterization and stabilization, Adv. Drug Del. Rev., 48 (2001) 27-42.

Yu, L., Mishra, D. S. and Rigsbee, D. R., Determination of the glass properties of D-mannitol using sorbitol as an impurity, J. Pharm. Sci., 87 (1998a) 774-777.

Yu, L., Reutzel, S. M. and Stephenson, G. A., Physical characterization of polymorphic drugs: an integrated characterization strategy, Pharm. Sci. Technol. Today, 1 (1998b) 118-127.

Zeng, X. M., Martin, G. P., Tee, S. K. and Marriott, C., The role of fine particle lactose on the dispersion and deaggregation of salbutamol sulphate in an air stream in vitro, Int. J. Pharm., 176 (1998) 99-110.

Zeng, X. M., Martin, G. P. and Marriott, C., Particulate interactions in dry powder formulations for inhalation, London, Taylor and Francis, (2001).

Zetterström, O., Buhl, R., Mellem, H., Perpiñá, M., Hedman, J., O'Neill, S. and Ekström, T., Improved asthma control with budesonide/formoterol in a single inhaler, compared with budesonide alone, Eur. Resp. J., 18 (2001) 262-268.

Zhang, J. and Zografi, G., Water vapor absorption into amorphous sucrose-poly(vinyl pyrrolidone) and trehalose-poly(vinyl pyrrolidone) mixtures, J. Pharm. Sci., 90 (2001) 1375-1385.

APPENDICES

APPENDIX I

Table 1 Spray drying conditions for the salbutamol base/excipient systems. Systems were prepared using mixtures of ethanol and deionised water. The lactose used in the preparation of all solutions for spray drying was lactose monohydrate and trehalose used was trehalose dihydrate.

System	Inlet temperature (°C)	Outlet temperature (°C)	Aspirator (%)	Airflow rate (Nl/h)	Pump rate (%)
Salbutamol base/lactose 10% containing 10% lactose by weight of total solids spray dried as a 1.25% w/v solution from 65% (v/v) ethanol	78	57-58	100	500	20
Salbutamol base/lactose 50% containing 50% lactose by weight of total solids spray dried as a 0.42% w/v solution from 69% (v/v) ethanol	78	42-44	70	500	22
Salbutamol base/trehalose 10% containing 10% trehalose by weight of total solids spray dried as a 1.36% w/v solution from 75% (v/v) ethanol	78-79	53-55	100	500	20
Salbutamol base/trehalose 50% containing 50% trehalose by weight of total solids spray dried as a 0.41% w/v solution from 68% (v/v) ethanol	78	43-45	70	500	20
Salbutamol base/maltodextrin 10% containing 10% maltodextrin by weight of total solids spray dried as a 1.15% w/v solution from 46% (v/v) ethanol	90	52-55	100	500	20
Salbutamol base/PVP 10000 10% containing 10% PVP 10000 by weight of total solids spray dried as a 2% w/v solution from 95% (v/v) ethanol	78	60	100	500	10
Salbutamol base/PVP 10000 30% containing 30% PVP 10000 by weight of total solids spray dried as a 2% w/v solution from 95% (v/v) ethanol	78	47-50	70	500	30
Salbutamol base/PVP 10000 50% containing 50% PVP 10000 by weight of total solids spray dried as a 2% w/v solution from 95% (v/v) ethanol	78	60	100	500	15
Salbutamol base/PVP 10000 70% containing 70% PVP 10000 by weight of total solids spray dried as a 2% w/v solution from 95% (v/v) ethanol	78	49-51	70	500	30
Salbutamol base/PVP 10000 90% containing 90% PVP 10000 by weight of total solids spray dried as a 2% w/v solution from 95% (v/v) ethanol	78	48-51	70	500	30

Table 2 Spray drying conditions for the formoterol fumarate (FF) and FF/excipient systems. Systems were prepared using mixtures of ethanol and deionised water. The formoterol fumarate used in the preparation of all solutions was formoterol fumarate dihydrate, trehalose used was trehalose dihydrate and raffinose used was raffinose pentahydrate.

System	Inlet temperature (°C)	Outlet temperature (°C)	Aspirator (%)	Airflow rate (Nl/h)	Pump rate (%)
FF spray dried as 0.2% w/v solution from 98% (v/v) ethanol	78-79	50-52	80	500	30
FF/PEG 20000 10% containing 10% PEG 20000 by weight of total solids spray dried as a 0.21% w/v solution from 98% (v/v) ethanol	78-79	49-51	80	500	30
FF/PEG 20000 30% containing 30% PEG 20000 by weight of total solids spray dried as a 0.27% w/v solution from 98% (v/v) ethanol	77-78	52-57	80	500	30
FF/PVP 10000 10% containing 10% PVP 10000 by weight of total solids spray dried as a 0.21% w/v solution from 98% (v/v) ethanol	78	50-54	80	500	25
FF/PVP 10000 30% containing 30% PVP 10000 by weight of total solids spray dried as a 0.27% w/v solution from 98% (v/v) ethanol	78	52-54	80	500	25
FF/trehalose 10% containing 10% trehalose by weight of total solids spray dried as a 0.21% w/v solution from 98% (v/v) ethanol	78	52-54	80	500	25
FF/trehalose 30% containing 30% trehalose by weight of total solids spray dried as a 0.27% w/v solution from 98% (v/v) ethanol	78	52-53	80	500	25
FF/raffinose 10% containing 10% raffinose by weight of total solids spray dried as a 0.21% w/v solution from 98% (v/v) ethanol	78	53-54	80	500	25
FF/raffinose 30% containing 30% raffinose by weight of total solids spray dried as a 0.27% w/v solution from 98% (v/v) ethanol	78	52-54	80	500	25
FF/HP-β-CYC 10% containing 10% HP-β-CYC by weight of total solids spray dried as a 0.21% w/v solution from 98% (v/v) ethanol	78	52-55	80	500	25
FF/HP-β-CYC 30% containing 30% HP-β-CYC by weight of total solids spray dried as a 0.27% w/v solution from 98% (v/v) ethanol	78	52-54	80	500	25

Table 3 Spray drying conditions for the formoterol fumarate (FF)/surfactant systems. Systems were prepared using mixtures of ethanol and deionised water. The formoterol fumarate used in the preparation of all solutions was formoterol fumarate dihydrate.

System	Inlet temperature (°C)	Outlet temperature (°C)	Aspirator (%)	Airflow rate (Nl/h)	Pump rate (%)
FF/Brij 58 0.5% containing 0.5% Brij 58 by weight of total solids spray dried as a 0.19% w/v solution from 98% (v/v) ethanol	78	53-54	80	500	25
FF/Brij 58 2% containing 2% Brij 58 by weight of total solids spray dried as a 0.19% w/v solution from 98% (v/v) ethanol	78	53-54	80	500	25
FF/Myrj 59 0.5% containing 0.5% Myrj 59 by weight of total solids spray dried as a 0.19% w/v solution from 98% (v/v) ethanol	78	54-55	80	500	25
FF/ Myrj 59 2% containing 2% Myrj 59 by weight of total solids spray dried as a 0.19% w/v solution from 98% (v/v) ethanol	78	54-55	80	500	25

Table 4 Spray drying conditions for various excipients. The lactose used in the preparation of a solution for spray drying was lactose monohydrate, trehalose used was trehalose dihydrate and raffinose used was raffinose pentahydrate.

System	Inlet temperature (°C)	Outlet temperature (°C)	Aspirator (%)	Airflow rate (Nl/h)	Pump rate (%)
Lactose spray dried as a 2% w/v solution from deionised water	130	85	100	600	15
PEG 20000 spray dried as a 5% w/v solution from dichloromethane	45	35-36	80	750	10
PVP 10000 spray dried as a 2.5% w/v solution from 95% (v/v) ethanol	78	57	100	600	20
Trehalose spray dried as a 2.5% w/v solution from deionised water	110	75-77	100	600	10
Raffinose spray dried as a 2.5% w/v solution from deionised water	110	77-78	100	600	10
Maltodextrin spray dried as a 2.5% w/v solution from deionised water	120	86	100	600	10

Table 5 Spray drying conditions for budesonide (Bud) and Bud/excipient systems. Systems were prepared using mixtures of ethanol and deionised water. The raffinose used in the preparation of a solution for spray drying was raffinose pentahydrate. Microcrystalline cellulose is abbreviated as m. cellulose.

System	Inlet temperature (°C)	Outlet temperature (°C)	Aspirator (%)	Airflow rate (Nl/h)	Pump rate (%)
Bud spray dried as 1% w/v solution from 95% (v/v) ethanol	77-78	56-57	85	600	15
Bud/raffinose 30% containing 30% raffinose by weight of total solids spray dried as a 1% w/v solution from 71% (v/v) ethanol	78	55	85	600	15
Bud/ HP-β-CYC 30% containing 30% HP-β-CYC by weight of total solids spray dried as a 1% w/v solution from 95% (v/v) ethanol	78	56-58	85	600	15
Bud/stearic acid 1% containing 1% stearic acid by weight of total solids spray dried as a 1% w/v solution from 95% (v/v) ethanol	78	58-59	85	600	15
Bud/stearic acid 2% containing 2% stearic acid by weight of total solids spray dried as a 1% w/v solution from 95% (v/v) ethanol	78	58-59	85	600	15
Bud/stearic acid 5% containing 5% stearic acid by weight of total solids spray dried as a 1% w/v solution from 95% (v/v) ethanol	78	57-58	85	600	15
Bud/stearic acid 10% containing 10% stearic acid by weight of total solids spray dried as a 1% w/v solution from 95% (v/v) ethanol	78	57-58	85	600	15
Bud/stearic acid 5%/PVP 10000 10% containing 5% stearic acid and 10% PVP 10000 by weight of total solids spray dried as a 1% w/v solution from 95% (v/v) ethanol	78	57-58	85	600	15
Bud/Aerosil 5% containing 5% Aerosil by weight of total solids spray dried as a 1% w/v suspension from 95% (v/v) ethanol	78	57-58	85	600	15
Bud/Aerosil 10% containing 10% Aerosil by weight of total solids spray dried as a 1% w/v suspension from 95% (v/v) ethanol	78	58	85	600	15
Bud/ascorbyl palmitate 5% containing 5% ascorbyl palmitate by weight of total solids spray dried as a 1% w/v solution from 95% (v/v) ethanol	78	58	85	600	15
Bud/ascorbyl palmitate 10% containing 10% ascorbyl palmitate by weight of total solids spray dried as a 1% w/v solution from 95% (v/v) ethanol	78	58	85	600	15
Bud/m. cellulose 5% containing 5% m. cellulose by weight of total solids spray dried as a 1% w/v suspension from 95% (v/v) ethanol	78	58	85	600	15
Bud/ m. cellulose 10% containing 10% m. cellulose by weight of total solids spray dried as a 1% w/v suspension from 95% (v/v) ethanol	78	58	85	600	15

Table 6 Spray drying conditions for magnesium stearate and the budesonide (Bud)/magnesium stearate systems. Systems were prepared using mixtures of ethanol and deionised water. Magnesium stearate Élan is abbreviated as Mg.st.E, magnesium stearate Aldrich as Mg.st.A and magnesium stearate RDH as Mg.st.R.

System	Inlet temperature (°C)	Outlet temperature (°C)	Aspirator (%)	Airflow rate (Nl/h)	Pump rate (%)
Mg.St.E spray dried as 0.5% w/v suspension from 95% (v/v) ethanol	78	53-55	85	600	15
Mg.St.A spray dried as 0.5% w/v suspension from 95% (v/v) ethanol	78	57-59	85	600	15
Mg.St.R spray dried as 0.5% w/v suspension from 95% (v/v) ethanol	78	57-58	85	600	15
Bud/ Mg.St.E 1% containing 1% Mg.St.E by weight of total solids spray dried as a 1% w/v suspension from 95% (v/v) ethanol	78	57	85	600	15
Bud/ Mg.St.E 2% containing 2% Mg.St.E by weight of total solids spray dried as a 1% w/v suspension from 95% (v/v) ethanol	78	58	85	600	15
Bud/ Mg.St.E 5% containing 5% Mg.St.E by weight of total solids spray dried as a 1% w/v suspension from 95% (v/v) ethanol	78	57-58	85	600	15
Bud/ Mg.St.E 5%/PVP 10000 10% containing 5% Mg.St.E and 10% PVP 10000 by weight of total solids spray dried as a 1% w/v suspension from 95% (v/v) ethanol	78	57-58	85	600	15
Bud/ Mg.St.A 5% containing 5% Mg.St.A by weight of total solids spray dried as a 1% w/v suspension from 95% (v/v) ethanol	78	57-59	85	600	15
Bud/ Mg.St.A 5%/PVP 10000 10% containing 5% Mg.St.A and 10% PVP 10000 by weight of total solids spray dried as a 1% w/v suspension from 95% (v/v) ethanol	78	57-59	85	600	15
Bud/ Mg.St.R 5% containing 5% Mg.St.R by weight of total solids spray dried as a 1% w/v suspension from 95% (v/v) ethanol	78	57-60	85	600	15
Bud/ Mg.St.R 5%/PVP 10000 10% containing 5% Mg.St.R and 10% PVP 10000 by weight of total solids spray dried as a 1% w/v suspension from 95% (v/v) ethanol	78	57-58	85	600	15

Table 7 Spray drying conditions for the drug/ammonium carbonate and drug/polymer/ammonium carbonate systems. Systems were prepared using mixtures of ethanol and deionised water.

System	Inlet temperature (°C)	Outlet temperature (°C)	Aspirator (%)	Airflow rate (Nl/h)	Pump rate (%)
Budesonide/ammonium carbonate 10% containing 10% ammonium carbonate by weight of total solids spray dried as a 1% w/v solution from 80% (v/v) ethanol	78	57-58	85	600	15
Budesonide/ammonium carbonate 10% containing 10% ammonium carbonate by weight of total solids spray dried as a 0.77% w/v solution from 80% (v/v) ethanol	85	60-64	85	600	15
Bendroflumethiazide/ammonium carbonate 10% containing 10% ammonium carbonate by weight of total solids spray dried as a 1.28% w/v solution from 80% (v/v) ethanol	85	59-61	85	600	15
Sulphadimidine/ammonium carbonate 10% containing 10% ammonium carbonate by weight of total solids spray dried as a 0.36% w/v solution from 80% (v/v) ethanol	78	53-56	85	600	15
Bendroflumethiazide/PVP 10000/ ammonium carbonate containing 10% PVP 1000 by weight of the total amount of the drug and polymer and containing 10% ammonium carbonate by weight of the total solids spray dried as a 1.27% w/v solution from 80% (v/v) ethanol	78	53-55	85	600	15

Table 8 Spray drying conditions for various excipients used in Chapter 7.

System	Inlet temperature (°C)	Outlet temperature (°C)	Aspirator (%)	Airflow rate (Nl/h)	Pump rate (%)
Mannitol I Mannitol spray dried as a 2.5% w/v solution from deionised water	120	78	100	600	10
Mannitol II Mannitol spray dried as a 1.5% w/v solution from deionised water	140	95-97	100	800	20
Xylitol spray dried as a 2.5% w/v solution from deionised water	120	79	100	600	10
HPMC E5 spray dried as a 2.5% w/v solution from deionised water	120	81	100	600	10
PVP 40000 I PVP 40000 spray dried as a 2.5% w/v solution from deionised water	120	79	100	600	10
PVP 40000 II PVP 40000 spray dried as a 2.5% w/v solution from 95% (v/v) ethanol	78	58	100	600	15
PVP 40000 III PVP 40000 spray dried as a 2.5% w/v solution from 95% (v/v) ethanol	78	58	100	800	15
PVP 40000 II PVP 40000 spray dried as a 1.5% w/v solution from 95% (v/v) ethanol	84	60-61	100	800	20

Table 9 Spray drying conditions for various binary mixtures of excipients used in Chapter 7.

System	Inlet temperature (°C)	Outlet temperature (°C)	Aspirator (%)	Airflow rate (Nl/h)	Pump rate (%)
Mannitol/PVP 40000 10% containing 10% PVP 40000 by weight of total solids spray dried as a 1.5% w/v solution from deionised water	140	84-88	100	800	20
Mannitol/PVP 40000 50% containing 50% PVP 40000 by weight of total solids spray dried as a 1.5% w/v solution from deionised water	140	85-88	100	800	20
Mannitol/HPMC 30% containing 30% HPMC by weight of total solids spray dried as a 1% w/v solution from deionised water	140	83-87	100	800	20

Table 10 Spray drying conditions for the formoterol fumarate (FF)/excipient(s) systems used in Chapter 7. The formoterol fumarate used in the preparation of all solution was formoterol fumarate dihydrate and calcium chloride ($CaCl_2$) was calcium chloride dihydrate.

System	Inlet temperature (°C)	Outlet temperature (°C)	Aspirator (%)	Airflow rate (Nl/h)	Pump rate (%)
Mannitol/FF 10% containing 10% FF by weight of total solids spray dried as a 0.86% w/v solution from deionised water	130	79-81	100	800	20
Mannitol/FF 20% containing 20% FF by weight of total solids spray dried as a 0.43% w/v solution from deionised water	130	79-82	100	800	20
Mannitol/FF 30% containing 30% FF by weight of total solids spray dried as a 0.29% w/v solution from deionised water	130	79-83	100	800	20
Mannitol/FF 10%/citrate buffer salts 1% containing 10% FF and 1% citrate buffer salts by weight of total solids spray dried as a 0.86% w/v solution from deionised water	120	72-74	100	800	20
Mannitol/FF 10%/phosphate buffer salts 1% containing 10% FF and 1% phosphate buffer salts by weight of total solids spray dried as a 0.86% w/v solution from deionised water	120	71-73	100	800	20
Mannitol/FF 10%/$CaCl_2$ 5% containing 10% FF and 5% $CaCl_2$ by weight of total solids spray dried as a 0.86% w/v solution from deionised water	120	70-71	100	800	20
Mannitol/FF 10%/citrate buffer salts 1%/ $CaCl_2$ 5% containing 10% FF, 1% citrate buffer salts and 5% $CaCl_2$ by weight of total solids spray dried as a 0.86% w/v solution from deionised water	120	67-68	100	800	20

APPENDIX II

HPLC calibration curves

(1) **Formoterol fumarate** (method described in Chapter 2.2.9.1)

Peak area = 99738*Concentration [µg/ml]

$R^2 = 0.9989$

(2) **Budesonide** (method described in Chapter 2.2.9.1)

Peak area = 447501*Concentration [µg/ml]

$R^2 = 0.9998$

(3) **Formoterol fumarate** (method described in Chapter 2.2.9.2)

Peak area = 609134*Concentration [µg/ml]

$R^2 = 0.9999$

APPENDIX IV

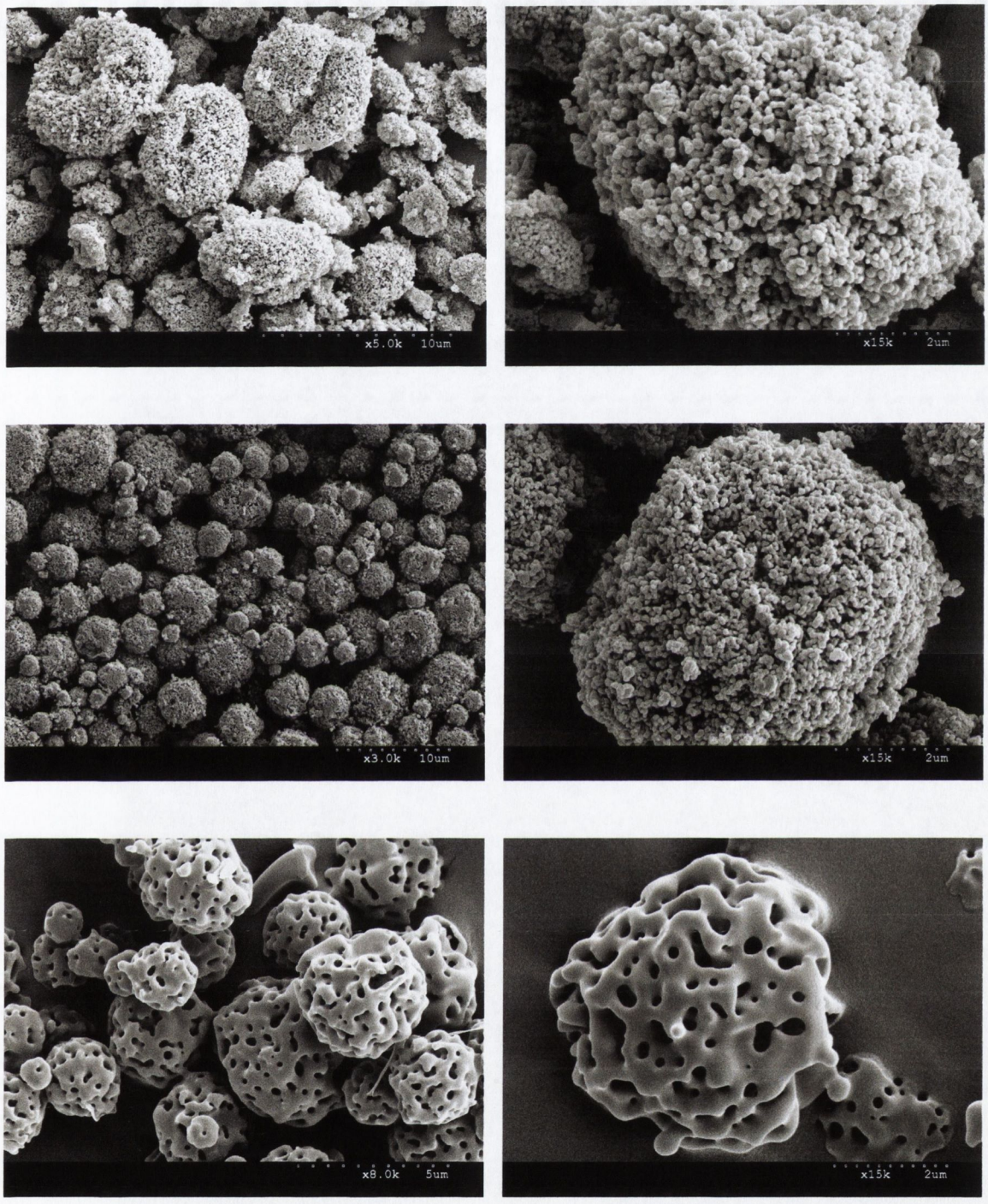

Figure 1 SEM micrographs of porous bendroflumethiazide (top), porous bendroflumethiazide/PVP 10000 10% (w/) (middle) and sulphadimidine (bottom) prepared by spray drying with ammonium carbonate. The processing conditions are given in Appendix 1.

APPENDIX V

Table 1 The retention time and assignment of decomposition products obtained in the Robinson-Britton buffer at 40°C (FF isomer, FFD, FFA and A-4 are the degradation product codes according to Table 7.1 in Chapter 7, question mark indicates that the interpretation is uncertain).

pH	Retention time [min]	Relative retention time	Compound
2.05	5.96	0.81	FFD
	7.40	1.00	FF
3.00	5.71	0.81	FFD
	6.28	0.89	
	7.06	1.00	FF
3.90	5.33	0.73	
	6.00	0.82	FFD
	6.85	0.93	FF isomer ?
	7.34	1.00	FF
	12.62	1.72	
5.00	5.20	0.73	
	5.91	0.83	FFD
	6.68	0.94	FF isomer ?
	7.14	1.00	FF
	11.92	1.67	
6.10	5.82	0.83	FFD
	6.64	0.95	FF isomer ?
	7.00	1.00	FF
6.70	5.81	0.82	FFD
	7.02	1.00	FF
	8.31	1.18	FFA
8.20	4.24	0.55	
	6.29	0.82	FFD
	6.76	0.88	
	7.65	1.00	FF
	8.85	1.16	FFA
	9.22	1.21	
	10.86	1.42	
8.70	3.34	0.47	
	4.04	0.57	
	4.54	0.64	A-4
	5.36	0.76	
	5.82	0.83	FFD
	6.29	0.89	
	7.05	1.00	FF
	7.61	1.08	
	8.22	1.17	FFA
	10.33	1.47	
	10.81	1.53	
9.60	3.98	0.56	
	4.45	0.64	A-4
	5.36	0.76	
	6.28	0.89	
	7.04	1.00	FF
	8.24	1.17	FFA
	8.99	1.28	

APPENDIX VI

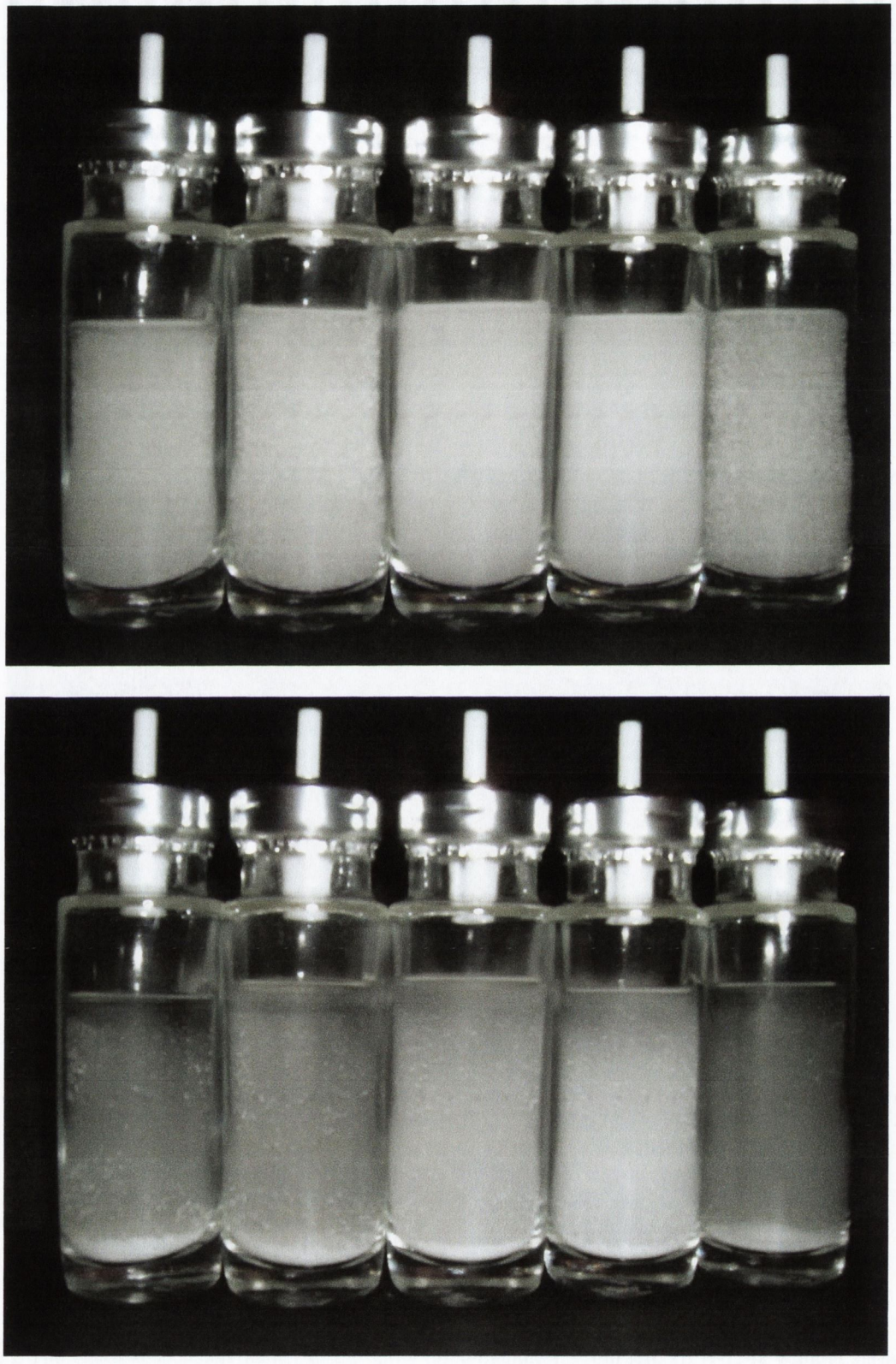

Figure 1 The visual suspension quality of the spray dried mannitol. From left: HFA-134a without ethanol, HFA-134a and 0.1% (w/w) ethanol, HFA-134a and 1% (w/w) ethanol, HFA-134a and 2% (w/w) ethanol, HFA-134a and 5% (w/w) ethanol.

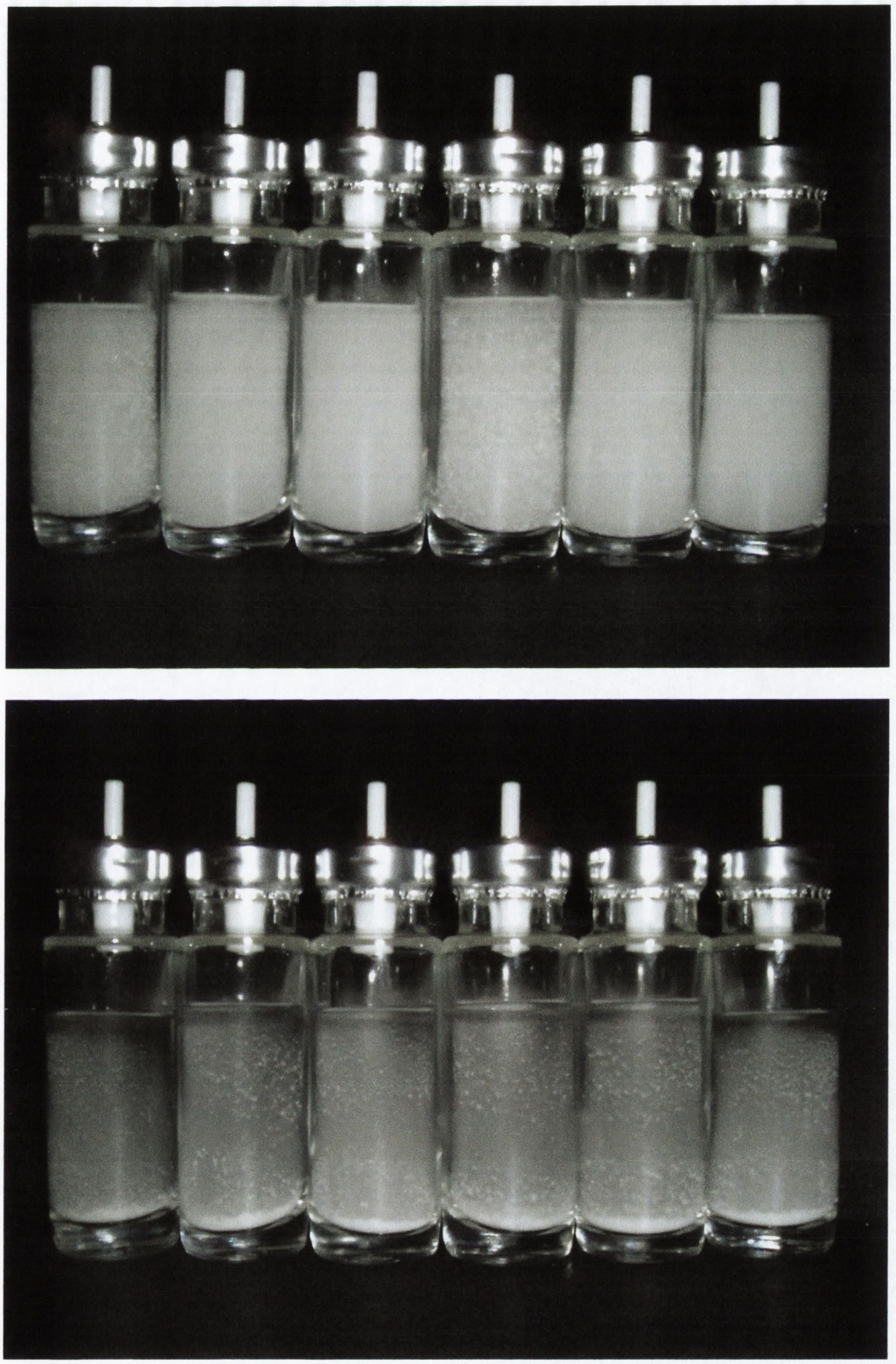

Figure 2 The visual suspension quality of the spray dried mannitol. From left: HFA-134a without surfactant, HFA-134a and 1% (w/w) PEG 300, HFA-134a and 1% (w/w) PEG 1000, HFA-134a and 1% (w/w) Capmul PG-12, HFA-134a and 1% (w/w) Brij 35, 1% (w/w) Brij 58.

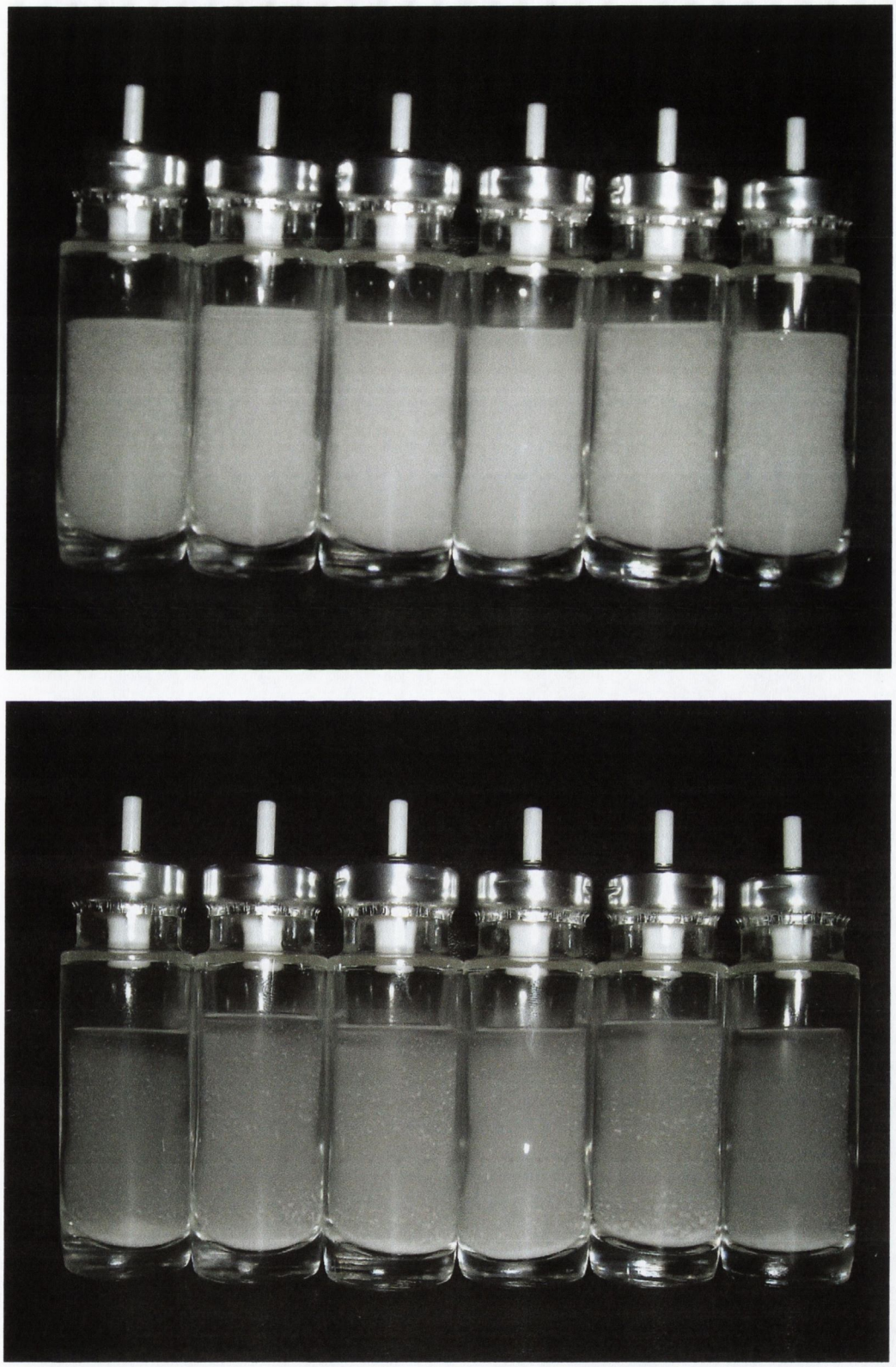

Figure 3 The visual suspension quality of the spray dried mannitol in HFA-134a containing 1% (w/w) ethanol. From left: HFA-134a without surfactant, HFA-134a and 1% (w/w) PEG 300, HFA-134a and 1% (w/w) PEG 1000, HFA-134a and 1% (w/w) Capmul PG-12, HFA-134a and 1% (w/w) Brij 35, 1% (w/w) Brij 58.

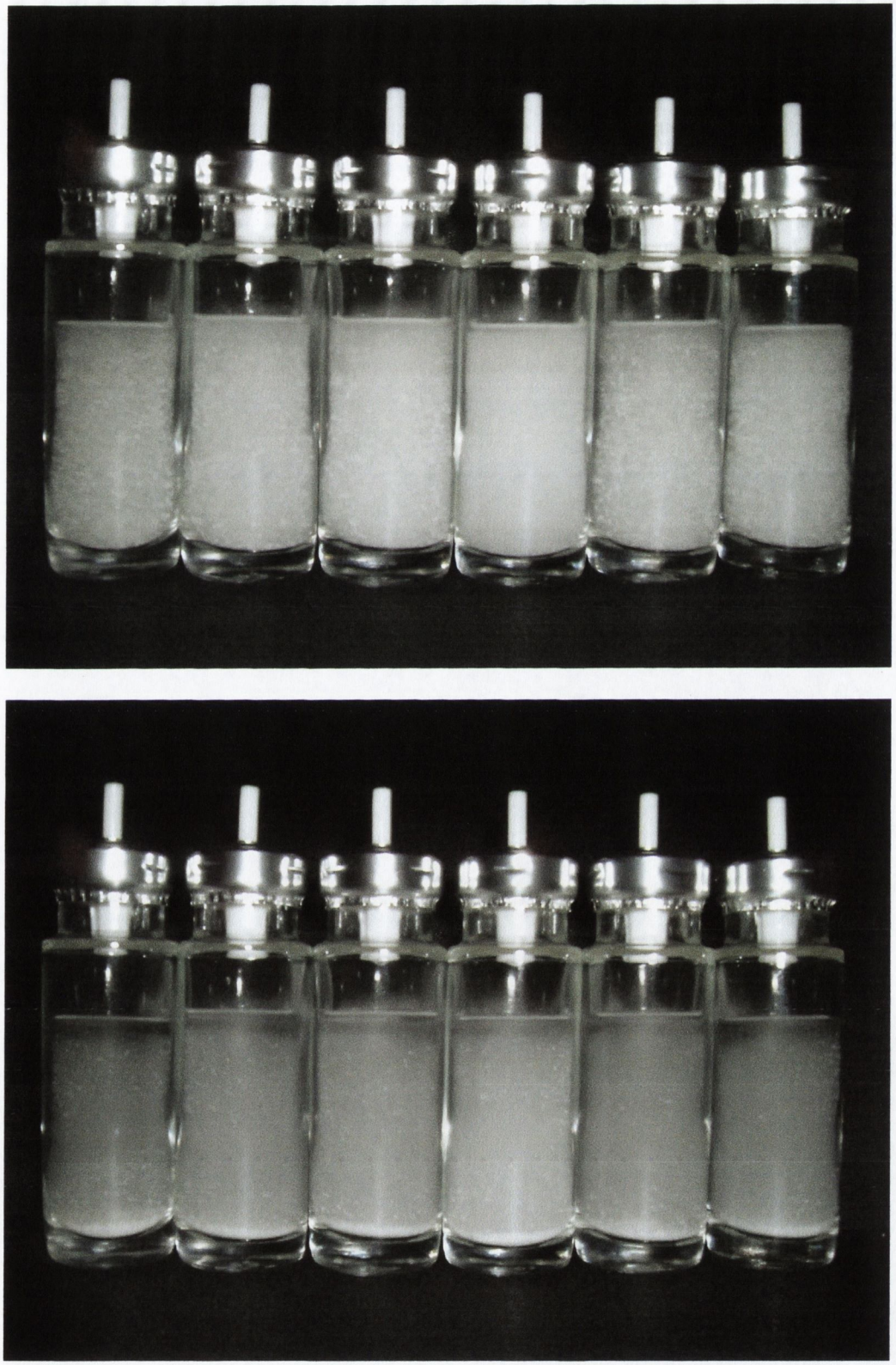

Figure 4 The visual suspension quality of the spray dried mannitol in HFA-134a containing 2% (w/w) ethanol. From left: HFA-134a without surfactant, HFA-134a and 1% (w/w) PEG 300, HFA-134a and 1% (w/w) PEG 1000, HFA-134a and 1% (w/w) Capmul PG-12, HFA-134a and 1% (w/w) Brij 35, 1% (w/w) Brij 58.

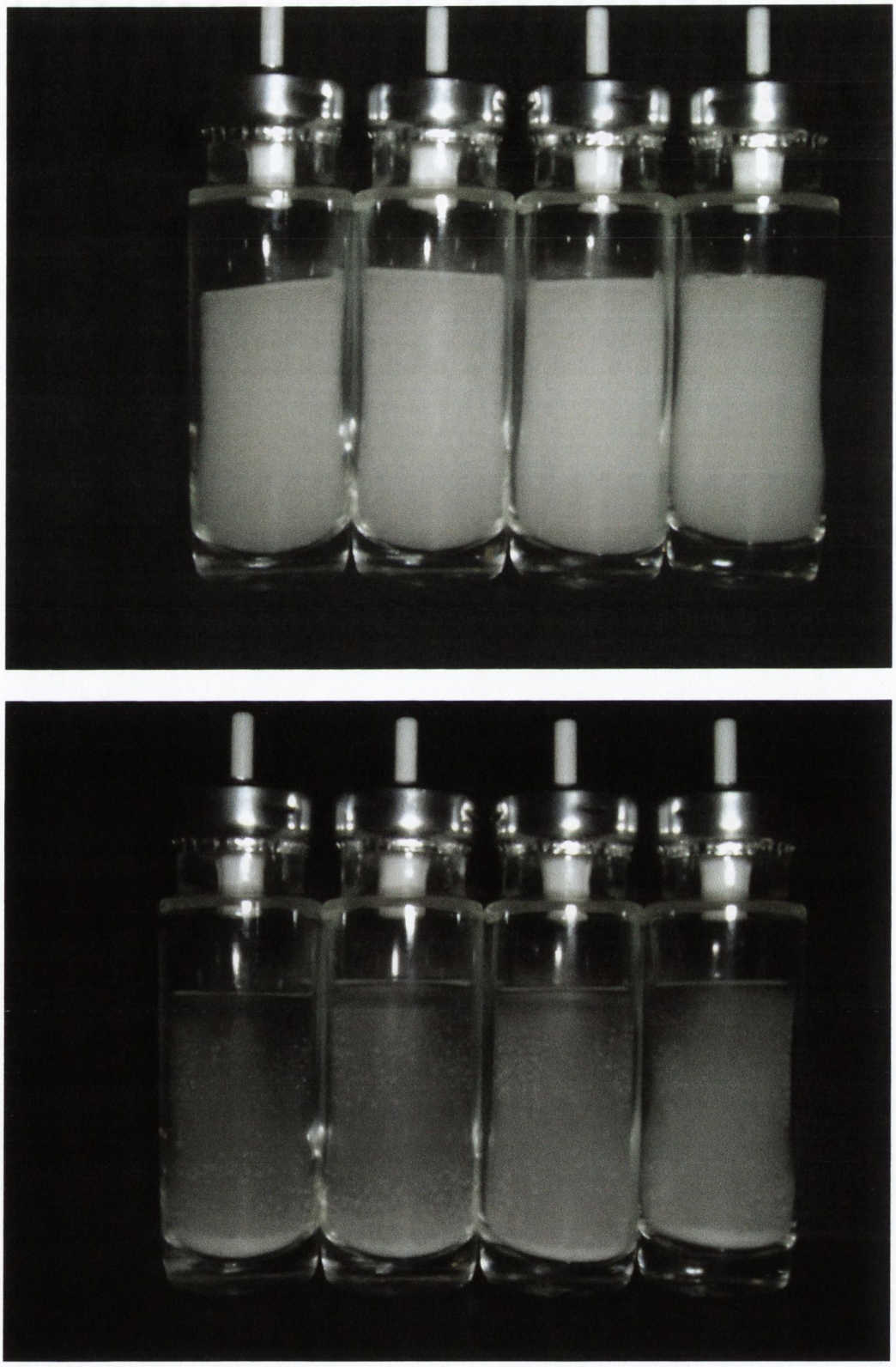

Figure 5 The visual suspension quality of the spray dried mannitol. From left: HFA-134a without ethanol and surfactant (control), HFA-134a with 1% (w/w) ethanol and 1% (w/w) Brij 97, HFA-134a with 2% (w/w) ethanol and 1% (w/w) Brij 97, HFA-134a with 2% (w/w) ethanol and 1% (w/w) Myrj 53.

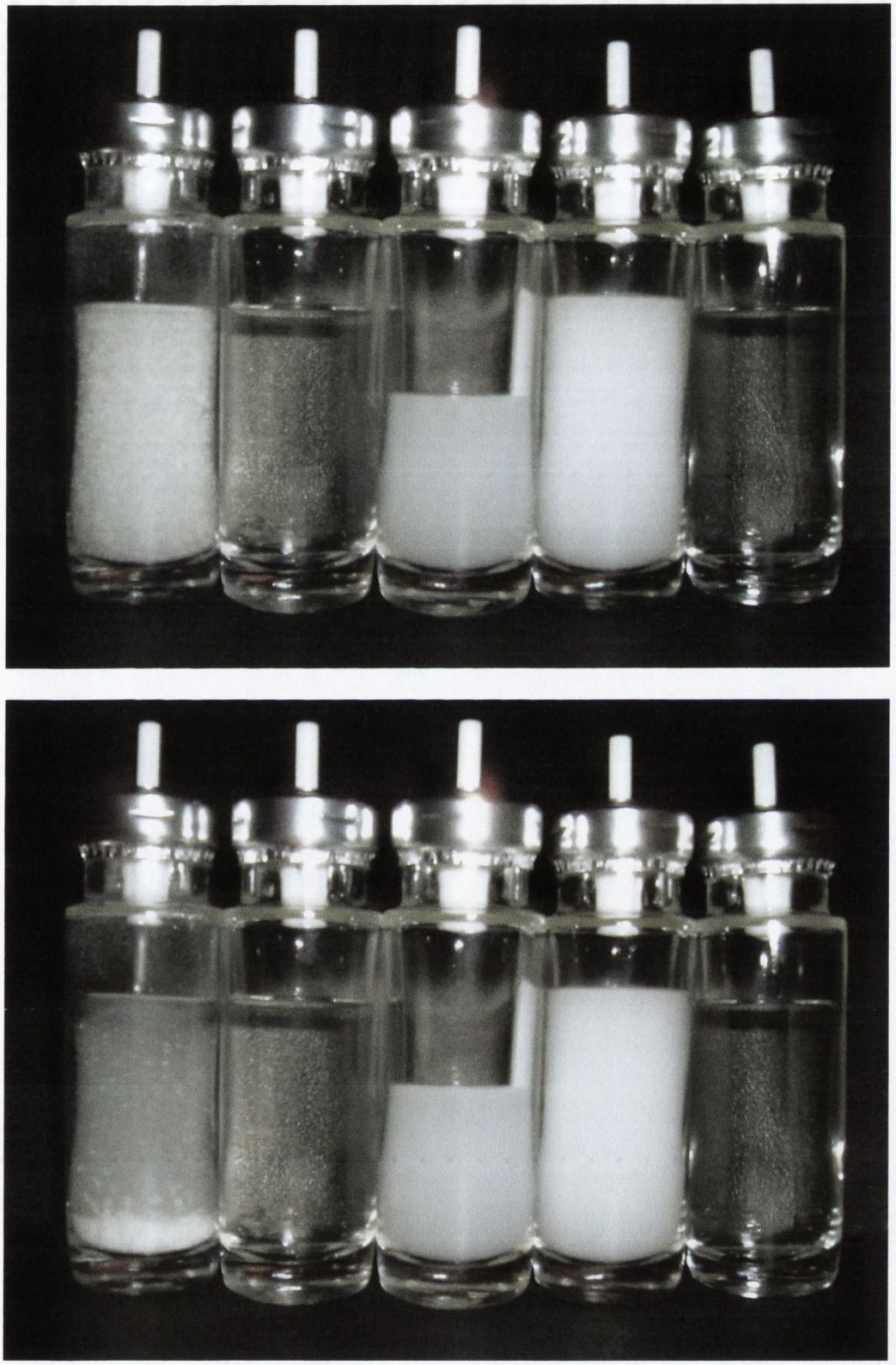

Figure 6 The visual suspension quality of the spray dried PVP. From left: HFA-134a without ethanol, HFA-134a and 0.1% (w/w) ethanol, HFA-134a and 1% (w/w) ethanol, HFA-134a and 2% (w/w) ethanol, HFA-134a and 5% (w/w) ethanol.

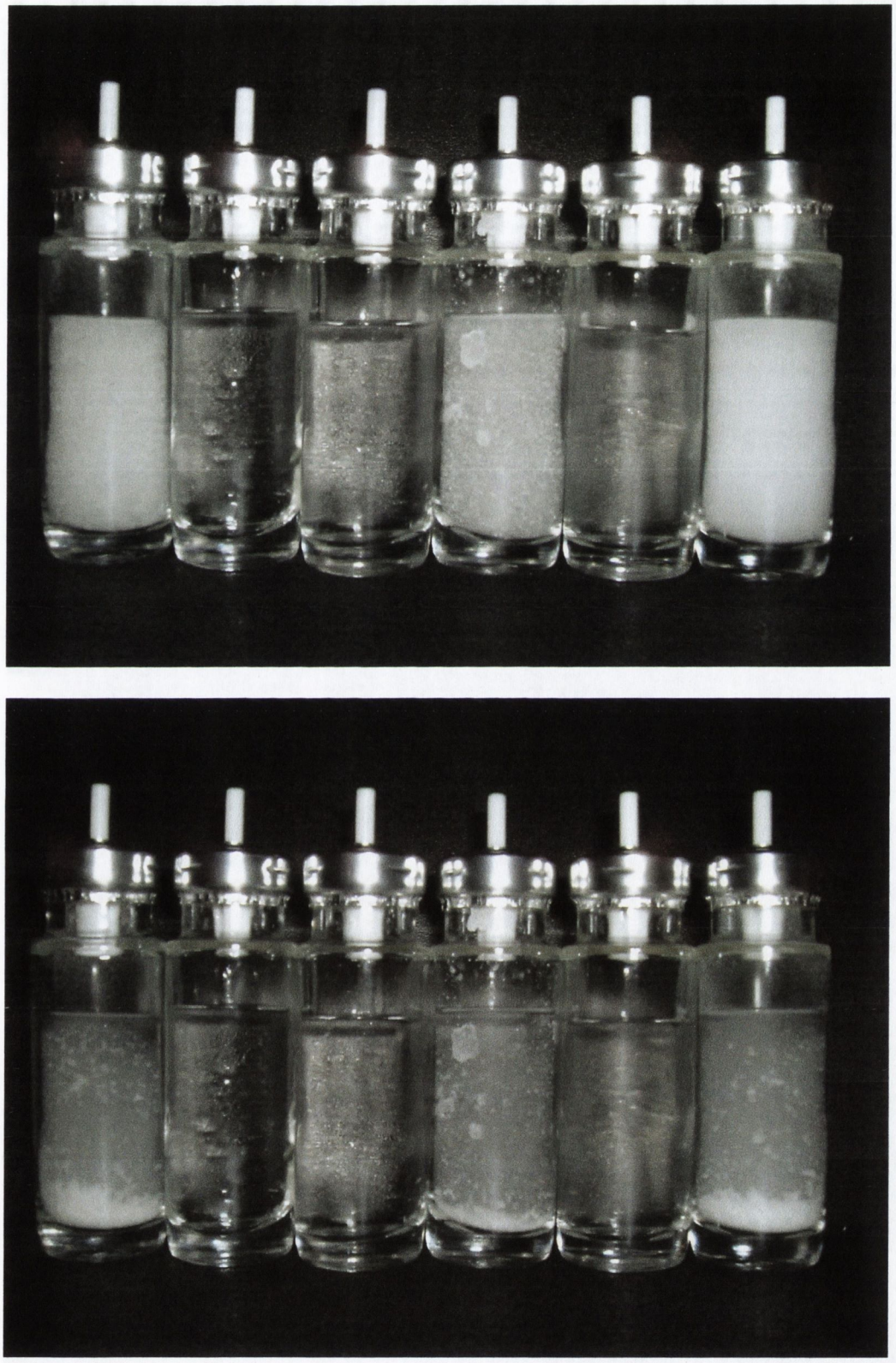

Figure 7 The visual suspension quality of the spray dried PVP. From left: HFA-134a without surfactant, HFA-134a and 1% (w/w) PEG 300, HFA-134a and 1% (w/w) PEG 1000, HFA-134a and 1% (w/w) Brij 58, HFA-134a and 1% (w/w) Capmul PG-12, 1% (w/w) Brij 35.

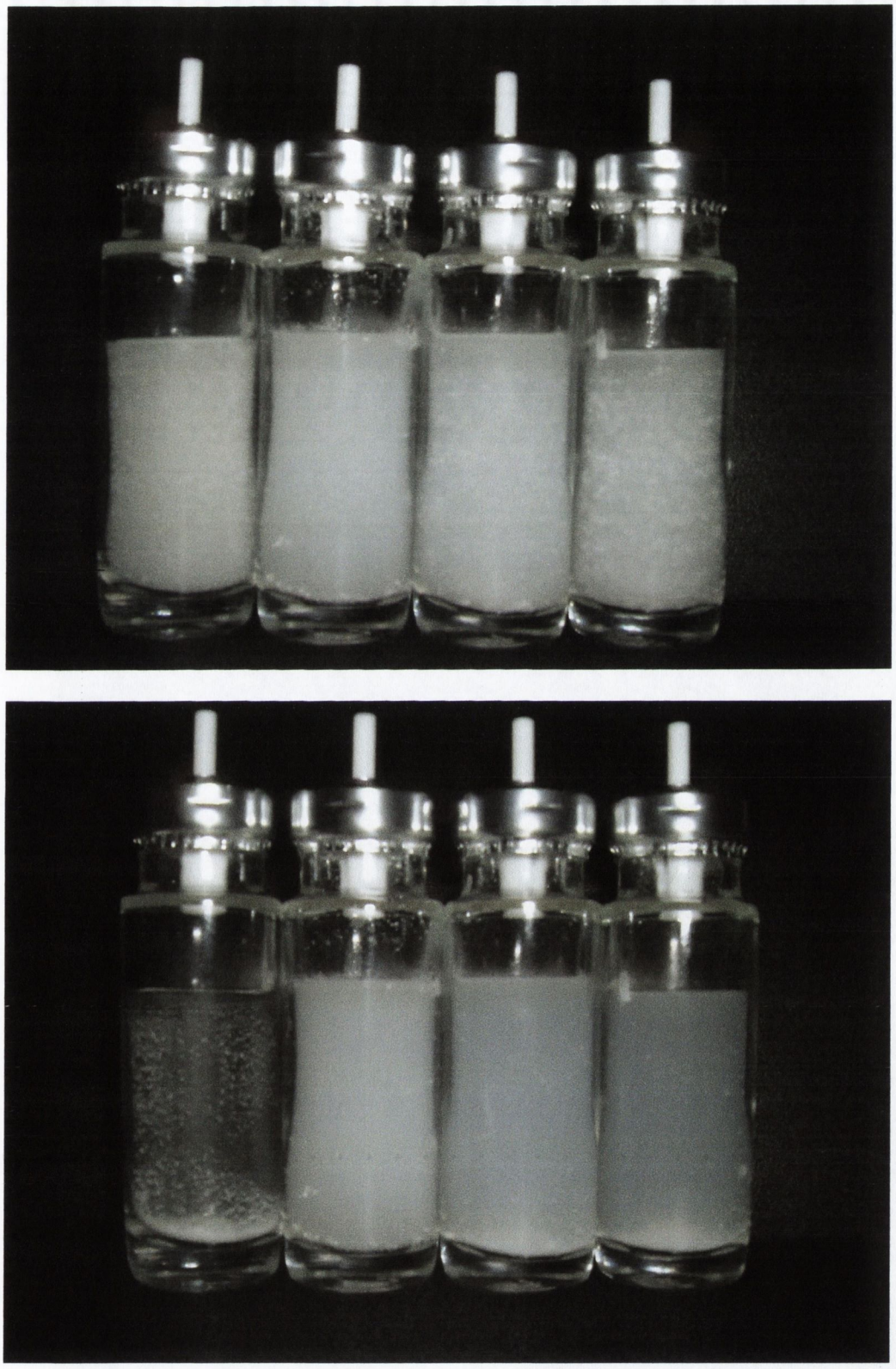

Figure 8 The visual suspension quality of the spray dried mannitol in HFA-134a containing 2% (w/w) ethanol. From left: mannitol in HFA-134a without ethanol and PVP (control), 2% (w/w) ethanol and 0.2% (w/w) PVP, 2% (w/w) ethanol and 0.1% (w/w) PVP, 2% (w/w) ethanol and 0.05% (w/w) PVP.

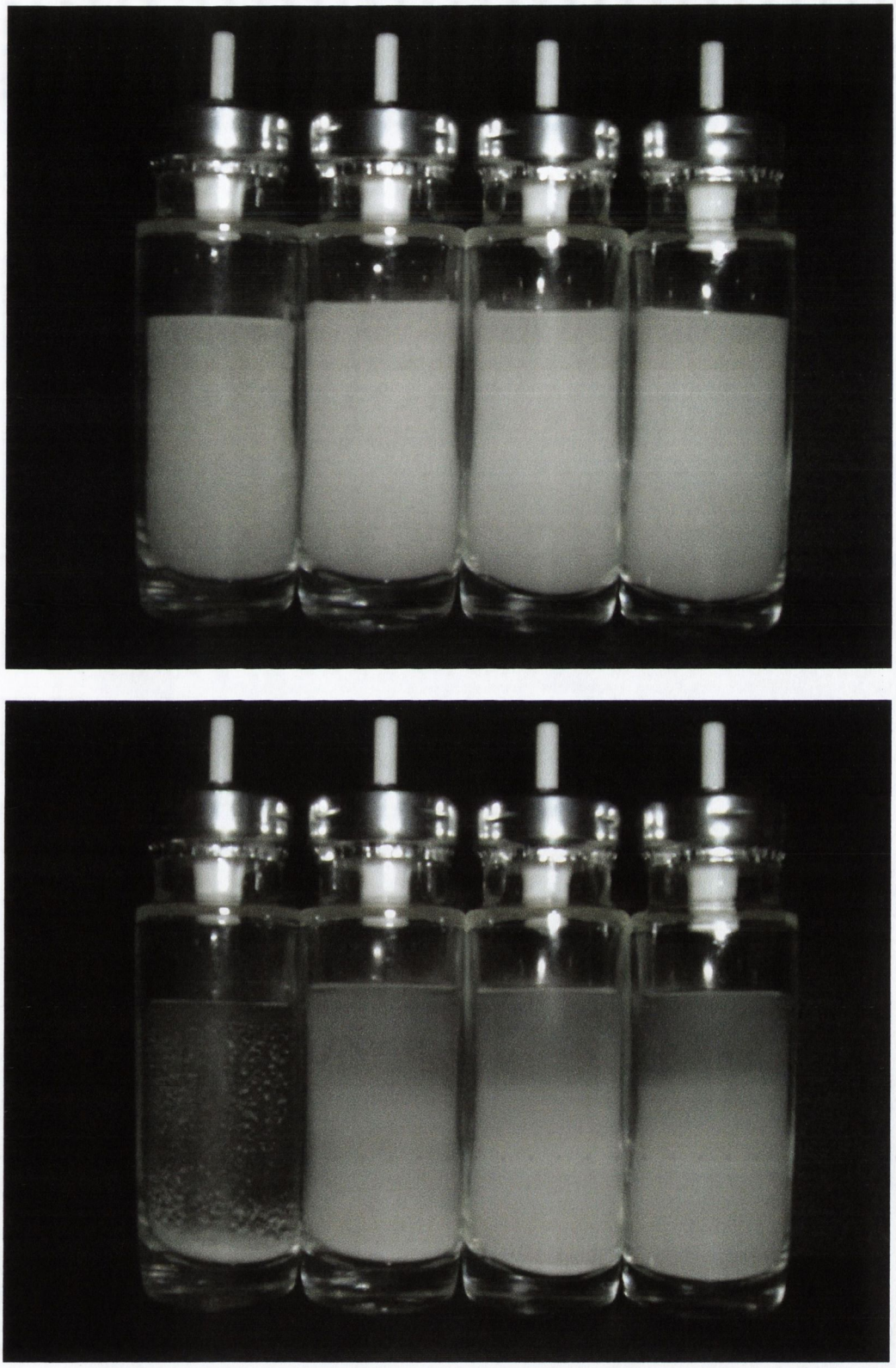

Figure 9 The visual suspension quality of the spray dried mannitol in HFA-134a containing 5% (w/w) ethanol. From left: mannitol in HFA-134a without ethanol and PVP (control), 5% (w/w) ethanol and 0.2% (w/w) PVP, 5% (w/w) ethanol and 0.1% (w/w) PVP, 5% (w/w) ethanol and 0.05% (w/w) PVP.



Figure 10 The visual suspension quality of the co-spray dried mannitol/HPMC E5 30%. From left: mannitol in HFA-134a without ethanol (reference), co-spray dried sample in HFA-134a without ethanol, co-spray dried sample in HFA-134a and 1% (w/w) ethanol.

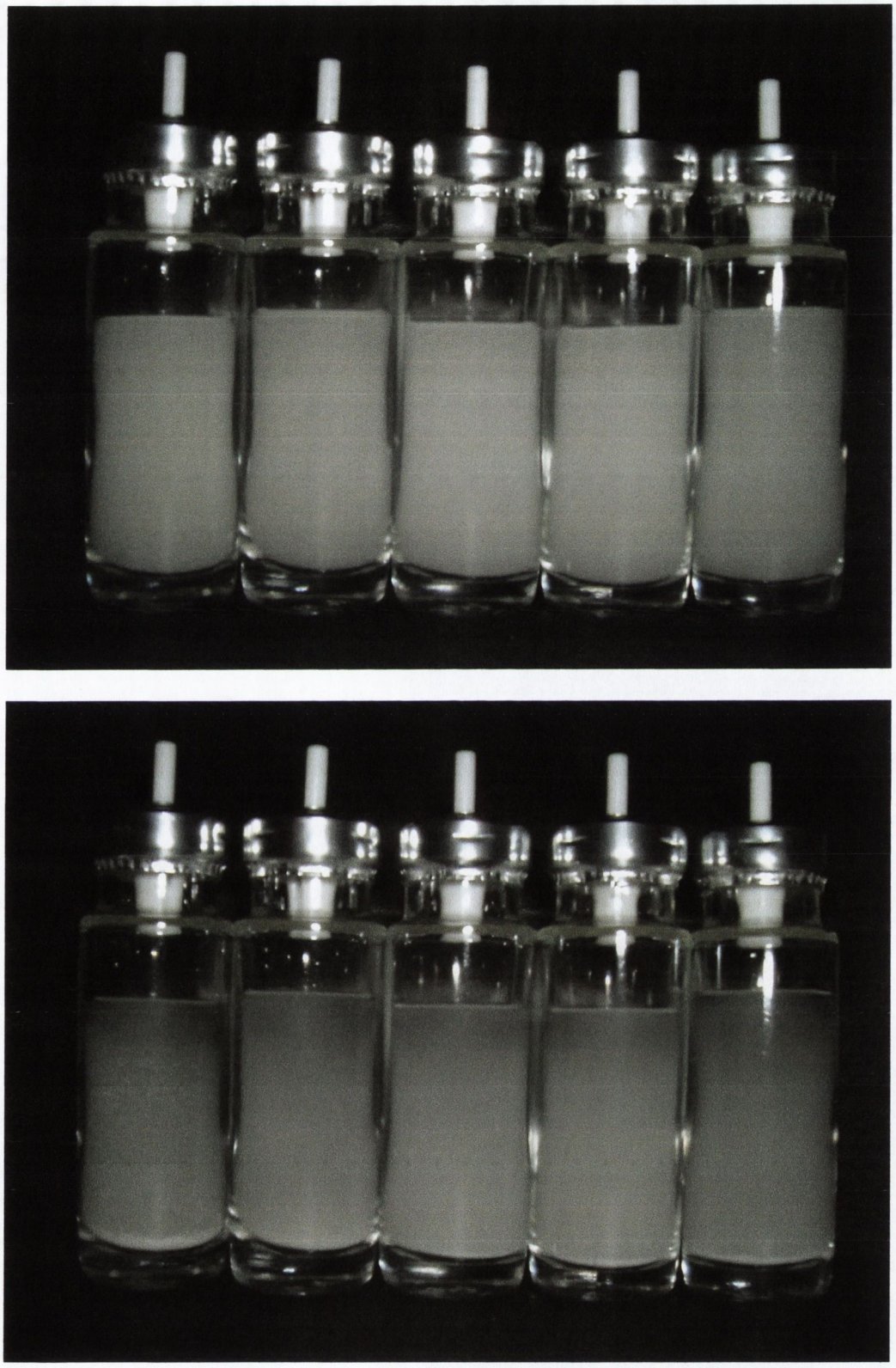

Figure 11 The visual suspension quality of the co-spray dried mannitol/PVP 10%. From left: HFA-134a without ethanol, HFA-134a and 0.1% (w/w) ethanol, HFA-134a and 1% (w/w) ethanol, HFA-134a and 2% (w/w) ethanol, HFA-134a and 5% (w/w) ethanol.



Figure 12 The visual suspension quality of the formoterol fumarate dihydrate starting material. From left: HFA-134a without ethanol, HFA-134a and 1% (w/w) ethanol, HFA-134a and 0.5% (w/w) oleic acid, HFA-134a and 0.5% (w/w) oleic acid with 1% (w/w) ethanol, HFA-134a and 0.2% (w/w) PVP with 5% (w/w) ethanol, HFA-134a and 0.01% (w/w) PVP with 1% (w/w) ethanol.

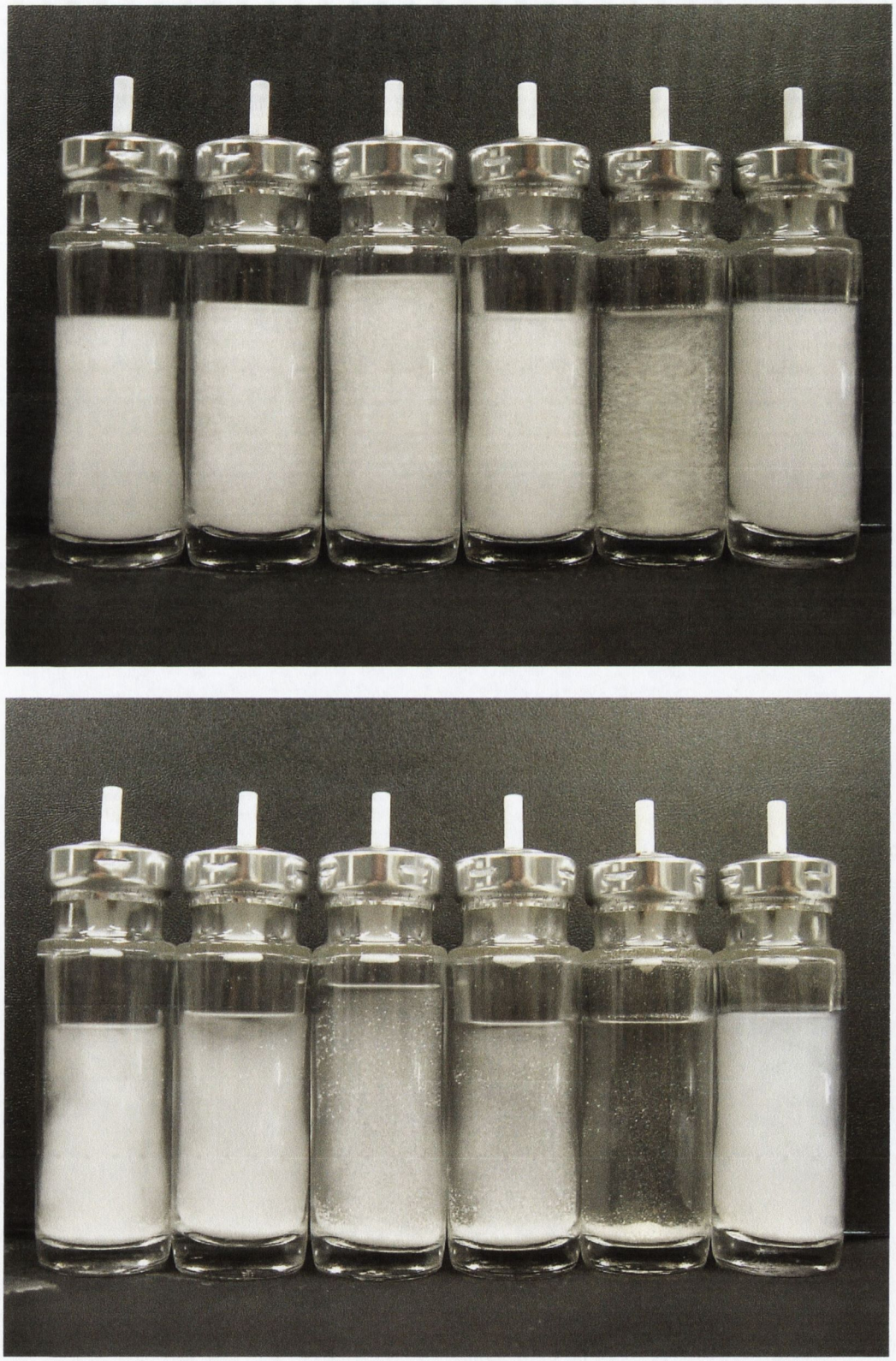

Figure 13 The visual suspension quality of the co-spray dried mannitol and formoterol fumarate dihydrate 10%. From left: HFA-134a without additives, HFA-134a and 1% (w/w) ethanol, HFA-134a and 1% (w/w) PEG 1000, HFA-134a and 1% (w/w) Brij 35, HFA-134a containing 5% (w/w) ethanol and 0.2 % (w/w) PVP, HFA-134a containing 1% (w/w) ethanol and 0.01% (w/w) PVP.

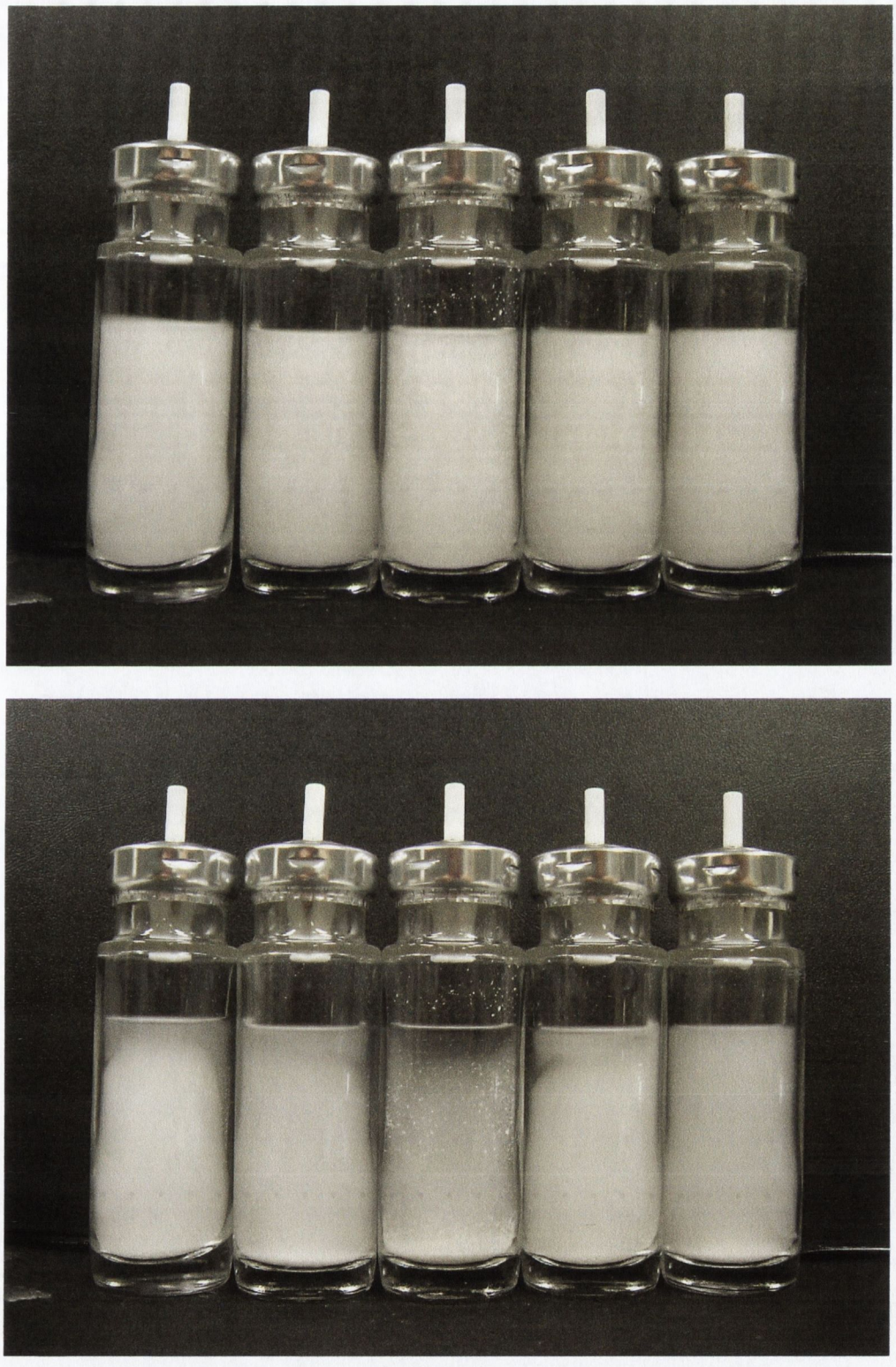

Figure 14 The visual suspension quality of the co-spray dried mannitol and formoterol fumarate dihydrate. From left: co-spray dried mannitol and formoterol fumarate dihydrate 20% in HFA-134a, co-spray dried mannitol and formoterol fumarate dihydrate 20% in HFA-134a and 1% (w/w) ethanol, co-spray dried mannitol and formoterol fumarate dihydrate 20% in HFA-134a and 1% (w/w) PEG 1000, co-spray dried mannitol and formoterol fumarate dihydrate 30% in HFA-134a, co-spray dried mannitol and formoterol fumarate dihydrate 30% in HFA-134a and 1% (w/w) ethanol.

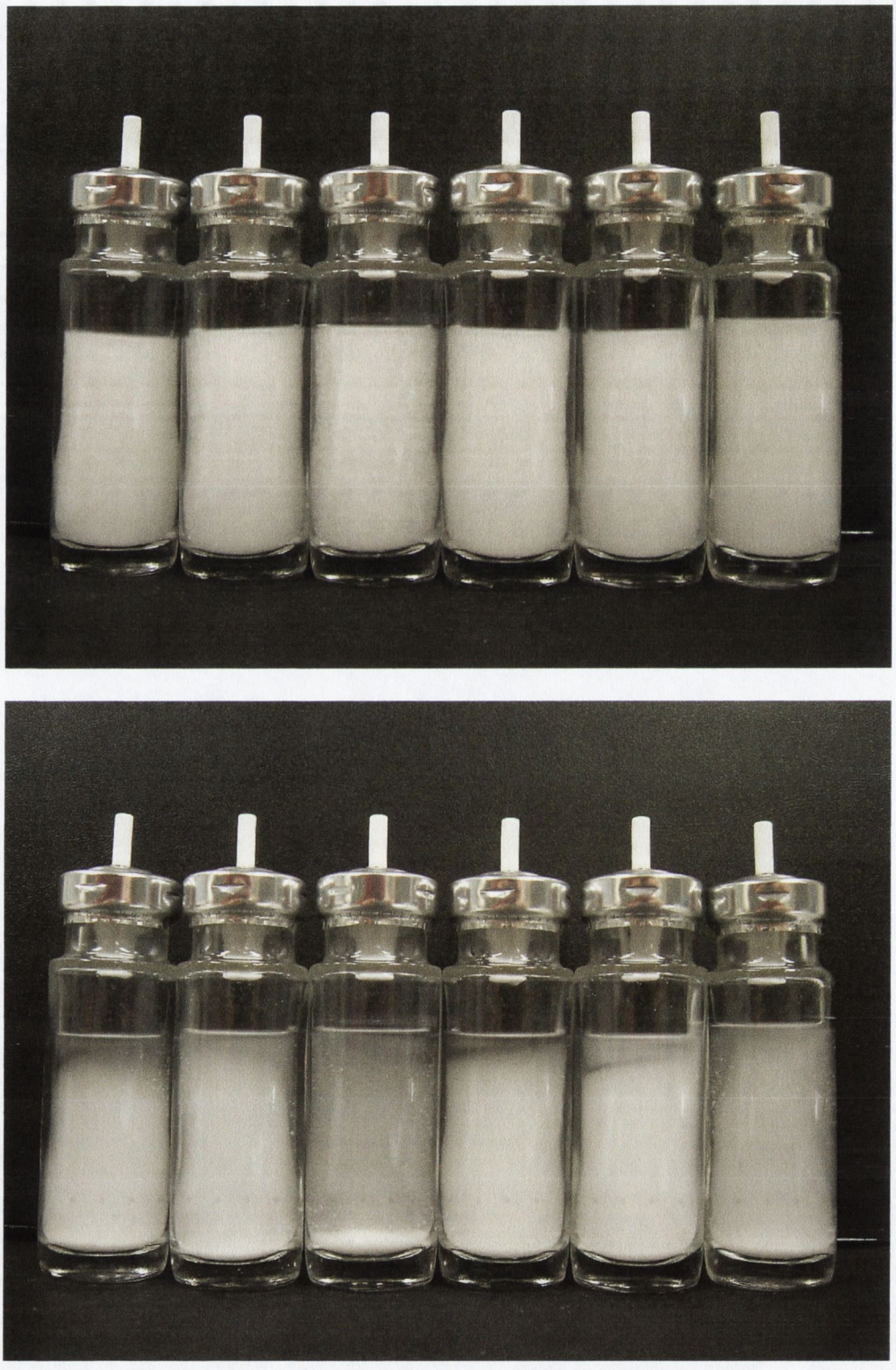

Figure 15 The visual suspension quality of the co-spray dried mannitol, formoterol fumarate dihydrate 10% and buffer salts 1%. From left: co-spray sample containing citrate buffer salts 1% in HFA-134a, co-spray sample containing citrate buffer salts 1% in HFA-134a and 1% (w/w) ethanol, co-spray sample containing citrate buffer salts 1% in HFA-134a and 5% (w/w) ethanol, co-spray dried sample containing phosphate buffer salts 1% in HFA-134a, co-spray dried sample containing phosphate buffer salts 1% in HFA-134a and 1% (w/w) ethanol, co-spray dried sample containing phosphate buffer salts 1% in HFA-134a and 5% (w/w) ethanol.

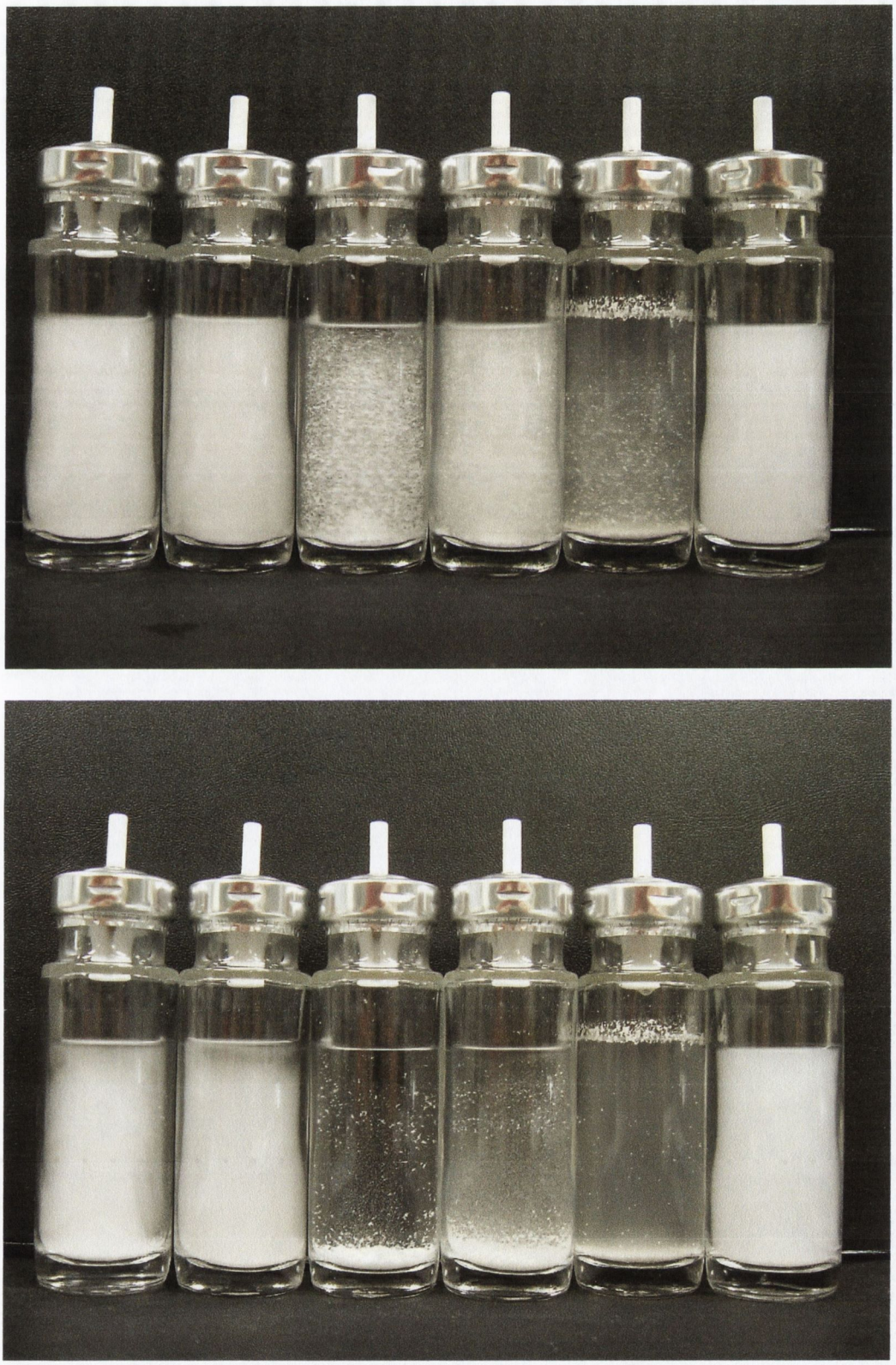

Figure 16 The visual suspension quality of the co-spray dried mannitol, formoterol fumarate dihydrate 10% and $CaCl_2 \cdot 2H_2O$ 5%. From left: HFA-134a without additives, HFA-134a and 1% (w/w) ethanol, HFA-134a and 1% (w/w) PEG 1000, HFA-134a and 1% (w/w) Brij 35, HFA-134a containing 5% (w/w) ethanol and 0.2 % (w/w) PVP, HFA-134a containing 1% (w/w) ethanol and 0.01 % (w/w) PVP.

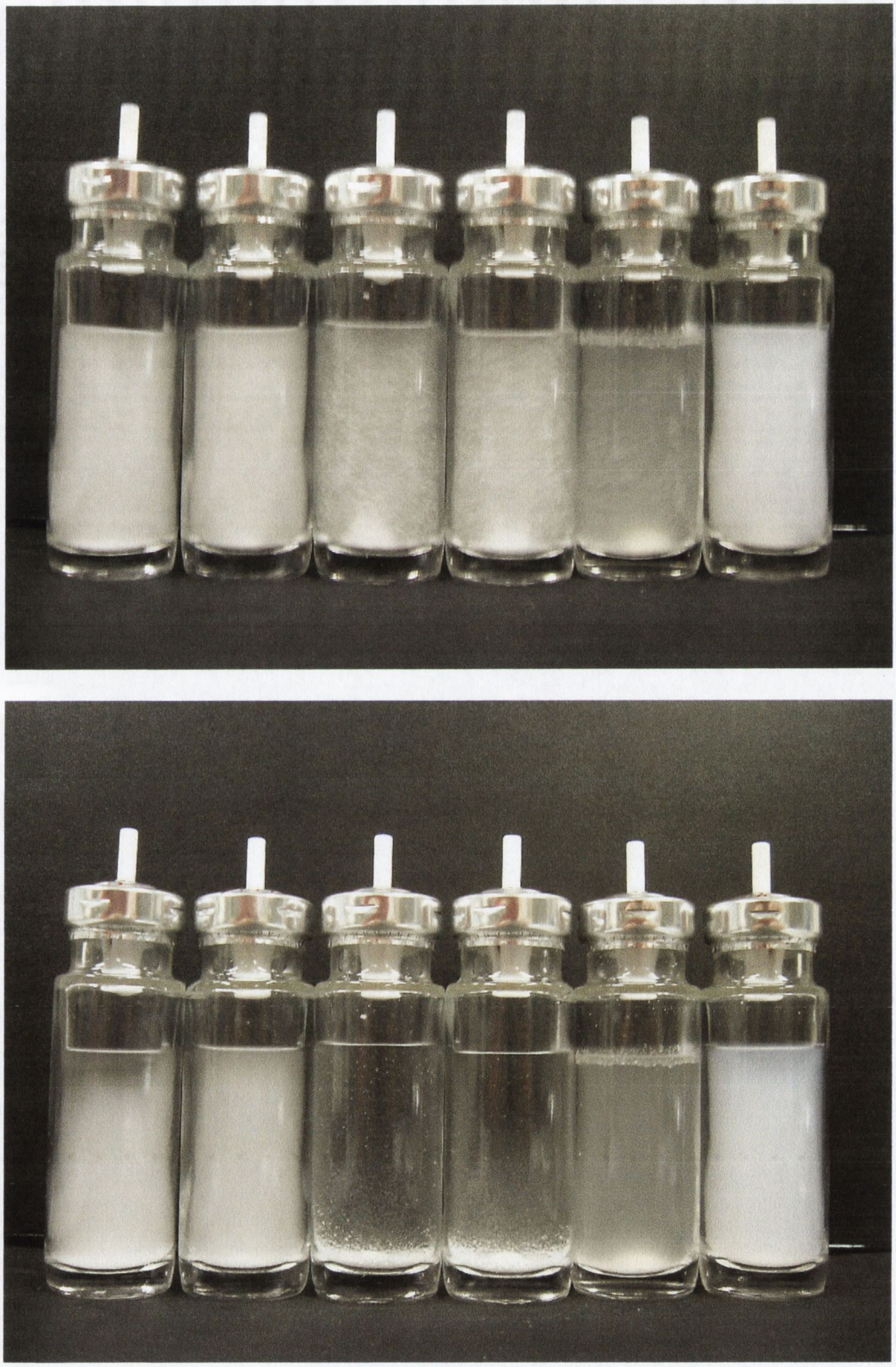

Figure 17 The visual suspension quality of the co-spray dried mannitol, formoterol fumarate dihydrate 10%, citrate buffer salts 1% and $CaCl_2 \cdot 2H_2O$ 5%. From left: HFA-134a without additives, HFA-134a and 1% (w/w) ethanol, HFA-134a and 1% (w/w) PEG 1000, HFA-134a and 1% (w/w) Brij 35, HFA-134a containing 5% (w/w) ethanol and 0.2 % (w/w) PVP, HFA-134a containing 1% (w/w) ethanol and 0.01 % (w/w) PVP.



Figure 18 The visual suspension quality of the budesonide systems in HFA-134a after mixing (top) and after 2 minutes (bottom). From left: budesonide "as received" powder, spray dried budesonide, porous budesonide spray dried at the inlet temperature of 78°C and porous budesonide spray dried at the inlet temperature of 85°C.